CONSTITUTIVE MODEL OF CONCRETE CONFINED BY ADVANCED FIBER COMPOSITE MATERIALS AND APPLICATIONS IN SEISMIC RETROFITTING

by

Hui Wu

A Dissertation Presented to the
FACULTY OF THE GRADUATE SCHOOL
UNIVERSITY OF SOUTHERN CALIFORNIA
In Partial Fulfillment of the
Requirements for the Degree
DOCTOR OF PHILOSOPHY
(CIVIL ENGINEERING)

August 2007

DEDICATION

To my wife, daughter, and parents.

ACKNOWLEDGMENTS

This dissertation is presented by the author under the supervision of Professor Yan Xiao, the dissertation committee also includes Professors G.R. Martin, and S. Nutt.

My special thanks go to Mr. Robert Bueche, previous manager of the USC Civil Engineering Laboratory, and to Mr. Lance Hill, current manager, for their technical expertise during the experimental phase of the research.

The author would like to thank Mr. Henry W. Yun and Mr. Tolga T. Yaprak, graduate research assistants at Structural Laboratory of the University of Southern California for their support during the construction and testing of the experiments.

The study described in this dissertation was conducted as one phase of the California Department of Transportation (Caltrans) evaluation program for various composite jacketing systems and other funding agencies. The tests on concrete sub columns confined by carbon fiber reinforced composite jackets were funded by Master Builders, Inc., Mitsubishi Corp., TYFO system, and XXsys Technologies Inc. The author would also like to thank Caltrans engineer Mr. L.H. Sheng for his valuable input.

TABLE OF CONTENTS

LIST OF TABLES

LIST OF FIGURES

ABSTRACT

Fiber Reinforced Polymer (FRP) or Fiber Reinforced Plastics have been widely utilized in civil infrastructures due to their unique properties. The advantages of FRP composites include superior strength or stiffness to weight ratio, ductile form in design, and sustained chemical inertness in most civil environments. However, the behavior mechanism of the FRP jacketing in reinforced concrete column is not yet fully understood. The current design of FRP confined concrete retrofit jacketing system is still limited to the experimental results of transversely reinforced steel in concrete confinement.

In this study, more than 200 concrete stub columns with composite jackets have been tested under axial compression. Experimental parameters include plain concrete strengths, types of composites, and jacket thickness. Axial and transverse strain responses were investigated. The confinement coefficient *k* was obtained from the test results, based on the Rechart equation. Hence a constitutive model of confined concrete is proposed and shown to compare well with the test results from previous studies by other researchers.

The overall goal of this research is to create a universal model of confined concrete through an analytical approach and intensive experimental studies. The proposed model is suitable not only for FRP jacketing but also steel confined concrete. Based on this model, concrete column confined with FRP or steel jackets can be predicted by a numerical method.

CHAPTER 1: INTRODUCTION

1.1 Overview and Problem Description

Advanced composite materials have been recently applied to bridge column retrofits. The general expectations from composite retrofit systems include lightweight, high stiffness or strength to weight ratios, etc. Several composite jacketing systems have been developed and validated in laboratory or field conditions. Matsuda et al. [1990] tested a system for bridge pier retrofit using unidirectional carbon fiber sheets wrapped longitudinally and transversely in the potential plastic hinge region or in the region of main bar cut-off. The carbon fiber sheets were bonded to the concrete surface using epoxy resin.

Another composite wrapping system using E-glass fiber, which is much more economical than carbon fiber, has been experimentally studied by Priestley and Seible [1991, 1993]. Priestley et al.'s test results on 40% scale bridge piers wrapped with the glass fiber composite jacketing demonstrated significant improvement of seismic performance with increased strength and ductility. Priestley and Seible also developed a full design package for seismic retrofit of existing columns using different retrofit jacketing systems. Saadatmanesh, et al. [1994] have proposed a wrapping technique using glass fiber composite straps for column retrofit. Seible et al. [1995] have experimentally validated a carbon fiber retrofit system, which utilizes an automated machine to wrap carbon bundles to form a continuous jacket. Successful field construction demonstration is also reported by Seible et al. [1995].

These composite retrofit measures can be categorized as in-situ fabricated jacketing, which involves manual or automated machine placement of epoxy saturated glass or carbon fibers on the surface of existing concrete. An in-situ fabricated jacket can then match the shape of the concrete column. However, due to the intricate process of in-situ fabrication, these systems may require special attention to job-site quality control and curing of the composite jackets.

Another category of the composite retrofit method can be classified as prefabricated (or preformed) jacketing system. The prefabricated jacketing system is expected to have superior constructability in terms of the quality control and the speed of installation. The prefabricated jackets are made by sticking together fiber sheets with fiber strands. With the roll of fiber encased in the fabric sheet, a composite laminate is created and can only bend in one direction. The laminate is then saturated in resin and placed onto a specially designed form, thus creating the prefabricated jacket shell. These types of jackets are custom designed based on different projects. Recently a prefabricated composite jacketing system for seismic retrofitting of reinforced concrete columns has been investigated at the University of Southern California [Xiao et al. 1996, 1997]. Nine half-scale bridge short columns have been tested. The as-built columns showed typical shear failure in cyclic loading. A similar preformed carbon shell system has also been studied at University of California, San Diego [Seible et al. 1997].

As the largest commercial application of FRP technology in the seismic retrofit in the US, over 3,000 columns on the Yolo causeway west of Sacramento, California, were wrapped with prefabricated E-glass fibers as reinforcement in a polyester matrix.

Despite the successful applications of various composite jacketing systems in retrofitting laboratory models as well as prototype bridge columns, research on the fundamental mechanisms of the interactions between the composite jackets and the confined concrete is still limited. Several stress strain models have been proposed and calibrated against several individual jacketing systems [Picher et al. 1996; Hosotani et al. 1996; Mirmiran et al. 1997, 1998; Harmon et al. 1998; Toutanji 1999]. However, they are not yet calibrated for general use due to the lack of sufficient data. Thus in many cases of structural retrofit design, engineers rely on the models developed based on the test results of concrete confined in transverse reinforcing steel.

1.2 Objective and Scope

The objective of the proposed research is to develop a general confined concrete model that is suitable not only for steel confined concrete but also for composite fiber confined concrete. Based on our constitutive model, the behavior of the RC structural components in cyclic loading can be better understood. To achieve these goals, the following tasks have been developed or will be performed in future studies:

(1) Develop a Universal Constitutive Model of Confined Concrete.

(2) Evaluate the behavior mechanism and failure modes of concrete columns confined with advanced fiber composite jackets. (Done, 1997~1998.)

(3) Investigate the influence of behavior mechanism in nine different types of jacketing systems. A total of 324 cylinders confined with fiber have been tested in USC Structural Lab. (Done.)

(4) Develop a constitutive model of confined concrete with advanced composite fibers. (Done, 1997. It has been published in ASCE J. of Material, 2000.)

(5) Experimental Program for Seismic Retrofit of RC Columns with Fiber or Steel.

(6) Test RC Columns Retrofitted with Composite on a large scale. (Done, 1997. The results have published in ASCE J of Structural Engineering, 2000. See Appendix B.)

(7) Develop a new steel jacketing system for seismic retrofitting of rectangular RC columns. (Done. Test in 1998, published in ASCE J of Structural Engineering 2003. See Appendix C.)

(8) Develop An Analytical Method Using the Universal Constitutive Confined Concrete Model to Predict the Mechanical Behavior of Concrete Confined by FRP or Steel.

(9) Based on FRP confined concrete test results, further investigate using elastic-plastic analysis.

(10) Transfer the proposed model to octahedral stress-strain coordinate to create a more general model for confined concrete.

(11) Using proposed confined concrete model to develop a numerical approach to predict the behavior of RC component confined by FRP as well as steel.

1.3 Research Approach

To achieve the objectives, the following tasks were performed:

(1) A systematic investigation of nine systems of concrete cylinders confined by FRP.

(2) Based on nonlinear elastic theory, a confined concrete model with FRP is developed in this research.

(3) Confined concrete behavior in principal coordinates and octahedral coordinates was investigated by the above model.

1.4 Organization of Dissertation

The objectives for the research in this dissertation are described in Chapter 1. A review of the state-of-the-art research on confined concrete is presented in Chapter 2. Chapter 3 introduces the experimental program, test setup, and instrumental measurements. Test results are presented in Chapter 4. Based on the test results, a nonlinear elastic concrete confined model with FRP is developed in Chapter 5.

Chapter 6 presents the confined concrete behavior in principal coordinates and the octahedral coordinates. The conclusion from this research is given in Chapter 7. Appendix A to Appendix J present the test results of nine systems of concrete confined with FRP. Some published papers of my research at the USC structural lab, completed under Professor Xiao's supervisions are available. One paper presents the application of FRP in seismic retrofitting for concrete columns. Another published paper of my research at the USC structural lab which has also been conducted under Professor Xiao's supervisions. This paper proposed the use of partially stiffened rectilinear steel jackets in seismic retrofitting for rectangular section of concrete columns.

CHAPTER 2: PREVIOUS RESEARCH ON CONFINED CONCRETE MODELING

2.1 Introduction

Concrete or reinforced concrete is one of the most popular construction materials in the world. It has been widely used in many major constructions, such as multistory and high-rise buildings, dams, bridges, marine structures, and nuclear containment structures. However, the high brittleness of concrete results in higher strength in compression and much lower strength in tension. In the last eight decades, scientists and researchers have performed extensive experimental studies to better understand the behavior of concrete and to improve upon the concrete failure model from brittle to ductile.

2.1.1 Confined Concrete and Seismic Design of Concrete Structures

The concept of modern seismic design of concrete structures is initiated by a paper on the use of energy concepts presented by Housner [Housner,1956] at the First World Conference on Earthquake (Berkeley, 1956) . The title of the paper was "Limit Design of Structures to Resist Earthquakes."

Based on Housner's energy concepts, from seismic design philosophy to element details, numerous investigations have been carried out in the last half-century. In seismic design of reinforced concrete structures, a primary focus is on the need to have a structure capable of deforming in a ductile manner when subjected to cyclic loading. The most important design consideration for ductility in plastic hinge regions of reinforced concrete columns is the provision of sufficient transverse reinforcements, in order to confine the compressed concrete and to prevent the buckling of longitudinal bars and shear failure. The latest development of energy concept in seismic design has been called a performance based design philosophy which has been developed in the last decades.

It is well known that the confined concrete by suitable arrangements of transverse reinforcement achieves a significant increase in both the strength and the ductility of compressed concrete. Therefore, the concept of confined concrete has been widely used in seismic retrofit and seismic design. The constitutive relationship of confined concrete is a long historical topic in concrete research especially in seismic resistant structures. Early studies date back to the 1920's. The pioneer work on the confinement concrete was conducted by Richart et al [1928, 1929]. Their research on concrete cylinders either confined by uniform hydrostatic pressure or spiral reinforcement, created a fundamental frame for confined concrete research. Richart et al. (1929) also found that the strength of concrete with active confinement from lateral (fluid) pressure was approximately the same as for concrete with passive confinement pressure from closely spaced circular steel spirals. Balmer (1947) conducted triaxial test at high confining stress level. Different investigators, such as Roy and Sozen (1963), Sargin (1971), Kent and Park (1971), Ahmad and Shah (1983), Mander et al (1984,1988), Xiao (1989), Saatcioglu et al (1992,1998), Xiao and Martirossyan (1997), have carried out numerous tests on confined concrete and developed several analytical models with various limitations.

The stress-strain model of Kent and Park (1971) for concrete confined by rectangular transverse reinforcement was based on the test results of Roy and Sozen (1964) and other available data at that time. The early tests were generally carried out on small-scale specimens at quasi-static rate of strain.

Mander's (1988) model is developed for concrete subjected to uniaxial compressive loading and confined with either circular or rectangular sections, under static or dynamic axial compressive loading. Thirty-one nearly full size reinforced concrete columns of circular, square, or rectangular wall cross section containing various arrangements of reinforcement were tested.

Xiao's (1989) model is developed from concrete filled steel tubes. A confined concrete stress-strain model in octahedral coordinates was proposed. The bilinear stress-strain phenomenon was observed by Xiao (1989) for concrete stub columns confined by steel tubes before the yielding of steel. His steel tubes provided transverse confinement only and were not loaded in an axial direction. Xiao's model can also predict the stress-strain behavior of confined concrete after steel yielding.

2.1.2 The State of the Art of FRP Confined Concrete

In recent years, advanced composite materials have been applied to retrofitting concrete columns in seismic regions. A great amount of research has been carried out on the use of fiber-reinforced plastic or polymer (FRP) composite for retrofitting of concrete structures. Two of the early researchers, Fardis and Khalili (1982) investigated concrete cylinders wrapped with FRP fabrics under uniaxial compression loading. A stress-strain model was proposed based on model for steel-confined concrete by Richart et al.(1928,1929). Since 1990s', more researchers such as Ahmad et al. (1991); Saadatmanesh et al. (1994), have proposed FRP confined concrete material model based on their test results. However, these models do not encompass the bilinear behavior of the stress-strain of FRP confined concrete. Based on the experimental investigations, Karbhari et al (1993), Mirmiran et al (1996), Xiao and Wu (1997), Hormon et al (1998) and Toutanji (1999), presented various analysis models for confined concrete with advanced composite materials. The bilinear phenomenon was also observed by Xiao et al. (1991) for concrete stub columns confined by steel tubes before the yielding of steel. In Chapter 6, an explanation will be presented for the difference of stress-strain behavior of confined concrete between steel and FRP. Samaan et al (1998) first used Richard four-parameter stress-strain curve for modeling the bilinear stress-strain behavior of confined concrete with FRP. However, this model is a regression of test data only. Xiao and Wu (1997), Wu and Xiao (2000), investigated the effect of confinement modulus of FRP to axial and transverse strains. Based on Richart's confined concrete strength equation, the authors also investigated the confinement coefficient k.

Beque et al. (2003) proposed a model based on Gerstle's (1981) octahedral stress-strain models with some modifications. Based on plasticity, Karabinis et al.

(2002) proposed a FRP confined concrete model, which requires numerical integration.

2.2 Mechanical Behavior of Concrete

Concrete is a composite material, consisting of coarse aggregate and a continuous matrix, which is a mixture of cement paste and fine aggregate. Due to the differential shrinkage and thermal mismatch between aggregate and matrix, tensile stress and initial de-bonding cracks have been observed by many researchers (Hsu et al. 1963). The mechanical behavior of concrete depends on the development of micro cracking.

2.2.1 Uniaxial Compression Loading and Stress Strain Behavior

Typical stress-strain curves for concrete under compression loadings are given in Fig. 2.1 (Wischers, 1978). These stress strain curves of concrete can be divided into three stages. In the first stage, the stress-strain curve has a nearly linear elastic behavior until 30% of its peak stress point f_c'. The existing cracks in the concrete before loading remain nearly unchanged. Based on thermodynamics, the available internal energy is less than the energy required for crack-release energy.

From the stress at 30% of peak stress, the second stage, the nonlinear response is observed. During this stage, the microcrack propagation is stable in the sense that crack lengths rapidly reach their final values under the constant applied stress. The internal energy is roughly balanced by the required crack-release energy.

During the third stage, the stress-strain curve shows a gradual increase in curvature up to about 75% to 90% f_c' . This stage is an unstable crack developing stage. If the load is kept constant, the cracks will continue to propagate with a decreasing rate to their final lengths until concrete failure. The available internal energy is larger than the required crack-release energy. The stress level of about 75% of f'_c is termed the onset of unstable fracture propagation of critical stress since it corresponds to the minimal value of volumetric strain.

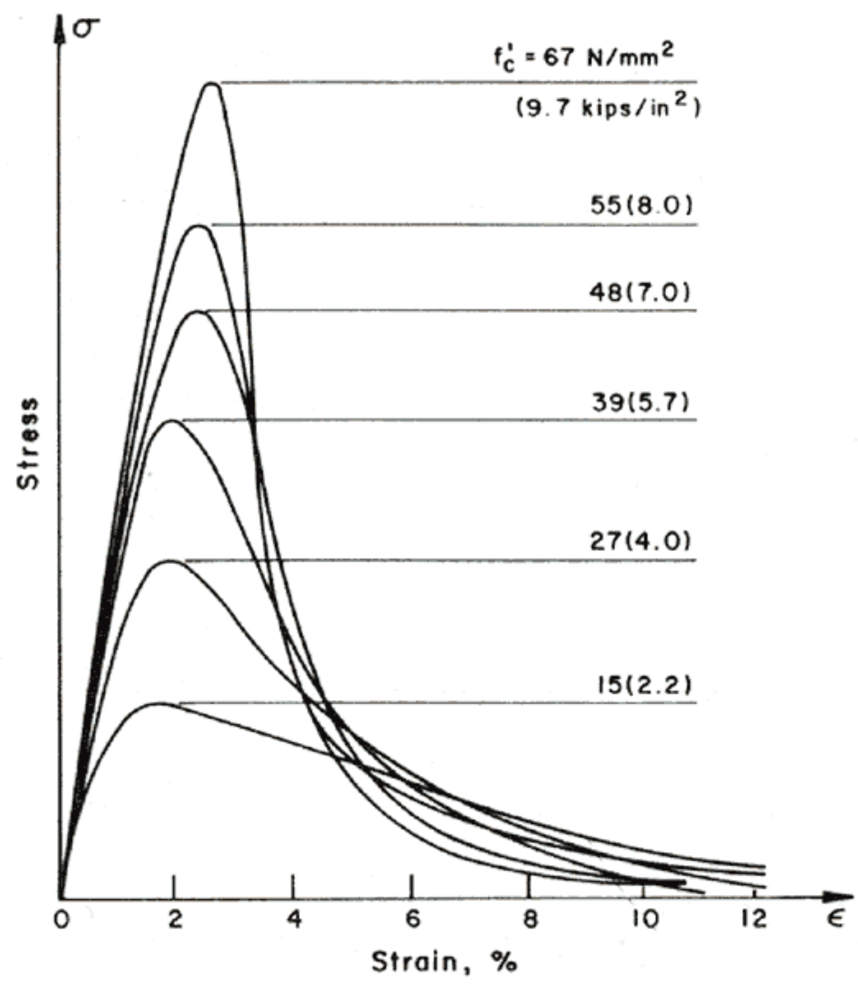

Figure 2.1: Complete compressive stress-strain curve. (*Wischers, 1978*)

2.2.2 Volume Dilatancy of Concrete

Fig. 2.2 shows the relationship between axial stress and volume strain under biaxial compression states (Kupfer, 1969). The test results show that under increasing compression, the material first compacts and eventually dilates due to microcracking (Newman et al.1969).

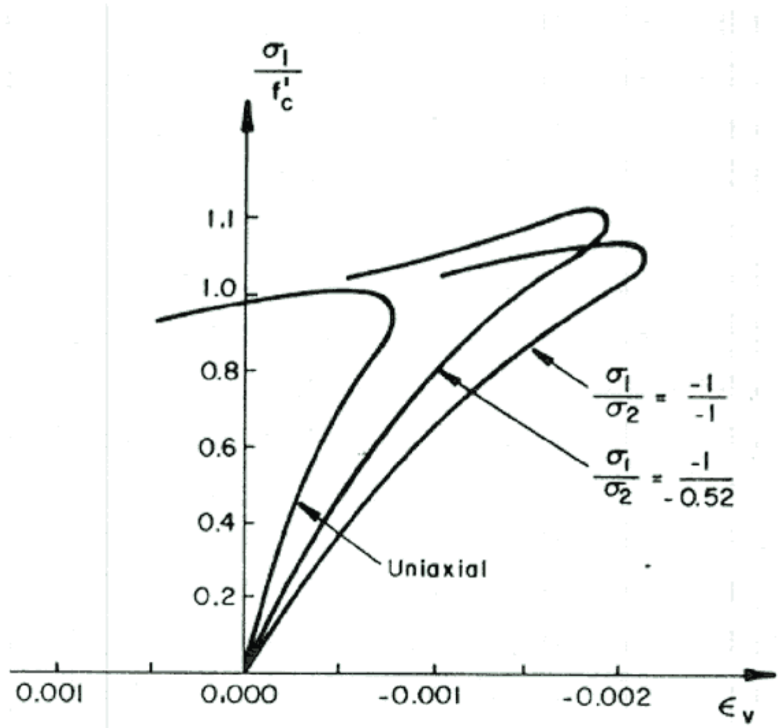

Figure 2.2: Volumetric Strain under Biaxal Compression (Kupfer et al., 1969)

2.2.3 Triaxial Compression Behavior

Fig 2.3 shows Stress-Strain curve under compression from the test results by Richart et al. (1928). The tests were conducted under low lateral (fluid) pressure. As these curves show, Richart et al (1929) also found that the strength of concrete with active confinement from lateral pressure was approximately the same as for concrete with passive confinement pressure from closely spaced circular steel spirals causing an equivalent lateral pressure.

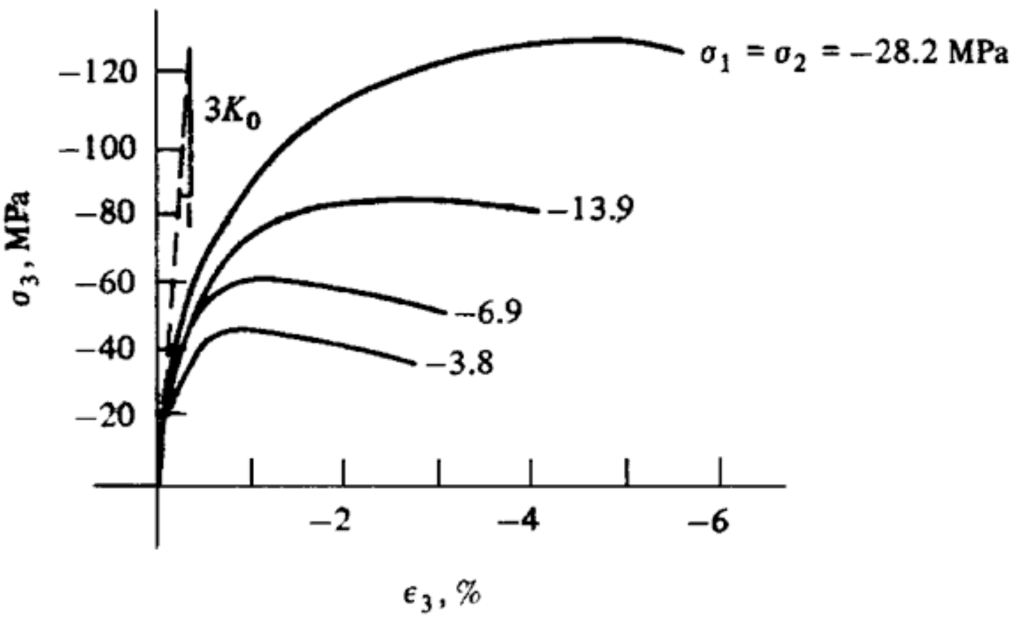

Figure 2.3: Stress-Strain curve under compression from the tests by Richart et al. (1928).

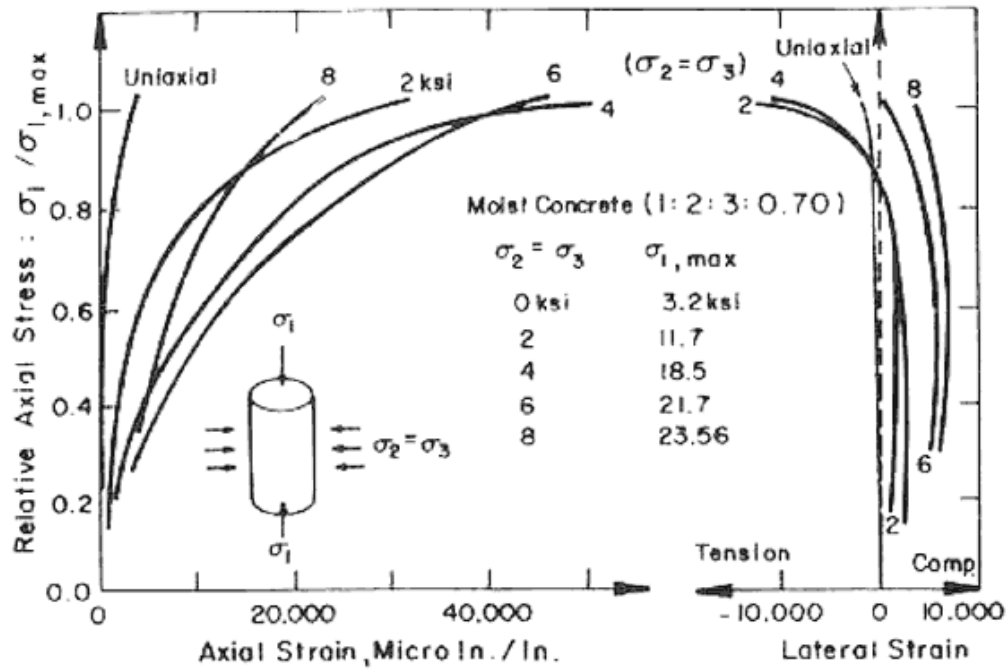

Figure 2.4: Stress-Strain curve under compression (Palmiswamy and Shah, 1974)

2.2.4 Behavior of FRP Confined Concrete

Fig.2.5 (a), (b) show axial stress versus axial and transverse strains for specimens with different unconfined concrete strengths and jacket layers. The axial stress strain relationships obtained from unconfined concrete stub columns are also shown in Fig.2.5. As shown in Fig.2.5, the initial portions of stress strain responses of confined concrete essentially followed the curves of unconfined concrete. After exceeding the unconfined concrete strength, the axial stress – axial strain as well as axial stress – transverse strain relationships of most specimens softened slightly and eventually exhibited an almost linear behavior until the sudden failure due to the rupture of carbon fiber composite jackets. Such near linear behavior of concrete confined in elastic materials has been observed in previous studies (Xiao 1989; Xiao et al. 1991; Hosotani et al. 1996; Mirmiran et al. 1997). For the three specimens of high strength concrete confined by one-layer jacket and one specimen with medium strength concrete confined by one-layer jacket, although the peak stress exceeded the unconfined concrete strength, the post peak behavior exhibited a sudden drop. Even for the specimens with a descending stress strain response, the post peak stress eventually stabilized at a lower stress level until the rupture of the jacket.

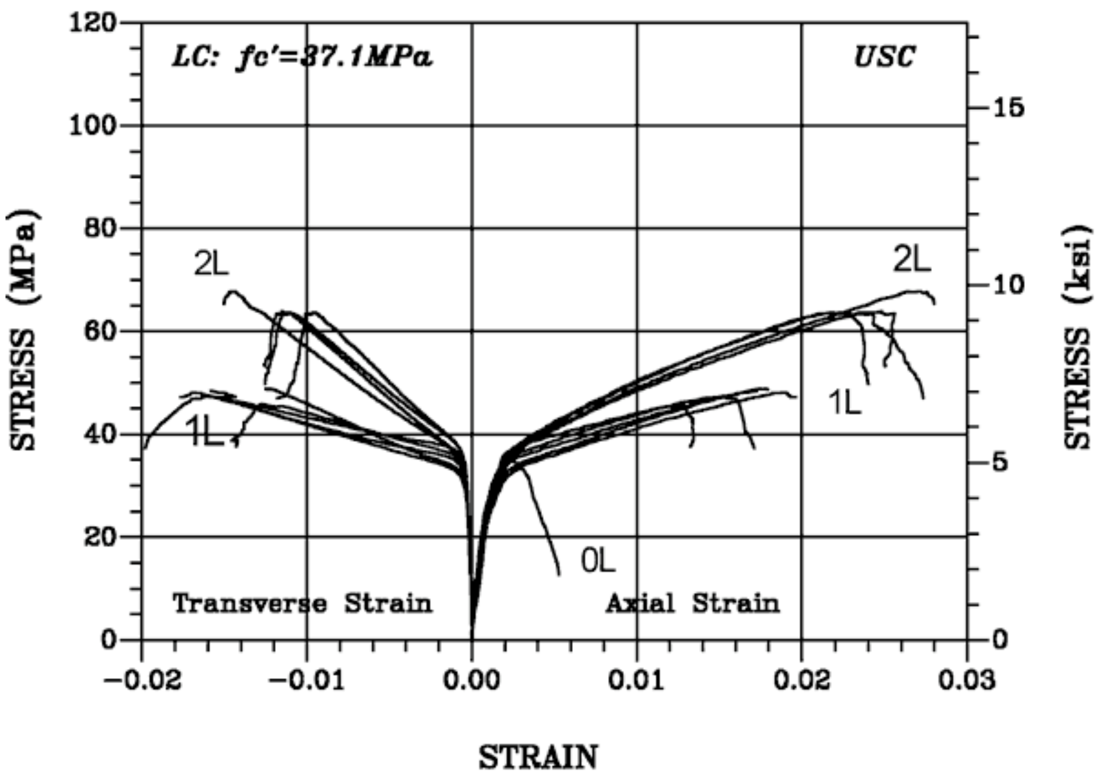

Figure 2.5a: Typical Stress-Strain Curve for Concrete Cylinder with Glass Fiber Composite Jacket

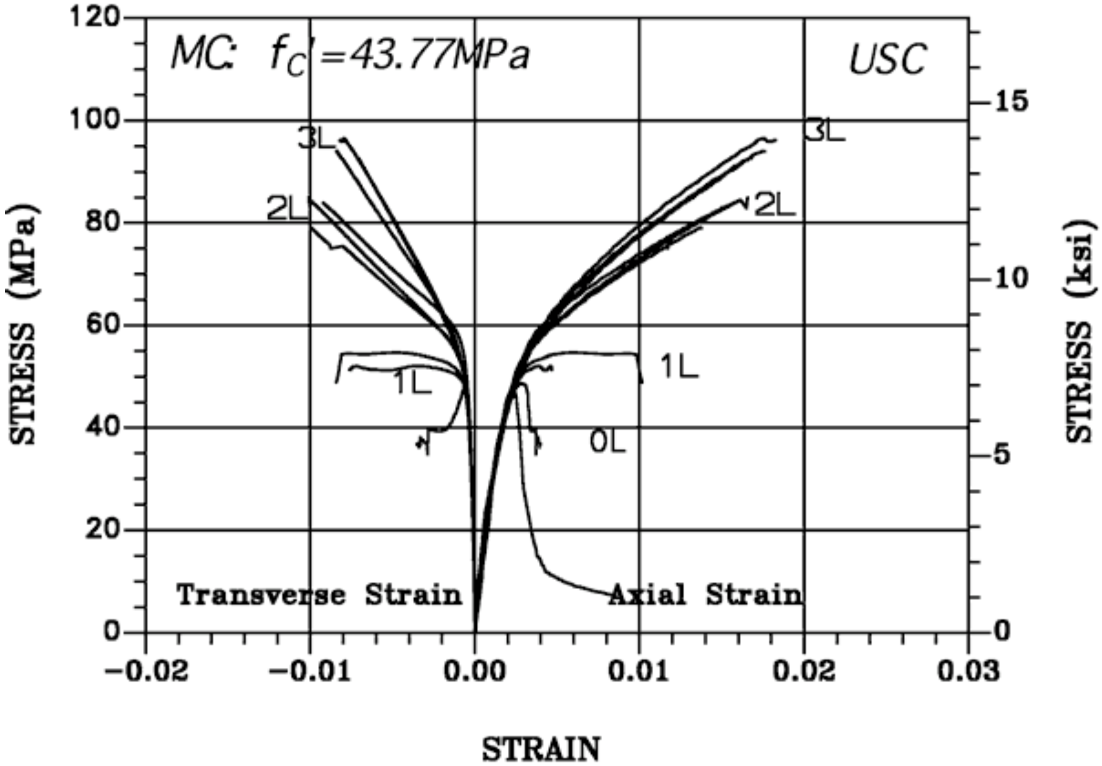

Figure 2.5b: Typical Stress-Strain Curve for Concrete Cylinder with Carbon Fiber Composite Jacket

The failure corresponding to the rupture of carbon fiber jacket was very explosive. For some specimens, the rupture of the jacket was accompanied by slight delamination of the layers. The recorded jacket strains corresponding to the failure ranged from 0.007 to 0.015, which were about 50% to 80% of the rupture strains obtained for the flat tensile coupons. The reduced rupture strains of the jackets most likely reflected the differences of the quality controls for flat coupons and the jackets, the dynamic development of concrete cracks, and delamination of the layers etc. The ultimate concrete axial strains corresponding to failure varied widely from 0.005 to

0.03, with a tendency of increase for specimens with lower strength and more jacket layers.

2.2.5 Seismic Retrofit Design of Concrete Structure and Confined Concrete

Confined concrete has been widely used in seismic retrofit of concrete structures since the Loma Prieta Earthquake (1989), the Northridge Earthquake (1994) and the Koba Earthquake (1995). Early research was focused on traditional retrofitting concrete columns with steel jacketing (Priestley and Seible, 1994 a,b). Fig.2.6 shows the freeway columns, which collapsed during the Northridge Earthquake (1994). Fig.2.7 shows retrofitted concrete columns with steel jacketing without damage during the same earthquake. However, it was also noted that the steel jacketed columns had substantially increased stiffness and higher capacity than the as built columns. The effects of the increased stiffness and strength are not always desirable because the retrofitted columns may attract more earthquake loads, although, as pointed out by Priestley et al. (1994b), such effects can be considered and utilized in the overall retrofit design of a bridge system.

As a conventional approach, steel jacketing has been widely adopted in bridge retrofit practices in California and elsewhere. Meanwhile, several retrofit jacketing systems using fiber reinforced polymer composites have been proposed and investigated (Matsuda et al. 1990; Priestley and Seible 1991; Saadatmanesh et at. 1994; Seible et al. 1995; Xiao et al. 1996; Xiao and Ma 1997; Xiao and Wu et al.1999). Because of their lightweight, high strength or stiffness to weight ratios, engineered properties, and performance, the fiber reinforced polymer composite-jacketing systems may provide some advantages compared to steel jacketing, in particular, the ease of construction. See Appendix B.

In the largest commercial application of FRP technology in the seismic retrofit in the USA, over 3,000 columns on the Yolo causeway west of Sacramento, California (2000), were wrapped with prefabricated E-glass fibers as reinforcement in a polyester matrix. See Fig 2.8 and Fig 2.9.

Despite the successful applications of various composite jacketing systems in the retrofitting laboratory models as well as prototype bridge columns, research on the fundamental interaction mechanisms between the composite jackets and the confined concrete is still limited. Although several stress strain models have been proposed and calibrated against several individual jacketing systems [Picher et al. 1996; Hosotani et al. 1996; Mirmiran et al. 1997, 1998; Harmon et al. 1998; Toutanji 1999;], they are not yet calibrated for general use due to the lack of sufficient data. As a result in many cases of structural retrofit design, engineers rely on the models based on test results of concrete confined in transverse reinforcing steel. Hence it is very important to understand concrete behavior and constitutive theory for seismic design and seismic retrofitting.

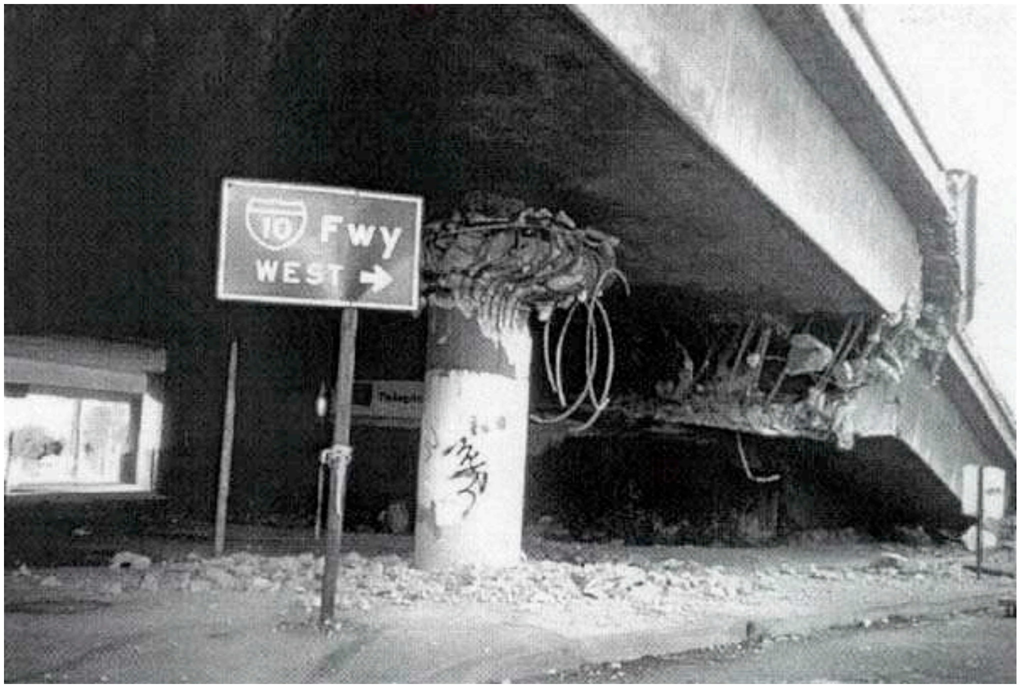

Figure 2.6: These non-ductile column failed in shear and collapsed
in Northridge Earthquake (1994) (from EERI Report)

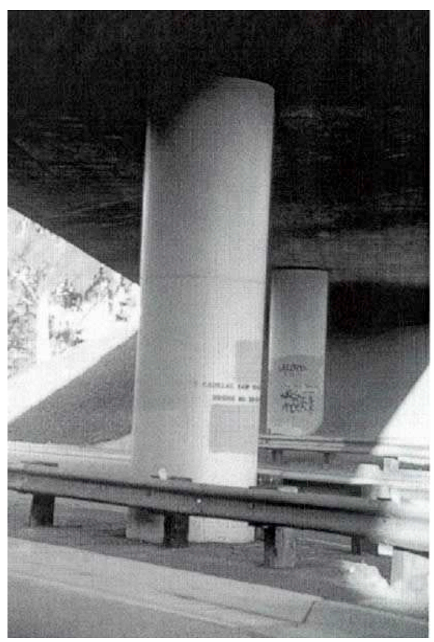

Figure 2.7: These columns retrofitted with steel jackets in 1990 were undamaged
in near location in Northridge Earthquake (1994) (from EERI Report)

Figure 2.8: The prefabricated jacketing system was installed

Figure 2.9: FRP technology in the seismic retrofit over 3,000 columns
on the Yolo causeway west of Sacramento, California

2.3 Concrete Constitutive Model

In the last three decades, there has been a tremendous effort aimed at developing analytical models that accurately predict the response of plain concrete to variable loading. Early models relied on elasticity theory. In the recent quarter century, more proposed models utilized general theories of solid mechanics including plasticity theory, fracture mechanics, and damage theory.

2.3.1 Nonlinear Elasticity Model of Concrete

For typical stress-strain behavior of concrete in the compression region, experiments have indicated that the nonlinear deformations of concrete are essentially inelastic, since upon unloading only a portion of strain can be recovered from total deformations. Therefore, the stress-strain behavior of concrete materials can be separated into recoverable elastic components and irrecoverable plastic components. And attempts have been made to treat each of these components individually. The recoverable behavior is treated within the framework of the theory of elasticity; the irrecoverable part is based on the theory of plasticity. Such separation is especially beneficial with cyclic loading and unloading. However, for problems in which a monotonically increasing proportional load prevails, elasticity-based models for concrete materials provide a much simpler approach.

The majority of these proposed models accurately predict particular aspects of concrete response with an acceptable level of accuracy and efficiency.

$$\sigma_{ij} = F_{ij}\,(\varepsilon_{kl}) \tag{2.3.1}$$

$$\sigma_{ij} = D_{ijkl}\,(\sigma_{pq})\,\varepsilon_{kl} \tag{2.3.2}$$

here D_{ijkl} defines the secant material. This approach is suggested by Ahmed and Shah[1982] and other researchers (Ottoson, 1978).

Such models may be used to represent the response of concrete subjected to moderate loading. However, this model implies a one-to-one correspondence between stress and strain. Hence it is not appropriate to predict the response of concrete subjected to severe loading in which case load reversals and monotonic loading past peak result in multiple strain states being associated with a single stress state.

A second approach is to characterize the tangent material stiffness and to define the stress and stain states incrementally:

$$\dot{\sigma}_{ij} = D_{ijkl}\left(\sigma_{pq}, \varepsilon_{kl}\right)\dot{\varepsilon}_{kl} \tag{2.3.3}$$

Here D_{ijkl} defines the tangent material stiffness. This approach is presented by Gerstle[1981] and other researchers.

Such an approach can be used to characterize the response of concrete subjected to variable load histories.

Stress-Strain Models

The most popular stress-strain expression proposed by Sargin (1971):

$$\frac{\sigma_c}{f'_{co}} = \frac{\dfrac{A\varepsilon_c}{\varepsilon_{co}} + (D-1)\left(\dfrac{\varepsilon_c}{\varepsilon_{co}}\right)^2}{1 + (A-2)\dfrac{\varepsilon_c}{\varepsilon_{co}} + D\left(\dfrac{\varepsilon_c}{\varepsilon_{co}}\right)^2} \qquad (2.3.4)$$

where *A* and *D* = constants controlling the initial slope and the descending path of the stress-strain curve, respectively. Fig.2.4 shows the Sargin's stress-strain curve, which is the most popular stress-strain curve for concrete design and analysis. It successfully exhibits strain-softening behavior beyond the peak stress. This equation has been used in Eurocode 2 (CEN 1991) for structural analysis and design, which is a special case of Eq(2.2.5) with A=2 and D=0, which is referred as Hognestad's (1951) parabola model. sylvanus.

Another popular stress-strain curve equation was proposed by Richard in (1975). This equation shows a typical bilinear stress-strain curve. For normal steel reinforced concrete however, this model does not predict the test results very well. As a result of after steel yielding, concrete stress- strain curve will show strain softening. After peak point the stress-strain curve usually can not keep a straight line. However, the test results of FRP confined concrete show typical bilinear stress-strain behavior. In recent years Richard's equations have been applied to most FRP confined concrete models. His bilinear equation will be introduced in Chapter 5.

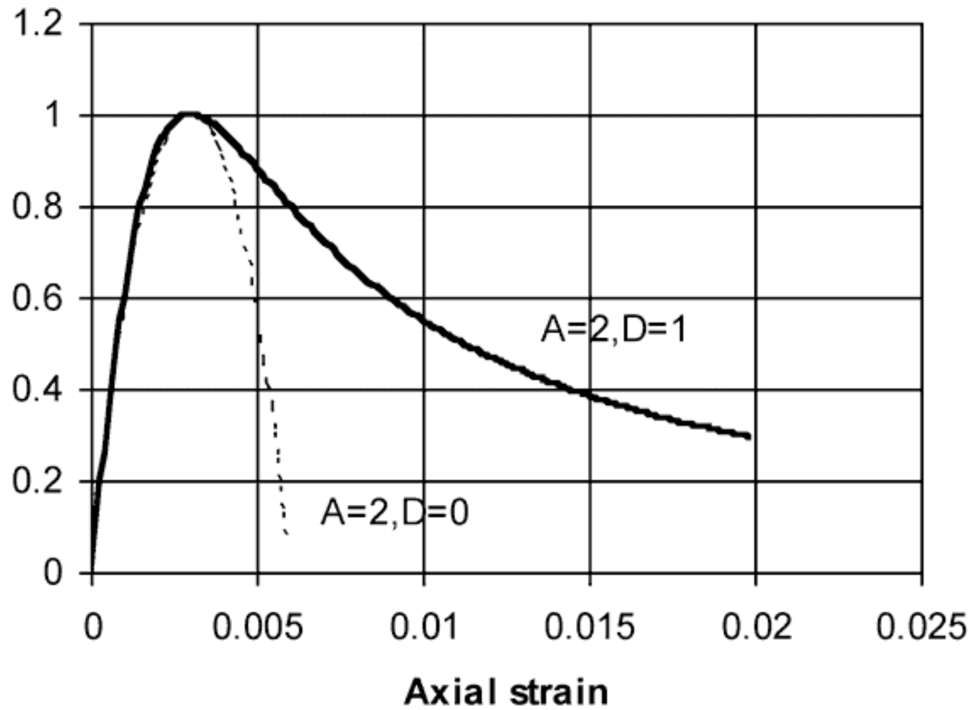

Figure 2.10: Sargin's general expression for stress-strain curve of unconfined concrete

Orthotropic Constitutive Model for Concrete

An orthotropic concrete constitutive model was proposed by Darwin and Pecknold (1977):

$$\begin{pmatrix} d\sigma_1 \\ d\sigma_2 \\ d\sigma_3 \end{pmatrix} = \frac{1}{1-\nu_1\nu_2}\begin{bmatrix} E_1 & \nu_2 E_1 & 0 \\ \nu_1 E_2 & E_2 & 0 \\ 0 & 0 & (1-\nu_1\nu_2)G \end{bmatrix}\begin{pmatrix} d\varepsilon_1 \\ d\varepsilon_2 \\ d\varepsilon_3 \end{pmatrix} \tag{2.3.5}$$

This model was developed to produce a two-dimensional state of stress. Incremental stress-strain relations for an orthotropic material take the above form, where $\nu_1 E_2 = \nu_2 E_1$, and subscripts 1 and 2 denote the current principal stress axes. After defining an "equivalent Poisson's ratio":

$$\nu^2 = \nu_1 \nu_2 \tag{2.3.6}$$

And assuming the shear modulus G to be independent of axis orientation,

$$(1-\nu^2)G = \frac{1}{4}\left(E_1 + E_2 - 2\nu\sqrt{E_1 E_2}\right) \tag{2.3.7}$$

The introduction of incremental equivalent uniaxial strains, measured in the principal stress directions,

$$d\varepsilon_{1u} = \frac{1}{1-\nu^2}\left[d\varepsilon_1 + \nu\sqrt{\frac{E_2}{E_1}}d\varepsilon_2\right] \tag{2.3.8}$$

$$d\varepsilon_{2u} = \frac{1}{1-\nu^2}\left[d\varepsilon_2 + \nu\sqrt{\frac{E_1}{E_2}}d\varepsilon_1\right] \tag{2.3.9}$$

leads to the uncoupling of the constitutive equations, (2-2.4) ,

$$d\sigma_1 = E_1 d\varepsilon_{1u}, \quad d\sigma_2 = E_2 d\varepsilon_{2u}, \quad d\tau_{12} = G d\gamma_{12} \tag{2.3.10}$$

For 3-D models, the work by Bazant and Tsubaki and Elwi and Murray should be mentioned. Based on orthotropic material model, Fujikake et al (2004) proposed an analytical model for concrete confined with FRP composite. See section 2.4.10.

2.3.2 Plasticity Model of Concrete

The classical theory of plasticity is conceived based on three main assumptions: an initial yield surface that defines the beginning of yielding, a hardening rule, and a flow rule.

The development of a plasticity-based constitutive model requires defining a rule for decomposition of the total strain, the constitutive relationship of the elastic material, the yield failure surfaces that bound the elastic domain, and the flow rules that define the evolution of the internal variables. Traditionally, the total strain is assumed to be the sum of the elastic strain and the accumulated plastic strain:

$$\varepsilon = \varepsilon^e + \varepsilon^p \tag{2.3.11}$$

It is reasonable to assume that concrete is a homogenous material; thus, the elastic material properties are readily defined on the basis of data collected from standard material tests and the elastic constitutive relationship follows Hooke's Law:

$$\sigma_{ij} = C_{ijkl}\varepsilon^{e}_{kl} \tag{2.3.12}$$

where C_{ijkl} is the rank four material stiffness tensor. The yield surface or surfaced bound the elastic domain. Following classical plasticity theory, the elastic domain is defined in terms of stress space. For concrete, the available material data facilitated the definition of the yield surface in stress space and it is most appropriate to consider a yield surface that evolves as a function of the loading history. A hardening rule defines the evolution of a set of internal variables that uniquely define the material state.

Failure Criterion of Concrete

A variety of yield surfaces have been proposed to characterize the response of plain concrete. The most well-known criterion was Mohr-Coulomb criterion [1800].

The simplest form of Mohr envelope is the straight line, illustrated in Fig. 2.3.1.

$$f\left(I_1, J_2, \theta\right) = \frac{1}{3} I_1 \sin\phi + \sqrt{J_2}\,\sin\left(\theta + \frac{\pi}{3}\right) + \frac{\sqrt{J_2}}{\sqrt{3}}\cos\left(\theta + \frac{\pi}{3}\right)\sin\phi - c\cos\phi \tag{2.3.13}$$

where I_1 and J_2 are invariants of the stress state as defined:

$$J_2 = \frac{1}{2} s_{ij} s_{ij} = \frac{1}{6}\left[(\sigma_1 - \sigma_2)^2 + (\sigma_2 - \sigma_3)^2 + (\sigma_3 - \sigma_1)^2\right] \tag{2.3.14}$$

$$I_1 = \sigma_1 + \sigma_2 + \sigma_3 \tag{2.3.15}$$

$$s_{ij} = \sigma_{ij} - \frac{1}{3}\sigma_{mm}\delta_{ij} = \begin{bmatrix} \sigma_{11} - \sigma_m & \sigma_{12} & \sigma_{13} \\ \sigma_{21} & \sigma_{22} - \sigma_m & \sigma_{23} \\ \sigma_{31} & \sigma_{32} & \sigma_{33} - \sigma_m \end{bmatrix} \tag{2.3.16}$$

δ is the Kroneker delta.

$$\theta = \frac{1}{3} a\cos\left[\frac{3\sqrt{3}}{2}\frac{J_3}{J_2^{3/2}}\right] \tag{2.3.17}$$

$$J_3 = \frac{1}{3} s_{ij} s_{jk} s_{ki} \tag{2.3.18}$$

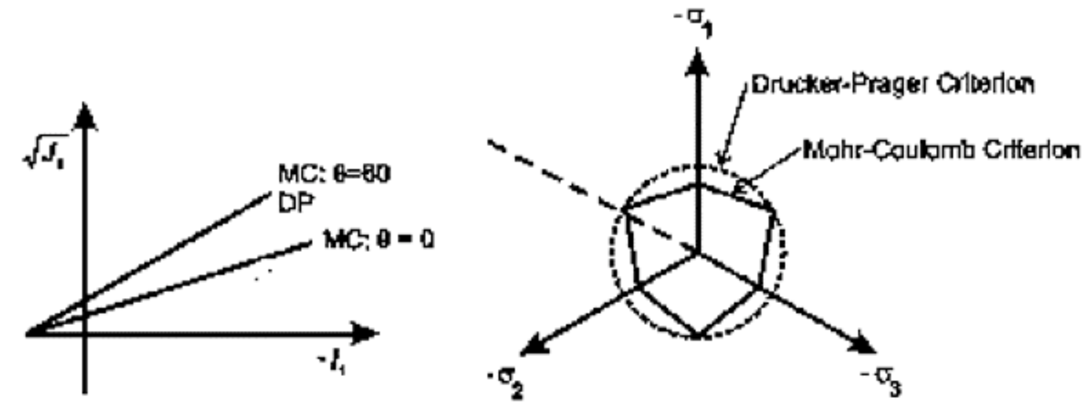

(a) (b)

Figure 2.11. Failure Criteria: (a) meridian plane; (b) deviatoric plane

Another important criterion is the Drucker-Prager criterion (1952). It presents moderately well the response of plain concrete subjected to multi-axial compression and provides a smooth yield surface.

$$\sqrt{J_2} + \alpha I_1 + y = 0 \tag{2.3.19}$$

Several concrete failure surfaces have been proposed in the recent three decades.

Willam and Warnk's model (1975)

$$\frac{\tau_{mt}}{f_c'} = \frac{\rho_t}{\sqrt{5} f_c'} = a_0 + a_1 \frac{\sigma_m}{f_c'} + a_2 \left(\frac{\sigma_m}{f_c'}\right)^2 \qquad \theta = 0^{\circ} \qquad (2.3.20a)$$

$$\frac{\tau_{mt}}{f_c'} = \frac{\rho_c}{\sqrt{5} f_c'} = b_0 + b_1 \frac{\sigma_m}{f_c'} + a_2 \left(\frac{\sigma_m}{f_c'}\right)^2 \qquad \theta = 60^{\circ} \qquad (2.3.20b)$$

$$\rho(\sigma_m, \theta) = \frac{2\rho_c\left(\rho_c^2 - \rho_t^2\right)\cos\theta + \rho_c(2\rho_c - \rho_c)\left[4\left(\rho_c^2 - \rho_t^2\right)\cos^2\theta + 5\rho_t^2 - 4\rho_t\rho_c\right]^{1/2}}{4\left(\rho_c^2 - \rho_t^2\right)\cos^2\theta + (\rho_c - 2\rho_t)^2}$$

(2.3.20c)

Ottosen's model (1977)

$$f(I_1, J_2, \theta) = \alpha J_2 + \lambda\sqrt{J_2} + bI_1 - 1 = 0 \qquad (2.3.21a)$$

where λ is a function of $\cos 3\theta$:

$$\lambda = k_1 \cos\left[\frac{1}{3} a\cos\left(k_2 \cos 3\theta\right)\right] \qquad \text{for } \cos 3\theta > 0 \qquad (2.3.21b)$$

$$\lambda = k_1 \cos\left[\frac{\pi}{3} - \frac{1}{3} a\cos\left(-k_2 \cos 3\theta\right)\right] \qquad \text{for } \cos 3\theta \le 0 \qquad (2.3.21c)$$

Podgorski's model (1985)

$$\sigma_{oct} = C_0 + C_1 P \tau_{oct} + C_2 \tau_{oct}^2 \qquad (2.3.22a)$$

$$P = cos\left(\frac{1}{3} arccos\, \alpha J - \beta\right) \qquad (2.3.22b)$$

Based on author's (Wu, 1990) comparison Ottosen's and Podgorski's model are most fit with test results. Willam and Warnk's model correlates with the test results very closely in lower hydro pressure. However, in higher hydro pressure Willam and Warnk's failure surface will cross hydro pressure axial. It is not fit test results.

Flow Rules for Concrete Plasticity Models

The definition of a plasticity-based constitutive model requires first establishing flow rules that define the evolution of a set of internal variables. The plastic flow rule that defines the orientation of the plastic strain is one of the most important aspects of this theory. The plastic strain rate is defined as follows:

$$\dot{\varepsilon}^p = \lambda \frac{\partial}{\partial \sigma} g(\sigma, q) \qquad (2.3.23)$$

where $\dot{\varepsilon}$ is the rate of plastic strain, λ is a positive scalar, q is the set of internal variables, and $g(\sigma, q)$ is the plastic potential function. Typically it is assumed that the orientation of plastic flow is normal to the yield surface in which case the plastic potential function is the yield function. Following this assumption of associated flow, the increment of plastic strain is defined as follows:

$$\dot{\varepsilon}^{p} = \lambda \frac{\partial}{\partial \sigma} f(\sigma, q) \tag{2.3.24}$$

A number of plastic models have been developed assuming associated flow [Ohtani and Chen, 1988; Salami, 1990].

Experimental data, however, indicate that associated flow may not be the most appropriate assumption for characterizing the response of concrete. Researchers have noted that concrete displays shear dilatancy characterized by volume change associated with shear distortion of the material. For typical yield functions, this characteristic is on the contrary to the assumption of associated flow. Additionally, data show that concrete subjected to compressive loading exhibits nonlinear volume change, displaying contraction at low load levels and dilation at higher load levels.

2.3.3 Fracture Mechanics of Concrete

It is generally accepted that most engineering materials contain some form of imperfection. More importantly, the propagation of these initial defects results in the failure of a structure. Thus, it may be significant to identify and characterize the behavior mechanism of crack behavior.

The behavior of a cracked body under load can be approached by fracture mechanics. Following Griffith theory, the elastic energy release is compared with the surface energy gain during crack extension. As long as the latter value is larger than the former, there is no crack propagation; otherwise, unstable (or catastrophic) failure occurs. The critical stress is given by

$$\sigma_c = \sqrt{\frac{2\gamma E}{\pi c}}.f \qquad (2.3.25)$$

with γ = surface energy, E = young's modulus, c = half crack length, *f* = a function taking account of the geometry.

Westergaard et al. analyzed the stress field near the crack tip and defined a parameter, which measures the intensity of the stresses,

$$K_I = \sigma\sqrt{\pi c}.g \qquad (2.3.26)$$

with K_I = stress intensity factor for mode I (crack opening), and g = geometrical function. Failure occurs when K_I approaches the critical stress intensity factor K_{Ic}, which is a material property.

For a brittle material, the two approaches converge to

$$K_I = \sigma\sqrt{2\gamma E} = \sqrt{G_c E} = \sqrt{RE} \tag{2.3.27}$$

with G_c = critical energy release rate, R = crack resistance. For other materials, G_c and R may include other energy contributions due to plastic, viscous, and frictional actions.

On a macro-scale, concrete does not follow the linear elastic fracture mechanics concept. But instead, it behaves more like a softening material than an ideal brittle material. A crack causes a process zone ahead of the crack tip with cohesive stresses and a crack band develops with dissipation of energy.

Hillerborg et al. first proposed a fictitious crack model for fracture of concrete in 1976. The principle for fictitious crack model is based on (a) a complete tensile stress-elongation curve, (b) stress-strain curve for uncracked section, and (c) stress-elongation curve for cracked section.

Bazant et al. (1983) modeled the fracture process zone by a band of uniformly and continuously distributed microcracks with a fixed width. This model was called crack band model in facture mechanics of concrete.

Since the fracture process zone in quasi-brittle materials such as concrete, is considerable, the validity of linear elastic fracture mechanics (LEFM) for these materials is limited to large structures. This localized zone consumes part of the energy provided by the applied load and induces nonlinearity in the response.

As a tool in the research of concrete failure, fracture mechanics of concrete is both powerful and useful. However, it is not applied to confine concrete modeling. In this study, fracture mechanics have not been used.

2.3.4 Elastic-Plastic-Damage Model for Concrete

Damage mechanics of Concrete has evolved as a sub-discipline of continuum mechanics. Its conception in 1958 is generally credited to Kachanov, who studied brittle creep rupture under uniaxial tension at elevated temperatures. The state of the material deterioration was characterized by a scale field variable ψ, referred to as "continuity". For a defect-free material, $\psi = 1$ and $\psi = 0$ characterize a material with no remaining load carrying capacity. Accordingly, damage D is defined as being complementary to continuity, $D = 1 - \psi$.

The defining characteristic of material damage is the reduced material stiffness. Experimental data exhibit material damage for concrete subjected to tensile loading, and to a lesser extent, compressive loading. Thus, it is appropriate to incorporate material damage into models characterizing the response of plain concrete to variable loading. Various proposed damage models differ in the definition of the damage surface and damage rules.

Lemaitre, et al have developed a series of damage mechanics models, based on the thermodynamics of irreversible processes. Each equilibrium state is defined by a scale thermodynamic potential,

$$\rho\psi = f\left(\varepsilon^{e}, D, \varepsilon^{p}\right) \tag{2.3.28}$$

Only the elastic properties of the material are assumed to be affected by damage.

2.4 Existing models for Confined Concrete

2.4.1 Richart's Model

Professor Rechart, F. E. of University of Illinois at Urbana-Champaign is a pioneer in the research of confined concrete. In his early work on the effect of transverse confinement on concrete compression behavior[1928,1929], Richart discovered that the strength of concrete with active confinement from lateral pressure was approximately the same as for concrete with passive confinement pressure from closely spaced circular steel spirals causing an equivalent lateral pressure. The strength and the corresponding longitudinal strain at the strength of concrete confined by an active hydrostatic fluid pressure can be represented by following simple relationships:

$$f'_{cc} = f'_{co} + k_1 f_l \tag{2.4.1}$$

$$\varepsilon_{cc} = \varepsilon_{co}\left(1 + k_2 \frac{f_l}{f'_{co}}\right) \tag{2.4.2}$$

where f'_{cc} and ε_{cc} are the strength of confined concrete and the corresponding strain, respectively. f'_{co} and ε_{co} are the strength of unconfined concrete and the corresponding strain. f_l is the lateral pressure. k_1 and k_2 are coefficients. Based on the test results, Richart et al. found the average values of the coefficients to be k_1=4.1 and k_2=5k_1.

2.4.2 Ahmad and Shah's Model

After considerable research had been conducted on plain concrete subjected to active pressure (cylindrical triaxial compressive stresses), S. H. Ahmad and S.P. Shah proposed their concrete model to predict the stress-strain curve of confined concrete based on properties of spiral reinforcement and constitutive relationship of plain concrete.

For active confining pressure tests, concrete specimens are subjected to an increasing axial stress while the lateral confining pressure is held constant. However, in practical concrete structures, when the lateral reinforced component is subject to an increasing axial stress, the confinement is termed passive.

In Shah's model, for concrete subjected to a general state of triaxial compression, the stress-stain relation equation is

$$y = \frac{A_i x_i + (D_i - 1)x_i^2}{1 + (A_i - 2)x_i + D_i x_i^2} \qquad (2.4.3)$$

where $y=f_1/f_{cc,}\ x_I=\varepsilon_i/\varepsilon_{ci}.$, f_1 = the most principal compressive stress, f_p = the most principal compressive strength, ε_i = the strain in the i-th principal direction (i =1, 2 or 3), ε_{ip} = the strain at the peak in the I-th direction, $A_i = E_i/E_{ip,}\ E_i$ is the initial slope of the stress-strain curve; $E_{ip} = f_p/\varepsilon_{ip.}\ D_i$ is the parameter that governs the descending part of the stress-strain curve.

Compressive strength f_p was determined by a strength criterion based on octahedral theory.

$$\frac{\tau_{oct}}{f_0} = 0.2261 + 0.7360\frac{f_{oct}}{f_0} \quad (2.4.4)$$

The equivalent equation is

$$f'_{cc}=f'_{co}+4.255\, f_l \quad (2.4.5)$$

2.4.3 Mander's Model

Mander et al. developed a general model for concrete confined by various type of transverse reinforcements (Mander, Priestley and Park,1986). This model has been widely used in analyzing reinforced concrete columns (Xiao, Priestley and Seible, 1993,1994). In this model, the load application can be either static or dynamic, and applied monotonically or by load cycles. The transverse reinforcement can also be of different types, for instance, circular or spiral, and rectangular hoops together with cross ties or without cross ties.

In Mander's model, the "five-parameter" tri-axial failure criterion described by William and Warnke (1975) were adopted. For confined concrete under triaxial compression with equal lateral effective confining stress by transverse steel, the confined compressive strength can be estimated by following equation:

$$f_{cc}^{'} = f_{c}^{'}\left(-1.254 + 2.254\sqrt{1 + \frac{7.94 f_{l}^{'}}{f_{co}^{'}}} - 2\frac{f_{l}^{'}}{f_{co}^{'}}\right) \tag{2.4.6}$$

where f'_{cc} = compressive strength of confined concrete. f_l' is the effective lateral confining stress.

Mander's model is base on a stress- strain equation proposed by Popovics(1973). The longitudinal compressive concrete stress f_c is given by

$$f_c = \frac{f_{cc}^{'} x r}{r - 1 + x^r} \tag{2.4.7}$$

$$x = \frac{\varepsilon_c}{\varepsilon_{cc}} \tag{2.4.8}$$

where ε_c = longitudinal compressive concrete strain.

$$\varepsilon_{cc} = \varepsilon_{co}\left(1 + 5\left(\frac{f'_{cc}}{f'_c} - 1\right)\right) \tag{2.4.9}$$

as suggested by Richart et al.(1929).

$$r = \frac{E_c}{E_c - E_{\sec}} \tag{2.4.10}$$

where

$$E_c = 5{,}000\sqrt{f'_{co}} \text{ Mpa} \tag{2.4.11}$$

is the modulus of the concrete.

$$E_{\sec} = \frac{f'_{cc}}{\varepsilon_{cc}} \tag{2.4.12}$$

This model is recommended for the design of columns with composite jackets in seismic retrofit (Priestly and Seible, 1991). However, when compared with the test results, the model is not verified (Fig.2.5).

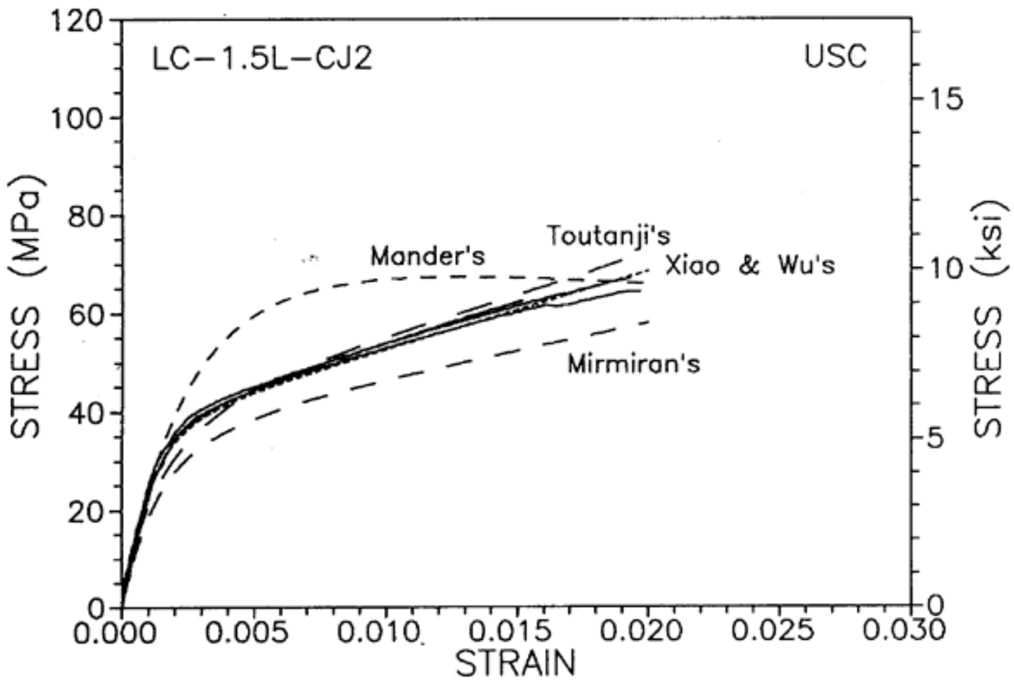

Figure 2.12: Comparison with test results in different models

2.4.4 Fardis and Khalili's Model

Fardis and Khalili (1981) studied the behavior of concrete-encased glass fiber tubes. The ultimate strength and ultimate strain of concrete confined by glass fiber were significantly increased with the number of the layers. A confined concrete model was proposed (1982)

$$f_{cc}^{'} = f_c^{'}\left(1 + 4.1\left(\frac{f_{com}t}{df_c^{'}}\right)\right) \tag{2.4.13}$$

$$\varepsilon_{cc} = 0.002 + 0.01\left(\frac{E_{com}t}{df_c^{'}}\right) \tag{2.4.14}$$

where E_{com} is the elastic modulus of the confinement in transverse direction.

This stress-strain model was proposed based on model for steel-confined concrete by Richart et al.(1928,1929). However, this model does not encompass the bilinear behavior of the stress-strain of FRP confined concrete.

2.4.5 Karbhari's Model

Karvhari et al. suggested the following equation to predict the ultimate stress and ultimate strain of advanced composite wrapped concrete cylinders under uniform compression.

$$f_{cc}^{'} = f_c^{'}\left(1 + 2.1\left(\frac{2tf_{com}}{df_c^{'}}\right)^{0.87}\right) \tag{2.4.15}$$

$$\varepsilon_{cc} = 0.002 + 0.01\left(\frac{2tf_{com}}{df_c^{'}}\right) \tag{2.4.16}$$

This stress-strain model was also proposed based on model for steel-confined concrete by Richart et al.(1928,1929). And this model does not encompass the bilinear behavior of the stress-strain of FRP confined concrete.

2.4.6 Mirmiran's Model

Mirmiran et al. developed a model of confined concrete with fiber composites. In this model, the four-parameter relationship of Richard and Abbott (1975) was used:

$$\sigma = \frac{(E_1 - E_2)\varepsilon}{\left(1 + \left|\frac{(E_1 - E_2)\varepsilon}{\sigma_0}\right|^n\right)^{1/n}} + E_2\varepsilon \qquad (2.4.17)$$

However, in this model E_2 and E_{2r} was regressed directly by experimental results. They do not have clear physical significance.

$$E_2 = 245.61 f_c^{'0.2} + 1.3456 \frac{E_j t_j}{D} \, [MPa] \qquad (2.4.18)$$

$$f_o = 0.872 f_{c'} + 0.371 f_r + 6.258 [MPa] \qquad (2.4.19)$$

2.4.7 Xiao and Wu's Model

Xiao and Wu (1997) investigated the behavior of confined concrete with advanced composite materials. They further explored the relationships of confined concrete in axial stress to transverse stress and in axial strain to transverse strain.

They derived expression of E_2 and E_{r2} and then established their physical meaning in the proposed model. The model will be shown in chapter 4 and further discussed in chapter 5.

$$f_{cc}^{'} = f_c^{'} + kf_l = f_c^{'} + \left(4.1 - 0.45\left(\frac{f_c^{'2}}{C_j}\right)^{1.4}\right)f_l \qquad (2.4.20)$$

$$\varepsilon_{\mathrm{r}} = \varepsilon'_{ro} - \nu'\varepsilon_{cz} \qquad (2.4.21)$$

$$\nu' = 10\left(\frac{f'_{co}}{C_j}\right)^{0.9} \qquad (2.4.22)$$

$$E_2 = kC_j\nu' \qquad (2.4.23)$$

$$E_{t2} = kC_j \qquad (2.4.24)$$

2.4.8 Harmon's Model

Harmon et al. (1998) developed a model for FRP-confined concrete based on the concept of crack slip and separation in the concrete.

To predict the radial strain, Harmon proposed the internal friction concept. Two models were proposed by Harmon et al (1998) based on the internal friction in the confined concrete. This model assumes that concrete strain is comprised of three parts

$$\varepsilon = \varepsilon_{elastic} + \varepsilon_{crack} + \varepsilon_{void} \tag{2.4.25}$$

where $\varepsilon_{elastic,}$ ε_{crack} and ε_{void} are elastic strain, crack strain, and void strain respectively.

This model shows that crack slip leads to crack separation due to crack surface roughness. Crack strain, ε and γ, equal the crack separation and slip divided by the average crack spacing, S. Slip leads to compressive axial strain and tensile radial strain, while separation leads to tensile strain in both directions.

Although this model presents a reasonable prediction of stress-strain response of FRP-confined concrete, it involves a complicated procedure and is difficult to predict each strain accurately. In this model, the relationship between lateral strain and axial strain is not explicit but dependent on the crack slip-separation path.

Two models were proposed by the author, the first model is stress ratio model. The other model is crack path model.

2.4.9 Toutanji's Model

A modified Ahamad and Shah's model was proposed by Toutanji (1998).

$$f = \frac{A\varepsilon}{1 + B\varepsilon + C\varepsilon^2} \tag{2.4.26}$$

$$f'_{cc} = f'_c\left(1 + 2.2\left(\frac{2tf_{com}}{df'_c}\right)^{0.84}\right) \tag{2.4.27}$$

where f_{com} is the tensile strength of composite confinement.

Based on the test results, a modified Rishart relationship was used in Toutanji's Model.

$$\varepsilon_{cc} = \varepsilon_{co}\left(1 + (537\varepsilon_l + 2.6)\left(\frac{f'_{cc}}{f'_c} - 1\right)\right) \tag{2.4.28}$$

2.4.10 Fujikake's Model

Based on Darwin's orthotropic constitutive model, Fujikake et al (2004) proposed an analytical model to predict the behavior of concrete confined with FRP under axial compression load.

A constitutive model for plain concrete was formulated based on past experimental results obtained from triaxial compression of concrete. Based on the concept of an equivalent uniaxial strain, this was an orthotropic constitutive model. The FRP was assumed to be a linear elastic material.

The orthotropic constitutive model is described in the principal stress directions, when the orthotropic axes coincide with the principal axes:

$$\begin{pmatrix} d\sigma_1 \\ d\sigma_2 \\ d\sigma_3 \end{pmatrix} = \frac{1}{\phi} \begin{bmatrix} E_1(1-\nu_{23}\nu_{32}) & E_1(\nu_{12}+\nu_{13}\nu_{32}) & E_1(\nu_{13}+\nu_{12}\nu_{23}) \\ E_2(\nu_{21}+\nu_{23}\nu_{31}) & E_2(1-\nu_{13}\nu_{31}) & E_2(\nu_{23}+\nu_{21}\nu_{13}) \\ E_3(\nu_{31}+\nu_{32}\nu_{21}) & E_3(\nu_{32}+\nu_{31}\nu_{12}) & E_3(1-\nu_{12}\nu_{21}) \end{bmatrix} \begin{pmatrix} d\varepsilon_1 \\ d\varepsilon_2 \\ d\varepsilon_3 \end{pmatrix} \qquad (2.4.29)$$

Where

$$\phi = 1 - \nu_{13}\nu_{31} - \nu_{23}\nu_{32} - \nu_{12}\nu_{21} - \nu_{21}\nu_{13}\nu_{31} - \nu_{12}\nu_{23}\nu_{31}$$

in which $d\sigma_i$ $(i = 1,2,3)$ = principal stress increments in the i direction; $d\varepsilon_i$ (i = 1,2,3) = principal strain increments in the i direction; E_i $(i = 1,2,3)$ = total secant modulus of elasticity in the i direction of orthotropy; ν_{ij} $(i,j = 1,2,3)$ = transverse strain ratio for strain in i direction caused by stress in the j direction.

Eq.(2.4.29) can be written in a simple form as:

$$\{d\sigma_i\} = [D]\{d\varepsilon_i\} \qquad (2.4.30)$$

where [D] = stiffness matrix.

Stress vs. equivalent uniaxial strain relationship

$$\sigma_i = \frac{AX_i + (B-1)X_i^{\,2}}{1 + (A-2)X_i + BX_i^{\,2}}\sigma_p \qquad (i = 1, 2, 3) \qquad (2.4.31)$$

where A, B = constants; X_i = normalized equivalent uniaxial strains; σ_p = ultimate strength associated with the current states. The constants A and B and X_i are defined in following equations:

$$A = \frac{E_0 \varepsilon_p}{\sigma_p} \qquad (2.4.32)$$

$$B = \frac{1}{\alpha^2 \beta (1-\beta)} \left[(A-1)^2 \alpha\beta + A^2 (1-\alpha) + \alpha(\alpha - 1)\beta \right] \qquad B \geq 1 - A \qquad (2.4.33)$$

where $\alpha = E_0 / E_c, \beta = 0.45 f_c^{'} / \sigma_p, X_i = \dfrac{\varepsilon_{ui}}{\varepsilon_p}$

$$B = \frac{\sigma_p}{\sigma_p - \sigma_R} \qquad (\varepsilon_{ui} > \varepsilon_p) \qquad (2.4.34)$$

$$X_i = \left(\frac{\varepsilon_{ui}}{\varepsilon_p} \right)^m \qquad (2.4.35)$$

where

$$m = 1.04 + 2.0 \left(\frac{f_c^{'}}{100} \right)^2 \qquad (2.4.36)$$

2.4.10 Beque's Model

Beque et al. (2003) proposed a model based on Gerstle's (1981) octahedral stress-strain models with some modifications. The elastic bulk and shear moduli are taken as scalar functions of the stress-, strain-tensor invariants. Thus, the stress state can be defined by the two octahedral stresses, the octahedral normal stress σ_0 and the octahedral shear stress τ_0 :

$$\sigma_m = K_s \varepsilon_{kk} \tag{2.4.37}$$

$$S_{ij} = 2G_s e_{ij} \tag{2.4.38}$$

where $\sigma_m = \sigma_{kk} /3 = \sigma_0$ is the mean normal stress and K_s and G_s are called the secant bulk modulus and secant shear modulus, respectively. Expressions for E_s and ν_s can be obtained from Ks and G_s

$$K_s = \frac{\sigma_{oct}}{3\varepsilon_{oct}} = \frac{E_s}{3(1-2\nu_s)} \tag{2.4.39a}$$

$$G_s = \frac{\tau_{oct}}{\gamma_{oct}} = \frac{E_s}{2(1+\nu_s)} \tag{2.4.39b}$$

The lateral-to-axial strain relationship in this model depends on the bulk modulus K_s and shear modulus G_s. Modifications to Gerstle's original models were made by taking K_s to be a constant value, and the failure surface using an equation proposed by Samaan et al. (1998).

CHAPTER 3: EXPERIMENTAL PROGRAM SUMMARY

3.1 Specimens

This chapter presents the experimental results on stress – strain behavior of concrete stub columns confined in advanced composite jackets and discusses issues related to the modeling of stress – strain relationships. Note that throughout the dissertation, compression is defined as positive while tension is defined as negative for forces, stresses, and deformations.

Nine concrete systems with different wrapping materials have been tested in this project (Table-1.0). A total of 36 standard concrete cylinders with diameter of 152 mm (6 in.) and height of 300 mm (about 12 in.) have been tested under uniaxial compression loading in each system. The main experimental parameters include unconfined concrete strength and thickness of in-situ fabricated carbon or glass fiber composite jackets. Table 1 summarizes the testing matrix (on the following pages).

Table 3.1: Test Matrix

System	Type of FRP	f'_c(Mpa)	Jacket Layers or Thickness	Specimen Name	Total Number
1	Carbon Fiber Sheet	33.7	0, 1, 2, 3 layers	LC-CJ1	12
		43.8	0, 1, 2, 3 layers	MC-CJ1	12
		55.2	0, 1, 2, 3 layers	HC-CJ1	12
2	Carbon Fiber Sheet	32.4	0, 0.5, 1, 1.5 Layers	LC-CJ2	12
		43.6	0, 0.5, 1, 1.5 Layers	MC-CJ2	12
		53.8	0, 0.5, 1, 1.5 Layers	HC-CJ2	12
3	Prefabricated Glass Fiber Jakets	31.3	0, 2, 3, 4 layers	LC-GJ3	12
		43.9	0, 2, 3, 4 layers	MC-GJ3	12
		60.1	0, 2, 3, 4 layers	HC-GJ3	12
4	Machine-Wound Carbon Fiber	32.7	0, 0.5, 1, 1.5 Layers	LC-CJ4	12
		46.3	0, 0.5, 1, 1.5 Layers	MC-CJ4	12
		58.4	0, 0.5, 1, 1.5 Layers	HC-CJ4	12
5	Carbon Fiber Sheet	32.1	0, 1, 2, 3 layers	LC-CJ5	12
		43.0	0, 1, 2, 3 layers	MC-CJ5	12
		64.2	0, 1, 2, 3 layers	HC-CJ5	12
6	Glass Fiber Sheet	37.1	0, 1, 2 Layers	LC-GJ6	12
		56.9	0, 1, 2 Layers	MC-GJ6	12
		63.3	0, 1, 2 Layers	HC-GJ6	12

Table 3.1, continued

		35.0	0, 0.318, 0.635, 1.270mm	LC-CJ7	12
7	Machine-Wound Carbon Fiber	50.0	0, 0.318, 0.635, 1.270mm	MC-CJ7	12
		63.2	0, 0.318, 0.635, 1.270mm	HC-CJ7	12
		34.5	0, 0.318, 0.635, 1.270mm	LC-CJ8	12
8	Machine-Wound Carbon Fiber	48.8	0, 0.318, 0.635, 1.270mm	MC-CJ8	12
		60.2	0, 0.318, 0.635, 1.270mm	HC-CJ8	12
		34.7	0, 0.318, 0.635, 1.270mm	LC-CJ9	12
9	Machine-Wound Carbon Fiber	54.3	0, 0.318, 0.635, 1.270mm	MC-CJ9	12
		61.9	0, 0.318, 0.635, 1.270mm	HC-CJ9	12

For each type of composite jacket system, three batches of concrete representing lower, medium, and higher strength concrete were prepared. Concrete mix design proportions are shown in Table 2.1. The maximum size of the coarse aggregates was approximately 13mm (about 0.5 in.). The target strengths at 28 days for the lower, medium, and higher strength concrete were 27.6 MPa (4ksi), 37.9 Mpa (5.5 ksi) and 48.2 Mpa (7 ksi), respectively. The actual concrete strength at testing ages, which ranges from 60 to 80 days after casting, was slightly higher than the mix design target strength. For each batch of concrete, 12 cylinders were made using the standard procedure. The specimens were cured in a close-can condition at room temperature. Three cylinders from each batch were tested without jacket to provide control data for the unconfined concrete, and nine others were wrapped with composite jackets at three different levels of thickness. For each combination of testing parameters, three identical specimens were fabricated and tested. The ends of the concrete cylinders were capped with high strength sulfur. The edge of the sulfur was trimmed in order to prevent the composite jacket from directly bearing the axial compression.

In this dissertation, the results of two typical carbon fiber systems were introduced mainly.

3.2 Composite Jackets

The CFRP jacket system under investigation involves hand layout of uni-direction fiber sheets on epoxy saturated surfaces or machine-wound uni-direction fiber jackets. The installed jackets had a fiber orientation configured along the circumferential direction. A thin layer of primer epoxy was first applied to the concrete surface. After the primer epoxy on the concrete surface was cured at the ambient temperature for several hours, the carbon fiber sheets were installed. For each layer of fiber sheets, two plies of epoxy, one on the cylinder surface prior to installing the sheet and the other on top of the installed sheet were applied using paint brushes to fully saturate the layers with epoxy. The extra epoxy for each layer was squeezed out using a flat plastic edge. After the required layers of the sheet were installed, the CFRP composite jacket was cured in the ambient condition. Fig. 3.1 shows the typical procedure for installing the jacket on cylinder specimens.

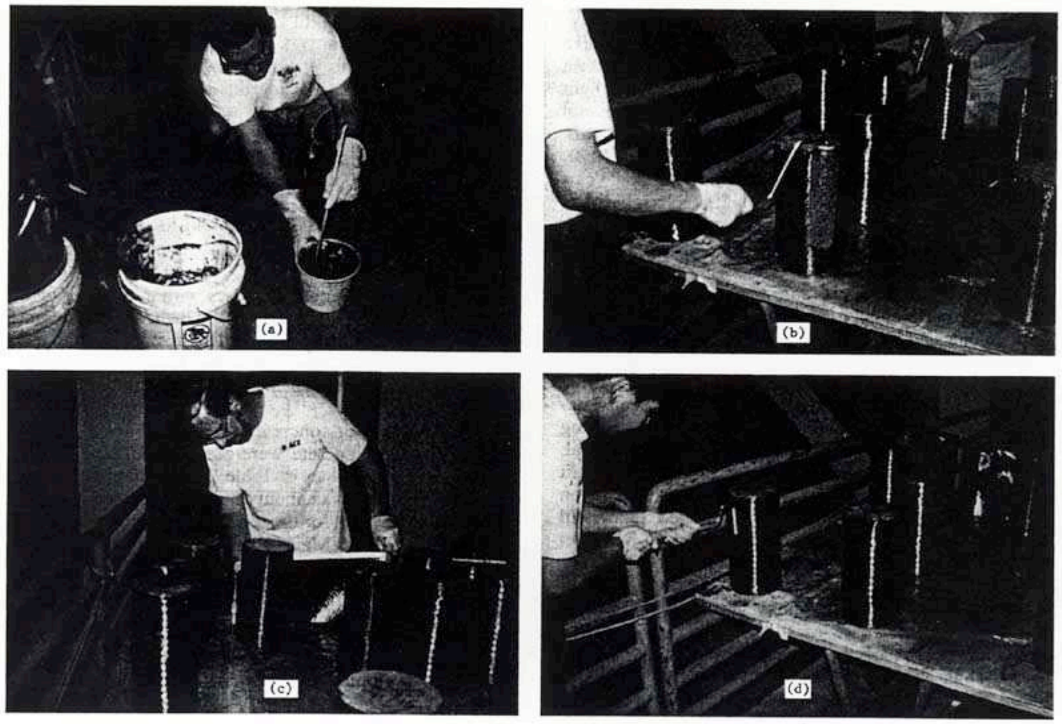

Figure 3.1: Installation Procedure of Carbon Fiber Composite Jackets:
(a) Mixing Epoxy; (b) Applying Epoxy on Specimen Surface;
(c) Installing Carbon Fiber Sheets; (d) Consolidating Jacket

The mechanical properties such as the modulus and the tensile strength of the composite jackets were obtained through tensile testing of flat coupons with fibers configured uni-directionally along the coupon axis. The tensile coupons were conducted following the ASTM specification D 3039-75 (Standards 1990). The tensile coupons were cut from a thin CFRP plate made simultaneously along with the installation of jackets. Prior to testing, aluminum flat bars were glued to the ends of the 12 mm wide coupons, as shown in Fig. 3.2, to avoid premature failure of the coupon ends, which were clamped in the jaws of the testing machine. Main mechanical properties were obtained from the averaged value of three tensile coupon tests and are summarized below:

Thickness (per ply): 0.381 mm

Modulus E_j: 1.05 x 10^5 MPa

Strength f_{ju}: 1,577 MPa

Strain ε_{ju}: 0.015

Note that the strength and modulus were defined based on the gross sectional area of the coupons. The strain was obtained as an average strain over a length of 50 mm in the middle portion of the coupon measured using a linear potentiometer. Table 3 summarizes the mechanical properties.

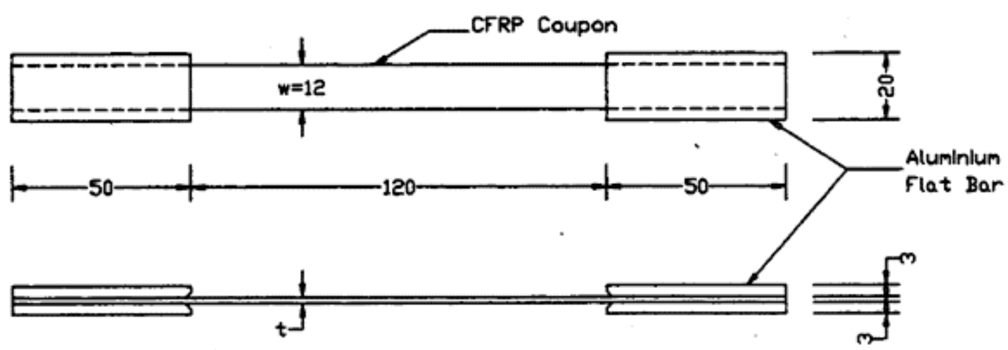

Figure 3.2: CFRP Tension Coupon Details

3.3 Confinement Modulus and Confinement Strength

In addition to the material properties of concrete, there are two significant factors affecting the performance of confined concrete. They can be defined as confinement modulus and confinement strength (Xiao et al. 1990). Based on the cylindrical coordinate system shown in Fig.1, the confinement modulus, C_j, can be defined as the ratio of the increments of confinement stress, Δf_r, and radial (transverse) strain, $\Delta\varepsilon_r$,

$$C_j = -\frac{\Delta f_r}{\Delta \varepsilon_r} \tag{3-1}$$

where, the "-" sigh represents the passive confinement. Using the equilibrium condition and the deformation compatibility condition in the cross section, the following two equations can be established,

$$f_r = -\frac{2t_j}{D} f_{j\theta} \tag{3-2}$$

$$\varepsilon_r = \varepsilon_{j\theta} \tag{3-3}$$

where, t_j is the thickness of the jacket; D is the diameter of the concrete cylindrical column; $f_{j\theta}$ and $\varepsilon_{j\theta}$ are the circumferential stress and strains of jacket, respectively. Using equations (3-2) and (3-3), the confinement modulus can be expressed as,

$$C_j = \frac{2t_j}{D}\frac{\Delta f_{j\theta}}{\Delta\varepsilon_{j\theta}} \tag{3-4}$$

Since the composite jacket is essentially a linear elastic material, $\Delta f_{j\theta}/\Delta\varepsilon_{r\theta}$ can be assumed to be equal to tensile modulus of E_j. Thus, a constant confinement modulus based on the thickness of jacket, diameter of column, and jacket modulus can be defined.

$$C_j = \frac{2t_j}{D}E_j \tag{3-5}$$

Based on the tensile coupon test results, for example, the confinement modulus is found to be 525 MPa, 1,050 MPa and 1,580 MPa for the jackets with one, two, and three plies (layers), respectively for system one.

On the other hand, the confinement strength limit, f_{ru}, is determined by the ultimate strength of the jacket, $f_{ju,}$ given by,

$$f_{ru} = -\frac{2t_j}{D}f_{ju} \tag{3-6}$$

Using the assumption that the composite is perfectly elastobrittle, the ultimate jacket strength f_{ju}, can be expressed by its ultimate strain, ε_{ju}, multiplied by the elastic modulus, E_j , and then (3-6) can be rewritten as

$$f_{ru} = -C_j \varepsilon_{ju} \tag{3-7}$$

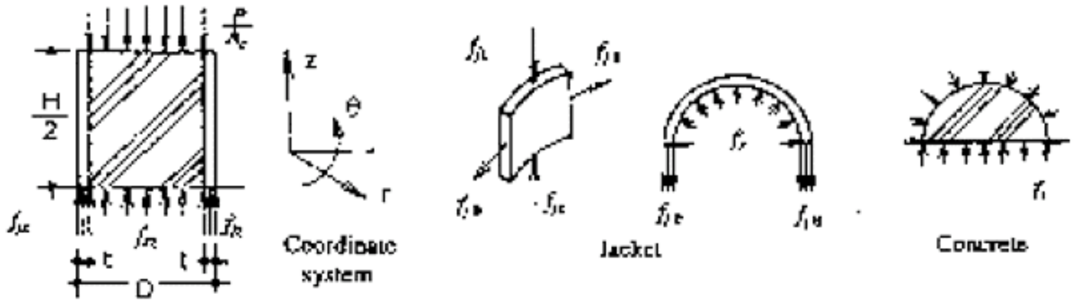

Figure 3.3: Definition of Mechanical Variables

3.4 Test Methods

As shown in Fig. 3.4, all the specimens were tested using the SATEC One Million Pounds Compression Machine at the Structural Laboratory of University of Southern California. This unique equipment has sufficient capacity and stiffness required for conducting such experiement. The extreme stiffness of the test frame makes it possible to measure the falling branch, if any, of the concrete stub columns. The machine is also equipped with a sophisticated computer control and data acquisition system. The tests were performed in uniaxial compression with the axial strain rate set at 0.001/min.

The acquired data included the applied axial strains of the jacket. As shown in Fig.3-4, in order to obtain data without the influence from the possible imperfect contacts as well as the end confinement due to the friction between the ends of the specimen and the loading platens, the axial deformation of the concrete was measured at the middle portion with a gauge length of 152 mm (6 in). The jacket strain was measured using a specially designed device composed of linear bearings and linear potentiometers. The jacket strains were measured using electrical resistance gauges with a gauge length of 30 mm(i.18 in.).

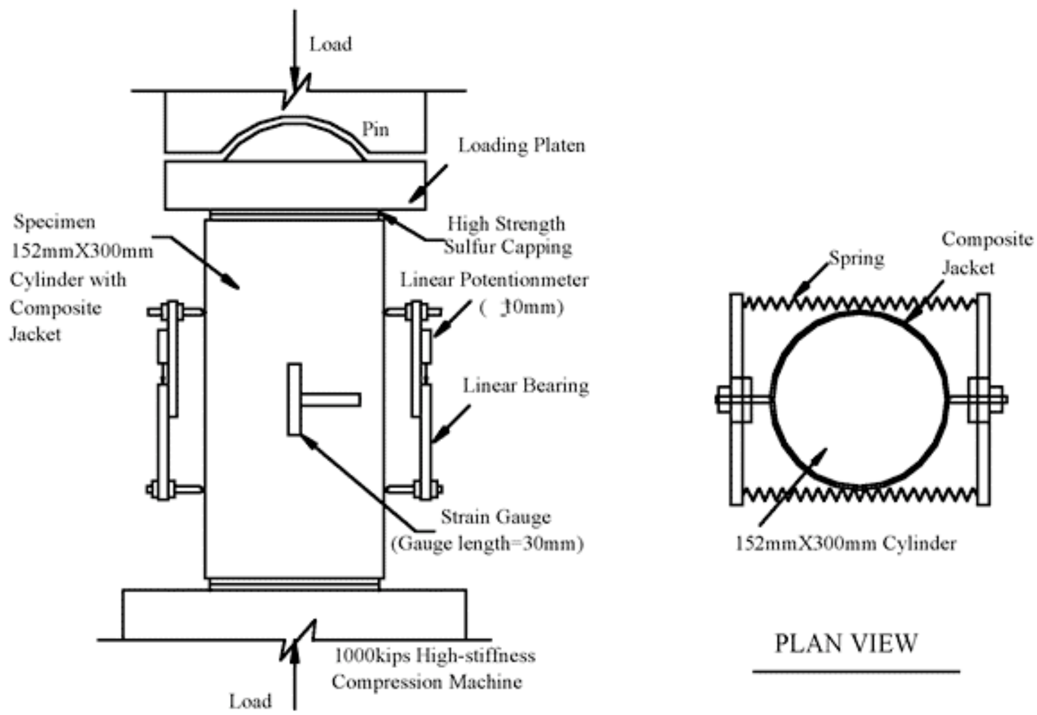

Figure 3.4: Test and Instrumentation Configurations

Figure 3.5: Test Setup

Determination of Concrete Stresses and Strains

The axial strain of concrete, ε_z , is determined based on the linear potentiometer measurements. The jacket axial and circumferential strains, ε_{jz}, and $\varepsilon_{j\theta}$, are directly measured using electrical resistance gauges. The concrete transverse (radial and circumferential) strains, ε_{cr} and $\varepsilon_{c\theta}$, are then obtained using the deformation compatibility condition in the cylinder cross section, which subjects to a confinement that is assumed to be uniform around the surface.

$$\varepsilon_{cr} = \varepsilon_{c\theta} = \varepsilon_r = \varepsilon_{j\theta} \tag{3-8}$$

The transverse (radial and circumferential) stresses of confined concrete, f_{cr} and $f_{c\theta}$ can be obtained using the equilibrium condition between the confined concrete core and the jacket:

$$f_{cr} = f_{c\theta} = f_r = -\frac{2t_j}{D} f_{j\theta} \tag{3-9}$$

Using (3-5) and (3-8), the following equation can be derived:

$$f_r = -C_j \varepsilon_{j\theta} \tag{3-10}$$

The axial stress of confined concrete, f_{cz}, is calculated using the equilibrium condition in the column axial direction ignoring the jacket axial stress:

$$f_{cz} = \frac{P}{A_c} \tag{3-11}$$

where A_c = sectional area of confined concrete. Note that although the jacket did not directly bear the loading plates at the ends, some axial stress existed in the jacket due to the bond transfer between the jacket and the concrete. The axial stress in the composite jacket is considered insignificant compared to that in the concrete as well as the circumferential stress in the jacket.

CHAPTER 4: EXPERIMENTAL RESULTS

In this study, nine confined concrete systems was been tested. Total 243 cylinders wrapped with carbon fiber or glass fiber, 81 concrete cylinders without confinements were tested. Based on the system one and system two' test data, a confined concrete model was proposed in Appendix A and B.

4.1 Experimental Behavior of Confined Concrete under Monotonic Loading

Axial stress versus axial and transverse strains of confined concrete are shown in Fig.4.1 (a) to (c). The average axial stress strain relationships obtained for unconfined concrete cylinders are also shown in Fig 4.1. As shown in Fig 4.1, the initial portions of stress strain responses of confined concrete essentially followed the curves of unconfined concrete. After exceeding the unconfined concrete strength, the axial stress – axial strain as well as axial stress – transverse strain relationships of most specimens softened slightly and eventually exhibited an almost linear behavior until the sudden failure due to the rupture of carbon fiber composite jackets. Such near linear behavior of concrete confined in elastic materials have been noticed in existing studies (Xiao 1989; Xiao et al. 1991; Hosotani et al. 1996; Mirmiran et al. 1997]. For the three specimens of high strength concrete confined by one-layer jacket and one specimen with medium strength concrete confined by one-layer jacket, although the peak stress exceeded the unconfined concrete strength, the post peak behavior exhibited a sudden drop. Even for the specimens with a descending stress strain response, the post peak stress eventually stabilized at a lower stress level until the rupture of the jacket.

The failure corresponding to the rupture of carbon fiber jacket was very explosive. For some specimens, the rupture of jacket was accompanied by slight delamination between the layers. The recorded jacket strains corresponding to the failure ranged from 0.007 to 0.012, which were about 50% to 80% of the rupture strains obtained for the tensile coupons. The following are among the most important reasons considered to have contributed to the reduction of ultimate strain.

Despite using the same materials, the process of making flat coupons is easier than that of making the cylindrical shaped jacket. As a result, the composites in the flat coupons may have a higher quality than those in the jacket.

Due to the existence of the confinement pressure acting on the internal surface of the jacket as well as axial stress in the jacket, the stress state is not a strictly pure tension condition as that for the flat coupon tension tests.

Concrete cracking and crushing beneath the jacket may have caused local stress concentrations in the jacket.

Based on the observation, the study shows that the onset of the jacket rupture was the due cause of the total failure.

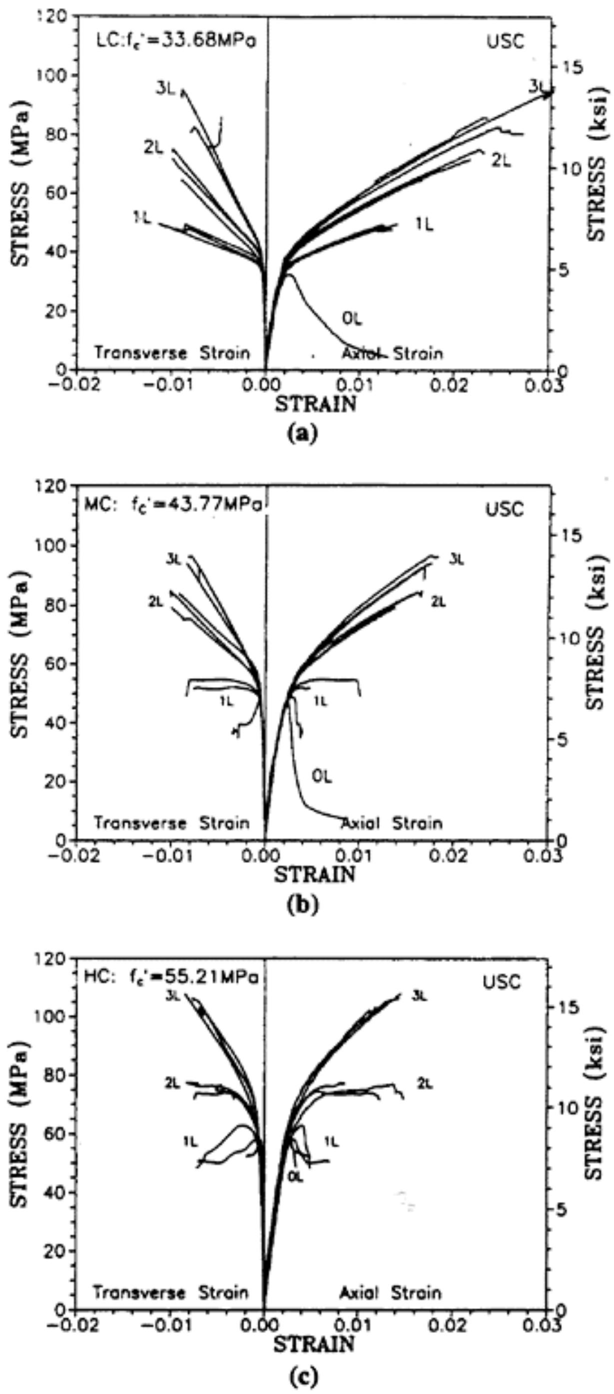

Figure 4.1: Axial Stress-Strain Relationships for CFRP Confined Concrete Cylinders with (a) Lower Unconfined Concrete Strength; (b) Medium Unconfined Concrete Strength; (c) Higher Unconfined Concrete Strength

Fig. 4.1 shows axial stress versus volume strain. Unconfined concrete decreases in volume until the stress reaches about 85% of f_c'. This occurs at a stress slightly higher than critical stress at which, in unconfined concrete, micro-cracks start to cause volumetric expansion. It has been generally accepted that under increasing compression, the material first compacts and eventually dilates due to micro cracking. In cylinders with low confinement (one layer), the expansion continues monotonically until the jacket bursts. With higher confinement values (two layers), the curve turns back again to the direction of reduction of volume. For high confinement ratio (three layers), the volumetric strain is always negative. For high strength concrete with high confinement values, the deformations are determined by the interaction of the jacket hoop stiffness and the bulk compressibility of the concrete, with the jacket exerting the greater influence.

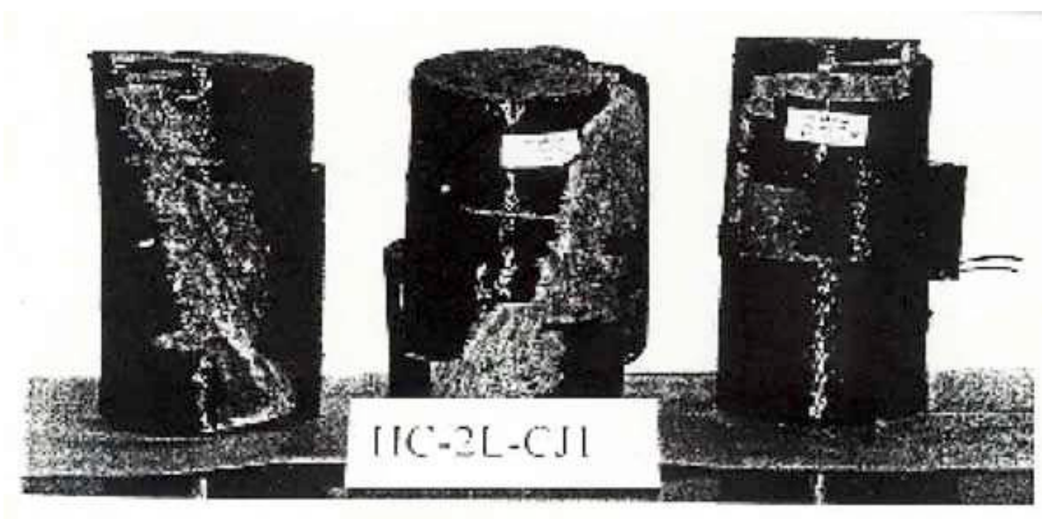

Figure 4.2: Typical Example of Failure Condition

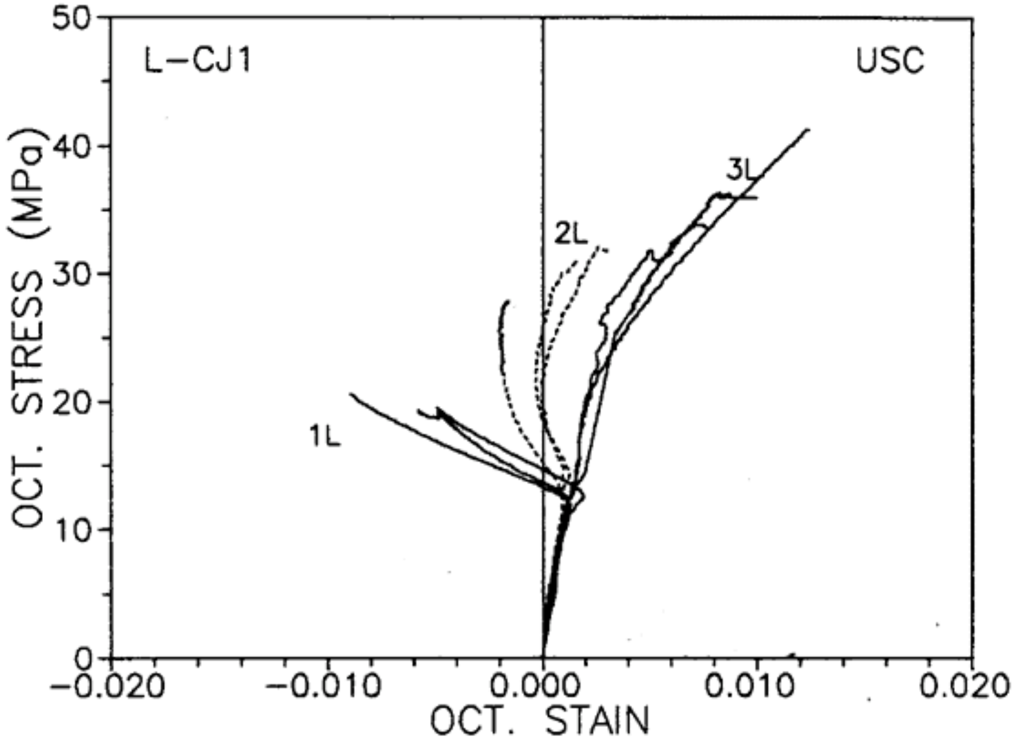

Figure 4.3: Volume Stress Versus Volume Strain

Fig. 4.4 shows axial stress versus effective confinement stress. The curve shows loading path in stress space. Due to the effect of confinement the loading path is along yield surface after yielding. Actually failure occurs suddenly due to fiber rupture.

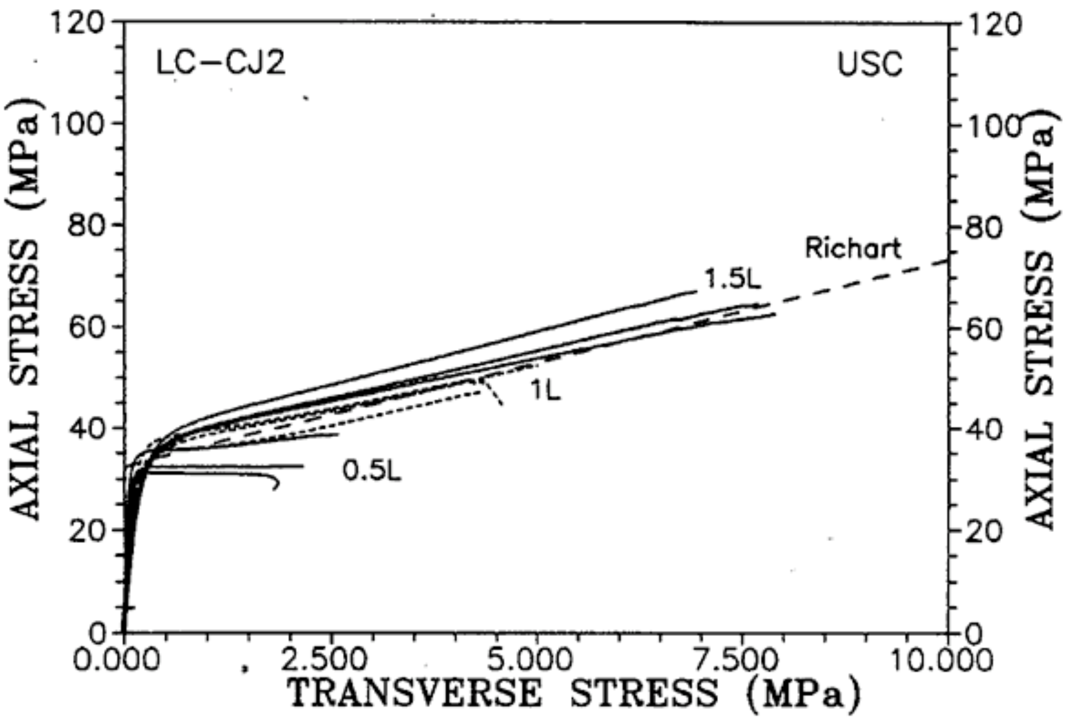

Figure 4.4: Axial Stress Effective Confinement Stress

4.2 Axial – Transverse Strain Responses

Typical relationships for axial and transverse strains are shown in Fig.4.5 for the three specimens with medium strength concrete and 3 layers of carbon fiber composite jacket. As shown in Fig.4.5, the initial slopes of the axial strain and transverse strain relationships are very close to dashed line corresponding to a slope value of 0.18, which represents the typical initial Poisson's ratio for concrete. This is consistent with the following theoretical equation based on generalized Hooke's law with C_j being sufficient smaller than E_c :

$$\varepsilon_r = -\frac{\nu_c}{1 + \left(C_j / E_c\right)\left(1 - \nu_c - 2\nu_c^2\right)}\varepsilon_z \tag{4-1}$$

where E_c = elastic modulus of unconfined concrete, taken as $4{,}733\sqrt{f_c'}$; and ν_c = initial Poisson's ratio, taken as 0.18.

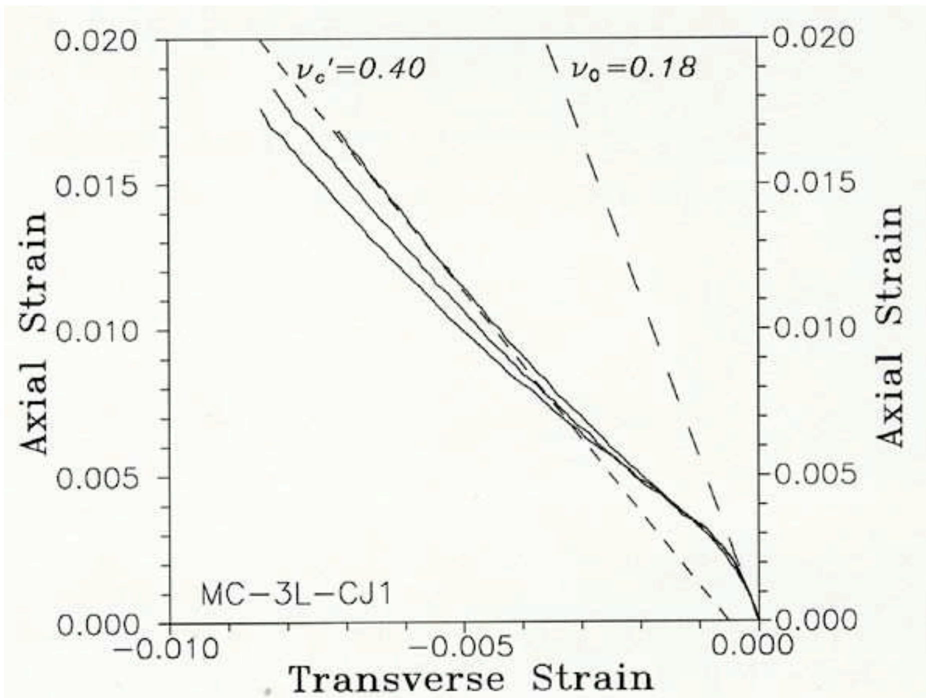

Figure 4.5: Typical Relationship between Axial Strain and Transverse Strain

As the axial strain increases, the ratio between the transverse strain and axial strain also increases, indicating the acceleration of lateral dilation of the concrete. The curves appear to eventually converge to lines, which can be empirically expressed as

$$\varepsilon_r = \varepsilon'_{ro} - \nu' \varepsilon_{cz} \tag{4-2}$$

where, ε'_{ro} is the intersection of the linear line at zero axial strain; and ν' is the slop value of the line. For all the 27 specimens with jackets, ε'_{ro} and ν_c' were calculated. Based on the test results, ε'_{ro} had an average value of about −0.0005. It was recognized that the value of slope, ν_c', increases for higher concrete strength, f'_{co} and lower confinement modulus, C_j, and can be given by the following equation obtained from regression analysis

$$\nu_c' = 10\left(\frac{f'_{co}}{C_j}\right)^{0.9} \tag{4-3}$$

Note that the value of ν_c' approaches to zero when C_j becomes infinity. This is consistent with experimental observations for concrete with significantly large confinement modulus [Bazant et al. 1986; Xiao 1989, 1991]. Comparison of equation (4-3) and all the test data is shown in Fig.5. The calculated value of 0.40 based on equation (4-3) is also shown in Fig.4 for the specimens with f'_{co} = 43.8Mpa and C_j=1.580Mpa. Table 4.1 shows the data of the correlation of equation (4-3).

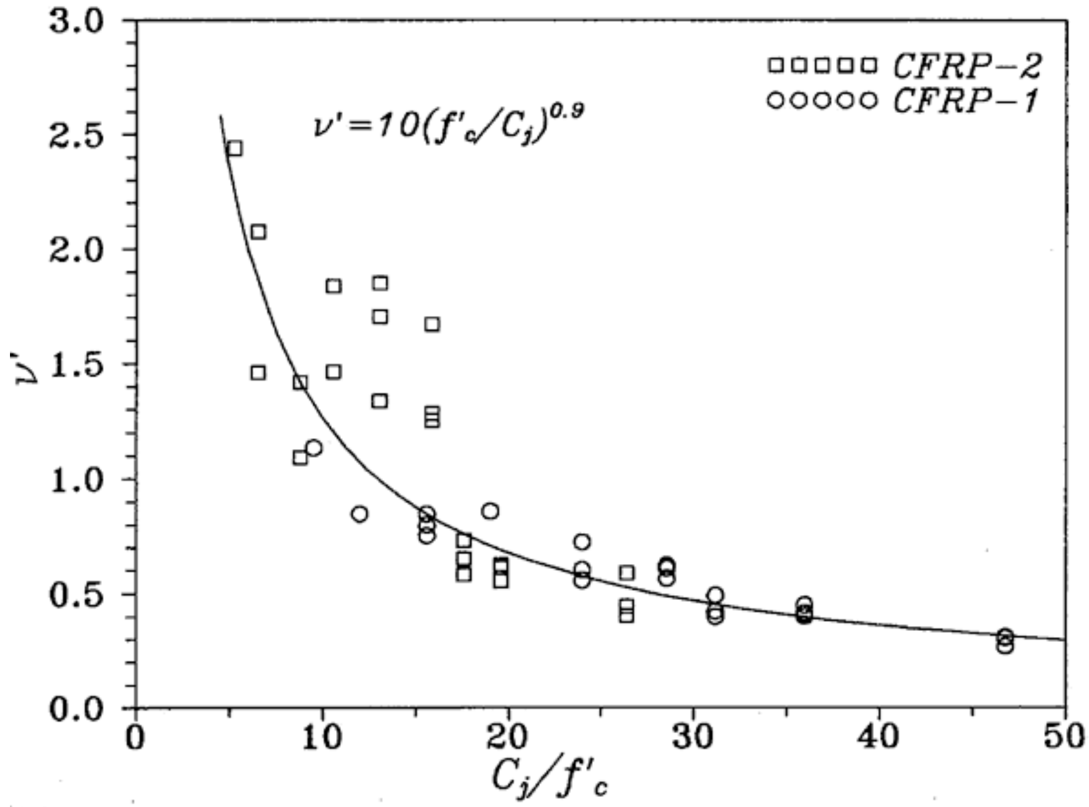

Figure 4.6: Test Data and Regression Equation for Coefficient ν_c'

All of above data obtained from following system one and system two test results. Both system are carbon fiber confined concrete.

Table 4.1: Data of the correlation of equation (4-3).

name	layer	f_c'	Cj	Cj/f_c'	ν’	name	layer	f_c'	Cj	Cj/f_c'	ν’
		MPa	MPa					MPa	MPa		
L-1-1	1	33.7	525	15.58	0.752	L-0.5-1	0.5	32.4	284.6	8.79	1.09
L-1-2	1	33.7	525	15.58	0.798	L-0.5-2	0.5	32.4	284.6	8.79	1.42
L-1-3	1	33.7	525	15.58	0.846	L-0.5-3	0.5	32.4	284.6	8.79	4.00
L-2-1	2	33.7	1050	31.16	0.491	L-1-1	1	32.4	569.2	17.58	0.58
L-2-2	2	33.7	1050	31.16	0.399	L-1-2	1	32.4	569.2	17.58	0.65
L-2-3	2	33.7	1050	31.16	0.423	L-1-3	1	32.4	569.2	17.58	0.73
L-3-1	3	33.7	1575	46.74	0.308	L-1.5-1	1.5	32.4	853.8	26.37	0.40
L-3-2	3	33.7	1575	46.74	0.303	L-1.5-2	1.5	32.4	853.8	26.37	0.44
L-3-3	3	33.7	1575	46.74	0.268	L-1.5-3	1.5	32.4	853.8	26.37	0.59
M-1-1	1	43.8	525	11.99	0.846	M-0.5-1	0.5	43.6	284.6	6.53	1.46
M-1-2	1	43.8	525	11.99	0.846	M-0.5-2	0.5	43.6	284.6	6.53	2.07
M-1-3	1	43.8	525	11.99	0.846	M-0.5-3	0.5	43.6	284.6	6.53	4.44
M-2-1	2	43.8	1050	23.97	0.556	M-1-1	1	43.6	569.2	13.06	1.33
M-2-2	2	43.8	1050	23.97	0.722	M-1-2	1	43.6	569.2	13.06	1.70
M-2-3	2	43.8	1050	23.97	0.602	M-1-3	1	43.6	569.2	13.06	1.99
M-3-1	3	43.8	1575	35.96	0.416	M-1.5-1	1.5	43.6	853.8	19.58	0.55
M-3-2	3	43.8	1575	35.96	0.402	M-1.5-2	1.5	43.6	853.8	19.58	0.59
M-3-3	3	43.8	1575	35.96	0.450	M-1.5-3	1.5	43.6	853.8	19.58	0.62
H-1-1	1	55.2	525	9.51	1.133	H-0.5-1	0.5	53.8	284.6	5.29	2.44
H-1-2	1	55.2	525	9.51	1.133	H-0.5-2	0.5	53.8	284.6	5.29	8.00
H-1-3	1	55.2	525	9.51	1.133	H-0.5-3	0.5	53.8	284.6	5.29	
H-2-1	2	55.2	1050	19.02	0.858	H-1-1	1	53.8	569.2	10.58	1.46
H-2-2	2	55.2	1050	19.02	0.858	H-1-2	1	53.8	569.2	10.58	1.84
H-2-3	2	55.2	1050	19.02	0.858	H-1-3	1	53.8	569.2	10.58	3.57
H-3-1	3	55.2	1575	28.53	0.564	H-1.5-1	1.5	53.8	853.8	15.87	1.33
H-3-2	3	55.2	1575	28.53	0.608	H-1.5-2	1.5	53.8	853.8	15.87	1.78
H-3-3	3	55.2	1575	28.53	0.621	H-1.5-3	1.5	53.8	853.8	15.87	2.27

4.3 Axial Stress – Confinement Stress Responses

As an example, the axial stress – confinement stress relationships for the specimens with medium concrete strength and 3-layer carbon composite jacket are depicted in Fig.4.7. The stresses in Fig.4.7 are shown as the ratios of stresses divided by unconfined concrete strength, f'_{co}. The initial slopes of the curves are very close to the dashed line with a slope of k_0, which was calculated based on the generalized Hooke's Law.

$$k_0 = \frac{df_z}{df_r} = \frac{E_c}{C_j \nu_0}\left(1 + 2\nu_c \nu_0 \frac{C_j}{E_c}\right) = \frac{E_c}{C_j \nu_c} + \frac{1-\nu_c}{\nu_c} \tag{4-4}$$

where E_c is the elastic modulus of unconfined concrete, taken as $4{,}733\sqrt{f'_{co}}$; ν_o is the initial ratio of transverse strain over axial strain,

$$\nu_0 = \frac{\nu_c}{1 + \frac{C_j}{E_c}\left(1 - 2\nu_c\right)\left(1 + \nu_c\right)} \tag{4-5}$$

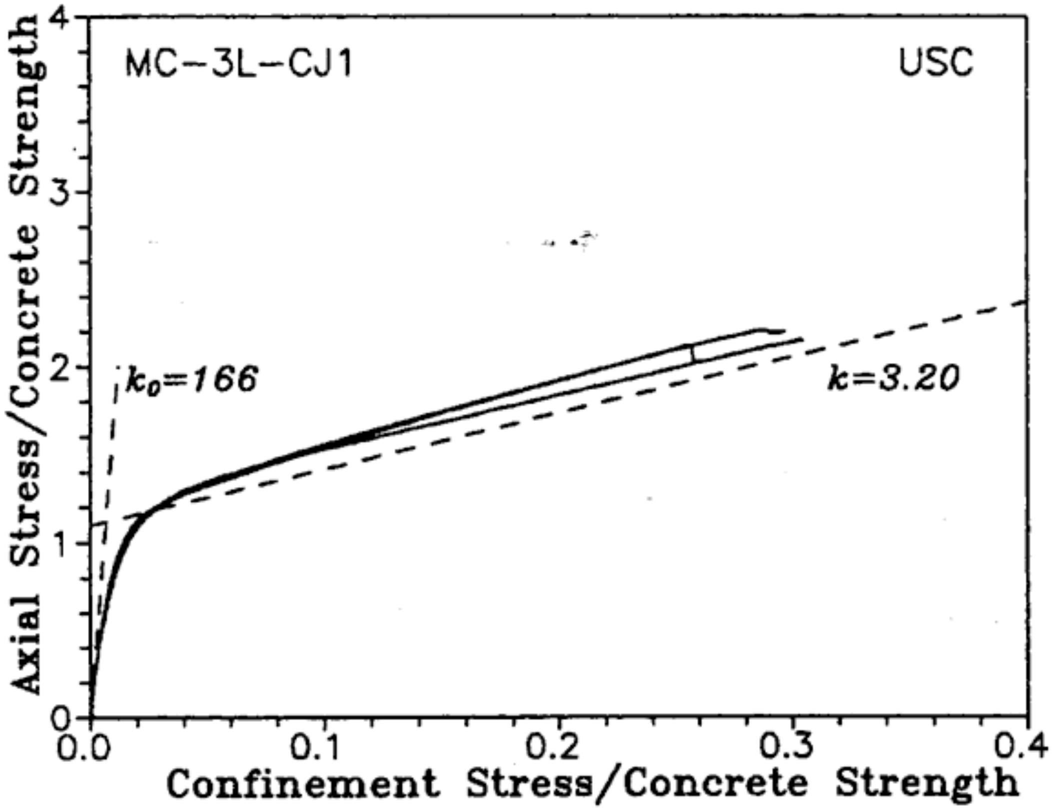

Figure 4.7: Typical Relationship between Axial Stress and Confining Stress

As shown in Fig 4.7, after the axial stresses exceed the unconfined concrete strength, the curves tend to converge into linear lines with much smaller slopes than the initial behaviors. The final linear portion of the axial and confinement stress relationships can be expressed by the following equation,

$$\frac{f_{cz}}{f'_{co}} = \alpha + k\frac{f_r}{f'_{co}} \tag{4-6}$$

where α and k represent the intersection with vertical axis and slope of the linear line, respectively. If taking , α=1.0, k=4.1 , the above equation becomes the well known Richart's failure criterion [Rechart et al. 1929]. The values of α for all the specimens vary around an average value of 1.10. Based on the regression analysis for all the specimens with setting the ultimate value of k to be 4.1 corresponding to infinite C_j, the following equation was obtained with a correlation factor of 80 percent.

$$k = 4.1 - 0.45\left(\frac{f'^{2}_{co}}{C_j}\right)^{1.4} \tag{4-7}$$

Fig 4.8 shows the correlation of equation (4-7) with test data. Note that the small or negative values for k corresponding to small values of C_j/f'_{co} were obtained for the final linear portions in the axial stress and confinement stress relationships rather than the points at peak axial stresses. The test data indicated that a boundary of $C_j/f'_{co} \approx 0.3$ exists to distinguish the performances with or without descending axial stresses after achieving f_c'. Table 4.2 shows the data of the correlation of equation (4-7).

Table 4.2: Data of the correlation of equation (4-7).

name	layer	f_c'	Cj	$Cj/f_c'^2$	□	name	layer	f_c'	Cj	$Cj/f_c'^2$	□
		MPa	MPa					MPa	MPa		
L-1-1	1	33.7	525	0.463	2.57	L-0.5-1	0.5	32.4	284.6	0.271	-0.04
L-1-2	1	33.7	525	0.463	2.77	L-0.5-2	0.5	32.4	284.6	0.271	0.01
L-1-3	1	33.7	525	0.463	3.05	L-0.5-3	0.5	32.4	284.6	0.271	1.80
L-2-1	2	33.7	1050	0.926	3.26	L-1-1	1	32.4	569.2	0.543	3.50
L-2-2	2	33.7	1050	0.926	3.39	L-1-2	1	32.4	569.2	0.543	3.20
L-2-3	2	33.7	1050	0.926	4.02	L-1-3	1	32.4	569.2	0.543	3.20
L-3-1	3	33.7	1575	1.389	3.87	L-1.5-1	1.5	32.4	853.8	0.814	3.37
L-3-2	3	33.7	1575	1.389	3.96	L-1.5-2	1.5	32.4	853.8	0.814	3.78
L-3-3	3	33.7	1575	1.389	4.39	L-1.5-3	1.5	32.4	853.8	0.814	4.20

M-1-1	1	43.8	525	0.274	0.33	M-0.5-1	0.5	43.6	284.6	0.150	
M-1-2	1	43.8	525	0.274	0.86	M-0.5-2	0.5	43.6	284.6	0.150	
M-1-3	1	43.8	525	0.274	0.78	M-0.5-3	0.5	43.6	284.6	0.150	
M-2-1	2	43.8	1050	0.548	2.77	M-1-1	1	43.6	569.2	0.299	0.39
M-2-2	2	43.8	1050	0.548	3.04	M-1-2	1	43.6	569.2	0.299	1.18
M-2-3	2	43.8	1050	0.548	3.24	M-1-3	1	43.6	569.2	0.299	0.66
M-3-1	3	43.8	1575	0.822	3.25	M-1.5-1	1.5	43.6	853.8	0.449	3.78
M-3-2	3	43.8	1575	0.822	3.83	M-1.5-2	1.5	43.6	853.8	0.449	4.25
M-3-3	3	43.8	1575	0.822	3.86	M-1.5-3	1.5	43.6	853.8	0.449	3.93

H-1-1	1	55.2	525	0.172	0.69	H-0.5-1	0.5	53.8	284.6	0.098	
H-1-2	1	55.2	525	0.172	-4.28	H-0.5-2	0.5	53.8	284.6	0.098	
H-1-3	1	55.2	525	0.172	-0.98	H-0.5-3	0.5	53.8	284.6	0.098	
H-2-1	2	55.2	1050	0.344	0.73	H-1-1	1	53.8	569.2	0.197	
H-2-2	2	55.2	1050	0.344	0.93	H-1-2	1	53.8	569.2	0.197	
H-2-3	2	55.2	1050	0.344	0.42	H-1-3	1	53.8	569.2	0.197	
H-3-1	3	55.2	1575	0.517	3.24	H-1.5-1	1.5	53.8	853.8	0.295	
H-3-2	3	55.2	1575	0.517	3.29	H-1.5-2	1.5	53.8	853.8	0.295	
H-3-3	3	55.2	1575	0.517	3.45	H-1.5-3	1.5	53.8	853.8	0.295	

However, higher strength concrete cylinders with lower confinement FRP showed very random behavior after concrete stress reached peak point. Because of lacking of confinement the concrete became unstable materials. In Table 4-2, the cells of κ are intentionally left blank.

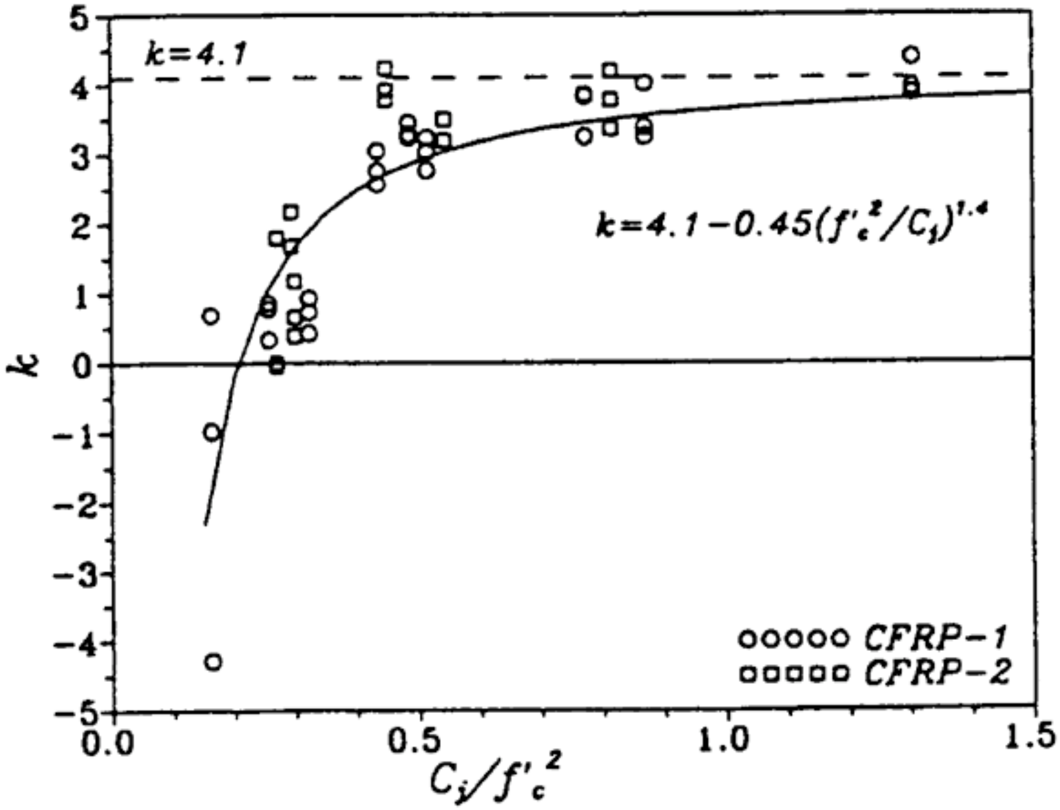

Figure 4.8: Test Data and Regression for Final Confinement Coeffient *k*

4.4 Bilinear Simulations for Stress – Strain Relationships of Confined Concrete

Cased on the test results and theoretical equations between the four mechanical variables of confined concrete, ε_{cz}, ε_r, f_{cz} and f_r, it is suggested to use the following two sets of linear equations to describe the mechanical natures of initial and final performances of concrete confined by composite jacket.

For initial performance,

$$f_{cz}=E_c\varepsilon_{cz} + 2\nu_c f_r \quad (4\text{-}8a)$$

$$\varepsilon_r = -\nu_o\varepsilon_{cz} \quad (4\text{-}8b)$$

$$f_r = -C_j\varepsilon_r \quad (4\text{-}8c)$$

For final performance,

$$f_{cz}=\alpha f'_{co}+kf_r \quad (4\text{-}9a)$$

$$\varepsilon_r=\varepsilon'_{ro}-\nu'_o\,\varepsilon_{cz} \quad (4\text{-}9b)$$

$$f_r=-C_j\varepsilon_r \quad (4\text{-}9c)$$

The ultimate condition of the confined concrete can be determined by substituting the ultimate rupture strain of jacket into equation (4-9). Based on the test results, it is conservatively suggested to use the 50% of the rupture strain measured for flat tensile coupon samples of carbon fiber composites.

The simple bilinear simulations based on equations (4-6) and (4-9) were performed for the test results conducted by Hosotani et al. (1996), as compared in Fig.4.9(a) and (b). As shown in Fig.4.9, the bilinear equations describe the trends of Hosotani et al.'s test data reasonably well.

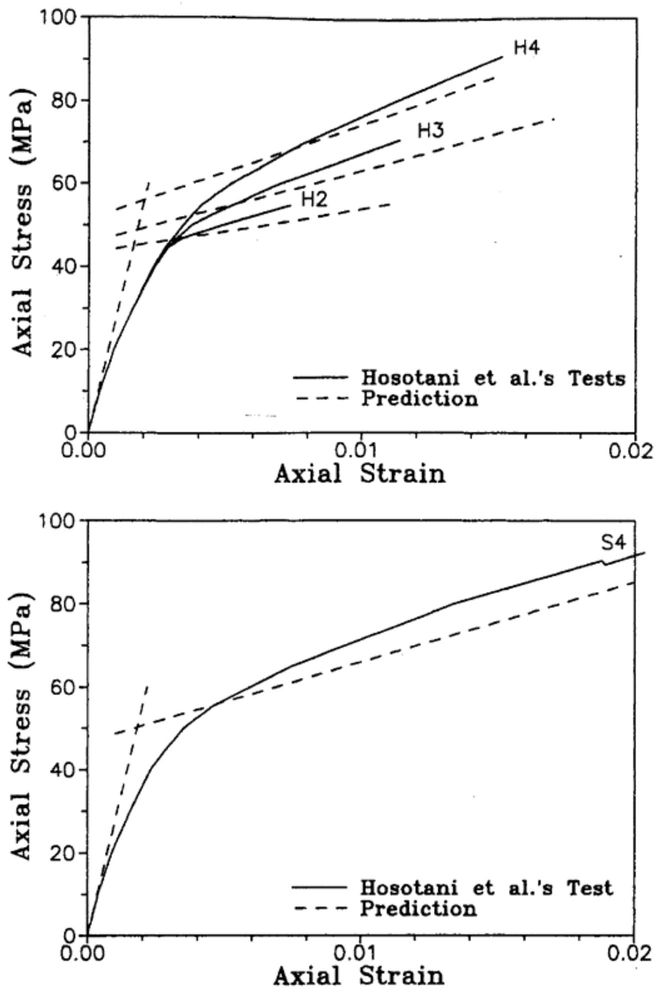

Figure 4.9: Bilinear Simulation of Hosotani et al.'s Test Results

From Table 4-3 to Table 3-11 are summary of total test results of nine systems.

Table 4.3: Test Results of System One

Series	Specimen	f_c' (MPa)	Jacket Layers	f_{cc}' (MPa)	ε_{cu}
L	LC-0L-CJ1-1	33.7	0	32.35	0.002591
	LC-0L-CJ1-2			33.43	0.002137
	LC-0L-CJ1-3			35.25	0.002441
	LC-1L-CJ1-1		1	47.87	0.01340
	LC-1L-CJ1-2			49.66	0.01397
	LC-1L-CJ1-3			49.38	0.01241
	LC-2L-CJ1-1		2	64.56	0.01650
	LC-2L-CJ1-2			75.23	0.02253
	LC-2L-CJ1-3			71.79	0.02160
	LC-3L-CJ1-1		3	82.94	0.02460
	LC-3L-CJ1-2			86.25	0.02329
	LC-3L-CJ1-3			95.38	0.03030
M	MC-0L-CJ1-1	43.8	0	47.01	0.002432
	MC-0L-CJ1-2			43.42	0.002157
	MC-0L-CJ1-3			40.87	0.002092
	MC-1L-CJ1-1		1	54.77	0.009805
	MC-1L-CJ1-2			52.05	0.004679
	MC-1L-CJ1-3			48.27	0.003360
	MC-2L-CJ1-1		2	83.95	0.01570
	MC-2L-CJ1-2			79.21	0.01376
	MC-2L-CJ1-3			84.97	0.01658
	MC-3L-CJ1-1		3	96.50	0.01744
	MC-3L-CJ1-2			92.60	0.01678
	MC-3L-CJ1-3			94.04	0.01759
H	HC-0L-CJ1-1	55.2	0	54.75	0.002266
	HC-0L-CJ1-2			53.44	0.002106
	HC-0L-CJ1-3			57.45	0.002840
	HC-1L-CJ1-1		1	56.97	0.00686
	HC-1L-CJ1-2			62.87	0.00406
	HC-1L-CJ1-3			58.06	0.00486
	HC-2L-CJ1-1		2	74.57	0.01230
	HC-2L-CJ1-2			77.50	0.00847
	HC-2L-CJ1-3			76.99	0.01390
	HC-3L-CJ1-1		3	106.5	0.01436
	HC-3L-CJ1-2			101.1	0.01452
	HC-3L-CJ1-3			103.3	0.01182

Note: (i) Example for specimen name designation:
LC-2L-CJ1-1: LC designates Lower strength Concrete; 2L designates 2 Layers; CJ1 designates Carbon fiber Jacket System 1; and the last number represents specimen number in same series.

(ii) f_c': Average plain concrete cylinder strength;

(iii) f_{cc}': Ultimate strength of confined concrete;

(iv) ε_{cu}: Ultimate strain

Table 4.4: Test Results of System Two

Series	Specimen	f_c' (MPa)	Jacket Layers	f_{cc}' (MPa)	ε_{cu}
L	LC-0L-CJ2-1	32.4	0	32.70	0.002061
	LC-0L-CJ2-2			32.08	0.001813
	LC-0L-CJ2-3			32.35	0.002096
	LC-0.5L-CJ2-1		0.5	32.37	0.006267
	LC-0.5L-CJ2-2			38.67	0.008592
	LC-0.5L-CJ2-3			31.26	0.003196
	LC-1L-CJ2-1		1	47.29	0.00980
	LC-1L-CJ2-2			52.41	0.01487
	LC-1L-CJ2-3			49.46	0.01138
	LC-1.5L-CJ2-1		1.5	67.00	0.01929
	LC-1.5L-CJ2-2			64.52	0.01970
	LC-1.5L-CJ2-3			62.46	0.01521
M	MC-0L-CJ2-1	43.6	0	41.23	0.002053
	MC-0L-CJ2-2			43.69	0.002431
	MC-0L-CJ2-3			45.88	0.002479
	MC-0.5L-CJ2-1		0.5	46.75	0.005899
	MC-0.5L-CJ2-2			46.15	0.004126
	MC-0.5L-CJ2-3			43.15	0.005111
	MC-1L-CJ2-1		1	51.87	0.005469
	MC-1L-CJ2-2			54.30	0.007883
	MC-1L-CJ2-3			52.31	0.006631
	MC-1.5L-CJ2-1		1.5	76.13	0.01374
	MC-1.5L-CJ2-2			67.97	0.01143
	MC-1.5L-CJ2-3			72.11	0.01240
H	HC-0L-CJ2-1	53.8	0	53.36	0.002268
	HC-0L-CJ2-2			54.60	0.002006
	HC-0L-CJ2-3			53.42	0.002382
	HC-0.5L-CJ2-1		0.5	61.01	0.002745
	HC-0.5L-CJ2-2			57.32	0.002417
	HC-0.5L-CJ2-3			62.54	0.005164
	HC-1L-CJ2-1		1	63.73	0.006188
	HC-1L-CJ2-2			67.90	0.005293
	HC-1L-CJ2-3			60.25	0.006209
	HC-1.5L-CJ2-1		1.5	78.65	0.007155
	HC-1.5L-CJ2-2			59.25	0.006460
	HC-1.5L-CJ2-3			71.32	0.007603

Note: (i) Example for specimen name designation:
LC-1L-CJ2-1: LC designates Lower strength Concrete; 1L designates 1 Layers; CJ2 designates Carbon fiber Jacket System 2; and the last number represents specimen number in same series.

(ii) f_c': Average plain concrete cylinder strength;

(iii) f_{cc}': Ultimate strength of confined concrete;

(iv) ε_{cu}: Ultimate strain

Table 4.5: Test Results of System Three

Series	Specimen	f_c' (MPa)	Jacket Layers	f_{cc}' (Mpa)	ε_{cu}
L	LC-0L-PGJ-1	31.3	0	29.84	0.001983
	LC-0L-PGJ-2			32.03	0.002011
	LC-0L-PGJ-3			32.03	0.001867
	LC-2L-PGJ-1		2	42.38	0.01931
	LC-2L-PGJ-2			43.89	0.01820
	LC-2L-PGJ-3			45.11	0.01326
	LC-3L-PGJ-1		3	58.92	0.01940
	LC-3L-PGJ-2			55.99	0.01996
	LC-3L-PGJ-3			61.05	0.02370
	LC-4L-PGJ-1		4	71.80	0.02806
	LC-4L-PGJ-2			78.09	0.02800
	LC-4L-PGJ-3			76.54	0.03370
M	MC-0L-PGJ-1	43.9	0	43.87	0.001754
	MC-0L-PGJ-2			44.53	0.001868
	MC-0L-PGJ-3			43.22	0.001935
	MC-2L-PGJ-1		2	55.26	0.007540
	MC-2L-PGJ-2			45.42	0.008781
	MC-2L-PGJ-3			47.86	0.003680
	MC-3L-PGJ-1		3	56.86	0.01400
	MC-3L-PGJ-2			59.76	0.02556
	MC-3L-PGJ-3			51.73	0.01920
	MC-4L-PGJ-1		4	49.90	0.01250
	MC-4L-PGJ-2			59.96	0.02070
	MC-4L-PGJ-3			73.09	0.02134
H	HC-0L-PGJ-1	60.1	0	56.95	0.001677
	HC-0L-PGJ-2			65.46	0.002218
	HC-0L-PGJ-3			57.83	0.001860
	HC-2L-PGJ-1		2	67.01	0.007952
	HC-2L-PGJ-2			65.86	0.005600
	HC-2L-PGJ-3			72.42	0.002550
	HC-3L-PGJ-1		3	70.14	0.00675
	HC-3L-PGJ-2			63.80	0.01330
	HC-3L-PGJ-3			67.52	0.00768
	HC-4L-PGJ-1		4	66.66	0.00239
	HC-4L-PGJ-2			70.98	0.02087
	HC-4L-PGJ-3			78.17	0.01561

Note: (i) Example for specimen name designation:

LC-2L-PGJ-1: LC designates Lower strength Concrete; 2L designates 2 Layers; PGJ designates Prefabricated Glass fiber Jacket System; and the last number represents specimen number in same series.

(ii) f_c': Average plain concrete cylinder strength;

(iii) f_{cc}': Ultimate strength of confined concrete;

(iv) ε_{cu}: Ultimate strain.

Table 4.6: Test Results of System Four

Series	Specimen	f_c' (MPa)	Jacket Layers	f_{cc}' (MPa)	ε_{cu}
L	LC-0L-CJ4-1	33.7	0	33.57	0.002035
	LC-0L-CJ4-2			31.66	0.001802
	LC-0L-CJ4-3			35.92	0.002094
	LC-0.5L-CJ4-1		0.5	39.89	0.009768
	LC-0.5L-CJ4-2			38.67	0.013576
	LC-0.5L-CJ4-3			41.39	0.009940
	LC-1L-CJ4-1		1	53.94	0.01841
	LC-1L-CJ4-2			53.21	0.01556
	LC-1L-CJ4-3			53.48	0.01754
	LC-1.5L-CJ4-1		1.5	59.90	0.01835
	LC-1.5L-CJ4-2			56.91	0.02537
	LC-1.5L-CJ4-3			57.33	0.02315
M	MC-0L-CJ4-1	46.2	0	45.03	0.001963
	MC-0L-CJ4-2			47.56	0.002472
	MC-0L-CJ4-3			46.03	0.001986
	MC-0.5L-CJ4-1		0.5	46.45	0.003850
	MC-0.5L-CJ4-2			50.44	0.010117
	MC-0.5L-CJ4-3			49.27	0.006072
	MC-1L-CJ4-1		1	58.37	0.007644
	MC-1L-CJ4-2			58.31	0.010075
	MC-1L-CJ4-3			55.56	0.008930
	MC-1.5L-CJ4-1		1.5	67.20	0.011047
	MC-1.5L-CJ4-2			61.26	0.006882
	MC-1.5L-CJ4-3			65.74	0.014089
H	HC-0L-CJ4-1	58.4	0	59.49	0.001940
	HC-0L-CJ4-2			58.42	0.002058
	HC-0L-CJ4-3			57.40	0.002035
	HC-0.5L-CJ4-1		0.5	61.50	0.003558
	HC-0.5L-CJ4-2			66.69	0.007595
	HC-0.5L-CJ4-3			64.30	0.008091
	HC-1L-CJ4-1		1	66.09	0.005902
	HC-1L-CJ4-2			71.59	0.008980
	HC-1L-CJ4-3			64.79	0.004165
	HC-1.5L-CJ4-1		1.5	74.74	0.015435
	HC-1.5L-CJ4-2			71.39	0.011705
	HC-1.5L-CJ4-3			70.99	0.009208

Note: (i) Example for specimen name designation:
LC-1L-CJ4-1: LC designates Lower strength Concrete; 1L designates 1 Layers; CJ4 designates Carbon fiber Jacket System 4; and the last number represents specimen number in same series.
(ii) f_c': Average plain concrete cylinder strength;
(iii) f_{cc}': Ultimate strength of confined concrete;
(iv) ε_{cu}: Ultimate strain

Table 4.7 Test Results of System Five

Series	Specimen	f_c' (MPa)	Jacket Layers	f_{cc}' (MPa)	ε_{cu}
L	LC-0L-CJ5-1	32.1	0	30.57	0.001976
	LC-0L-CJ5-2			33.92	0.002039
	LC-0L-CJ5-3			31.84	0.002109
	LC-1L-CJ5-1		1	58.46	0.014378
	LC-1L-CJ5-2			58.53	0.014216
	LC-1L-CJ5-3			64.64	0.020299
	LC-2L-CJ5-1		2	76.91	0.020043
	LC-2L-CJ5-2			77.02	0.016284
	LC-2L-CJ5-3			82.26	0.021005
	LC-3L-CJ5-1		3	94.68	0.026652
	LC-3L-CJ5-2			99.58	0.029076
	LC-3L-CJ5-3			103.48	0.014948
M	MC-0L-CJ5-1	43.0	0	44.11	0.002622
	MC-0L-CJ5-2			41.40	0.002374
	MC-0L-CJ5-3			43.44	0.002440
	MC-1L-CJ5-1		1	75.63	0.020223
	MC-1L-CJ5-2			75.47	0.020542
	MC-1L-CJ5-3			73.52	0.017513
	MC-2L-CJ5-1		2	98.04	0.025506
	MC-2L-CJ5-2			94.81	0.020595
	MC-2L-CJ5-3			96.72	0.021858
	MC-3L-CJ5-1		3	116.62	0.030397
	MC-3L-CJ5-2			108.29	0.025646
	MC-3L-CJ5-3			108.05	0.023363
H	HC-0L-CJ5-1	64.2	0	64.26	0.002483
	HC-0L-CJ5-2			65.58	0.002585
	HC-0L-CJ5-3			62.89	0.003062
	HC-1L-CJ5-1		1	70.91	0.005223
	HC-1L-CJ5-2			80.78	0.007379
	HC-1L-CJ5-3			75.00	0.003827
	HC-2L-CJ5-1		2	94.14	0.007873
	HC-2L-CJ5-2			111.98	0.014643
	HC-2L-CJ5-3			116.71	0.013276
	HC-3L-CJ5-1		3	105.36	0.007659
	HC-3L-CJ5-2			142.85	0.016566
	HC-3L-CJ5-3			111.94	0.010766

Note: (i) Example for specimen name designation:
LC-2L-CJ5-1: LC designates Lower strength Concrete; 2L designates 2 Layers; CJ5 designates Carbon fiber Jacket System 1; and the last number represents specimen number in same series.
(ii) f_c': Average plain concrete cylinder strength;
(iii) f_{cc}': Ultimate strength of confined concrete;
(iv) ε_{cu}: Ultimate strain

Table 4.8: Test Results of System Six

Series	Specimen	f_c' (MPa)	Jacket Layers	f_{cc}' (MPa)	ε_{cu}
L	LC-0L-GJ6-1	37.1	0	38.22	0.002609
	LC-0L-GJ6-2			34.87	0.002367
	LC-0L-GJ6-3			38.16	0.002228
	LC-1L-GJ6-1		1	48.81	0.012715
	LC-1L-GJ6-2			48.97	0.017447
	LC-1L-GJ6-3			48.40	0.017224
	LC-1L-GJ6-4			48.10	0.019018
	LC-1L-GJ6-5			47.42	0.015266
	LC-2L-GJ6-1		2	63.72	0.021822
	LC-2L-GJ6-2			63.56	0.021680
	LC-2L-GJ6-3			63.92	0.024826
	LC-2L-GJ6-4			63.73	0.026472
M	MC-0L-GJ6-1	56.9	0	60.07	0.002605
	MC-0L-GJ6-2			55.12	0.002072
	MC-0L-GJ6-3			55.62	0.002463
	MC-1L-GJ6-1		1	60.52	0.003005
	MC-1L-GJ6-2			60.18	0.003146
	MC-1L-GJ6-3			60.74	0.003496
	MC-1L-GJ6-4			59.33	0.002973
	MC-1L-GJ6-5			61.68	0.002980
	MC-2L-GJ6-1		2	79.59	0.013982
	MC-2L-GJ6-2			71.20	0.008680
	MC-2L-GJ6-3			78.52	0.013995
	MC-2L-GJ6-4			73.46	0.012079
H	HC-0L-GJ6-1	63.5	0	6515	0.002469
	HC-0L-GJ6-2			58.26	0.002105
	HC-0L-GJ6-3			67.19	0.002268
	HC-1L-GJ6-1		1	73.59	0.002907
	HC-1L-GJ6-2			77.22	0.003435
	HC-1L-GJ6-3			72.61	0.003064
	HC-1L-GJ6-4			67.24	0.002744
	HC-1L-GJ6-5			74.33	0.003088
	HC-2L-GJ6-1		2	77.40	0.003620
	HC-2L-GJ6-2			79.91	0.004984
	HC-2L-GJ6-3			81.47	0.008276
	HC-2L-GJ6-4			78.61	0.006011

Note: (i) Example for specimen name designation:
LC-2L-GJ6-1: LC designates Lower strength Concrete; 2L designates 2 Layers; GJ6 designates Glass fiber Jacket System 6; and the last number represents specimen number in same series.
(ii) f_c': Average plain concrete cylinder strength;
(iii) f_{cc}': Ultimate strength of confined concrete;
(iv) ε_{cu}: Ultimate strain

Table 4.9: Test Results of System Seven

Series	Specimen	f_c' (MPa)	Jacket Equivalent Thickness (mm)	f_{cc}' (MPa)	ε_{cu}
L	LC-0L-CJ7-1	35.0	0	35.81	0.002062
	LC-0L-CJ7-2			37.15	0.002089
	LC-0L-CJ7-3			31.91	0.001649
	LC-0.0125-CJ7-1		0.318	51.23	0.011886
	LC-0.0125-CJ7-2			51.52	0.012269
	LC-0.0125-CJ7-3			46.71	0.011299
	LC-0.0250-CJ7-1		0.635	68.94	0.016742
	LC-0.0250-CJ7-2			68.44	0.016611
	LC-0.0250-CJ7-3			68.80	0.017898
	LC-0.0500-CJ7-1		1.270	94.75	0.028350
	LC-0.0500-CJ7-2			81.38	0.023747
	LC-0.0500-CJ7-3			93.92	0.025394
M	MC-0L-CJ7-1	50.0	0	47.65	0.002427
	MC-0L-CJ7-2			51.48	0.002572
	MC-0L-CJ7-3			50.74	0.002609
	MC-0.0125-CJ7-1		0.318	59.87	0.006471
	MC-0.0125-CJ7-2			61.40	0.007581
	MC-0.0125-CJ7-3			62.94	0.008547
	MC-0.0250-CJ7-1		0.635	78.67	0.013224
	MC-0.0250-CJ7-2			82.99	0.012878
	MC-0.0250-CJ7-3			81.70	0.014147
	MC-0.0500-CJ7-1		1.270	114.29	0.022076
	MC-0.0500-CJ7-2			105.85	0.017131
	MC-0.0500-CJ7-3			110.06	0.019049
H	HC-0L-CJ7-1	63.2	0	63.88	0.002344
	HC-0L-CJ7-2			60.00	0.002440
	HC-0L-CJ7-3			65.69	0.002615
	HC-0.0125-CJ7-1		0.318	65.87	0.003242
	HC-0.0125-CJ7-2			64.44	0.003023
	HC-0.0125-CJ7-3			69.85	0.003210
	HC-0.0250-CJ7-1		0.635	90.29	0.008567
	HC-0.0250-CJ7-2			81.70	0.005932
	HC-0.0250-CJ7-3			80.15	0.004764
	HC-0.0500-CJ7-1		1.270	114.65	0.013034
	HC-0.0500-CJ7-2			118.48	0.013383
	HC-0.0500-CJ7-3			130.14	0.016651

Note: (i) Example for specimen name designation:
LC-0.0250-CJ7-1: LC designates Lower strength Concrete; 0.0250 designates jacket equivalent thickness in inches; CJ7 designates Carbon fiber Jacket System 7; and the last number represents specimen number in same series.
(ii) f_c': Average plain concrete cylinder strength;
(iii) f_{cc}': Ultimate strength of confined concrete;
(iv) ε_{cu}: Ultimate strain

Table 4.10: Test Results of System Eight

Series	Specimen	f_c' (MPa)	Jacket Equivalent Thickness (mm)	f_{cc}' (MPa)	ε_{cu}
L	LC-0L-CJ8-1	34.5	0	34.68	0.001569
	LC-0L-CJ8-2			36.03	0.001877
	LC-0L-CJ8-3			32.74	0.001513
	LC-0.0125-CJ8-1		0.318	49.93	0.009149
	LC-0.0125-CJ8-2			41.36	0.005343
	LC-0.0125-CJ8-3			49.33	0.009913
	LC-0.0250-CJ8-1		0.635	63.77	0.014026
	LC-0.0250-CJ8-2			59.85	0.013206
	LC-0.0250-CJ8-3			62.84	0.014535
	LC-0.0500-CJ8-1		1.270	96.05	0.031151
	LC-0.0500-CJ8-2			91.59	0.023993
	LC-0.0500-CJ8-3			76.12	0.022242
M	MC-0L-CJ8-1	48.8	0	46.35	0.002026
	MC-0L-CJ8-2			48.70	0.002102
	MC-0L-CJ8-3			51.32	0.002278
	MC-0.0125-CJ8-1		0.318	46.77	0.002381
	MC-0.0125-CJ8-2			53.58	0.003963
	MC-0.0125-CJ8-3			58.12	0.006554
	MC-0.0250-CJ8-1		0.635	56.51	0.003294
	MC-0.0250-CJ8-2			60.43	0.004222
	MC-0.0250-CJ8-3			75.14	0.009706
	MC-0.0500-CJ8-1		1.270	108.18	0.018290
	MC-0.0500-CJ8-2			105.36	0.020808
	MC-0.0500-CJ8-3			114.63	0.023628
H	HC-0L-CJ8-1	60.2	0	65.13	0.002887
	HC-0L-CJ8-2			53.56	0.001831
	HC-0L-CJ8-3			62.02	0.002569
	HC-0.0125-CJ8-1		0.318	57.45	0.002358
	HC-0.0125-CJ8-2			58.57	0.002767
	HC-0.0125-CJ8-3			57.50	0.002255
	HC-0.0250-CJ8-1		0.635	84.29	0.009113
	HC-0.0250-CJ8-2			67.70	0.004402
	HC-0.0250-CJ8-3			73.32	0.005954
	HC-0.0500-CJ8-1		1.270	124.05	0.013835
	HC-0.0500-CJ8-2			128.62	0.015697
	HC-0.0500-CJ8-3			103.12	0.006560

Note: (i) Example for specimen name designation:
LC-0.0250-CJ8-1: LC designates Lower strength Concrete; 0.0250 designates jacket equivalent thickness in inches; CJ8 designates Carbon fiber Jacket System 8; and the last number represents specimen number in same series.
(ii) f_c': Average plain concrete cylinder strength;
(iii) f_{cc}': Ultimate strength of confined concrete;
(iv) ε_{cu}: Ultimate strain.

Table 4.11: Test Results of System Nine

Series	Specimen	f_c' (MPa)	Jacket Equivalent Thickness (mm)	f_{cc}' (MPa)	ε_{cu}
L	LC-0L-CJ9-1	34.7	0	33.19	0.002140
	LC-0L-CJ9-2			35.85	0.002440
	LC-0L-CJ9-3			34.91	0.001841
	LC-0.0125-CJ9-1		0.318	37.06	0.007121
	LC-0.0125-CJ9-2			35.09	0.002770
	LC-0.0125-CJ9-3			43.01	0.004712
	LC-0.0250-CJ9-1		0.635	60.01	0.016185
	LC-0.0250-CJ9-2			58.28	0.009641
	LC-0.0250-CJ9-3			54.40	0.012779
	LC-0.0500-CJ9-1		1.270	81.79	0.030770
	LC-0.0500-CJ9-2			61.95	0.013448
	LC-0.0500-CJ9-3			75.76	0.021571
M	MC-0L-CJ9-1	54.3	0	53.24	0.002585
	MC-0L-CJ9-2			56.29	0.002761
	MC-0L-CJ9-3			53.27	0.002830
	MC-0.0125-CJ9-1		0.318	53.51	0.002840
	MC-0.0125-CJ9-2			49.91	0.002206
	MC-0.0125-CJ9-3			50.85	0.002789
	MC-0.0250-CJ9-1		0.635	84.67	0.013935
	MC-0.0250-CJ9-2			67.95	0.007421
	MC-0.0250-CJ9-3			54.90	0.003690
	MC-0.0500-CJ9-1		1.270	96.14	0.014837
	MC-0.0500-CJ9-2			95.78	0.016359
	MC-0.0500-CJ9-3			109.46	0.020639
H	HC-0L-CJ9-1	61.9	0	64.55	0.002714
	HC-0L-CJ9-2			63.16	0.002685
	HC-0L-CJ9-3			57.97	0.002344
	HC-0.0125-CJ9-1		0.318	61.95	0.002467
	HC-0.0125-CJ9-2			59.69	0.002353
	HC-0.0125-CJ9-3			65.47	0.002829
	HC-0.0250-CJ9-1		0.635	68.67	0.003585
	HC-0.0250-CJ9-2			69.21	0.003119
	HC-0.0250-CJ9-3			69.14	0.003433
	HC-0.0500-CJ9-1		1.270	84.79	0.005570
	HC-0.0500-CJ9-2			98.93	0.007854
	HC-0.0500-CJ9-3			92.55	0.008013

Note: (i) Example for specimen name designation:
LC-0.0250-CJ9-1: LC designates Lower strength Concrete; 0.0250 designates jacket equivalent thickness in inches; CJ9 designates Carbon fiber Jacket System 9; and the last number represents specimen number in same series.
(ii) f_c': Average plain concrete cylinder strength;
(iii) f_{cc}': Ultimate strength of confined concrete;
(iv) ε_{cu}: Ultimate strain.

CHAPTER 5: NONLINEAR ELASTIC MODELING OF CONFINED CONCRETE

In Chapter 2, the literature of confined concrete modeling has been reviewed. All classifications of theoretical models have been applied in confined concrete. Based on the nonlinear elastic theory and previous chapter's research results, a constitutive relationship of FRP confined concrete will be proposed in this Chapter. To achieve bilinear stress-strain behavior of FRP confined concrete, Richard bilinear Equation (1975) has been used in this model.

5.1 Nonlinear Elasticity, Hyperelastic and Hypoelastic Model for concrete

Three different types of elastic constitutive approaches are used in the model of concrete material behavior. Most popular approach is Cauchy elastic material. The current state of stress depends only on the state of deformation:

$$\sigma_{ij} = F_{ij}\left(\varepsilon_{kl}\right) \tag{5-1}$$

There is no dependency of the behavior on the stress and strain histories followed to reach the current state of the stress or strain. It may generate energy under certain loading-unloading cycles. It violates the laws of thermodynamics.

A second type of approach is Hyperelastic (Green Material). This method is based on the assumption that the existence of a strain energy-density function W (or a complementary energy-density function Ω) such that

$$\sigma_{ij} = \frac{\partial W}{\partial \varepsilon_{ij}} \tag{5-2}$$

$$\varepsilon_{ij} = \frac{\partial \Omega}{\partial \sigma_{ij}} \tag{5-3}$$

This ensures that no energy can be generated through load cycles, and the laws of thermodynamics are always satisfied.

The last approach is incremental (hypoelastic) type. This type of formulation is often used to describe the mechanical behavior of a class of materials in which the state of stress depends on the current state of strain as well as the stress path that follows to reach that state. It can be written as

$$\dot{\sigma}_{ij} = F_{ij}(\dot{\varepsilon}_{kl}, \sigma_{mn}) \tag{5-4}$$

5.2 Bilinear Response Model

A bilinear stress-strain formula was represented by Richard et al. (1975):

$$\sigma = \frac{(E_1 - E_2)\varepsilon}{\left(1 + \left|\frac{(E_1 - E_2)\varepsilon}{\sigma_0}\right|^n\right)^{1/n}} + E_2\varepsilon \tag{5-5}$$

where E_1, E_2, and σ_0 are three independent parameters. n is a shape parameter of the stress-strain curve. Fig.5.1 is a nondimensional plot of Eq.(5-5) showing how the value of n affects the shape of the curve.

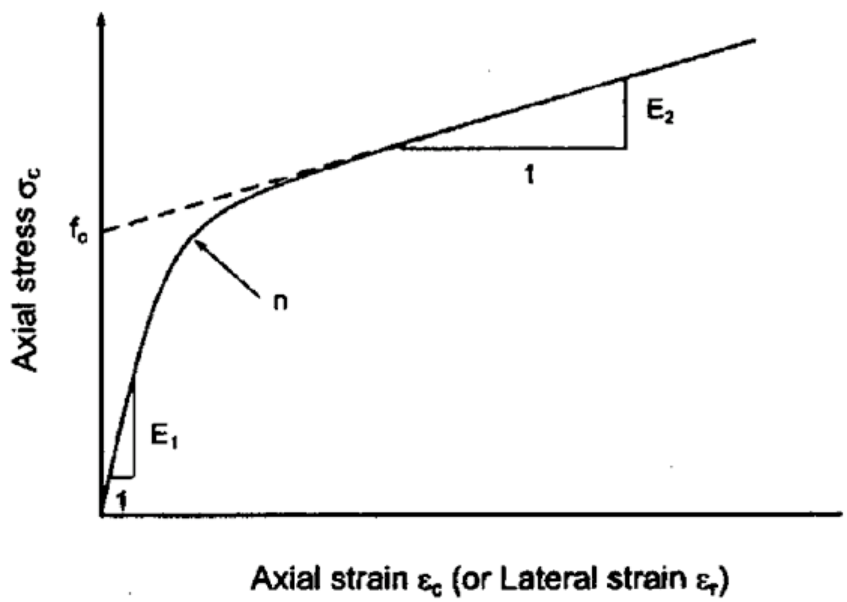

Figure 5.1: Richard's Stress-Strain Equation and Parameters

This formula was used in many referenced literatures. It is very convenient to express bilinear curve.

The Richard formula was applied in Mirmiran's model initially. However, in Mirmiran's model, E_1, E_2 and σ_0 were derived by empirical regression directly. Previous research in confined concrete does not have sufficient results to substantiate whether E_2 holds any physical meaning. In this Chapter, a new constitutive confined concrete model with clear physical meaning is presented. This model defines the stress-strain model for concrete confined by FRP based on Richard et al.'s equation and parameter with clear physical meaning. The behavior of FRP confined concrete predicted by this model is consistent with previous research in confined concrete. Proposed Model of Confined Concrete with Advanced Composite Materials.

Richard' bilinear curve equation was used in the proposed model with n equals 2.

$$f_{cz} = \frac{(E_1 - E_2)\varepsilon}{\left(1 + \left(\frac{(E_1 - E_2)\varepsilon}{f_0}\right)^2\right)^{1/2}} + E_2\varepsilon \tag{5-6}$$

where

$$E_1 = E_c\left(1 + 2\nu_c\nu_0\frac{C_j}{E_c}\right) \approx E_c = 4{,}733\sqrt{f_{co}^{'}} \tag{5-7}$$

ε is strain in loading direction.

From Eq.(4-9b) and Eq.(4-9a), we can derive E_2 easily. After concrete stress reached plastic yield surface, the concrete final behavior can be expressed as

$$f_{cc}^{'} = f_{co}^{'} + k_1 f_r = f_{co}^{'} + k_1 C_j \left(\nu^{'} \varepsilon_{cz} - \varepsilon_{r0} \right) \tag{5-8}$$

then, we have

$$E_2 = kC_j \nu' \tag{5-9}$$

from test results, we have

$$f_0 = \beta f_c^{'} \tag{5-10}$$

where β is the reference plastic strength increase coefficient. The values of the coefficient β were plotted as a function of the C_j, as seen in Fig.4.7. The effect of concrete strength can be ignored. Using a regression analysis, an equation for β is obtained with a correlation factor of 81 percent

$$\beta = 1 + 4.8 \times 10^{-4} C_j^{0.85} \tag{5-11}$$

In transverse direction, we have

$$f_{cz} = \frac{(E_{t1} - E_{t2})\varepsilon_t}{\left(1 + \left(\frac{(E_{t1} - E_{t2})\varepsilon_t}{f_0}\right)^2\right)^{1/2}} + E_{t2}\varepsilon_t \tag{5-6'}$$

where

$E_{t1} = E_1/\nu_0 \approx 4{,}733\sqrt{f'_{co}}\,/\nu'$; (5-7')

ε_t is strain in transverse (circumferential) direction.

From Eq.(4-9b) and Eq.(4-9a), we have

$E_{t2} = E_2/\nu' = kC_j$ (5-5')

From Eq. (5-5) and Eq. (5-5'), the E_2 and E_{2t} *'s* physical meaning become very clear. In order to fully understand the confined concrete behavior, more discussion on the principal stress coordinate and octahedral stress-strain coordinate will be presented in Chapter 6.

5.4 Comparison between analytical and experimental results

Fig 5.2 shows consistency between the test results and the proposed model. The solid lines indicate the stress-strain curve of the test results, where as the dash lines indicate theoretical prediction of the proposed model. The proposed model also predicts the results from other studies.

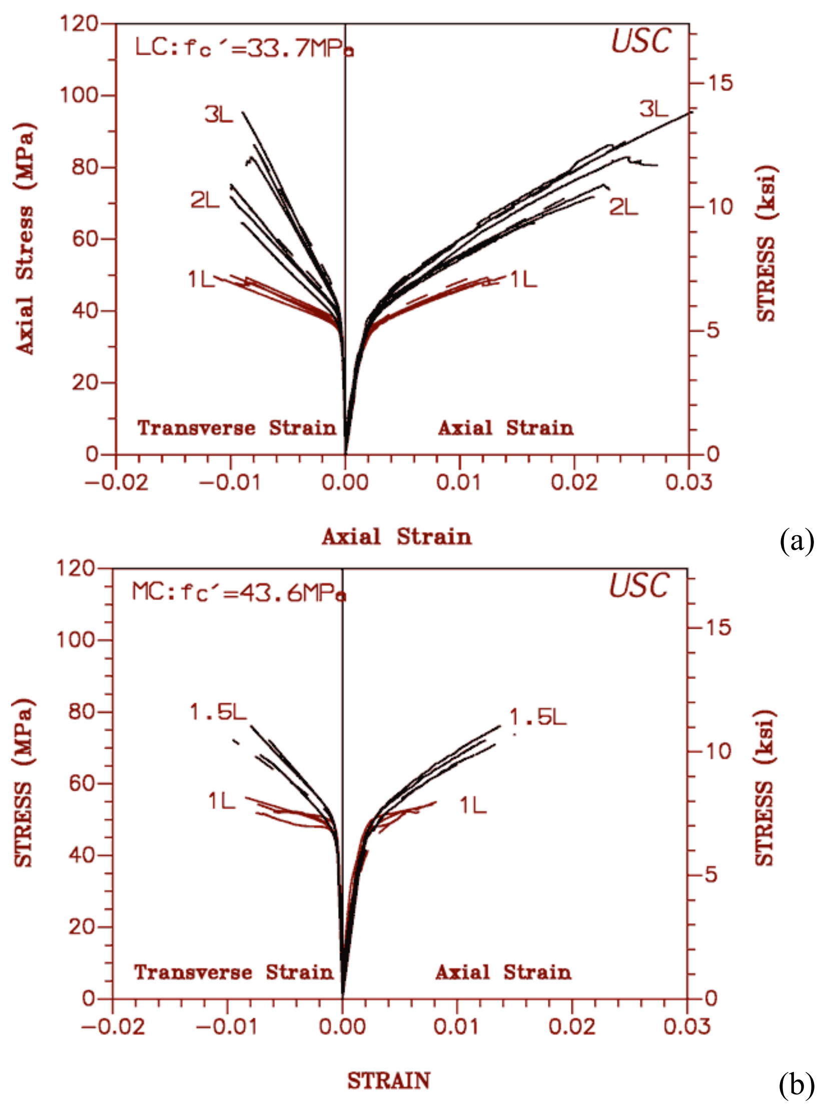

Figure 5.2: Comparison between proposed model to test results, dash line is theoretical predict. (a) Lower strength concrete; (b) Medium strength concrete.

Since the proposed model was published in 1997, and revised in 2000 and 2003, many researchers have proposed additional models. Many researchers have performed many experiments to compare the different models with their test results. Fig 5.3 and Fig 5.4 show the comparison by Teng and Lam (2003). As shown on the comparison graph, our theoretical model is among one of the best to correspond with the test results. Fig 5.3 also indicates that the ultimate rupture strain of FRP wrapped on cylinder should be smaller than the coupon test results because the FRP stress distribution may be uneven.

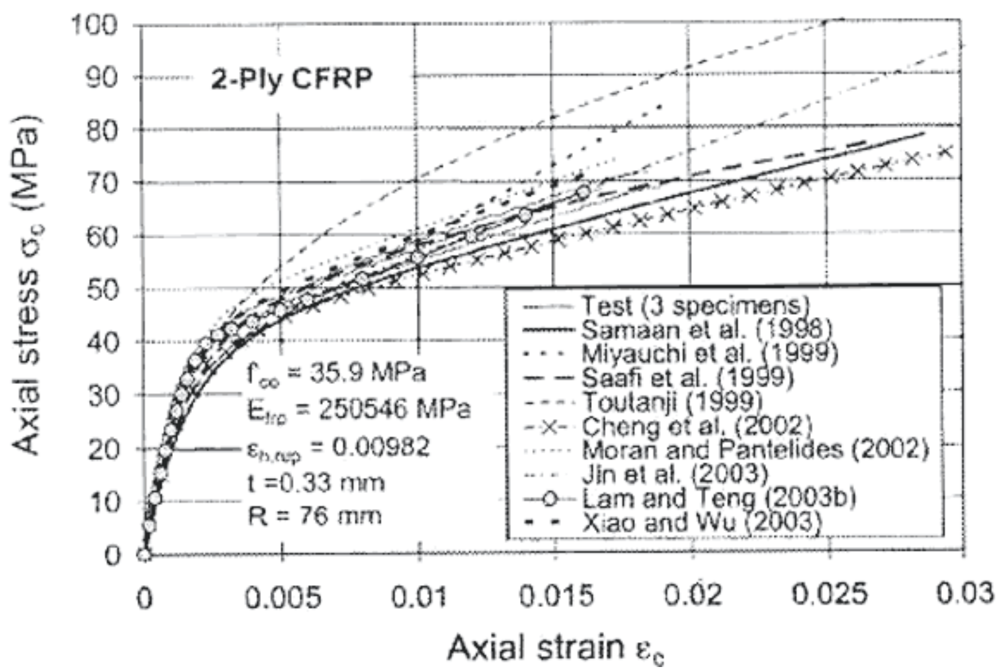

Figure 5.3: Performance of model using test original deflections of fiber reinforced polymer hoop rupture strain (Teng et al , 2004)

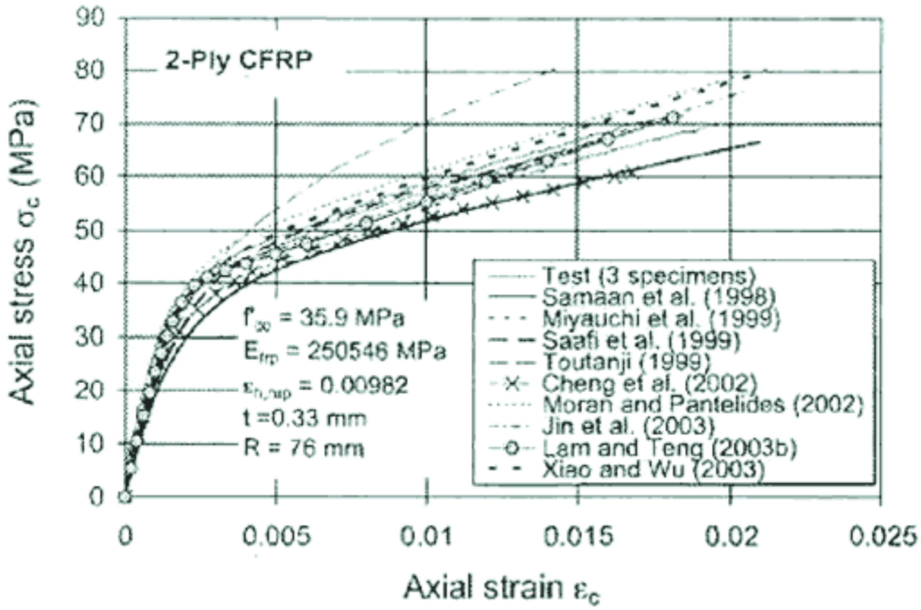

(a) Specimens confined by 2 plies of CFRP

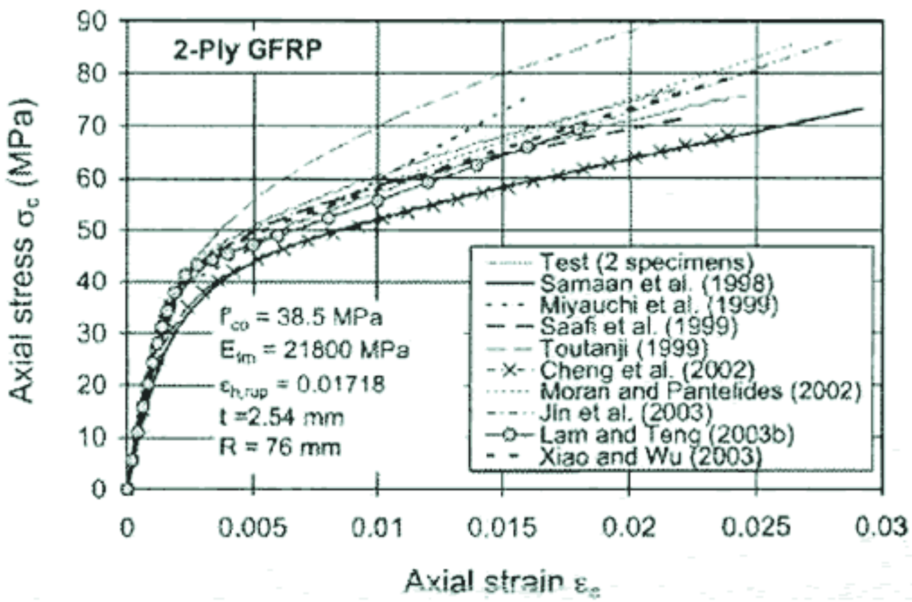

(b) Specimens confined by 2 plies of GFRP

Figure 5.4: Performance of models using test fiber reinforce polymer hoop rupture strain (Teng et al, 2004)

CHAPTER 6: ELASTIO-PLASTIC ANALYSIS OF CONFINED CONCRETE

A nonlinear elastic confined concrete material model was proposed in Chapter 5. However, this model is limited to the application of FRP confined concrete test results. Further research is needed to calibrate the model to be appropriate for other composite materials in confined concrete and to obtain a deeper understanding on the behavior of confined concrete after yielding.

Based on the elastic-plasticity theory, this chapter shows the mechanical behavior of confined concrete with FRP or steel. A universal confined concrete material analysis approach will be proposed based on the previous model. The analysis of concrete filled steel tube has been completed by the proposed approach.

6.1 Basic Concept of Concrete Plasticity

In chapter 2, the plastic model of concrete has been introduced briefly. In the following section, based on elastic-plastic theory, further analysis for confined concrete will be presented.

The defining characteristic of material plasticity is the accumulation of irreversible deformation upon loading beyond the yield limit. The test results show that concrete exhibits this characteristic when loaded in compression. Thus, it is appropriate that a constitutive model for confined concrete incorporates the plasticity theory.

Plasticity model of concrete is based on three basic assumptions:

There is an initial yield surface and a failure surface in stress space.

A hardening rule, which defines the change of the loading surface and the change of the hardening properties of the material during the course of plastic flow.

A flow rule, which is related to a plastic potential function, leads to an incremental plastic stress-strain relation.

The development of a plasticity-based constitutive model requires defining a rule for decomposition of the total strain. It is assumed to be the sum of the elastic strain and the accumulated plastic strain:

$$\varepsilon = \varepsilon^{e} + \varepsilon^{p} \tag{6.1.1}$$

It is reasonable to assume that concrete is a homogenous material; thus, the elastic material properties are readily defined on the basis of data collected from standard material tests and the elastic constitutive relationship follows Hooke's Law:

$$\sigma_{ij} = C_{ijkl}\varepsilon_{kl}^{e} \tag{6.1.2}$$

where C_{ijkl} is the rank four material stiffness tensor. The yield surface or surfaced bound the elastic domain. Following classical plasticity theory, the elastic domain is defined in terms of stress space. For concrete, the available material data facilitated the definition of the yield surface in stress space and it is most appropriate to consider a yield surface that evolves as a function of the loading history. A hardening rule defines the evolution of a set of internal variables that uniquely define the material state.

However, for the plasticity approach model, the numerical integration makes it more complicated and the plasticity cannot predict the volume change very well after the onset of micro cracking.

Let's take a look at the test results under plasticity view first.

6.2 Yield Surface and Failure Criteria

To fully understand the behavior of confined concrete, further research is necessary. Fig 6.1, Fig 6.2 and Fig 6.3 shows axial stress versus transverse confined stresses of lower strength, medium strength and higher strength concrete cylinders confined by FRP respectively. Noticeably, from the graphs with higher FRP confinement cylinder exhibits a higher slope after concrete yielding. In fact, the graphs show the loading path of cylinders in axial stress versus transverse confinement stress coordinate. The different slopes after concrete yielding represent different confinement stress loading paths and stress states. When FRP confinement stiffness increases, the slope approaches the maximum slope, which was proposed by Richart in (1928). The slope is 4.1:1. All of the above phenomenon can be explained very well by the Mohr-Coulomb theory. Although the Mohr-Coulomb theory is conceived more than one hundred years ago, it is still a powerful conceptual tool to understand the properties of engineering material.

The Mohr-Coulomb failure envelope is shown in Fig 6.4. According to Mohr's criterion, failure of material will occur for all states of stress for which the largest of Mohr's circles is just tangent to the envelope. However, in FRP-confined cylinders, the slip may lead to an increase in radial strain and therefore an increase in confining stress. In fact, failure of FRP-confined concrete generally occurs when the hoop rupture ultimate strain of the FRP jacket is reached.

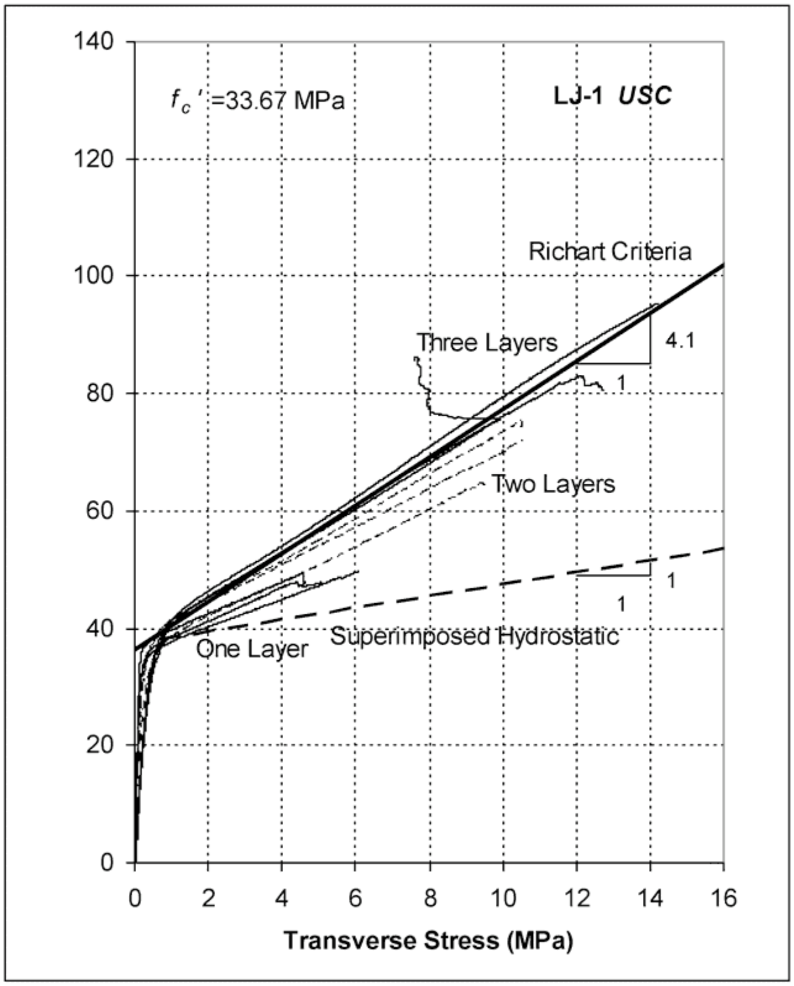

Figure 6.1: Axial Stress versus Confinement Stress for Lower Strength Concrete Confined by CFRP

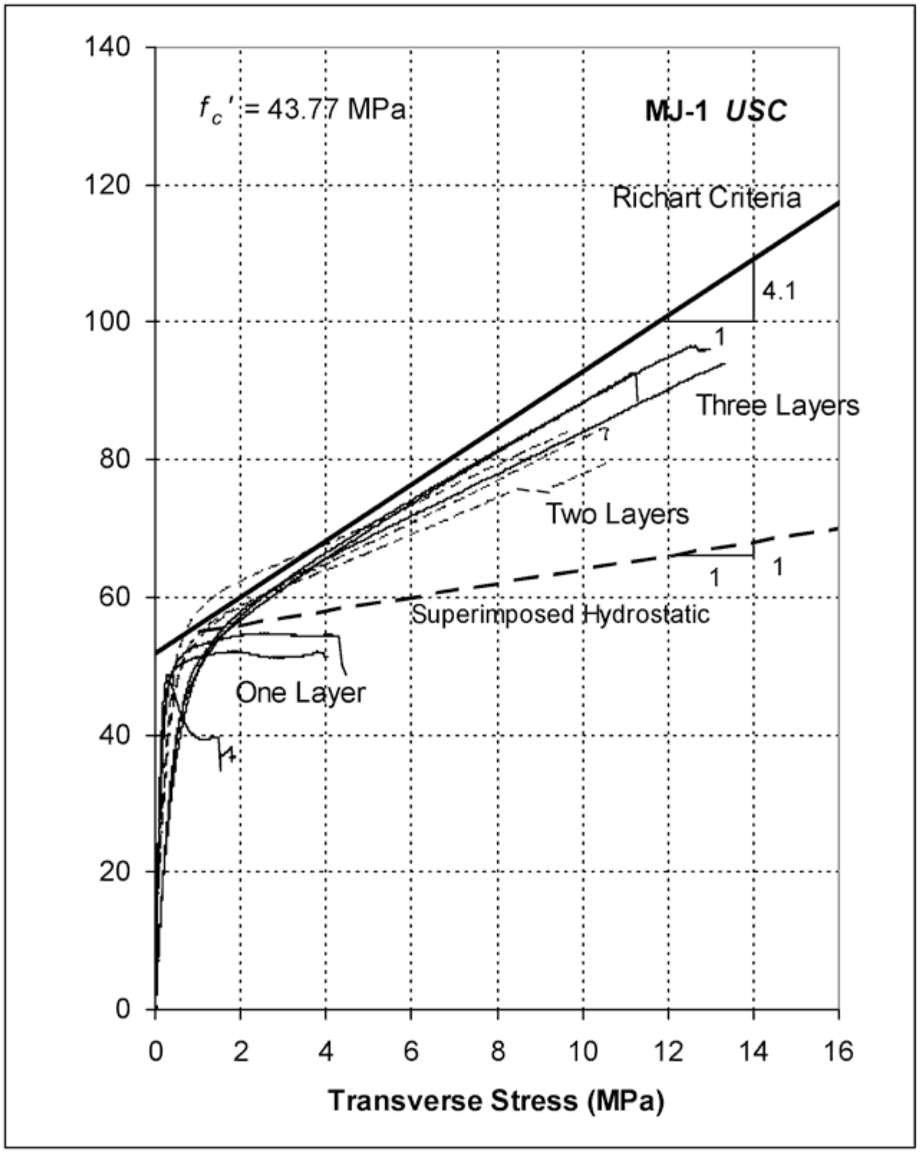

Figure 6.2: Axial Stress versus Confinement Stress for Medium Strength Concrete Confined by CFRP

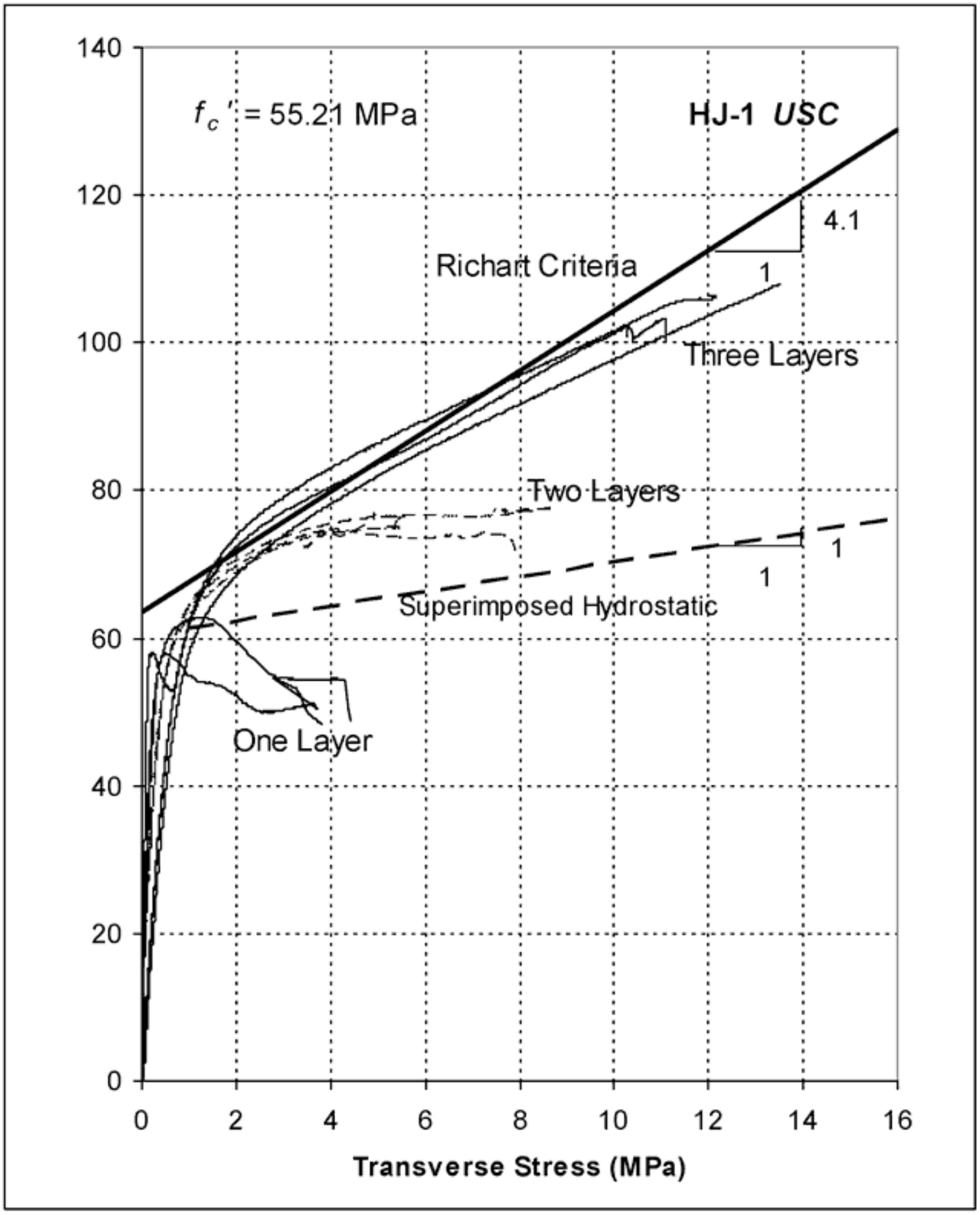

Figure 6.3: Axial Stress versus Confinement Stress for Higher Strength Concrete Confined by CFRP

When the concrete sustains internal shear slip, the axial stress, σ_z and the transverse confining stress, σ_r can be expressed as

$$\sigma_r = \sigma_z\left(\frac{1-\sin\phi}{1+\sin\phi}\right) + 2C\left(\frac{\cos\phi}{1+\sin\phi}\right) \tag{6-5}$$

where C = the cohesive strength of the concrete, given by the intercept on the vertical (shear stress) axis, and ϕ = angle of internal friction.

In reality, the different slopes after concrete yielding represent different concrete angles of internal friction under different confinement pressures.

Assuming that the concrete completely loses stiffness after yielding, the loading path should be along with what is called superimposed hydrostatic. In this case, concrete behaves like water in the FRP tube. When axial loading equals $d\sigma_z$, FRP tube will provide equivalent hydrostatic pressure. Thus, the slope should be 1:1.

When the confinement ratio reduces, the concrete may enter into softening mode because of the lack of lateral confinement pressure. From Fig. 6.2, the stress draped rapidly after it has reached the strength of the unconfined concrete for one layer FRP confined cylinder.

The author suggests that the superimposed hydrostatic line can be defined as the minimum confinement ratio for practical design. When the confinement ratio is less than the value, the concrete will become unstable after the stress reaches the peak point of unconfined concrete. The test results exhibit randomness, for which the reliability can not meet the code requirement.

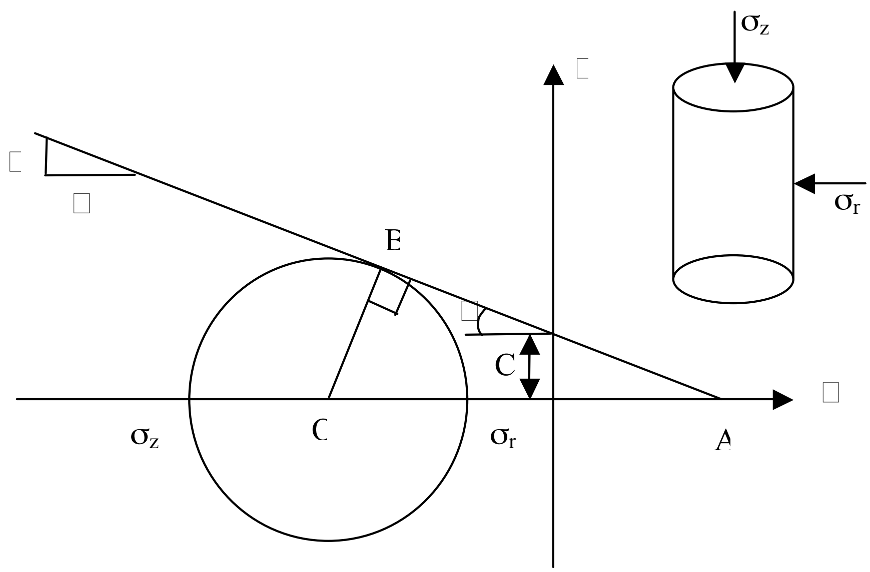

Figure 6.4: Mohr-Coulomb Failure Envelop

6.3 Flow Rules

Definition of a plasticity-based connotative model requires establishing flow rules that necessarily connect between the loading function *f* and the stress-strain relations. The flow rule of plasticity theory is expressed mathematically as,

$$d\varepsilon_{ij}^{p} = \lambda \frac{\partial f}{\partial \sigma_{ij}} \qquad (6\text{-}6)$$

where $\lambda > 0$ is a scalar proportionality factor and $f(\sigma_{ij})$ the yield surface function. The plastic flow develops along the normal to the loading surface. This normality condition assumes a unique solution for a given boundary-value problem using any stress-strain relations developed on the basis of Eq. (6-6). Relation (6-6) is called *the associated flow rule* because it is associated with the loading surface. Experimental data indicate that the associated flow may not be the most appropriate assumption for the modeling of the behavior of the concrete. Researchers have discovered that concrete displays shear dilatancy characterized by volume change associated with shear distortion of the material. This characteristic is contrary to the assumption of associated flow. Fig. 4.3 shows that concrete subjected to compressive loading exhibits nonlinear volume change, displaying contraction at low load levels and dilation at higher load levels. For higher confined concrete the dilation of concrete does not occur until failure. These characteristics of concrete may be difficult to represent by the assumption of associated flow. The experimental evidence also shows that both the associated flow rule and the normality requirement do not apply strictly for concrete. Thus, non-associated flow rules are gaining popularity.

Fig 6.5 shows the typical test results in Haigh – Westergard coordinate. Although the test results of different layered cylinders show different slope in Fig 6.1 and Fig. 6.2. In fact the concrete has yielded. Clearly it is flowing on the yielding surface. The yielding surface is very close Richart Criteria.

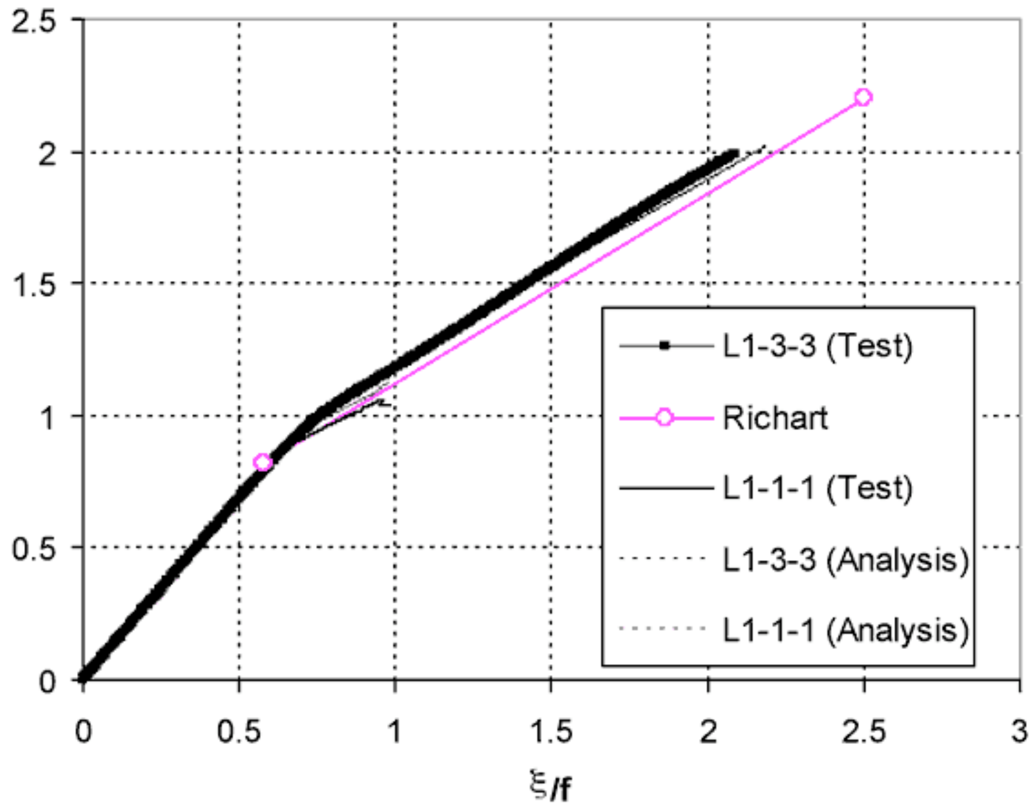

Figure 6.5: The Compression Test Results of Typical FRP Confined Concrete Cylinders in Haigh – Westergard Coordinate. (The name L1-3-3 means system one, three layer, third specimen.)

6.4 Proposed Analysis Approach for Universal Confined Concrete

Gerstle (1973) and Cedolin (1977), proposed a concrete stress-strain model in octahedral coordinate. However, their model can only predict concrete behavior until 80% of its peak strength. Beyond that stage, the dilatancy occurs, for which their model cannot predict the outcome. Xiao (1989) discovered that Cedolin's model is not consistent with the test results of the concrete filled steel tubes and hence proposed a confined concrete model with non-associate flow rule. However, this model does not correspond with the current test results of concrete confined by FRP.

Based on the previous confined concrete model, an analytical approach is proposed here.

For given ε_{zi} , f_{zi} can be calculated by Eq. (5-6); $\longrightarrow$ ε_{ti} can be calculated by a small solver from Eq. (5-6').

After all variables have been solved, octahedral stress and octahedral strain can be calculated easily. A short numerical program has been engineered to solve ε_{ti} from Eq. (5-6') for given f_{zi}. From Eq. (5-6'), we have following numerical equation by Newton-Raphson method.

$$\varepsilon_{\theta,n+1} = \varepsilon_{\theta,n} - \frac{f(\varepsilon_{\theta,n})}{f'(\varepsilon_{\theta,n})} \qquad (6\text{-}7)$$

Fig 6.6 shows the comparison of typical analysis results with test data in octahedral stress-strain coordinate. The analytical results can predict the volume compression and dilatancy behavior very well.

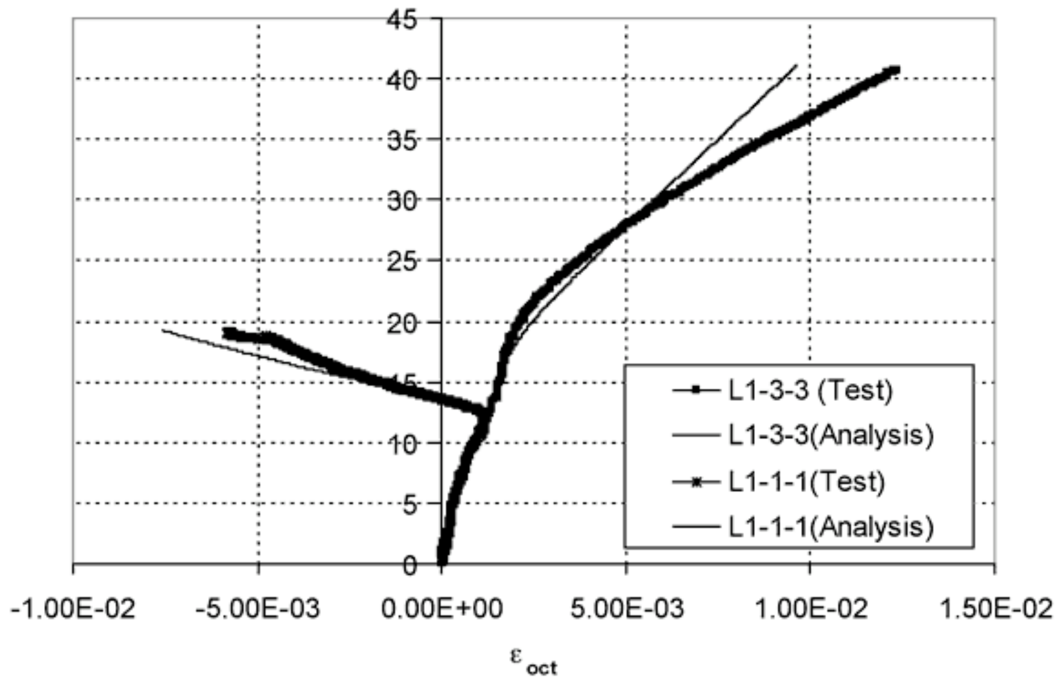

Figure 6.6: Comparison of Analytical with Experimental Results in Octahedral Normal Stress And Strain

Fig. 6.7 shows 3-layer and 1-layer CFRP confined concrete cylinders octahedral shear stress and shear strain relationship. Good agreements are generally observed.

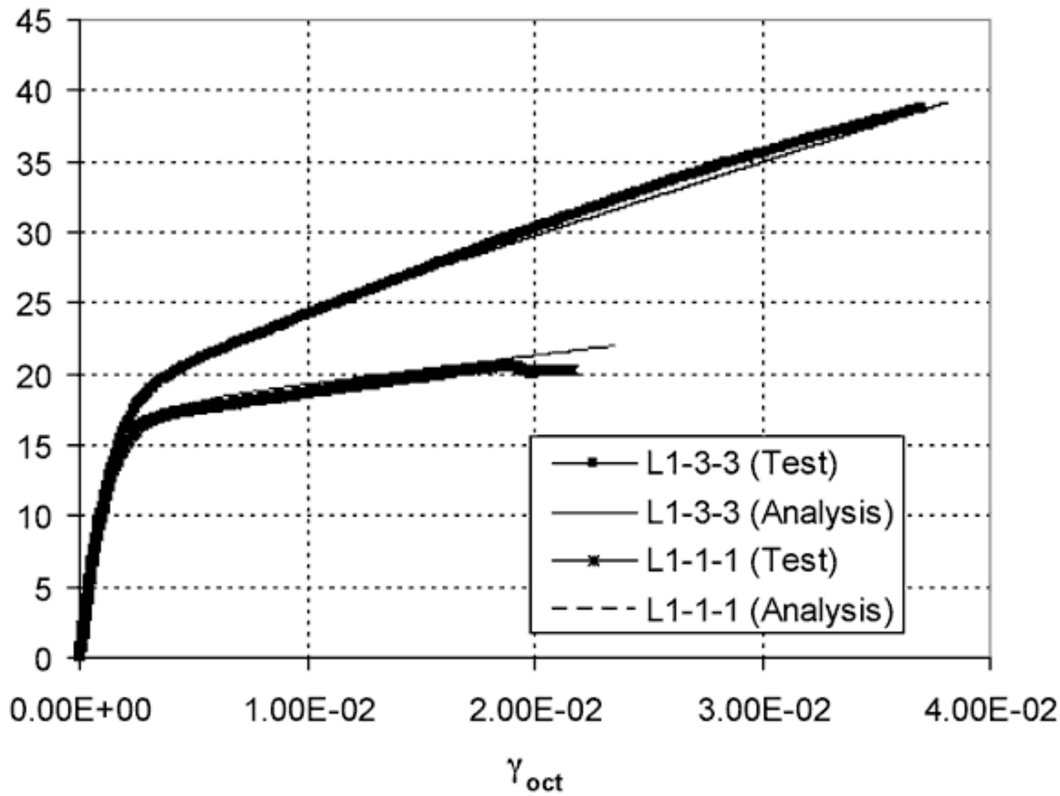

Figure 6.7: Comparison of Analytical with Experimental Results in Octahedral Shear Stress and Shear Strain

Figure 6.8 shows 3-layer and 1-layer CFRP confined concrete cylinders octahedral normal strain and shear strain relationship. It correlates with the test results very closely.

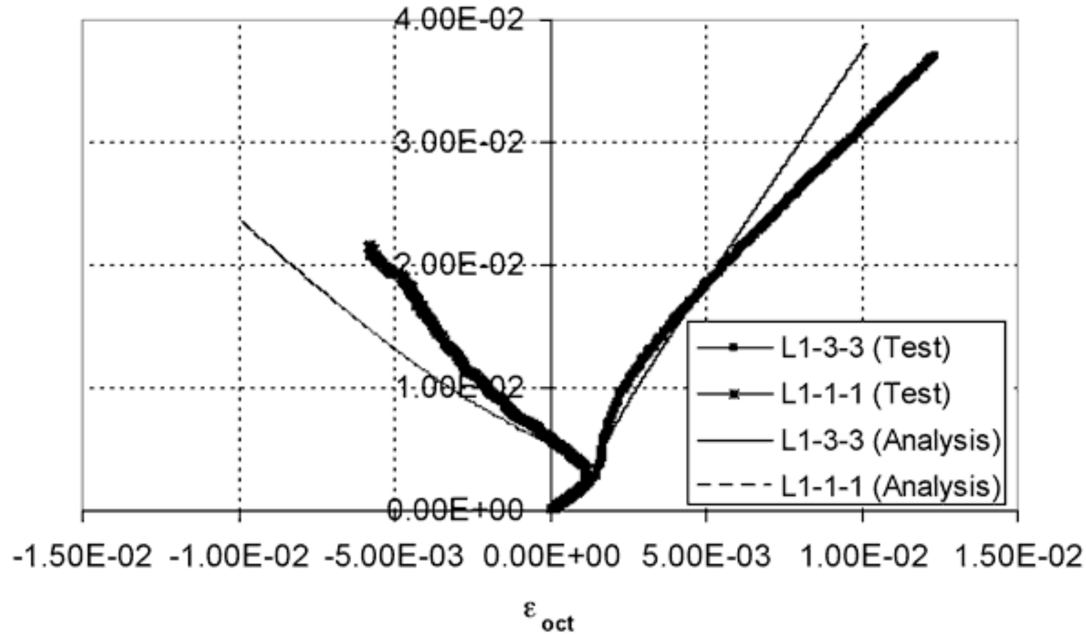

Figure 6.8: Comparison of Analytical with Experimental Results in Octahedral Normal Strain and Shear Strain

However, for higher strength concrete with lower FRP confinement, test results shows very random behavior after concrete reached peak point. Proposed model can not predict this behavior very well. Fig. 6.9 shows higher strength concrete analysis results with test data in octahedral stress-strain coordinate. For three layers FRP confined higher strength concrete specimen the prediction is close test result. For one layer FRP confined higher strength concrete specimen the prediction is far from test result.

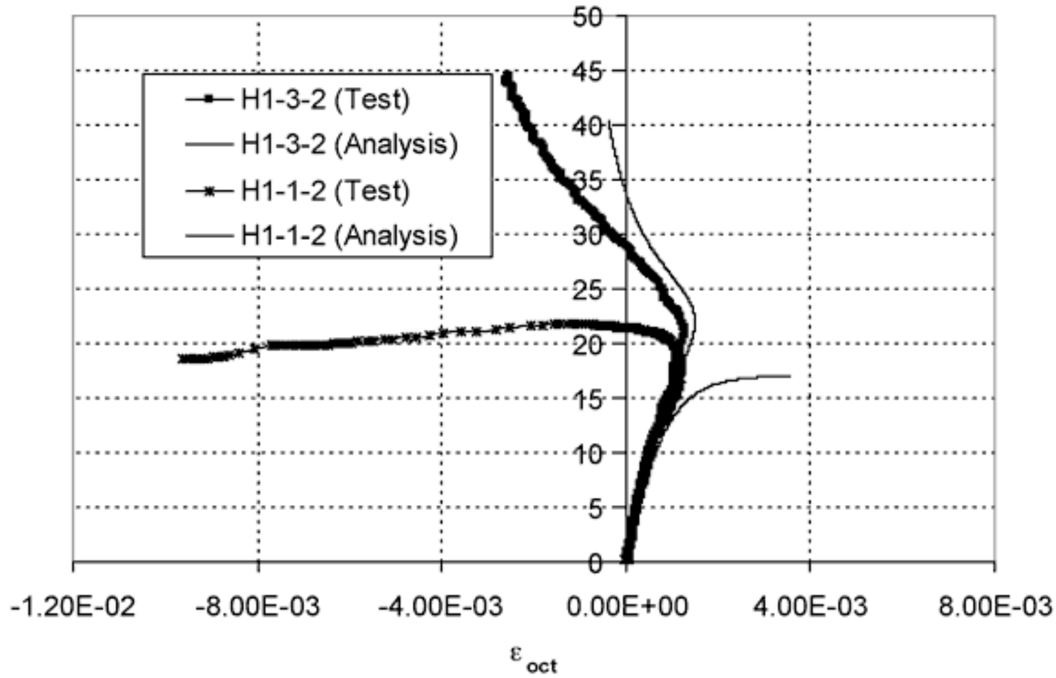

Figure 6.9: Comparison of Analytical with Experimental Results in Octahedral Normal Stress and Strain for Higher Strength Concrete Cylinders

Fig. 6.10 shows higher strength concrete analysis results with test data in octahedral shear stress - shear strain coordinate. Fig. 6.11 shows comparison of analytical with experimental results in octahedral normal strain and shear strain for higher strength concrete

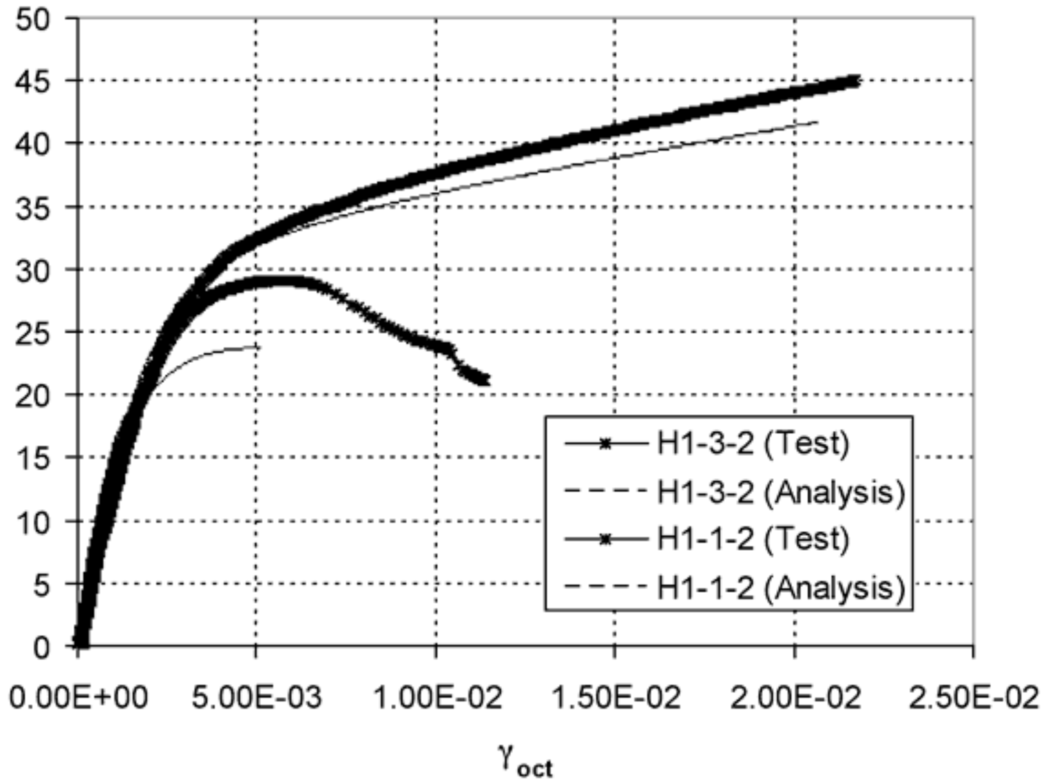

Figure 6.10: Comparison of Analytical with Experimental Results in Octahedral Shear Stress and Shear Strain for Higher Strength Concrete

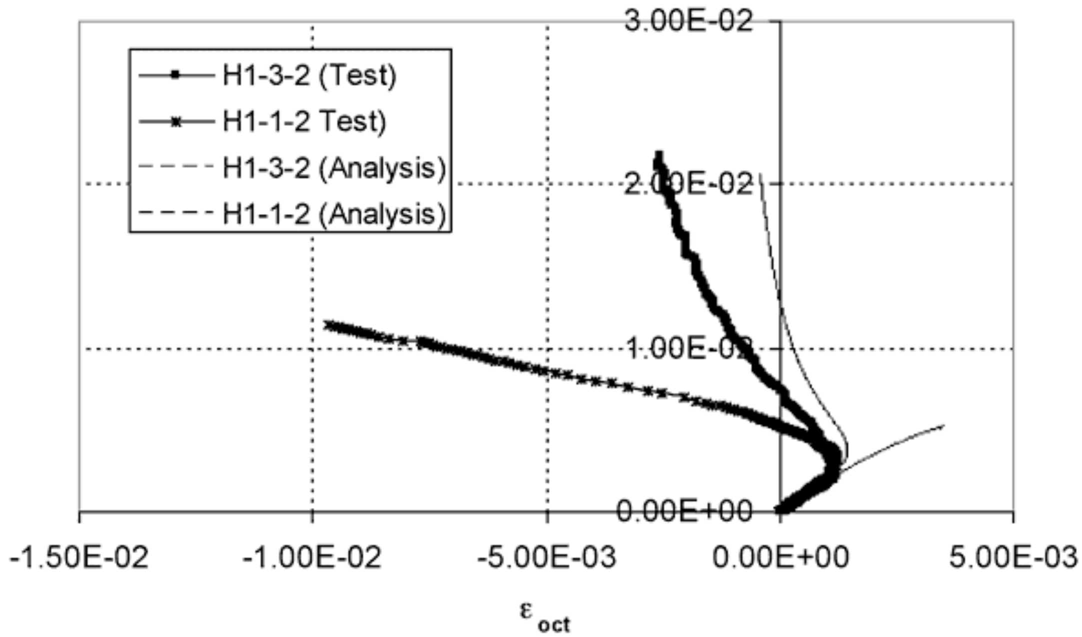

Figure 6.11: Comparison of Analytical with Experimental Results in Octahedral Normal Strain and Shear Strain for Higher Strength Concrete

6.5 Comparison between Analytical and Experimental Results

Based on the proposed approach, an elastic-plastic analysis has been performed for concrete filled steel tube. Fig 6.12 shows the analysis flow chart.

Table 6.13 shows two concrete filled steel tube test matrix in Kyushu University, Japan. The test setup shows that the loading platen does not touch the steel tube directly and concrete core sustain the loading platen in Fig 6.10. The loading transferred to steel tube by bound between concrete and steel tube. The steel tube was in circumferential tension stress and axial compression stress. Based on test results in Kyushu University, , $\varepsilon_\theta/\varepsilon_z$ kept constant in the loading.

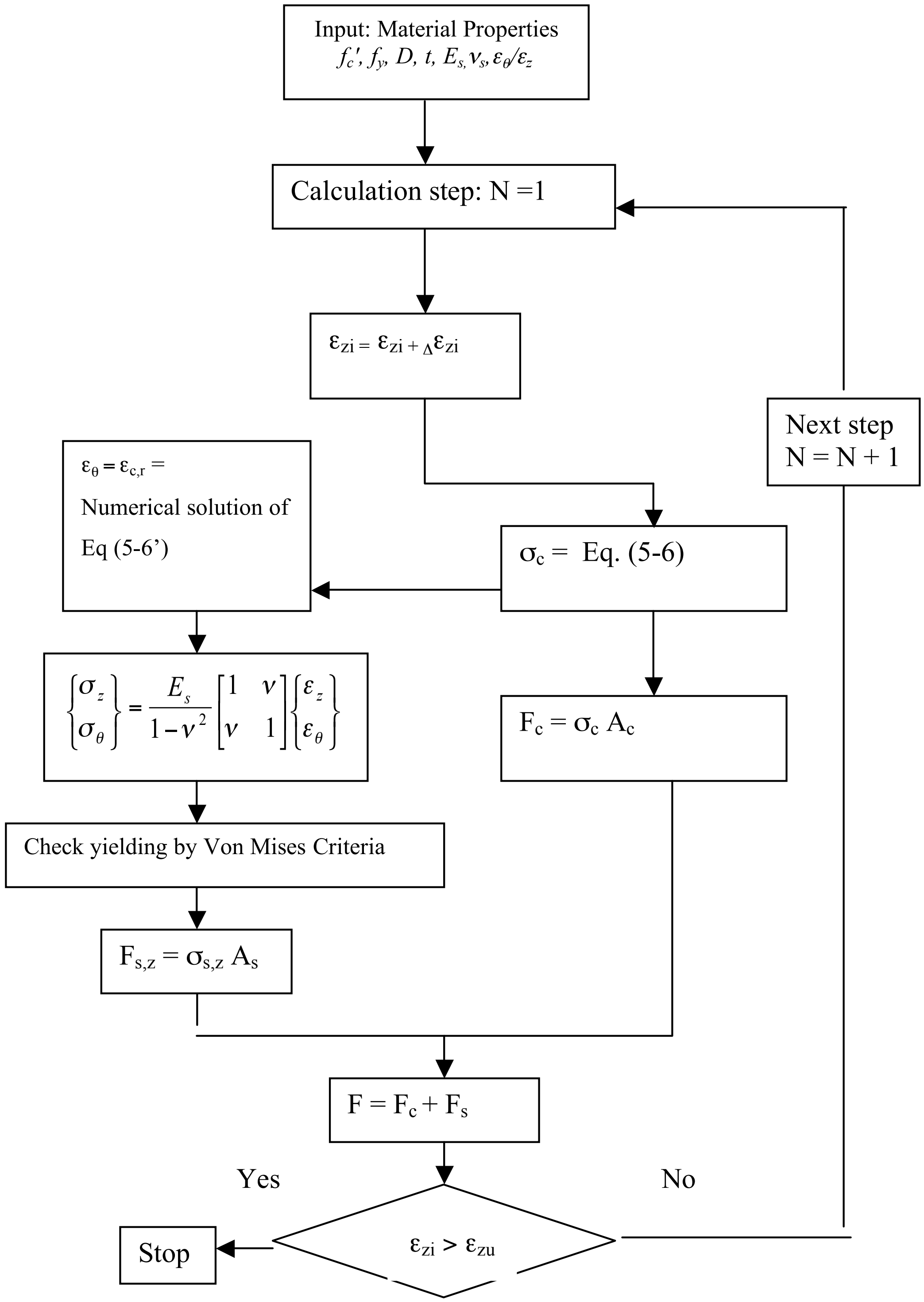

Figure 6.12: Analysis Flow Chart for Concrete filled Steel Tubes

From Hooke's Law:

$$\begin{Bmatrix} \sigma_z \\ \sigma_\theta \end{Bmatrix} = \frac{E_s}{1-\nu^2} \begin{bmatrix} 1 & \nu \\ \nu & 1 \end{bmatrix} \begin{Bmatrix} \varepsilon_z \\ \varepsilon_\theta \end{Bmatrix} \tag{6-8}$$

then

$$\sigma_\theta = \frac{E_s}{1-\nu^2}(\nu(\varepsilon_z / \varepsilon_\theta) + 1)\varepsilon_\theta \tag{6-9}$$

From above Eq. (6-9), equivalent confinement stiffness C_j can be calculated.

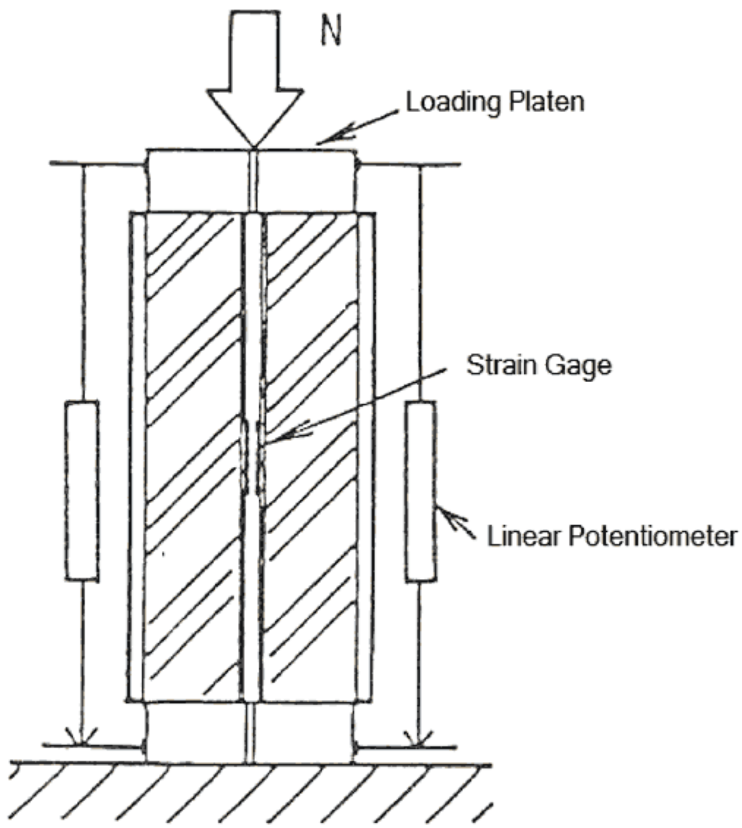

Figure 6.13: Test set up in Kyushu University, Japan

Fig.6.14 shows comparison the elastic-plastic analysis results with test results in Kyushu University. The prediction is good with test results before steel tube yielding. After steel tube yielding, the confinement stiffness reduced significantly.

Table 6.1: Test Matrix Kyushu University

	f_c'	E_c	D/t	D	H	A_s	A_c	f_y
	MPa	$x10^5$MPa		(mm)	(mm)	(mm^2)	(mm^2)	MPa
L-20-1	26.46	3.05	20	178	355	4810	20,090	260.7
L-20-2	26.46	3.05	20	178	355	4810	20,090	260.7
H-20-1	45.57	3.64	20	178	355	4810	20,090	260.7
H-20-2	45.57	3.64	20	178	355	4810	20,090	260.7

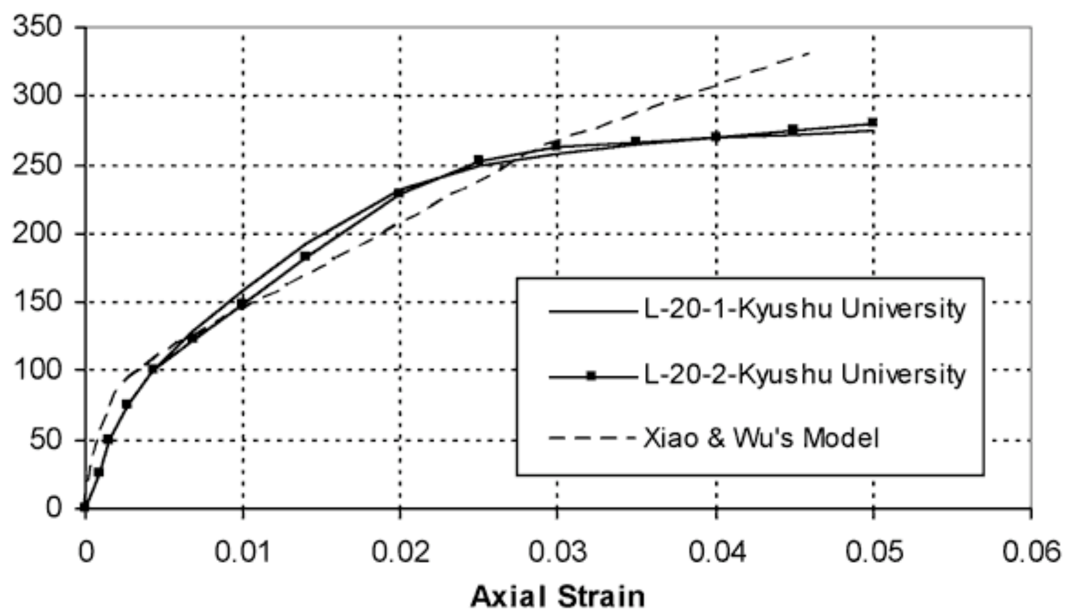

Figure 6.14: Comparison of analysis with test results of concrete filled steel tubes with lower strength concrete.

Fig.6.15 shows the comparison of results obtained from analysis using elasto-plastic approach and testing in Kyushu University.

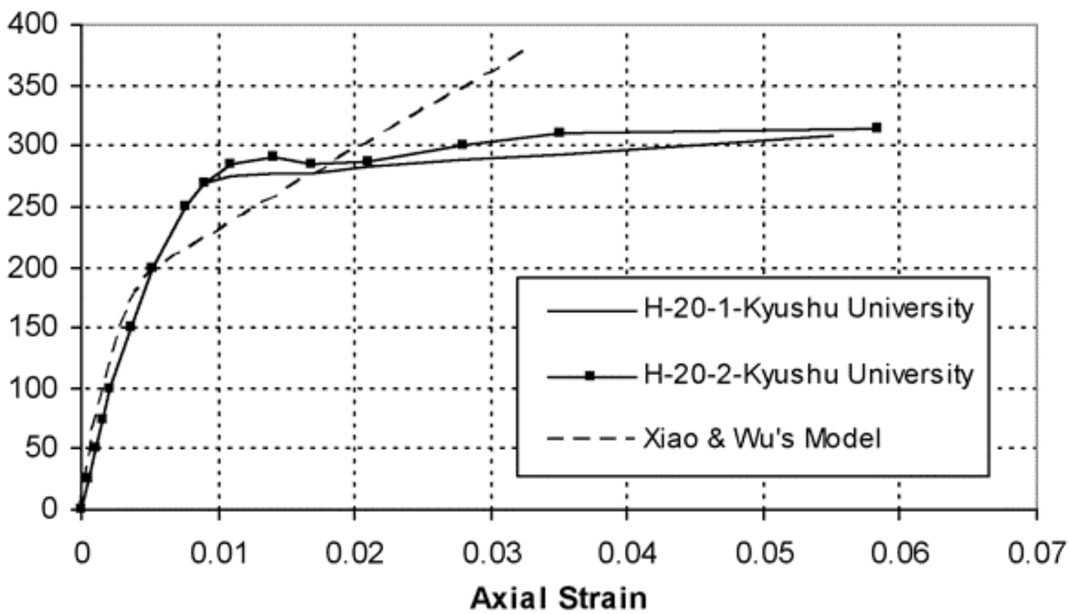

Figure 6.15: Comparison of analysis of concrete core stress strain with test results with higher strength concrete

However, the model still can not predict the behavior of concrete confined by other materials with plastic deformations such as steel after yielding, especially for high strength concrete filled steel tube, since steel tube can not provide enough confinement for high strength concrete after steel tube yield. The softening of concrete is very complex problem. So far the plasticity theory still can not apply in unstable material.

CHAPTER 7: CONCLUSION AND FURTHER RESEARCH

The aim of this research is to obtain a deeper understanding on the behavior mechanism of composite jacketing systems in concrete retrofit. Through intensive experimental testing of more than 200 concrete stub columns confined with advanced composite fibers under axial compression, much insight is gained on the interactions between the composite jackets and the confined concrete. An analytical approach is utilized to develop a universal constitutive model of confined concrete. Based on this model, researchers will be able to predict numerically the behavior of RC component for concrete confined by both FRP and steel. The validity of this model is further strengthened by close correlation with test results from other researchers.

The conclusions from this research are presented below:

Significant increase in strength and ductility of concrete can be achieved by carbon fiber composite jacketing.

As the parameters to describe the confinement effectiveness, the confinement modulus and the confinement strength of the composite jacketing have been defined.

Besides the material properties such as concrete strength, the performance of the confined concrete is dominated by the confinement modulus.

The ultimate condition of the confined concrete is determined by the rupture of the composite jacket. The rupture strain of the jacket is much lower than the rupture strain obtained for flat tensile coupon samples.

The final stress strain performances of confined concrete with carbon fiber composite jacketing exhibit a linear behavior. Equations to define the relationships between the mechanical variables of the confined concrete are proposed.

The proposed equations together with the equations for elastic behavior of unconfined concrete are suggested to provide the simple bilinear simulation to the mechanical behavior of confined concrete.

The proposed model, not only suitable for confined concrete with FRP but also steel tube before steel yielding.

The general confined concrete model is a long studied yet complex topic in concrete research that has not been fully grasped. The proposed model of confined concrete, though provides a valuable analytical tool for FRP jacketing system, may also exhibit some limitations in the practical design applications due to several factors such as the instability of the stiffness of confinement, transverse steel yielding, and the existing gap between jacket and concrete columns. Further investigation on the behavior of concrete softening may help to unravel some of these concerns.

REFERENCES

Ahmad, S. M., and Shah, S. P. (1982). "Complete triaxial stress-strain curves of concrete confined by spiral reinforcement," *J. Struct.Div. ASCE,* 108(4), 728-742.

Ahmad, S. M., and Shah, S. P. (1982). "Stress-strain curves of concrete confined by spiral reinforcement," *ACI Struct. J.,* 79(6),484-490.

Anderson, James C. and Bertero, Vitelmo V. (2006), "Use of Energy Concepts in Earthquake Engineering: a Historical Review" *Proceeding of the 8th U.S. National Conference on Earthquake Engineering* April 18-22, 2006, San Francisco, California, USA

Bazant,Z.P.; Bishop, F.C. and Chang, T.P., (1986), "Confined Compression Tests of Cement Paste and Concrete up to 300ksi," *ACI Journal,* V.83, July- August, pp. 553-560.

Bazant,Z.P. and T. Tsubaki, (1980), "Total strain theory and path-dependence of concrete," *ASCE J.Eng. Mech. Div.,* Vol. 106, No. 6, November/December 1980, pp. 1151-1173

Becque, J., Patnaik, A. K., and Rizkalla, S. H. (2003), " Analytical models for concrete confined with FRP tubes," *J. compos. Constr.,* 7(1), pp 31-38.

Bisby, Luke A., Dent, Aaron J. S., and Green, Mark F., (2006), "Comparison of Confinement Models for Fiber-Reinforced Polymer-Wrapped Concrete," *ACI Structural Journal,* V. 102, No. 1, pp 62-72.

Chen, W.F., "Plasticity in Reinforced Concrete," McGraw-Hill, New York, 1982.

Cheng, H. L., Sotelino, E. D., and Chen, W. F., (2002) "Strength estimation for FRP wrapped reinforced concrete columns," *Steel Compos Struc.,* 2(1), pp 1-20.

Darwin, D. and Pecknold, D. A. (1977), "Nonlinear Biaxial Law for Concrete", *Journal of the Engineering Mechanics Division, ASCE*, 103(EM2), 229-241.

de Borst, R., (1986), "No-linear Analysis of Frictional Materials," Ph. D. Dissertation, Delft University of Technology, delft, The Netherlands.

Elwi, A.A. and D.W. Murray, (1979), "A 3D Hypoelastic Concrete Constitutive Relationship," *Journal of the Engineering Mechanics Division, ASCE*, Vol. 105, No. 4, July/August 1979, pp. 623-641

Fam, A. Z., and Rizkalla, S. H. (2001), "Behavior of Axially Loaded Concrete-Filled Circular Fiber-Reinforced Polymer Tubes," *ACI Structrual Journal,* 98(3), 280-289.

Fam, A. Z., and Rizkalla, S. H. (2001), "Confinement Model for Axially Loaded Concrete Confined by Circular Fiber-Reinforced Polymer Tubes," *ACI Structrual Journal,* 98(4), 451-461.

Fardis, M.N., and Khalili, H. (1981) "Concrete encased in fiberglass-reinforced plastic." *ACI J.,* 78(6), 44-446.

Fujikake, Kazunori; Mindess, Sidney and Xu, Hanfeng (2004), "Analytical Model for Concrete Confined with Fiber Reinforced Polymer Composite," *J. Compos. for Constr*., Volume 8, Issue 4, pp. 341-351 July/August 2004

Gerstle, K. H. (1981a), "Simple Formulation of Biaxial Concrete Behavior," *ACI J.,* 78 (1), 62-68.

Gerstle, K. H. (1981b), "Simple Formulation of Triaxial Concrete Behavior," *ACI J.,* 78 (5), 382-378.

Harmon, T. G.; Ramakrishnan, S. and Wang, E. H., (1998), "Confined Concrete Subjected to Uniaxial Monotonic Loading," *ASCE Journal of Structural Engineering*, Vol. 124, No. 12, December, 1303-1309.

Harmon, T. G., and Alattery, K. T. (1992), "Advanced Composite Confinedment of Concrete," *Proc. Int. Conf. on Advanced Composite Materials in Bridges and Structures,* Canadian Society for Civil Engineering, pp 299-306.

Hosotani, M., Kawashima, K., and Hoshikuma, J., (1996), "Seismic Retrofit of Reinforced Concrete Bridge Piers by Carbon Fiber Sheets," *Proc., 3rd US-Japan Workshop of Seismic Retrofit of Bridges*, ISSN 0368-5878, Technical Memorandum of PWRI, No. 3481.

Hsu, T. T. C., Slate, F. O., Sturman, G. M. and Winter, G. (1963), "Microcracking of Plain Concrete and Shape of the Stress-Strain Curve," *ACI Journal* Vol. 60, pp. 209-223.

Karabinis, A. I., and Rousakis, T. C. (2002), “Concrete Confined by FRP Materials: a Plasticity Approach,” *Engineering Structures*, 24, 923-932.

Karbhari, V. M., and Gao, Y. (1997), “Composite jacketed concrete under uniaxial compression –Verification of simple design equations.” *J. Mater. Civ. Eng.*, 9(4), 185-193.

Kazunori Fujikake, Sidney Mindess, and Hanfeng Xu, (2004), “Analytical Model for Concrete Confined with Fiber Reinforced Polymer Composite” *Journal of Composites for Construction*, Vol. 8, No. 4, July/August 2004, pp. 341-351

Kupfer, H., H. K. Hilsdorf, and H. Rusch (1969), “Behavior of concrete under biaxial stresses,” *ACI J.* 66(8), 656-666.

Lemaitre, J., “A Course on Damage Mechanics”, Springer Verlag, Berlin 1992.

Lemaitre, Jean; Desmorat, Rodrigue; “Engineering Damage Mechanics: Ductile, Creep, Fatigue and Brittle Failures”, Springer Verlag, May 2005. pp 380.

Lam, L., and Teng, J. G. (2002), “Strength Models for Fiber-Reinforced Plastic-Confined Concrete,” *Journal of Structural Engineering,* ASCE, May 2002 612-623.

Lowes, Laura Nicole, (1999), “Finite Element Modeling of Reinforced Concrete Beam-Column Bridge Connections”, Ph.D. Dissertation, University of California, Berkeley.

Mander, J. B., Priestley, M. J. N., and Park, R. (1988). “Theoretical Stress-Strain Model for Confined Concrete.” *J. Struct. Engrg.,* ASCE, 114(8), 1804-1826.

Mander, J. B., Priestley, M. J. N., and Park, R. (1988). “Observed Stress-Strain Behavior of Confined Concrete.” *J. Struct. Engrg.,* ASCE, 114(8), 1827-1849.

Matsuda, T.; Sato, H.; Fujiwara, H.; and Higashira, N., (1990), “Effect of Carbon Fiber Reinforcement as a Strengthening Measure for Reinforced Concrete Bridge Piers,” *Proceeding of the First U.S.-Japan Workshop on Seismic Retrofit of Bridges*, Public Works Research Institute, Ministry of Construction, Tsukuba Science City, Japan, December 17-18.

Meyer, Christian, “Modeling and Analysis of Reinforced Concrete Structures for Dynamic Loading,” Columbia University, Springer Wien, NewYork, 1998.

Mirmiran, A., and Shahawy, M. (1996),"A New Concrete-filled Hollow FRP Composite Column," *Composites Part B: Engineering*, Special Issue on Infrastructure, 27B(3-4) 263-268.

Mirmiran, A., and Shahawy, M., (1997), "Behavior of Concrete Columns Confined by Fiber Composites," *ASCE Journal of Structural Engineering*, Vol. 123, No. 5, 583-590.

Moran, Domingo A., and Pantelides, Chris P., "Damage-Based Stress-Strain Model for Fiber-Reinforced Polymer-Confined Concrete," *ACI Structural Journal,* V.102, No. 1, pp. 54-61.

Neville, A. M., "Properties of concrete," 4th Ed., John Wiley & Sons, Inc., New York, USA. 1996.

Newman, K., and Newman, J. B. (1969), "Failure Theories and Design Criteria for Plain concrete," *Eng. Des, Civ. Eng. Mater pap*. 83, Southampton, 1969.

Palaniswamy, R., and Shah, S.P., "fracture and Stress-Strain Relationship of Concrete under Trixial Compression," Journal of Structural Engineering, ASCE, Vol.100, No.ST5, May 1974. pp 901- 916

Park, R. and Paulay, T. "Reinforced Concrete Structures," John Wiley and Sons, New York, 1975.

Paulay, T. and Priestley, M. J. N. "Seismic Design of Reinforced Concrete and Masonry Buildings". John Wiley and Sons, New York, 1992..

Picher, F., Rochette, P., and Labossiere, P. (1996), "Confinement of Concrete Cylinders with CFRP," *Proc, 1st Int. Conf. Composites in Infrastructure*, H. Saadatmanesh and M.R. Ehsani, eds., University of Arizona, Tuson, Ariz., 829-841.

Priestley, M.J.N.; and Seible, F., (1991), "Seismic Assessment and Retrofit of Bridges," Edited by M.J.N. Priestley and F. Seible, University of California at San Diego, *Structural Systems Research Project*, Report No. SSRP-91/03, July, 418p.

Richard, Ralph M. and Abbott, Barry J., (1975), "Versatile Elastic – Plastic Stress-Strain Fomula," *Journal Engineering Mechanics Division,* ASCE Vol. 101 No. EM4, August, 1975, pp.511~515.

Richart, F.E.; Brantzaeg, A.; and Brown, R.L., (1928), "A study of the failure of concrete under combined compressive stresses." Bulletin No. 185, Engineering Experiment Station, University of Illinois, Urbana, April.

Richart, F.E.; Brantzaeg, A.; and Brown, R.L., (1929), "The Failure of Plain and Spirally Reinforced Concrete in Compression," Bulletin No. 190, Engineering Experiment Station, University of Illinois, Urbana, April.

Saadatmanesh, H.; Ehsani, M.R.; and Li, M.W. (1994), "Strength and Ductility of Concrete Columns Externally Reinforced with Fiber Composite Straps," *ACI Structural Journal*, July-August Issue, pp.434.

Samaan, M., Mirmiran, A., and Shahaway, M., (1998), "Model of concrete confined by Fiber composites," *J. Struct. Eng.,* 124(9), pp 1025-1031.

Sargin, M., (1971), "Stress-Strain Relationship for Concrete and the Analysis of Structural Concrete Section," Ph.D. thesis, Univ. of Waterloo, Ontario, Canada.

Seible, F. and Priestley, M.J.N., (1993), "Retrofit of Rectangular Flexural Columns with Composite Fiber Jackets," California Department of Transportation, *Proceedings of the Second Annual Seismic Research Workshop*, Sacramento, March 16-18.

Seible, F.; Hegemier, G.A.; and Innamorato, D., (1995), "Developments in Bridge Column Jacketing Using Advance Composites," *Proceedings of the National Seismic Conference on Bridges and Highways*, Federal Highway Administration and California Department of Transportation, San Diego, California, December 10-13.

Stanton, J. F.; and Owen, L.M., (2006),"The Influence of concrete Strength and Confinement Type on the Response of FRP-Confined Concrete Cylinders," *International Symposium on Confined Concrete,* Y. Xiao, Sashi Kunnath,and Weijian Yi, eds ACI SP-238, pp347 – 362.

Teng, J. G., and Lam, L. (2004), "Behavior and Modelong of Fiber Reinforced Polymer-confined Concrete," *J. of Struct. Eng.,* ASCE, November 2004.

Toutanji, Houssam A., (1999), "Stress-Strain Characteristics of concrete Columns Externally Confined with Advanced Fiber Composite Sheets," *ACI Material Journal,* V.96, No. 3, May-June 1999, pp. 397-404.

Wu, H., and Xiao, Y., (2000), “Compressive Stress Strain Behavior of Concrete Comfined by Carbon Fiber Jackets,” *Proceedings of the Sixth ASCCS Conference on Composite and Hybrid Structures,* Y. Xiao, and S. A. Mahin, eds., Los Angeles, Calif., Mar. 22-24, 2000. pp.

Xiao, Y., (1989), “Experimental Study and Analytical Modeling of Triaxial Behavior of Confined Concrete,” Ph.D. Thesis, Kyushu University, Japan.

Xiao,Yan; and Wu, Hui (2003), “Compressive Stress Behavior of Concrete Comfined by Various Types of FRP Composite Jackets,” *J. Reinf. Plast. Compos.,* 22(13), 1187-1202.

Xiao,Yan; and Wu, Hui (2003), “Retrofit of reinforced concrete columns using partially stiffened steel jackets,” *ASCE Journal of Structural Engineering*, Vol. 129 No.6 pp 725-732.

Xiao,Yan; Wu, Hui; and Martin, G. R., (1999), “Prefabricated Composite Jacketing of RC Columns for Enhanced Shear Strength,” *ASCE Journal of Structural Engineering*, Vol.125 No. 3, pp255-264.

Xiao, Y., and Wu, H., (1997), “Compressive Behavior of Concrete Stub Columns Confined by Carbon Fiber Composite Jackets,” *Proceedings of the 13th U.S.-Japan Bridge Engineering Workshop*, ISSN 0386-5878, October, Japan, pp. 421-435.

Xiao, Y., and Wu, H., (2000), “Compressive Behavior of Concrete Confined by Carbon Fiber Composite Jackets,” *Journal of Materials in Civil Engineering*, ASCE, 12(2) 139-146.

Wu, Hui, (1990), “Nonlinear Finite Element Analysis of Reinforced Concrete and Application in Combined Torsion”, Master thesis, Tsinghua University, Beijing, China.

APPENDIX A: TEST RESULTS OF SYSTEM ONE

Part A-A General Information

Table A-A1 Test Matrix

Type of Jacket	Concrete Strength	Jacket Layers	Specimen Numbers
Carbon fiber sheet reinforced composite jacket	Lower	Plain concrete	3 specimens each
		1-layer	
		2-layer	
		3-layer	
	Medium	Plain concrete	
		1-layer	
		2-layer	
		3-layer	
	Higher	Plain concrete	
		1-layer	
		2-layer	
		3-layer	

Table A-A2 Mix Proportion of Concrete

Series	Target f'_{co} (MPa)	W/C	Water (kg/m^3)	Cement (kg/m^3)	Fine Aggregates (kg/m^3)	Coarse Aggregates (kg/m^3)
L	27.6	0.68	196	288	1087	853
M	37.9	0.48	196	408	986	853
H	48.2	0.38	197	515	857	853

Table A-A3 Mechanical Properties Based on Carbon Fiber Composite Tensile Coupon Tests

Type of Jacket	Thickness/Ply (mm)	Modulus E_j (MPa)	Modulus E_j (kN/cm)	Strength f_{ju} (MPa)	Strength f_{ju} (kN/cm)
Carbon (FTS C1-30)	0.381	1.1x10^5	259	1,577	6.01

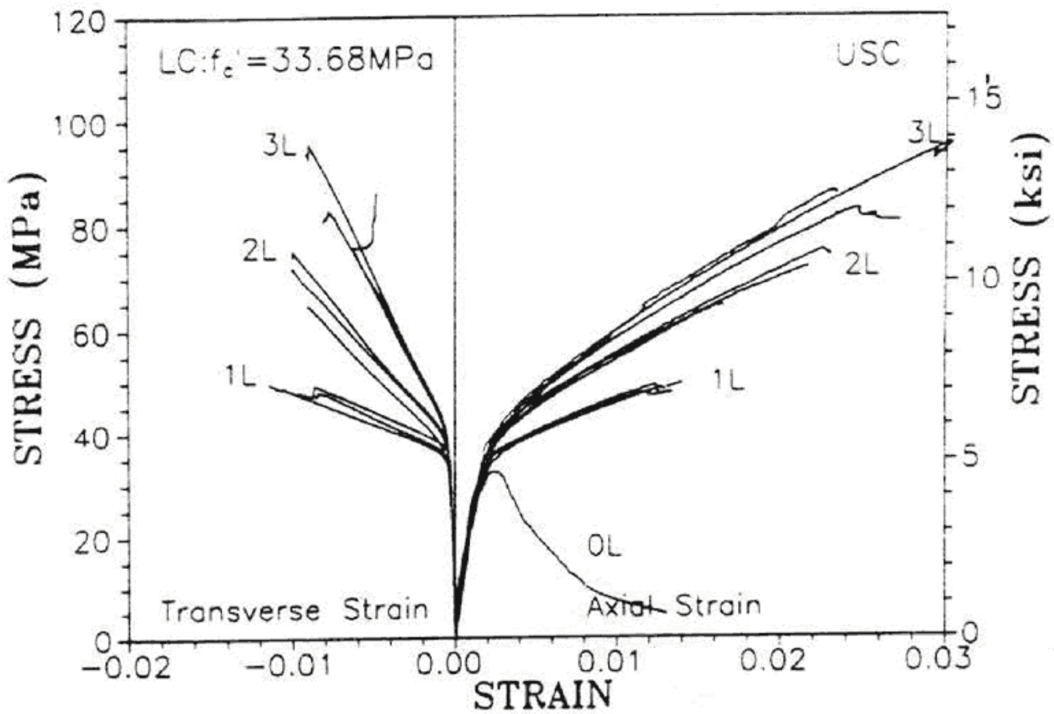

Fig.A-A1. Test Results of Lower-Strength Specimens

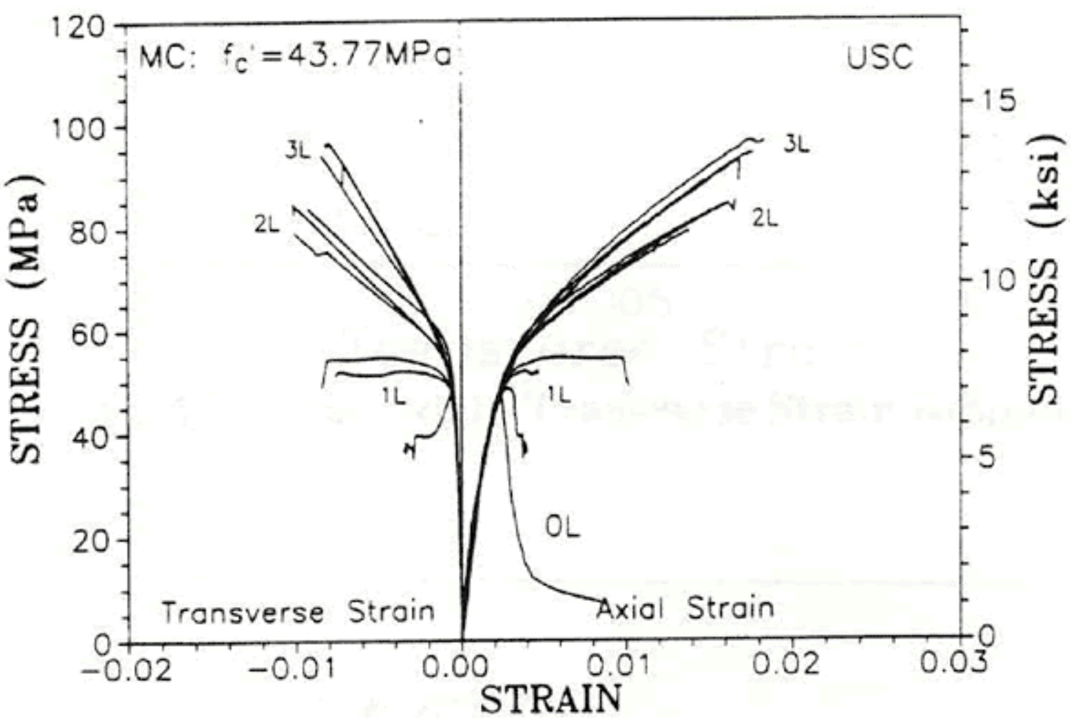

Fig.A-A2. Test Results of Medium-Strength Specimens

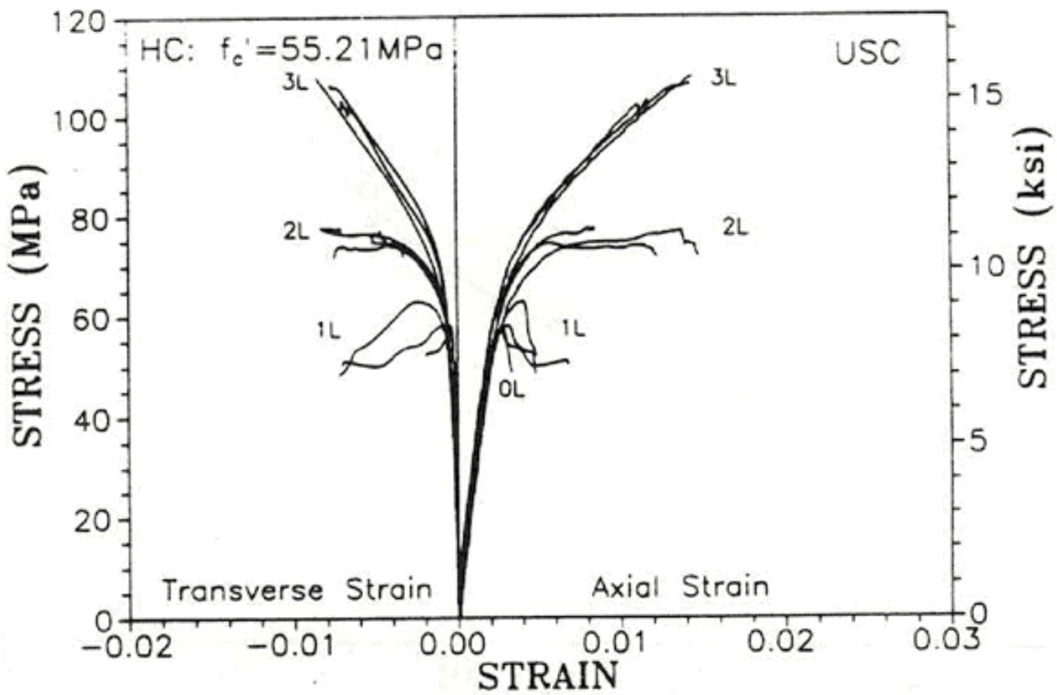

Fig.A-A3. Test Results of Higher-Strength Specimens

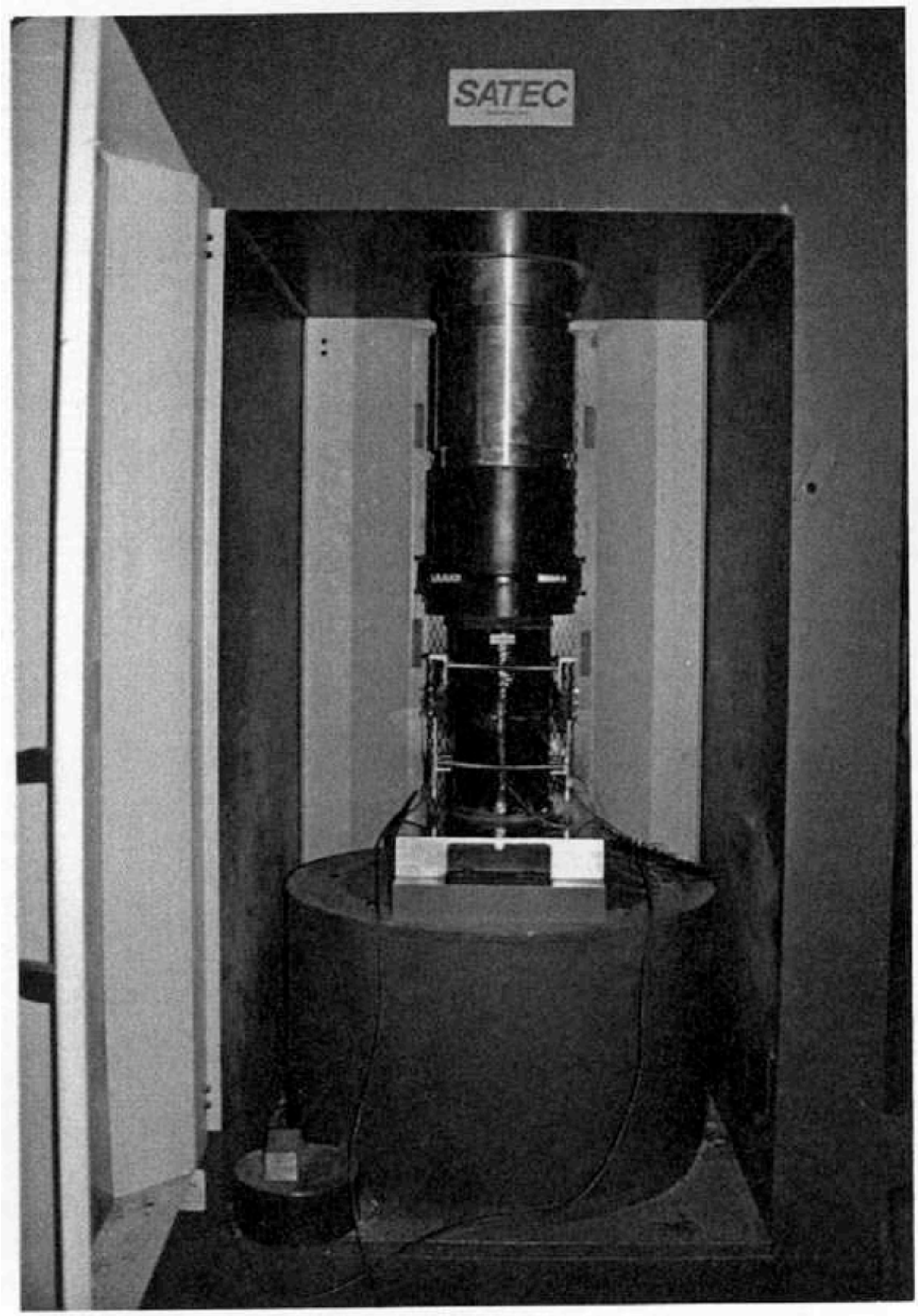

Fig A-A4. Test Setup

Table A-A4 Test Results

Series	Specimen	f_c' (MPa)	Jacket Layers	f_{cc}' (MPa)	ε_{cu}
L	LC-0L-CJ1-1	33.7	0	32.35	0.002591
	LC-0L-CJ1-2			33.43	0.002137
	LC-0L-CJ1-3			35.25	0.002441
	LC-1L-CJ1-1		1	47.87	0.01340
	LC-1L-CJ1-2			49.66	0.01397
	LC-1L-CJ1-3			49.38	0.01241
	LC-2L-CJ1-1		2	64.56	0.01650
	LC-2L-CJ1-2			75.23	0.02253
	LC-2L-CJ1-3			71.79	0.02160
	LC-3L-CJ1-1		3	82.94	0.02460
	LC-3L-CJ1-2			86.25	0.02329
	LC-3L-CJ1-3			95.38	0.03030
M	MC-0L-CJ1-1	43.8	0	47.01	0.002432
	MC-0L-CJ1-2			43.42	0.002157
	MC-0L-CJ1-3			40.87	0.002092
	MC-1L-CJ1-1		1	54.77	0.009805
	MC-1L-CJ1-2			52.05	0.004679
	MC-1L-CJ1-3			48.27	0.003360
	MC-2L-CJ1-1		2	83.95	0.01570
	MC-2L-CJ1-2			79.21	0.01376
	MC-2L-CJ1-3			84.97	0.01658
	MC-3L-CJ1-1		3	96.50	0.01744
	MC-3L-CJ1-2			92.60	0.01678
	MC-3L-CJ1-3			94.04	0.01759
H	HC-0L-CJ1-1	55.2	0	54.75	0.002266
	HC-0L-CJ1-2			53.44	0.002106
	HC-0L-CJ1-3			57.45	0.002840
	HC-1L-CJ1-1		1	56.97	0.00686
	HC-1L-CJ1-2			62.87	0.00406
	HC-1L-CJ1-3			58.06	0.00486
	HC-2L-CJ1-1		2	74.57	0.01230
	HC-2L-CJ1-2			77.50	0.00847
	HC-2L-CJ1-3			76.99	0.01390
	HC-3L-CJ1-1		3	106.5	0.01436
	HC-3L-CJ1-2			101.1	0.01452
	HC-3L-CJ1-3			103.3	0.01182

Note: (i) Example for specimen name designation:
LC-2L-CJ1-1: LC designates Lower strength Concrete; 2L designates 2 Layers; CJ1 designates Carbon fiber Jacket System 1; and the last number represents specimen number in same series.
(ii) f_c': Average plain concrete cylinder strength;
(iii) f_{cc}': Ultimate strength of confined concrete;
(iv) ε_{cu}: Ultimate strain

Part A-B Test Results of Lower Strength Concrete Cylinders

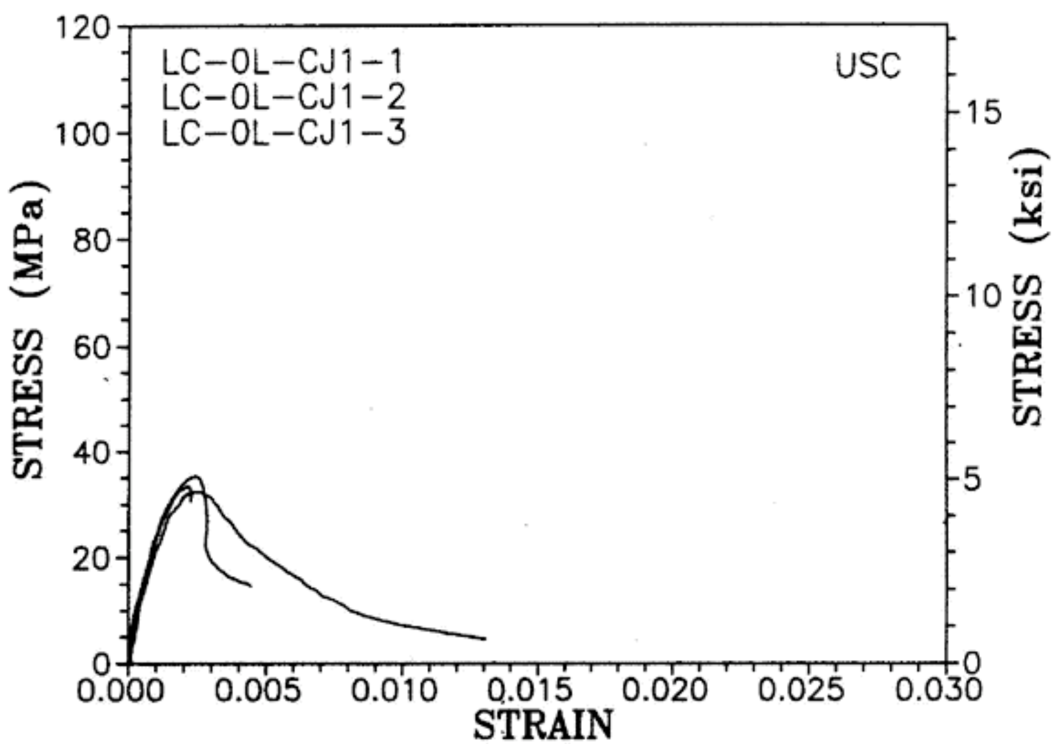

Fig.A-B1. Stress-Strain Relationship for Lower Strength Plain Concrete Cylinders

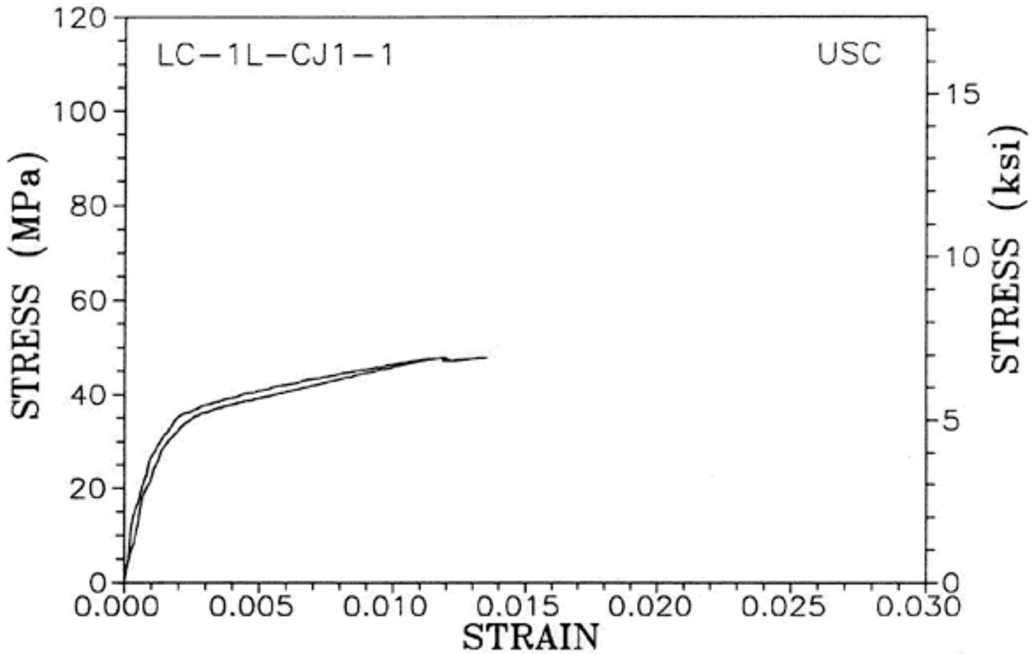

(a)

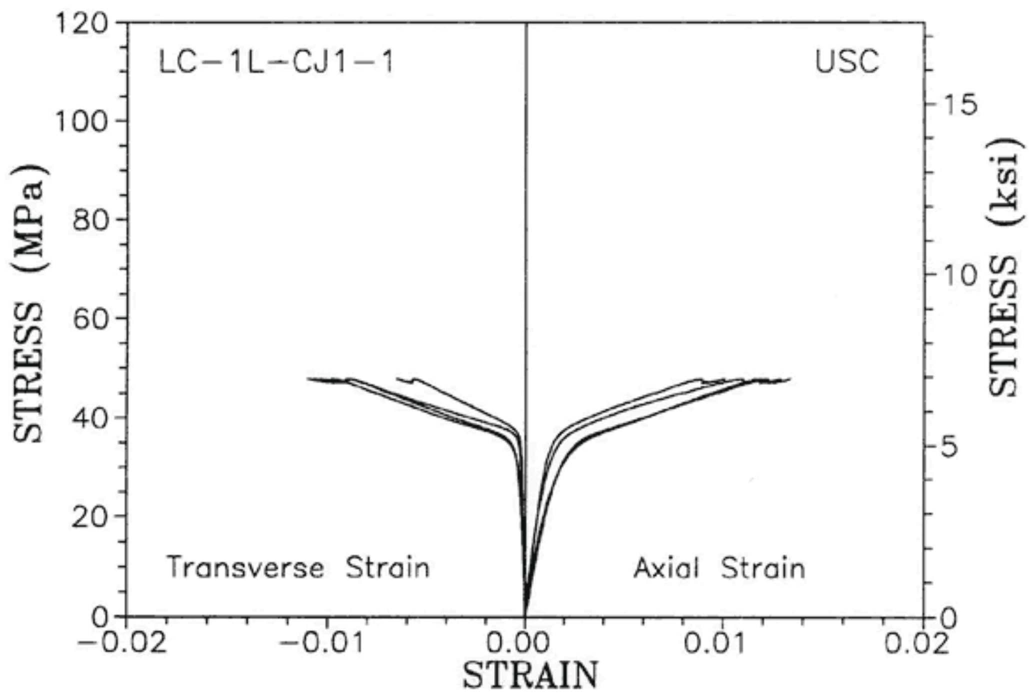

(b)

Fig A-B2.Stress-Strain Relationships for Lower Strength Concrete with One-layer Carbon Fiber Composite Jacket (LC-1L-CJ1-1)
(a) Strain measured by LP (b) Strain measured by strain gages

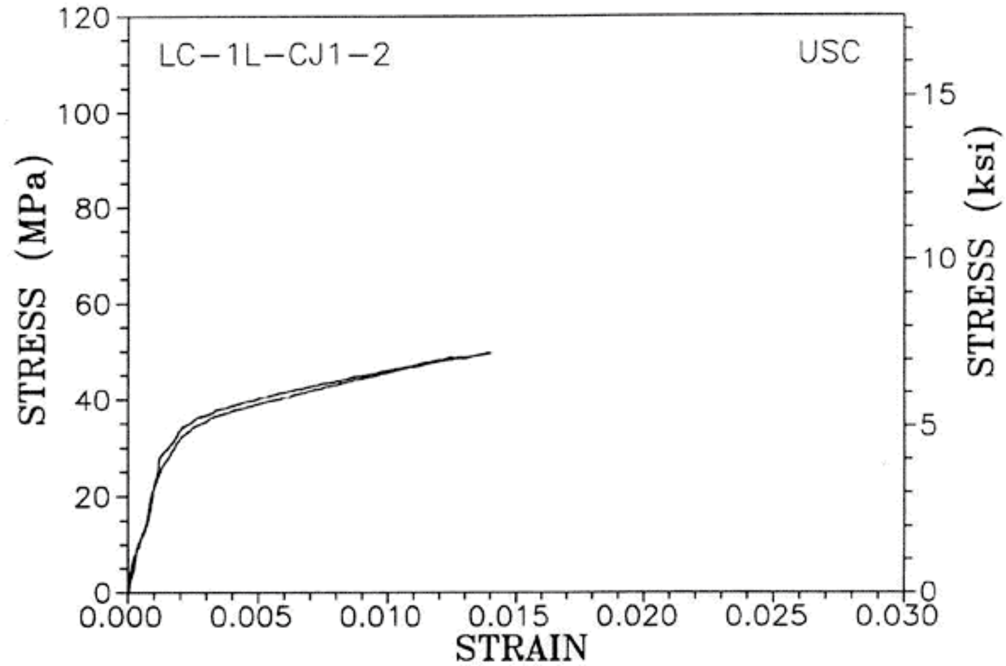

(a)

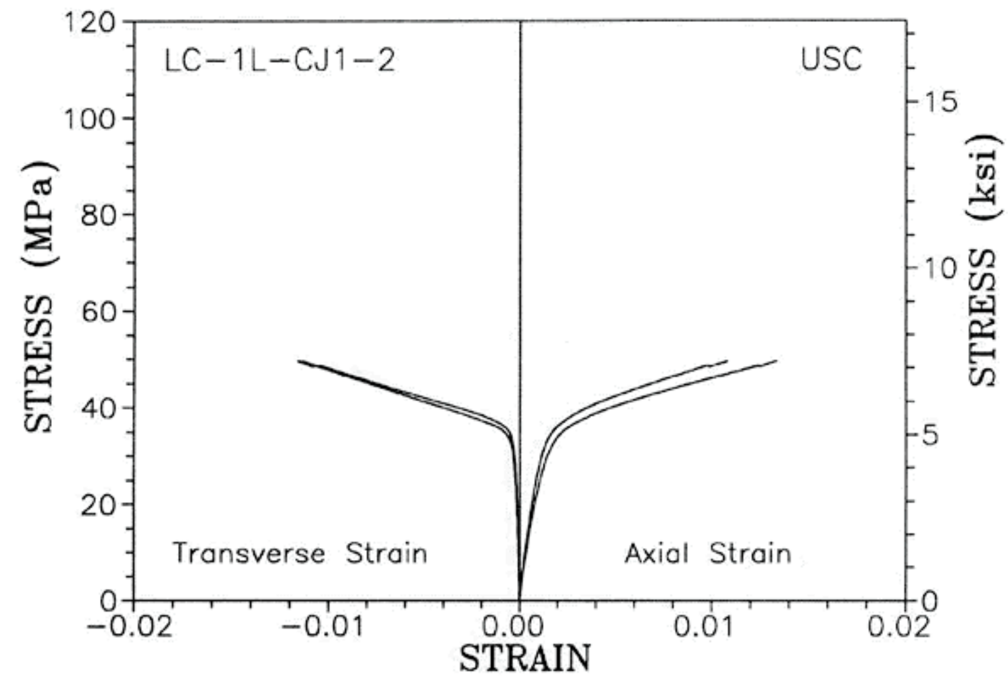

(b)

Fig A-B2.Stress-Strain Relationships for Lower Strength Concrete with One-layer Carbon Fiber Composite Jacket (LC-1L-CJ1-2)
(a) Strain measured by LP (b) Strain measured by strain gages

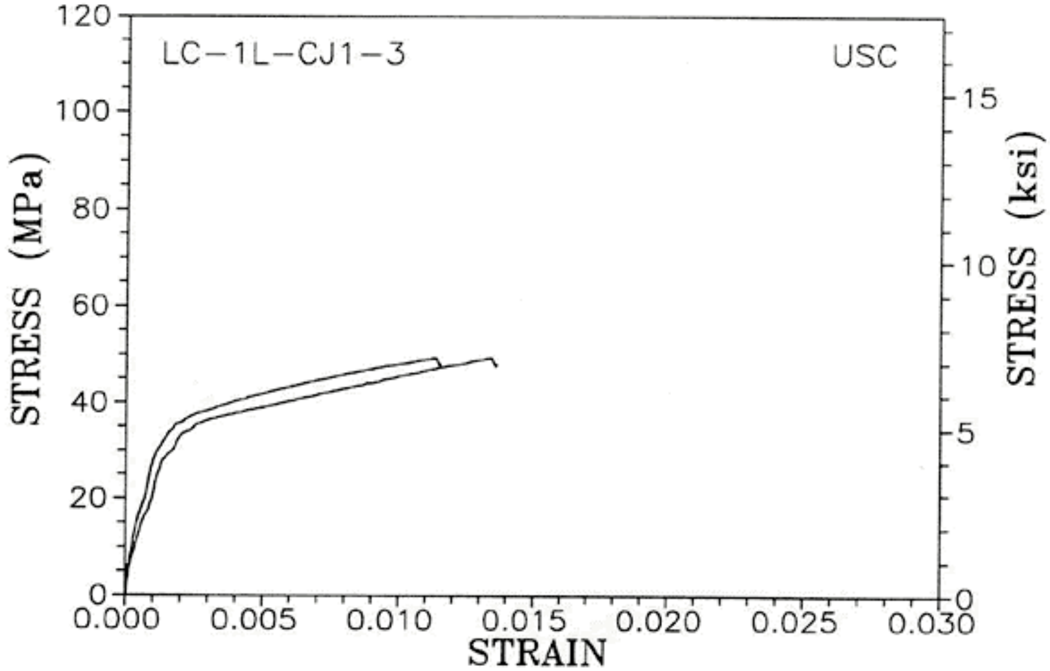

(a)

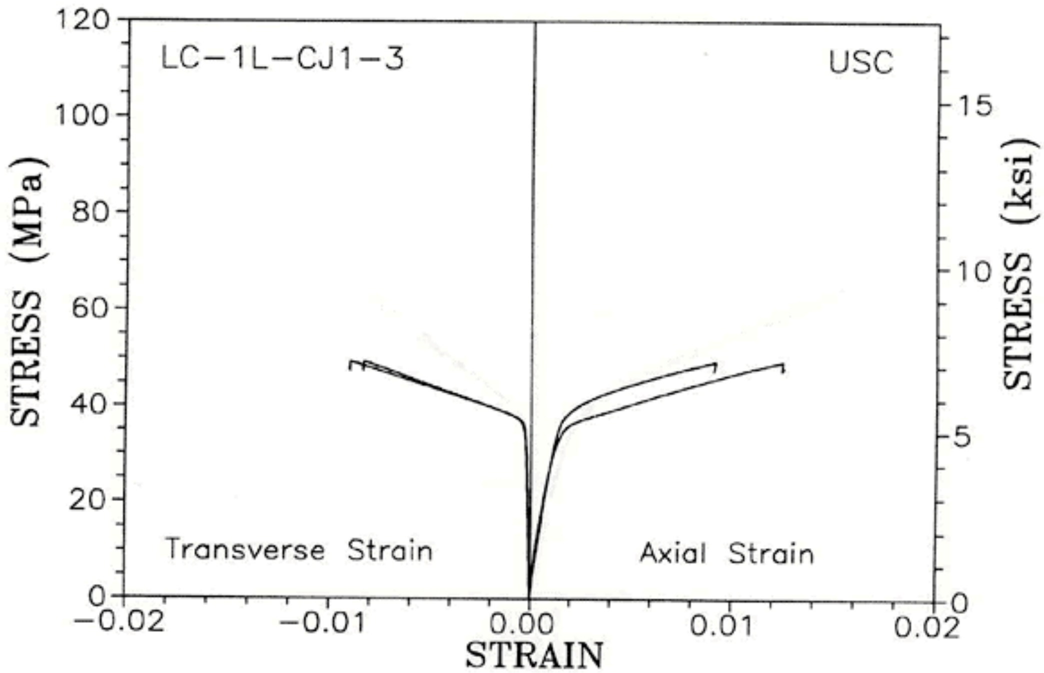

(b)

Fig A-B2.Stress-Strain Relationships for Lower Strength Concrete with One-layer Carbon Fiber Composite Jacket (LC-1L-CJ1-3)
(a) Strain measured by LP (b) Strain measured by strain gages

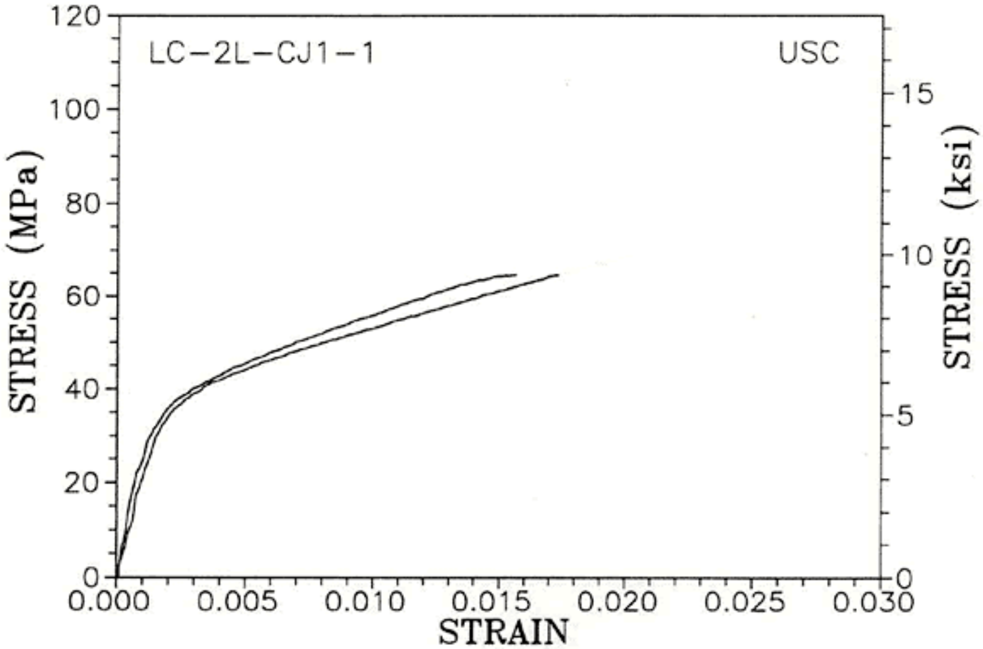

(a)

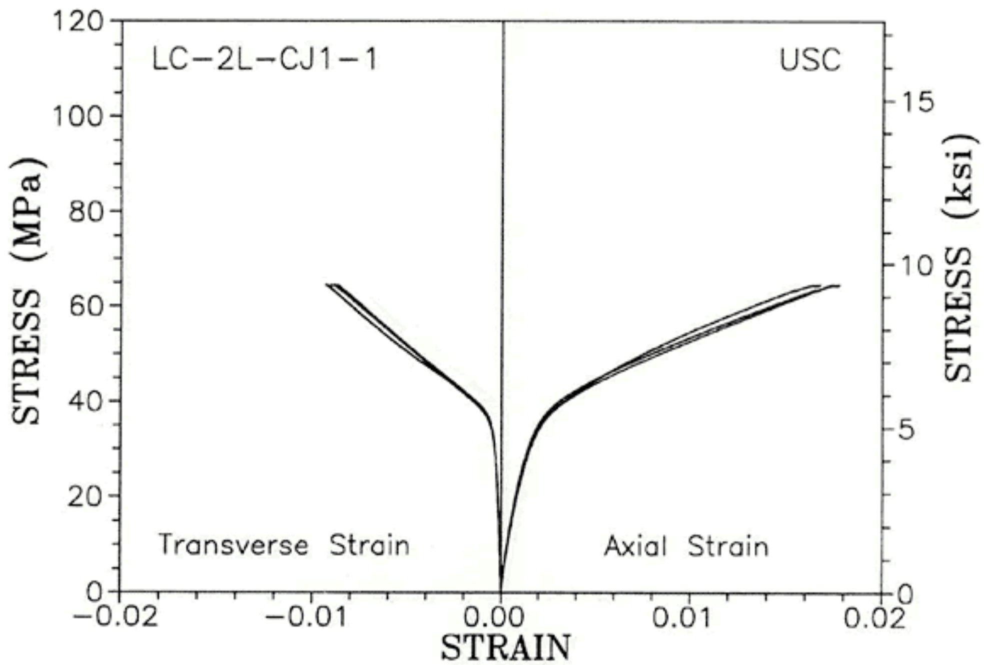

(b)

Fig A-B3.Stress-Strain Relationships for Lower Strength Concrete with Two-layer Carbon Fiber Composite Jacket (LC-2L-CJ1-1)
(a) Strain measured by LP (b) Strain measured by strain gages

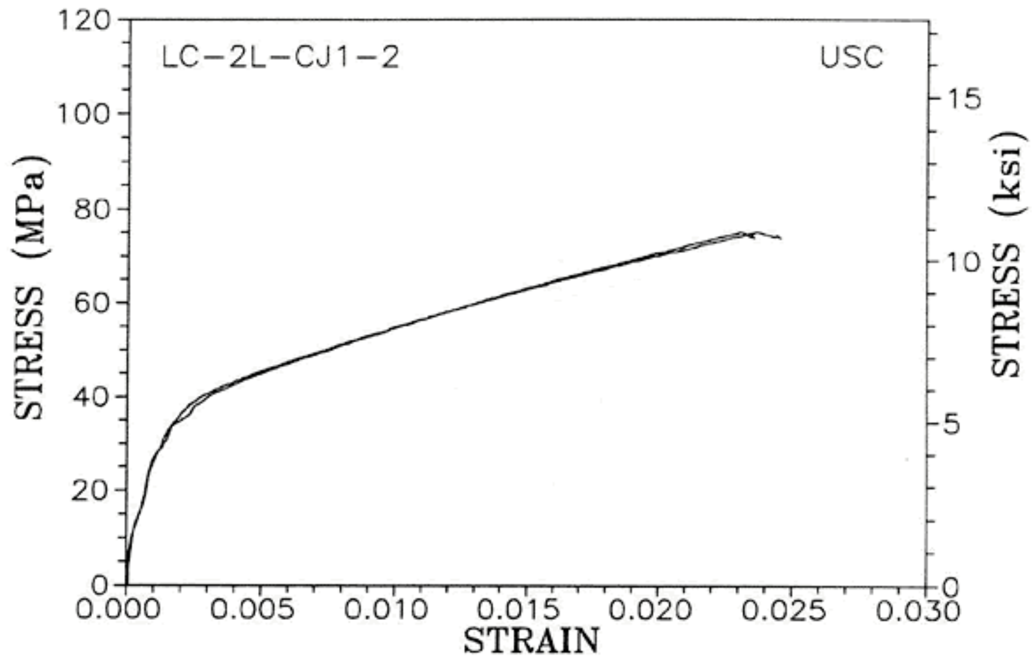

(a)

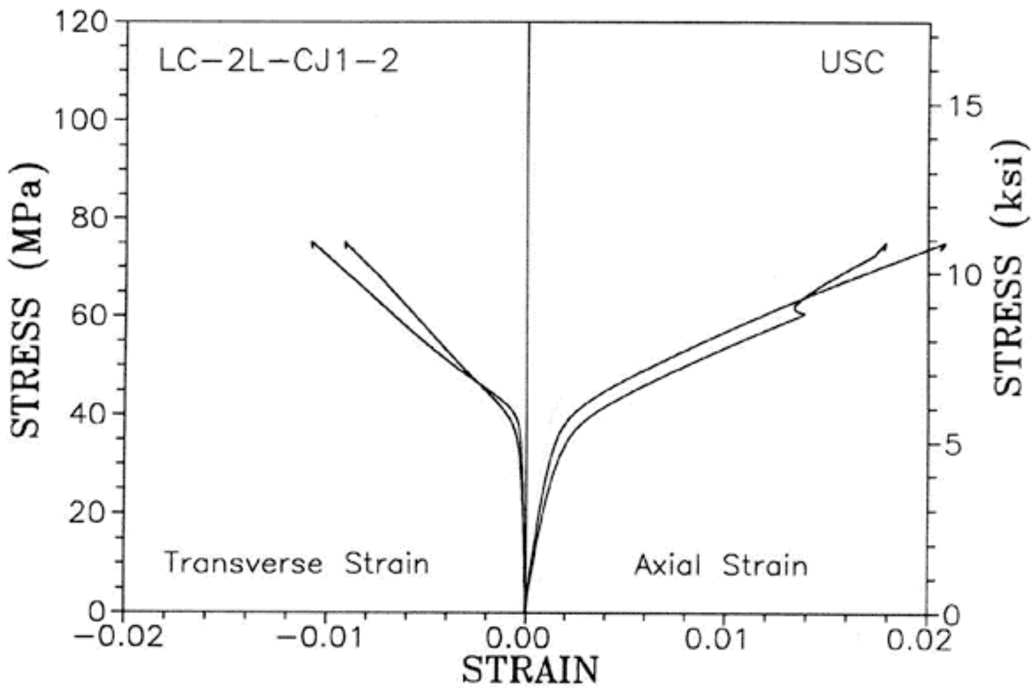

(b)

Fig A-B3.Stress-Strain Relationships for Lower Strength Concrete with Two-layer Carbon Fiber Composite Jacket (LC-2L-CJ1-2)
(a) Strain measured by LP (b) Strain measured by strain gages

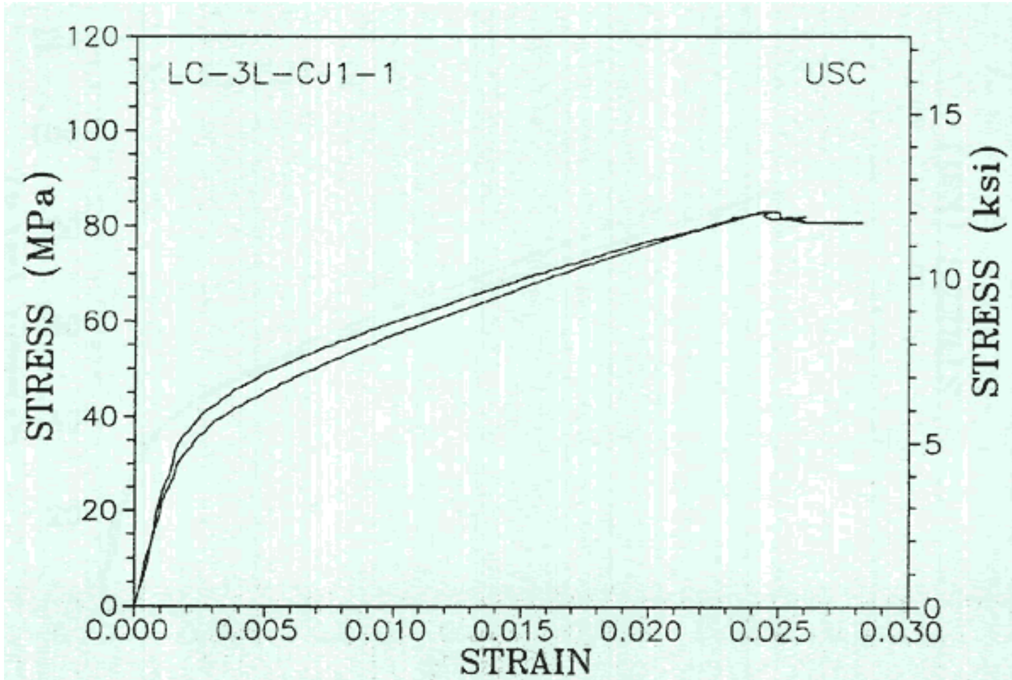

(a)

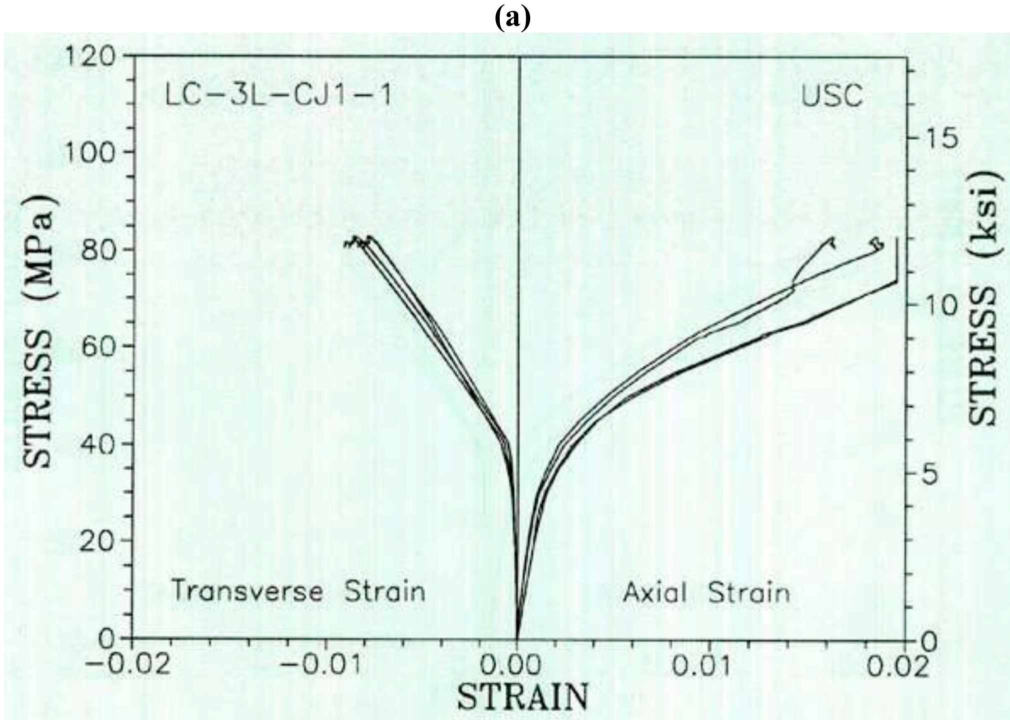

(b)

Fig A-B4.Stress-Strain Relationships for Lower Strength Concrete with Three-layer Carbon Fiber Composite Jacket (LC-3L-CJ1-1)
(a) Strain measured by LP (b) Strain measured by strain gages

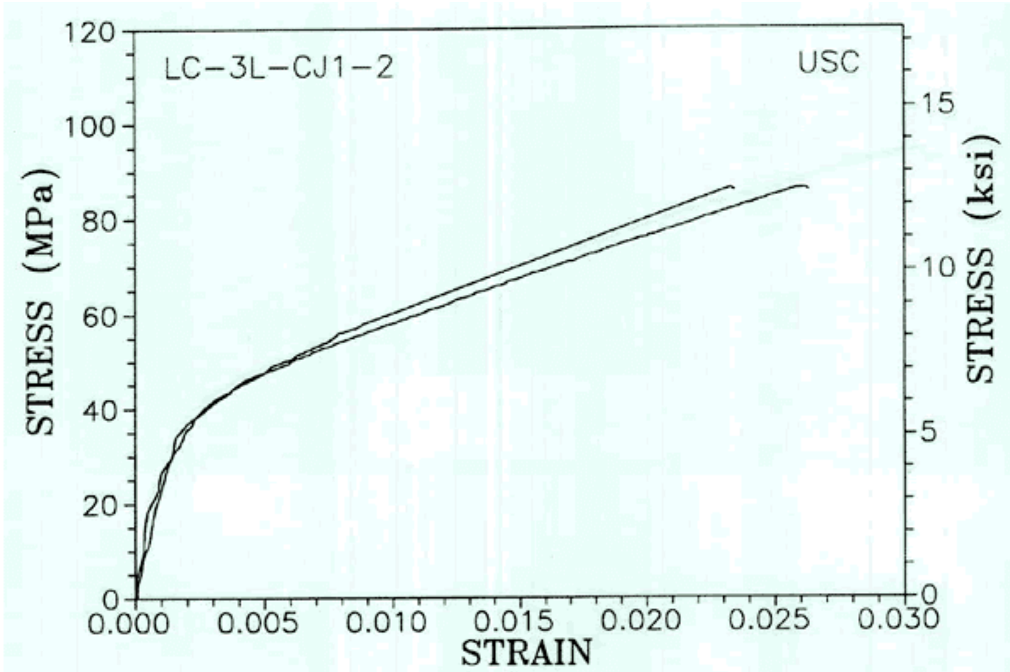

(a)

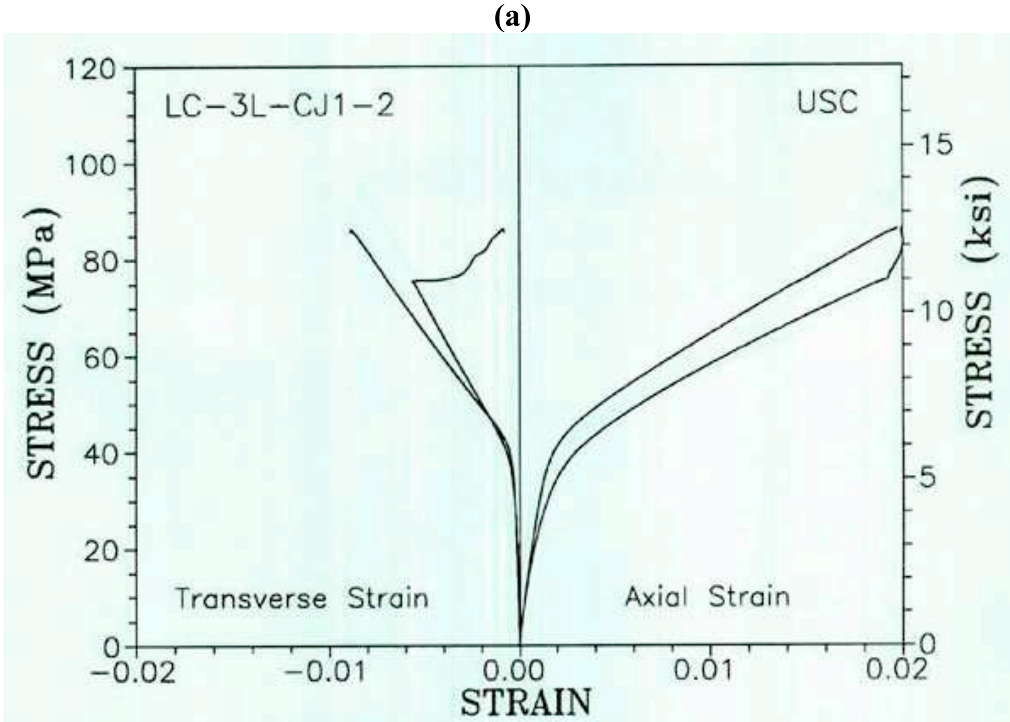

(b)

Fig A-B4.Stress-Strain Relationships for Lower Strength Concrete with Three-layer Carbon Fiber Composite Jacket (LC-3L-CJ1-2)
(a) Strain measured by LP (b) Strain measured by strain gages

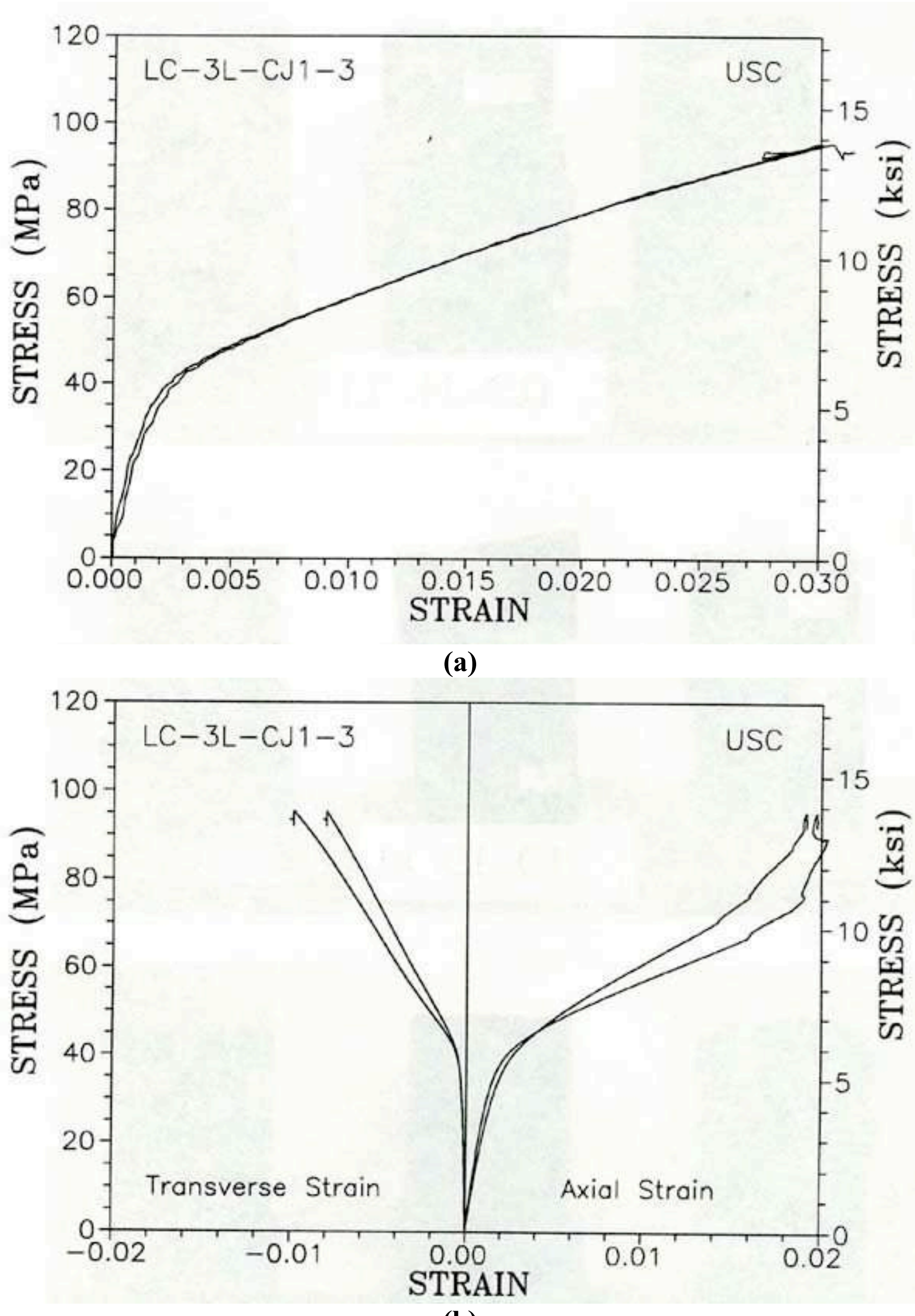

Fig A-B4.Stress-Strain Relationships for Lower Strength Concrete with Three-layer Carbon Fiber Composite Jacket (LC-3L-CJ1-3)
(a) Strain measured by LP (b) Strain measured by strain gages

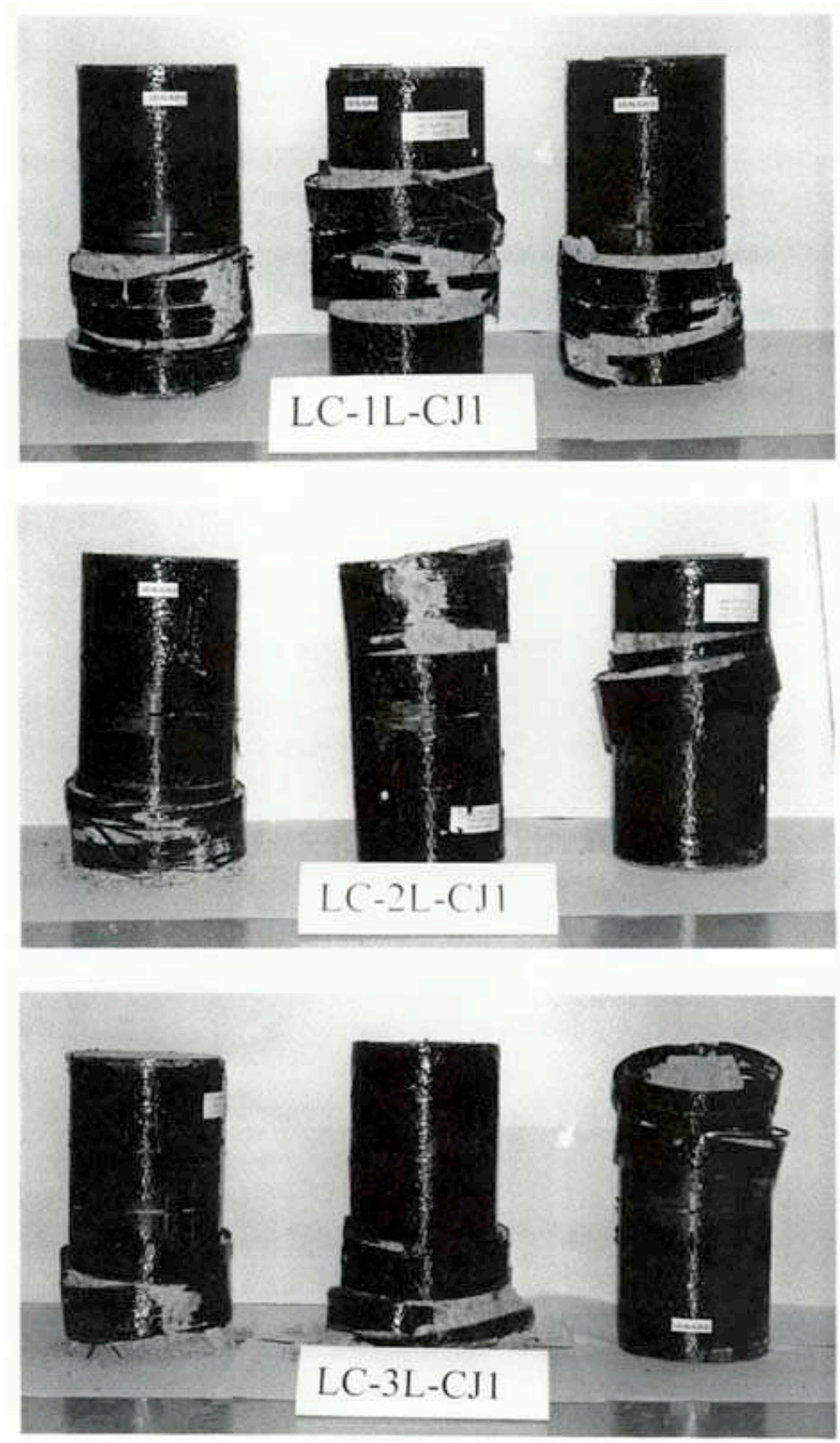

Fig.A-B5. Specimens after Testing

Part A-C Test Results of Medium Strength Concrete Cylinders

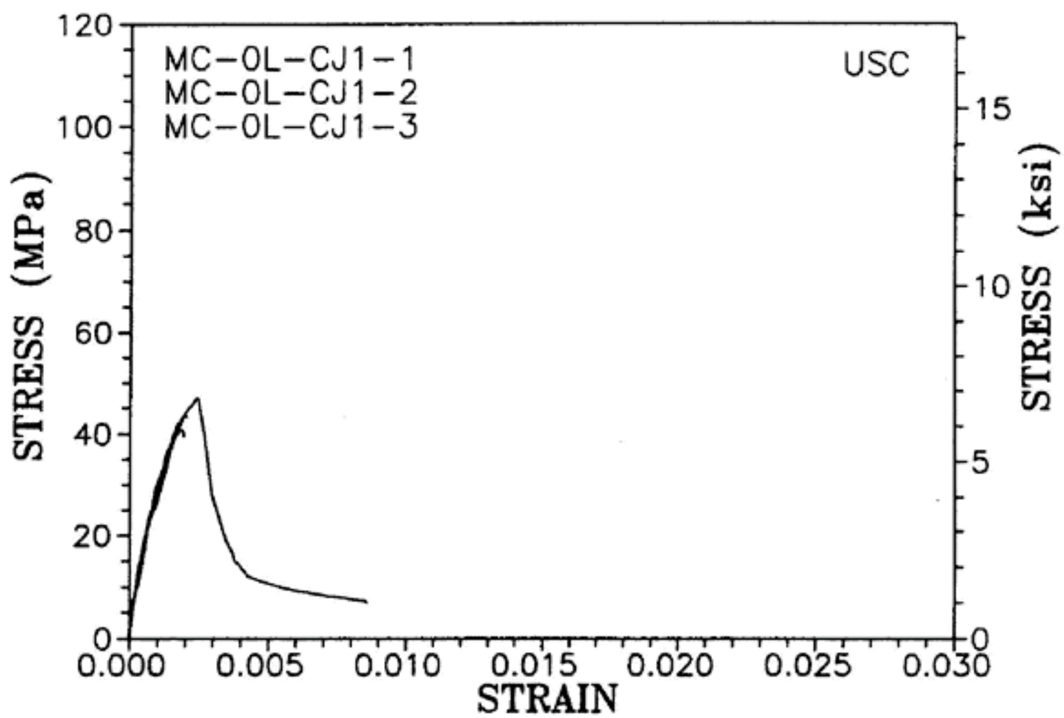

Fig.A-C1. Stress-Strain Relationship for Medium Strength Plain Concrete Cylinders

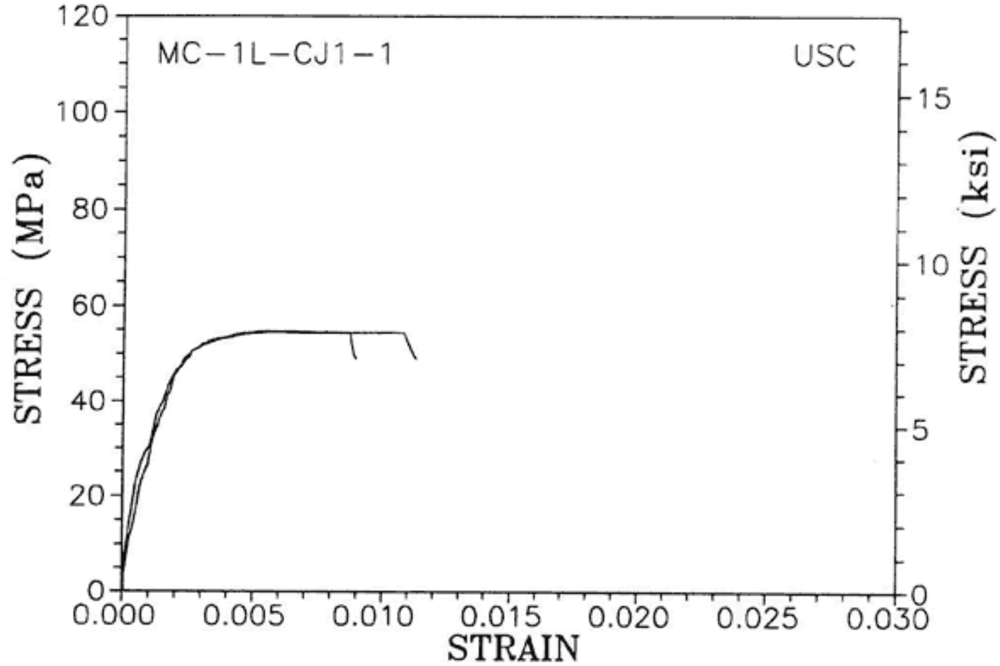

(a)

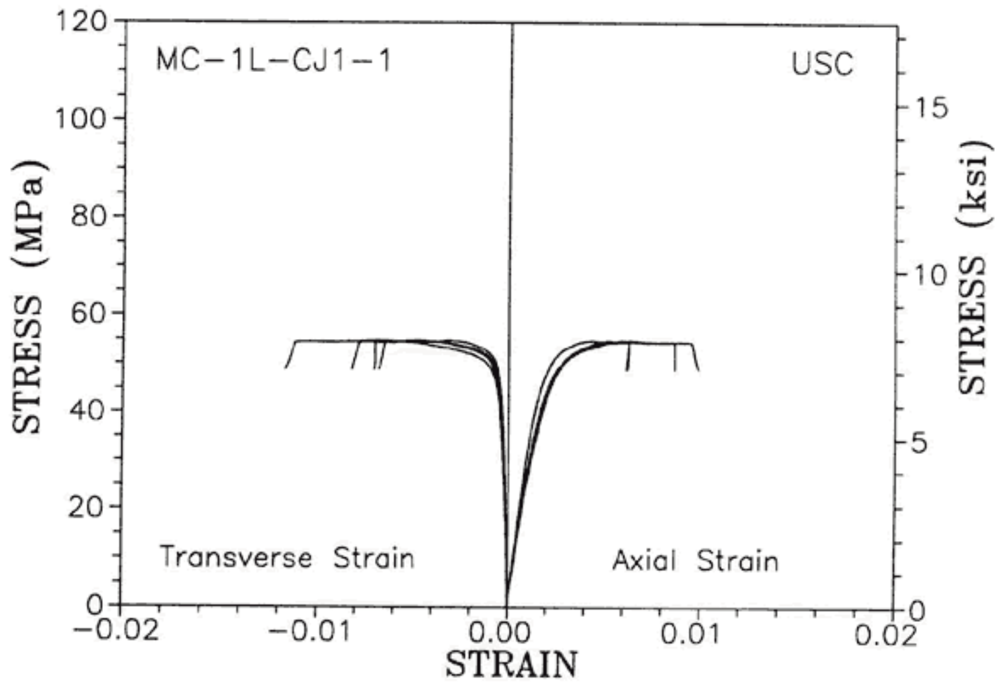

(b)

Fig A-C2.Stress-Strain Relationships for Medium Strength Concrete with One-layer Carbon Fiber Composite Jacket (MC-1L-CJ1-1)
(a) Strain measured by LP (b) Strain measured by strain gages

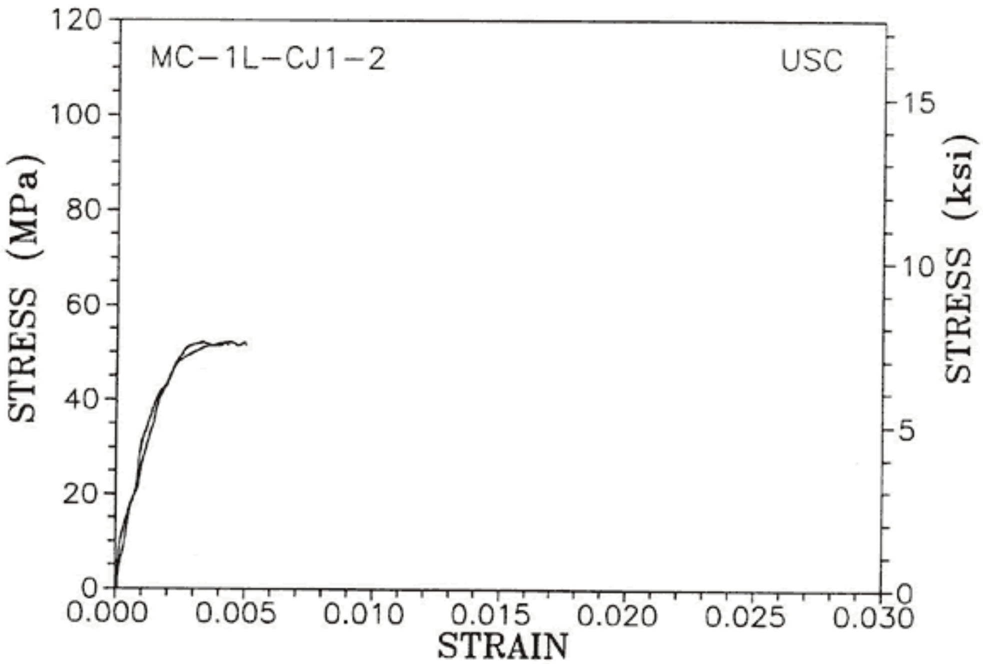

(a)

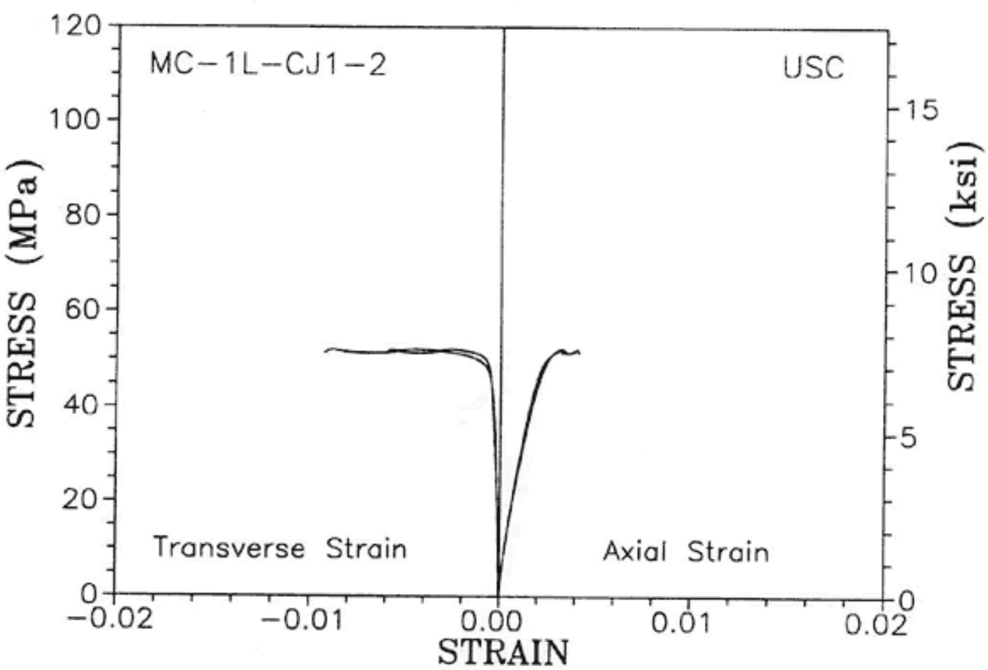

(b)

Fig A-C2.Stress-Strain Relationships for Medium Strength Concrete with One-layer Carbon Fiber Composite Jacket (MC-1L-CJ1-2)
(a) Strain measured by LP (b) Strain measured by strain gages

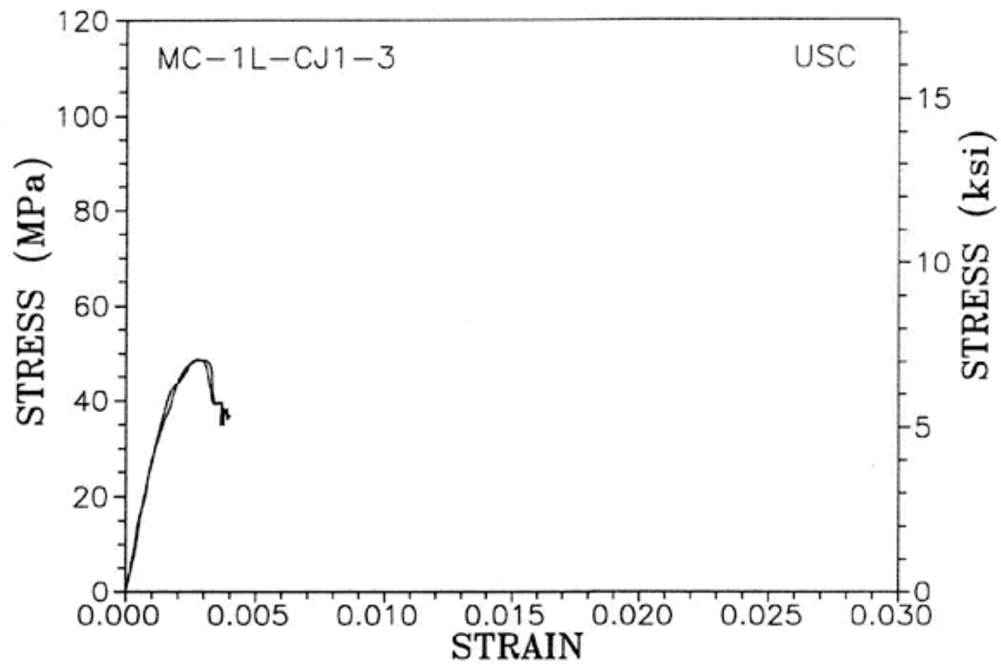

(a)

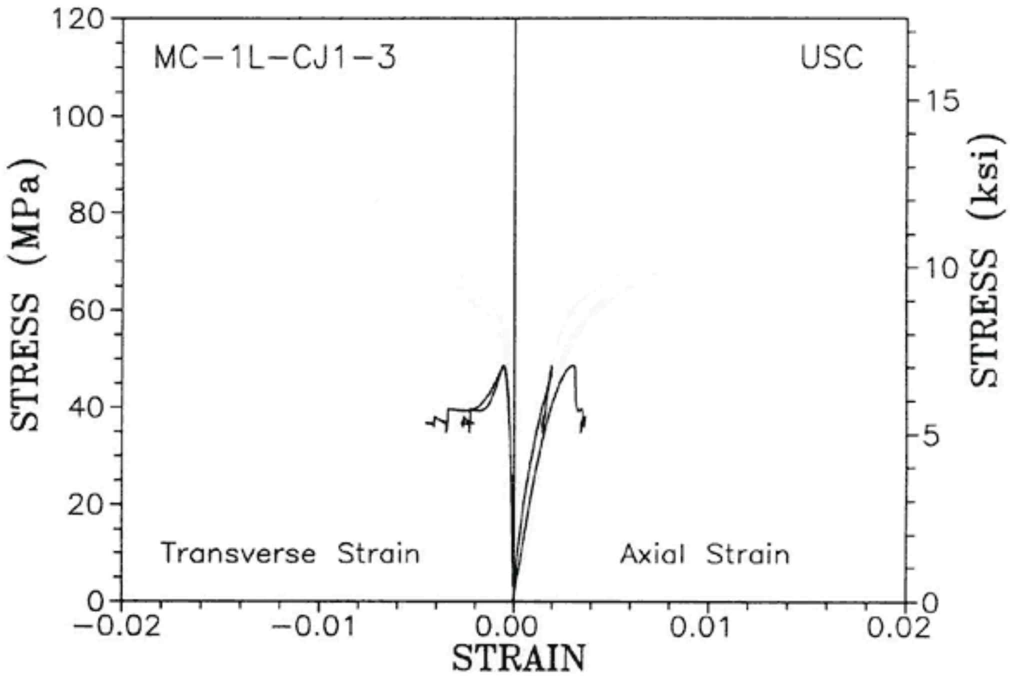

(b)

Fig A-C2.Stress-Strain Relationships for Medium Strength Concrete with One-layer Carbon Fiber Composite Jacket (MC-1L-CJ1-3)
(a) Strain measured by LP (b) Strain measured by strain gages

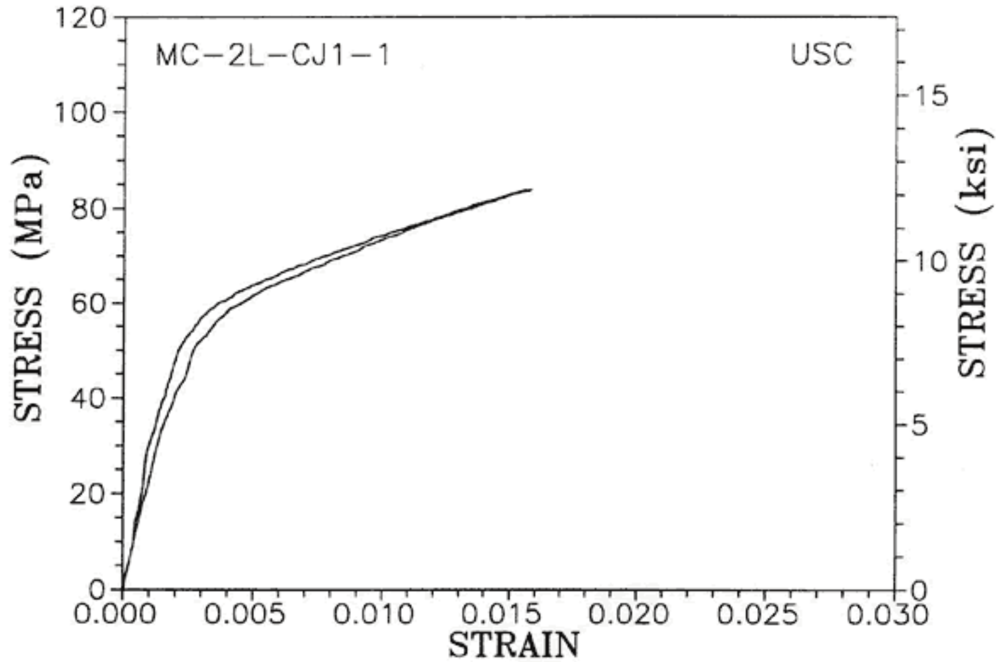

(a)

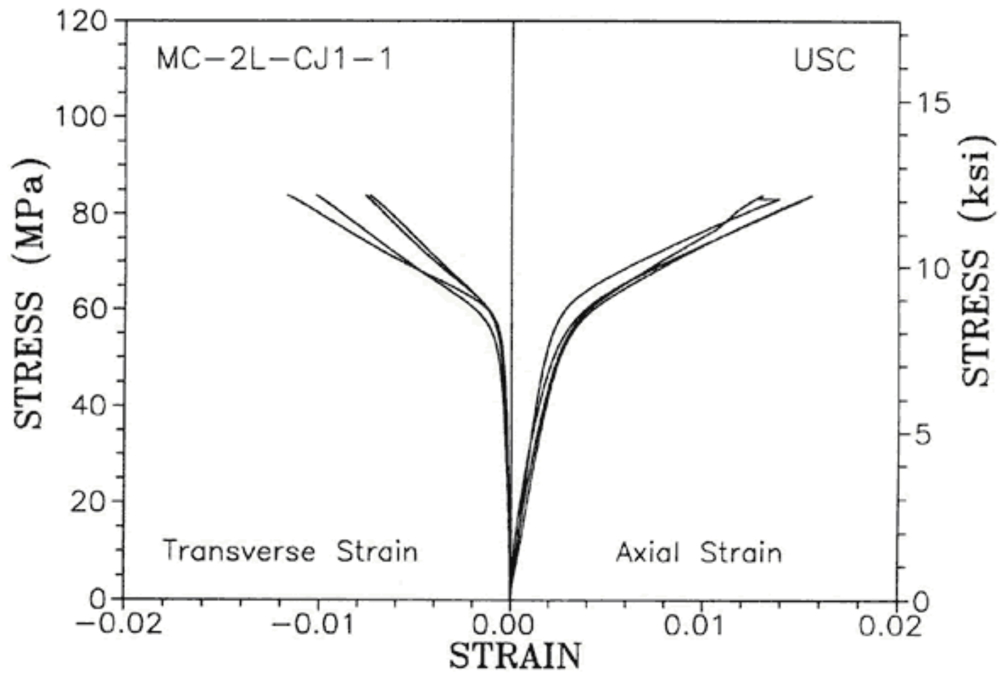

(b)

Fig A-C3.Stress-Strain Relationships for Medium Strength Concrete with Two-layer Carbon Fiber Composite Jacket (MC-2L-CJ1-1)
(a) Strain measured by LP (b) Strain measured by strain gages

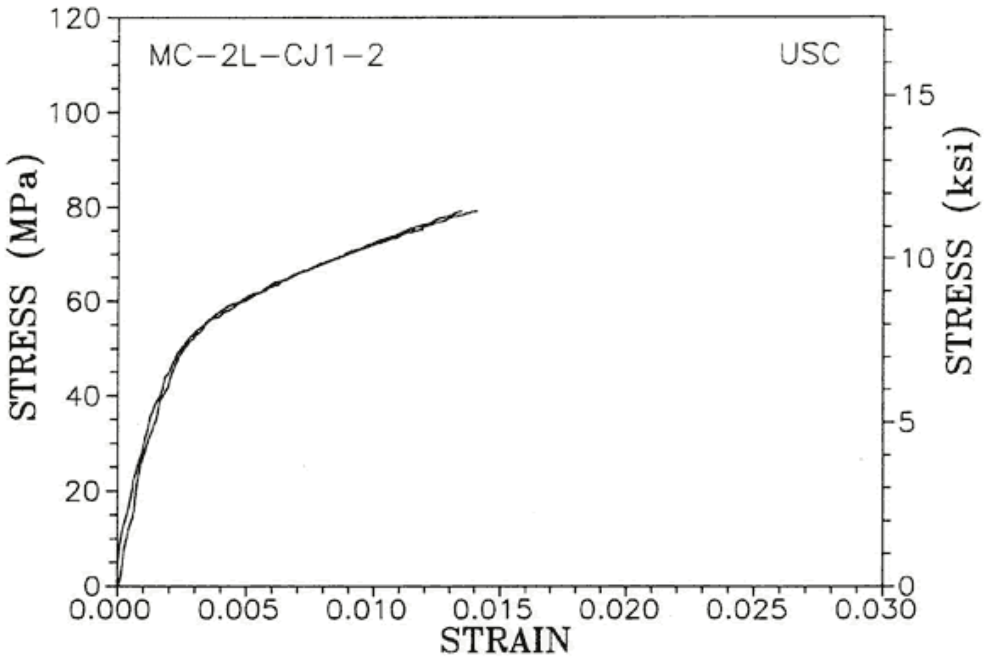

(a)

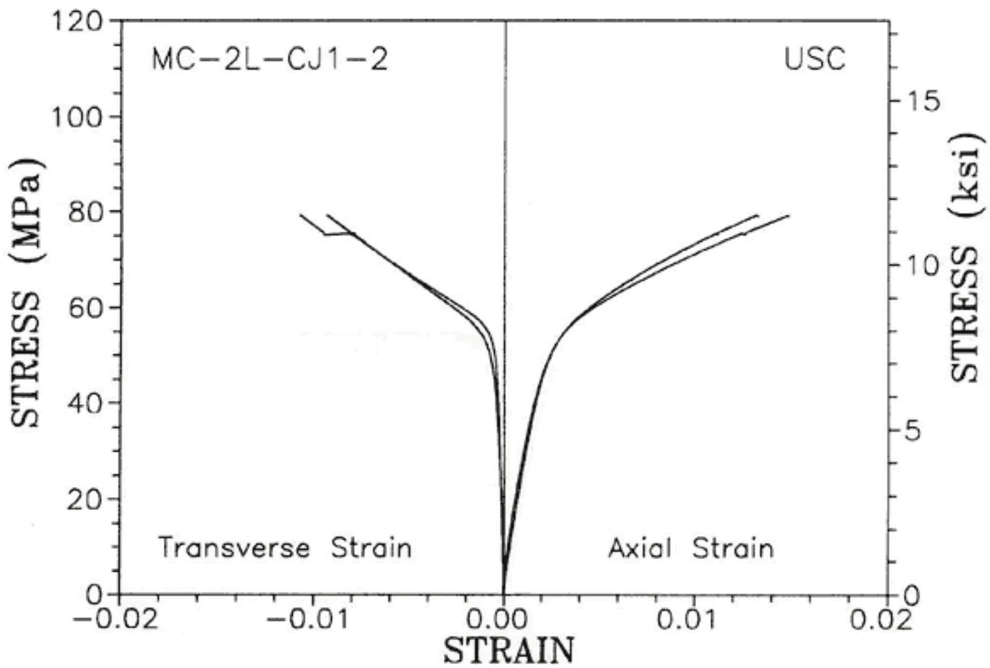

(b)

Fig A-C3.Stress-Strain Relationships for Medium Strength Concrete with Two-layer Carbon Fiber Composite Jacket (MC-2L-CJ1-2)
(a) Strain measured by LP (b) Strain measured by strain gages

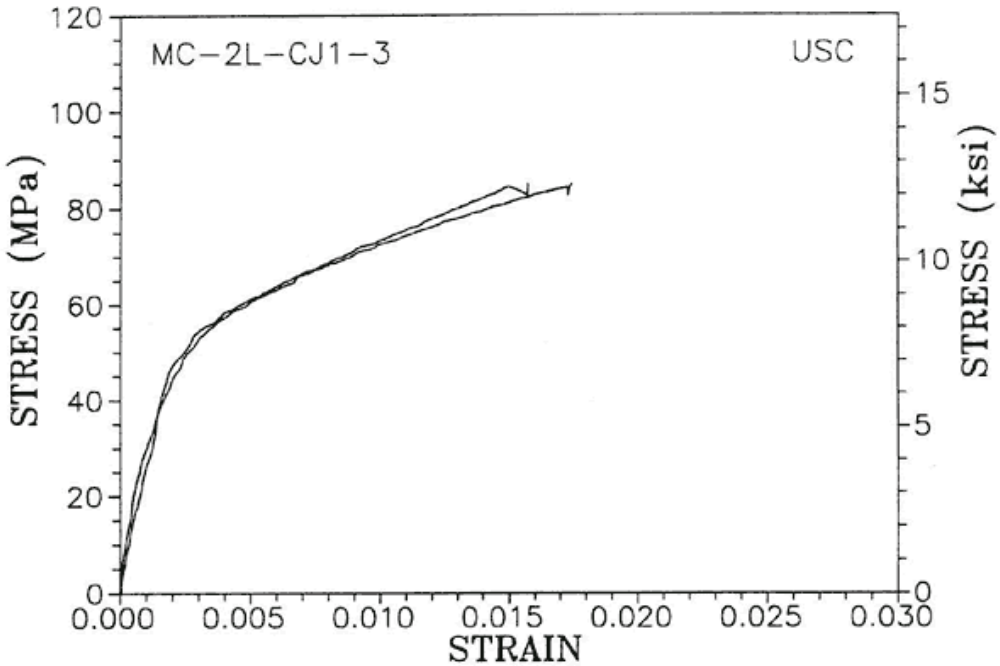

(a)

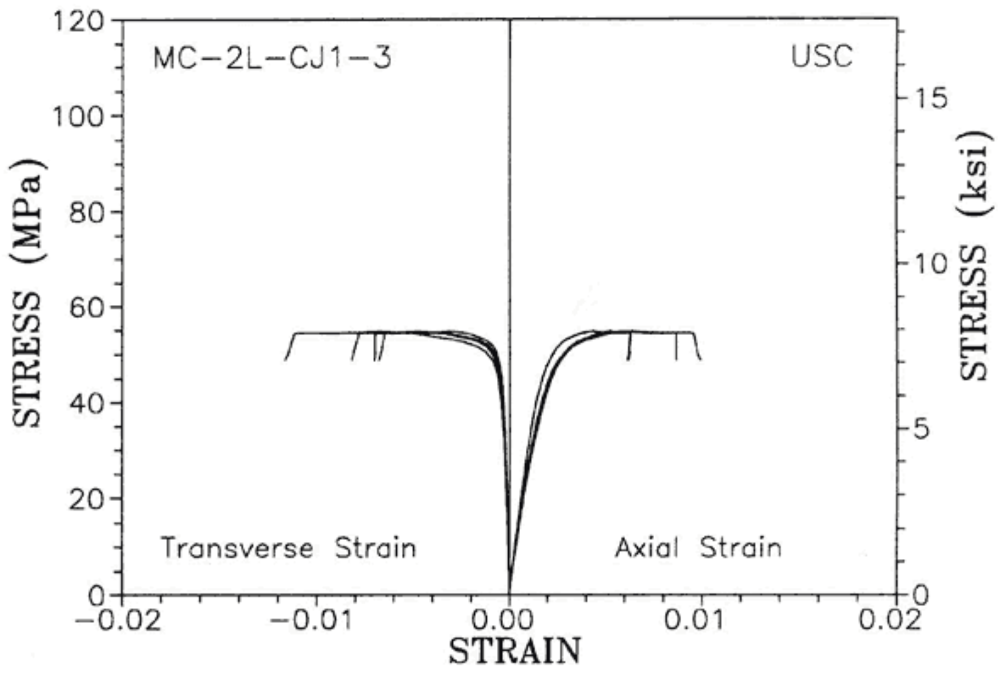

(b)

Fig A-C3.Stress-Strain Relationships for Medium Strength Concrete with Two-layer Carbon Fiber Composite Jacket (MC-2L-CJ1-3)
(a) Strain measured by LP (b) Strain measured by strain gages

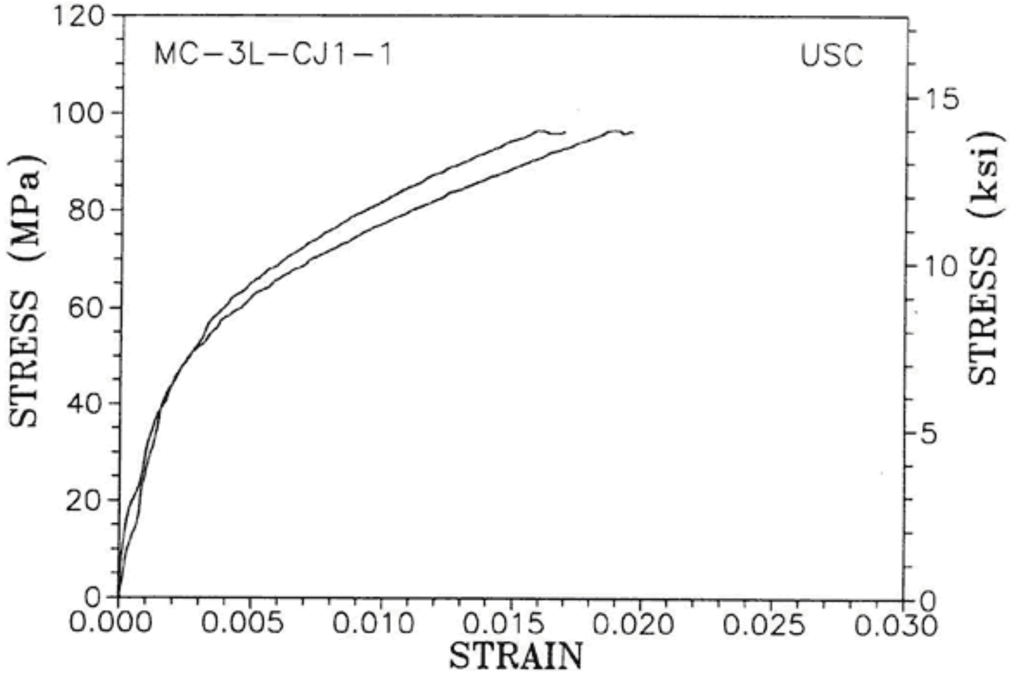

(a)

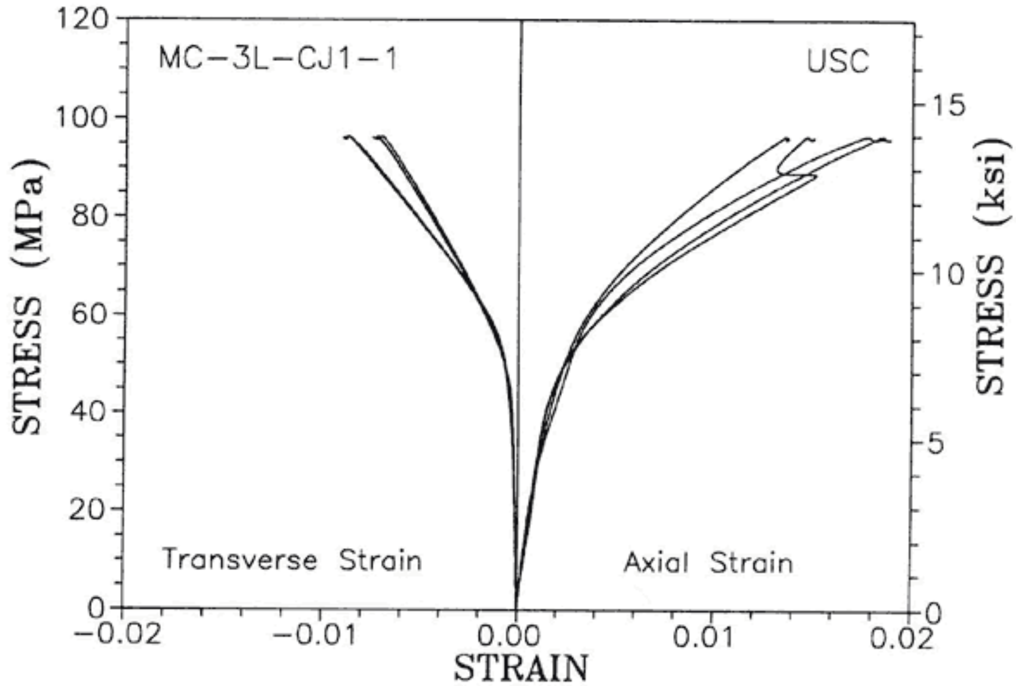

(b)

Fig A-C4.Stress-Strain Relationships for Medium Strength Concrete with Three-layer Carbon Fiber Composite Jacket (MC-3L-CJ1-1)
(a) Strain measured by LP (b) Strain measured by strain gages

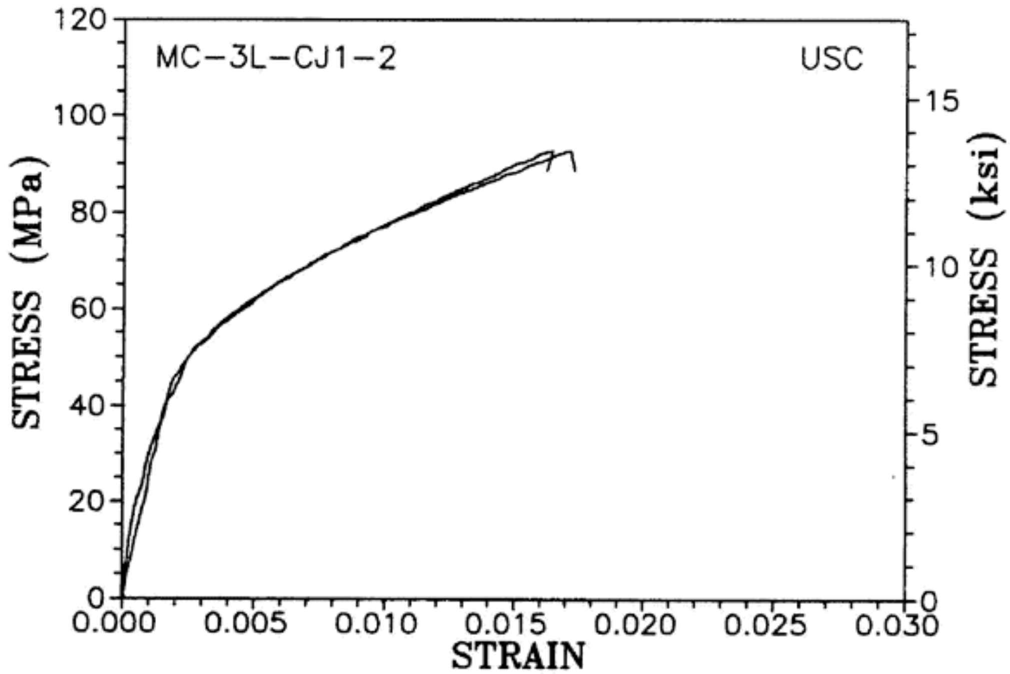

(a)

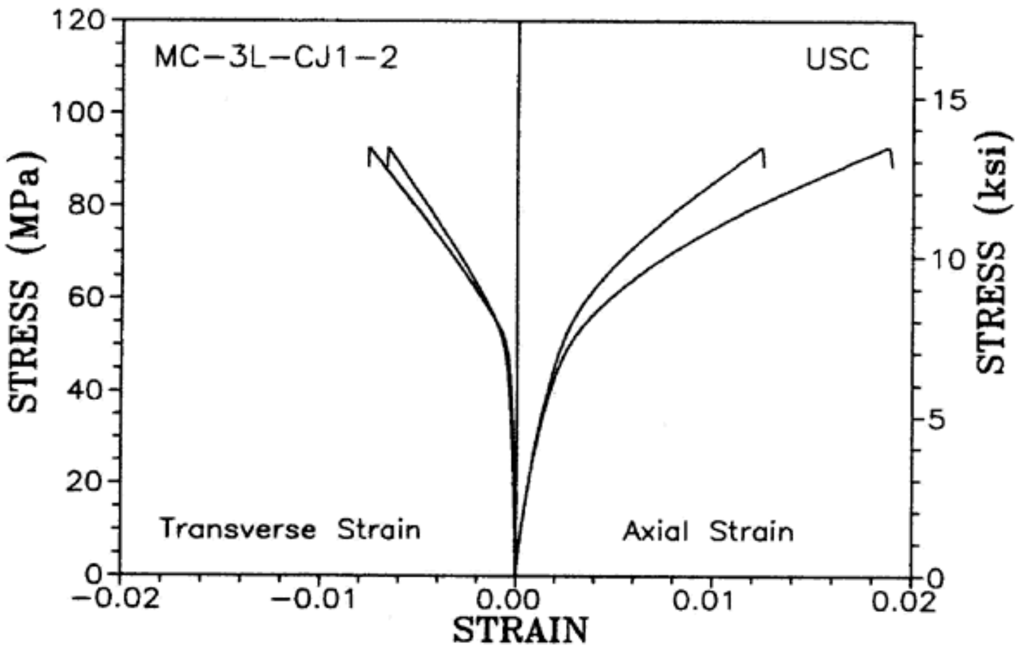

(b)

Fig A-C4.Stress-Strain Relationships for Medium Strength Concrete with Three-layer Carbon Fiber Composite Jacket (MC-3L-CJ1-2)
(a) Strain measured by LP (b) Strain measured by strain gages

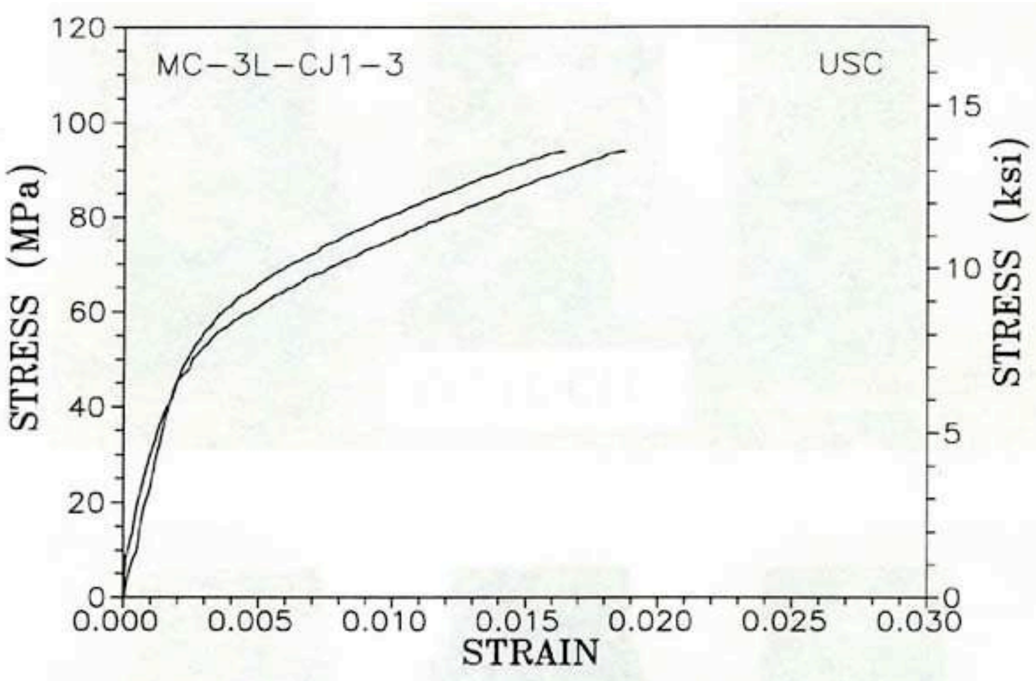

(a)

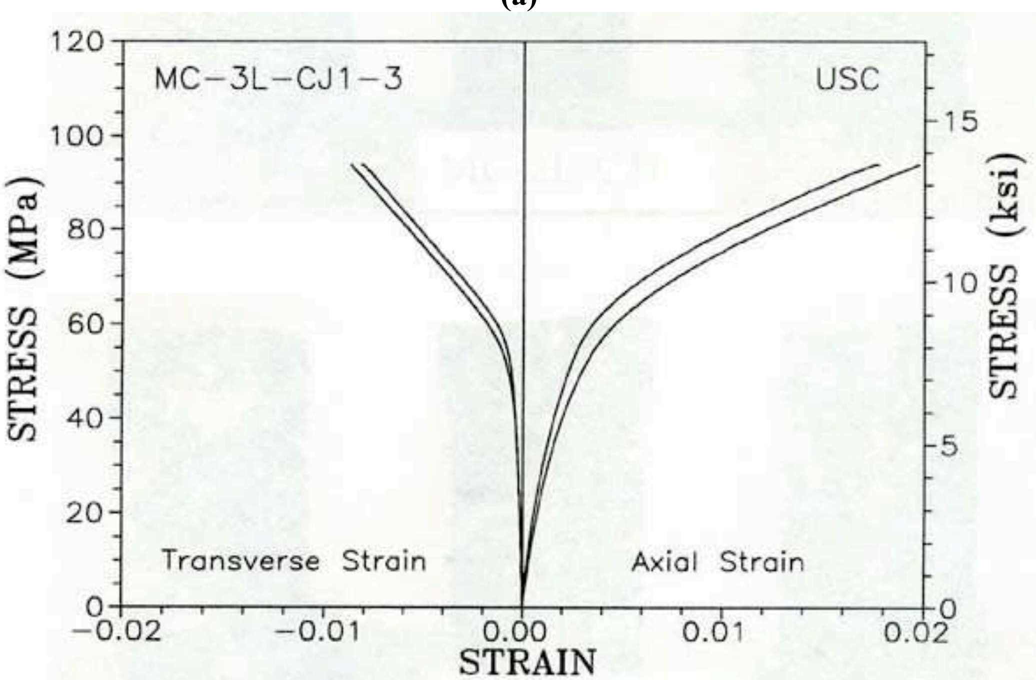

(b)

Fig A-C4.Stress-Strain Relationships for Medium Strength Concrete with Three-layer Carbon Fiber Composite Jacket (MC-3L-CJ1-3)
(a) Strain measured by LP (b) Strain measured by strain gages

Part A-D Test Results of Higher Strength Concrete Cylinders

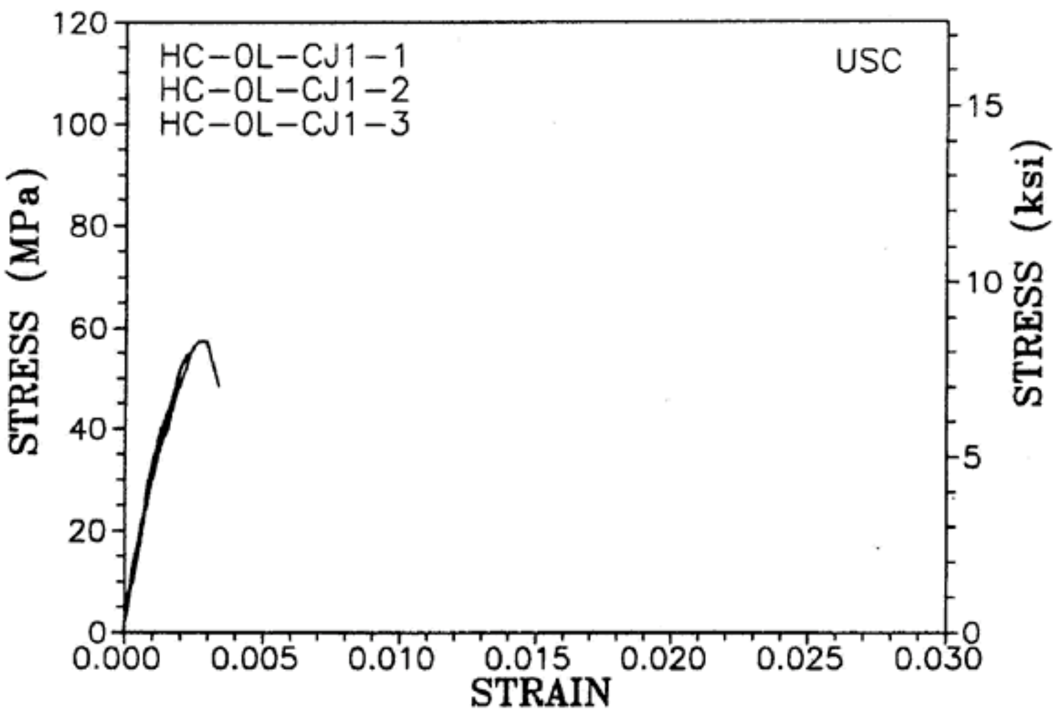

Fig.A-D1. Stress-Strain Relationship for Higher Strength Plain Concrete Cylinders

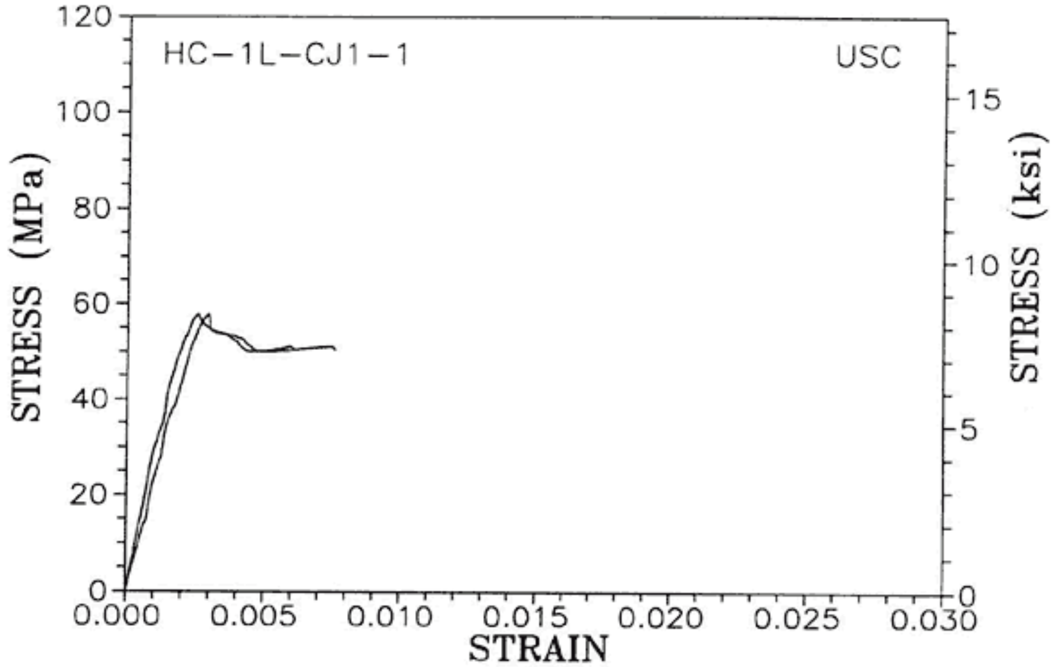

(a)

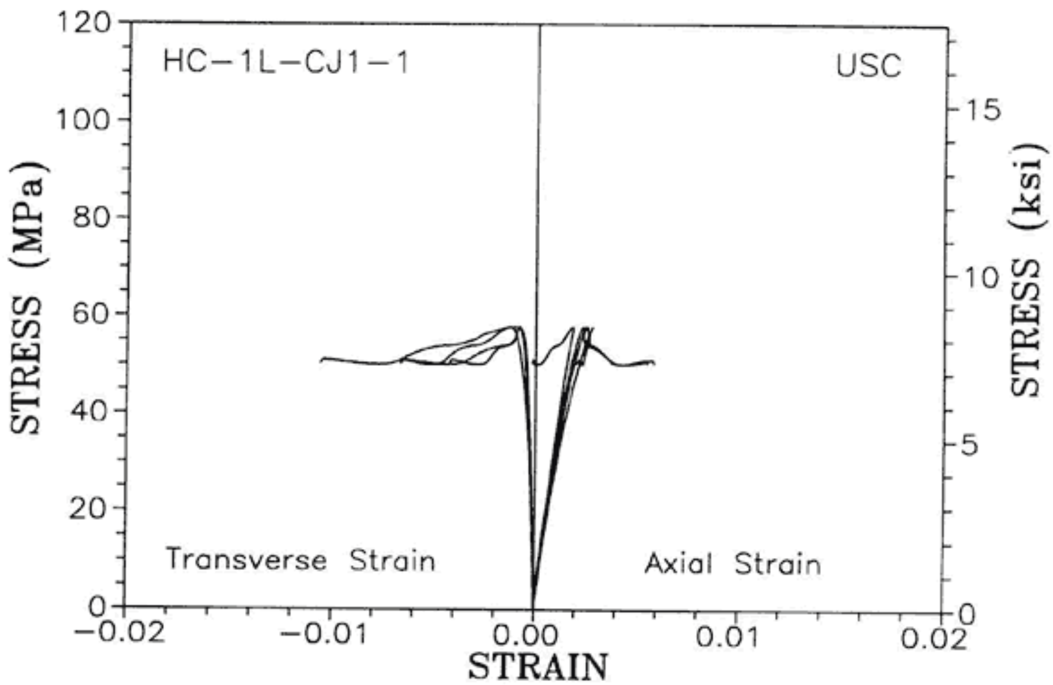

(b)

Fig A-D2.Stress-Strain Relationships for Higher Strength Concrete with One-layer Carbon Fiber Composite Jacket (HC-1L-CJ1-1)
(a) Strain measured by LP (b) Strain measured by strain gages

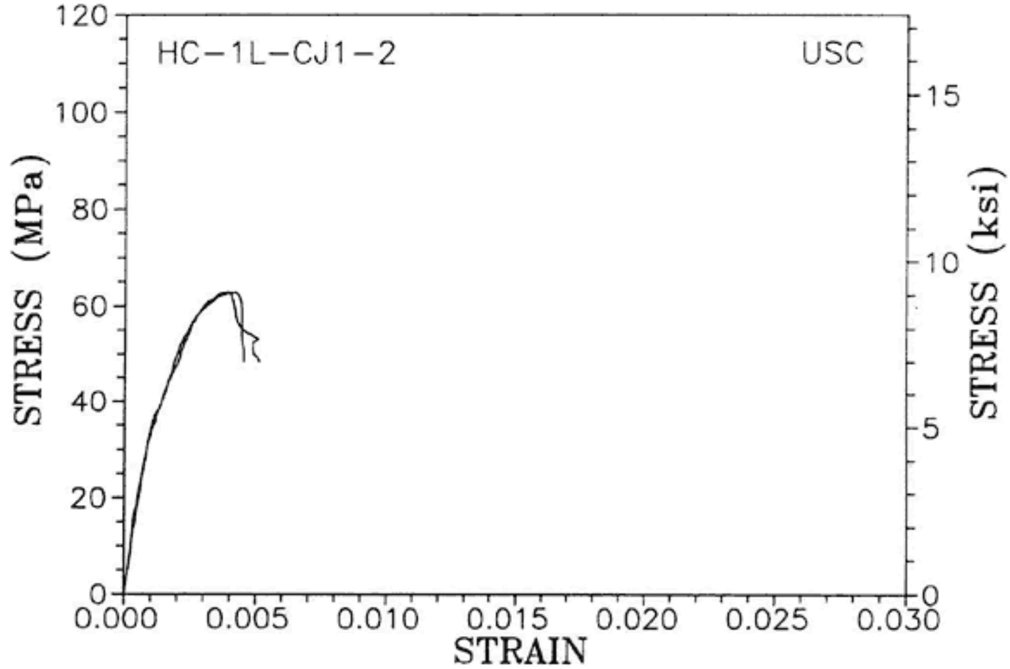

(a)

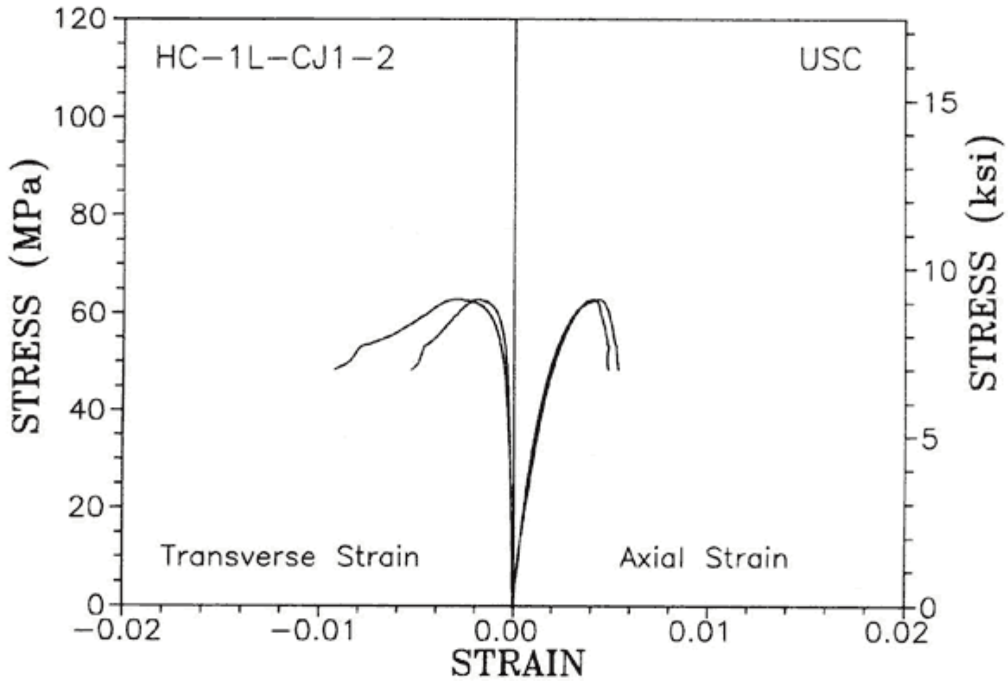

(b)

Fig A-D2.Stress-Strain Relationships for Higher Strength Concrete with One-layer Carbon Fiber Composite Jacket (HC-1L-CJ1-2)
(a) Strain measured by LP (b) Strain measured by strain gages

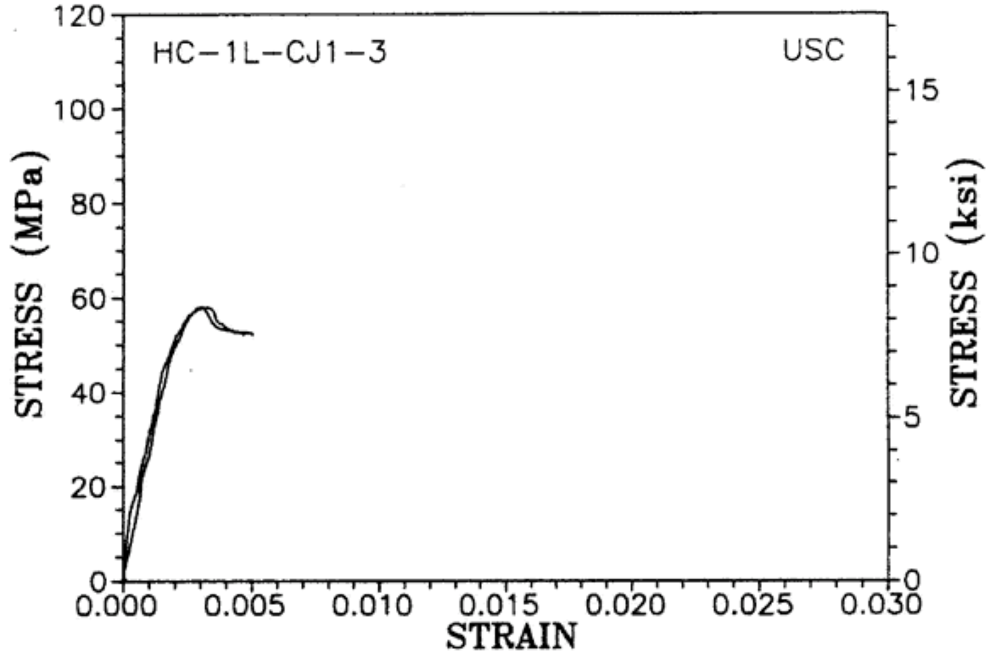

(a)

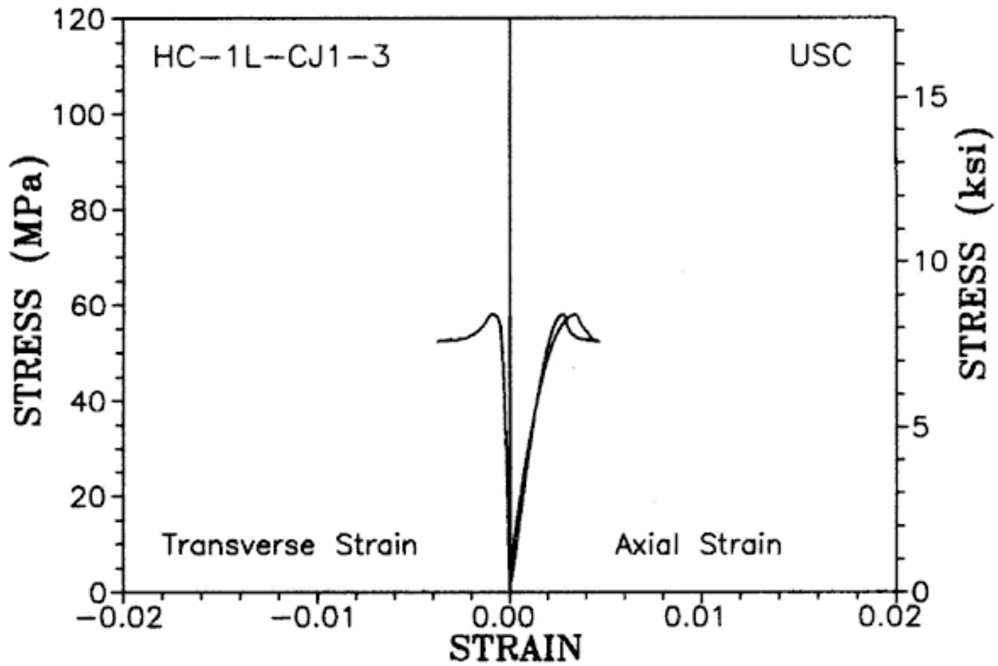

(b)

Fig A-D2.Stress-Strain Relationships for Higher Strength Concrete with One-layer Carbon Fiber Composite Jacket (HC-1L-CJ1-3)
(a) Strain measured by LP (b) Strain measured by strain gages

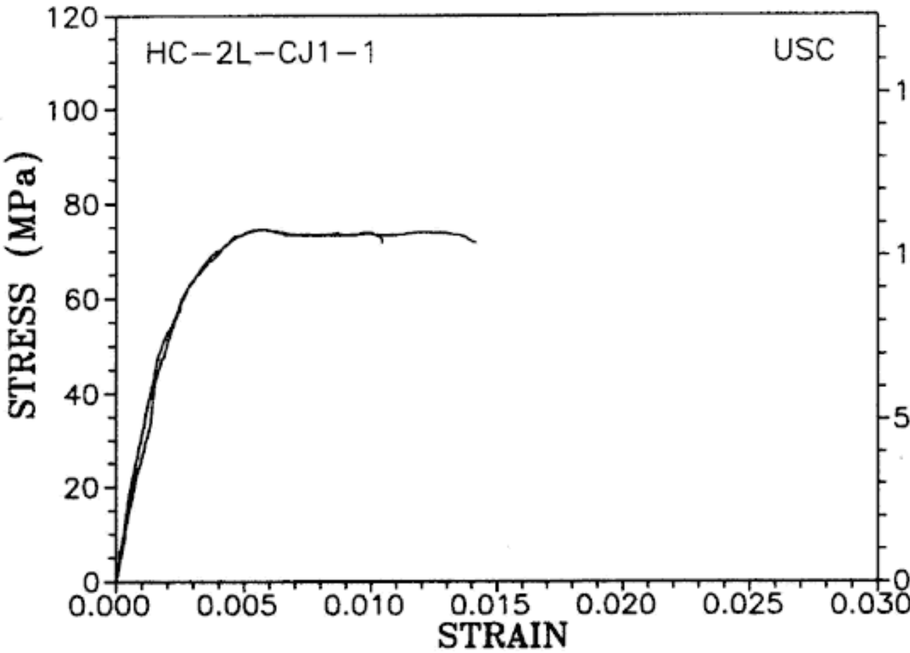

(a)

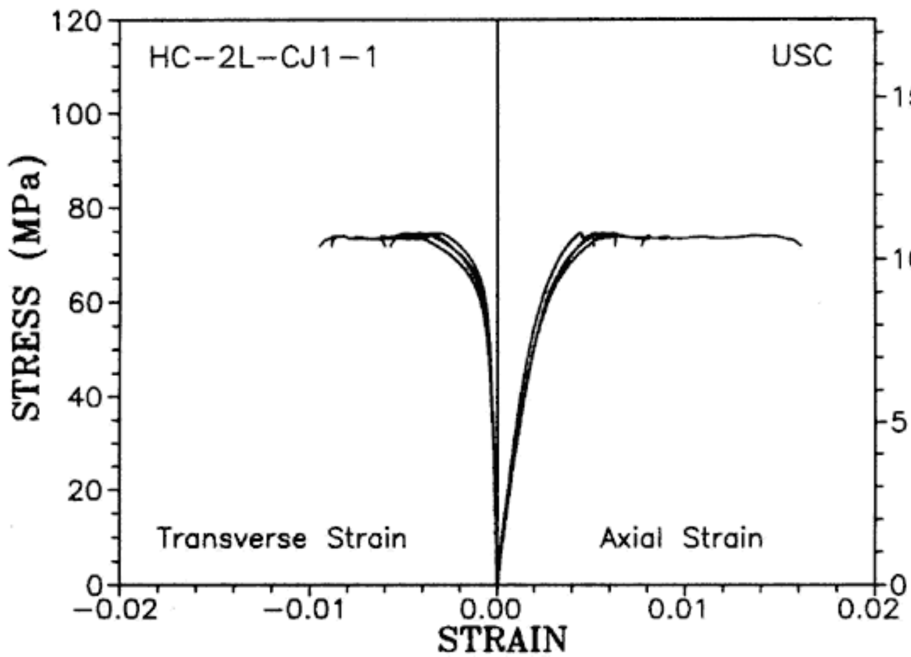

(b)

Fig A-D3.Stress-Strain Relationships for Higher Strength Concrete with Two-layer Carbon Fiber Composite Jacket (HC-2L-CJ1-1)
(a) Strain measured by LP (b) Strain measured by strain gages

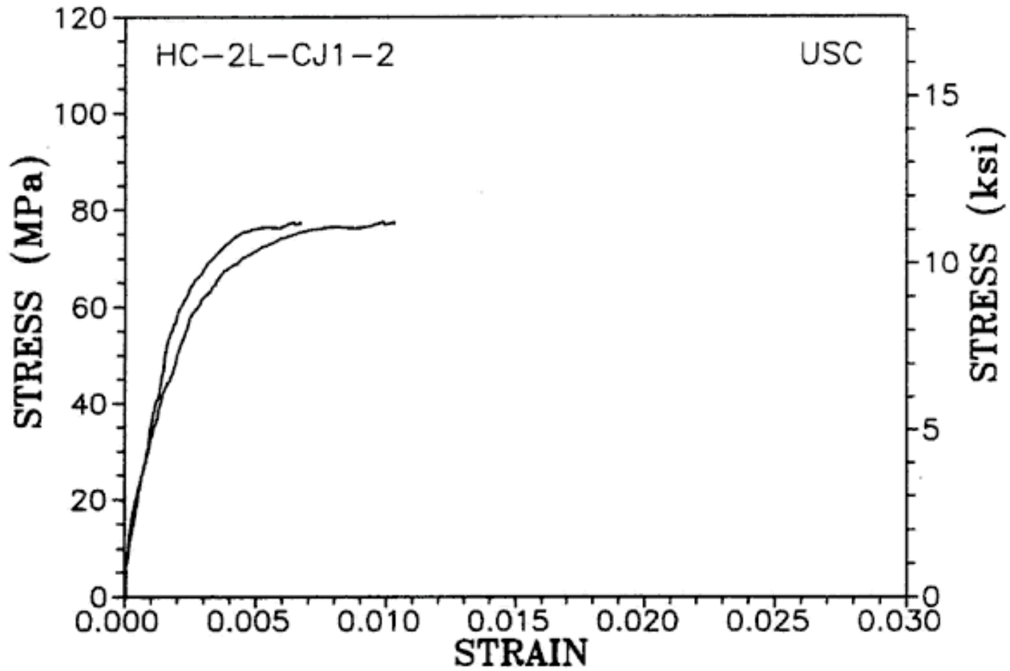

(a)

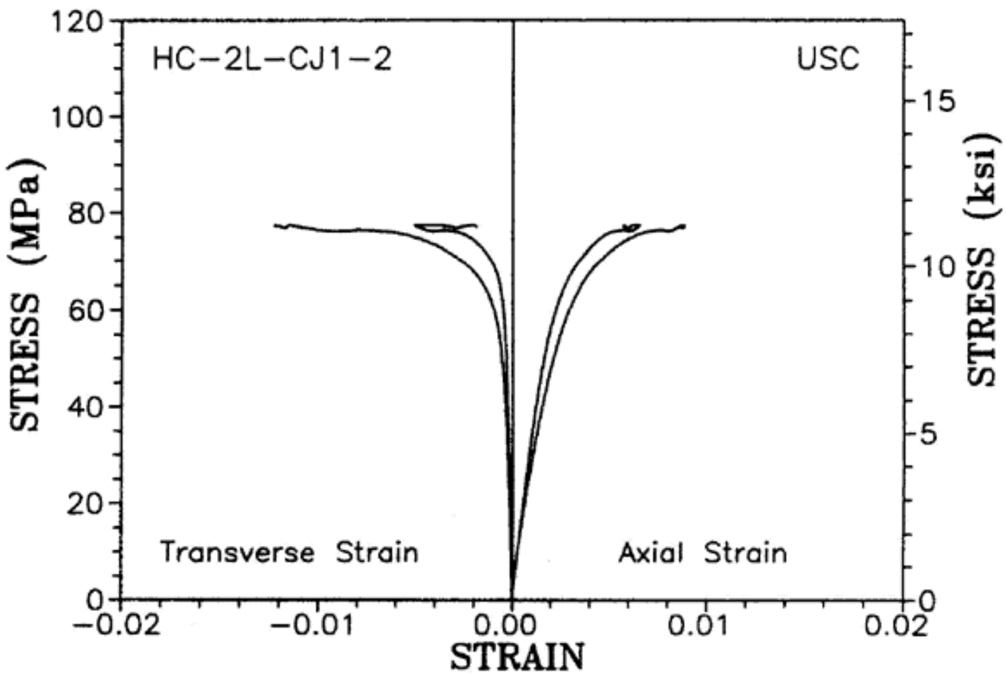

(b)

Fig A-D3.Stress-Strain Relationships for Higher Strength Concrete with Two-layer Carbon Fiber Composite Jacket (HC-2L-CJ1-2)
(a) Strain measured by LP (b) Strain measured by strain gages

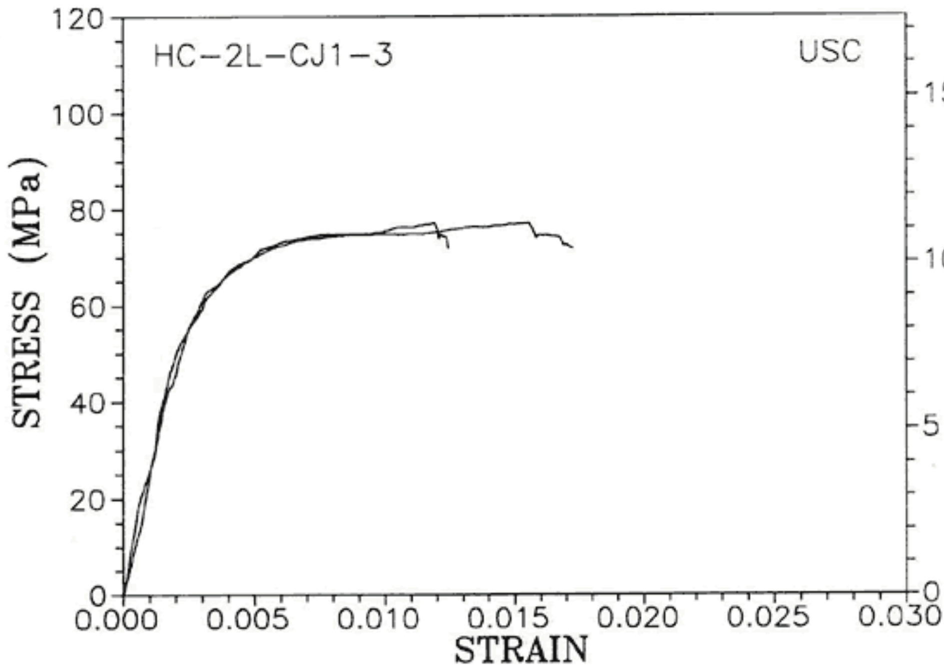

(a)

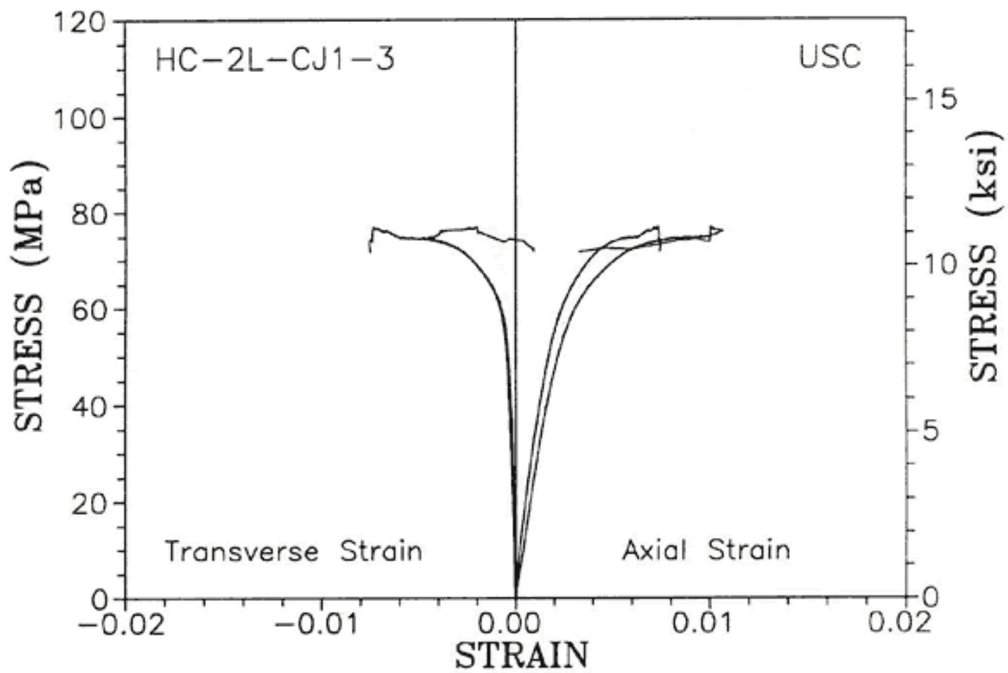

(b)

Fig A-D3.Stress-Strain Relationships for Higher Strength Concrete with Two-layer Carbon Fiber Composite Jacket (HC-2L-CJ1-3)
(a) Strain measured by LP (b) Strain measured by strain gages

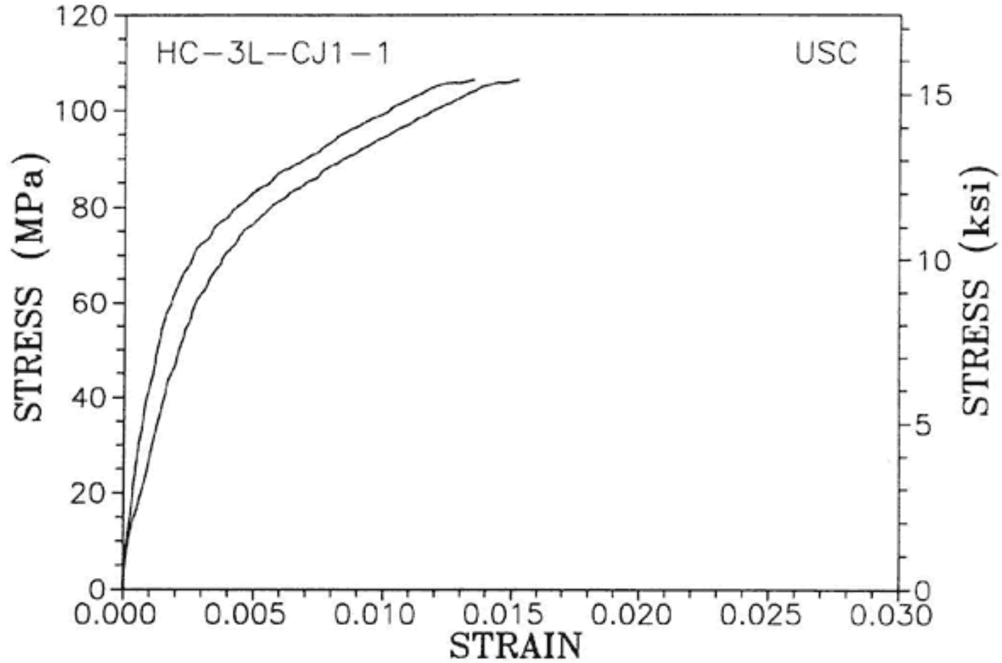

(a)

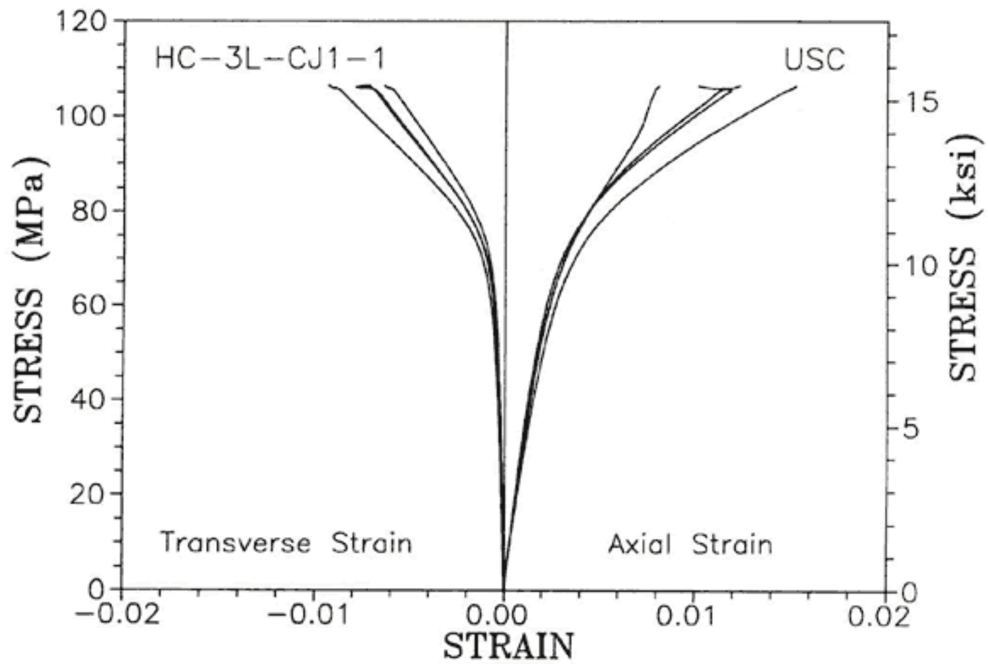

(b)

Fig A-D4.Stress-Strain Relationships for Higher Strength Concrete with Three-layer Carbon Fiber Composite Jacket (HC-3L-CJ1-1)
(a) Strain measured by LP (b) Strain measured by strain gages

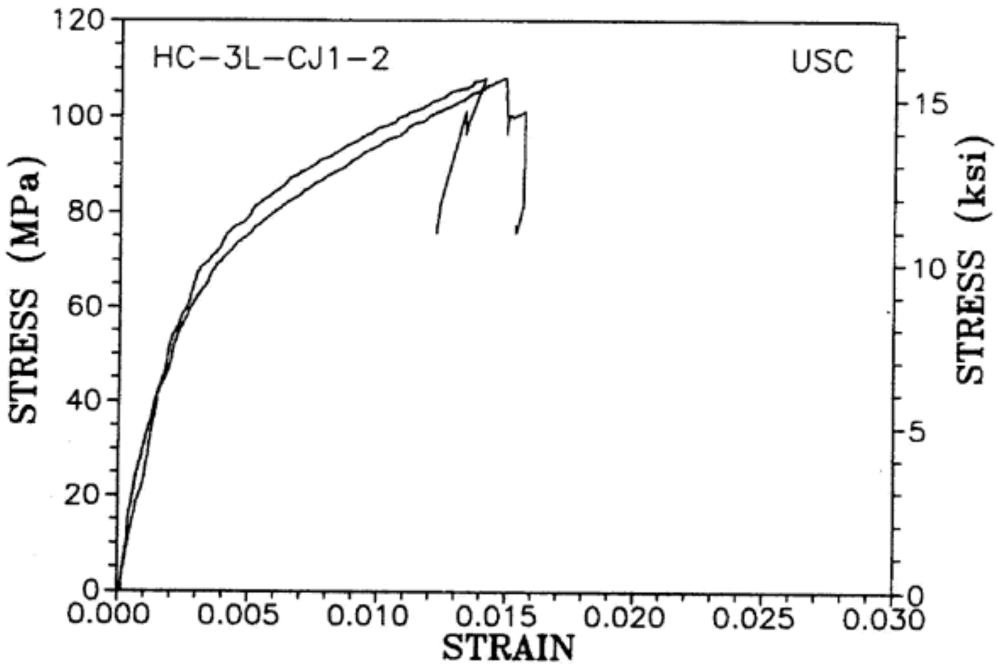

(a)

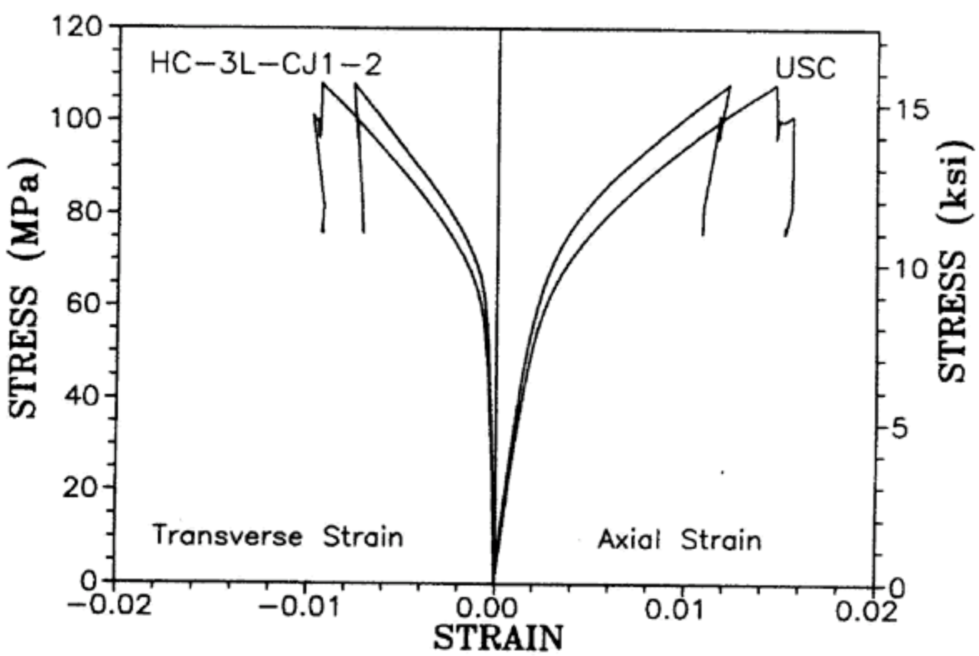

(b)

Fig A-D4.Stress-Strain Relationships for Higher Strength Concrete with Three-layer Carbon Fiber Composite Jacket (HC-3L-CJ1-2)
(a) Strain measured by LP (b) Strain measured by strain gages

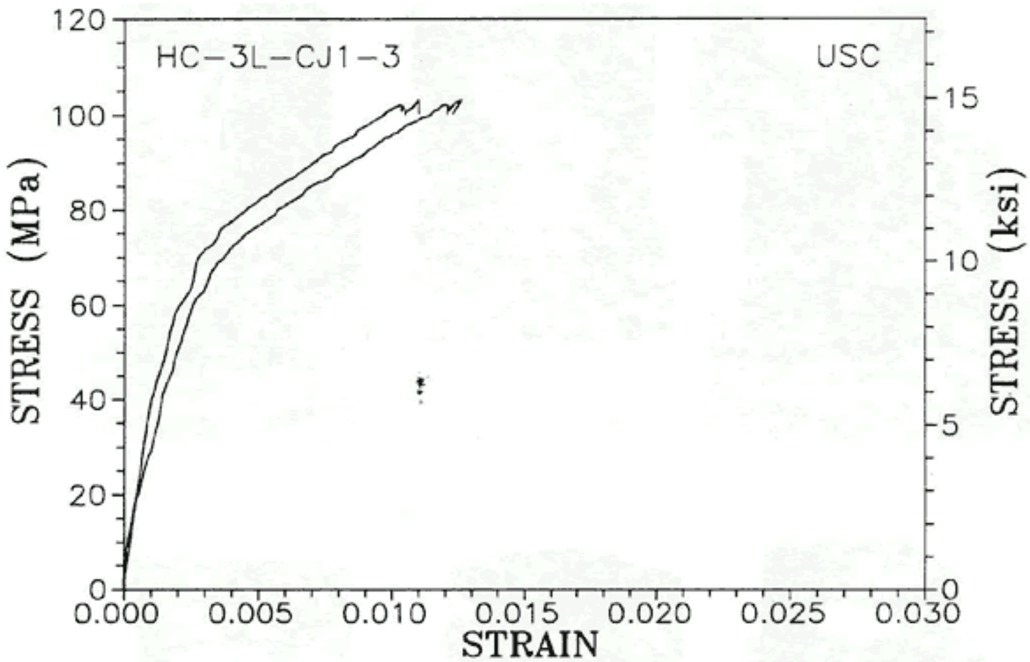

(a)

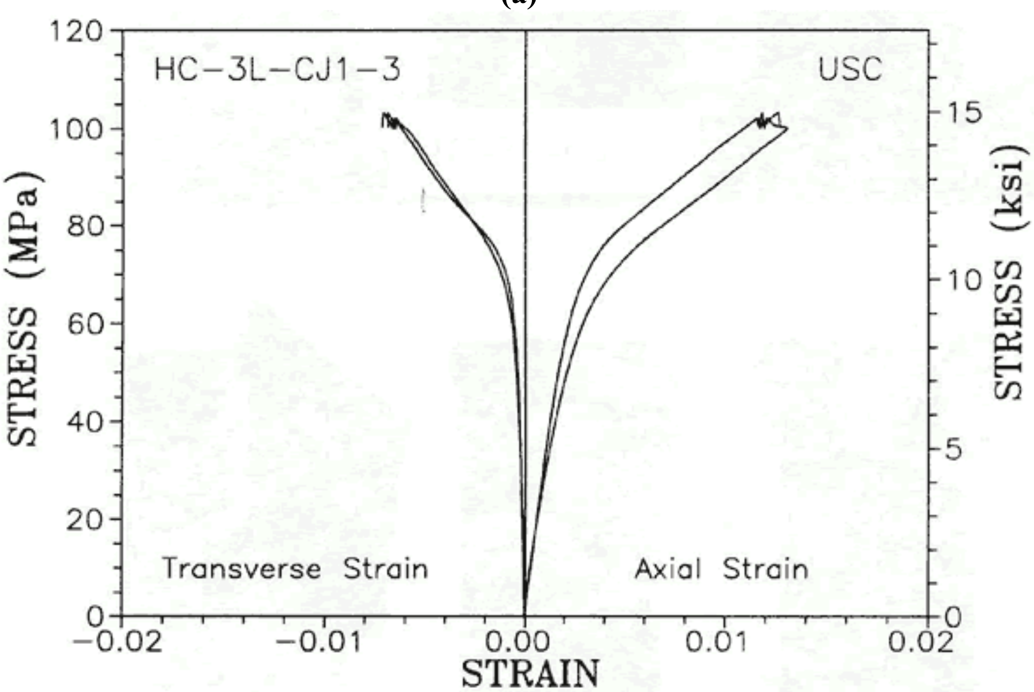

(b)

Fig A-D4.Stress-Strain Relationships for Higher Strength Concrete with Three-layer Carbon Fiber Composite Jacket (HC-3L-CJ1-3)
(a) Strain measured by LP (b) Strain measured by strain gages

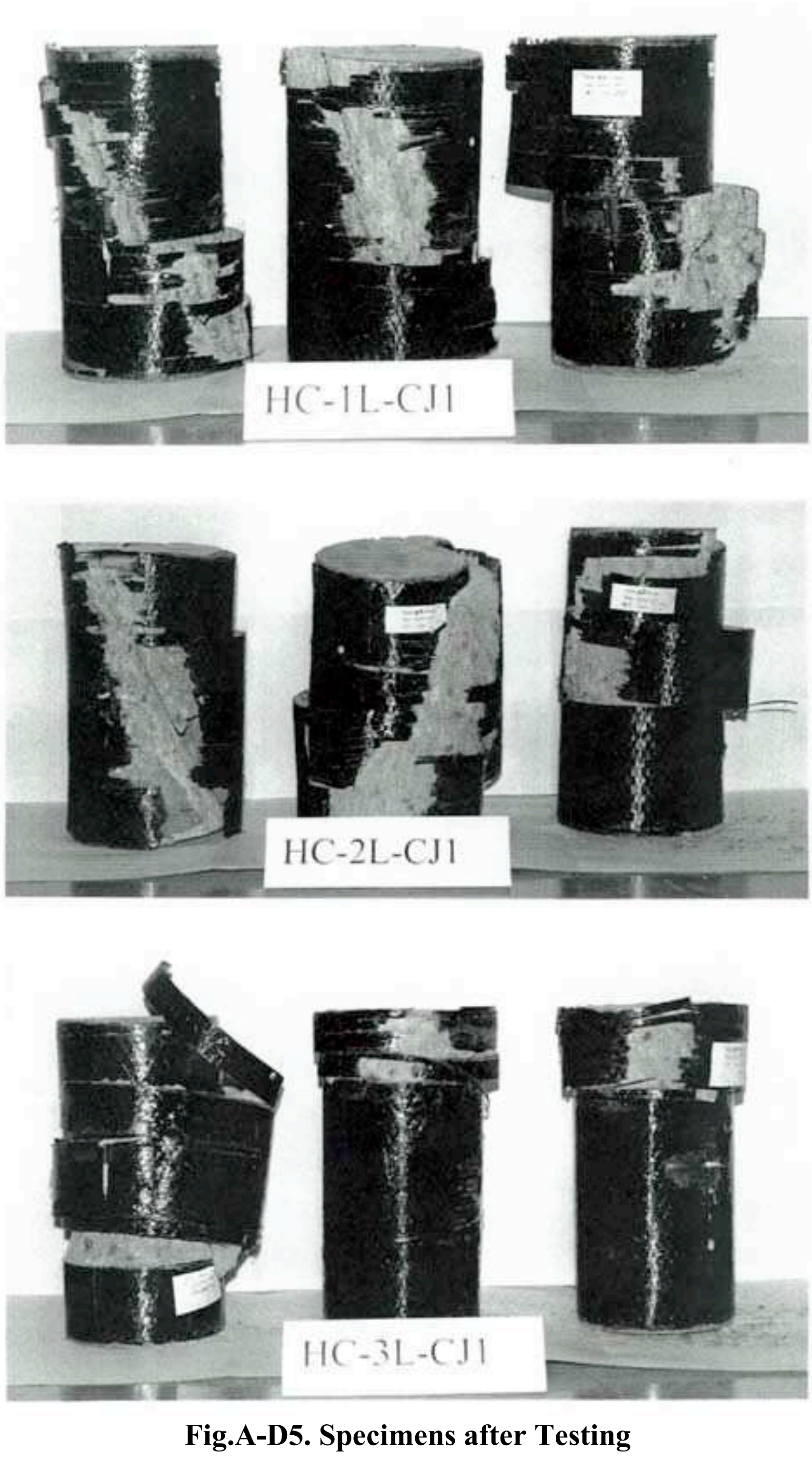

Fig.A-D5. Specimens after Testing

APPENDIX B: TEST RESULTS OF SYSTEM TWO

Part B-A General Information

Table B-A1 Test Matrix

Type of Jacket	Concrete Strength	Jacket Layers	Specimen Numbers
Carbon fiber sheet reinforced composite jacket	Lower	Plain concrete	3 specimens each
		0.5-layer	
		1-layer	
		1.5-layer	
	Medium	Plain concrete	
		0.5-layer	
		1-layer	
		1.5-layer	
	Higher	Plain concrete	
		0.5-layer	
		1-layer	
		1.5-layer	

Table B-A2 Mix Proportion of Concrete

Series	Target f'_{co} (MPa)	W/C	Water (kg/m^3)	Cement (kg/m^3)	Fine Aggregates (kg/m^3)	Coarse Aggregates (kg/m^3)
L	27.6	0.68	196	288	1087	853
M	37.9	0.48	196	408	986	853
H	48.2	0.38	197	515	857	853

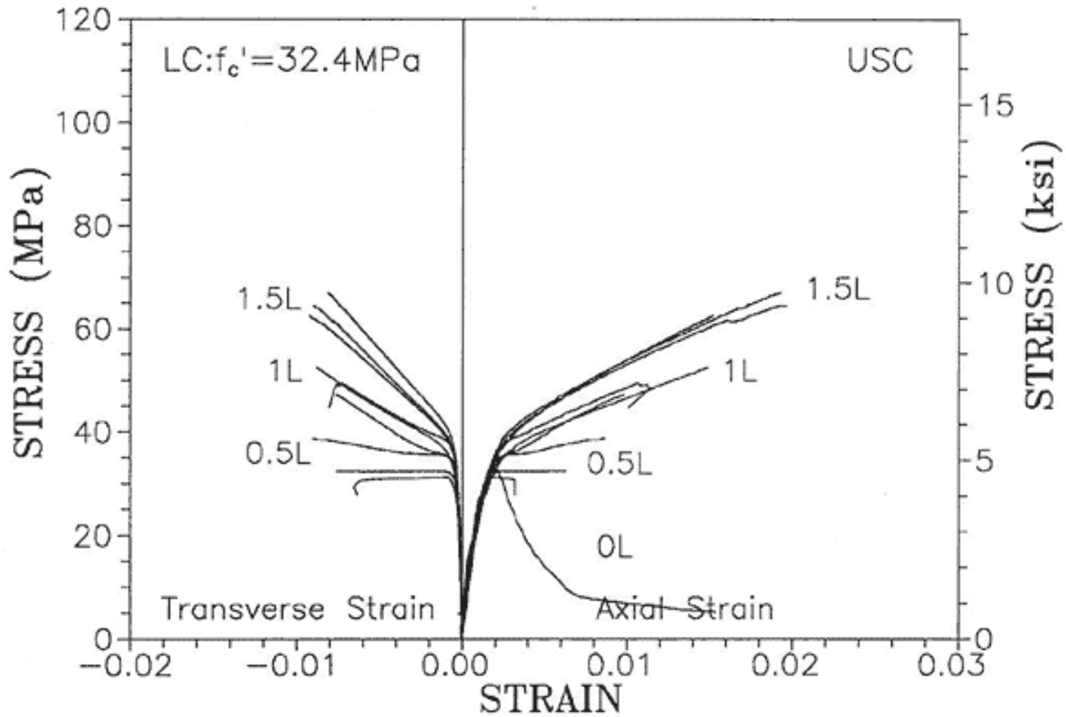

Fig.B-A1. Test Results of Lower-Strength Specimens

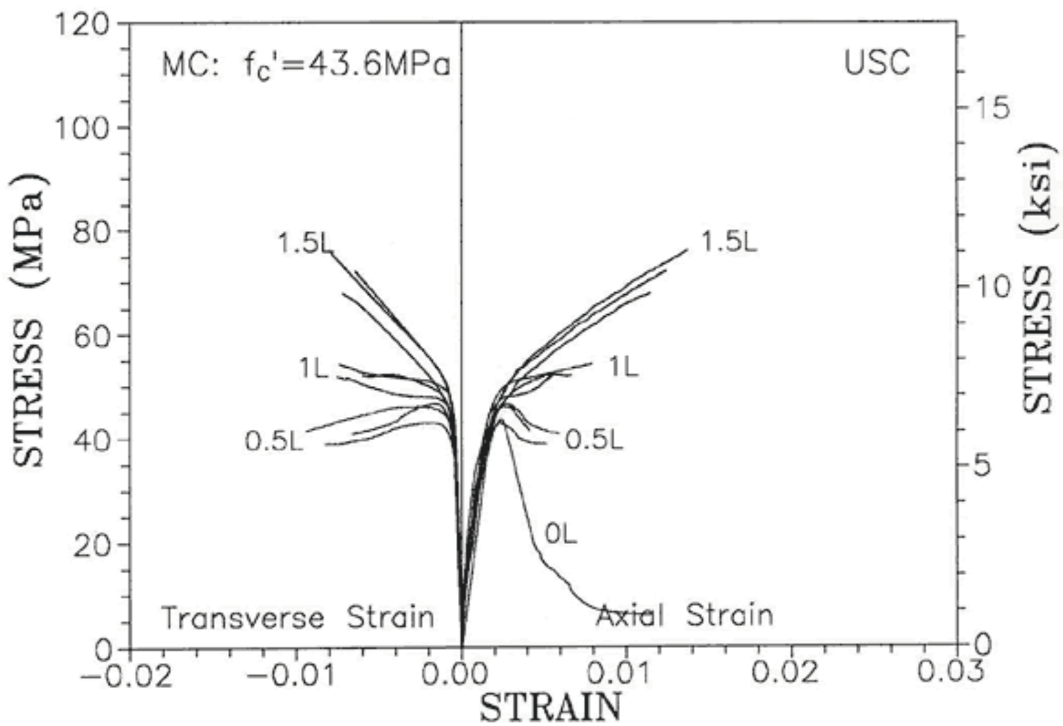

Fig.B-A2. Test Results of Medium-Strength Specimens

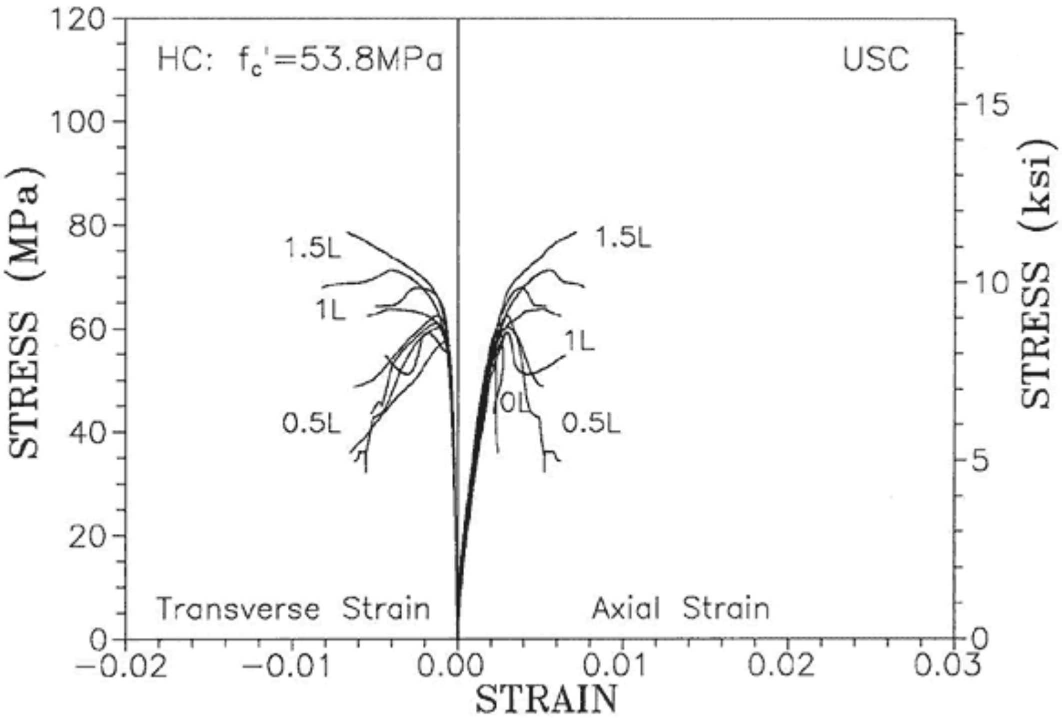

Fig.B-A3. Test Results of Higher-Strength Specimens

Table B-A3 Test Results

Series	Specimen	f_c' (MPa)	Jacket Layers	f_{cc}' (MPa)	ε_{cu}
L	LC-0L-CJ2-1	32.4	0	32.70	0.002061
	LC-0L-CJ2-2			32.08	0.001813
	LC-0L-CJ2-3			32.35	0.002096
	LC-0.5L-CJ2-1		0.5	32.37	0.006267
	LC-0.5L-CJ2-2			38.67	0.008592
	LC-0.5L-CJ2-3			31.26	0.003196
	LC-1L-CJ2-1		1	47.29	0.00980
	LC-1L-CJ2-2			52.41	0.01487
	LC-1L-CJ2-3			49.46	0.01138
	LC-1.5L-CJ2-1		1.5	67.00	0.01929
	LC-1.5L-CJ2-2			64.52	0.01970
	LC-1.5L-CJ2-3			62.46	0.01521
M	MC-0L-CJ2-1	43.6	0	41.23	0.002053
	MC-0L-CJ2-2			43.69	0.002431
	MC-0L-CJ2-3			45.88	0.002479
	MC-0.5L-CJ2-1		0.5	46.75	0.005899
	MC-0.5L-CJ2-2			46.15	0.004126
	MC-0.5L-CJ2-3			43.15	0.005111
	MC-1L-CJ2-1		1	51.87	0.005469
	MC-1L-CJ2-2			54.30	0.007883
	MC-1L-CJ2-3			52.31	0.006631
	MC-1.5L-CJ2-1		1.5	76.13	0.01374
	MC-1.5L-CJ2-2			67.97	0.01143
	MC-1.5L-CJ2-3			72.11	0.01240
H	HC-0L-CJ2-1	53.8	0	53.36	0.002268
	HC-0L-CJ2-2			54.60	0.002006
	HC-0L-CJ2-3			53.42	0.002382
	HC-0.5L-CJ2-1		0.5	61.01	0.002745
	HC-0.5L-CJ2-2			57.32	0.002417
	HC-0.5L-CJ2-3			62.54	0.005164
	HC-1L-CJ2-1		1	63.73	0.006188
	HC-1L-CJ2-2			67.90	0.005293
	HC-1L-CJ2-3			60.25	0.006209
	HC-1.5L-CJ2-1		1.5	78.65	0.007155
	HC-1.5L-CJ2-2			59.25	0.006460
	HC-1.5L-CJ2-3			71.32	0.007603

Note: (i) Example for specimen name designation:

LC-1L-CJ2-1: LC designates Lower strength Concrete; 1L designates 1 Layers; CJ2 designates Carbon fiber Jacket System 2; and the last number represents specimen number in same series.

(ii) f_c': Average plain concrete cylinder strength;

(iii) f_{cc}': Ultimate strength of confined concrete;

(iv) ε_{cu}: Ultimate strain

Part B-B Test Results of Lower Strength Concrete Cylinders

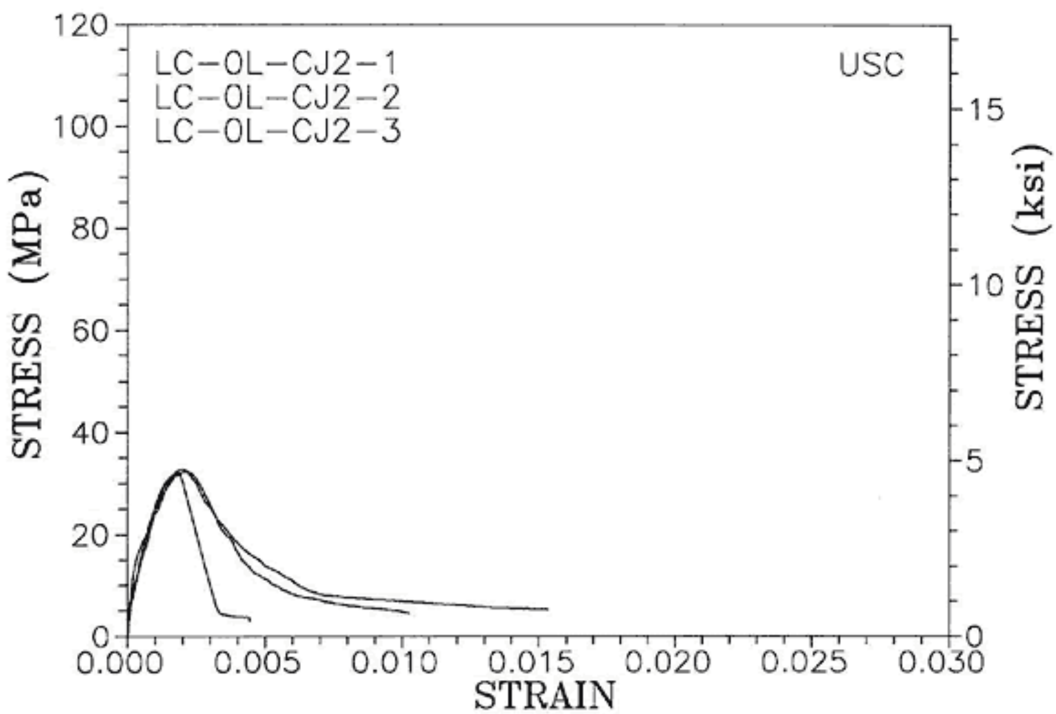

Fig. B-B1. Stress-Strain Relationships for Lower Strength Plain Concrete Cylinders

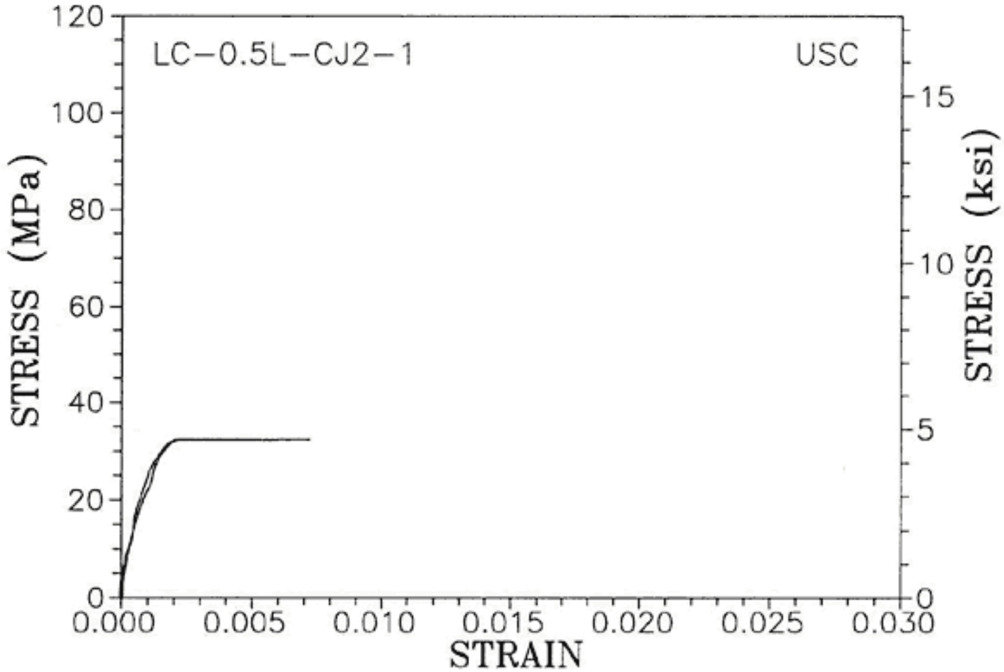

(a)

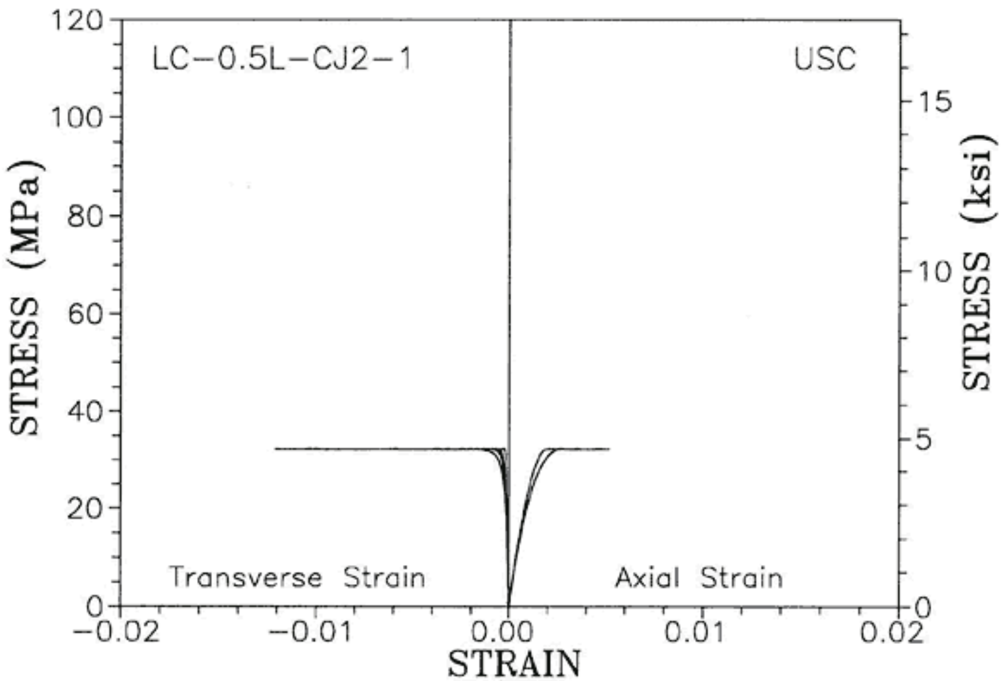

(b)

Fig.B-B2. Stress-Strain Relationships for Lower Strength Concrete with Half-Layer Carbon Fiber Composite Jacket (LC-0.5L-CJ2-1)
(a) Strain Measured by LP (b) Strain Measured by Strain Gages

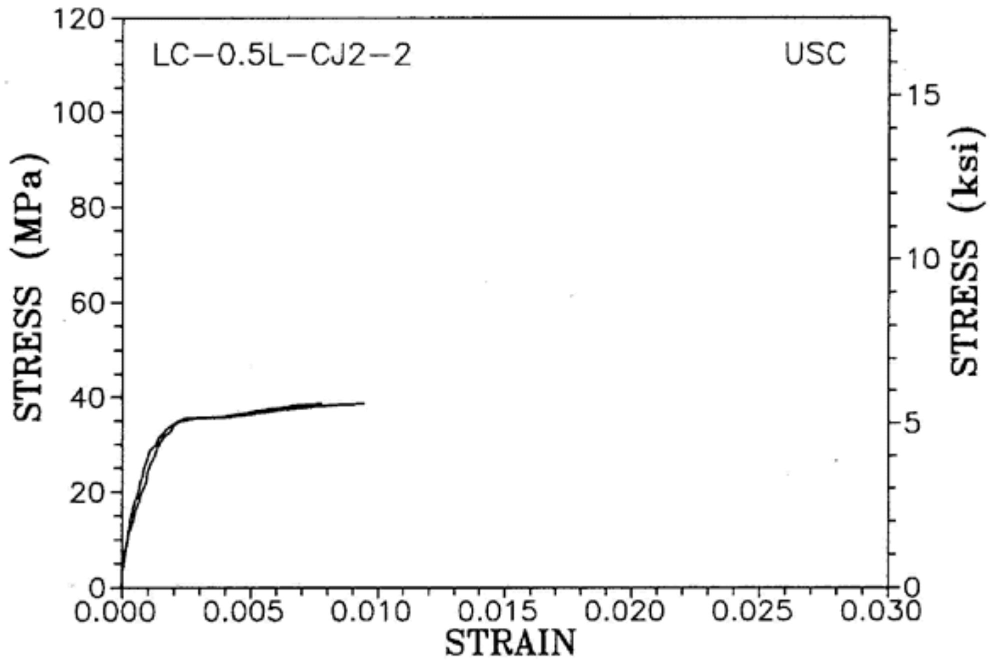

(a)

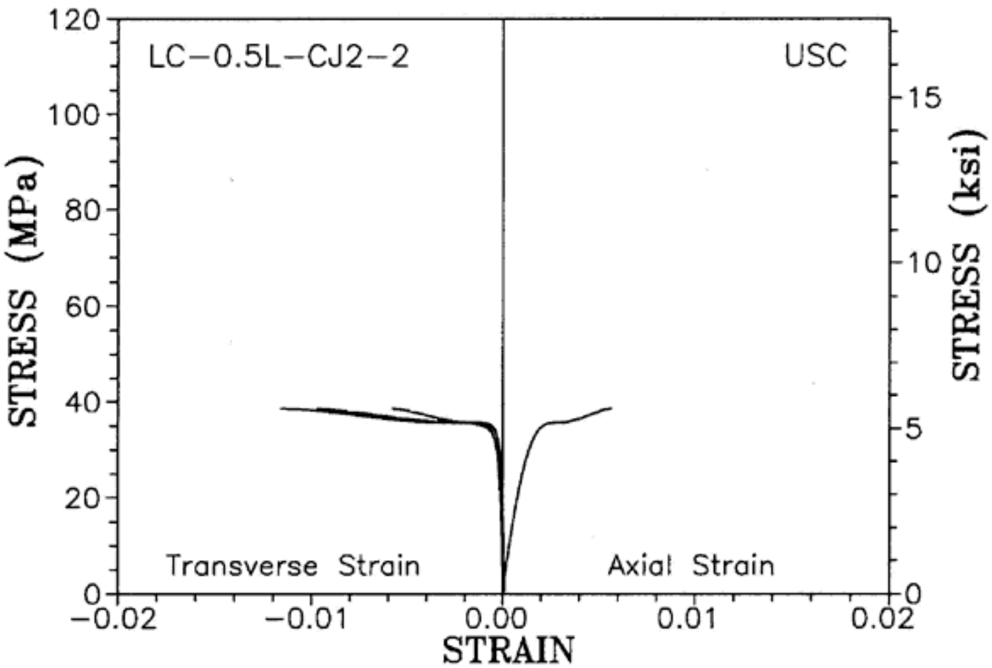

(b)

Fig.B-B2. Stress-Strain Relationships for Lower Strength Concrete with Half-Layer Carbon Fiber Composite Jacket (LC-0.5L-CJ2-2)
(a) Strain Measured by LP (b) Strain Measured by Strain Gages

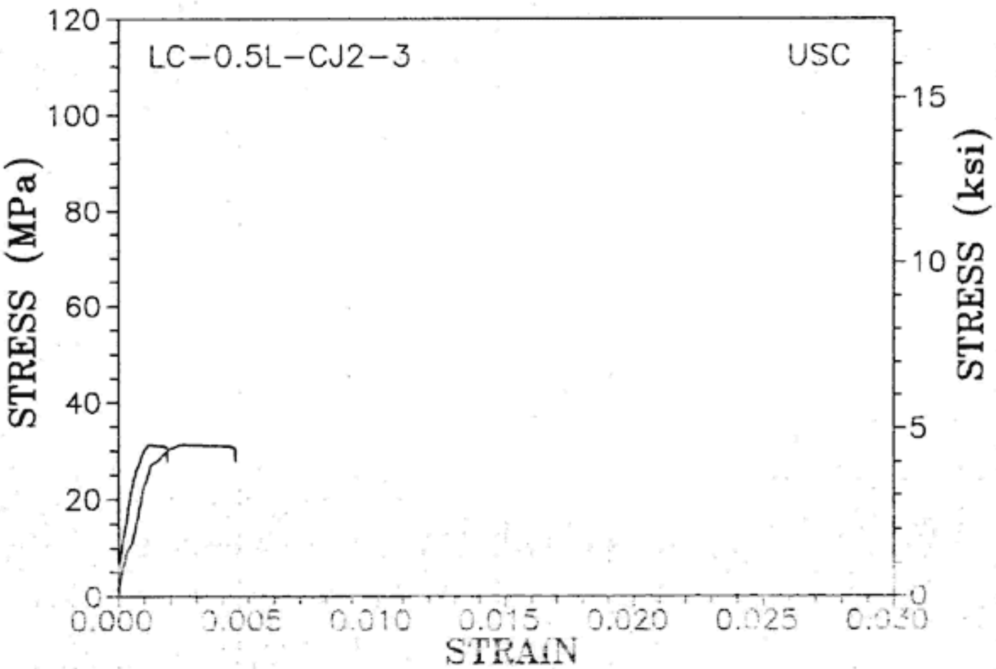

(a)

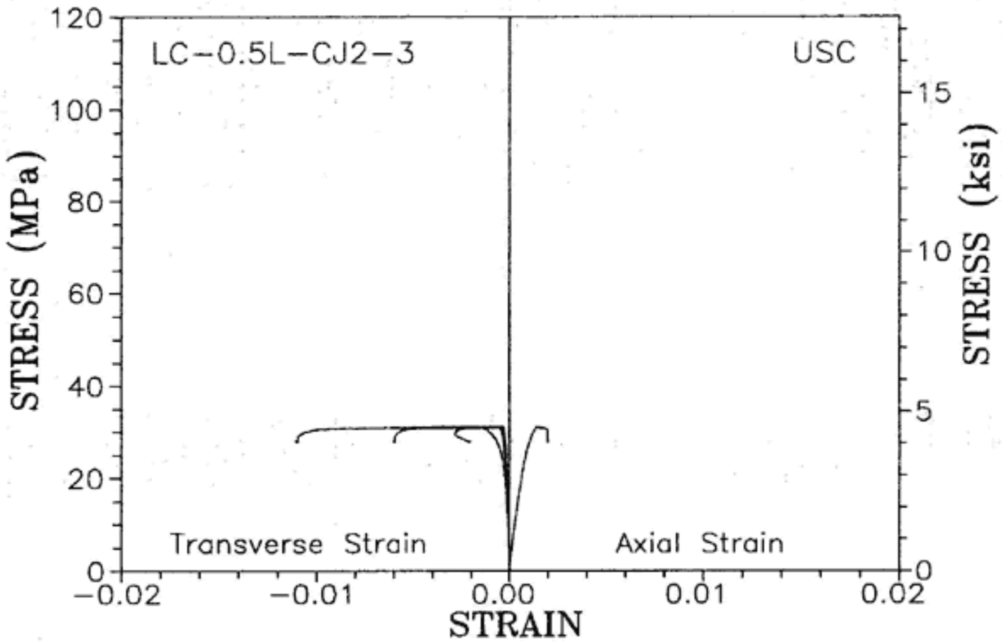

(b)

Fig.B-B2. Stress-Strain Relationships for Lower Strength Concrete with Half-Layer Carbon Fiber Composite Jacket (LC-0.5L-CJ2-3)
(a) Strain Measured by LP (b) Strain Measured by Strain Gages

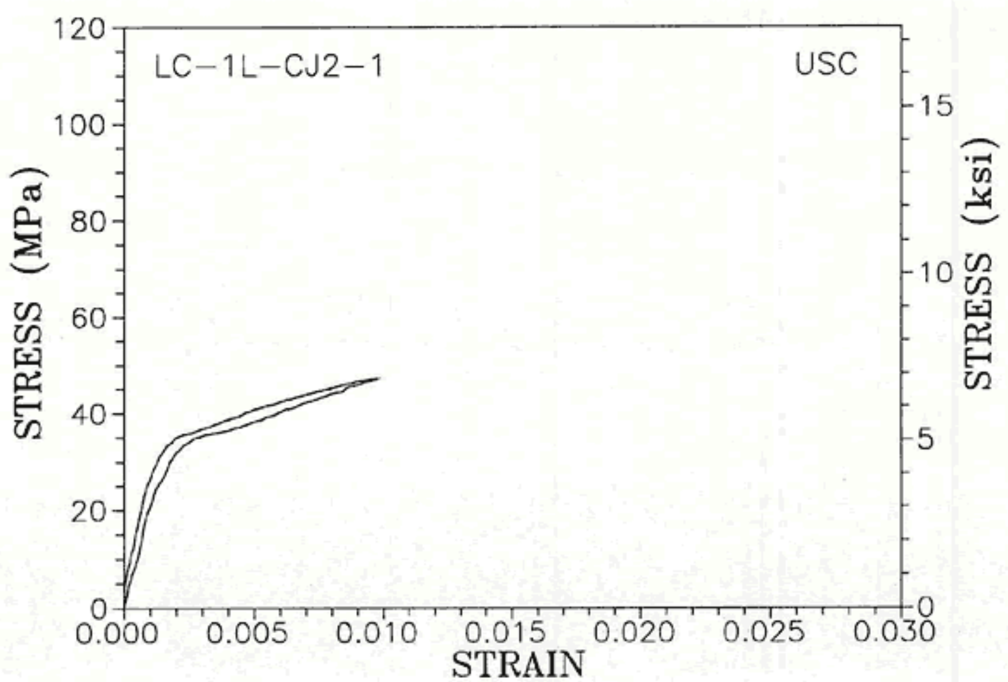

(a)

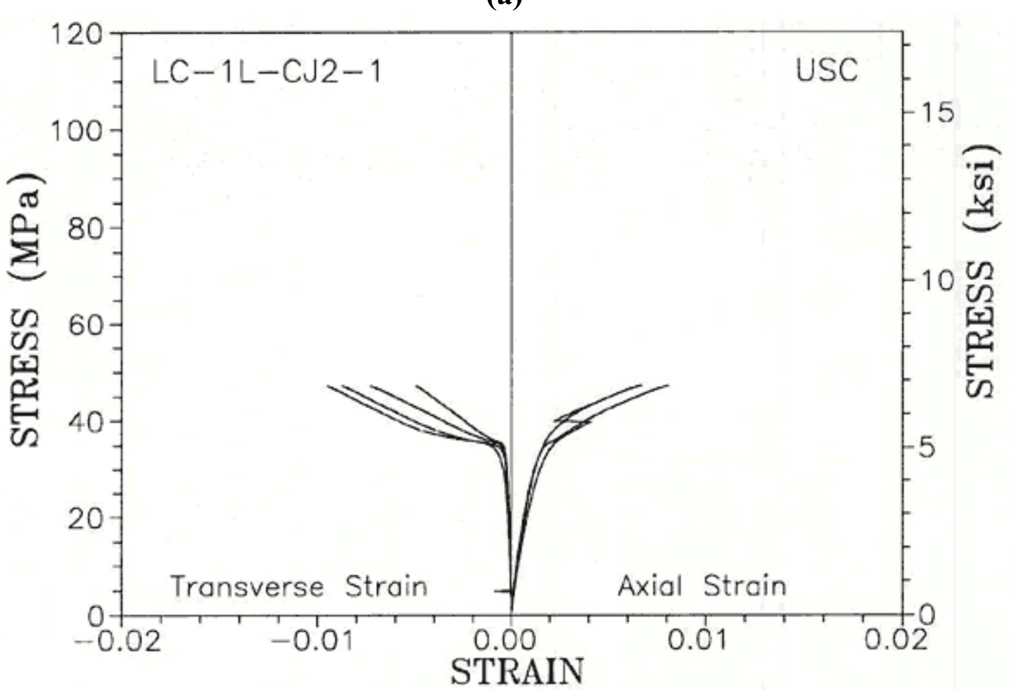

(b)

Fig.B-B3. Stress-Strain Relationships for Lower Strength Concrete with One-Layer Carbon Fiber Composite Jacket (LC-1L-CJ2-1)
(a) Strain Measured by LP (b) Strain Measured by Strain Gages

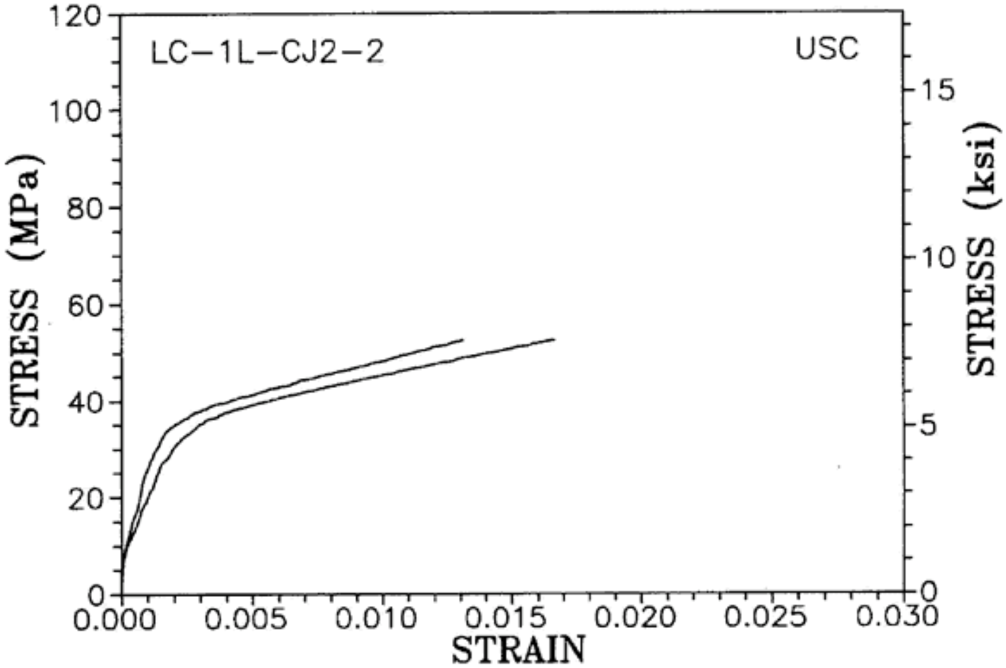

(a)

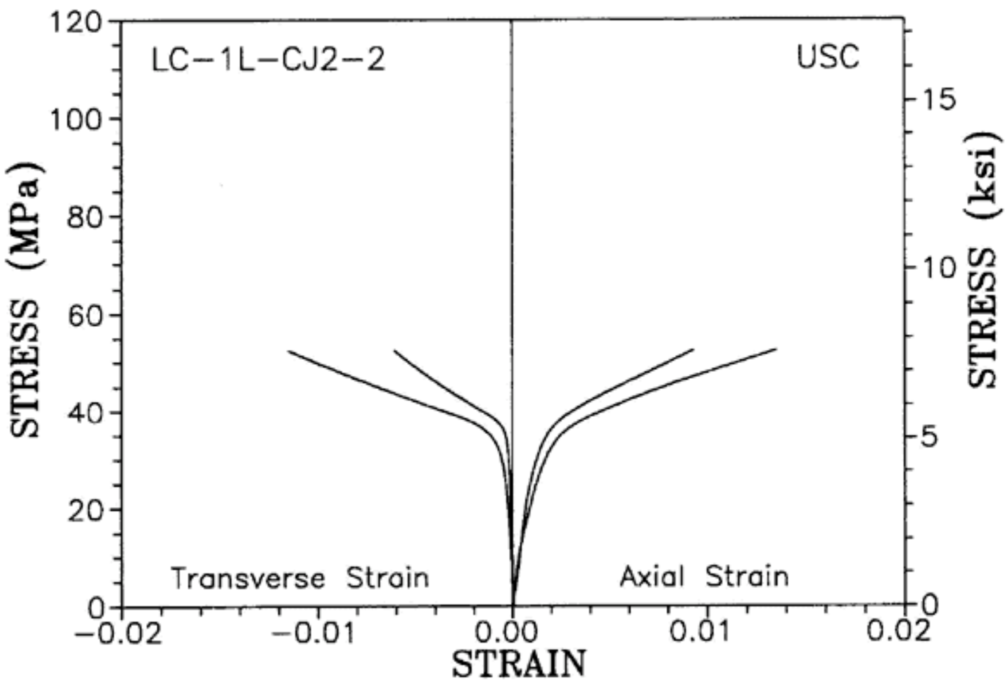

(b)

Fig.B-B3. Stress-Strain Relationships for Lower Strength Concrete with One-Layer Carbon Fiber Composite Jacket (LC-1L-CJ2-2)
(a) Strain Measured by LP (b) Strain Measured by Strain Gages

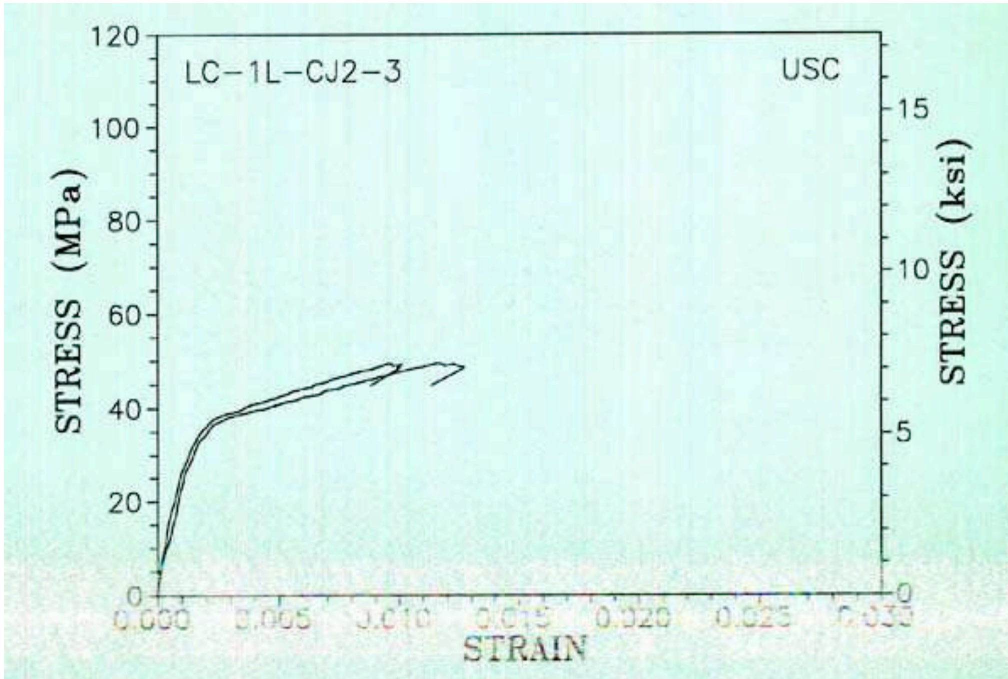

(a)

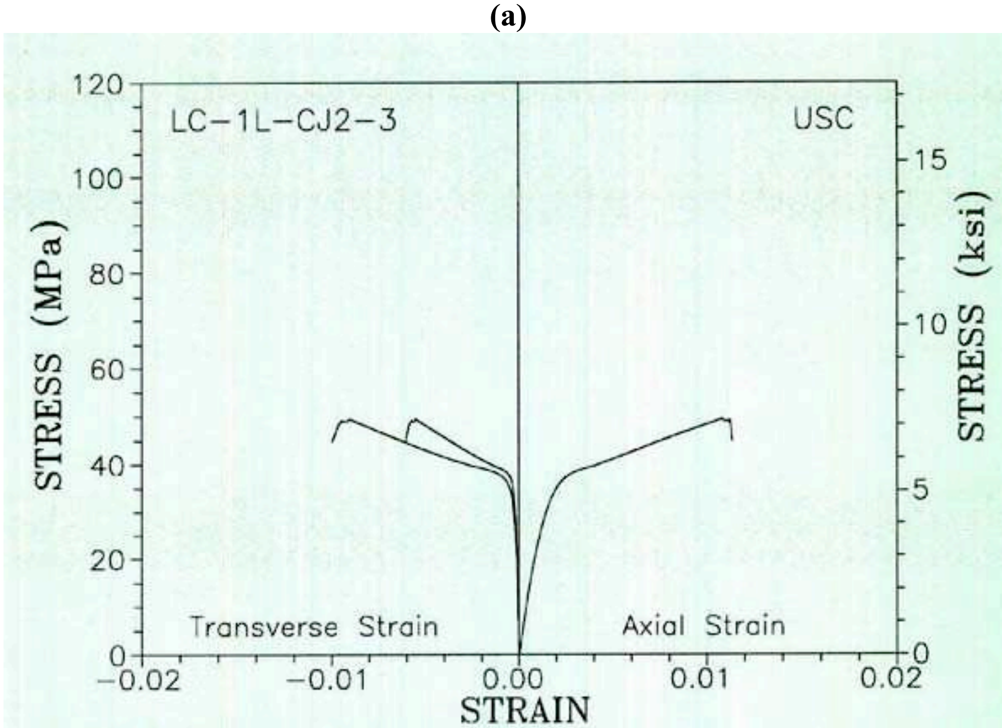

(b)

Fig.B-B3. Stress-Strain Relationships for Lower Strength Concrete with One-Layer Carbon Fiber Composite Jacket (LC-1L-CJ2-3)
(a) Strain Measured by LP (b) Strain Measured by Strain Gages

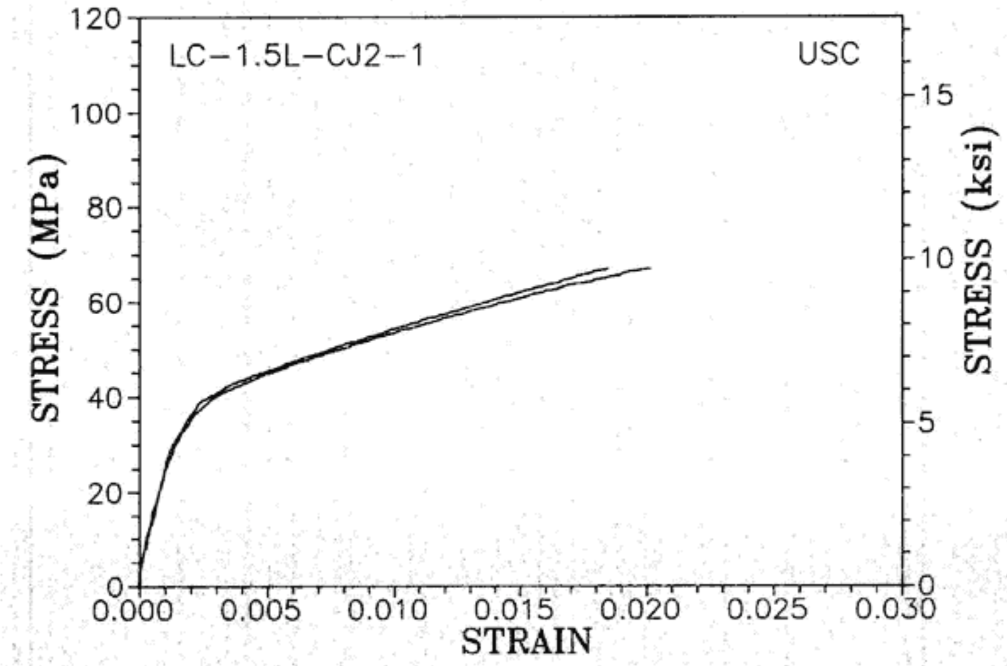

(a)

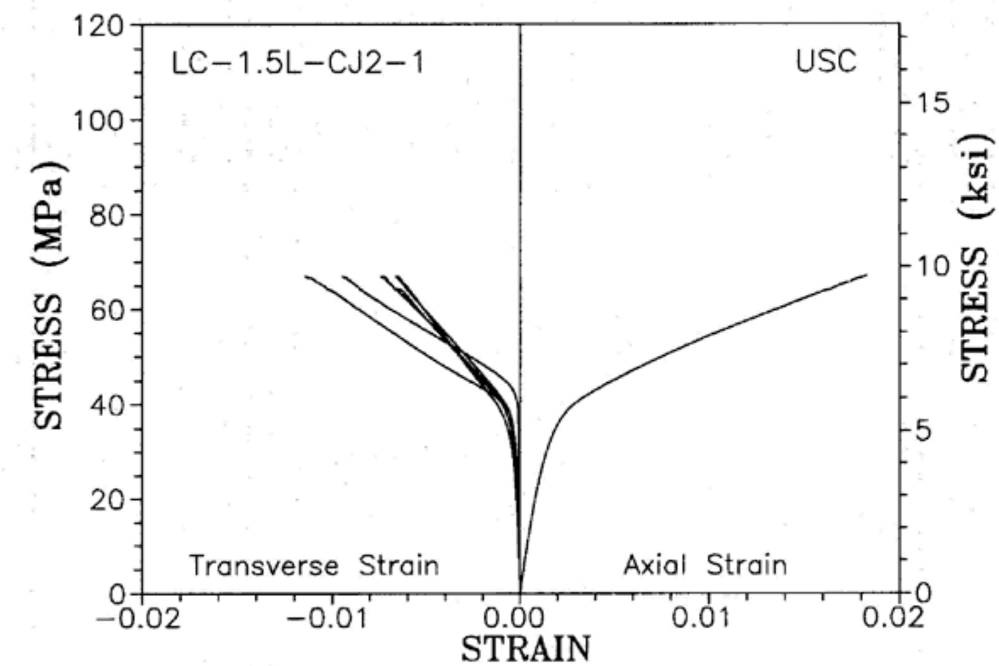

(b)

Fig.B-B4. Stress-Strain Relationships for Lower Strength Concrete with One and a Half-Layer Carbon Fiber Composite Jacket (LC-1.5L-CJ2-1)
(a) Strain Measured by LP (b) Strain Measured by Strain Gages

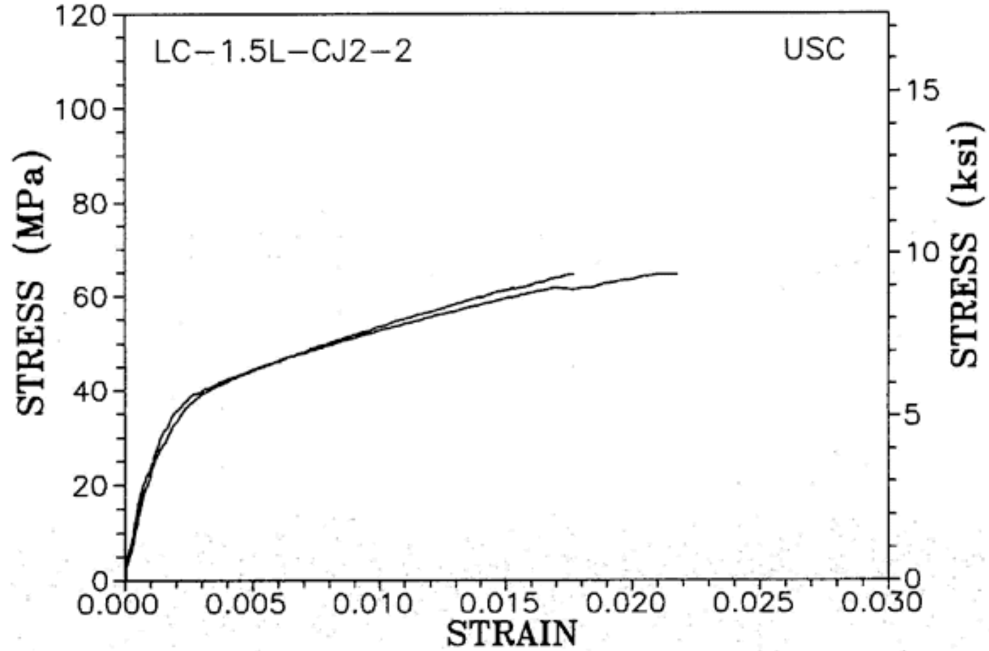

(a)

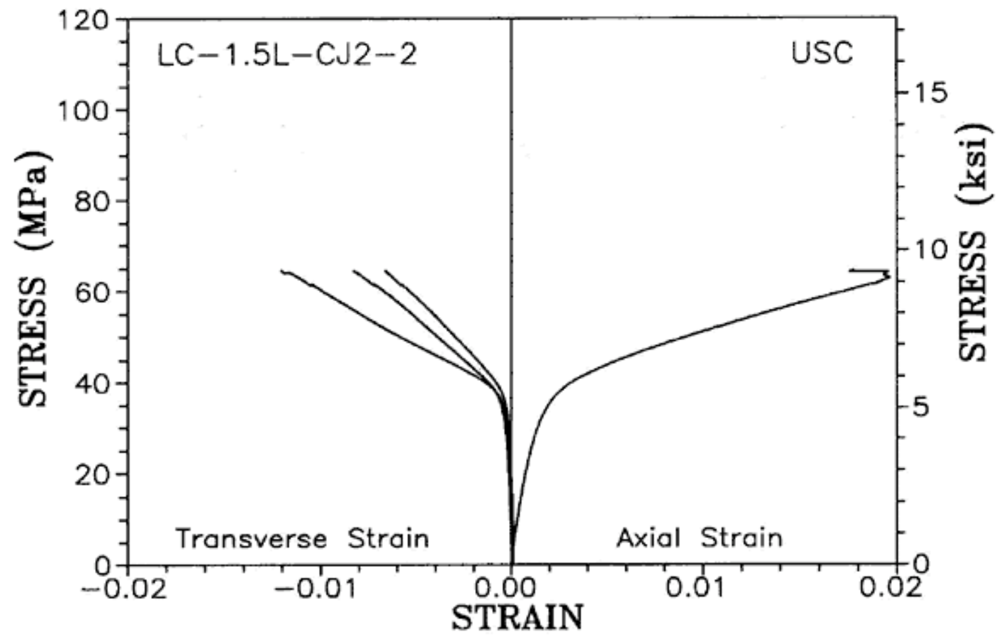

(b)

Fig.B-B4. Stress-Strain Relationships for Lower Strength Concrete with One and a Half-Layer Carbon Fiber Composite Jacket (LC-1.5L-CJ2-2)
(a) Strain Measured by LP (b) Strain Measured by Strain Gages

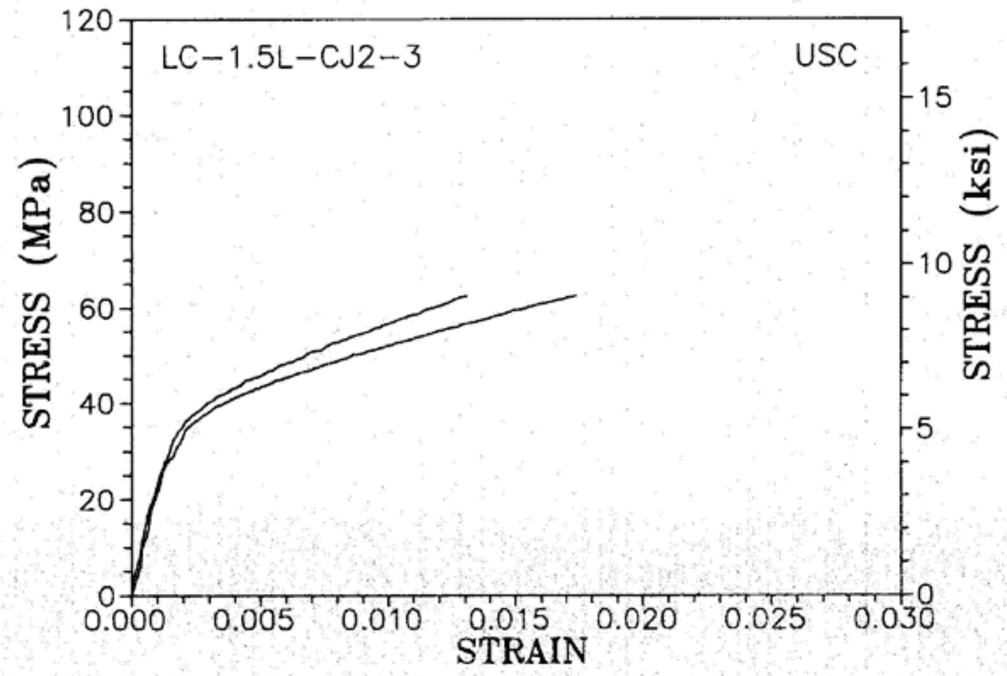

(a)

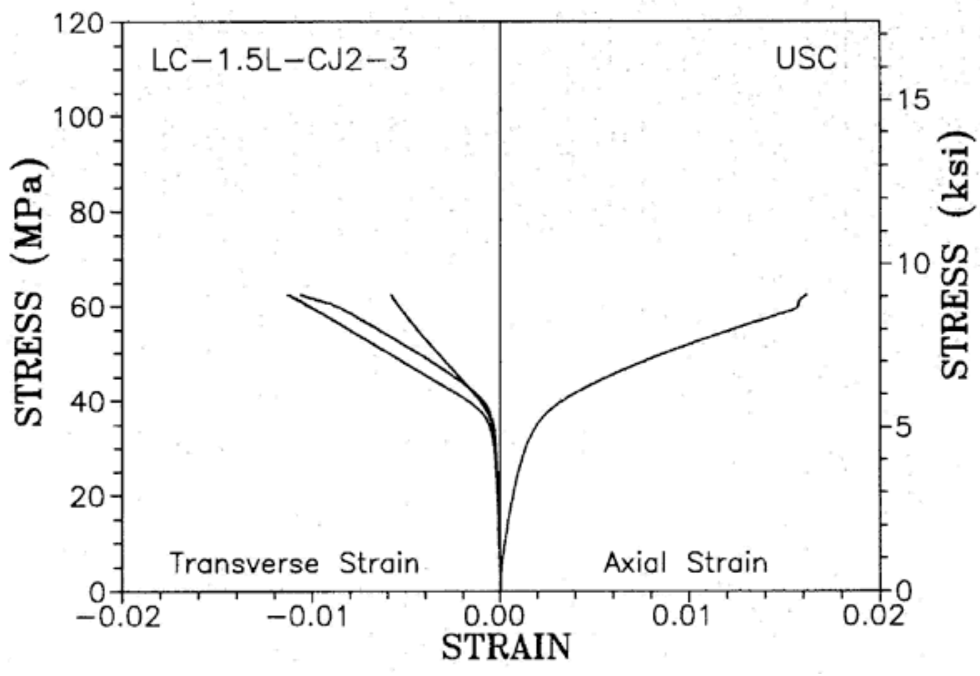

(b)

Fig.B-B4. Stress-Strain Relationships for Lower Strength Concrete with One and a Half-Layer Carbon Fiber Composite Jacket (LC-1.5L-CJ2-3)
(a) Strain Measured by LP (b) Strain Measured by Strain Gages

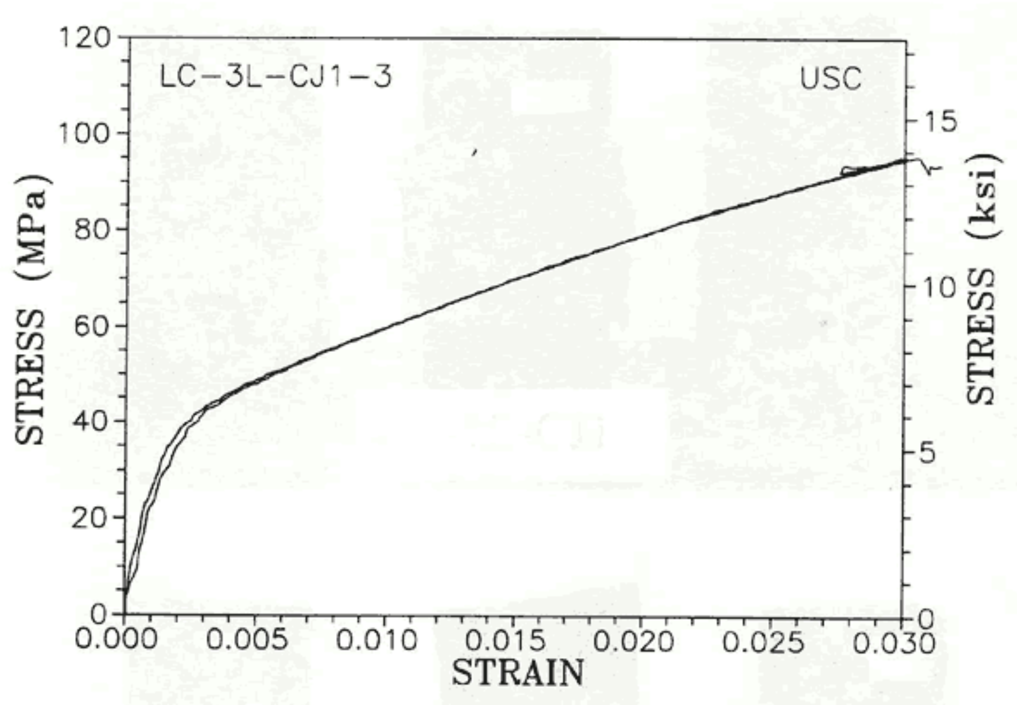

(a)

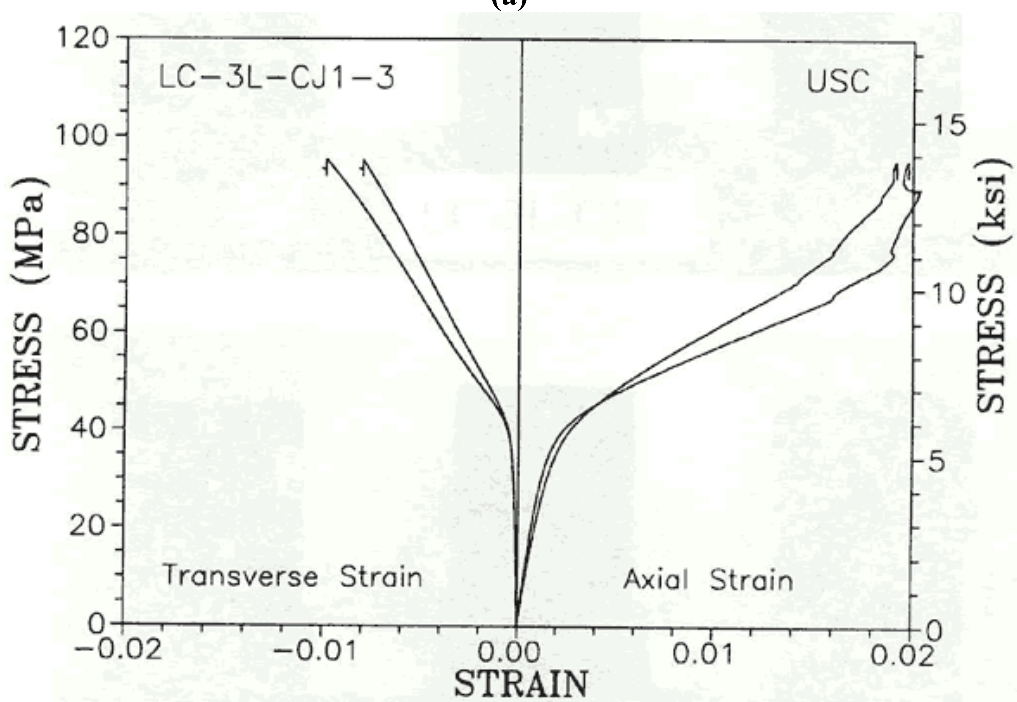

(b)

Fig B-B4.Stress-Strain Relationships for Lower Strength Concrete with Three-layer Carbon Fiber Composite Jacket (LC-3L-CJ2-3)
(a) Strain measured by LP (b) Strain measured by strain gages

Fig.B-B5. Specimens after Testing

Part B-C Test Results of Medium Strength Concrete Cylinders

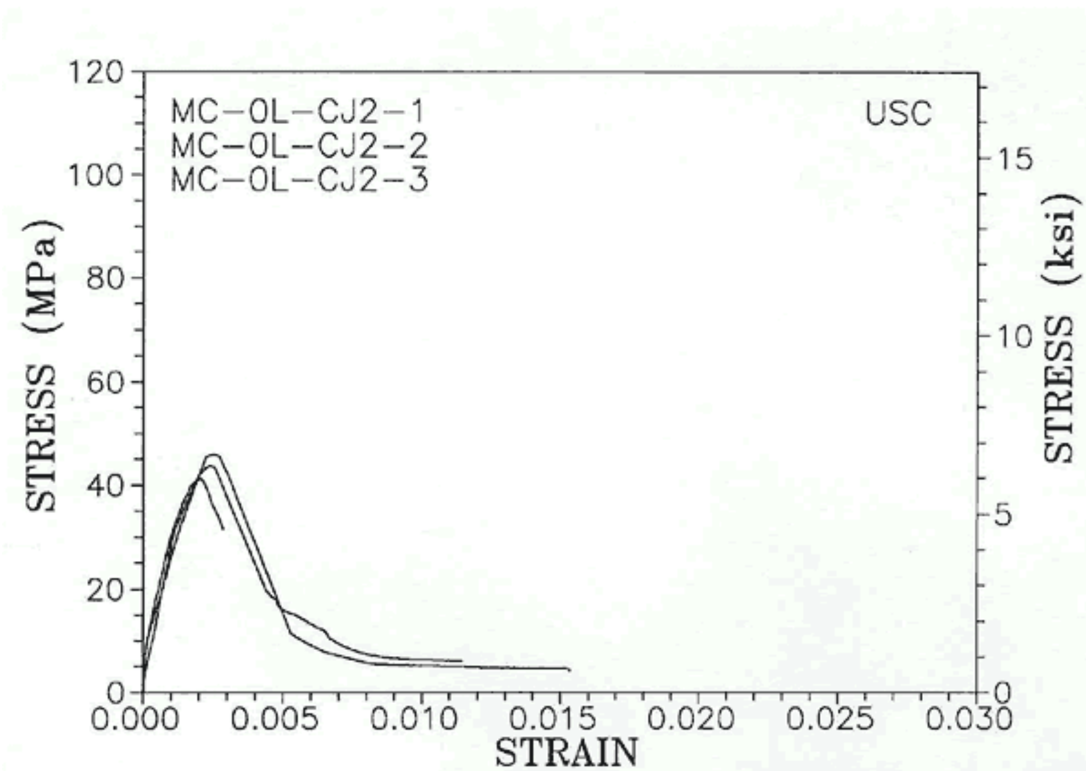

Fig. B-C1. Stress-Strain Relationships for Medium Strength Plain Concrete Cylinders

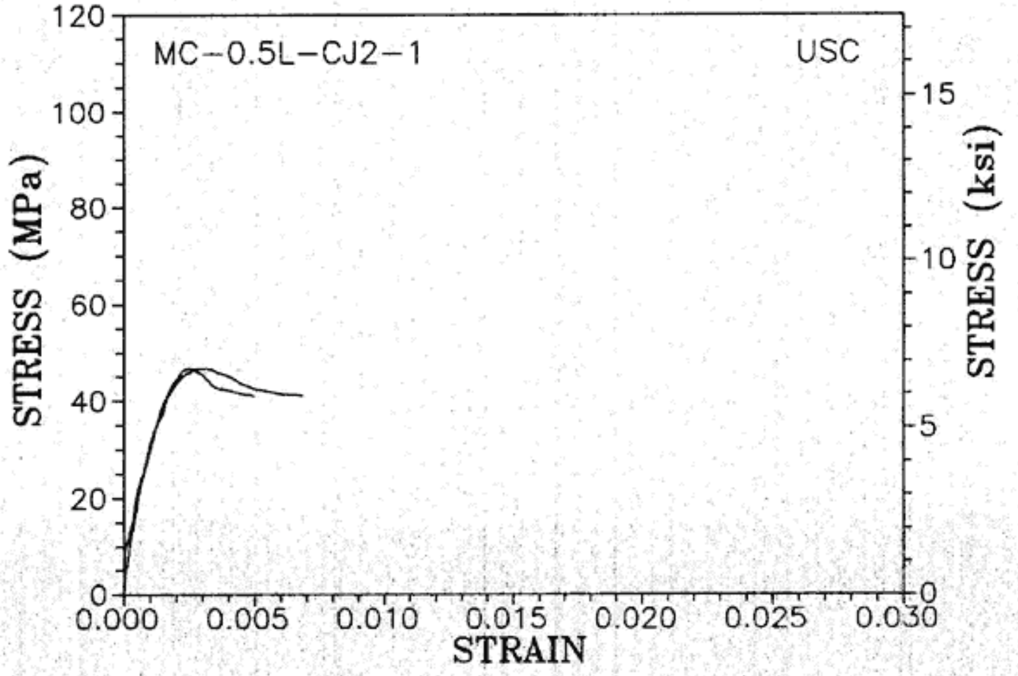

(a)

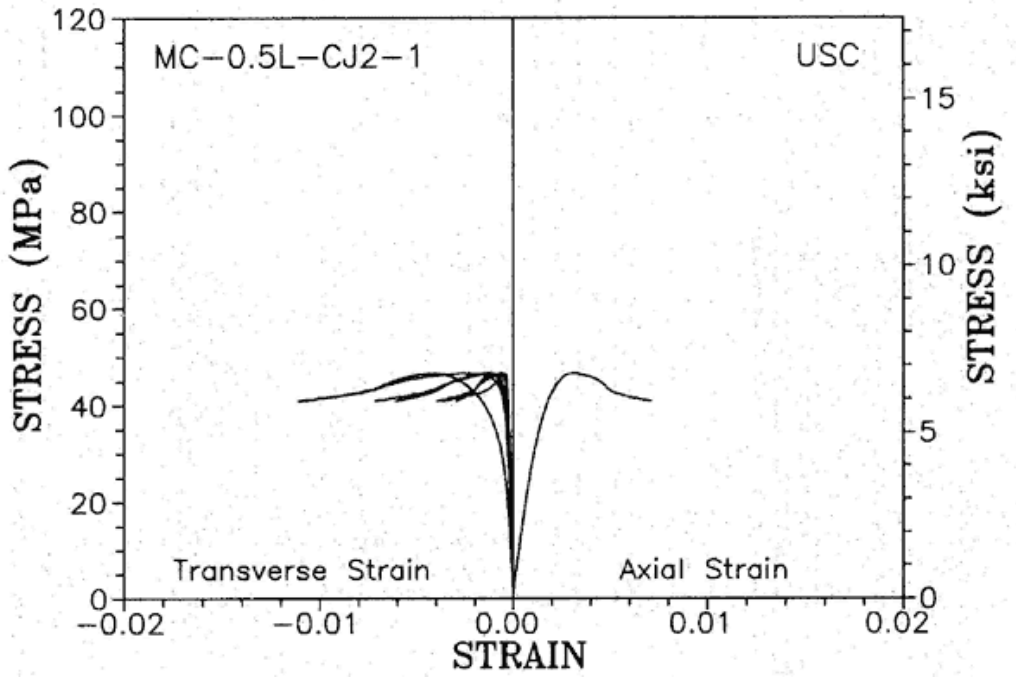

(b)

Fig.B-C2. Stress-Strain Relationships for Medium Strength Concrete with Half-Layer Carbon Fiber Composite Jacket (MC-0.5L-CJ2-1)
(a) Strain Measured by LP (b) Strain Measured by Strain Gages

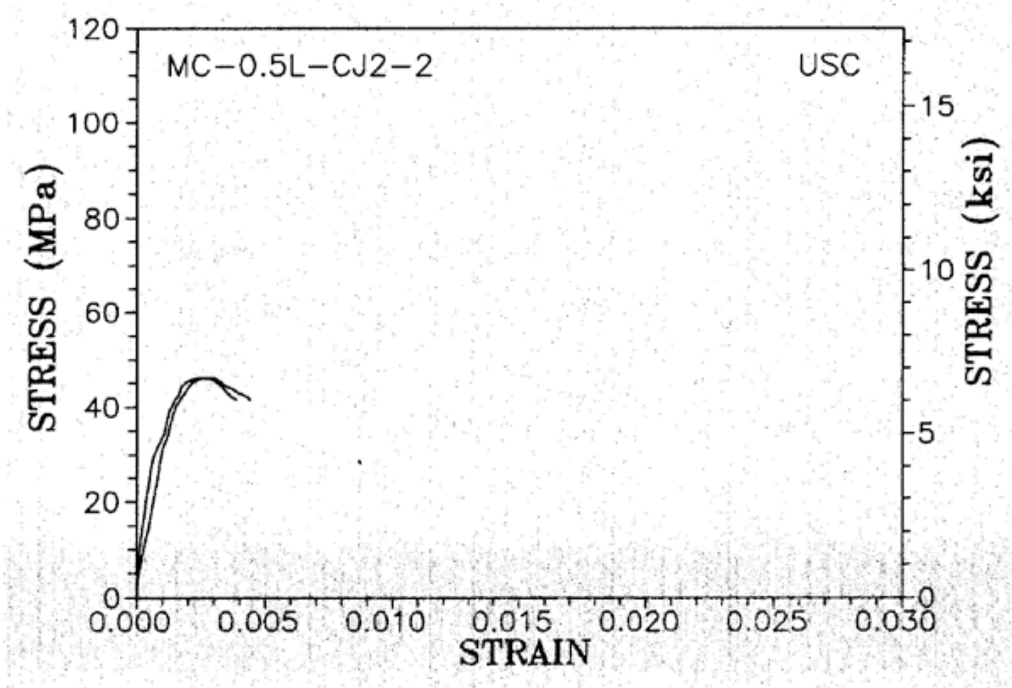

(a)

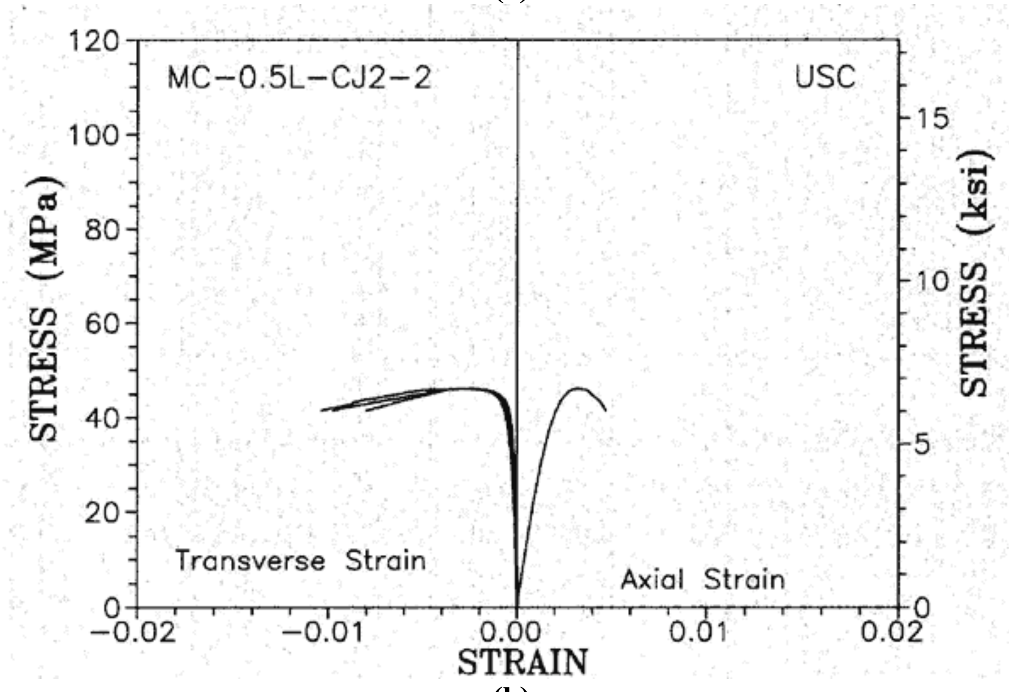

(b)

Fig.B-C2. Stress-Strain Relationships for Medium Strength Concrete with Half-Layer Carbon Fiber Composite Jacket (MC-0.5L-CJ2-2)
(a) Strain Measured by LP (b) Strain Measured by Strain Gages

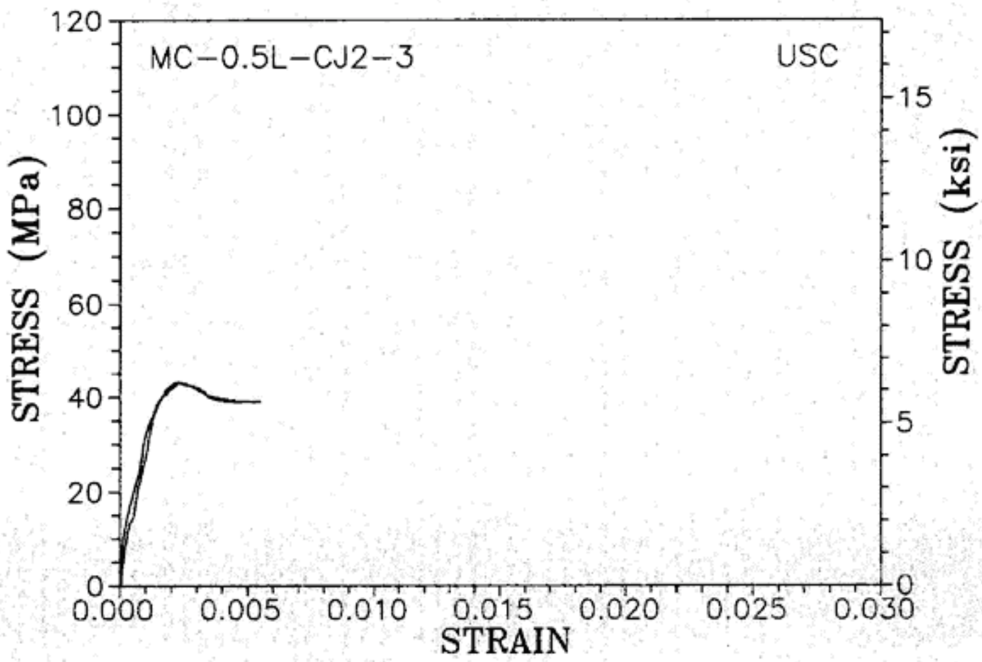

(a)

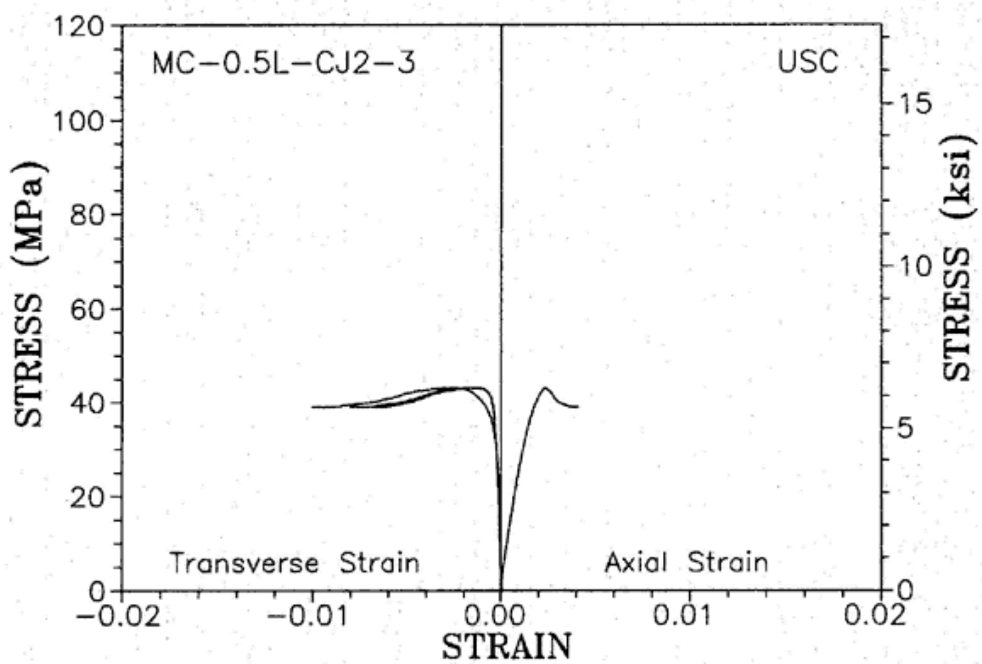

(b)

Fig.B-C2. Stress-Strain Relationships for Medium Strength Concrete with Half-Layer Carbon Fiber Composite Jacket (MC-0.5L-CJ2-3)
(a) Strain Measured by LP (b) Strain Measured by Strain Gages

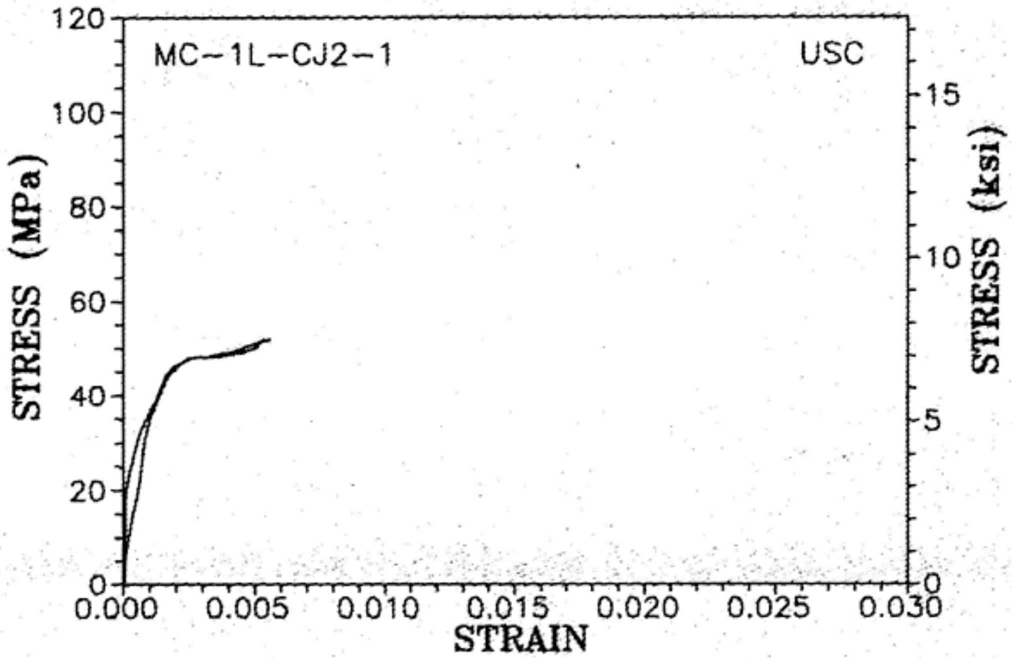

(a)

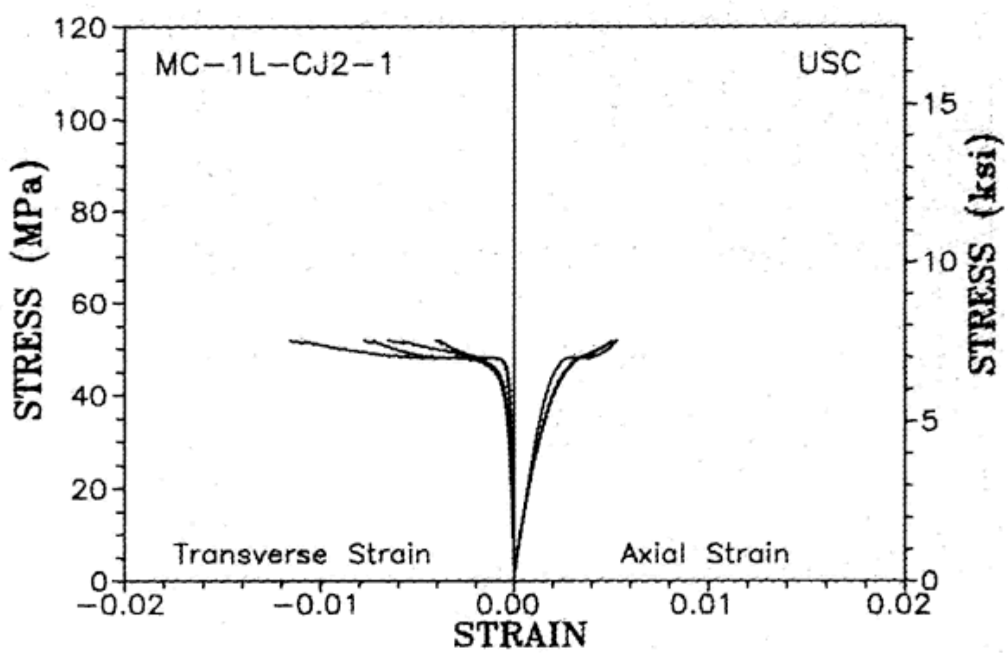

(b)

Fig.B-C3. Stress-Strain Relationships for Medium Strength Concrete with One-Layer Carbon Fiber Composite Jacket (MC-1L-CJ2-1)
(a) Strain Measured by LP (b) Strain Measured by Strain Gages

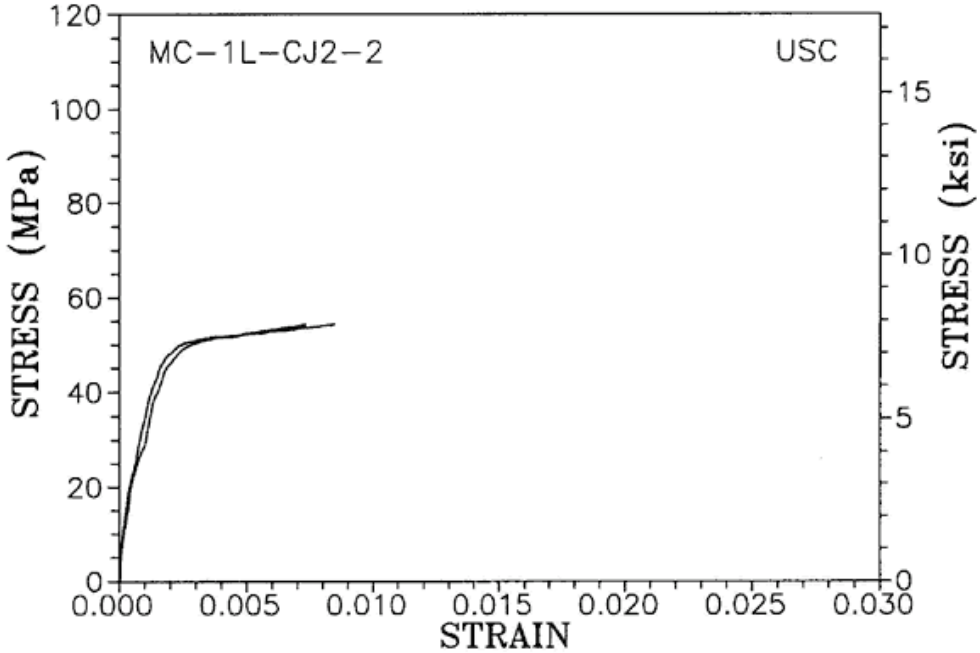

(a)

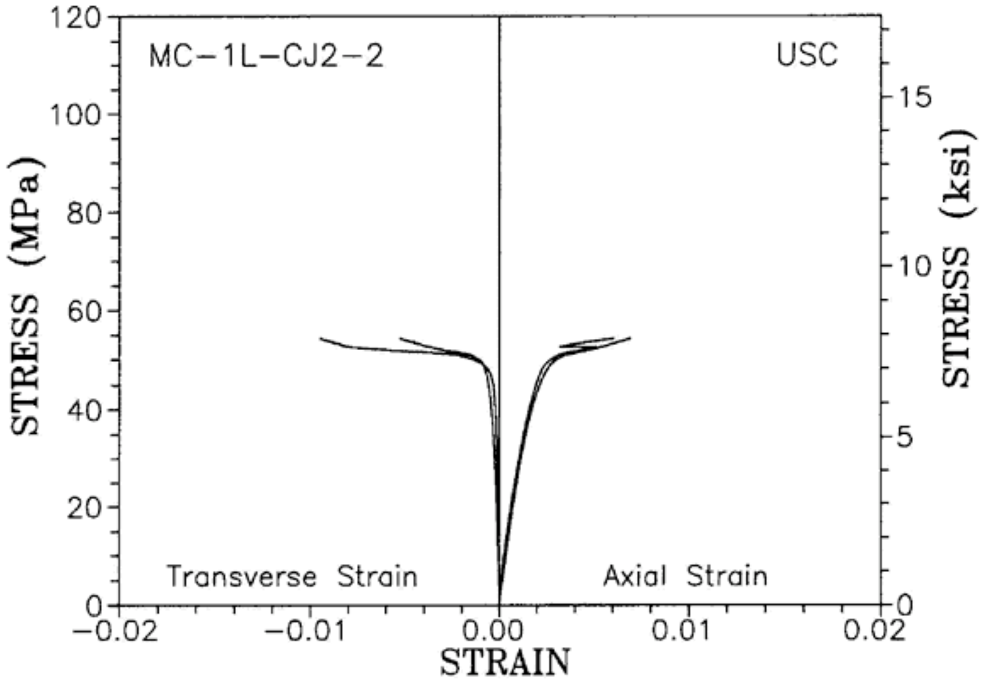

(b)

Fig.B-C3. Stress-Strain Relationships for Medium Strength Concrete with One-Layer Carbon Fiber Composite Jacket (MC-1L-CJ2-2)
(a) Strain Measured by LP (b) Strain Measured by Strain Gages

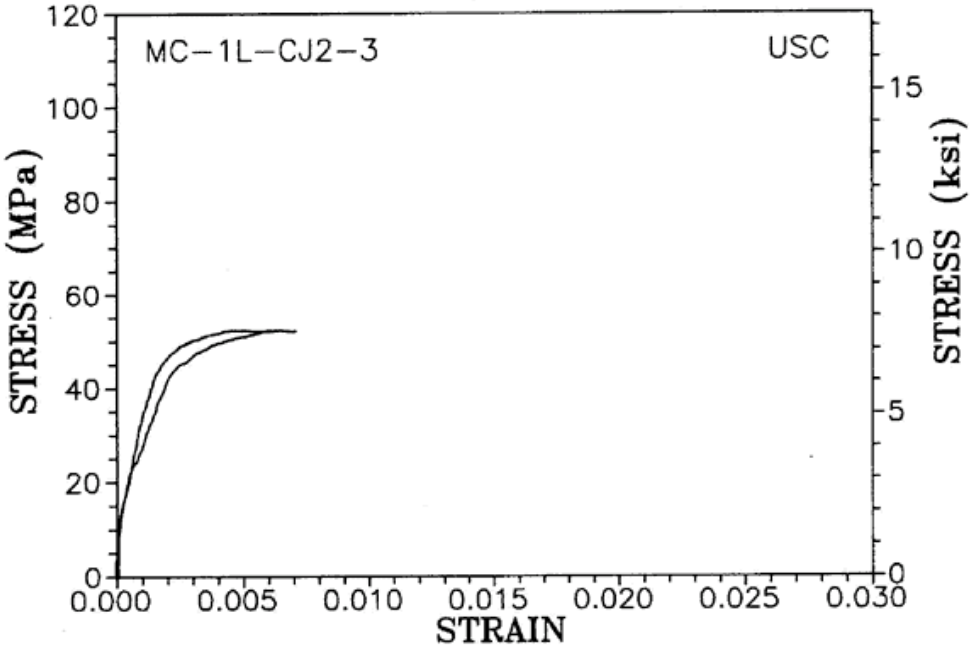

(a)

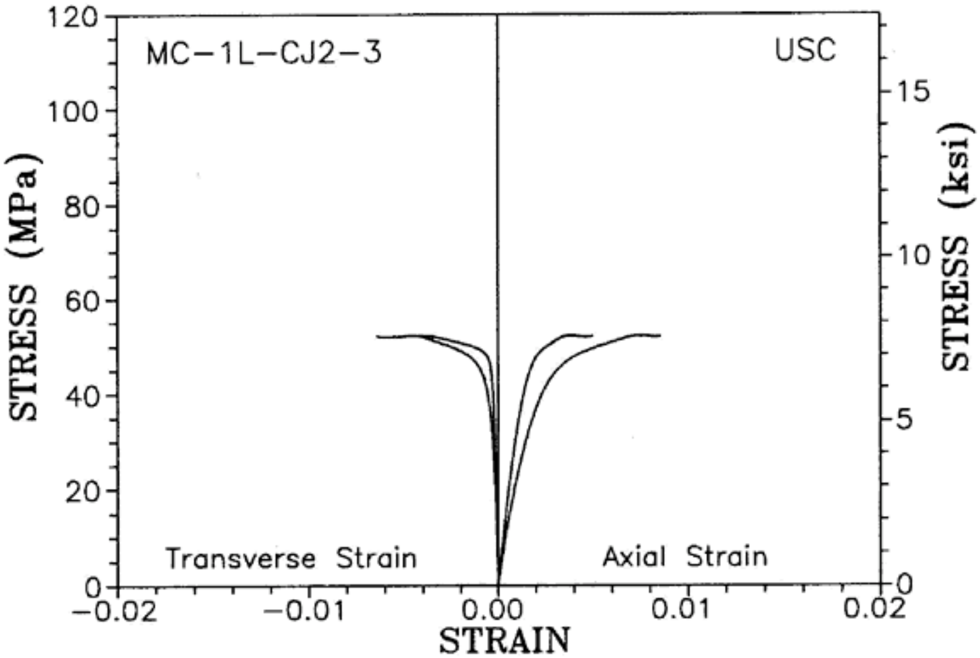

(b)

Fig.B-C3. Stress-Strain Relationships for Medium Strength Concrete with One-Layer Carbon Fiber Composite Jacket (MC-1L-CJ2-3)
(a) Strain Measured by LP (b) Strain Measured by Strain Gages

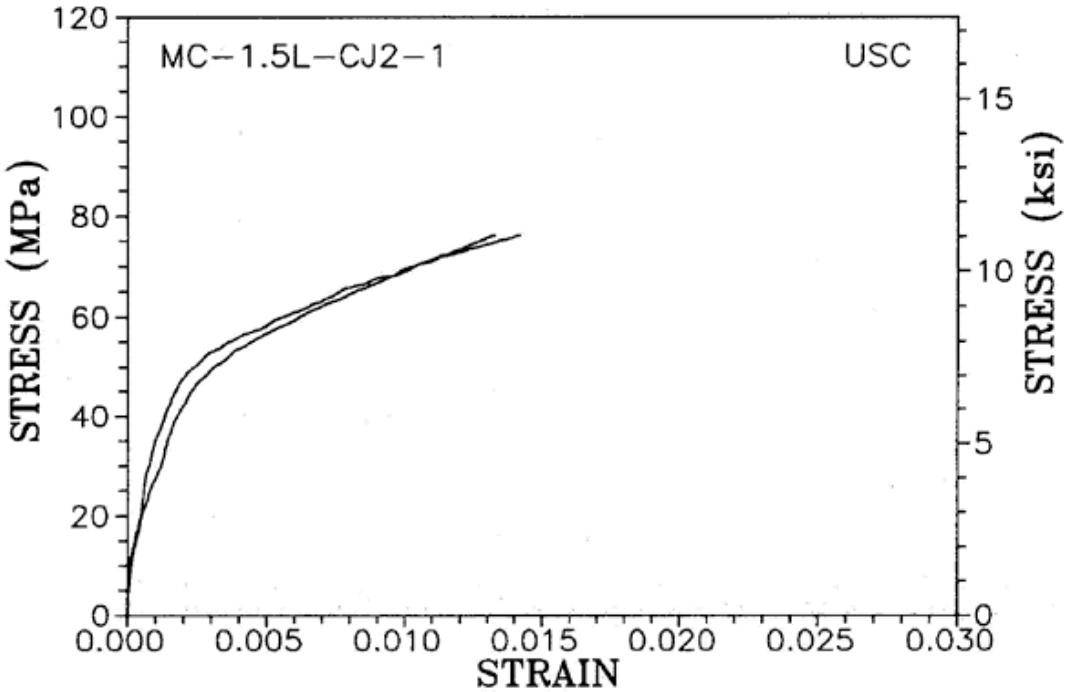

(a)

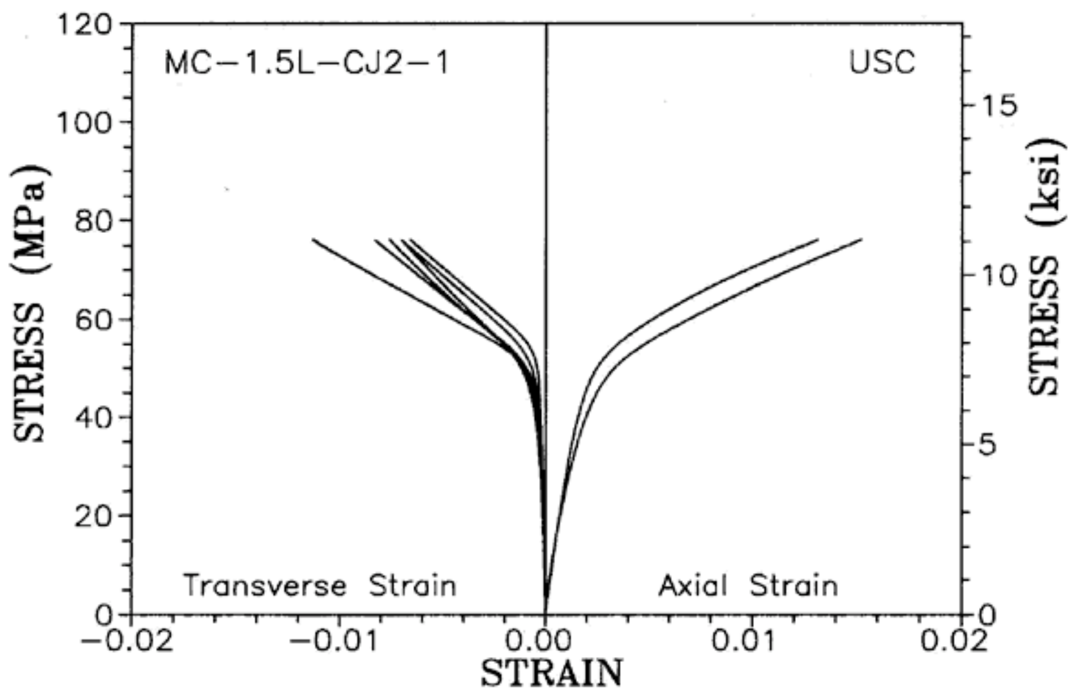

(b)

Fig.B-C4. Stress-Strain Relationships for Medium Strength Concrete with One and a Half-Layer Carbon Fiber Composite Jacket (MC-1.5L-CJ2-1)
(a) Strain Measured by LP (b) Strain Measured by Strain Gages

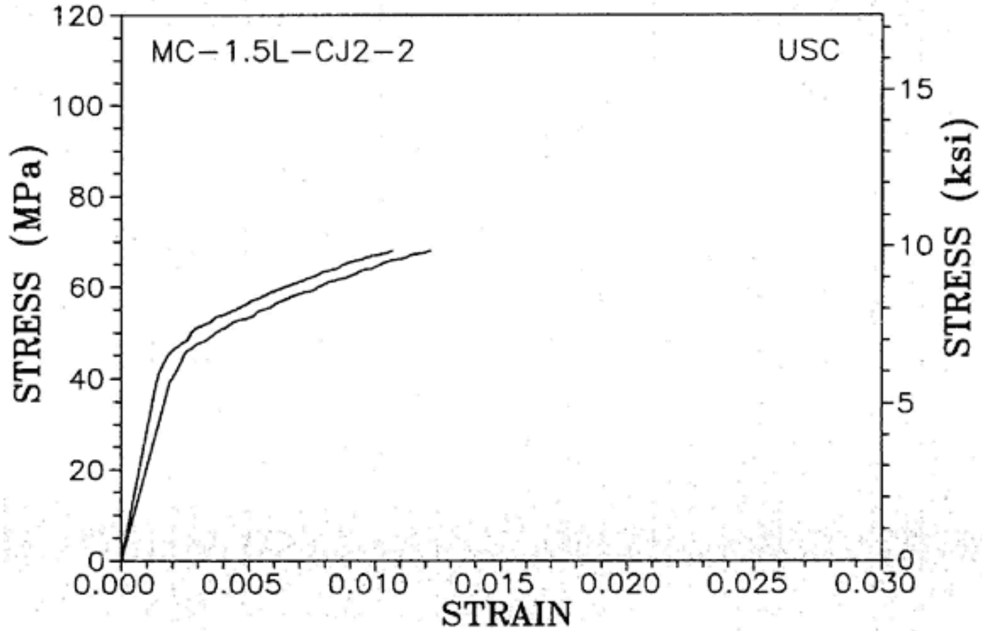

(a)

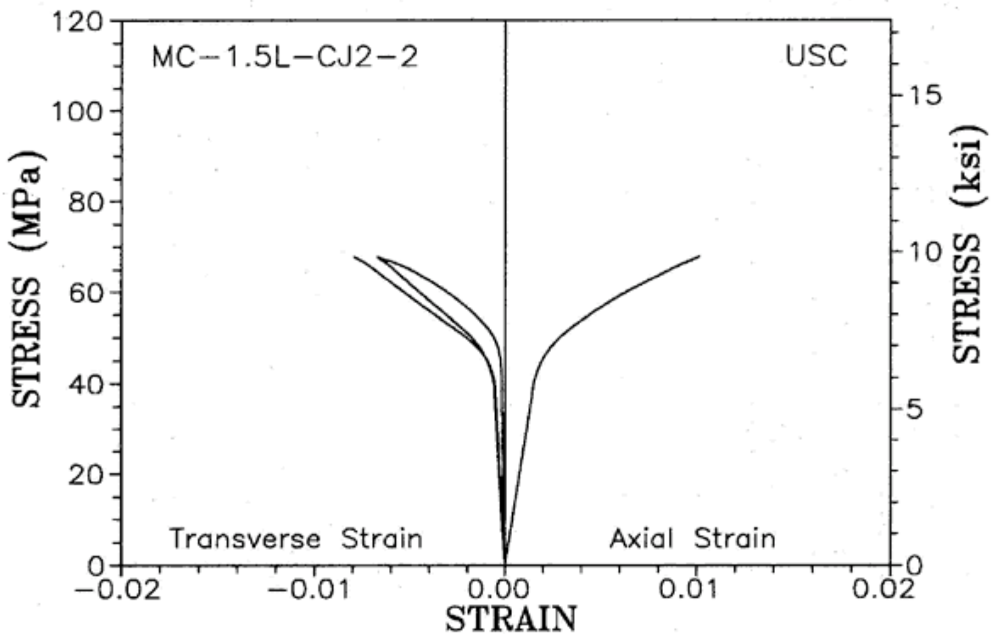

(b)

Fig.B-C4. Stress-Strain Relationships for Medium Strength Concrete with One and a Half-Layer Carbon Fiber Composite Jacket (MC-1.5L-CJ2-2)
(a) Strain Measured by LP (b) Strain Measured by Strain Gages

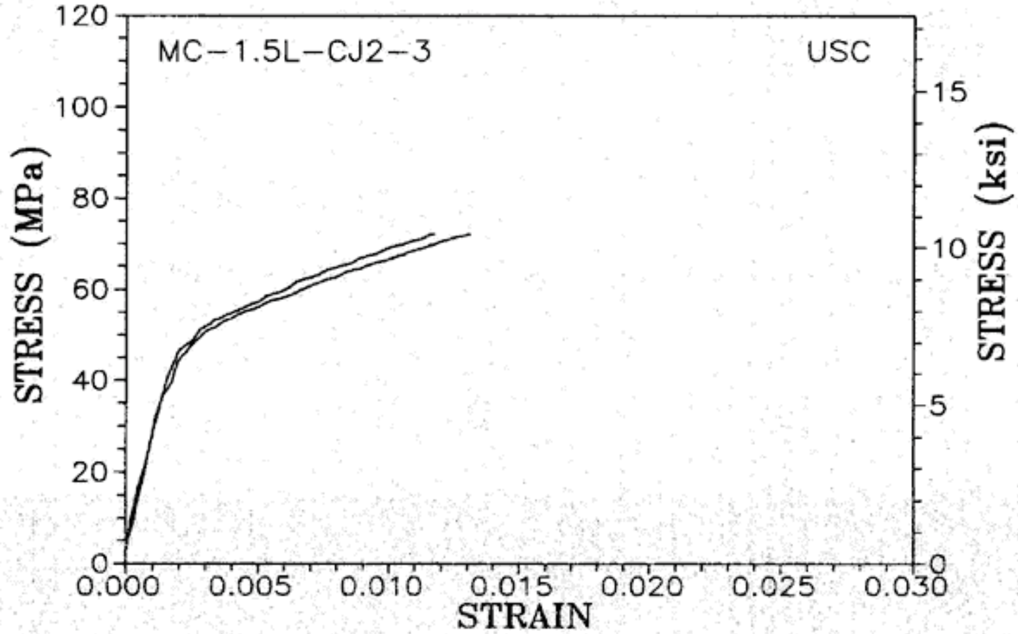

(a)

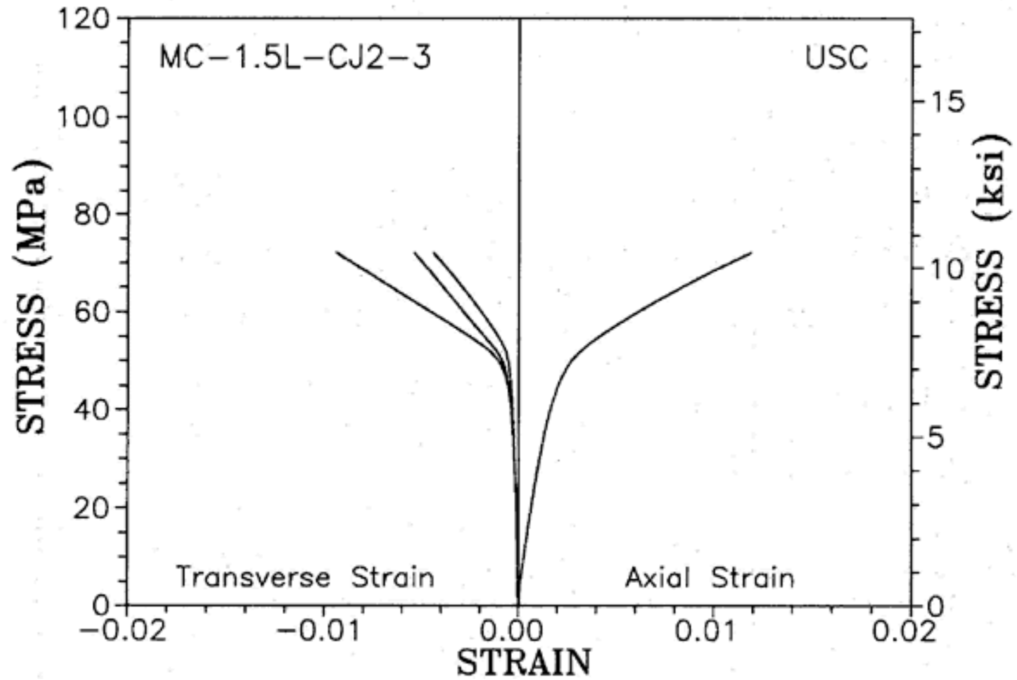

(b)

Fig.B-C4. Stress-Strain Relationships for Medium Strength Concrete with One and a Half-Layer Carbon Fiber Composite Jacket (MC-1.5L-CJ2-3)
(a) Strain Measured by LP (b) Strain Measured by Strain Gages

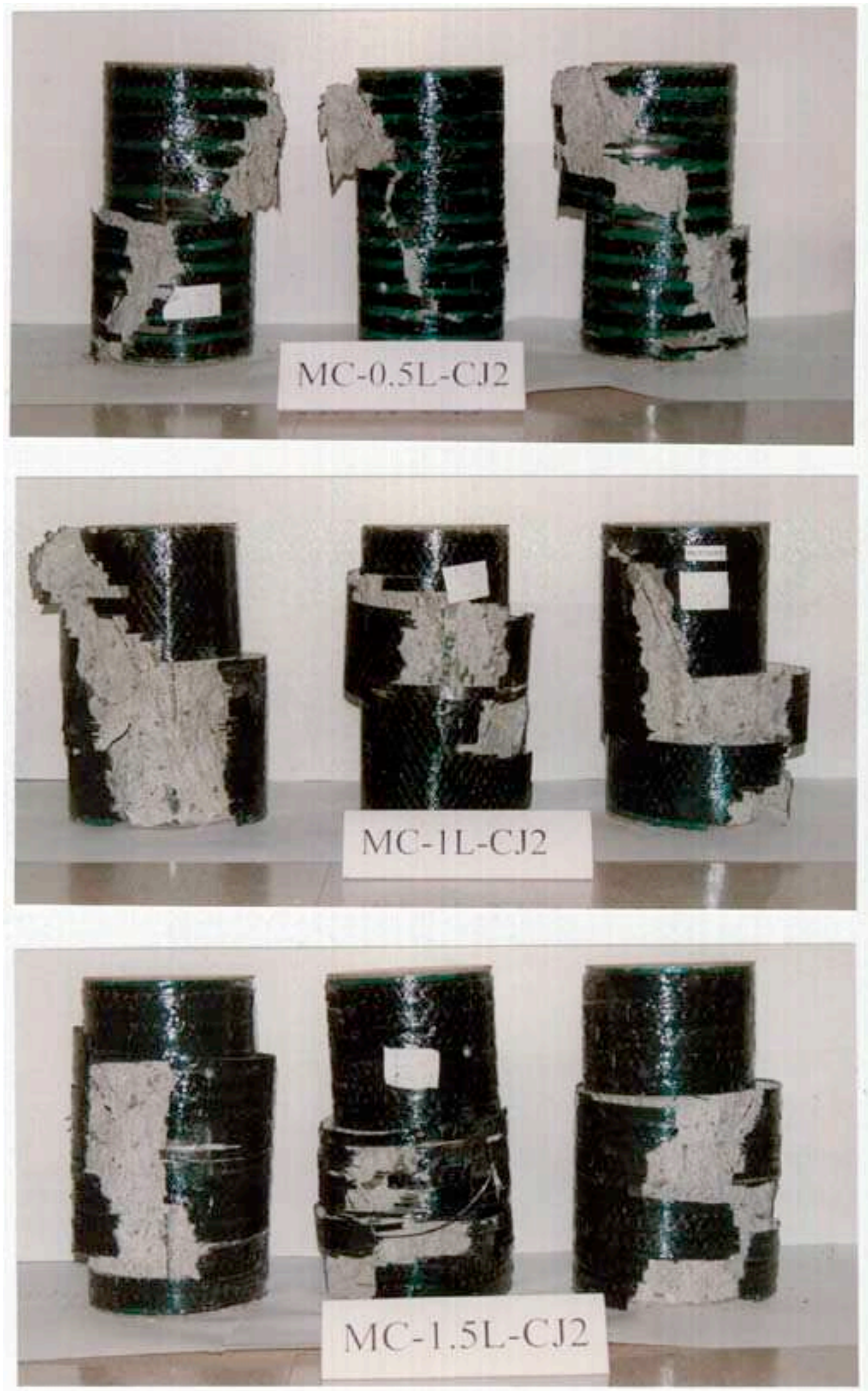

Fig.B-C5. Specimens after Testing

Part B-D Test Results of Higher Strength Concrete Cylinders

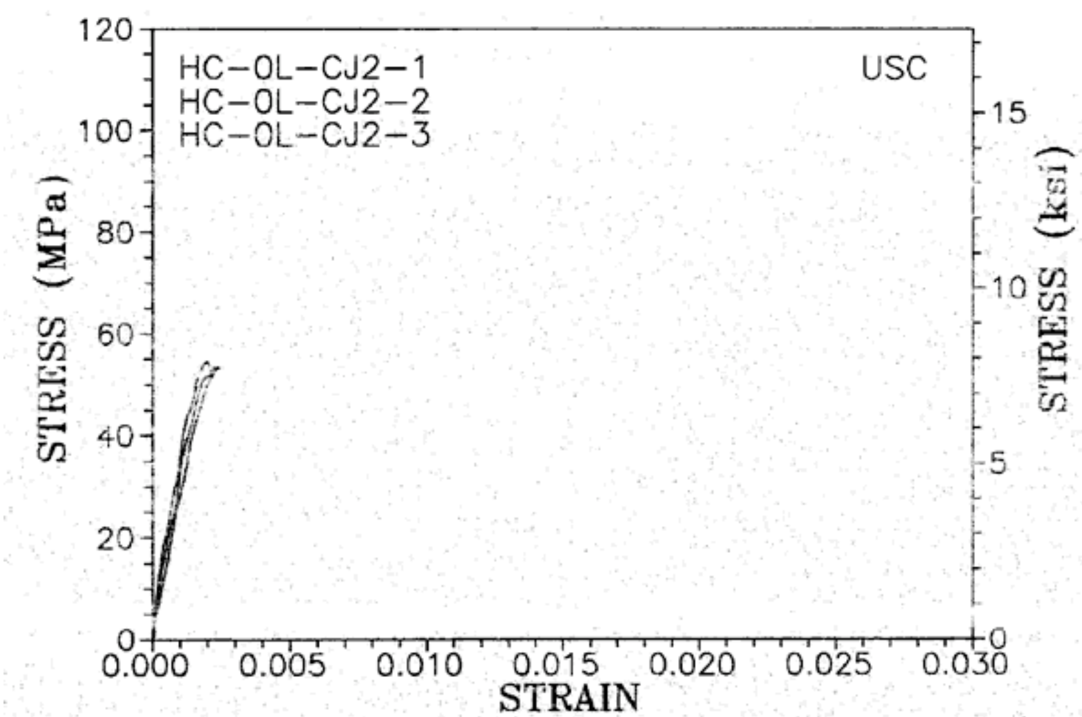

Fig.B-D1. Stress-Strain Relationships for Higher Strength Plain Concrete Cylinders

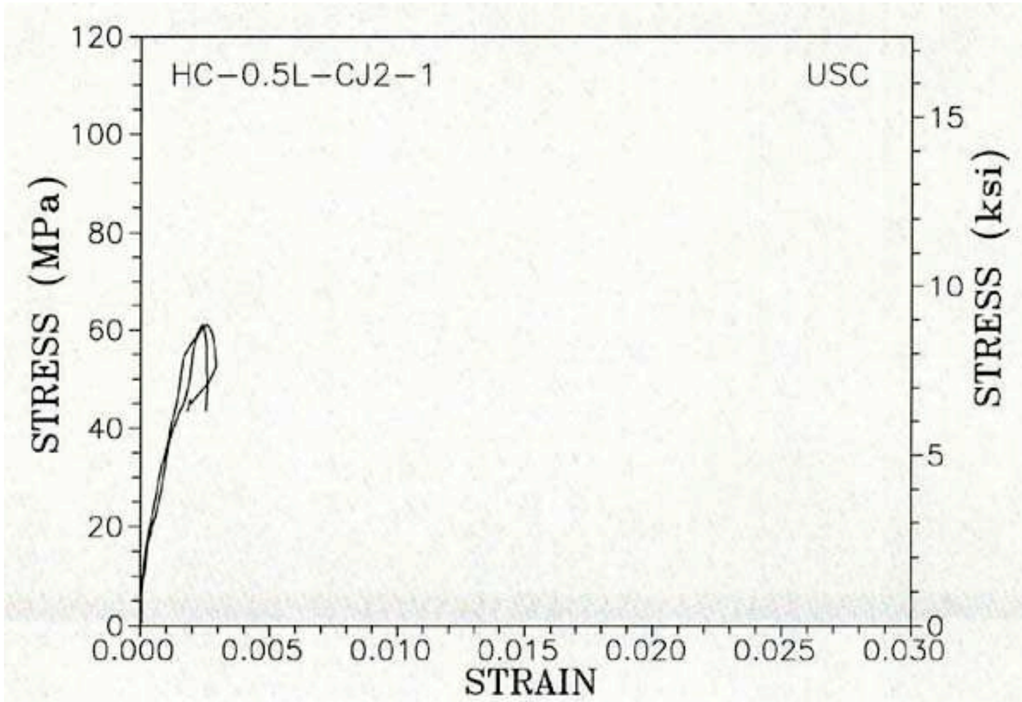

(a)

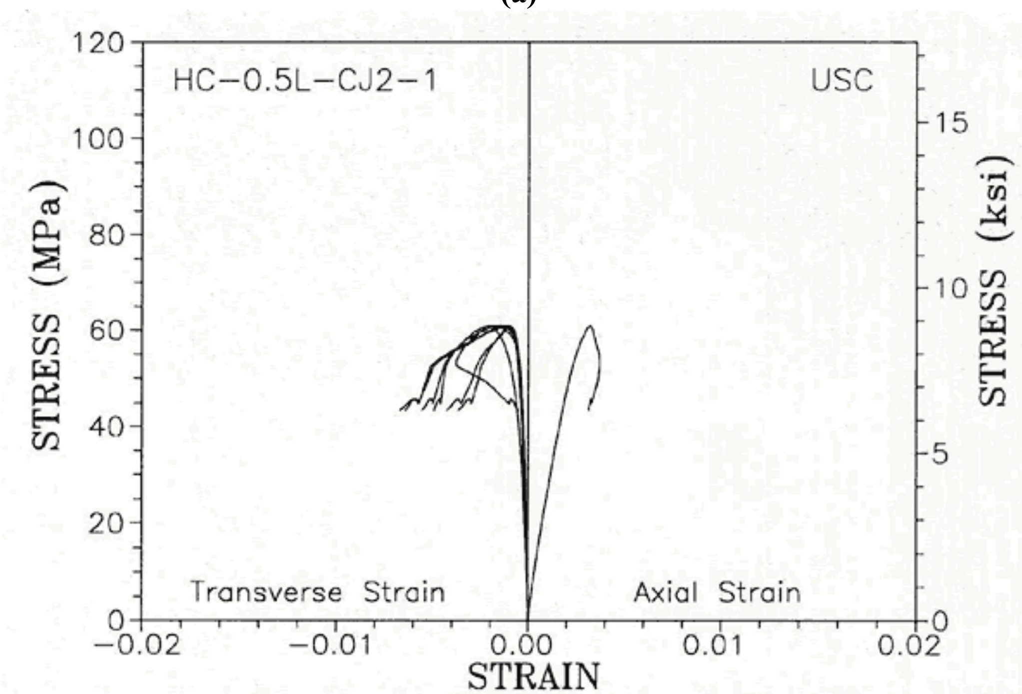

(b)

Fig.B-D2. Stress-Strain Relationships for Higher Strength Concrete with Half-Layer Carbon Fiber Composite Jacket (HC-0.5L-CJ2-1)
(a) Strain Measured by LP (b) Strain Measured by Strain Gages

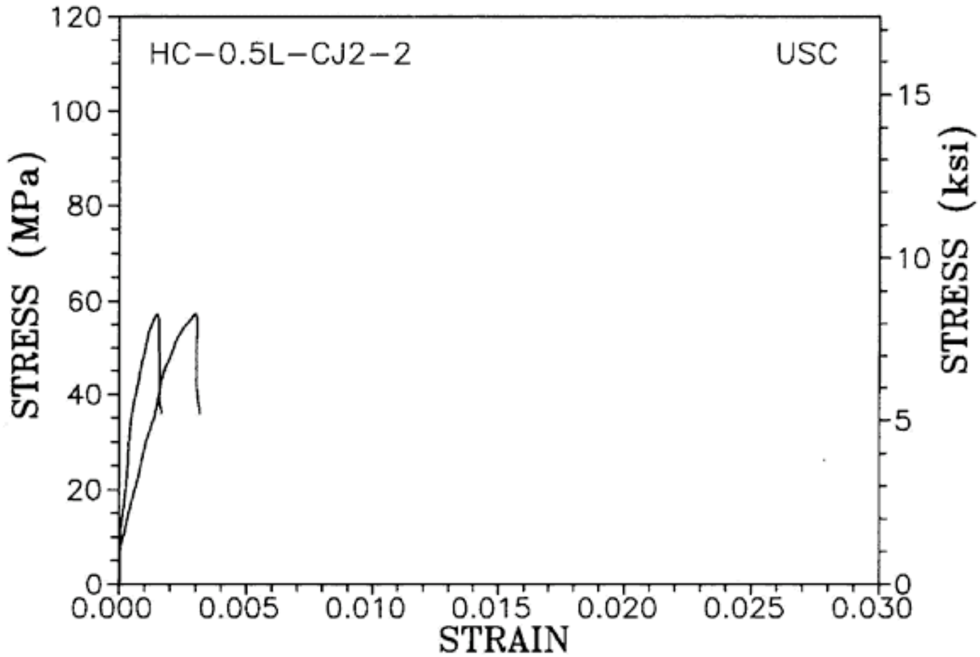

(a)

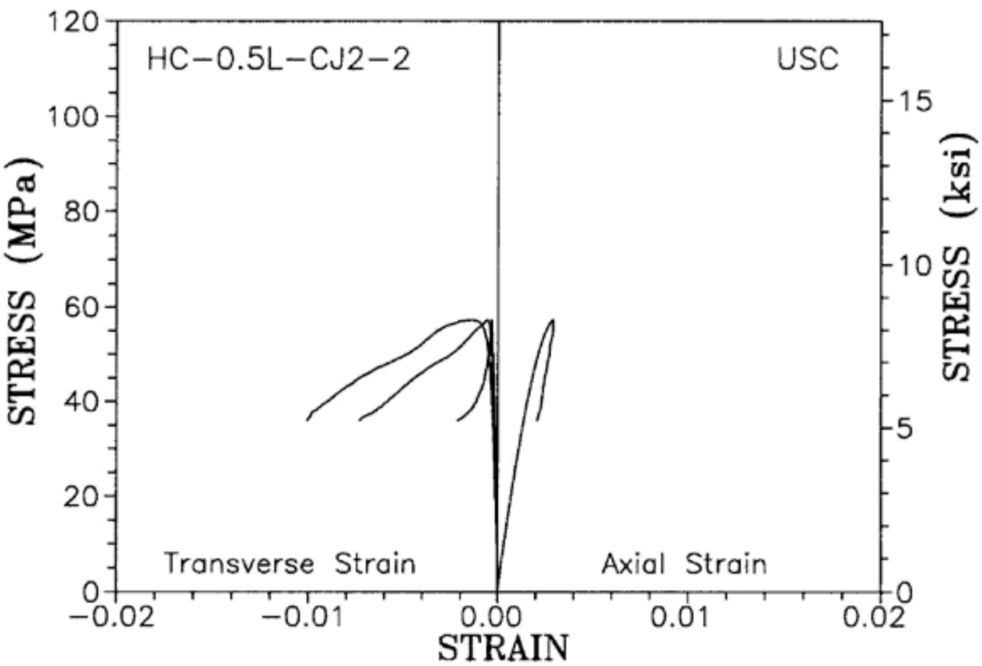

(b)

Fig.B-D2. Stress-Strain Relationships for Higher Strength Concrete with Half-Layer Carbon Fiber Composite Jacket (HC-0.5L-CJ2-2)
(a) Strain Measured by LP (b) Strain Measured by Strain Gages

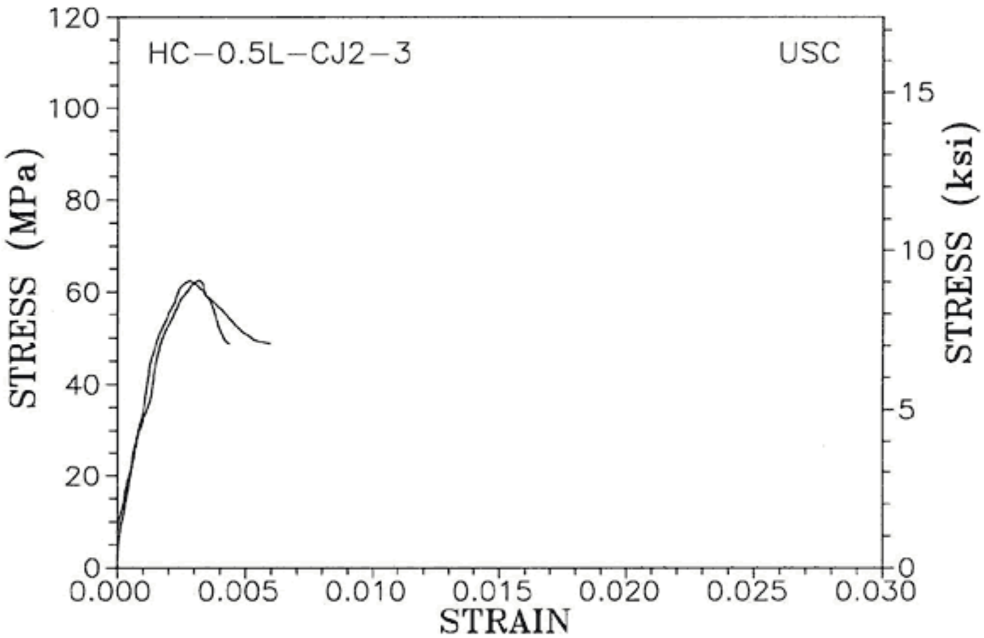

(a)

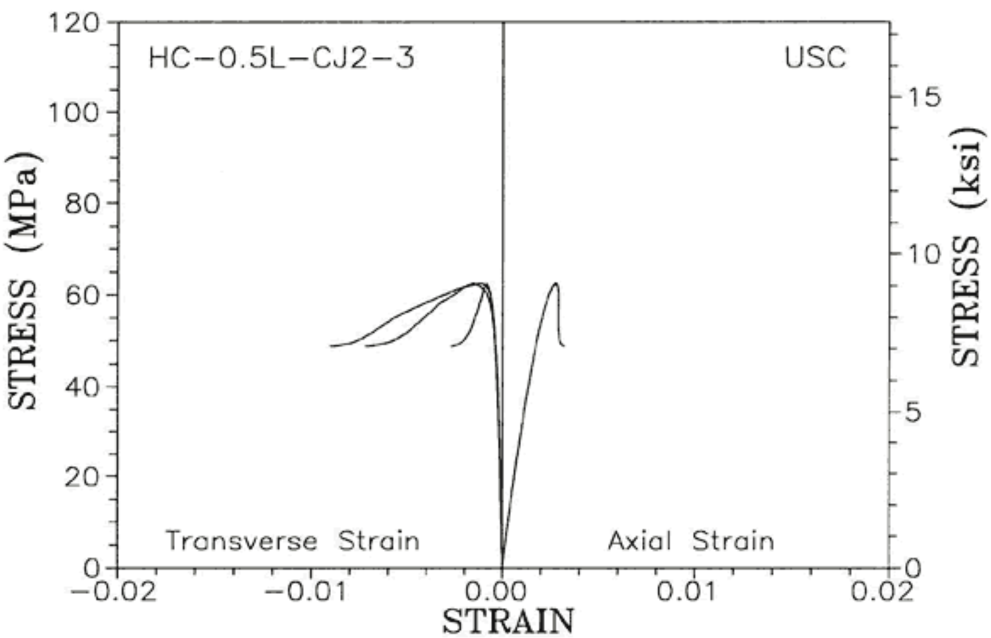

(b)

Fig.B-D2. Stress-Strain Relationships for Higher Strength Concrete with Half-Layer Carbon Fiber Composite Jacket (HC-0.5L-CJ2-3)
(a) Strain Measured by LP (b) Strain Measured by Strain Gages

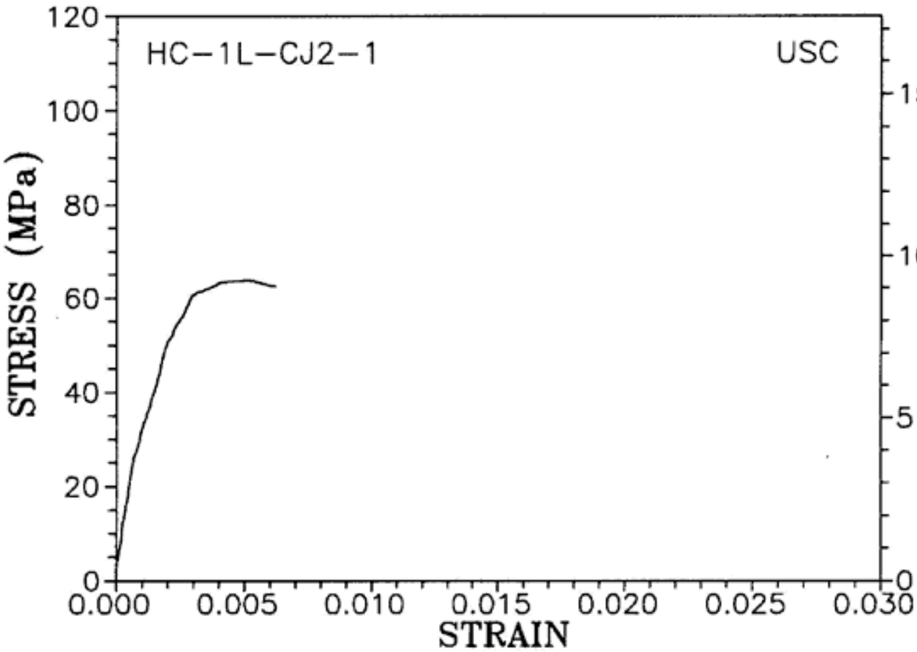

(a)

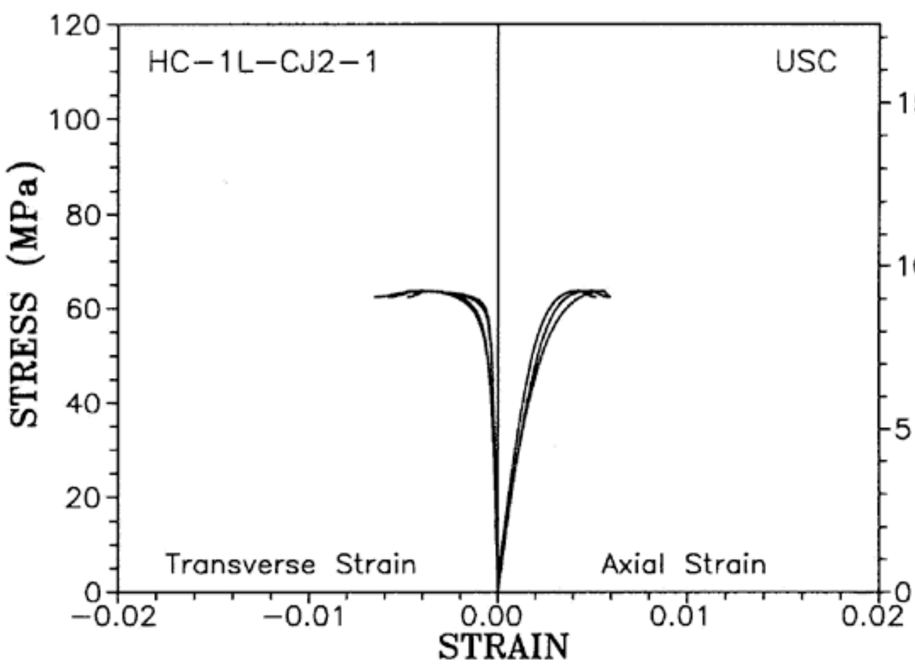

(b)

Fig.B-D3. Stress-Strain Relationships for Higher Strength Concrete with One-Layer Carbon Fiber Composite Jacket (HC-1L-CJ2-1)
(a) Strain Measured by LP (b) Strain Measured by Strain Gages

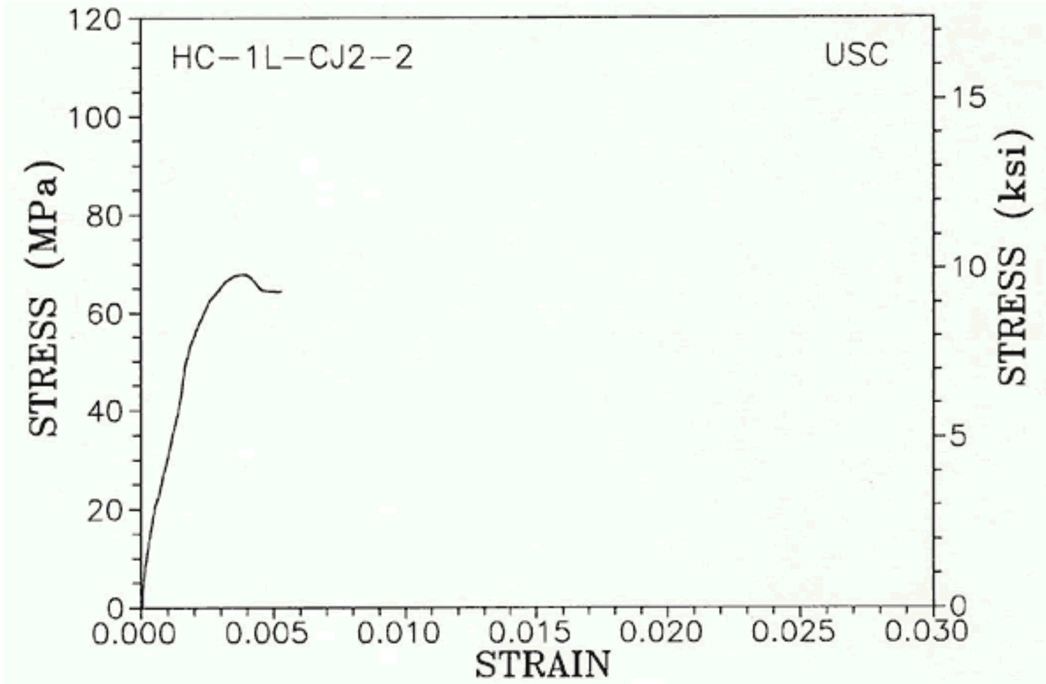

(a)

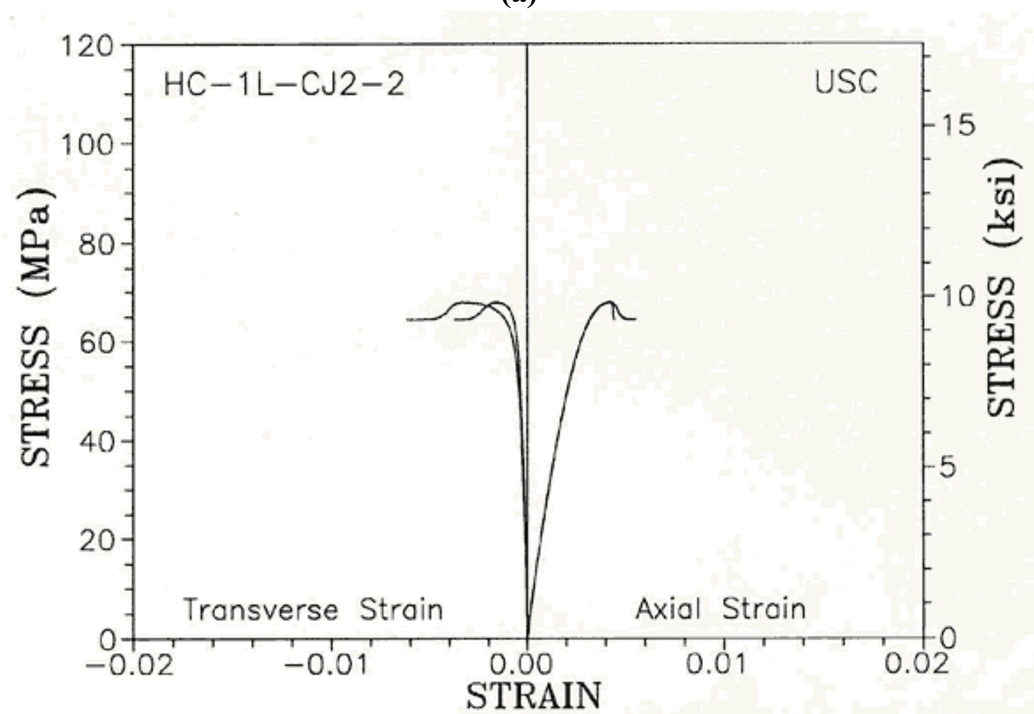

(b)

Fig.B-D3. Stress-Strain Relationships for Higher Strength Concrete with One-Layer Carbon Fiber Composite Jacket (HC-1L-CJ2-2)
(a) Strain Measured by LP (b) Strain Measured by Strain Gages

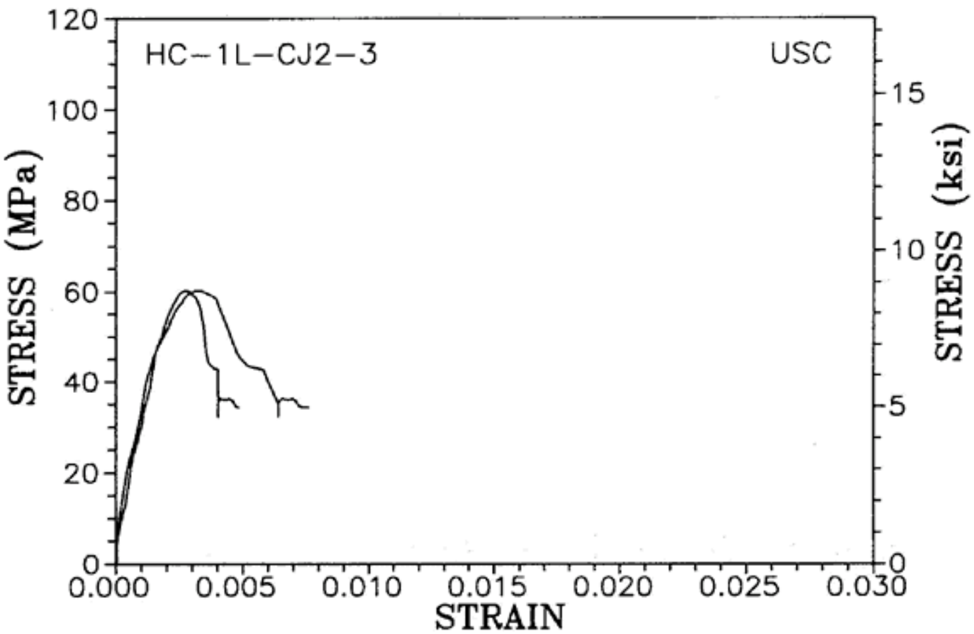

(a)

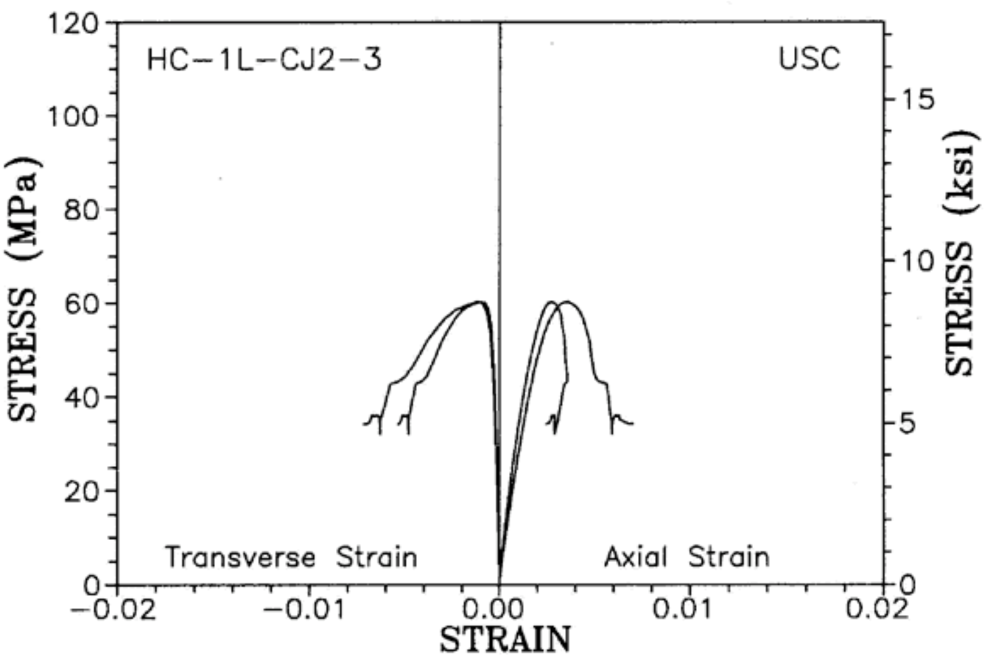

(b)

Fig.B-D3. Stress-Strain Relationships for Higher Strength Concrete with One-Layer Carbon Fiber Composite Jacket (HC-1L-CJ2-3)
(a) Strain Measured by LP (b) Strain Measured by Strain Gages

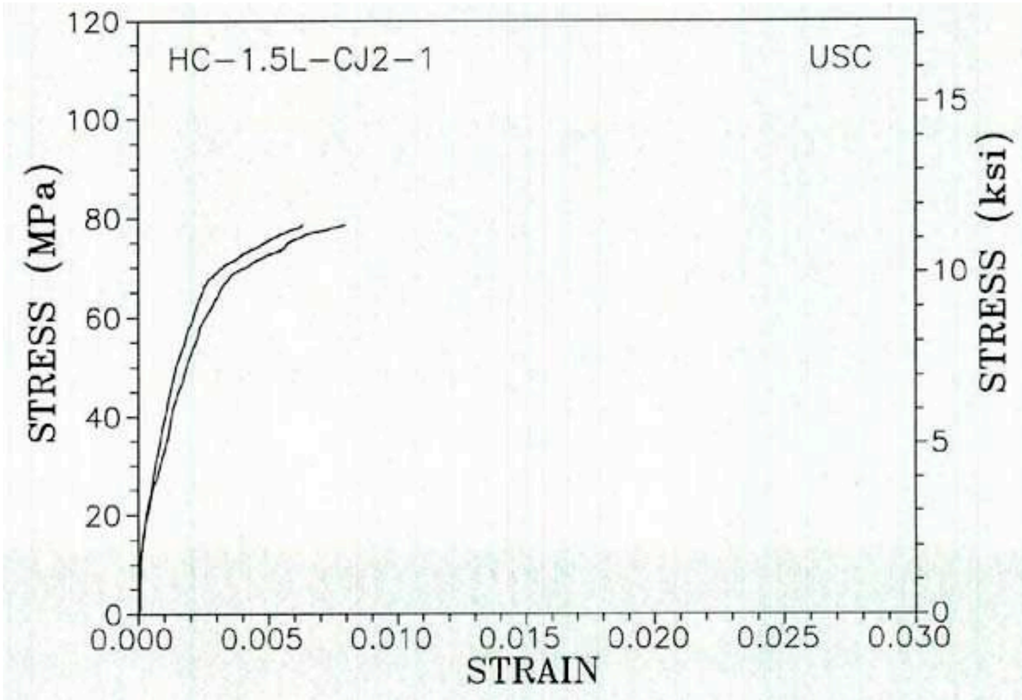

(a)

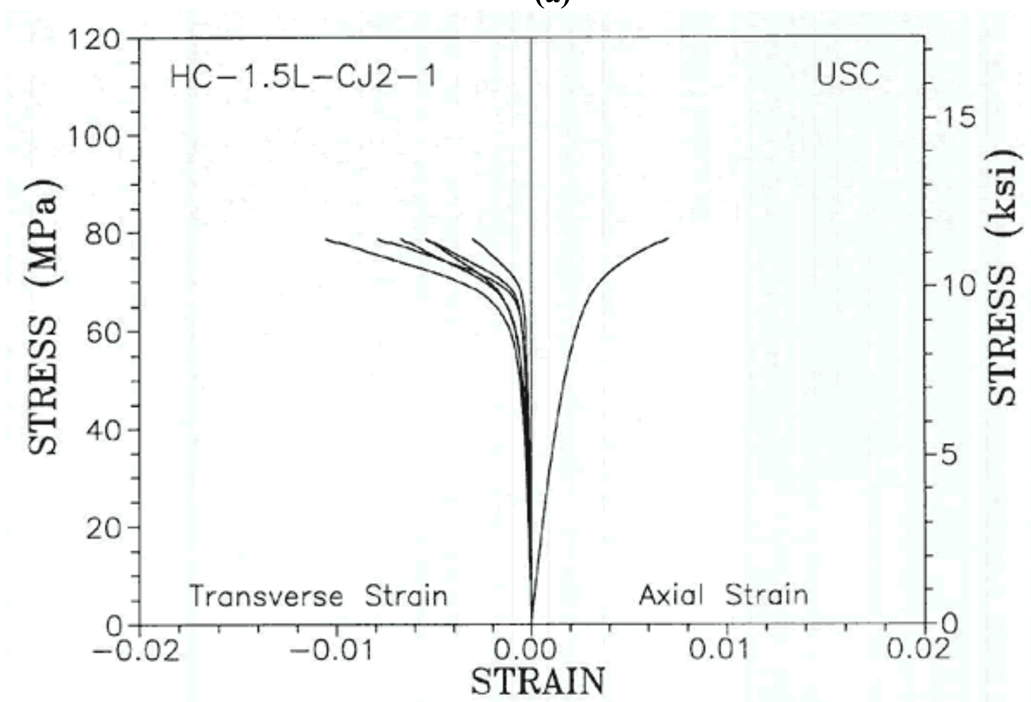

(b)

Fig.B-D4. Stress-Strain Relationships for Higher Strength Concrete with One and Half-Layer Carbon Fiber Composite Jacket (HC-1.5L-CJ2-1)
(a) Strain Measured by LP (b) Strain Measured by Strain Gages

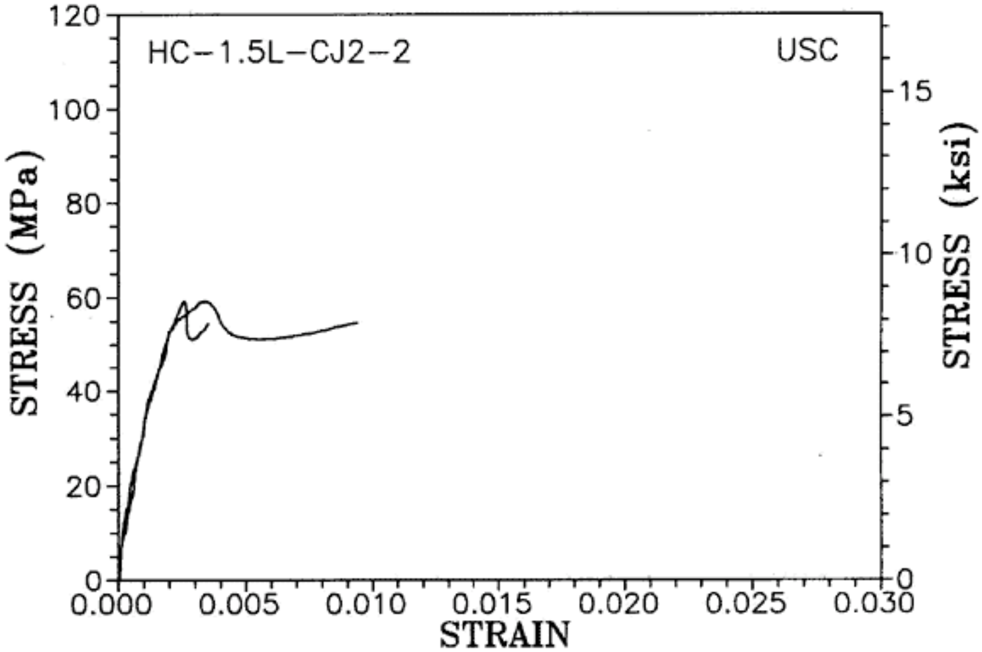

(a)

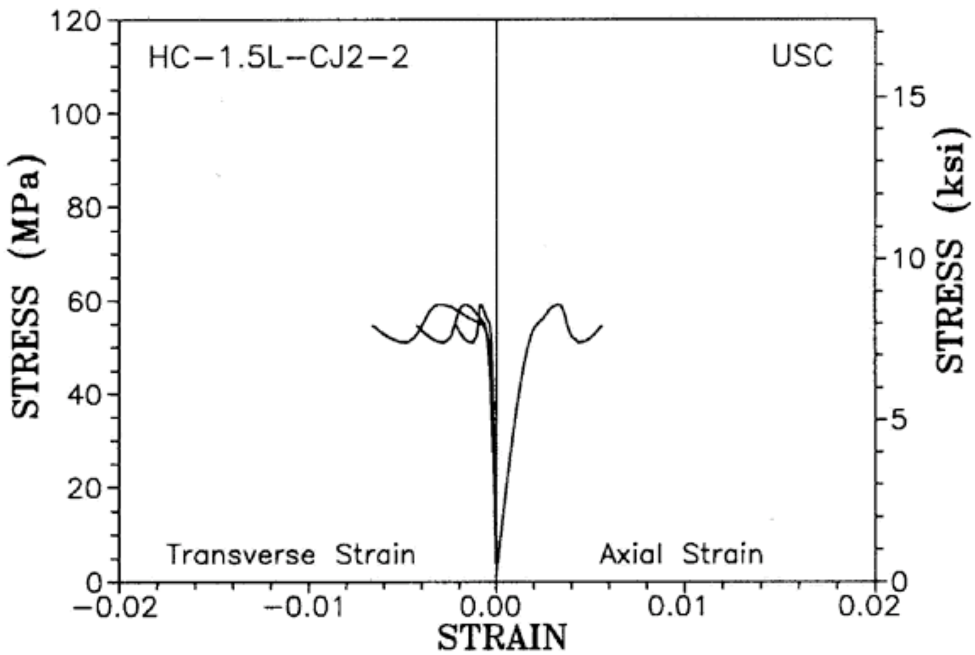

(b)

Fig.B-D4. Stress-Strain Relationships for Higher Strength Concrete with One and Half-Layer Carbon Fiber Composite Jacket (HC-1.5L-CJ2-2) (a) Strain Measured by LP (b) Strain Measured by Strain Gages

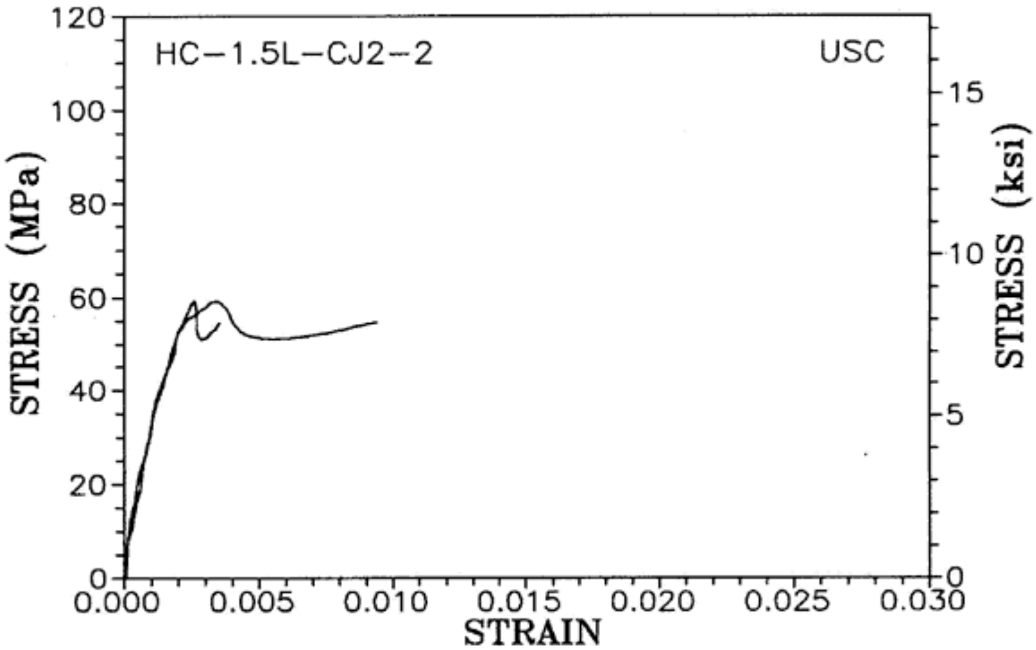

(a)

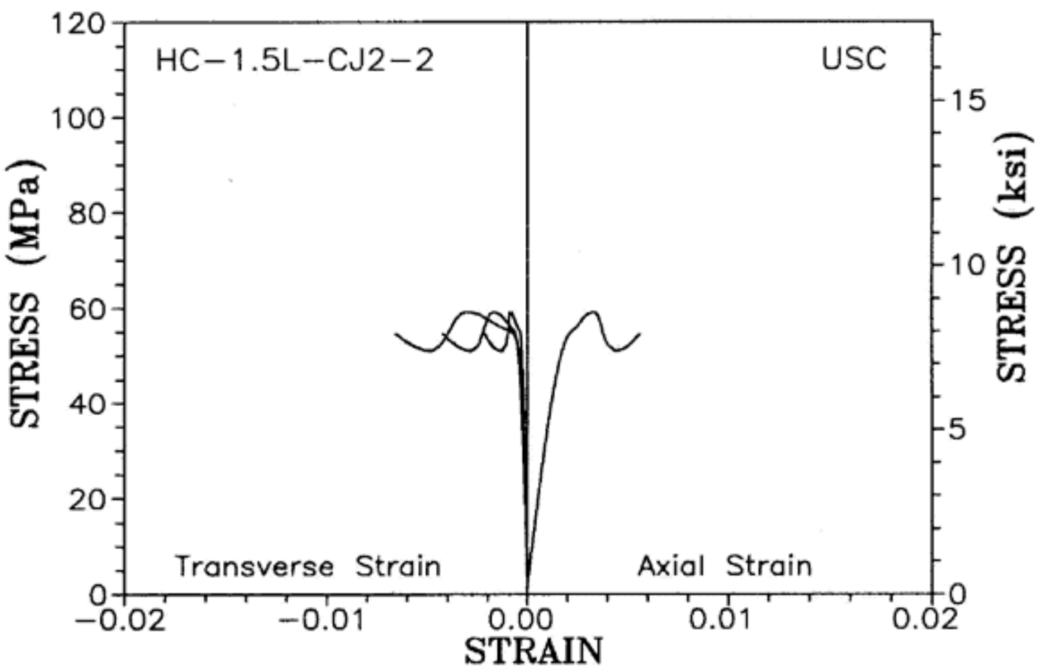

(b)

Fig.B-D4. Stress-Strain Relationships for Higher Strength Concrete with One and Half-Layer Carbon Fiber Composite Jacket (HC-1.5L-CJ2-2) (a) Strain Measured by LP (b) Strain Measured by Strain Gages

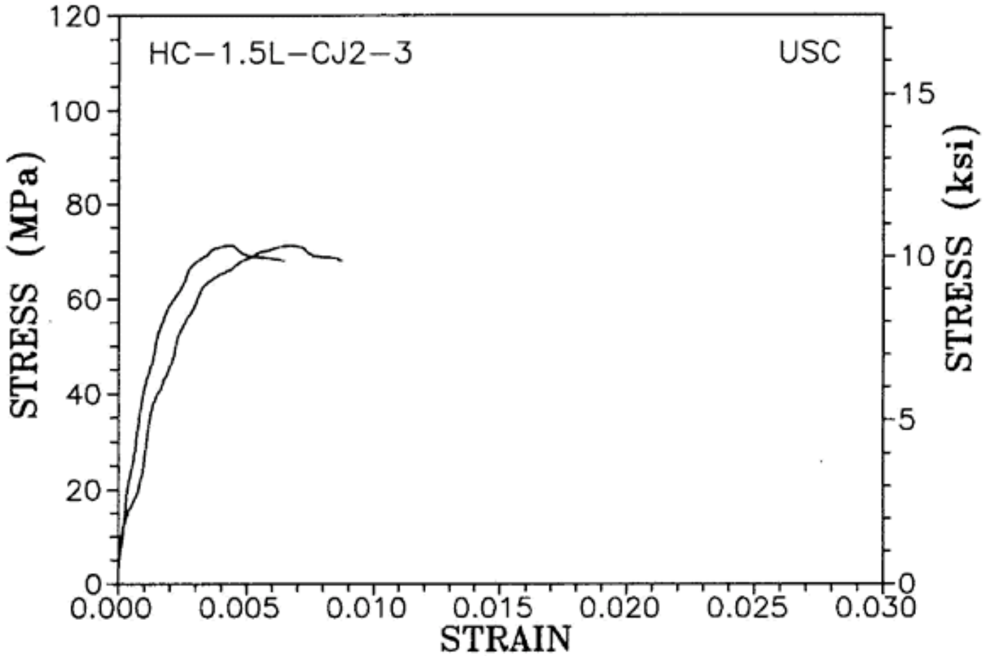

(a)

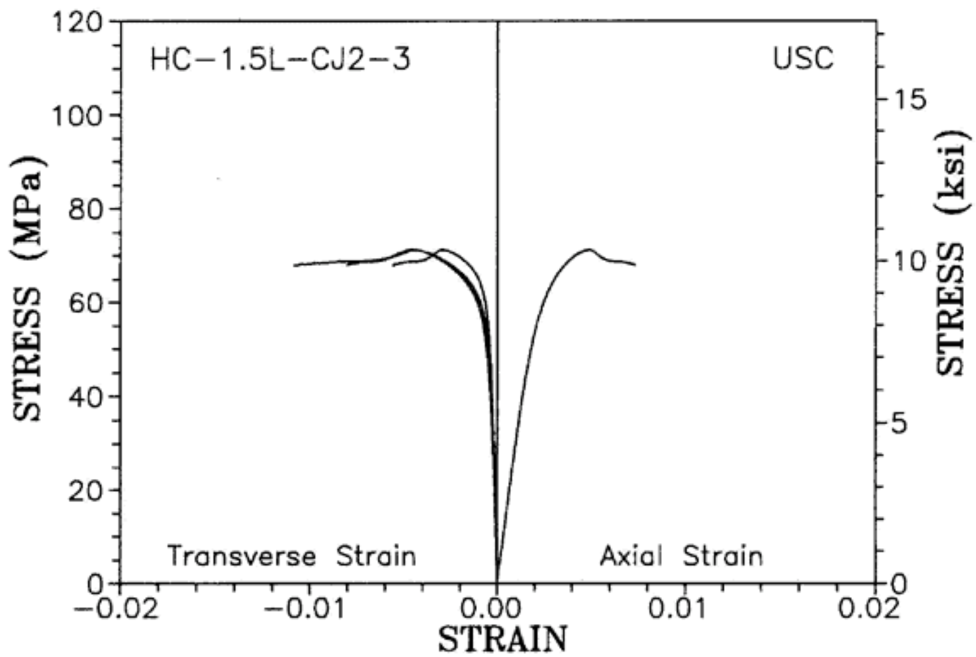

(b)

Fig.B-D4. Stress-Strain Relationships for Higher Strength Concrete with One and Half-Layer Carbon Fiber Composite Jacket (HC-1.5L-CJ2-3)
(a) Strain Measured by LP (b) Strain Measured by Strain Gages

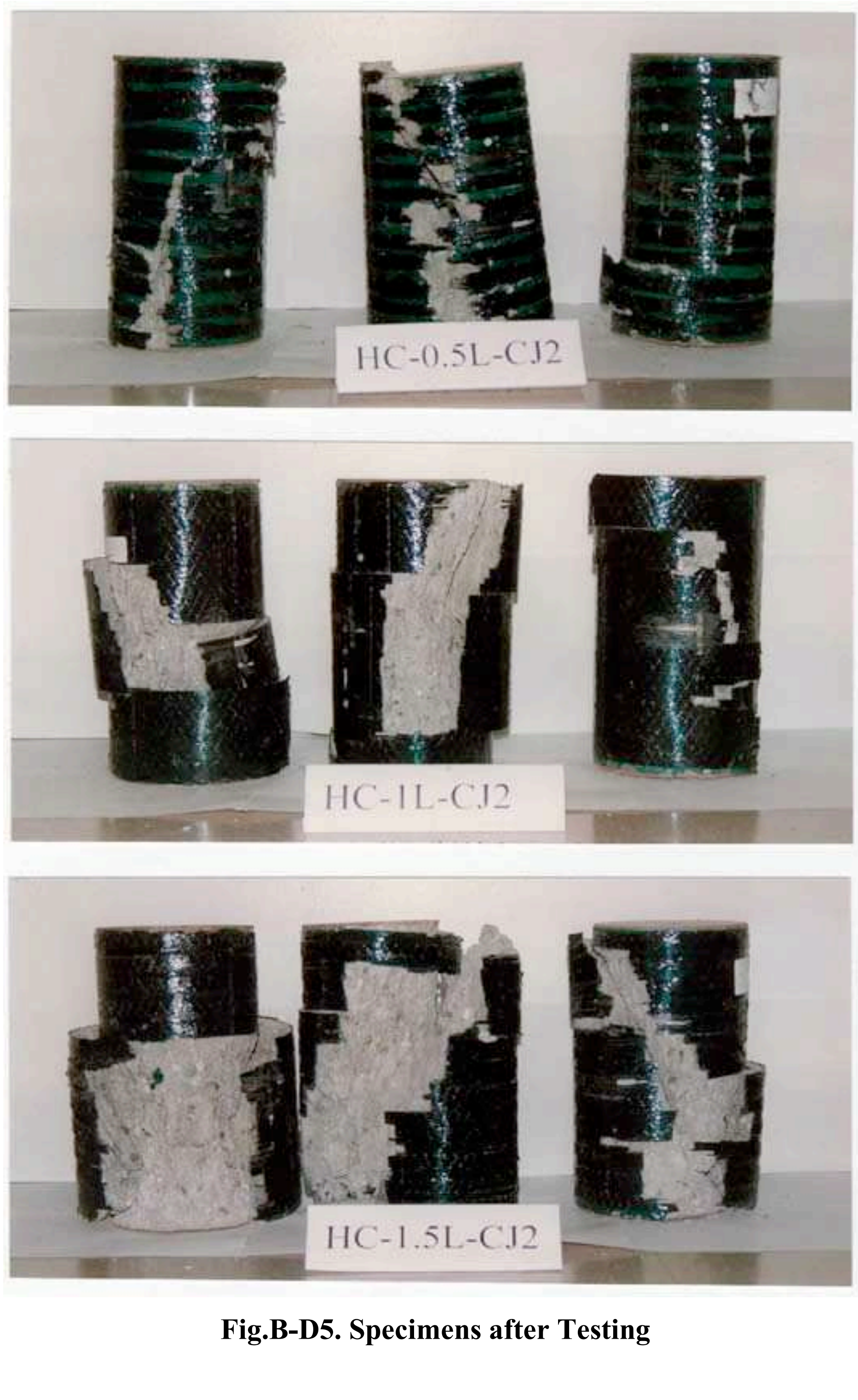

Fig.B-D5. Specimens after Testing

APPENDIX C: TEST RESULTS OF SYSTEM THREE

Part C-A General Information

Table C-A4 Test Results

Series	Specimen	f_c' (MPa)	Jacket Layers	f_{cc}' (Mpa)	ε_{cu}
L	LC-0L-PGJ-1	31.3	0	29.84	0.001983
	LC-0L-PGJ-2			32.03	0.002011
	LC-0L-PGJ-3			32.03	0.001867
	LC-2L-PGJ-1		2	42.38	0.01931
	LC-2L-PGJ-2			43.89	0.01820
	LC-2L-PGJ-3			45.11	0.01326
	LC-3L-PGJ-1		3	58.92	0.01940
	LC-3L-PGJ-2			55.99	0.01996
	LC-3L-PGJ-3			61.05	0.02370
	LC-4L-PGJ-1		4	71.80	0.02806
	LC-4L-PGJ-2			78.09	0.02800
	LC-4L-PGJ-3			76.54	0.03370
M	MC-0L-PGJ-1	43.9	0	43.87	0.001754
	MC-0L-PGJ-2			44.53	0.001868
	MC-0L-PGJ-3			43.22	0.001935
	MC-2L-PGJ-1		2	55.26	0.007540
	MC-2L-PGJ-2			45.42	0.008781
	MC-2L-PGJ-3			47.86	0.003680
	MC-3L-PGJ-1		3	56.86	0.01400
	MC-3L-PGJ-2			59.76	0.02556
	MC-3L-PGJ-3			51.73	0.01920
	MC-4L-PGJ-1		4	49.90	0.01250
	MC-4L-PGJ-2			59.96	0.02070
	MC-4L-PGJ-3			73.09	0.02134
H	HC-0L-PGJ-1	60.1	0	56.95	0.001677
	HC-0L-PGJ-2			65.46	0.002218
	HC-0L-PGJ-3			57.83	0.001860
	HC-2L-PGJ-1		2	67.01	0.007952
	HC-2L-PGJ-2			65.86	0.005600
	HC-2L-PGJ-3			72.42	0.002550
	HC-3L-PGJ-1		3	70.14	0.00675
	HC-3L-PGJ-2			63.80	0.01330
	HC-3L-PGJ-3			67.52	0.00768
	HC-4L-PGJ-1		4	66.66	0.00239
	HC-4L-PGJ-2			70.98	0.02087
	HC-4L-PGJ-3			78.17	0.01561

Note: (i) Example for specimen name designation:

LC-2L-PGJ-1: LC designates Lower strength Concrete; 2L designates 2 Layers; PGJ designates

Prefabricated Glass fiber Jacket System; and the last number represents specimen number in same series.

(ii) f_c': Average plain concrete cylinder strength;

(iii) f_{cc}': Ultimate strength of confined concrete;

(iv) ε_{cu}: Ultimate strain.

Part C-B Test Results of Lower Strength Concrete Cylinders

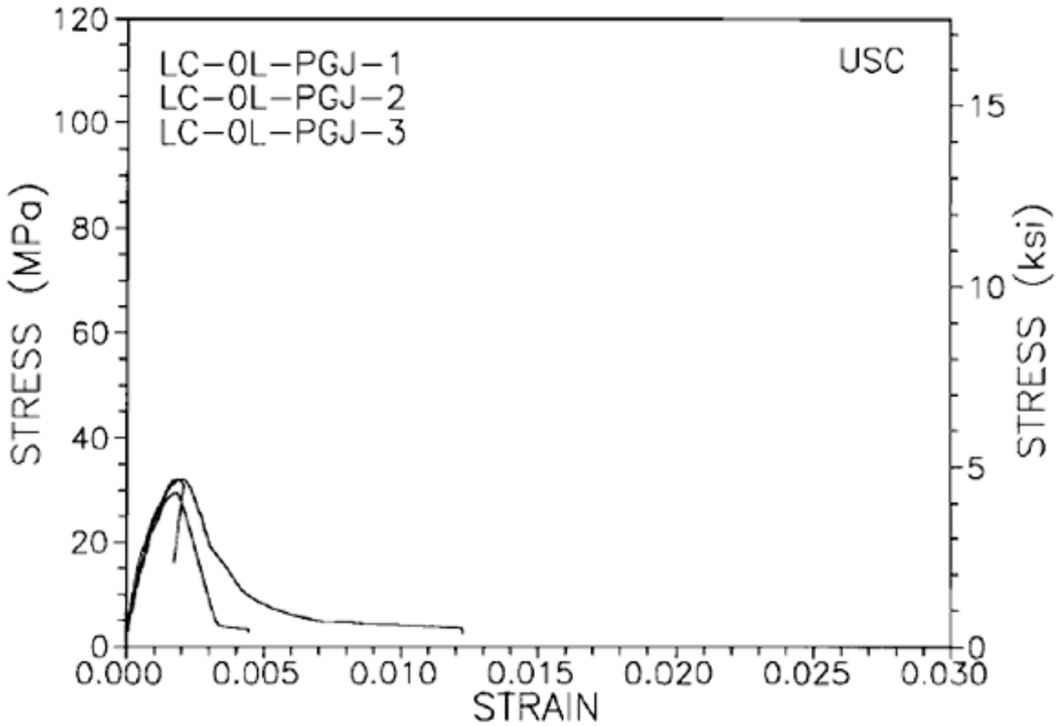

Fig. C-B1. Stress-Strain Relationships for Lower Strength Plain Concrete Cylinders

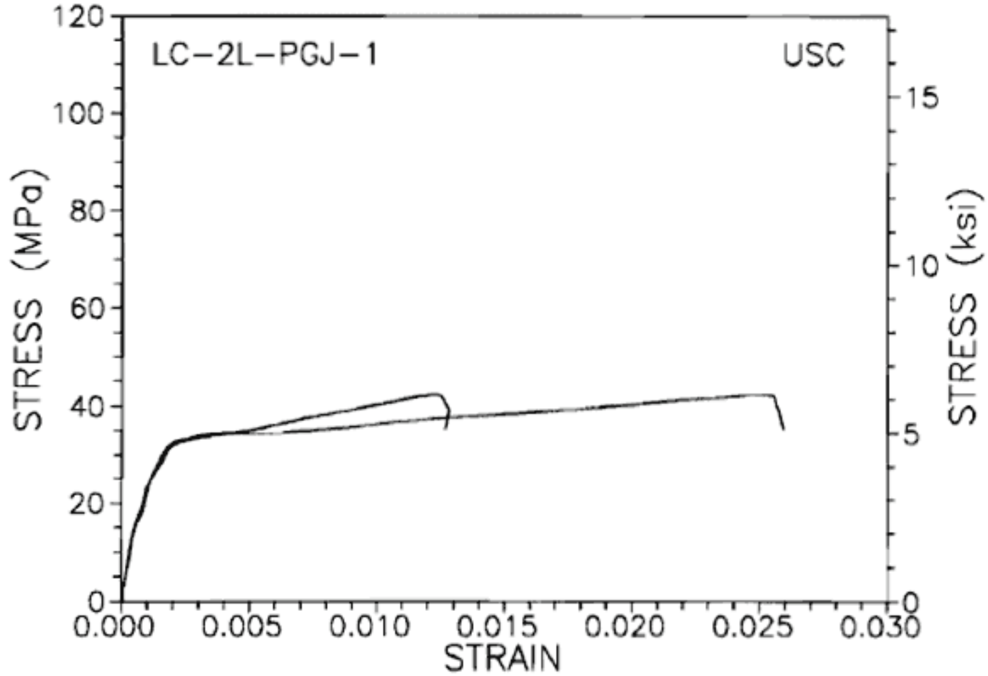

(a)

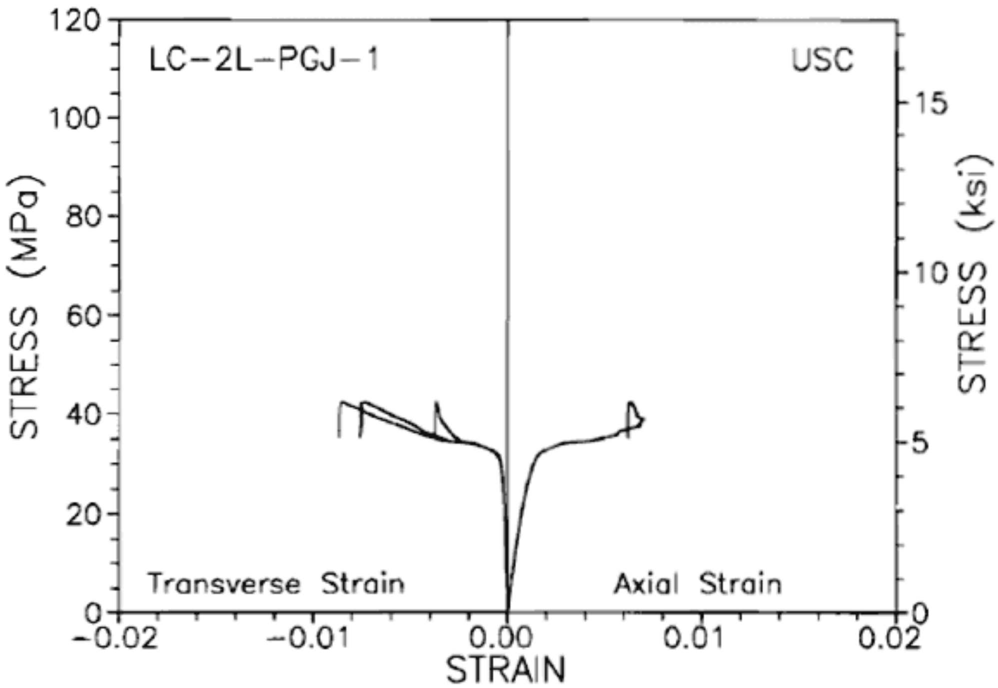

(b)

Fig.C-B2. Stress-Strain Relationships for Lower Strength Concrete with Two-Layer Prefabricated Glass Fiber Composite Jacket (LC-2L-PGJ-1)
(a) Strain Measured by LP (b) Strain Measured by Strain Gages

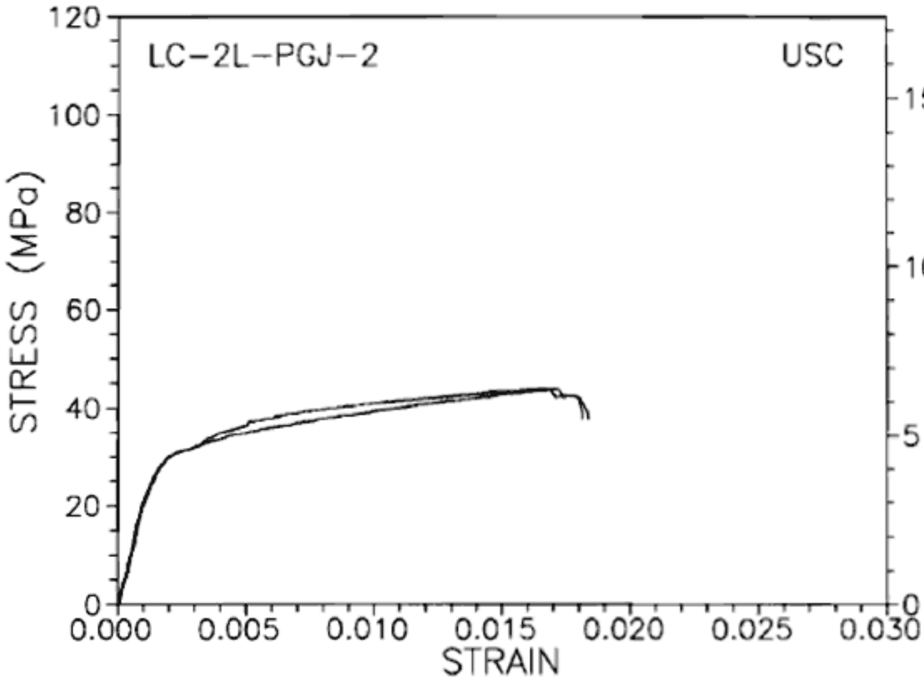

(a)

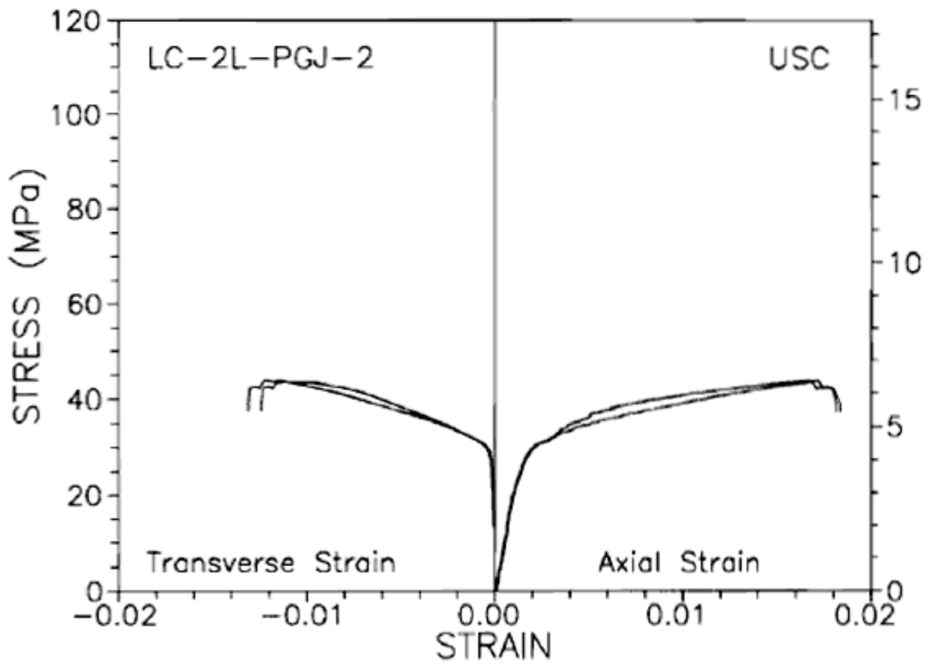

(b)

Fig.C-B2. Stress-Strain Relationships for Lower Strength Concrete with Two-Layer Prefabricated Glass Fiber Composite Jacket (LC-2L-PGJ-2)
(a) Strain Measured by LP (b) Strain Measured by Strain Gages

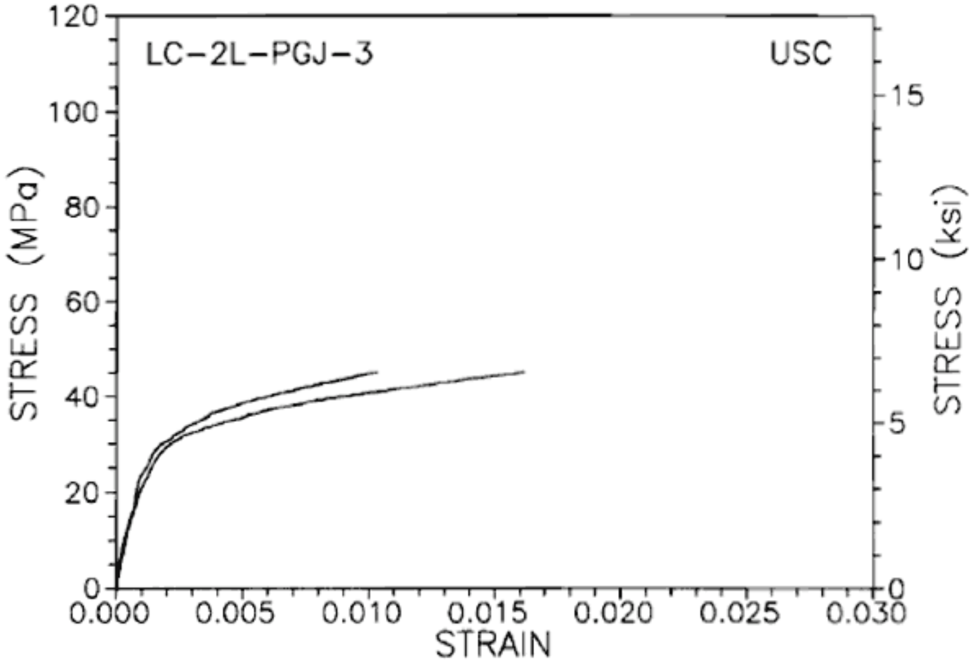

(a)

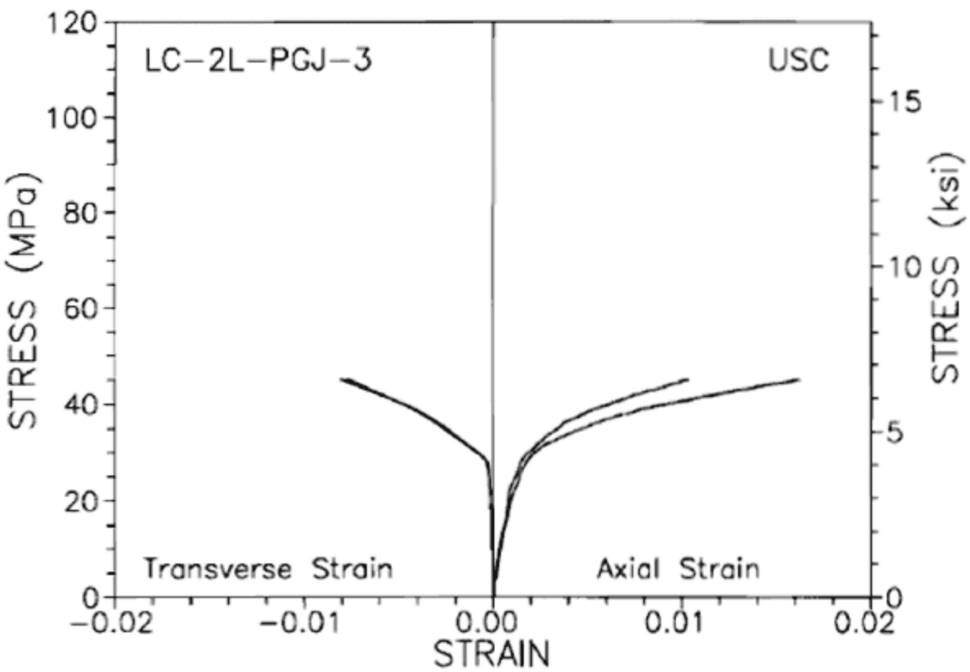

(b)

Fig.C-B2. Stress-Strain Relationships for Lower Strength Concrete with Two-Layer Prefabricated Glass Fiber Composite Jacket (LC-2L-PGJ-3)
(a) Strain Measured by LP (b) Strain Measured by Strain Gages

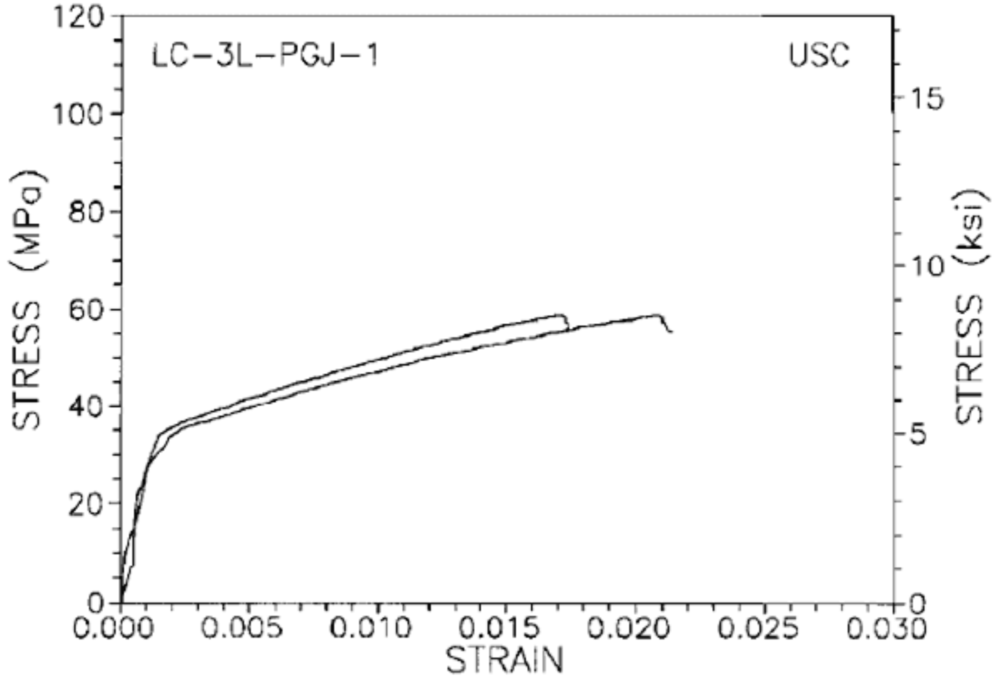

(a)

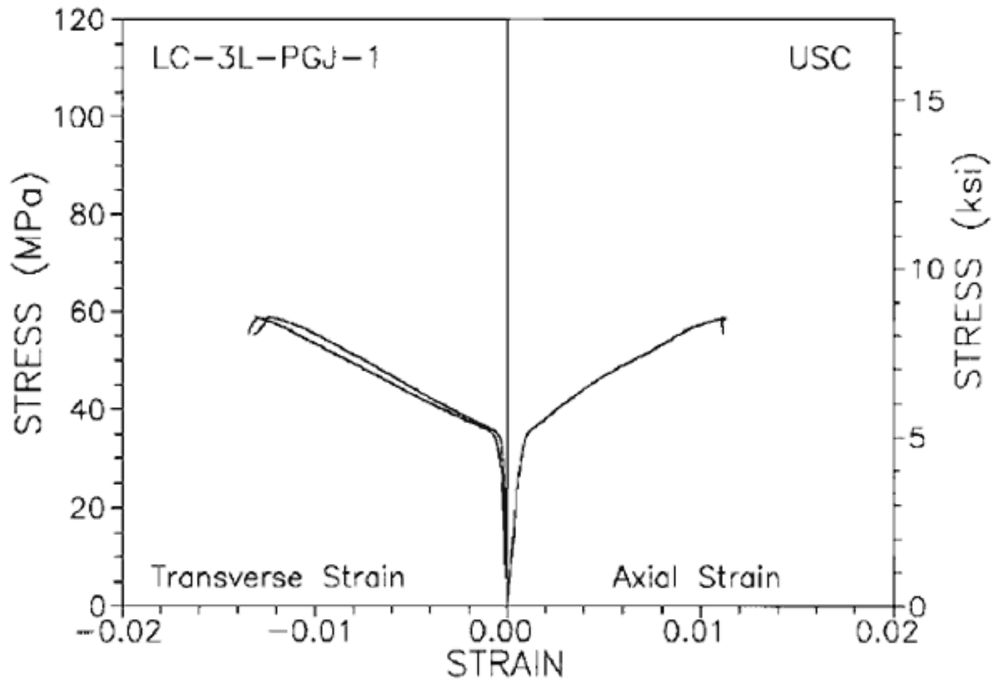

(b)

Fig.C-B3. Stress-Strain Relationships for Lower Strength Concrete with Three-Layer Prefabricated Glass Fiber Composite Jacket (LC-3L-PGJ-1)
(a) Strain Measured by LP (b) Strain Measured by Strain Gages

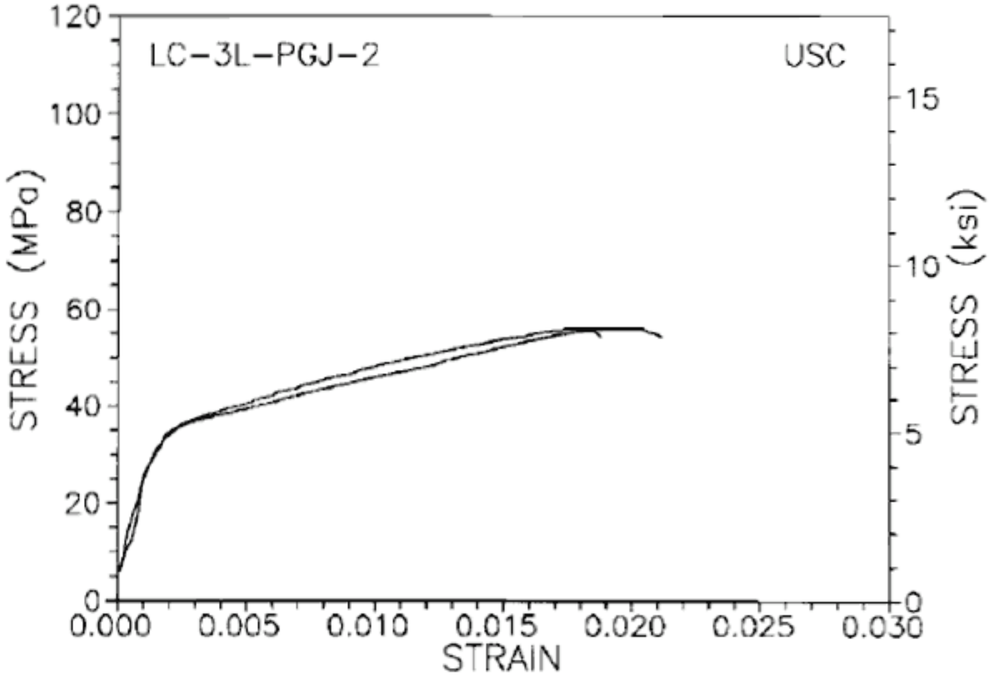

(a)

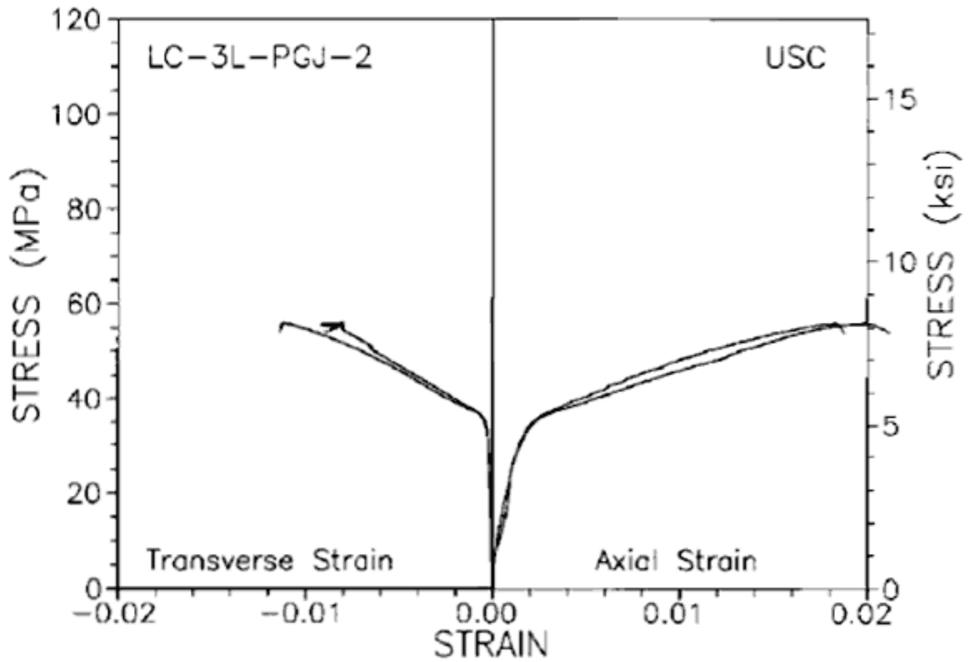

(b)

Fig.C-B3. Stress-Strain Relationships for Lower Strength Concrete with Three-Layer Prefabricated Glass Fiber Composite Jacket (LC-3L-PGJ-2)
(a) Strain Measured by LP (b) Strain Measured by Strain Gages

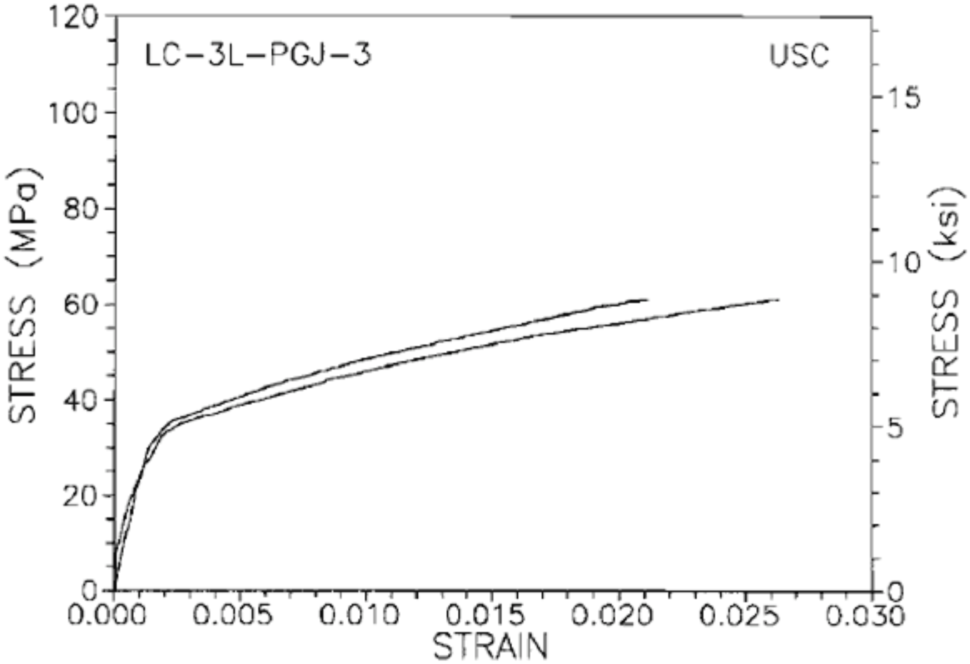

(a)

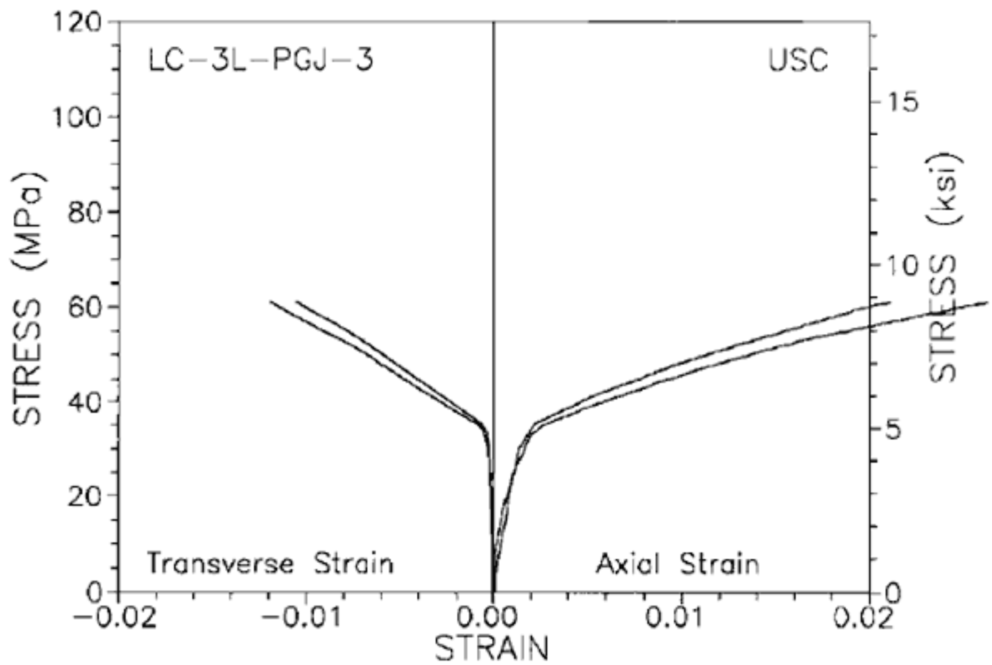

(b)

Fig.C-B3. Stress-Strain Relationships for Lower Strength Concrete with Three-Layer Prefabricated Glass Fiber Composite Jacket (LC-3L-PGJ-3)
(a) Strain Measured by LP (b) Strain Measured by Strain Gages

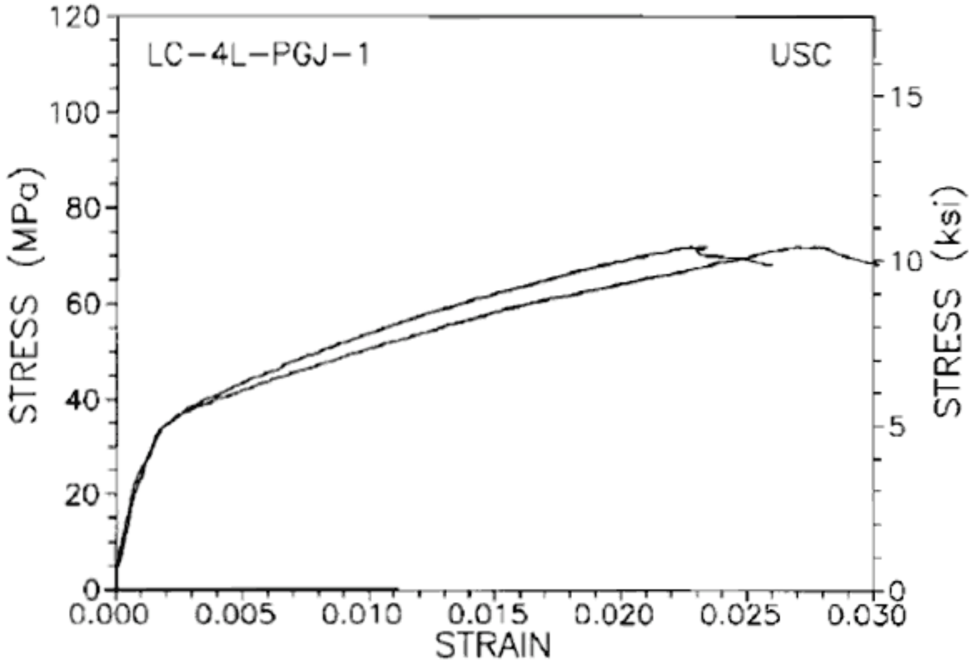

(a)

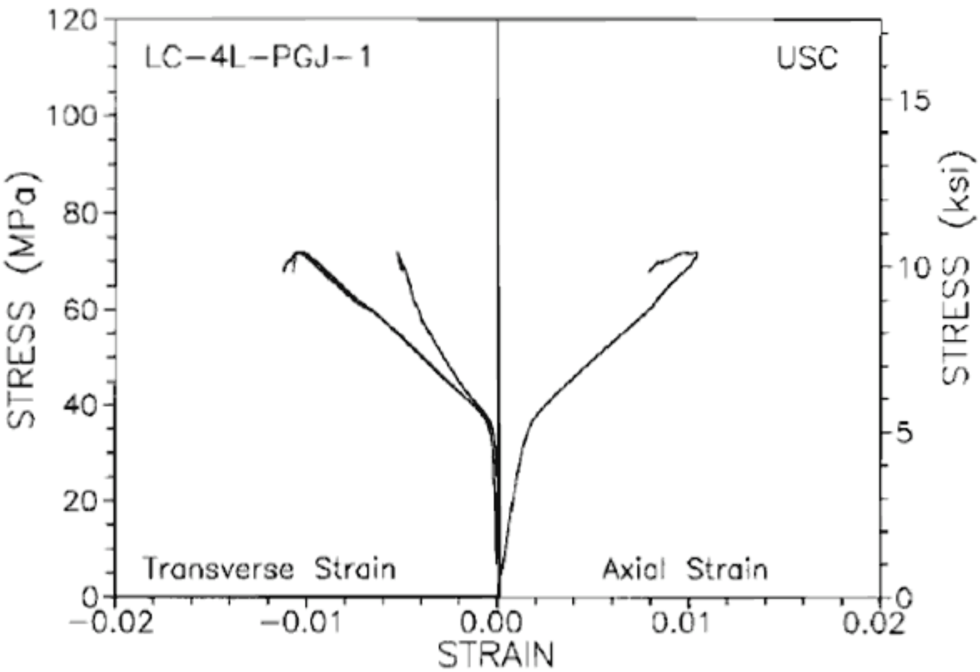

(b)

Fig.C-B4. Stress-Strain Relationships for Lower Strength Concrete with Four-Layer Prefabricated Glass Fiber Composite Jacket (LC-4L-PGJ-1)
(a) Strain Measured by LP (b) Strain Measured by Strain Gages

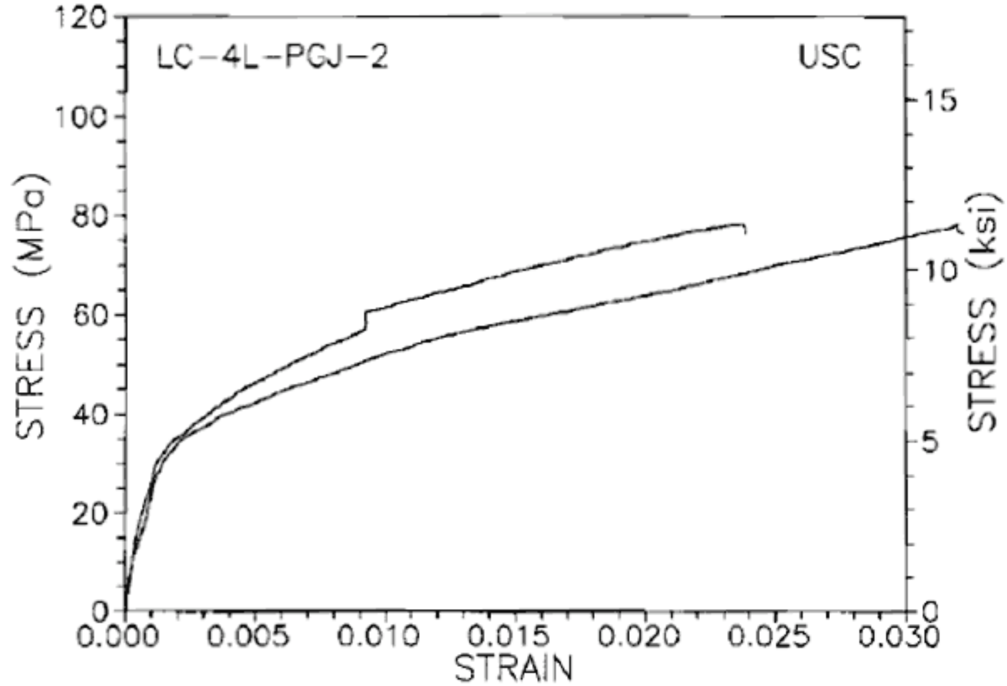

(a)

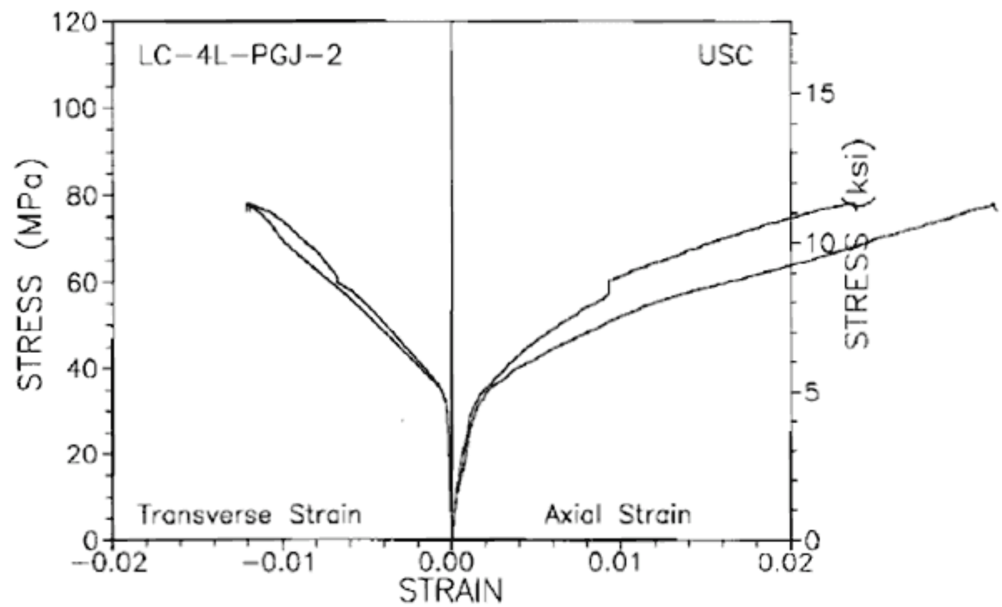

(b)

Fig.C-B4. Stress-Strain Relationships for Lower Strength Concrete with Four-Layer Prefabricated Glass Fiber Composite Jacket (LC-4L-PGJ-2)
(a) Strain Measured by LP (b) Strain Measured by Strain Gages

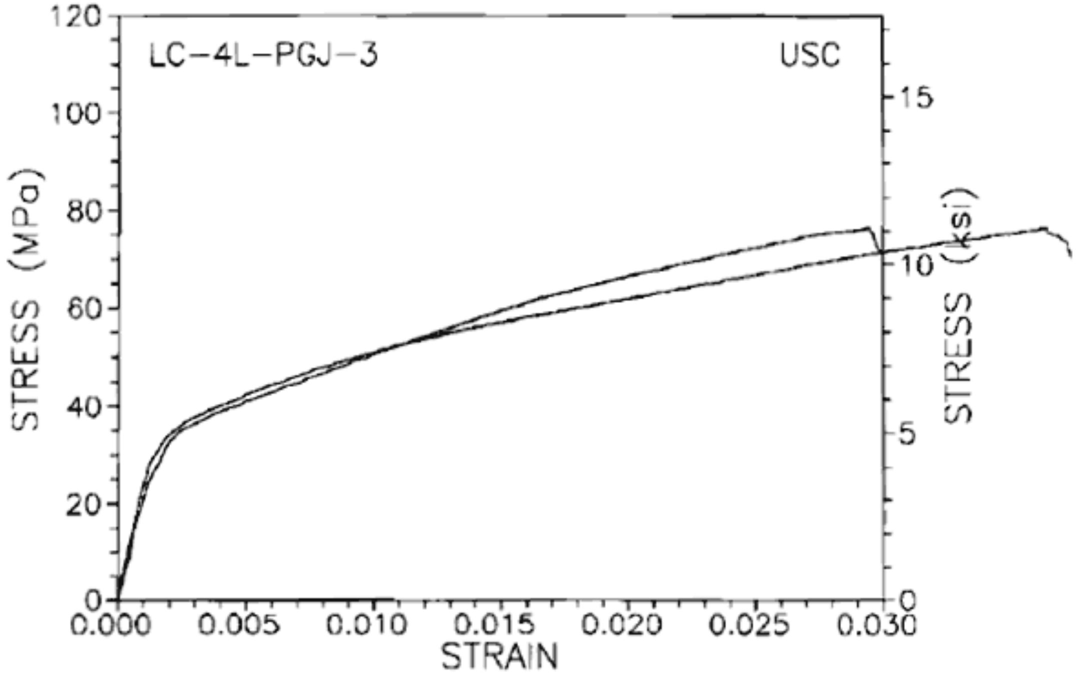

(a)

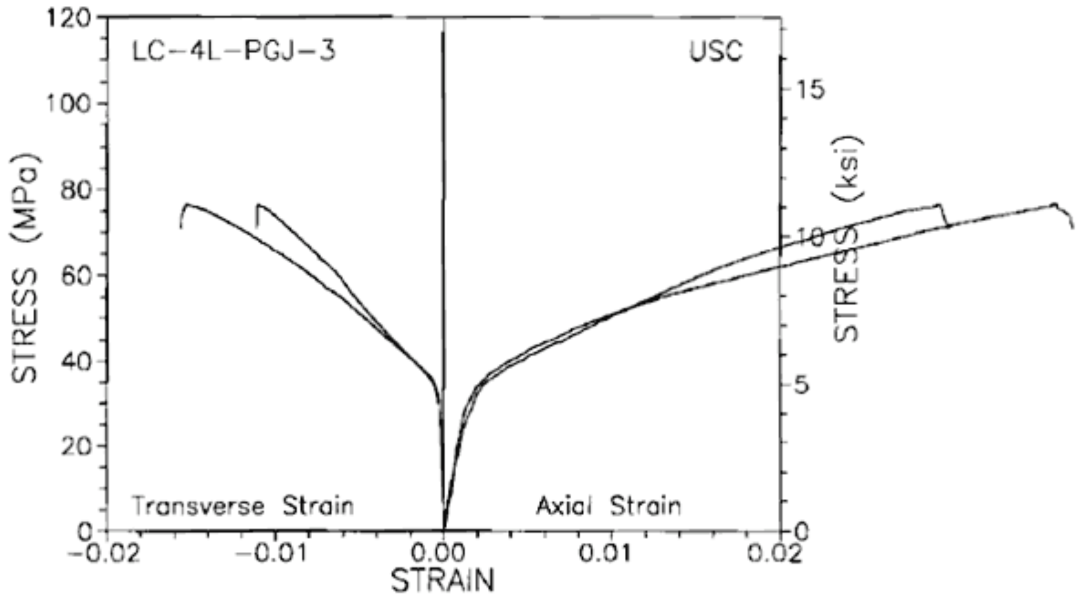

(b)

Fig.C-B4. Stress-Strain Relationships for Lower Strength Concrete with Four-Layer Prefabricated Glass Fiber Composite Jacket (LC-4L-PGJ-3)
(a) Strain Measured by LP (b) Strain Measured by Strain Gages

Part C-C Test Results of Medium Strength Concrete Cylinders

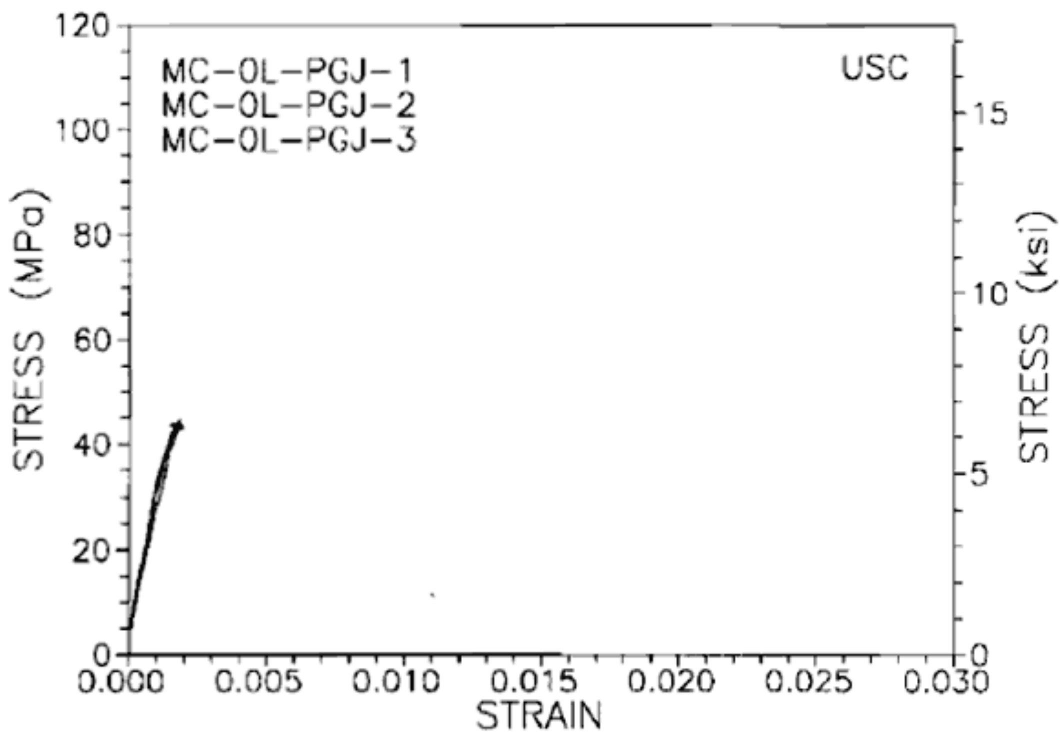

Fig. C-C1. Stress-Strain Relationships for Medium Strength Plain Concrete Cylinders

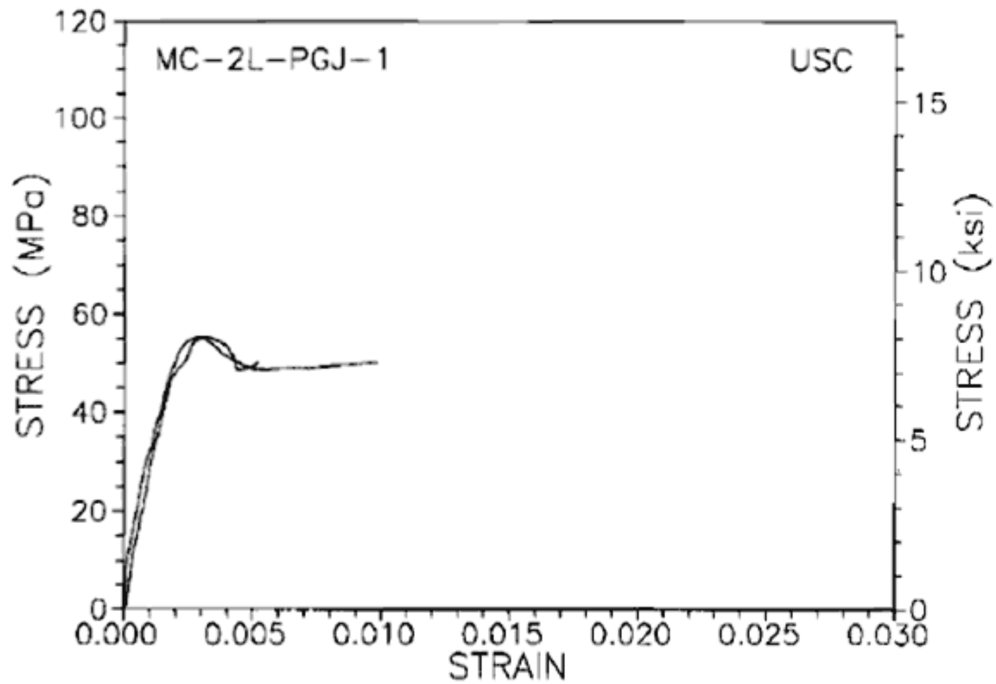

(a)

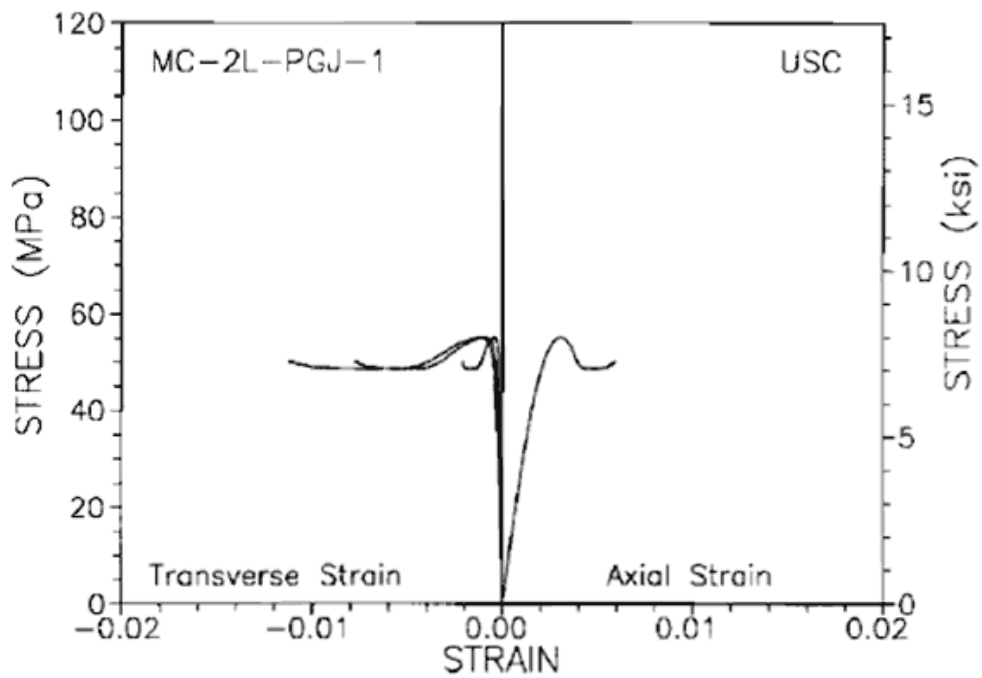

(b)

Fig.C-C2. Stress-Strain Relationships for Medium Strength Concrete with Two-Layer Prefabricated Glass Fiber Composite Jacket (MC-2L-PGJ-1)
(a) Strain Measured by LP (b) Strain Measured by Strain Gages

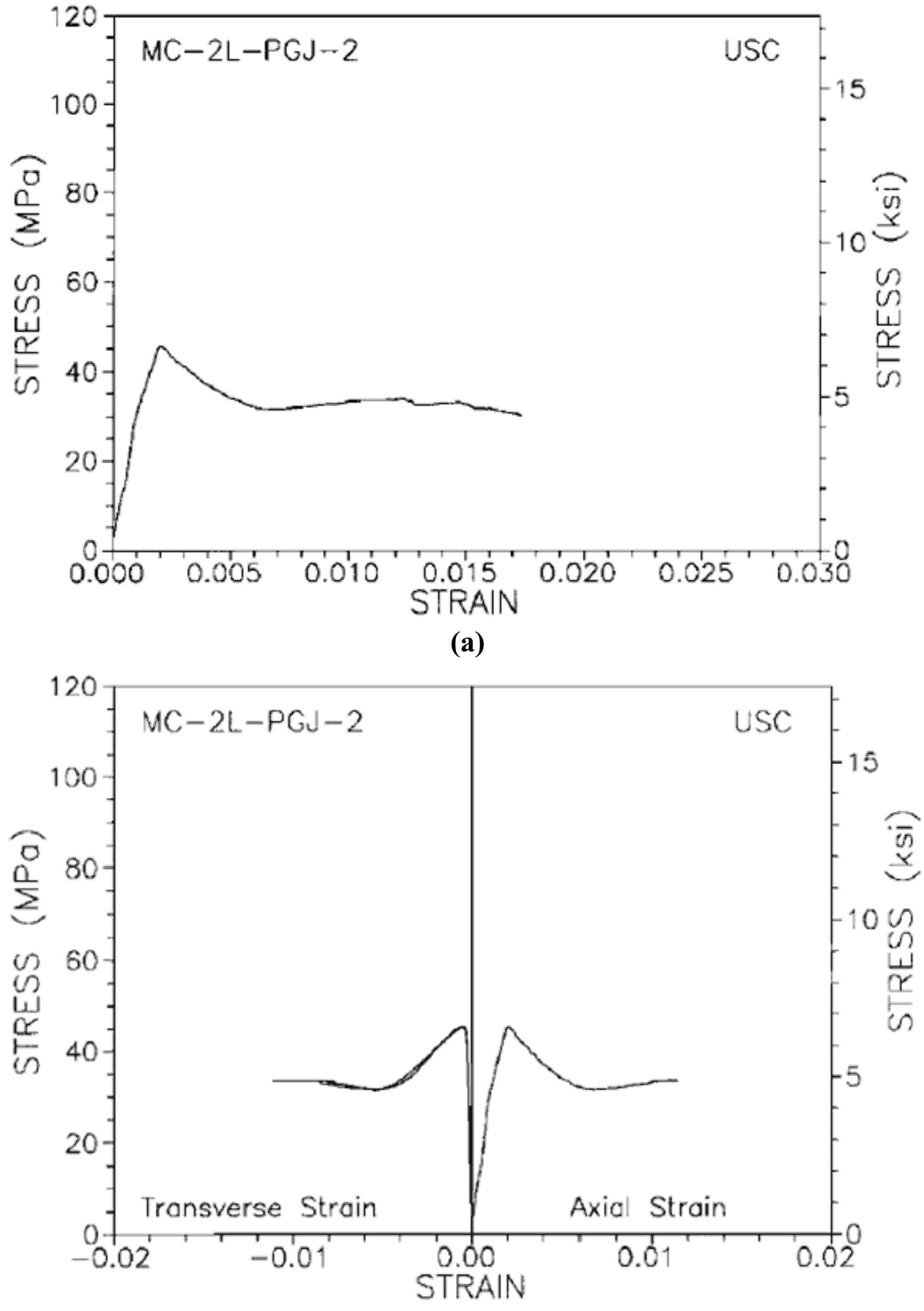

(a)

(b)

Fig.C-C2. Stress-Strain Relationships for Medium Strength Concrete with Two-Layer Prefabricated Glass Fiber Composite Jacket (MC-2L-PGJ-2)
(a) Strain Measured by LP (b) Strain Measured by Strain Gages

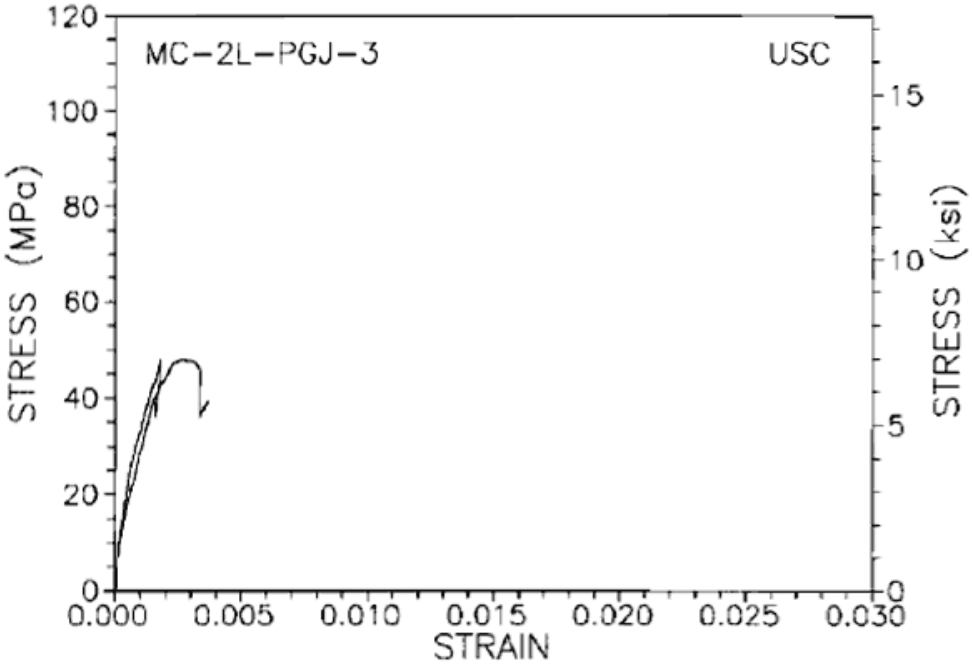

(a)

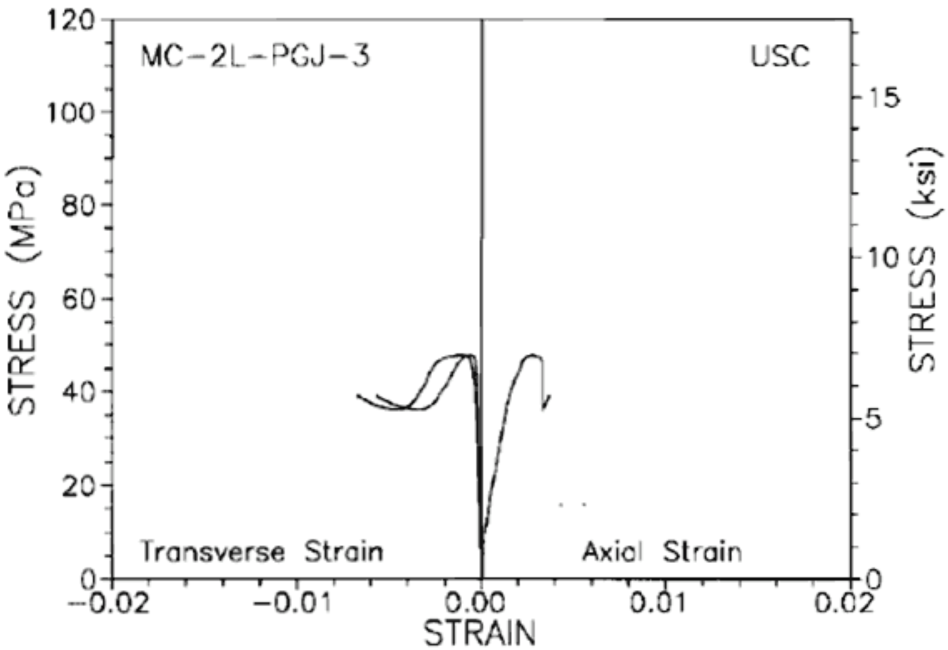

(b)

Fig.C-C2. Stress-Strain Relationships for Medium Strength Concrete with Two-Layer Prefabricated Glass Fiber Composite Jacket (MC-2L-PGJ-3)
(a) Strain Measured by LP (b) Strain Measured by Strain Gages

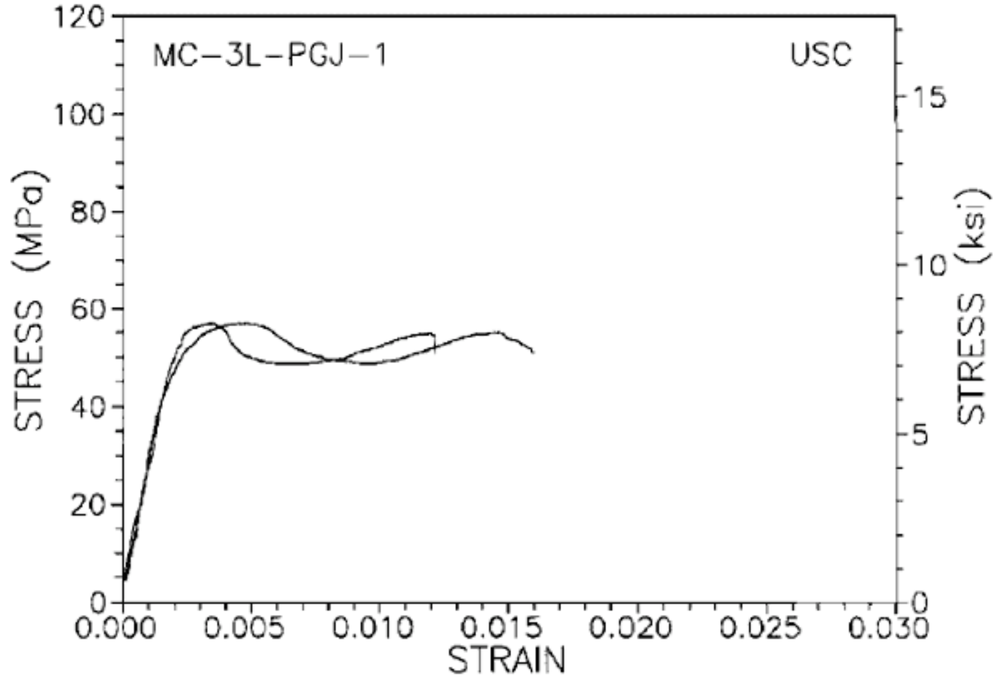

(a)

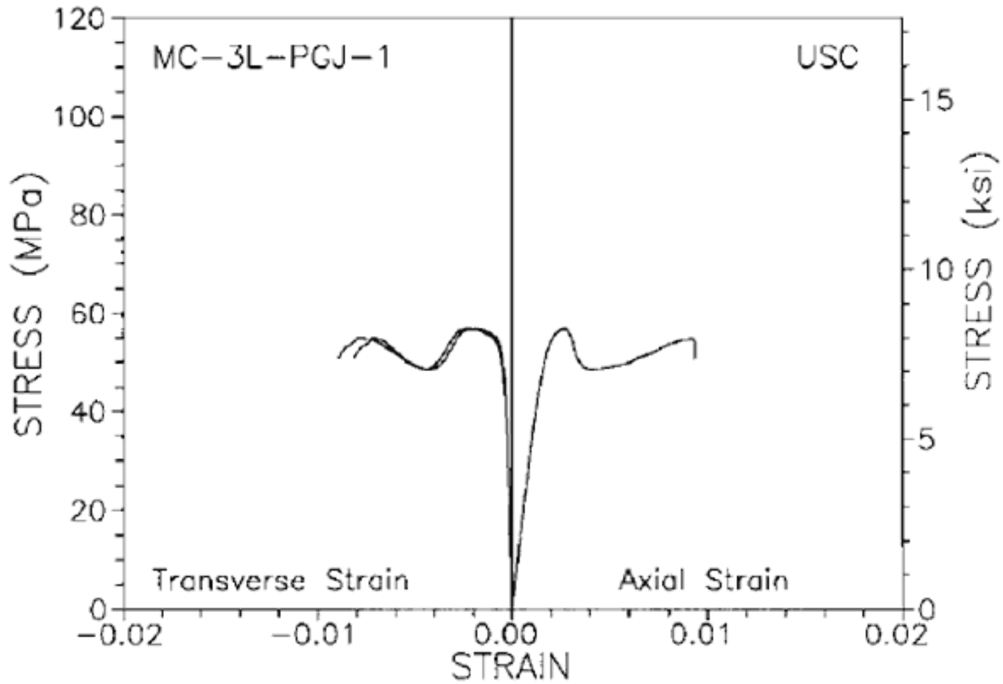

(b)

Fig.C-C3. Stress-Strain Relationships for Medium Strength Concrete with Three-Layer Prefabricated Glass Fiber Composite Jacket (MC-3L-PGJ-1) (a) Strain Measured by LP (b) Strain Measured by Strain Gages

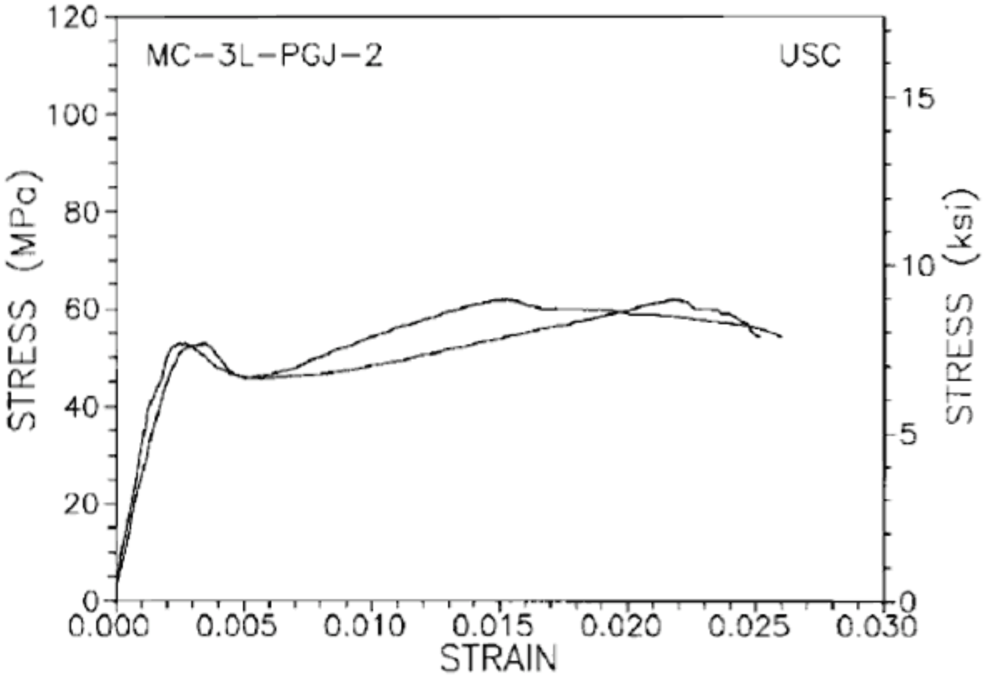

(a)

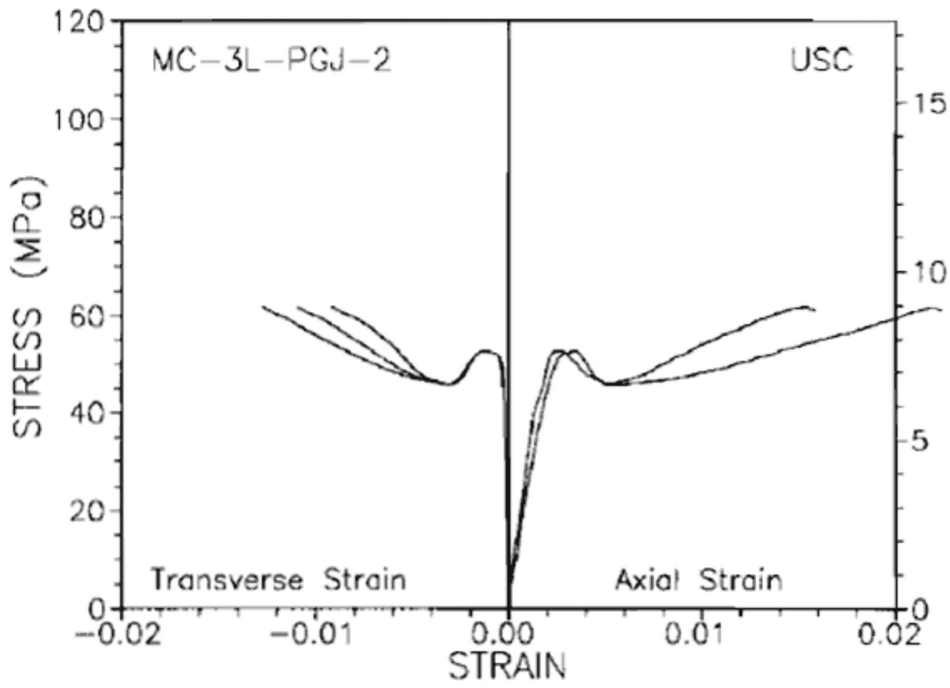

(b)

Fig.C-C3. Stress-Strain Relationships for Medium Strength Concrete with Three-Layer Prefabricated Glass Fiber Composite Jacket (MC-3L-PGJ-2) (a) Strain Measured by LP (b) Strain Measured by Strain Gages

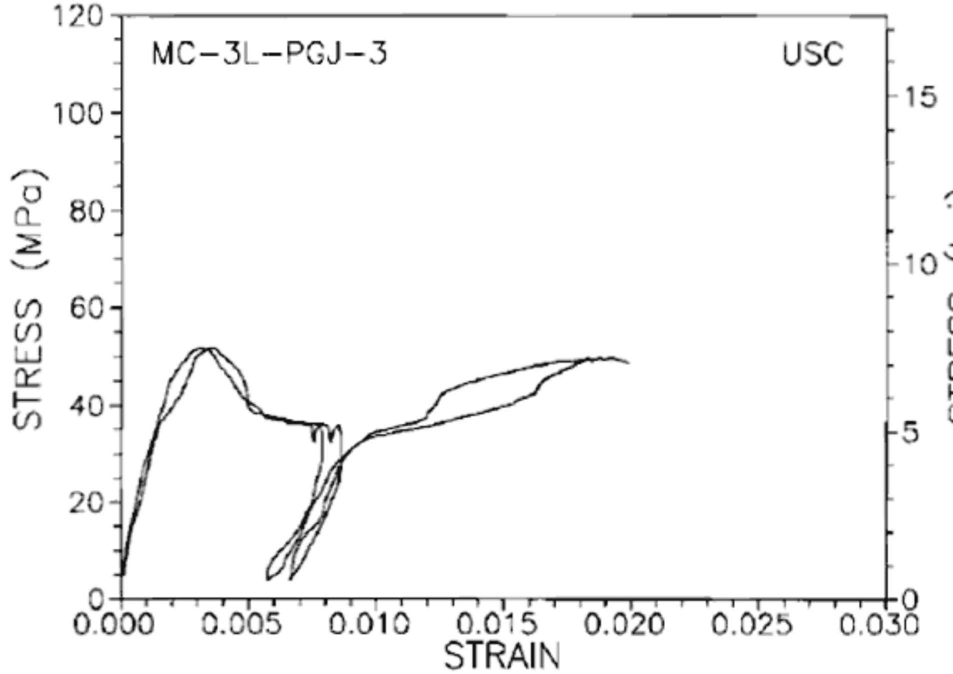

(a)

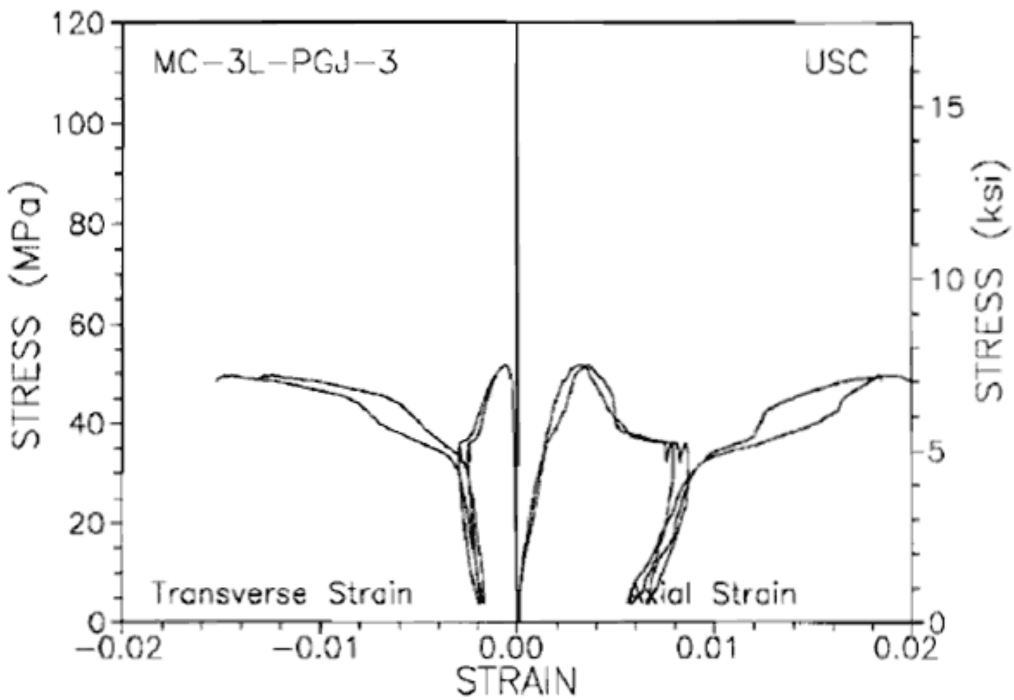

(b)

Fig.C-C3. Stress-Strain Relationships for Medium Strength Concrete with Three-Layer Prefabricated Glass Fiber Composite Jacket (MC-3L-PGJ-3) (a) Strain Measured by LP (b) Strain Measured by Strain Gages

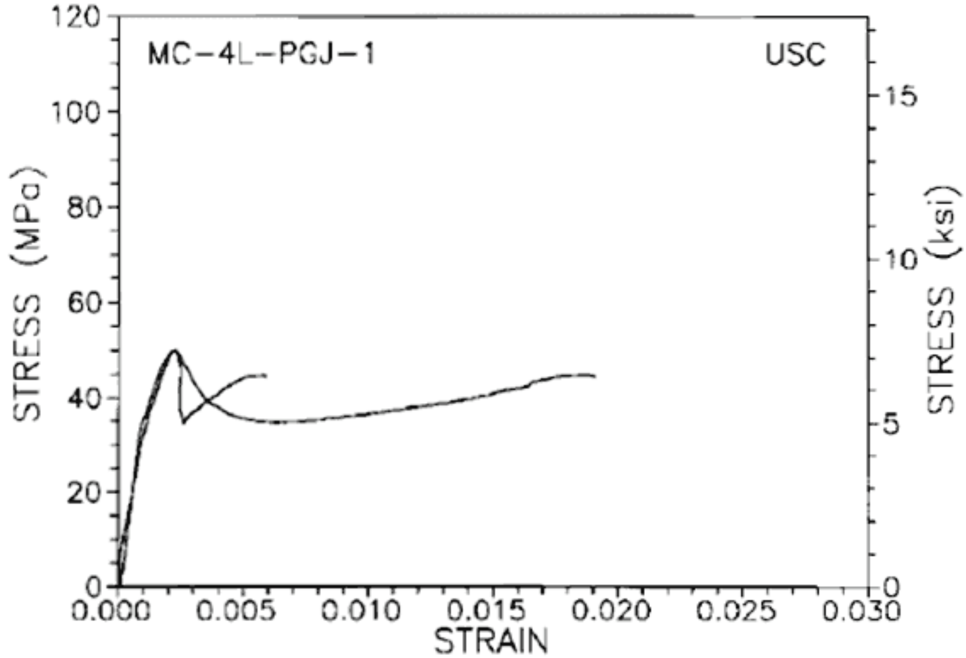

(a)

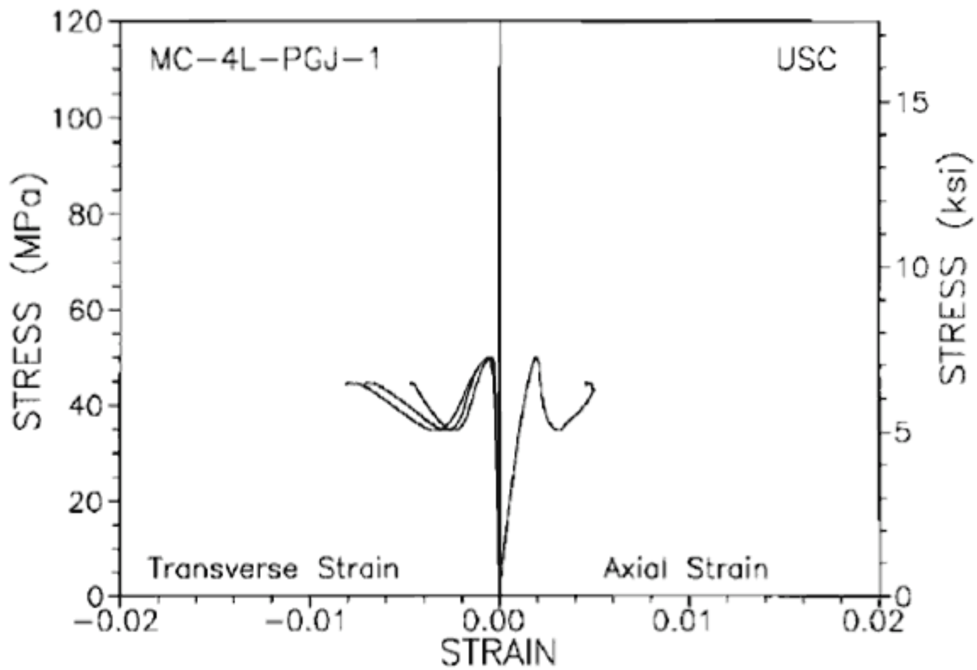

(b)

Fig.C-C4. Stress-Strain Relationships for Medium Strength Concrete with Four-Layer Prefabricated Glass Fiber Composite Jacket (MC-4L-PGJ-1) (a) Strain Measured by LP (b) Strain Measured by Strain Gages

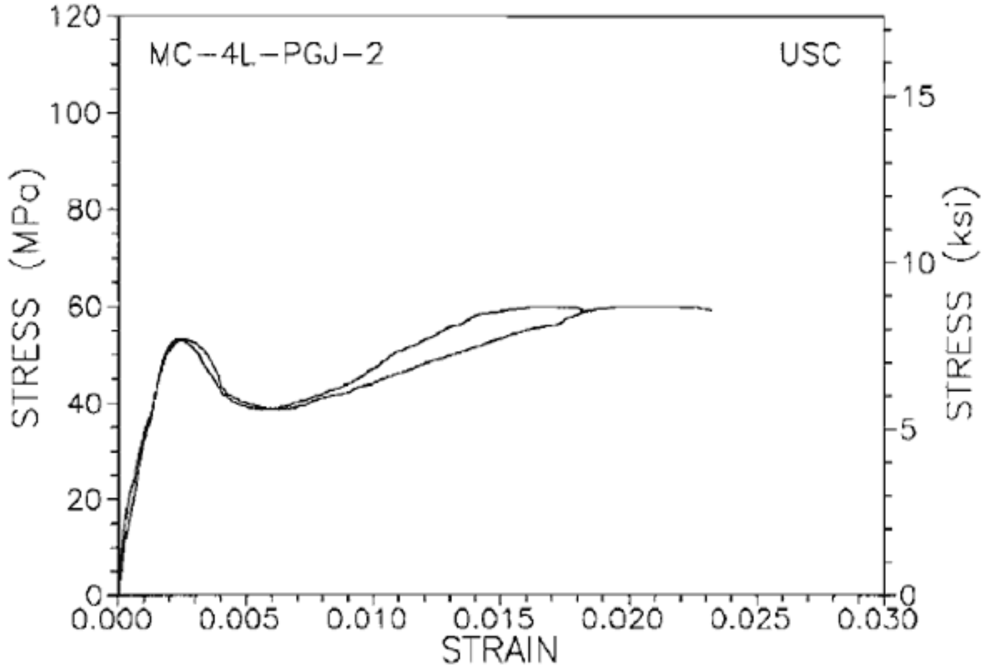

(a)

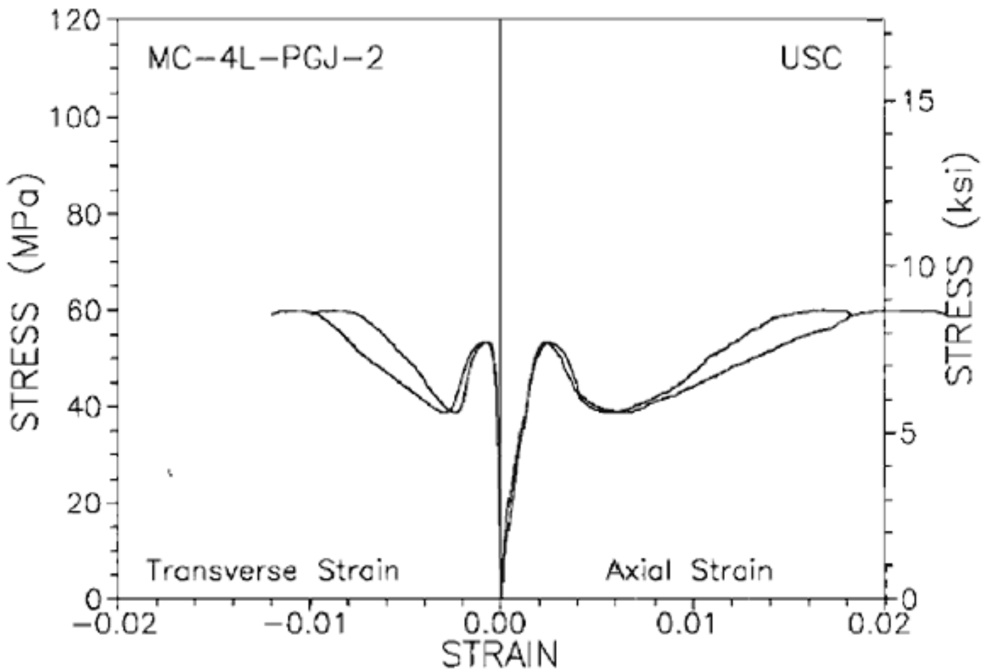

(b)

Fig.C-C4. Stress-Strain Relationships for Medium Strength Concrete with Four-Layer Prefabricated Glass Fiber Composite Jacket (MC-4L-PGJ-2) (a) Strain Measured by LP (b) Strain Measured by Strain Gages

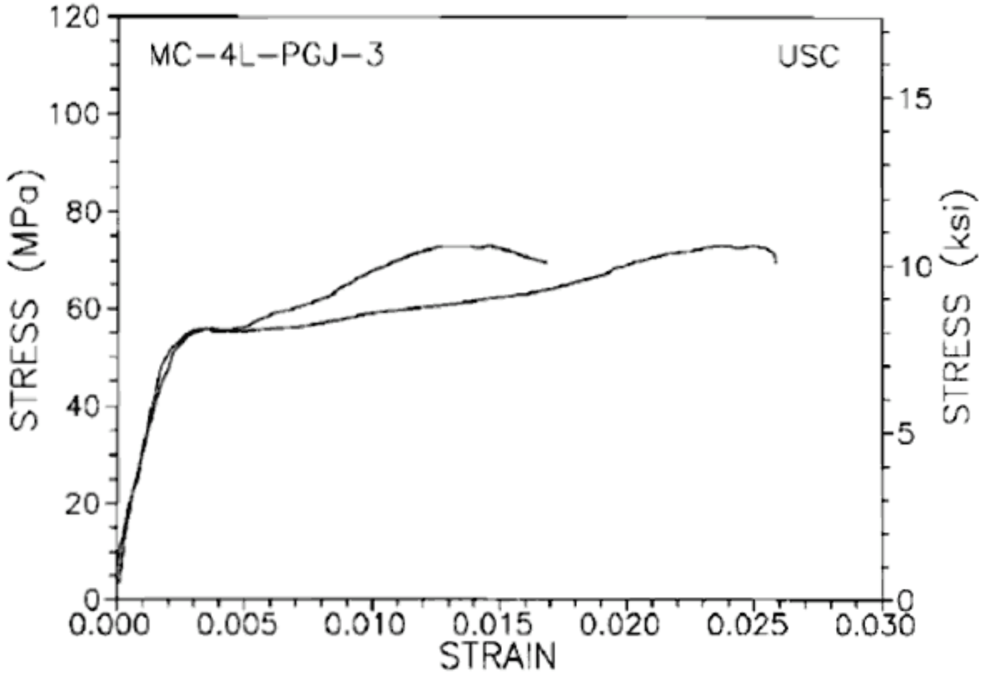

(a)

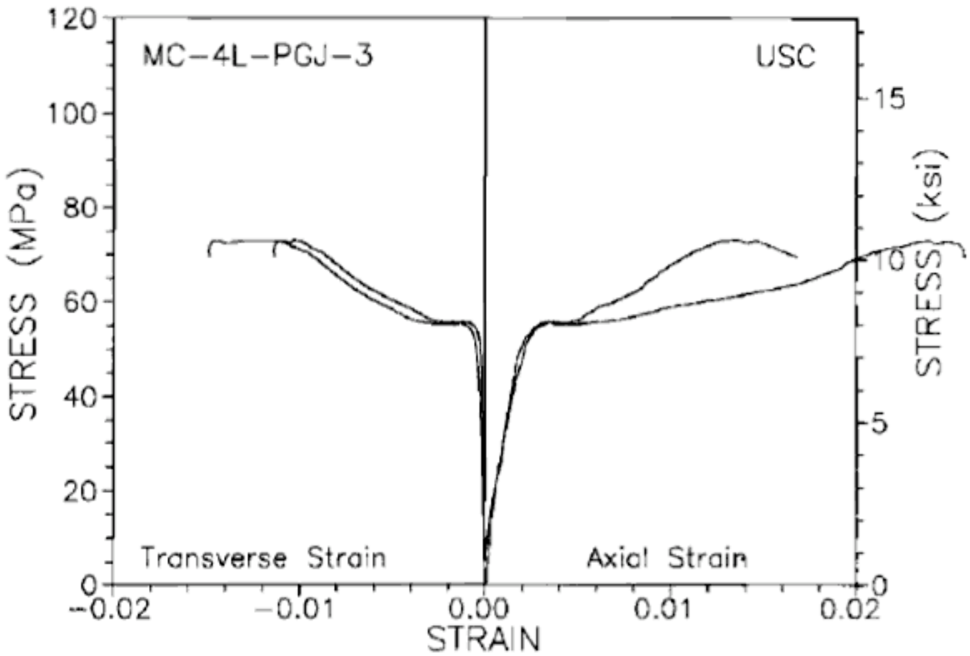

(b)

Fig.C-C4. Stress-Strain Relationships for Medium Strength Concrete with Four-Layer Prefabricated Glass Fiber Composite Jacket (MC-4L-PGJ-3) (a) Strain Measured by LP (b) Strain Measured by Strain Gages

Part C-D Test Results of Higher Strength Concrete Cylinders

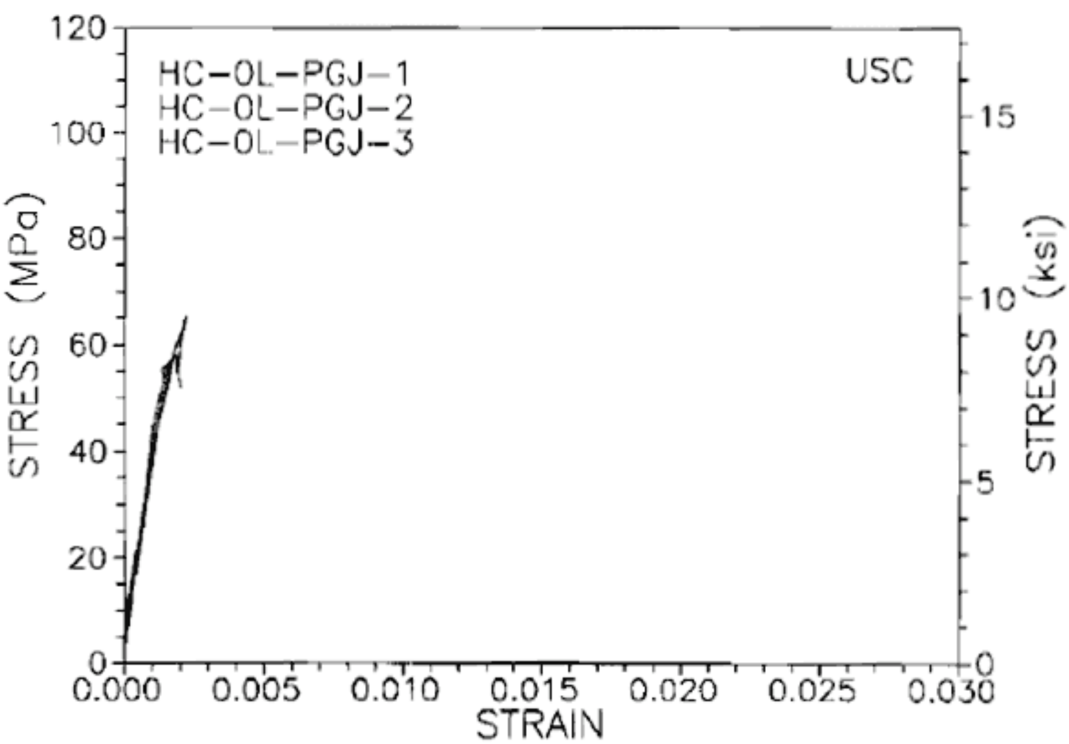

Fig.C-D1. Stress-Strain Relationships for Higher Strength Plain Concrete Cylinders

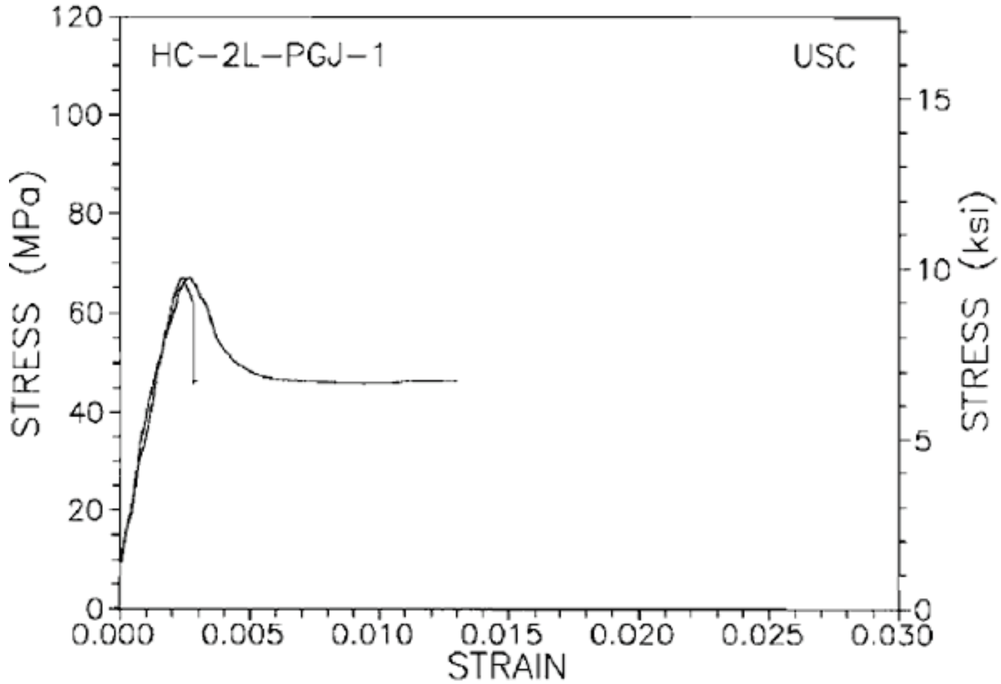

(a)

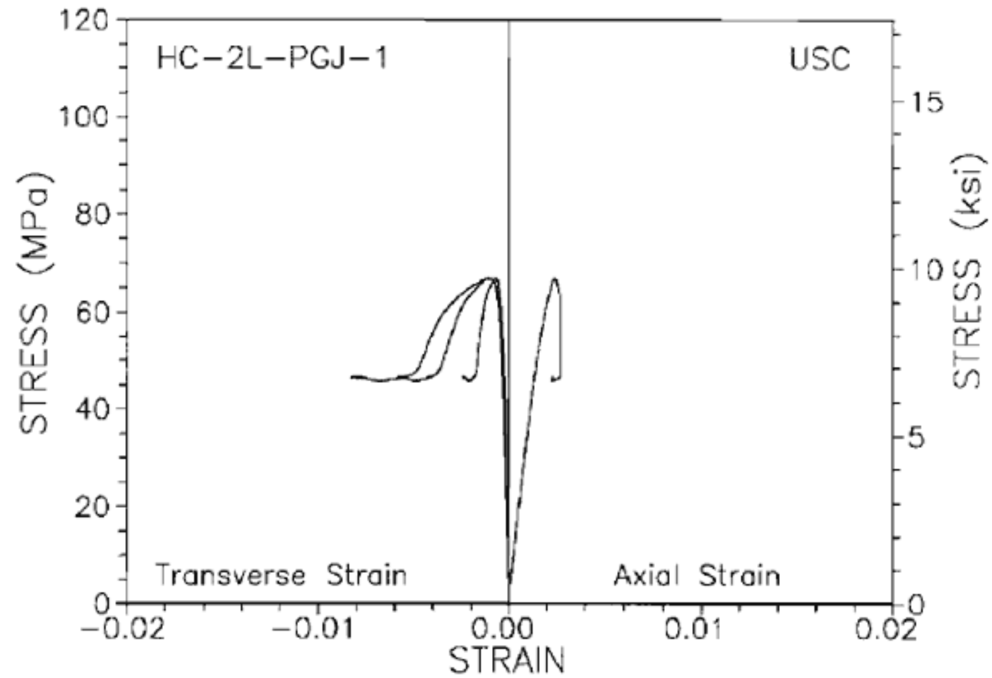

(b)

Fig.C-D2. Stress-Strain Relationships for Higher Strength Concrete with Two-Layer Prefabricated Glass Fiber Composite Jacket (HC-2L-PGJ-1)
(a) Strain Measured by LP (b) Strain Measured by Strain Gages

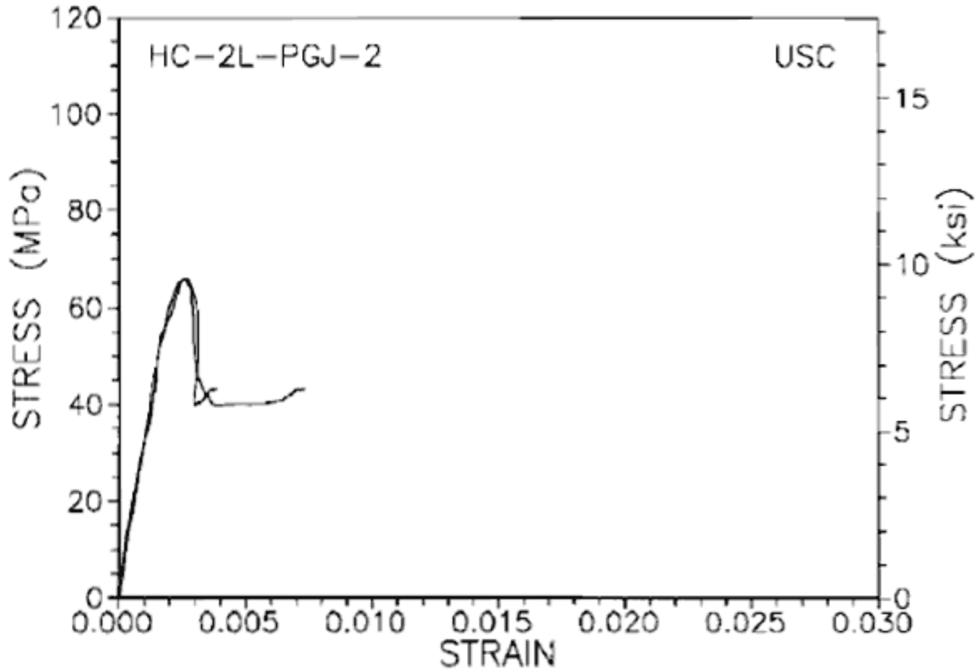

(a)

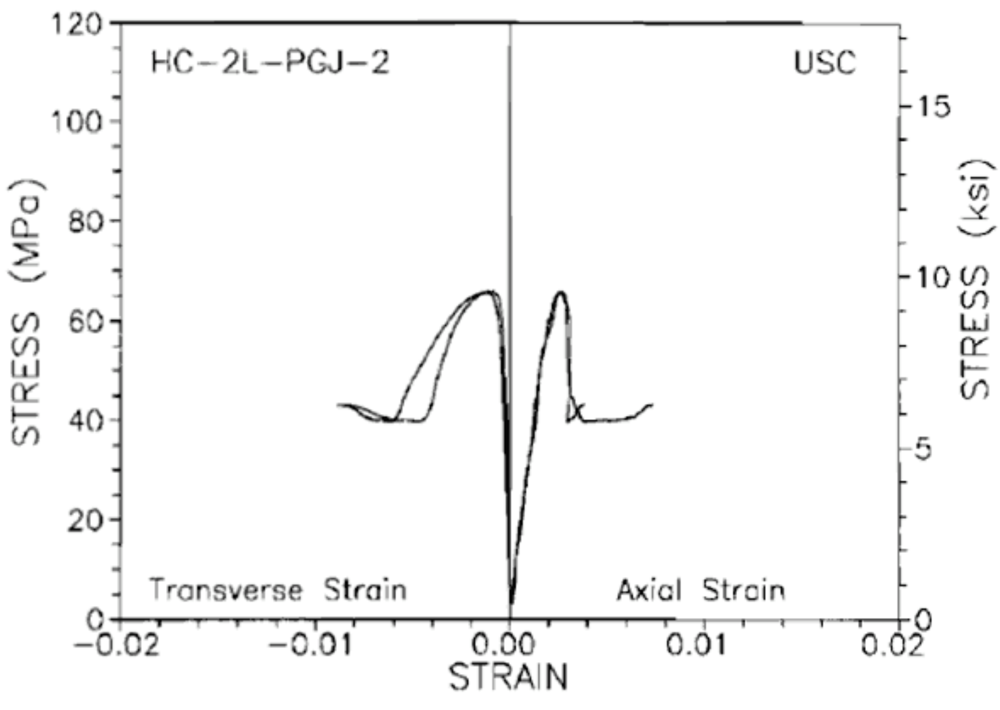

(b)

Fig.C-D2. Stress-Strain Relationships for Higher Strength Concrete with Two-Layer Prefabricated Glass Fiber Composite Jacket (HC-2L-PGJ-2)
(a) Strain Measured by LP (b) Strain Measured by Strain Gages

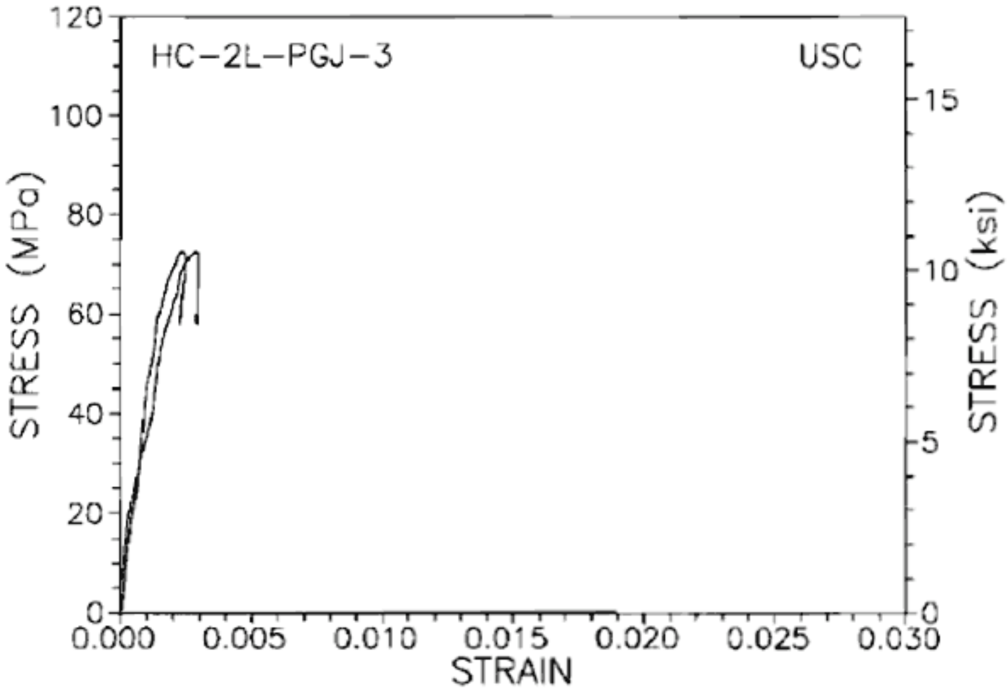

(a)

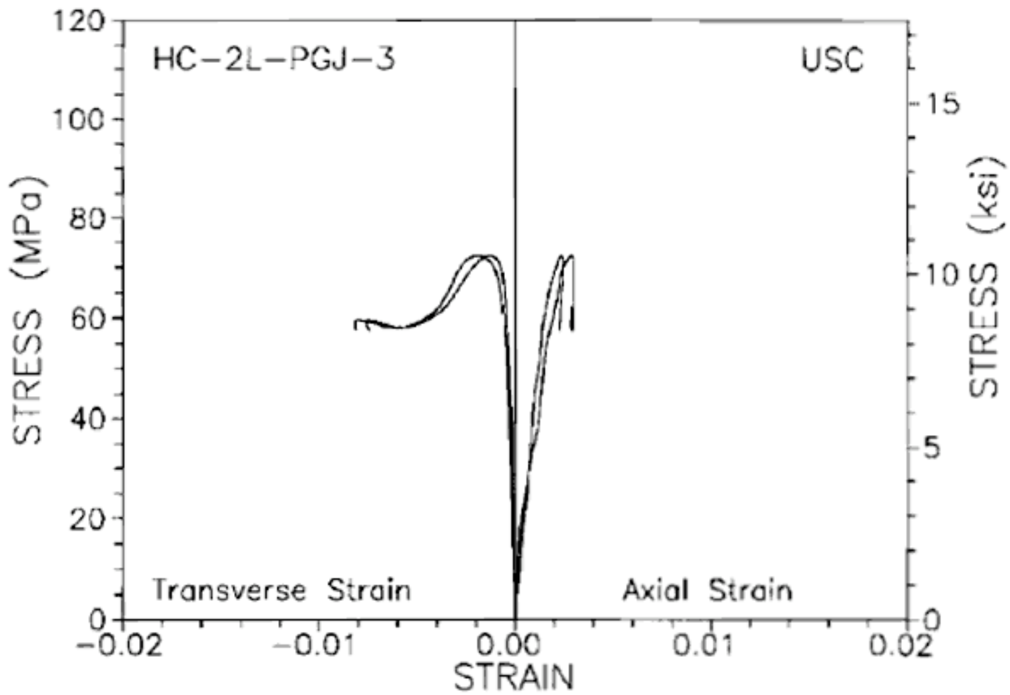

(b)

Fig.C-D2. Stress-Strain Relationships for Higher Strength Concrete with Two-Layer Prefabricated Glass Fiber Composite Jacket (HC-2L-PGJ-3)
(a) Strain Measured by LP (b) Strain Measured by Strain Gages

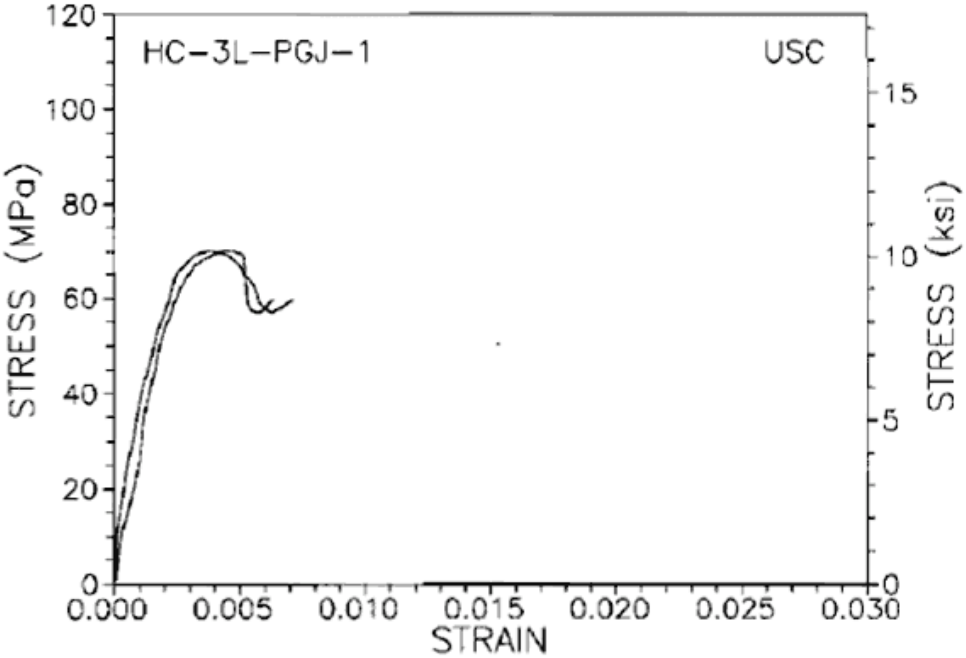

(a)

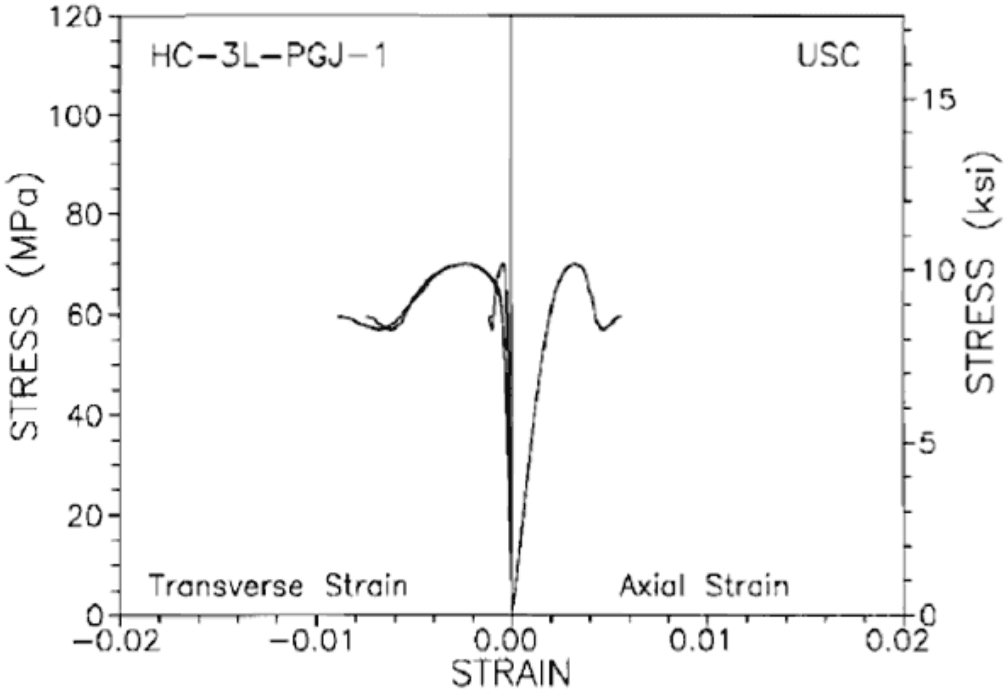

(b)

Fig.C-D3. Stress-Strain Relationships for Higher Strength Concrete with Three-Layer Prefabricated Glass Fiber Composite Jacket (HC-3L-PGJ-1)
(a) Strain Measured by LP (b) Strain Measured by Strain Gages

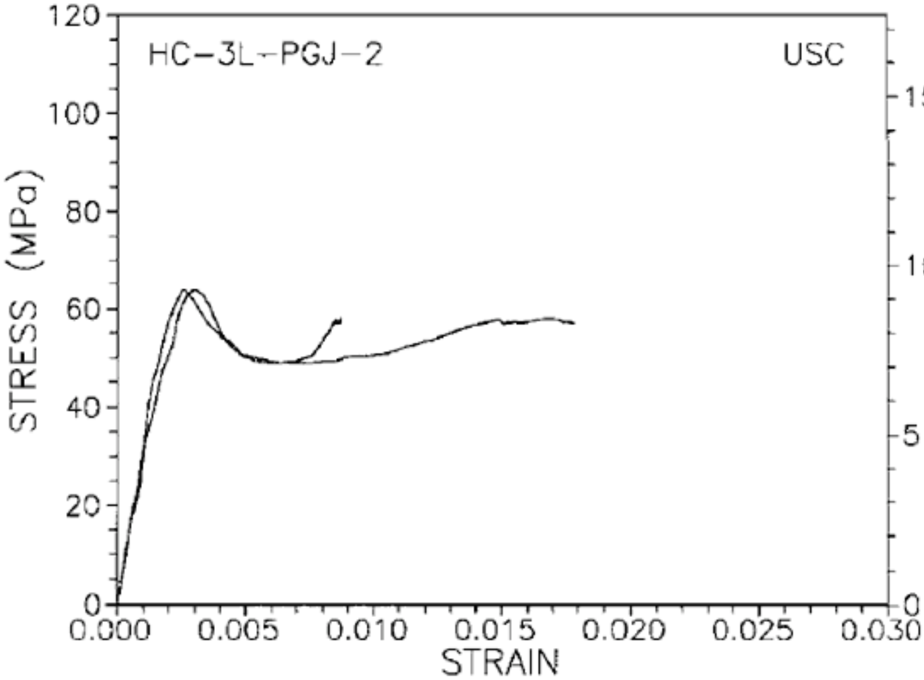

(a)

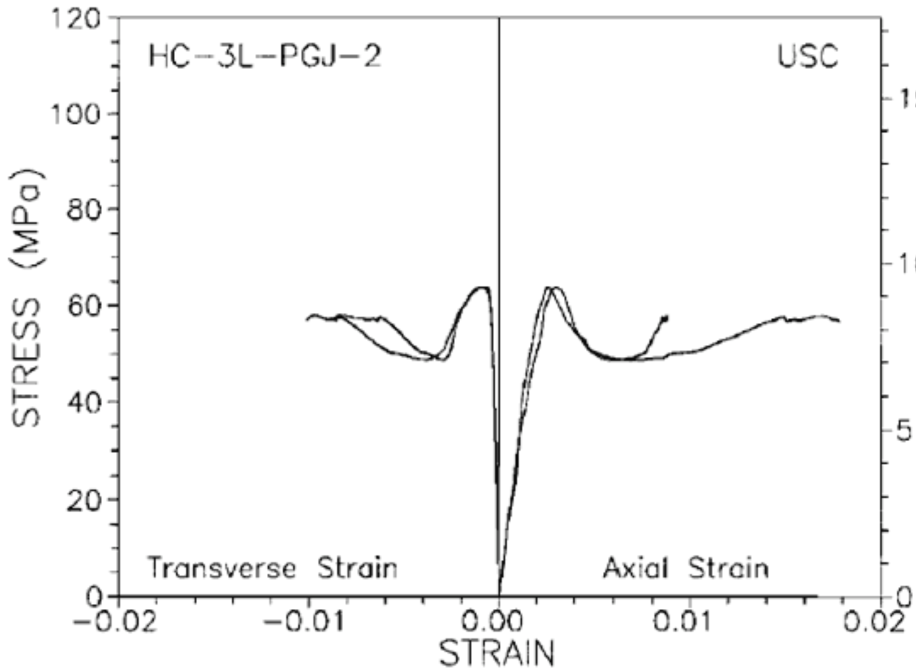

(b)

Fig.C-D3. Stress-Strain Relationships for Higher Strength Concrete with Three-Layer Prefabricated Glass Fiber Composite Jacket (HC-3L-PGJ-2)
(a) Strain Measured by LP (b) Strain Measured by Strain Gages

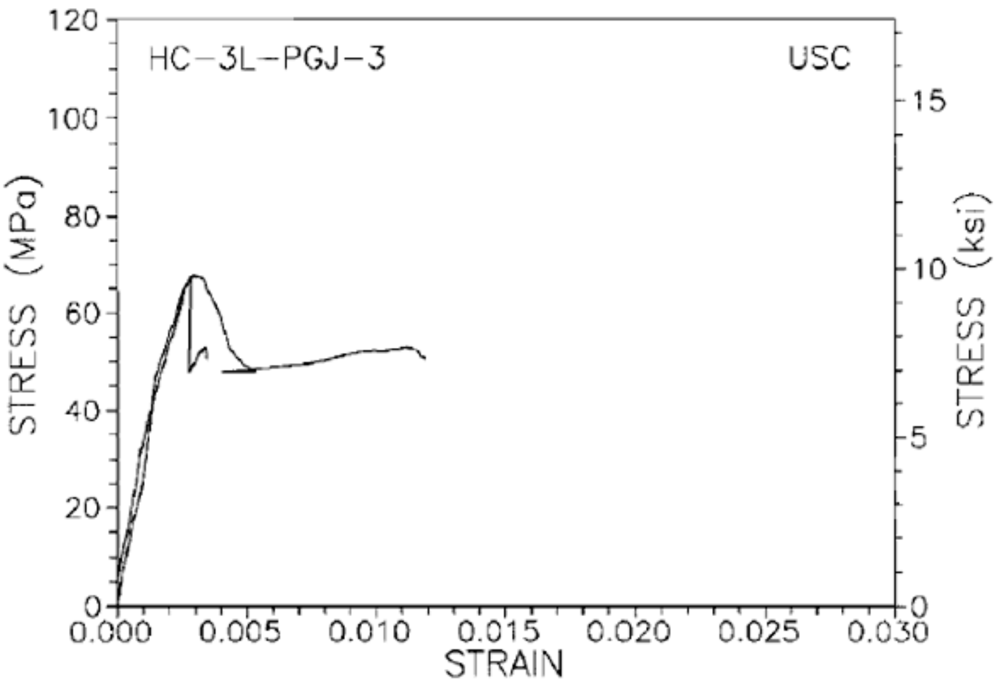

(a)

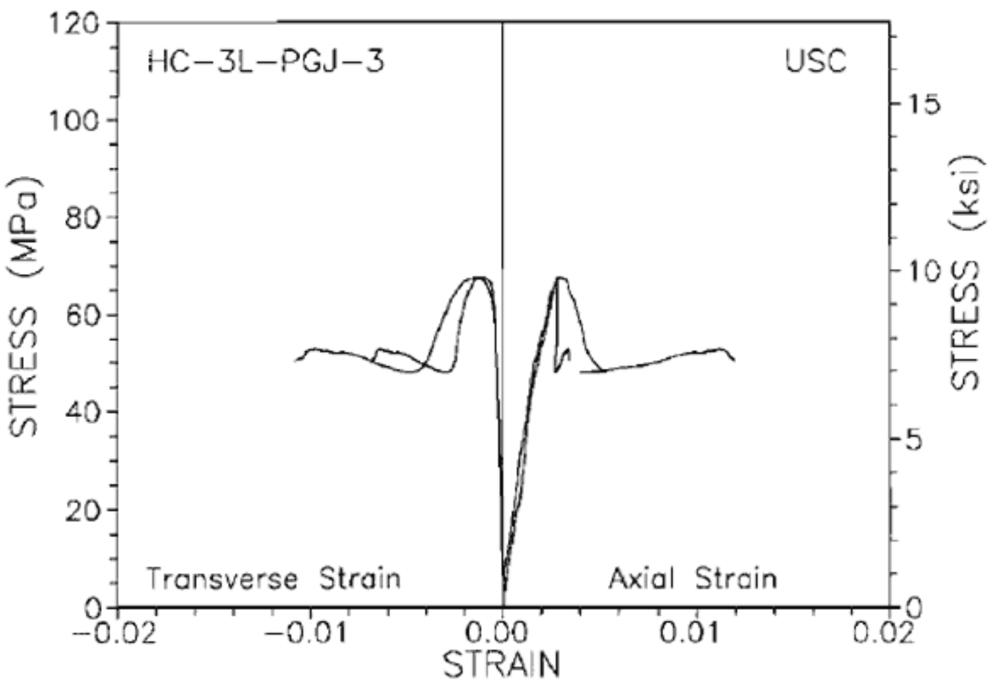

(b)

Fig.C-D3. Stress-Strain Relationships for Higher Strength Concrete with Three-Layer Prefabricated Glass Fiber Composite Jacket (HC-3L-PGJ-3)
(a) Strain Measured by LP (b) Strain Measured by Strain Gages

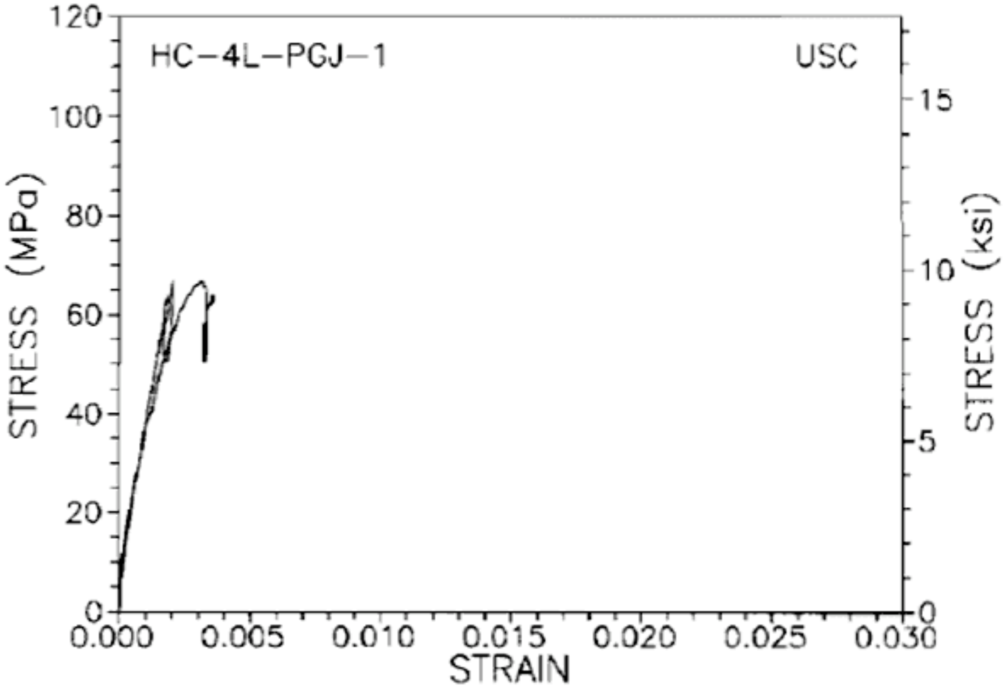

(a)

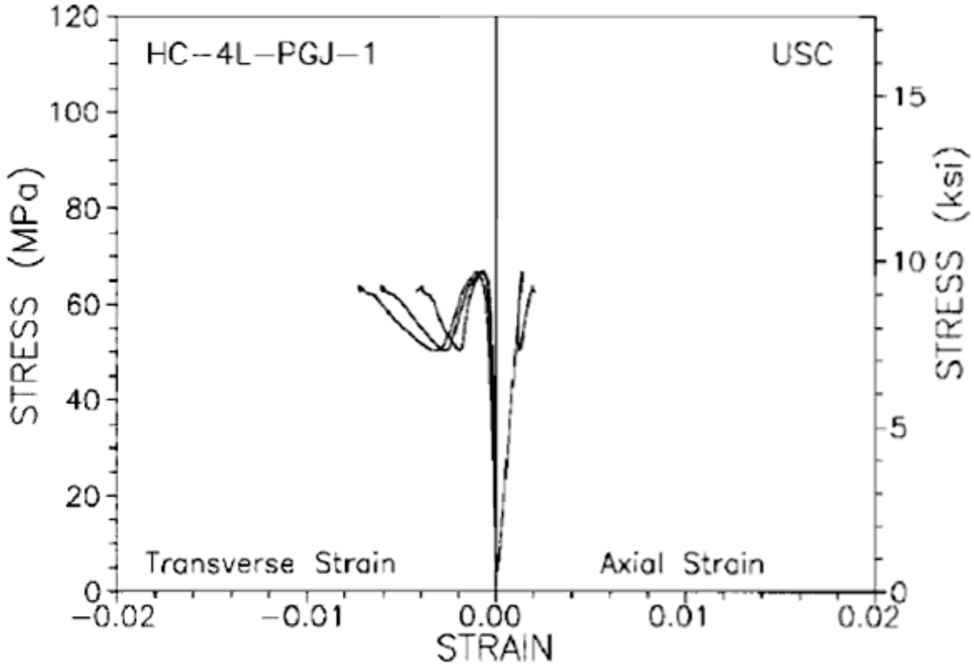

(b)

Fig.C-D4. Stress-Strain Relationships for Higher Strength Concrete with Four-Layer Prefabricated Glass Fiber Composite Jacket (HC-4L-PGJ-1)
(a) Strain Measured by LP (b) Strain Measured by Strain Gages

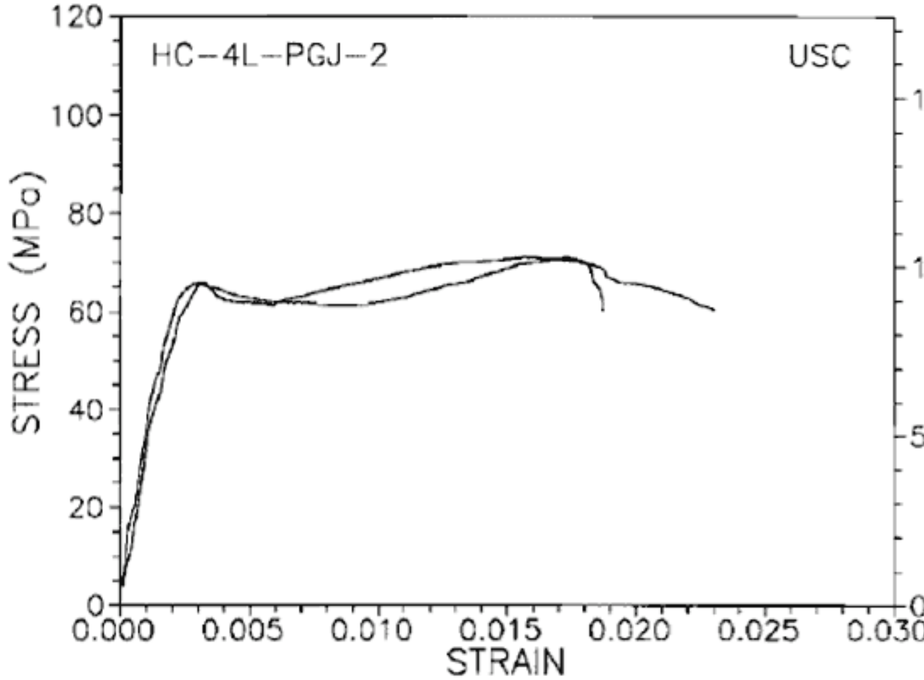

(a)

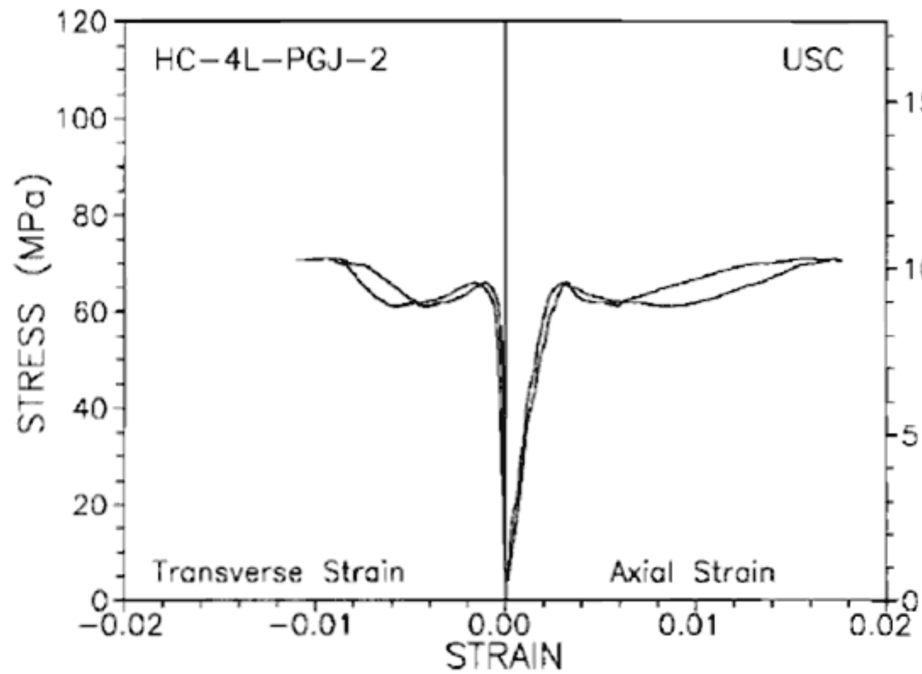

(b)

Fig.C-D4. Stress-Strain Relationships for Higher Strength Concrete with Four-Layer Prefabricated Glass Fiber Composite Jacket (HC-4L-PGJ-2) (a) Strain Measured by LP (b) Strain Measured by Strain Gages

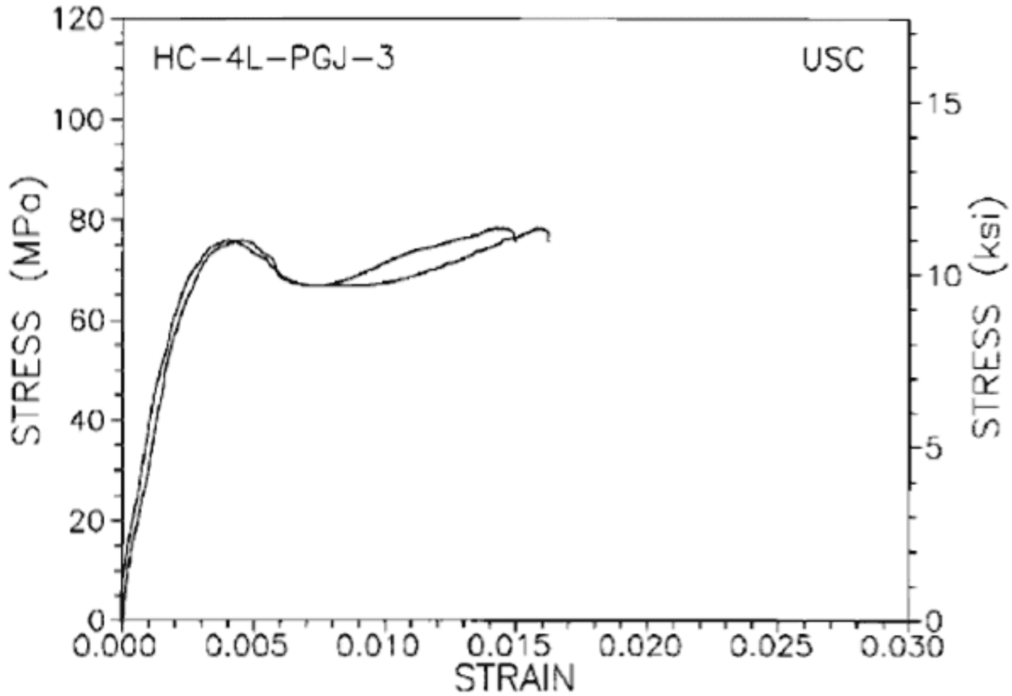

(a)

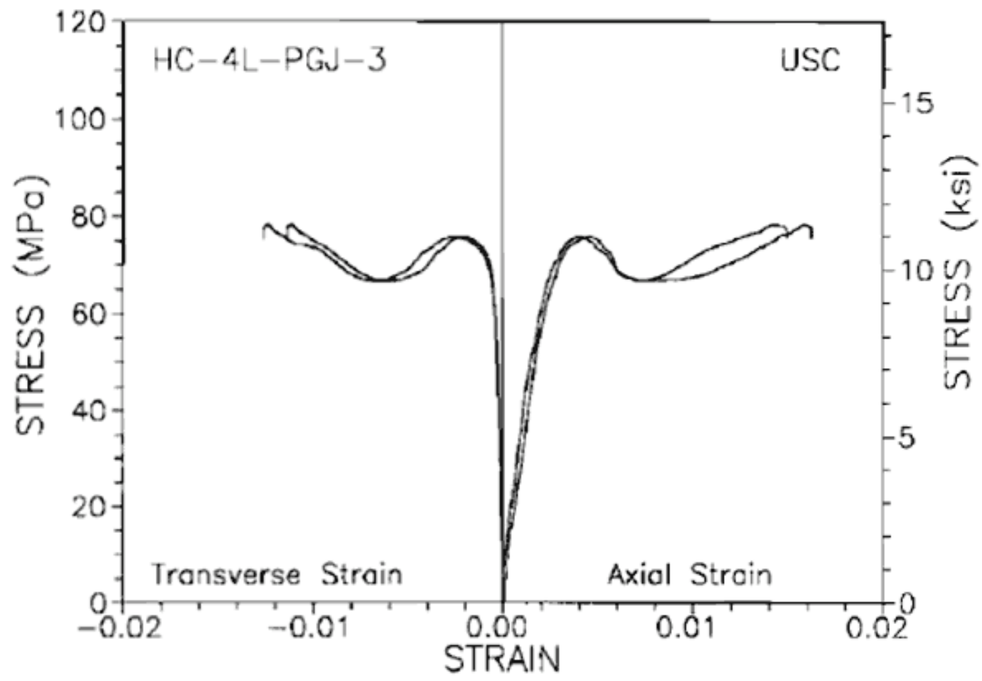

(b)

Fig.C-D4. Stress-Strain Relationships for Higher Strength Concrete with Four-Layer Prefabricated Glass Fiber Composite Jacket (HC-4L-PGJ-3)
(a) Strain Measured by LP (b) Strain Measured by Strain Gages

APPENDIX D: TEST RESULTS OF SYSTEM FOUR

Part D-A General Information

Table D-A1 Test Matrix

Type of Jacket	Concrete Strength	Jacket Layers	Specimen Numbers
Carbon fiber sheet reinforced composite jacket	Lower	Plain concrete	3 specimens each
		0.5-layer	
		1-layer	
		1.5-layer	
	Medium	Plain concrete	
		0.5-layer	
		1-layer	
		1.5-layer	
	Higher	Plain concrete	
		0.5-layer	
		1-layer	
		1.5-layer	

Table D-A2 Mix Proportion of Concrete

Series	Target f'_{co} (MPa)	W/C	Water (kg/m^3)	Cement (kg/m^3)	Fine Aggregates (kg/m^3)	Coarse Aggregates (kg/m^3)
L	27.6	0.68	196	288	1087	853
M	37.9	0.48	196	408	986	853
H	48.2	0.38	197	515	857	853

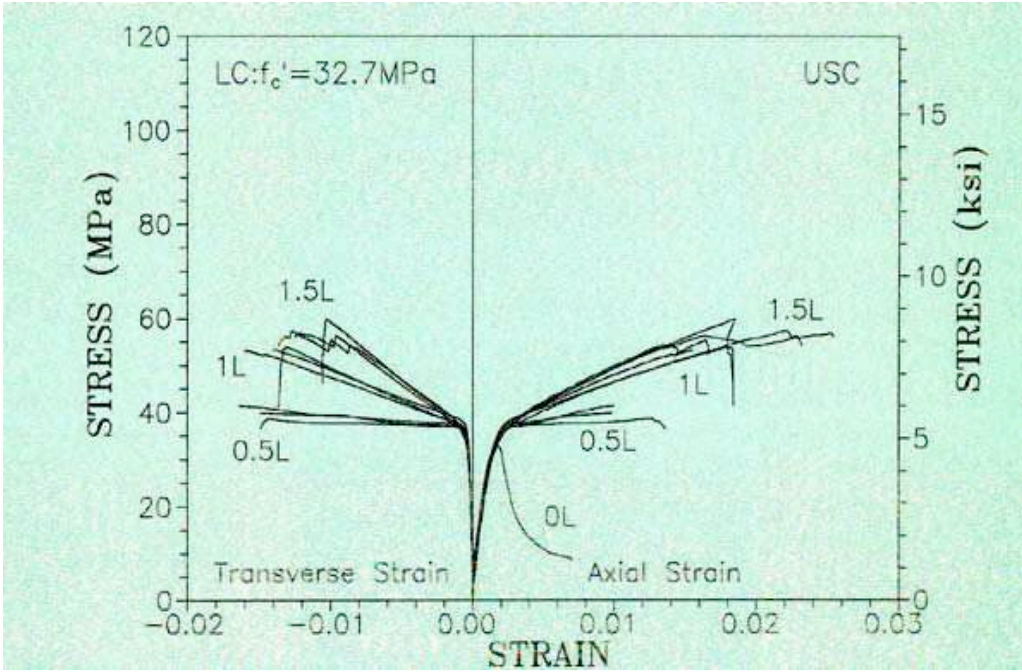

Fig.D-A1. Test Results of Lower-Strength Specimens

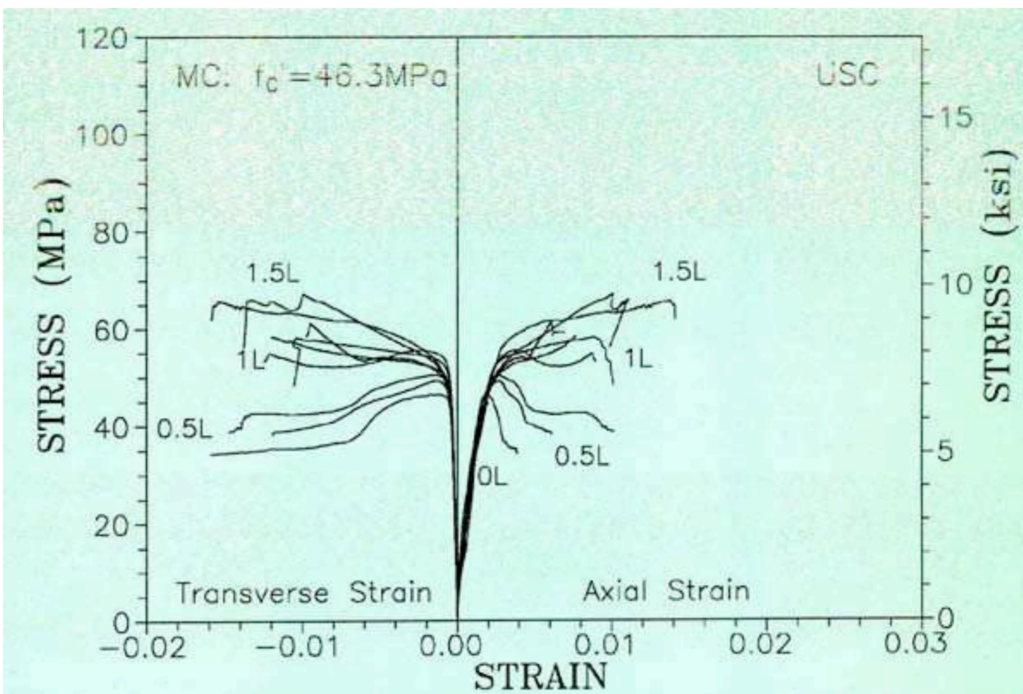

Fig.B-A2. Test Results of Medium-Strength Specimens

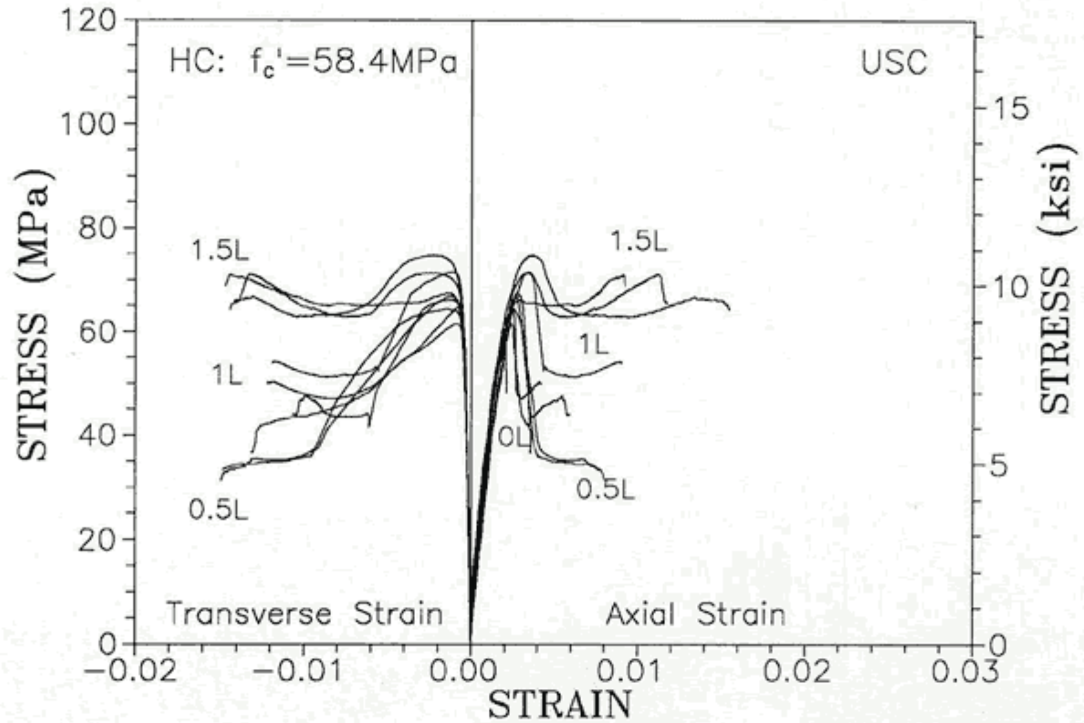

Fig.D-A3. Test Results of Higher-Strength Specimens

Table D-A4 Test Results

Series	Specimen	f_c' (MPa)	Jacket Layers	f_{cc}' (MPa)	ε_{cu}
L	LC-0L-CJ4-1	32.7	0	33.57	0.002035
	LC-0L-CJ4-2			31.66	0.001802
	LC-0L-CJ4-3			35.92	0.002094
	LC-0.5L-CJ4-1		0.5	39.89	0.009768
	LC-0.5L-CJ4-2			38.67	0.013576
	LC-0.5L-CJ4-3			41.39	0.009940
	LC-1L-CJ4-1		1	53.94	0.01841
	LC-1L-CJ4-2			53.21	0.01556
	LC-1L-CJ4-3			53.48	0.01754
	LC-1.5L-CJ4-1		1.5	59.90	0.01835
	LC-1.5L-CJ4-2			56.91	0.02537
	LC-1.5L-CJ4-3			57.33	0.02315
M	MC-0L-CJ4-1	46.3	0	45.03	0.001963
	MC-0L-CJ4-2			47.56	0.002472
	MC-0L-CJ4-3			46.03	0.001986
	MC-0.5L-CJ4-1		0.5	46.45	0.003850
	MC-0.5L-CJ4-2			50.44	0.010117
	MC-0.5L-CJ4-3			49.27	0.006072
	MC-1L-CJ4-1		1	58.37	0.007644
	MC-1L-CJ4-2			58.31	0.010075
	MC-1L-CJ4-3			55.56	0.008930
	MC-1.5L-CJ4-1		1.5	67.20	0.011047
	MC-1.5L-CJ4-2			61.26	0.006882
	MC-1.5L-CJ4-3			65.74	0.014089
H	HC-0L-CJ4-1	58.4	0	59.49	0.001940
	HC-0L-CJ4-2			58.42	0.002058
	HC-0L-CJ4-3			57.40	0.002035
	HC-0.5L-CJ4-1		0.5	61.50	0.003558
	HC-0.5L-CJ4-2			66.69	0.007595
	HC-0.5L-CJ4-3			64.30	0.008091
	HC-1L-CJ4-1		1	66.09	0.005902
	HC-1L-CJ4-2			71.59	0.008980
	HC-1L-CJ4-3			64.79	0.004165
	HC-1.5L-CJ4-1		1.5	74.74	0.015435
	HC-1.5L-CJ4-2			71.39	0.011705
	HC-1.5L-CJ4-3			70.99	0.009208

ote: (i) Example for specimen name designation:

LC-1L-CJ4-1: LC designates Lower strength Concrete; 1L designates 1 Layers; CJ4 designates Carbon fiber Jacket System 4; and the last number represents specimen number in same series.

(ii) f_c': Average plain concrete cylinder strength;

(iii) f_{cc}': Ultimate strength of confined concrete;

(iv) ε_{cu}: Ultimate strain

Part D-B Test Results of Lower Strength Concrete Cylinders

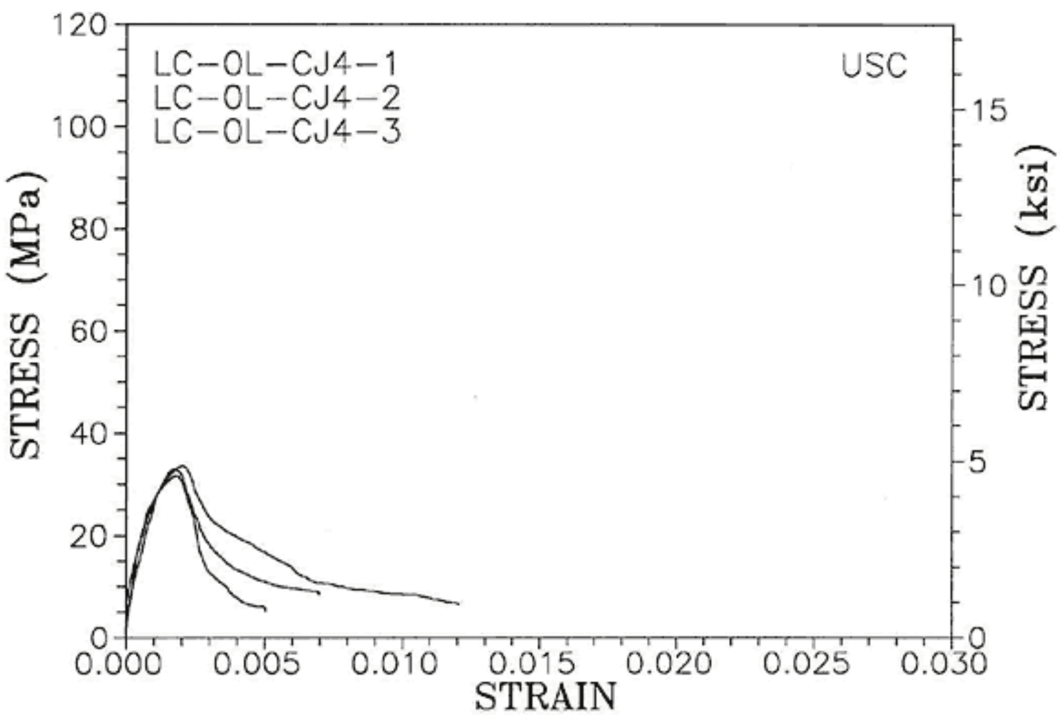

Fig.D-B1. Stress-Strain Relationship for Lower Strength Plain Concrete Cylinders

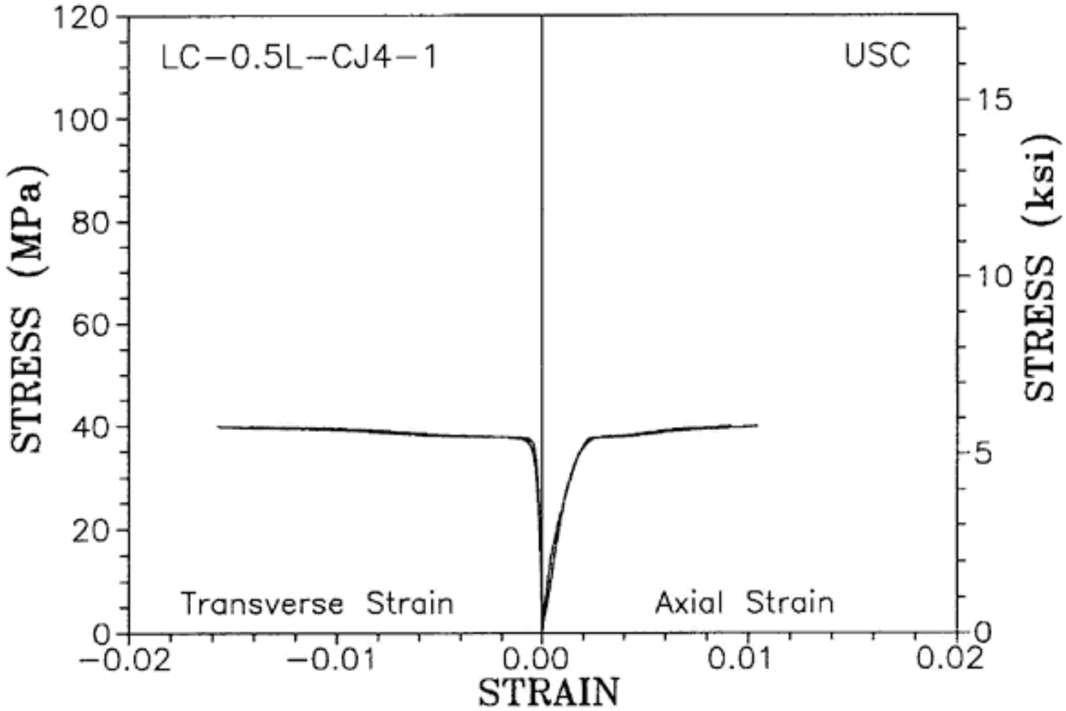

Fig D-B2.Stress-Strain Relationships for Lower Strength Concrete with Half-layer Carbon Fiber Composite Jacket (LC-0.5L-CJ4-1)

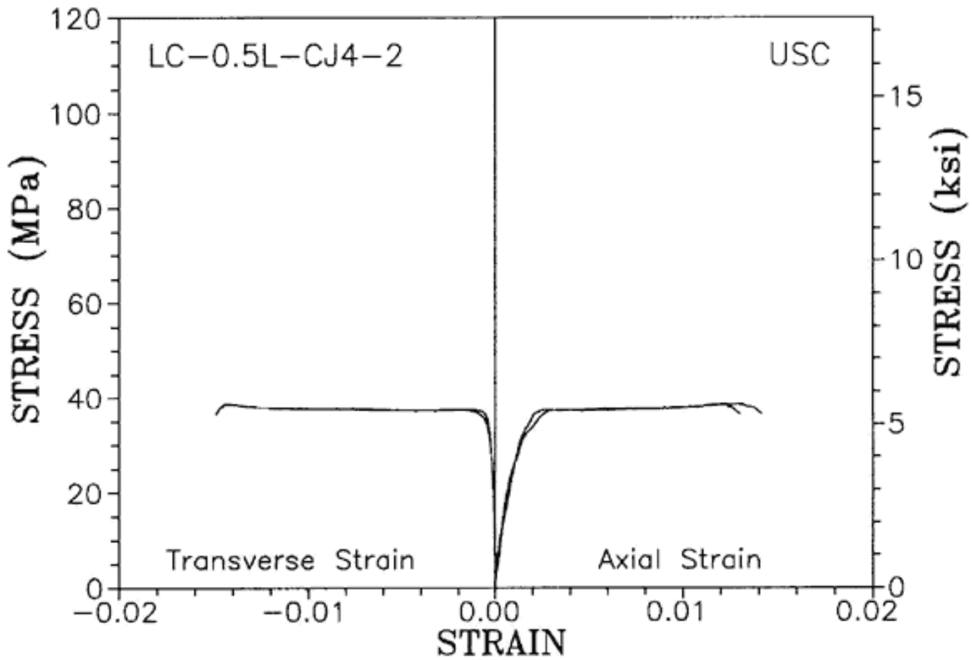

Fig D-B2.Stress-Strain Relationships for Lower Strength Concrete with Half-layer Carbon Fiber Composite Jacket (LC-0.5L-CJ4-2)

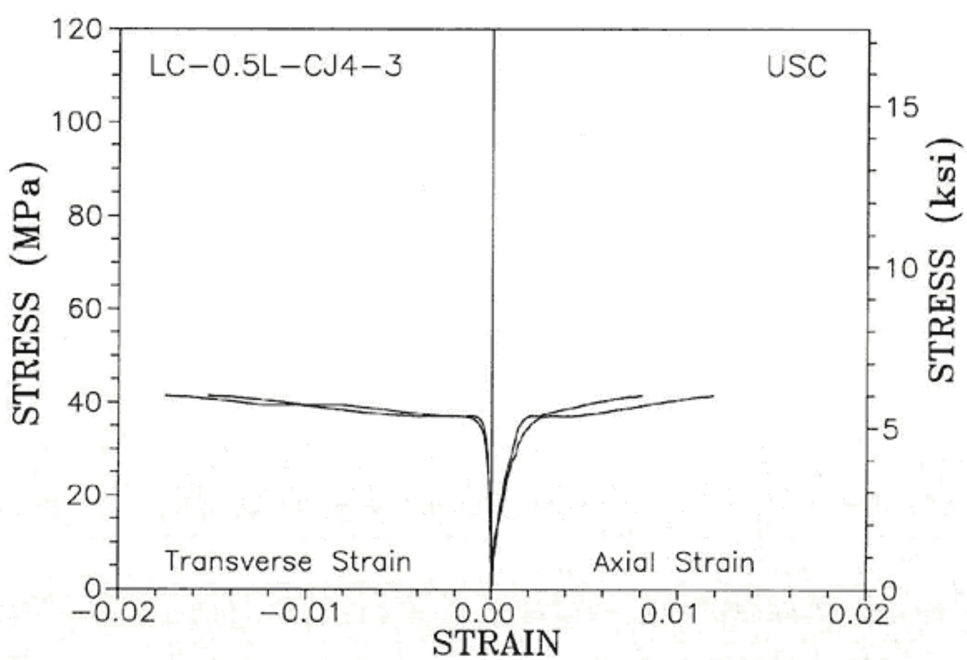

Fig D-B2.Stress-Strain Relationships for Lower Strength Concrete with Half-layer Carbon Fiber Composite Jacket (LC-0.5L-CJ4-3)

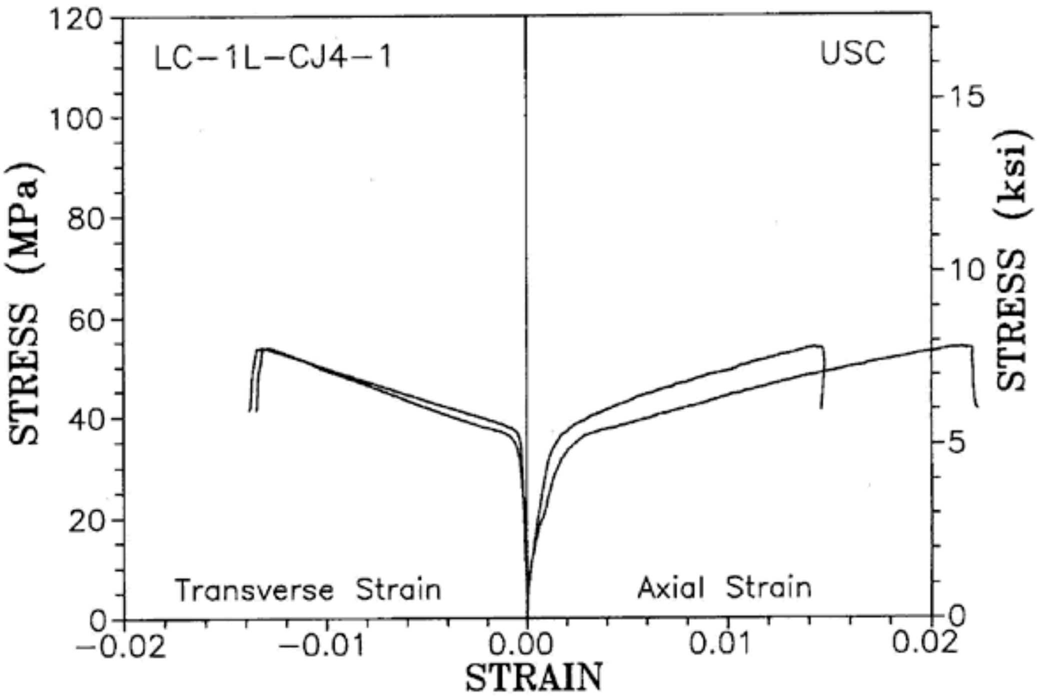

Fig D-B3.Stress-Strain Relationships for Lower Strength Concrete with One-layer Carbon Fiber Composite Jacket (LC-1L-CJ4-1)

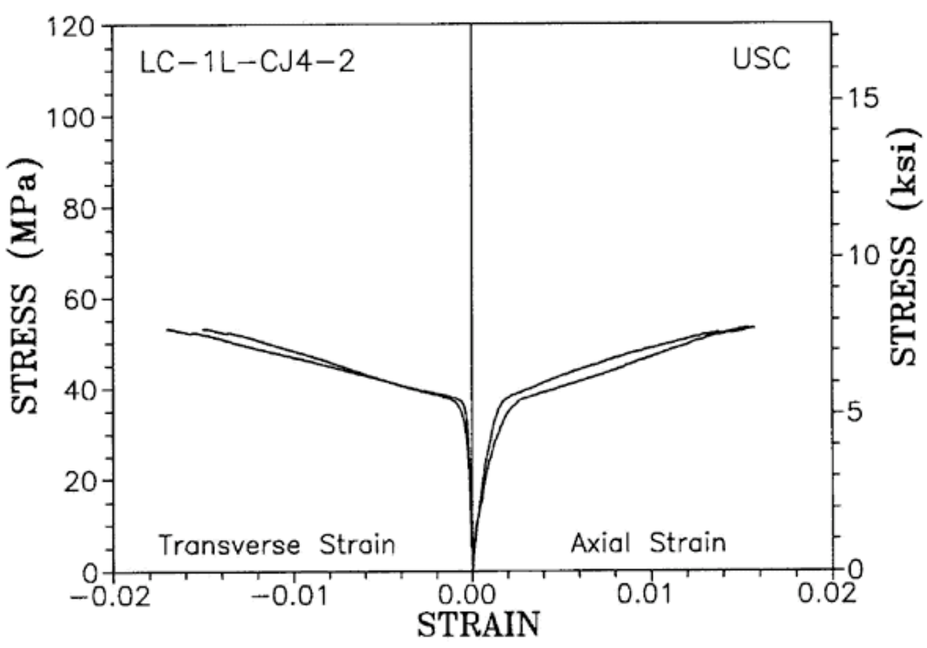

Fig D-B3.Stress-Strain Relationships for Lower Strength Concrete with One-layer Carbon Fiber Composite Jacket (LC-1L-CJ4-2)

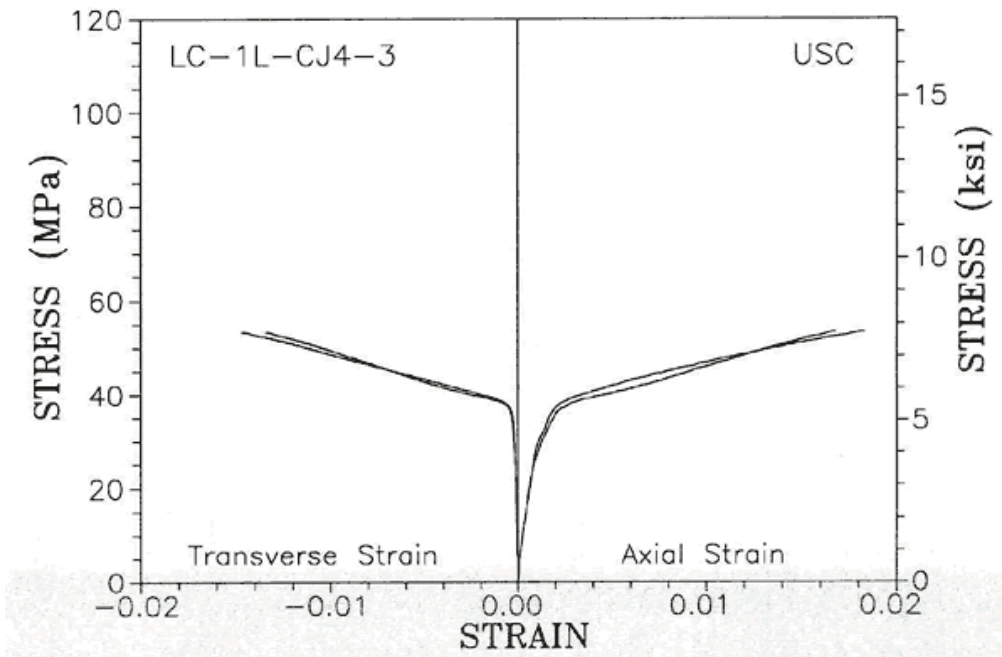

Fig D-B3.Stress-Strain Relationships for Lower Strength Concrete with One-layer Carbon Fiber Composite Jacket (LC-1L-CJ4-3)

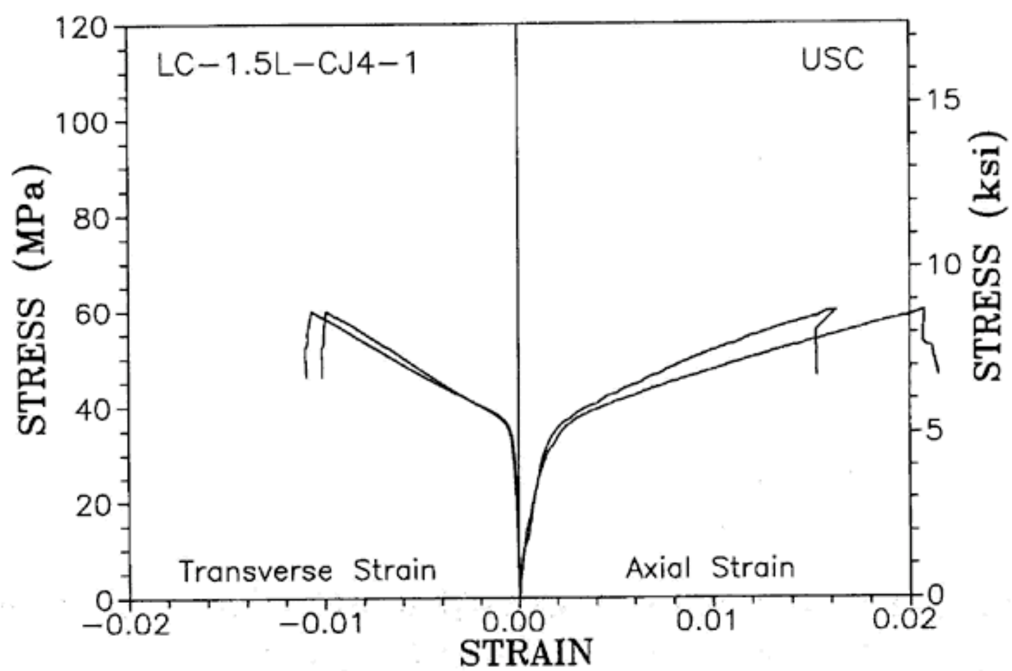

Fig D-B4.Stress-Strain Relationships for Lower Strength Concrete with One and a Half-layer Carbon Fiber Composite Jacket (LC-1.5L-CJ4-1)

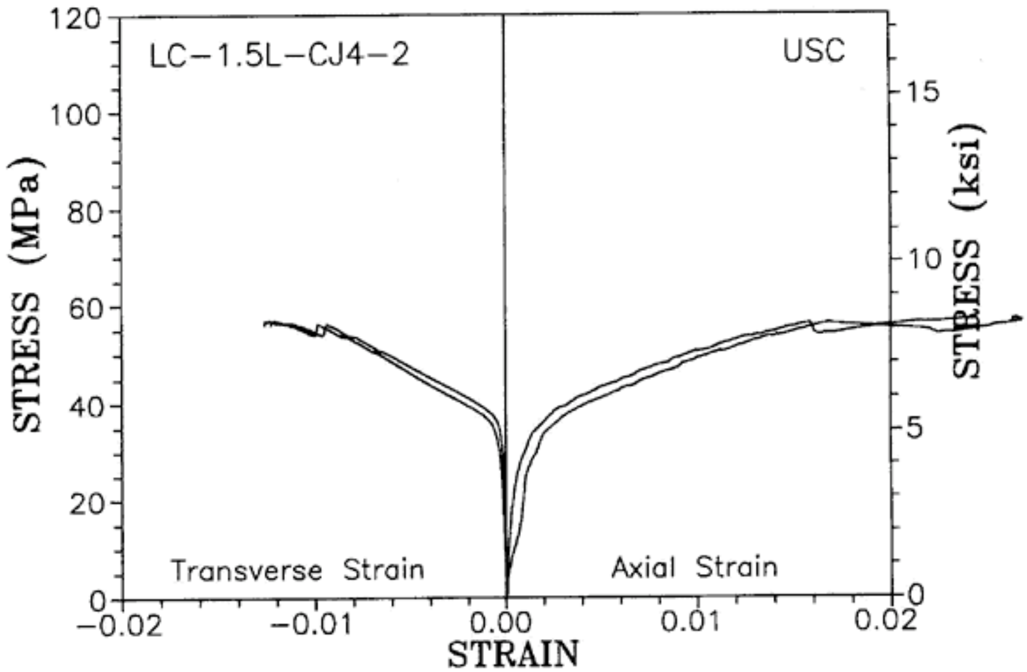

Fig D-B4.Stress-Strain Relationships for Lower Strength Concrete with One and a Half-layer Carbon Fiber Composite Jacket (LC-1.5L-CJ4-2)

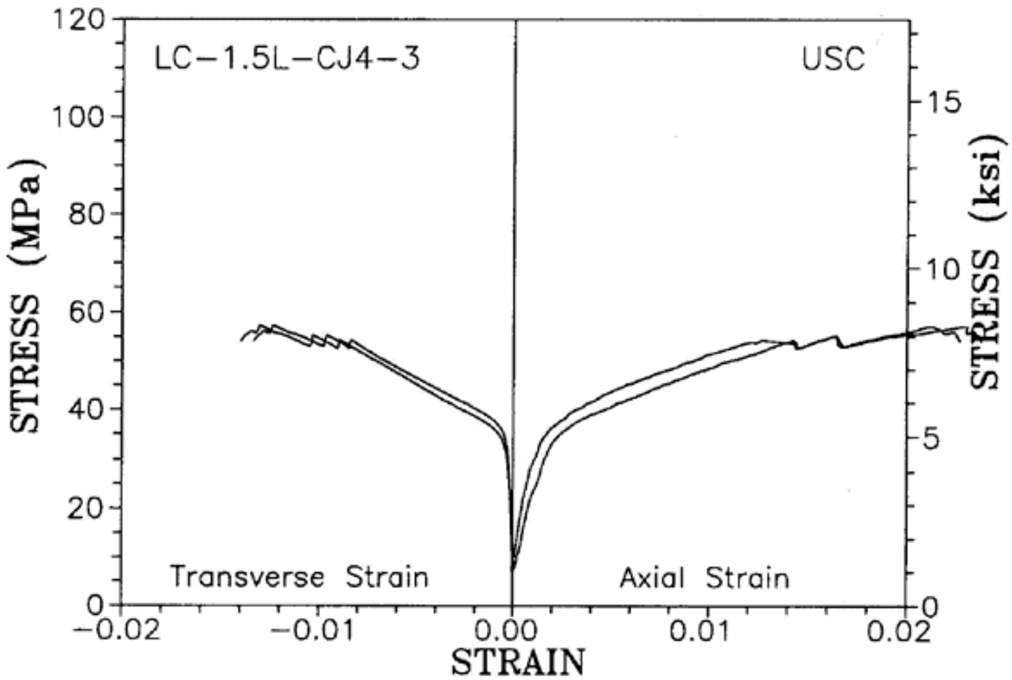

Fig D-B4.Stress-Strain Relationships for Lower Strength Concrete with One and a Half-layer Carbon Fiber Composite Jacket (LC-1.5L-CJ4-3)

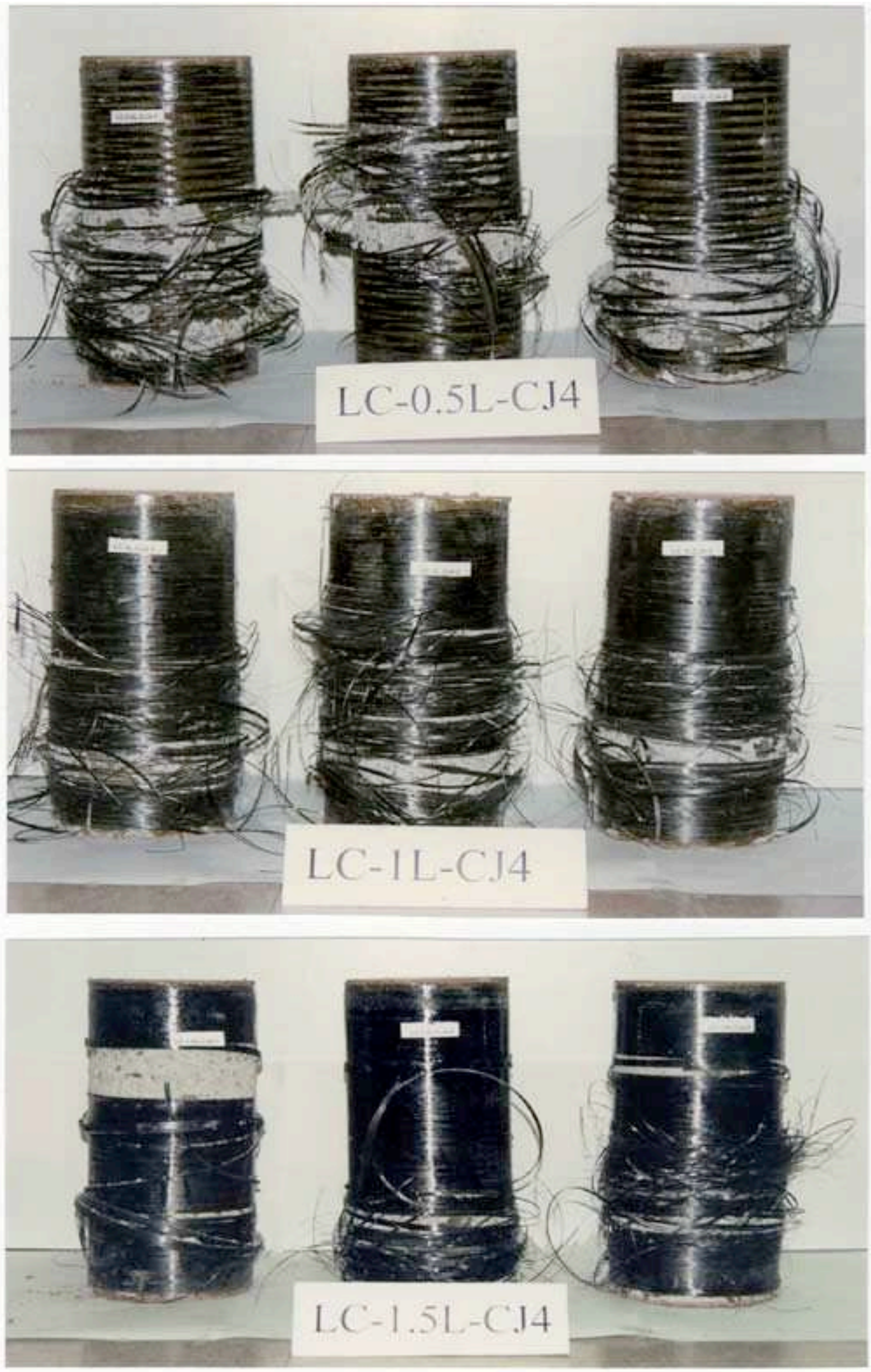

Fig.D-B5. Specimens after Testing

Part D-C Test Results of Medium Strength Concrete Cylinders

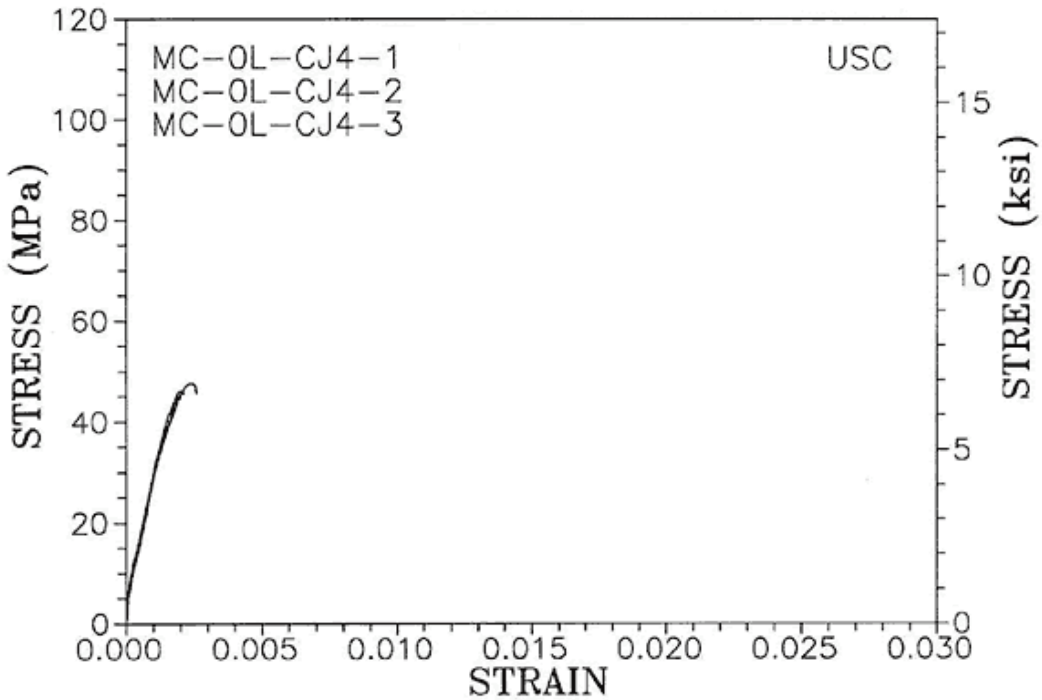

Fig.D-C1. Stress-Strain Relationship for Medium Strength Plain Concrete Cylinders

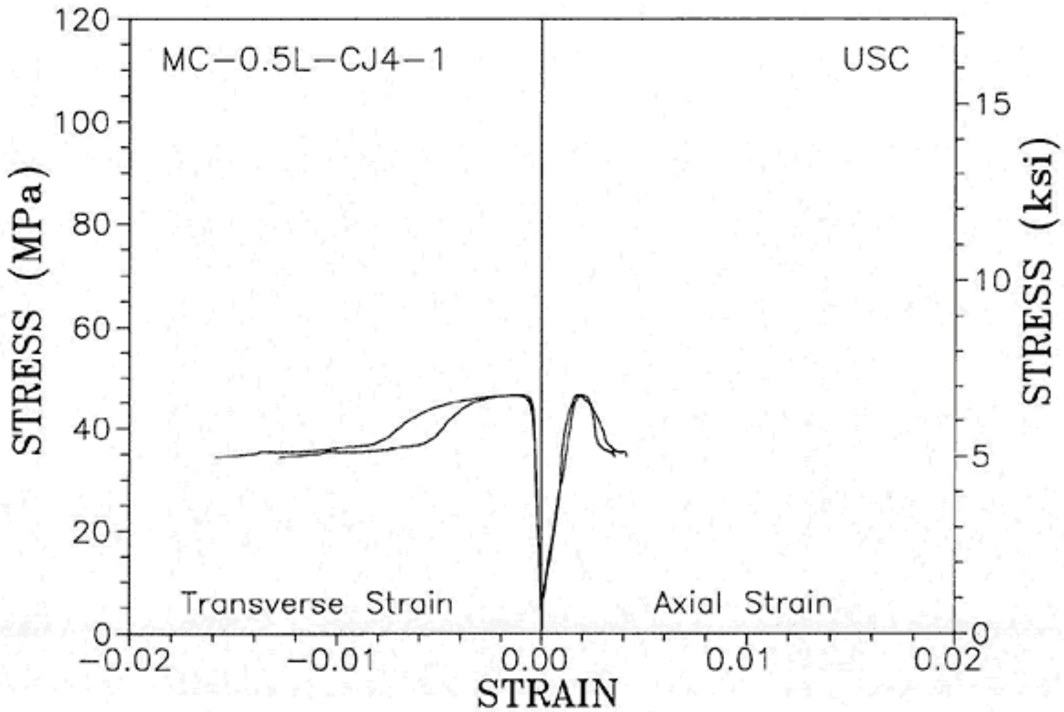

Fig D-C2.Stress-Strain Relationships for Medium Strength Concrete with Half-layer Carbon Fiber Composite Jacket (MC-0.5L-CJ4-1)

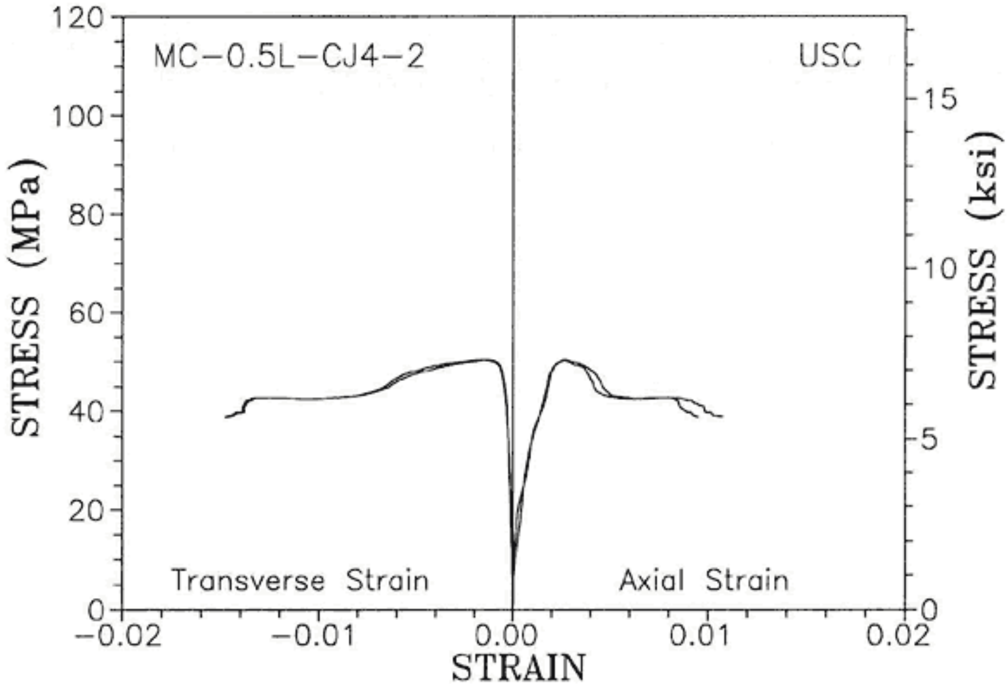

Fig D-C2.Stress-Strain Relationships for Medium Strength Concrete with Half-layer Carbon Fiber Composite Jacket (MC-0.5L-CJ4-2)

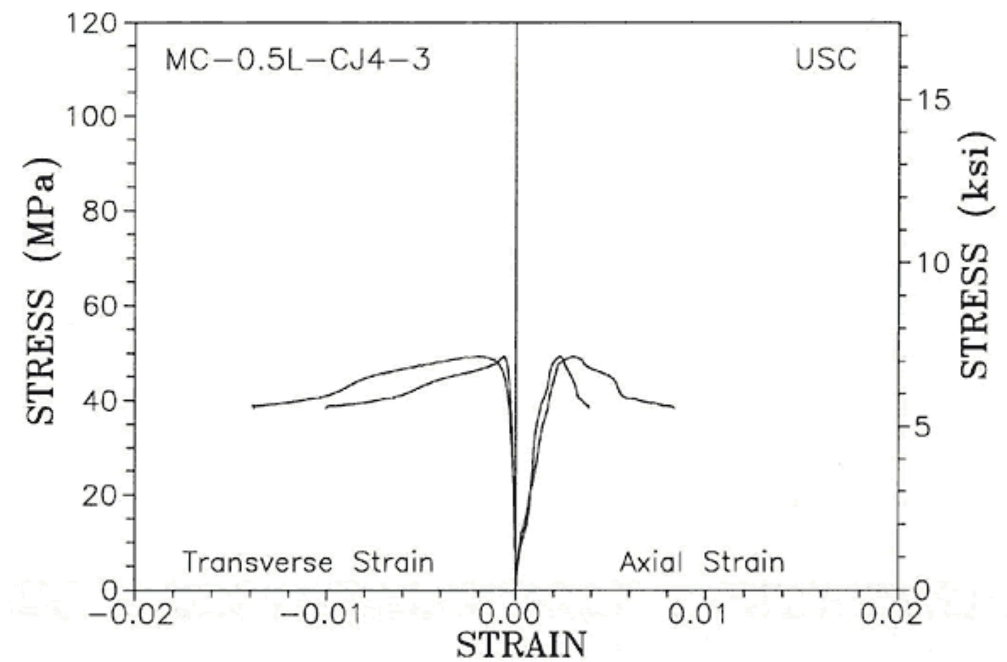

Fig D-C2.Stress-Strain Relationships for Medium Strength Concrete with Half-layer Carbon Fiber Composite Jacket (MC-0.5L-CJ4-3)

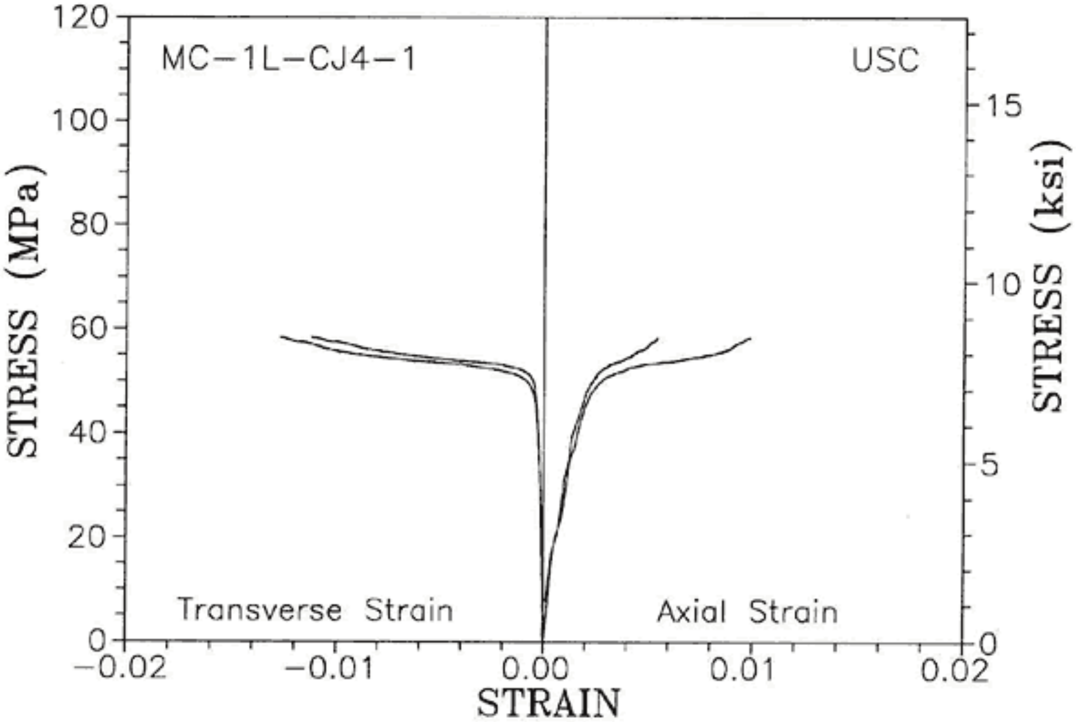

Fig D-C3.Stress-Strain Relationships for Medium Strength Concrete with One-layer Carbon Fiber Composite Jacket (MC-1L-CJ4-1)

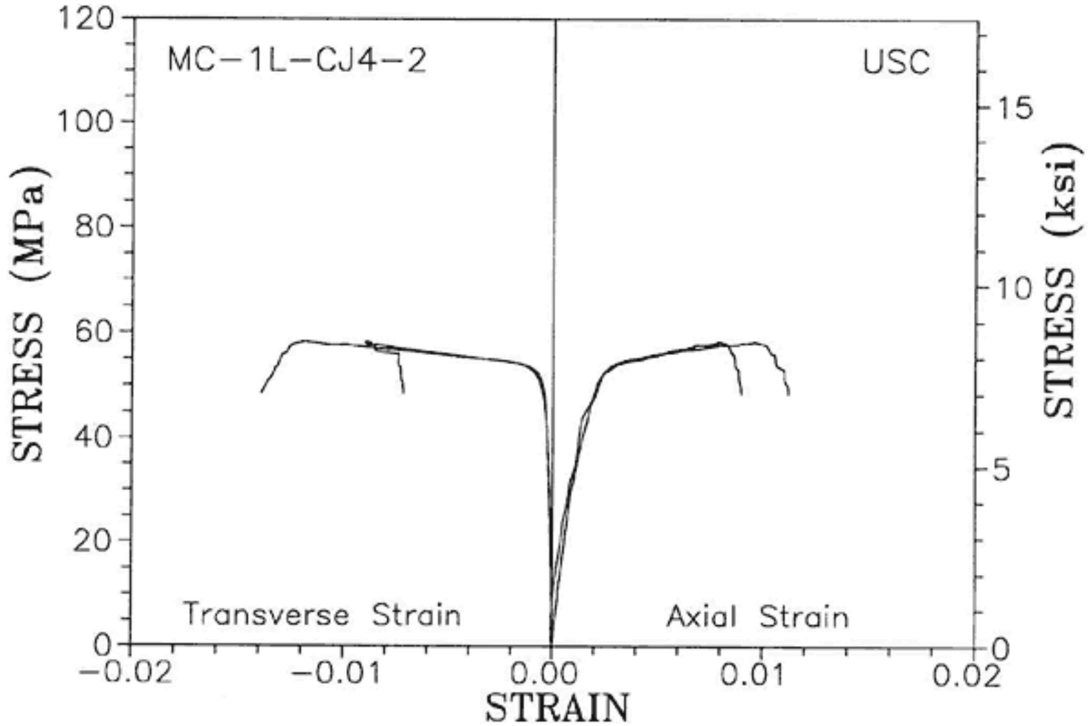

Fig D-C3.Stress-Strain Relationships for Medium Strength Concrete with One-layer Carbon Fiber Composite Jacket (MC-1L-CJ4-2)

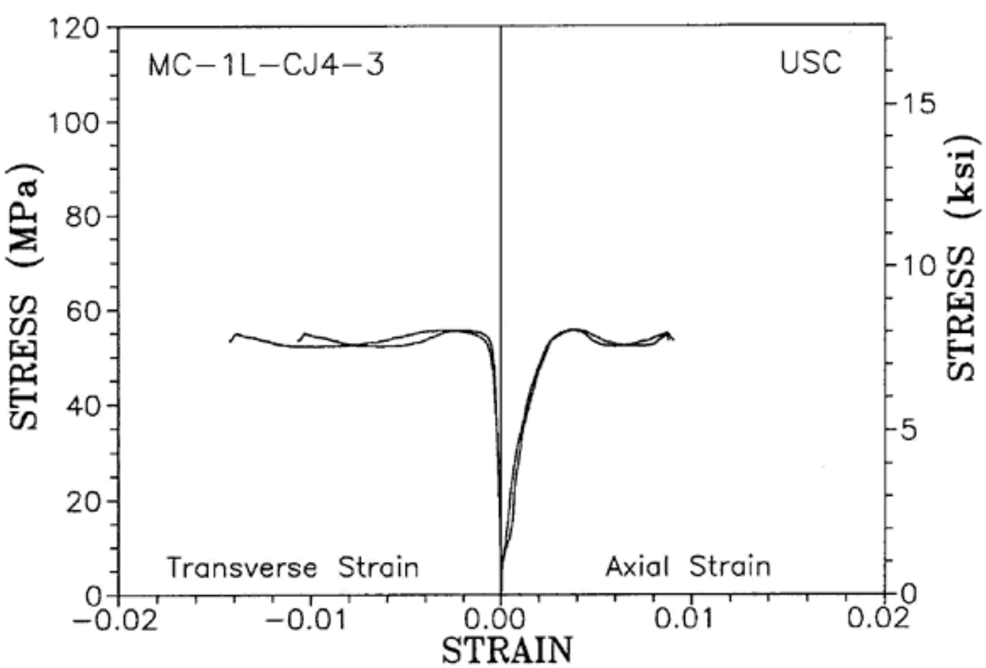

Fig D-C3.Stress-Strain Relationships for Medium Strength Concrete with One-layer Carbon Fiber Composite Jacket (MC-1L-CJ4-3)

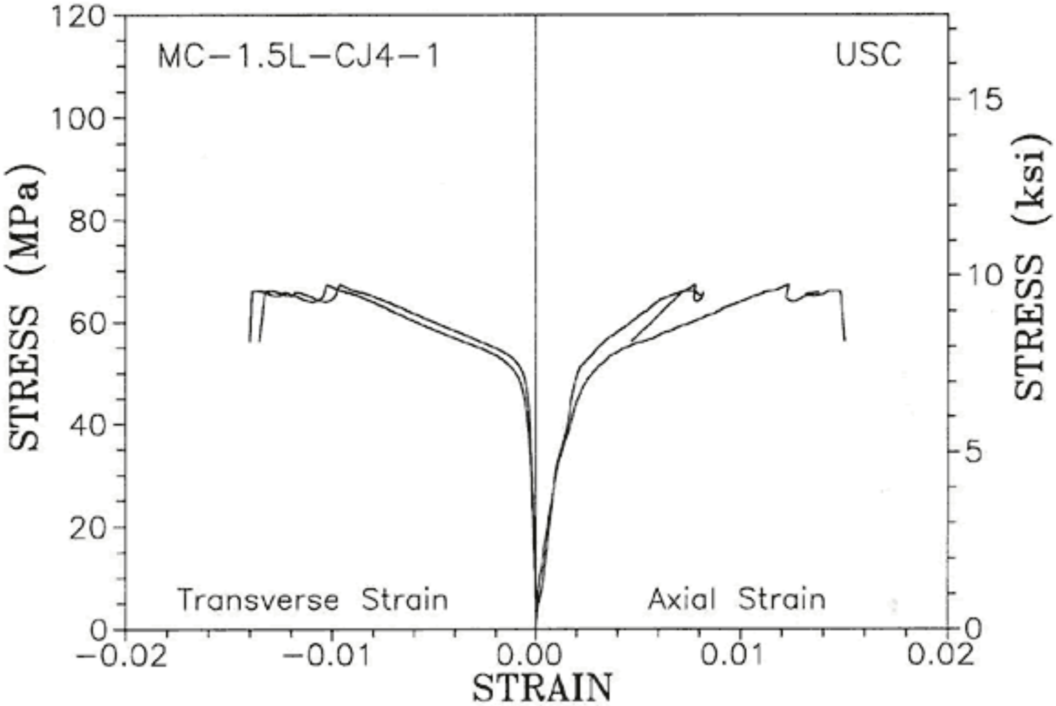

Fig D-C4.Stress-Strain Relationships for Medium Strength Concrete with One and a Half-layer Carbon Fiber Composite Jacket (MC-1.5L-CJ4-1)

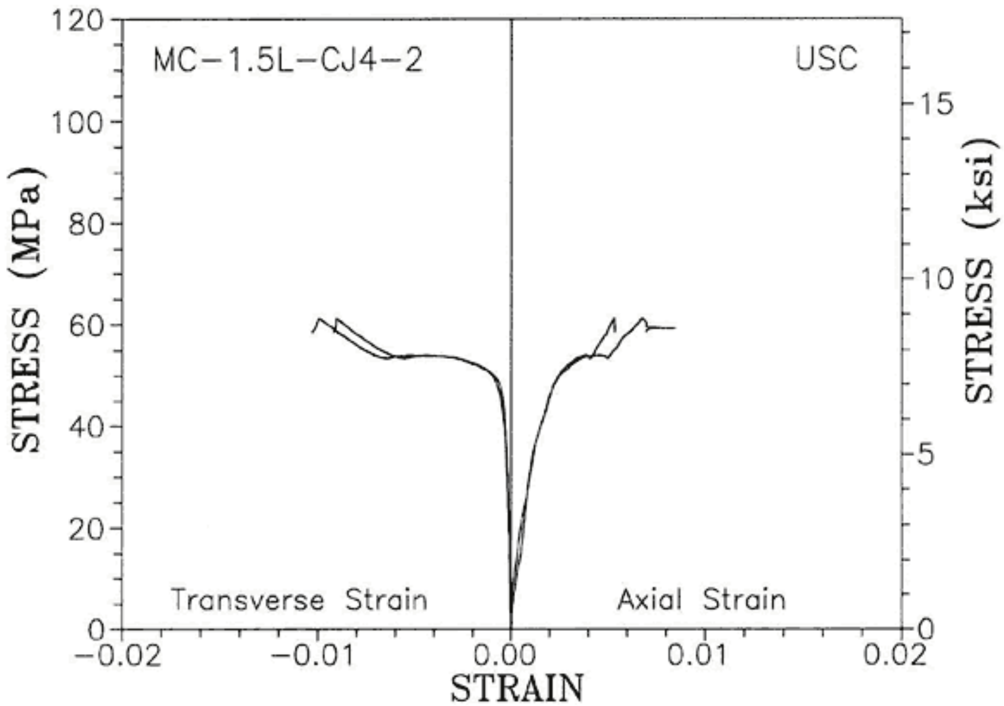

Fig D-C4.Stress-Strain Relationships for Medium Strength Concrete with One and a Half-layer Carbon Fiber Composite Jacket (MC-1.5L-CJ4-2)

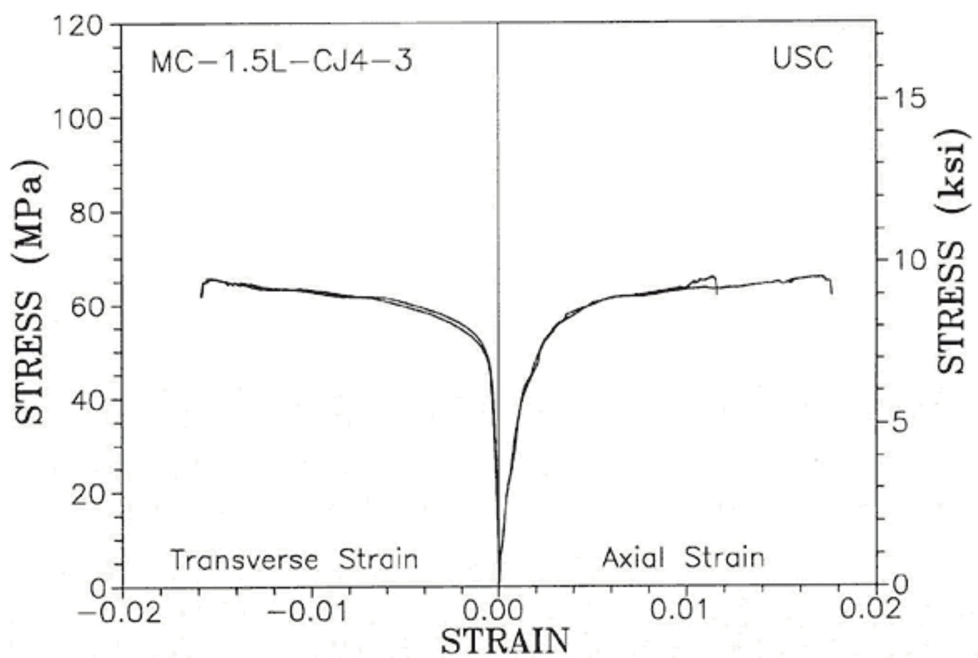

Fig D-C4.Stress-Strain Relationships for Medium Strength Concrete with One and a Half-layer Carbon Fiber Composite Jacket (MC-1.5L-CJ4-3)

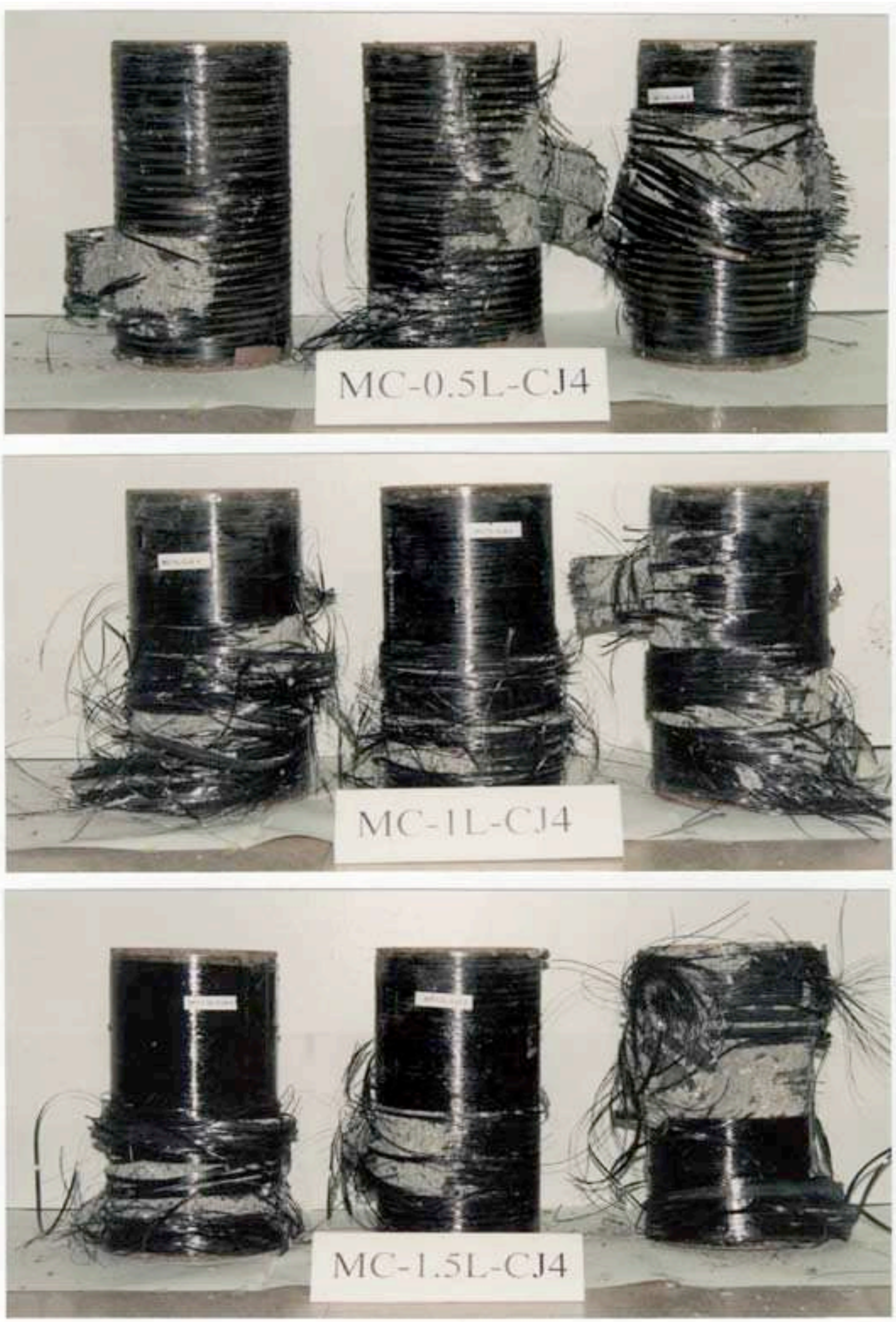

Fig.D-C5. Specimens after Testing

Part D-D Test Results of Higher Strength Concrete Cylinders

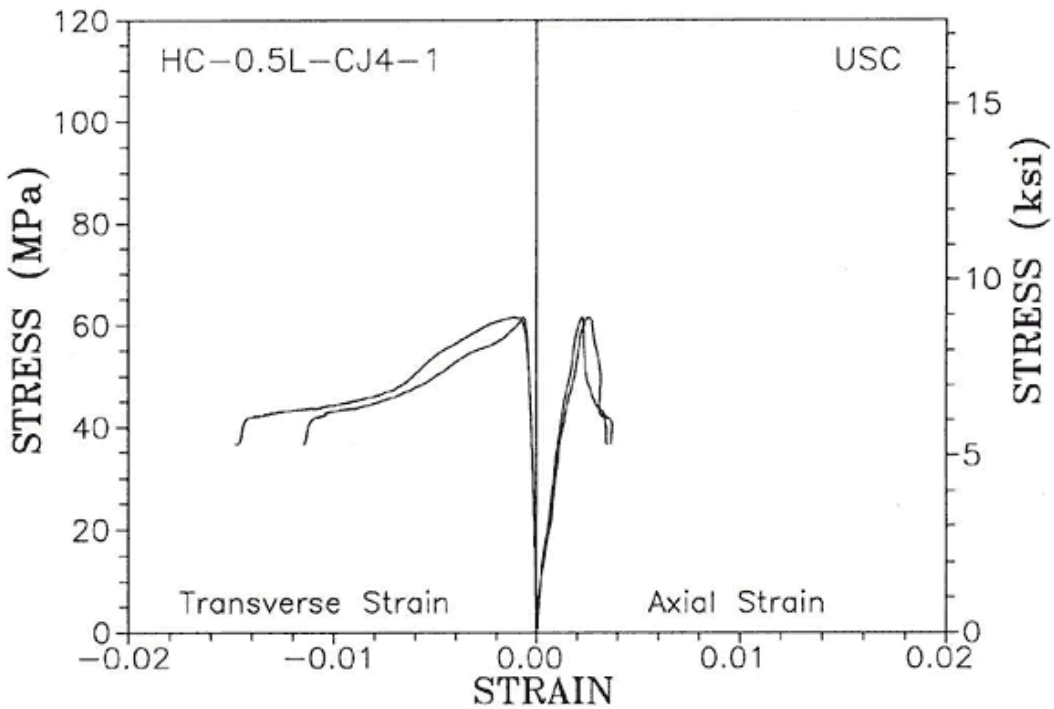

Fig D-D2.Stress-Strain Relationships for Higher Strength Concrete with Half-layer Carbon Fiber Composite Jacket (HC-0.5L-CJ4-1)

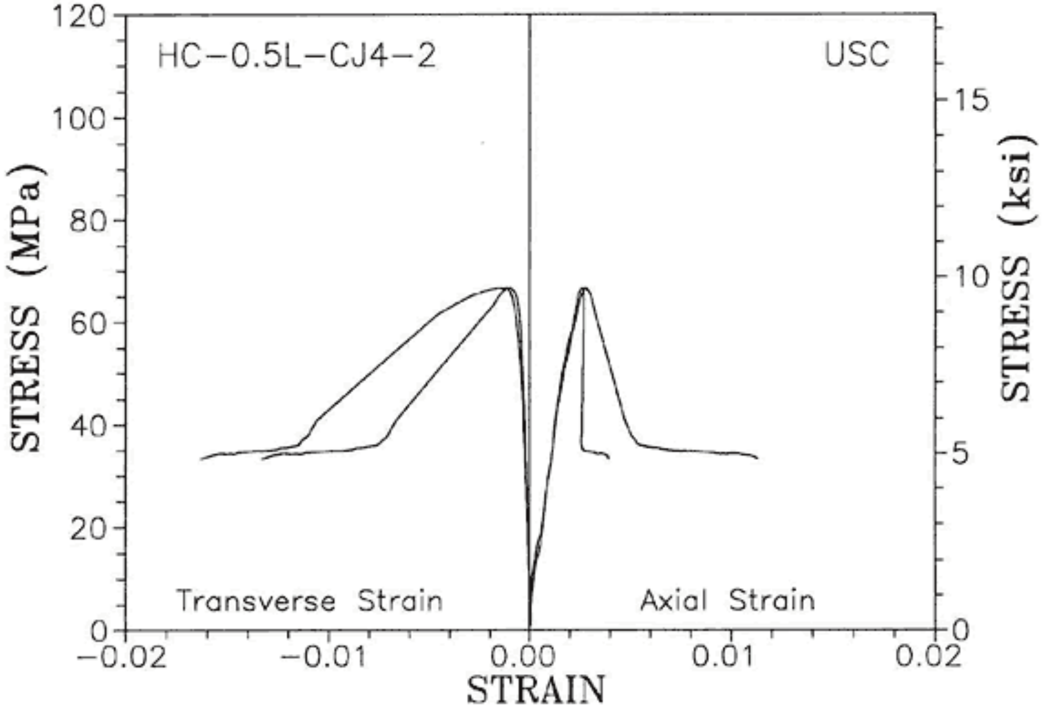

Fig D-D2.Stress-Strain Relationships for Higher Strength Concrete with Half-layer Carbon Fiber Composite Jacket (HC-0.5L-CJ4-2)

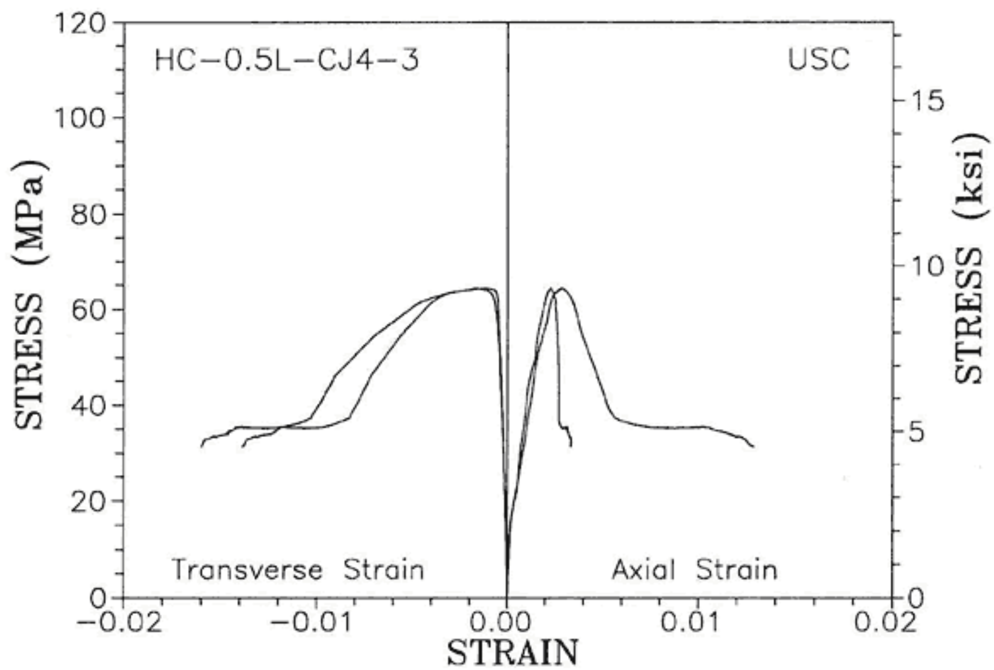

Fig D-D2.Stress-Strain Relationships for Higher Strength Concrete with Half-layer Carbon Fiber Composite Jacket (HC-0.5L-CJ4-3)

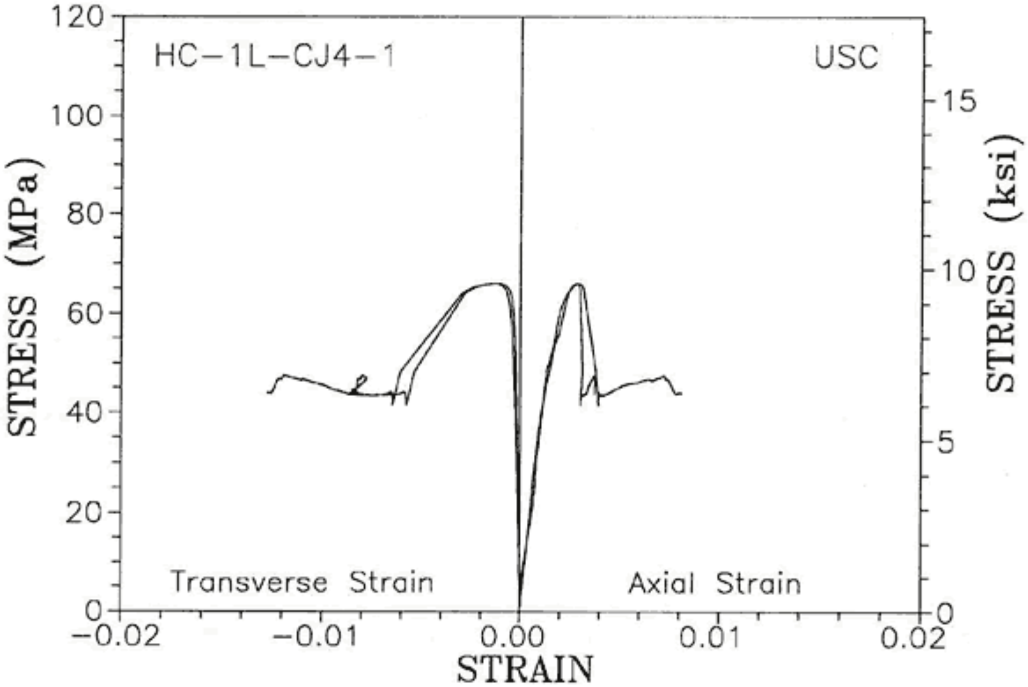

Fig D-D3.Stress-Strain Relationships for Higher Strength Concrete with One-layer Carbon Fiber Composite Jacket (HC-1L-CJ4-1)

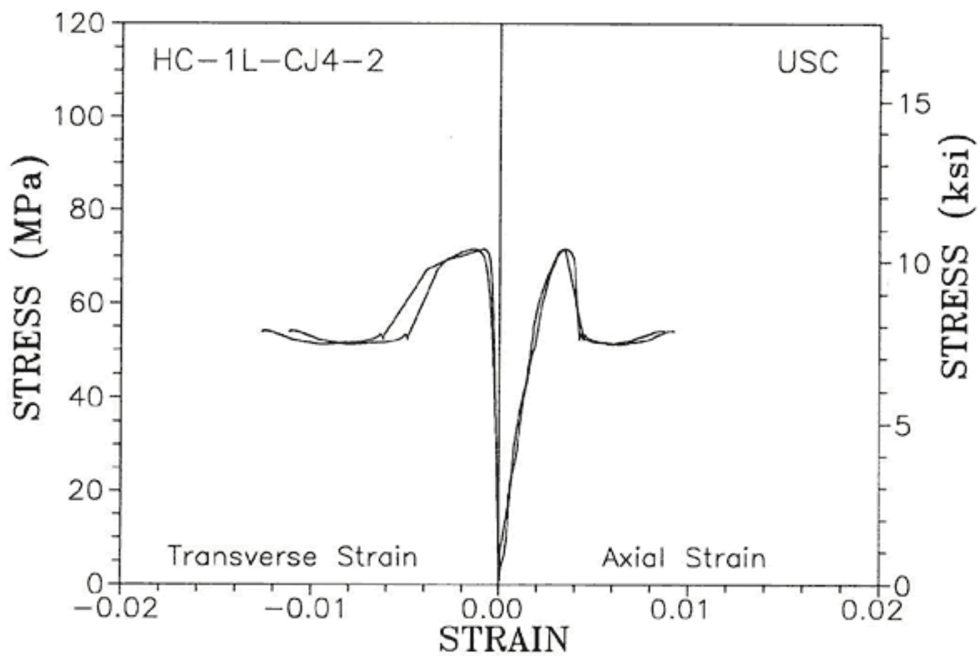

Fig D-D3.Stress-Strain Relationships for Higher Strength Concrete with One-layer Carbon Fiber Composite Jacket (HC-1L-CJ4-2)

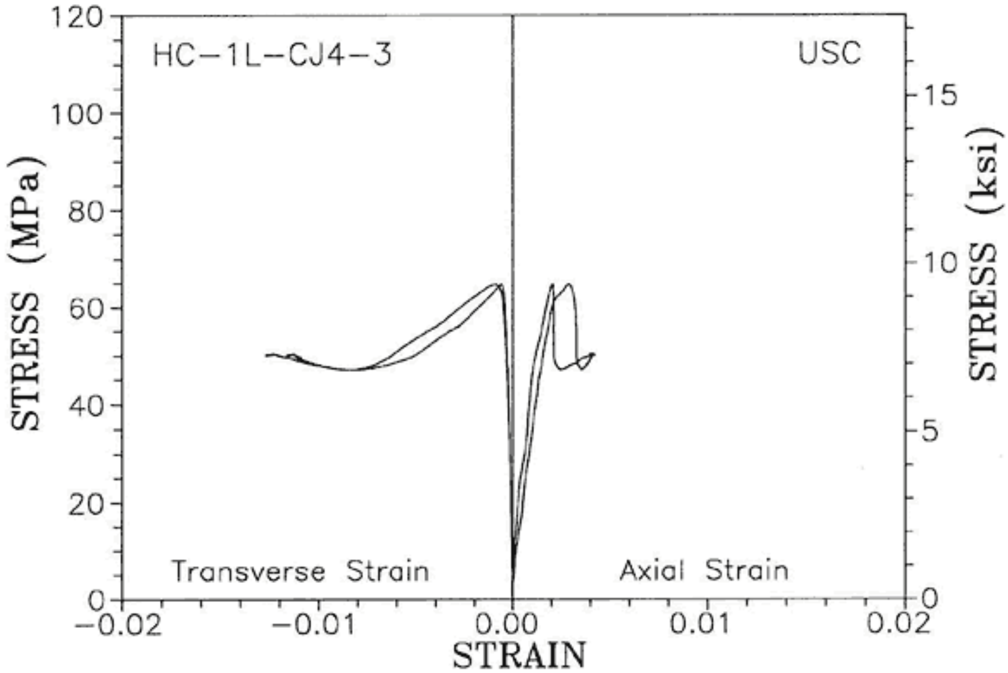

Fig D-D3.Stress-Strain Relationships for Higher Strength Concrete with One-layer Carbon Fiber Composite Jacket (HC-1L-CJ4-3)

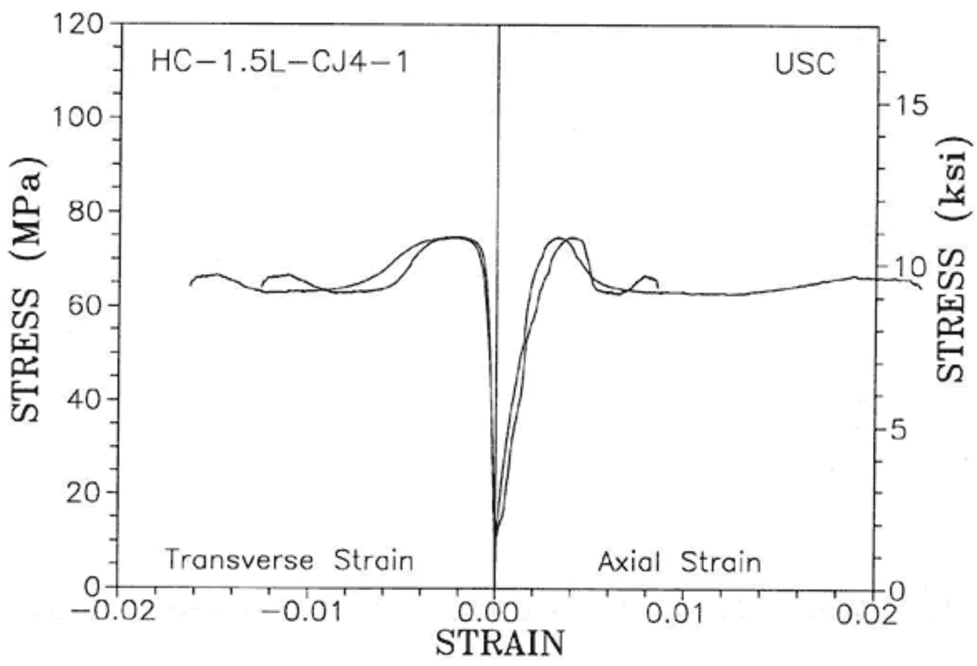

Fig D-D4.Stress-Strain Relationships for Higher Strength Concrete with One and a Half-layer Carbon Fiber Composite Jacket (HC-1.5L-CJ4-1)

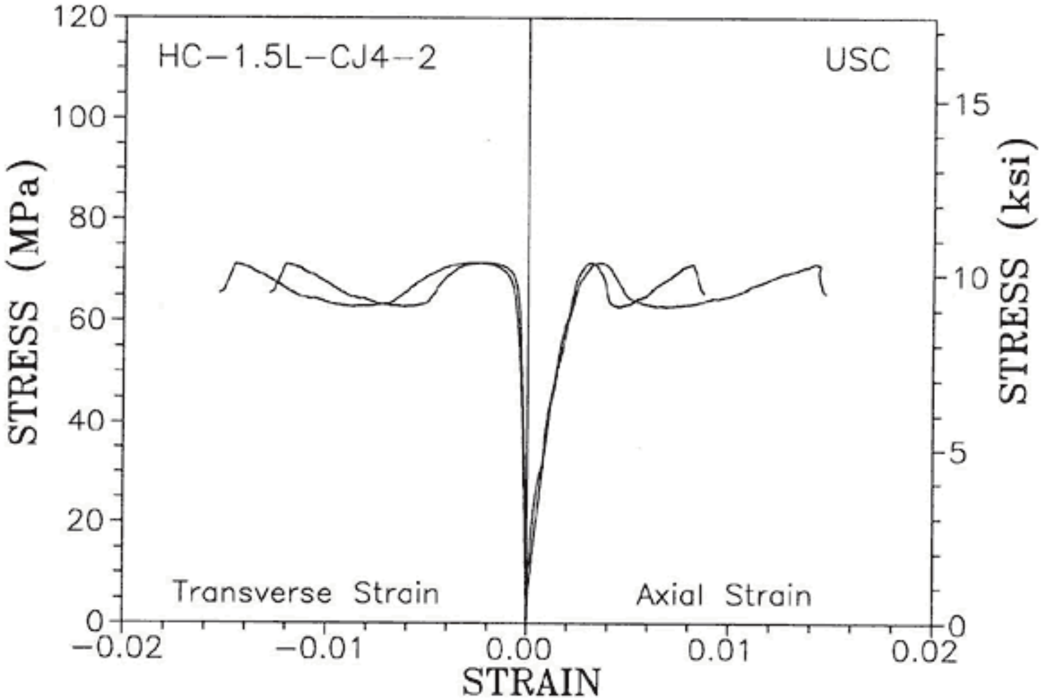

Fig D-D4.Stress-Strain Relationships for Higher Strength Concrete with One and a Half-layer Carbon Fiber Composite Jacket (HC-1.5L-CJ4-2)

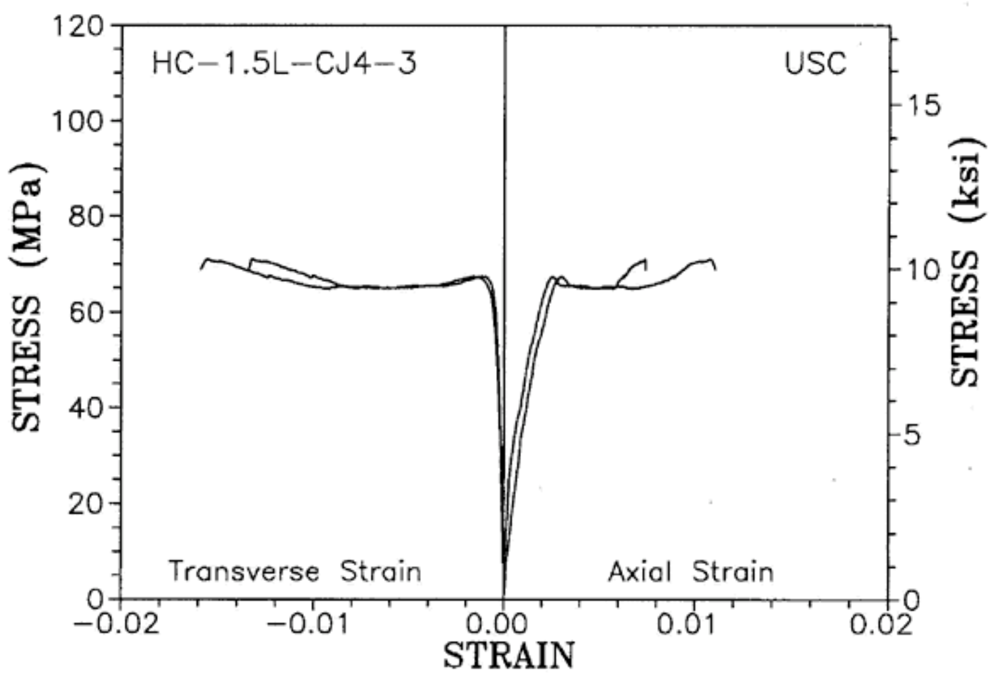

Fig D-D4.Stress-Strain Relationships for Higher Strength Concrete with One and a Half-layer Carbon Fiber Composite Jacket (HC-1.5L-CJ4-3)

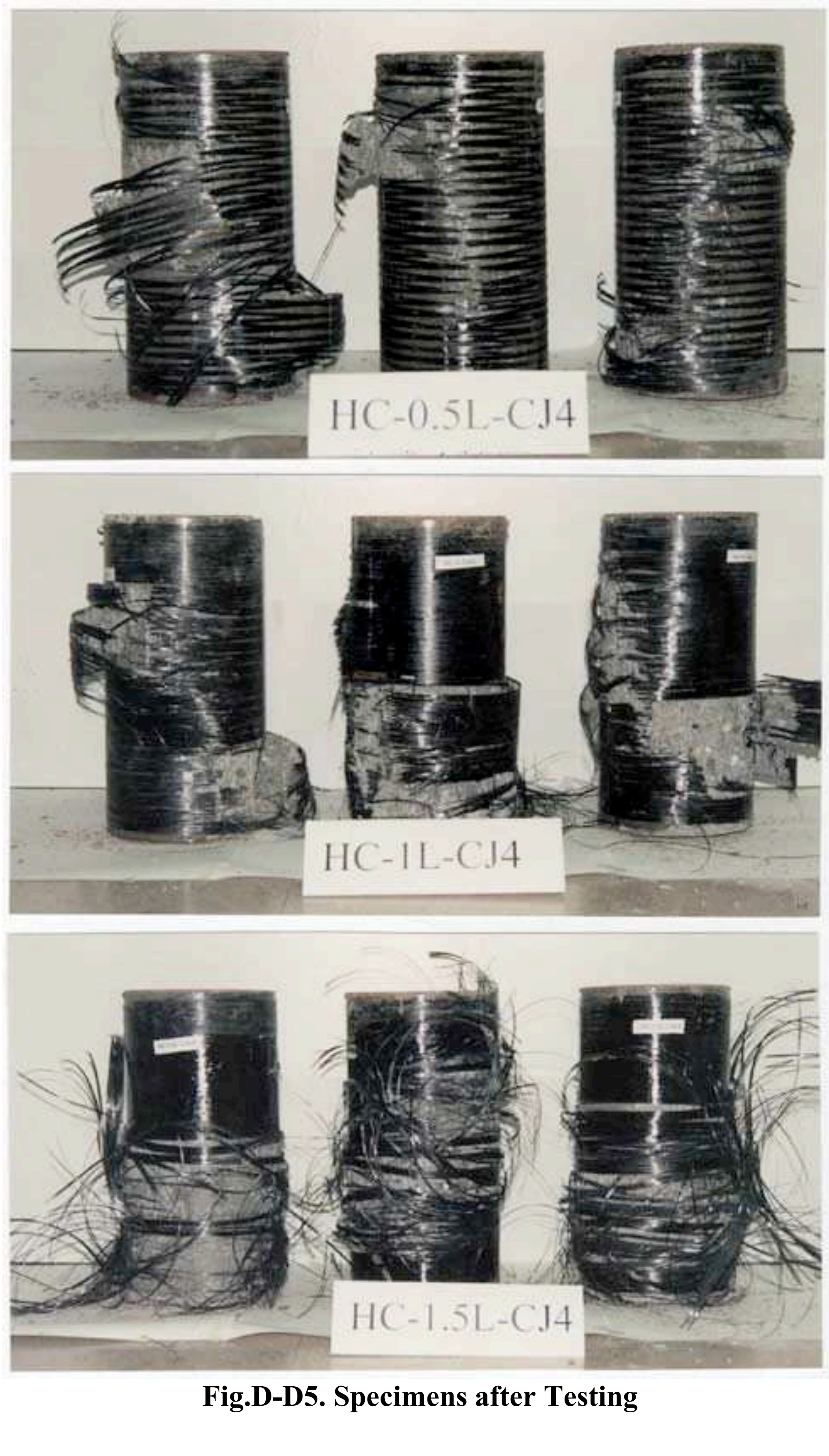

Fig.D-D5. Specimens after Testing

APPENDIX E: TEST RESULTS OF SYSTEM FIVE

Part E-A General Information

Table E-A1 Test Matrix

Type of Jacket	Concrete Strength	Jacket Layers	Specimen Numbers
Tyfo -Carbon fiber reinforced composite Jacket	Lower	Plain concrete	3 specimens each
		1-layer	
		2-layer	
		3-layer	
	Medium	Plain concrete	
		1-layer	
		2-layer	
		3-layer	
	Higher	Plain concrete	
		1-layer	
		2-layer	
		3-layer	

Table E-A2 Mix Proportion of Concrete

Series	Target f'_{co} (MPa)	W/C	Water (kg/m^3)	Cement (kg/m^3)	Fine Aggregates (kg/m^3)	Coarse Aggregates (kg/m^3)
L	27.6	0.68	196	288	1087	853
M	37.9	0.48	196	408	986	853
H	48.2	0.38	197	515	857	853

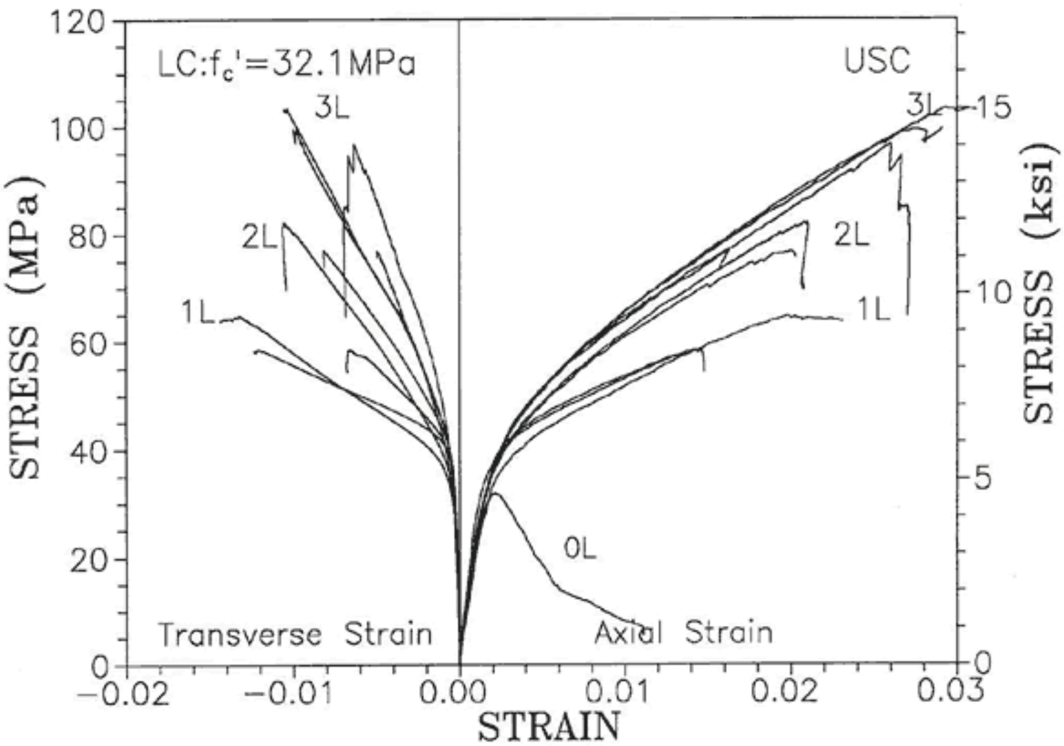

Fig.E-A1. Test Results of Lower-Strength Specimens

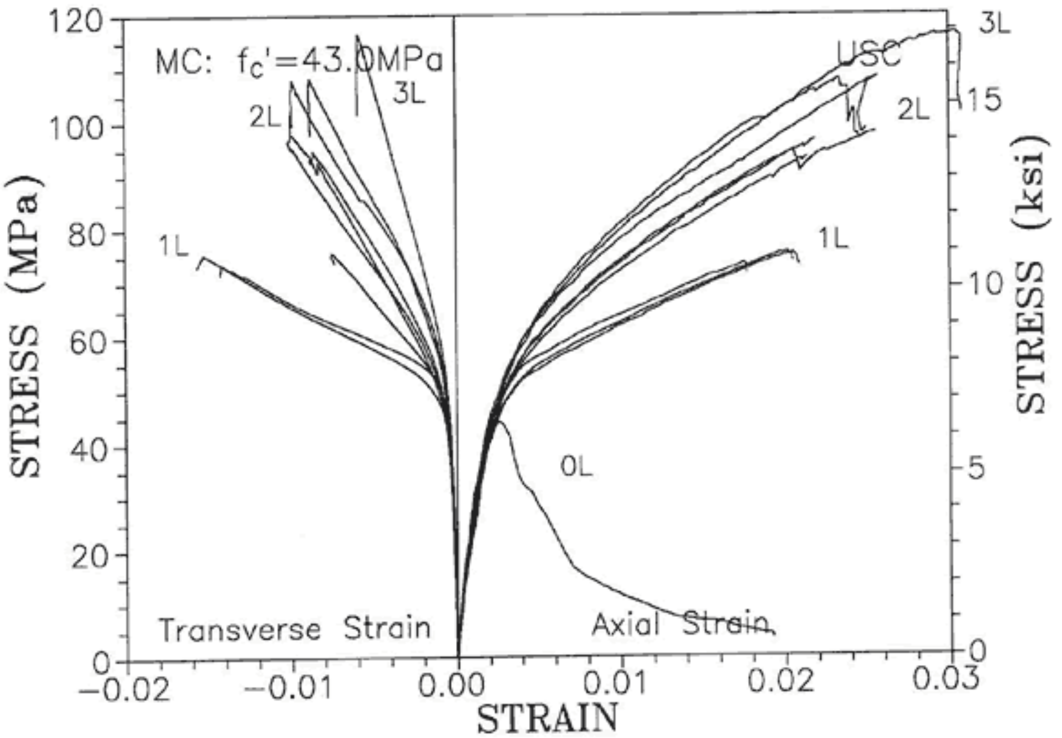

Fig.E-A2. Test Results of Medium-Strength Specimens

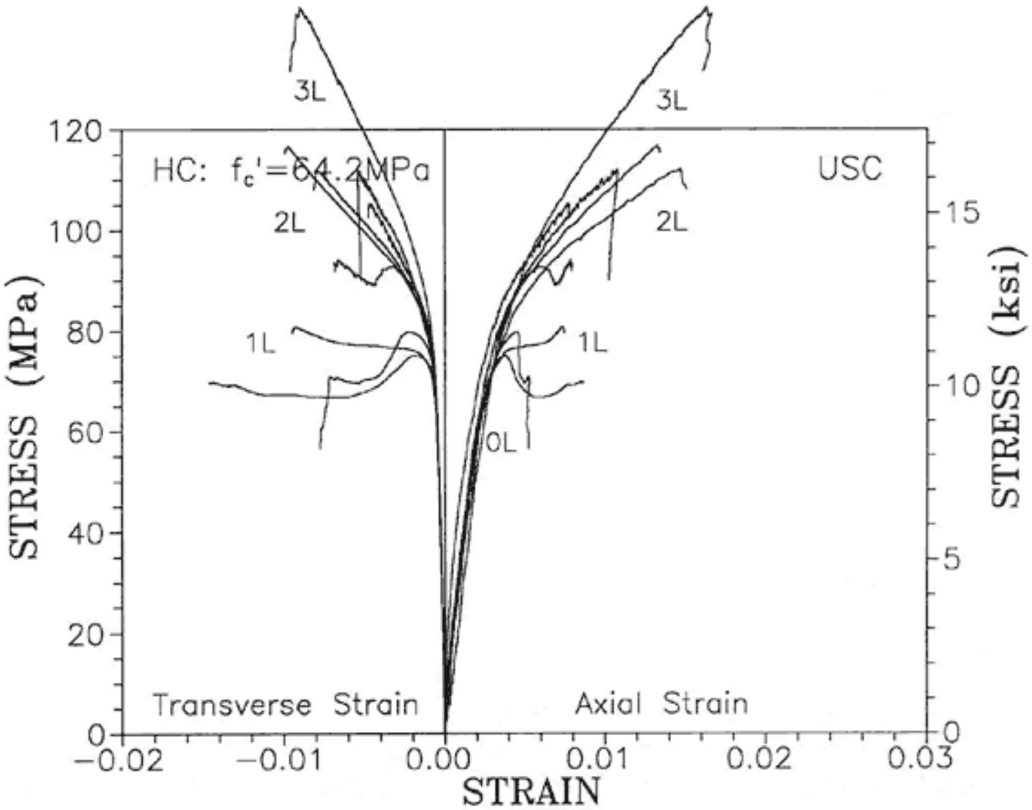

Fig.E-A3. Test Results of Higher-Strength Specimens

Table E-A4 Test Results

Series	Specimen	f_c' (MPa)	Jacket Layers	f_{cc}' (MPa)	ε_{cu}
L	LC-0L-CJ5-1	32.1	0	30.57	0.001976
	LC-0L-CJ5-2			33.92	0.002039
	LC-0L-CJ5-3			31.84	0.002109
	LC-1L-CJ5-1		1	58.46	0.014378
	LC-1L-CJ5-2			58.53	0.014216
	LC-1L-CJ5-3			64.64	0.020299
	LC-2L-CJ5-1		2	76.91	0.020043
	LC-2L-CJ5-2			77.02	0.016284
	LC-2L-CJ5-3			82.26	0.021005
	LC-3L-CJ5-1		3	94.68	0.026652
	LC-3L-CJ5-2			99.58	0.029076
	LC-3L-CJ5-3			103.48	0.014948
M	MC-0L-CJ5-1	43.0	0	44.11	0.002622
	MC-0L-CJ5-2			41.40	0.002374
	MC-0L-CJ5-3			43.44	0.002440
	MC-1L-CJ5-1		1	75.63	0.020223
	MC-1L-CJ5-2			75.47	0.020542
	MC-1L-CJ5-3			73.52	0.017513
	MC-2L-CJ5-1		2	98.04	0.025506
	MC-2L-CJ5-2			94.81	0.020595
	MC-2L-CJ5-3			96.72	0.021858
	MC-3L-CJ5-1		3	116.62	0.030397
	MC-3L-CJ5-2			108.29	0.025646
	MC-3L-CJ5-3			108.05	0.023363
H	HC-0L-CJ5-1	64.2	0	64.26	0.002483
	HC-0L-CJ5-2			65.58	0.002585
	HC-0L-CJ5-3			62.89	0.003062
	HC-1L-CJ5-1		1	70.91	0.005223
	HC-1L-CJ5-2			80.78	0.007379
	HC-1L-CJ5-3			75.00	0.003827
	HC-2L-CJ5-1		2	94.14	0.007873
	HC-2L-CJ5-2			111.98	0.014643
	HC-2L-CJ5-3			116.71	0.013276
	HC-3L-CJ5-1		3	105.36	0.007659
	HC-3L-CJ5-2			142.85	0.008283
	HC-3L-CJ5-3			111.94	0.010766

Note: (i) Example for specimen name designation:

LC-2L-CJ5-1: LC designates Lower strength Concrete; 2L designates 2 Layers; CJ5 designates Carbon fiber Jacket System 1; and the last number represents specimen number in same series.

(ii) f_c': Average plain concrete cylinder strength;

(iii) f_{cc}': Ultimate strength of confined concrete;

(iv) ε_{cu}: Ultimate strain

Part E-B Test Results of Lower Strength Concrete Cylinders

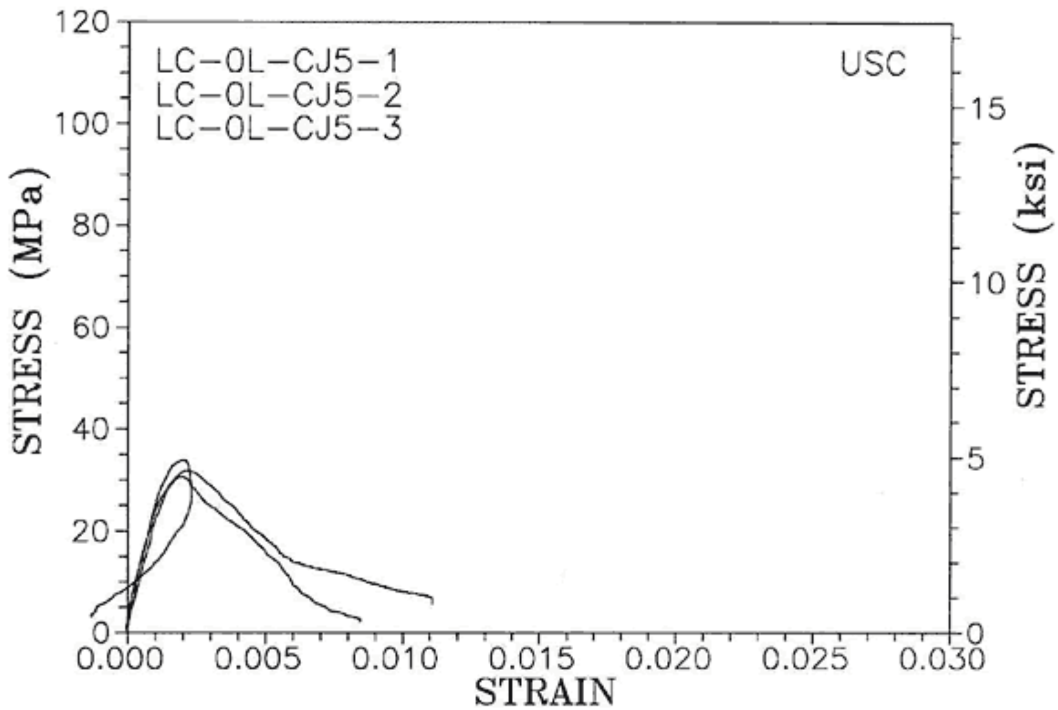

Fig.E-B1. Stress-Strain Relationship for Lower Strength Plain Concrete Cylinders

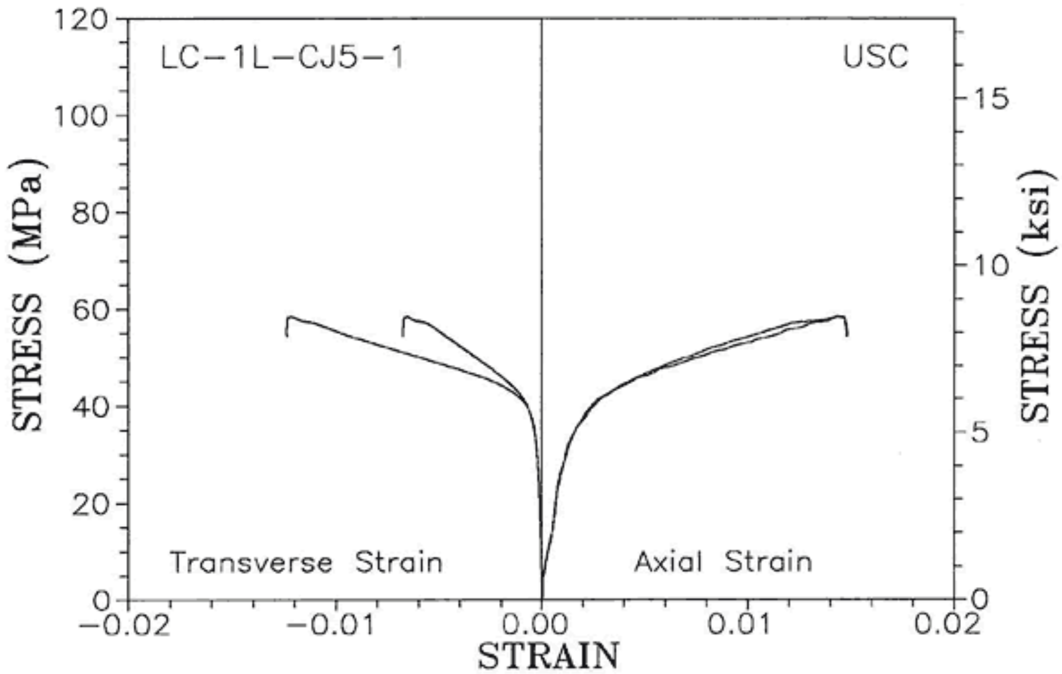

Fig E-B2.Stress-Strain Relationships for Lower Strength Concrete with One-layer Carbon Fiber Composite Jacket (LC-1L-CJ5-1)

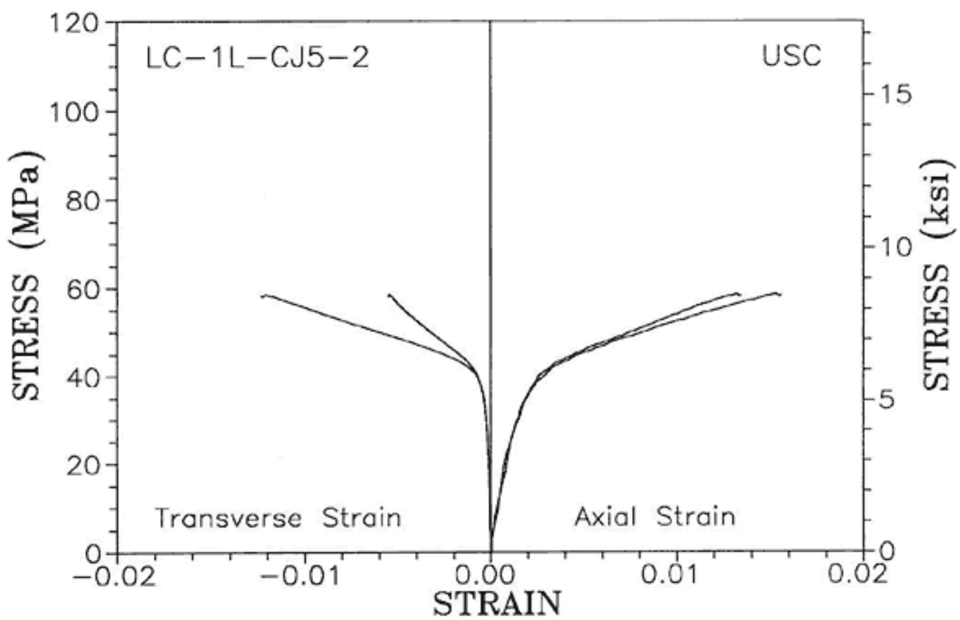

Fig e-B2.Stress-Strain Relationships for Lower Strength Concrete with One-layer Carbon Fiber Composite Jacket (LC-1L-CJ5-2)

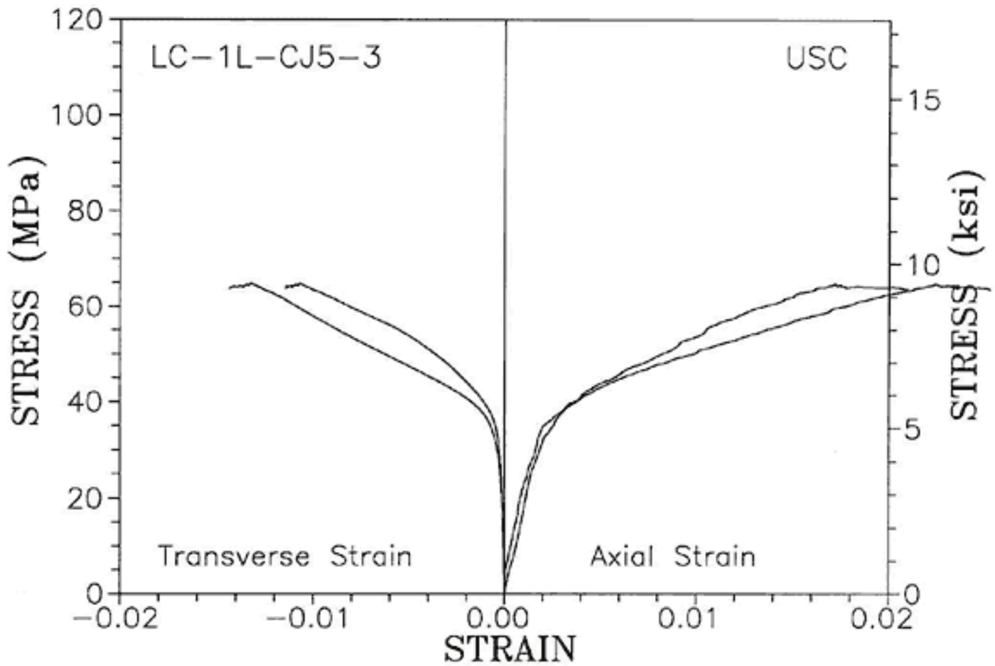

Fig E-B2.Stress-Strain Relationships for Lower Strength Concrete with Half-layer Carbon Fiber Composite Jacket (LC-1L-CJ5-3)

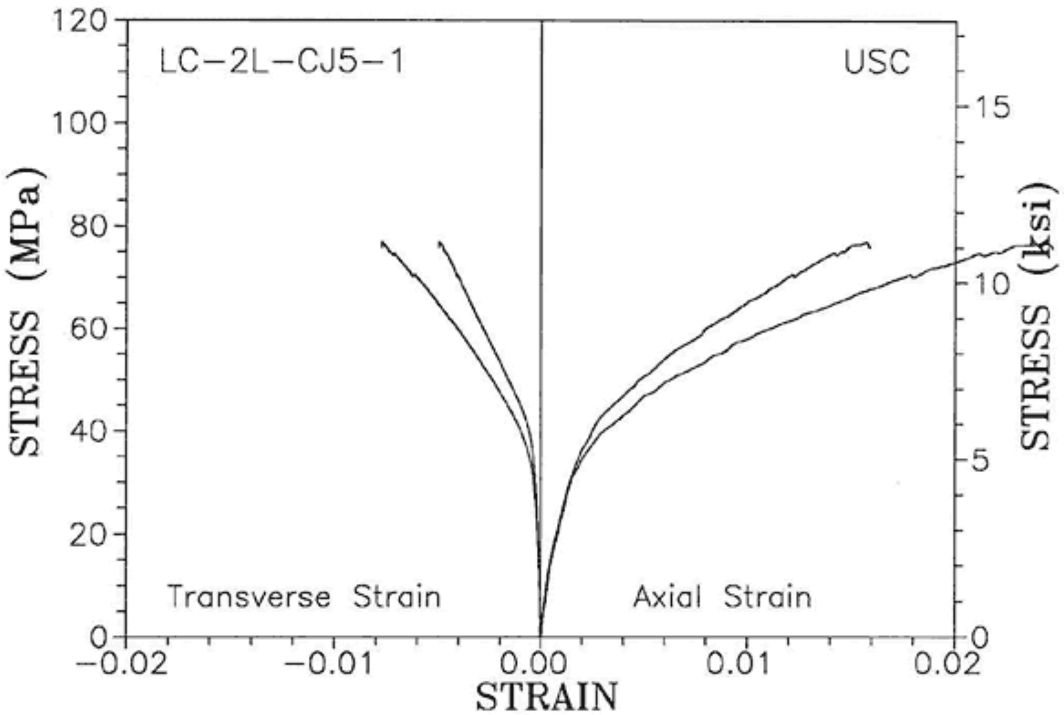

Fig E-B3.Stress-Strain Relationships for Lower Strength Concrete with Two-layer Carbon Fiber Composite Jacket (LC-2L-CJ5-1)

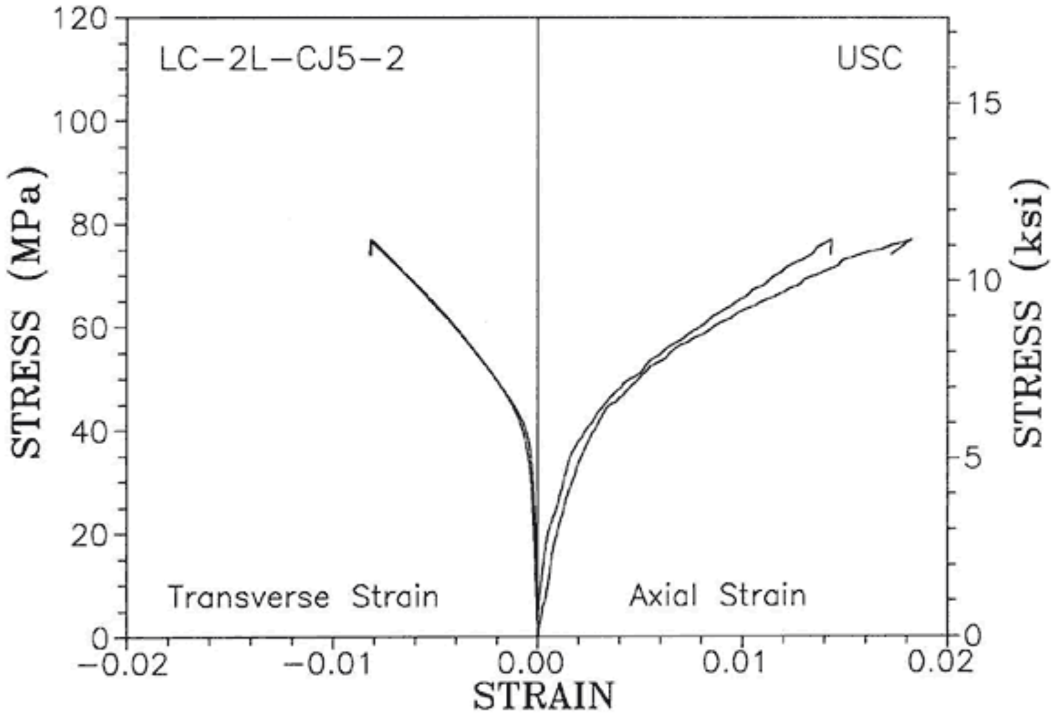

Fig E-B3.Stress-Strain Relationships for Lower Strength Concrete with Two-layer Carbon Fiber Composite Jacket (LC-2L-CJ5-2)

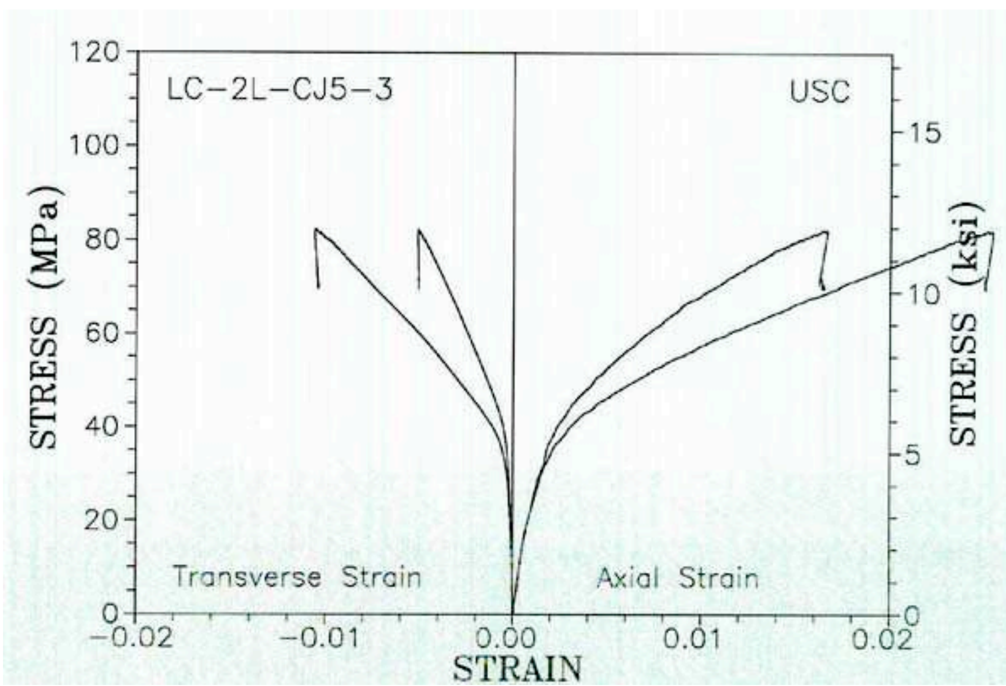

Fig E-B3.Stress-Strain Relationships for Lower Strength Concrete with Two-layer Carbon Fiber Composite Jacket (LC-2L-CJ5-3)

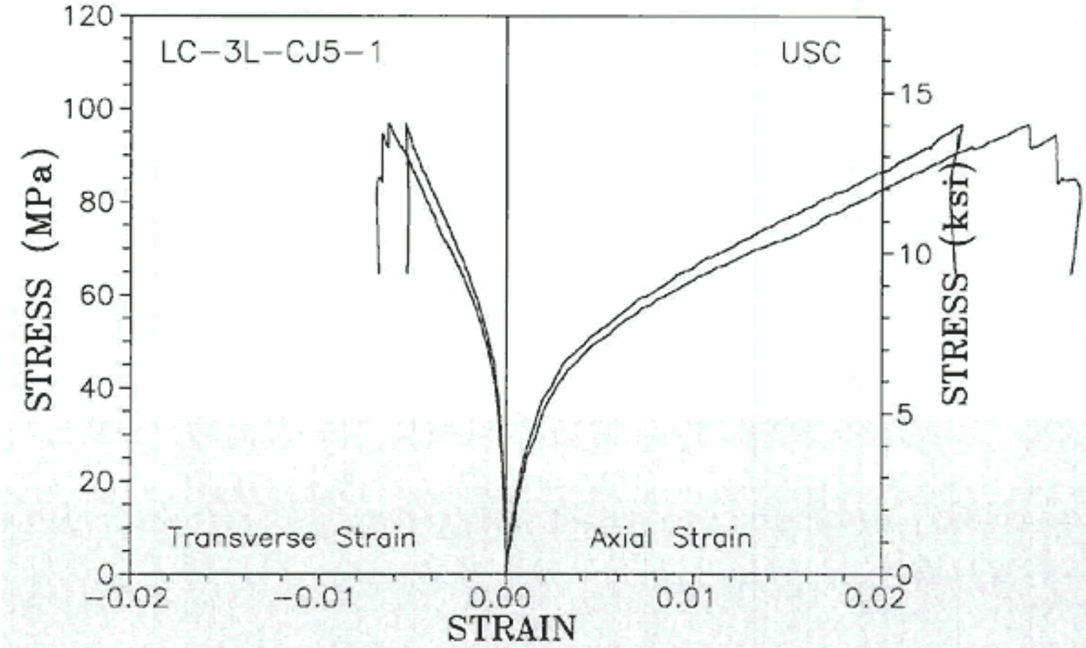

Fig E-B4.Stress-Strain Relationships for Lower Strength Concrete with Three-layer Carbon Fiber Composite Jacket (LC-3L-CJ5-1)

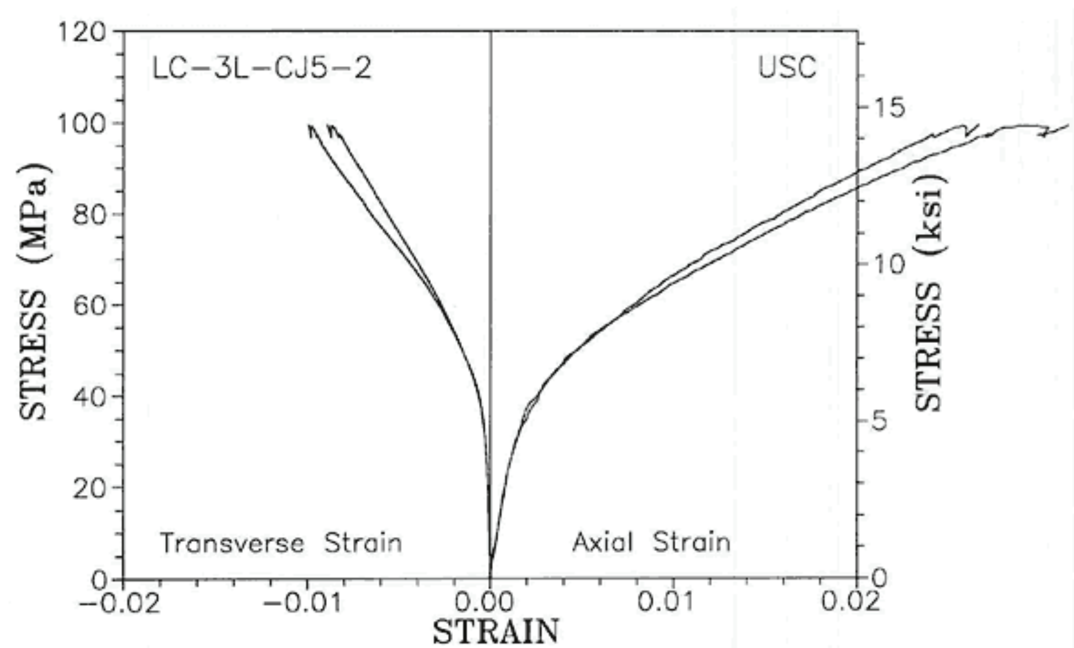

Fig E-B4.Stress-Strain Relationships for Lower Strength Concrete with Three-layer Carbon Fiber Composite Jacket (LC-3L-CJ5-2)

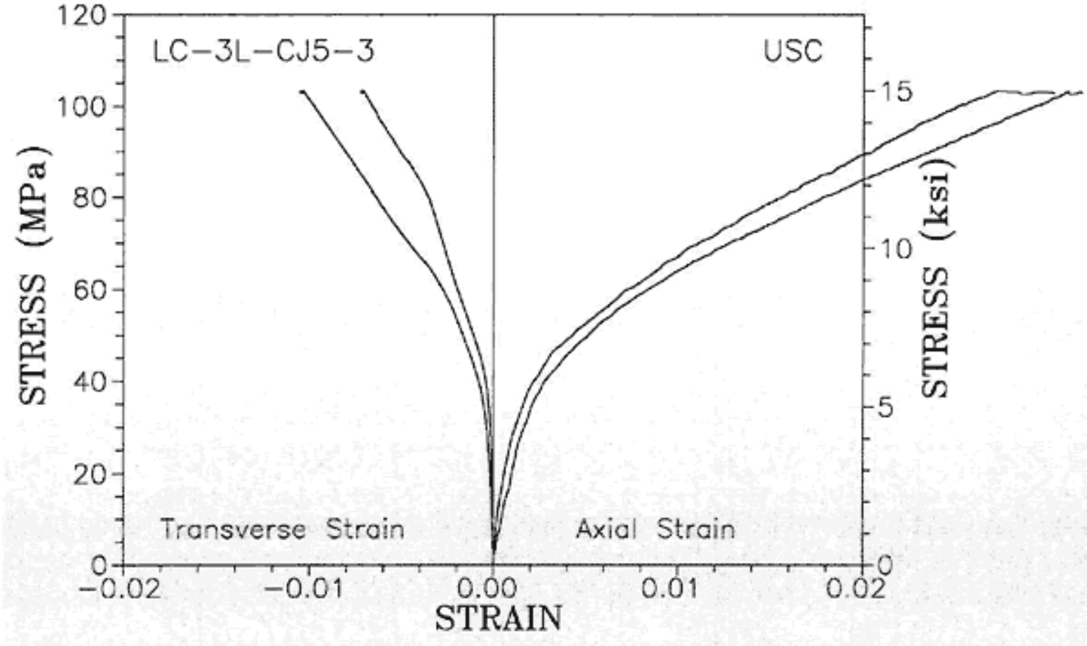

Fig E-B4.Stress-Strain Relationships for Lower Strength Concrete with Three-layer Carbon Fiber Composite Jacket (LC-3L-CJ5-3)

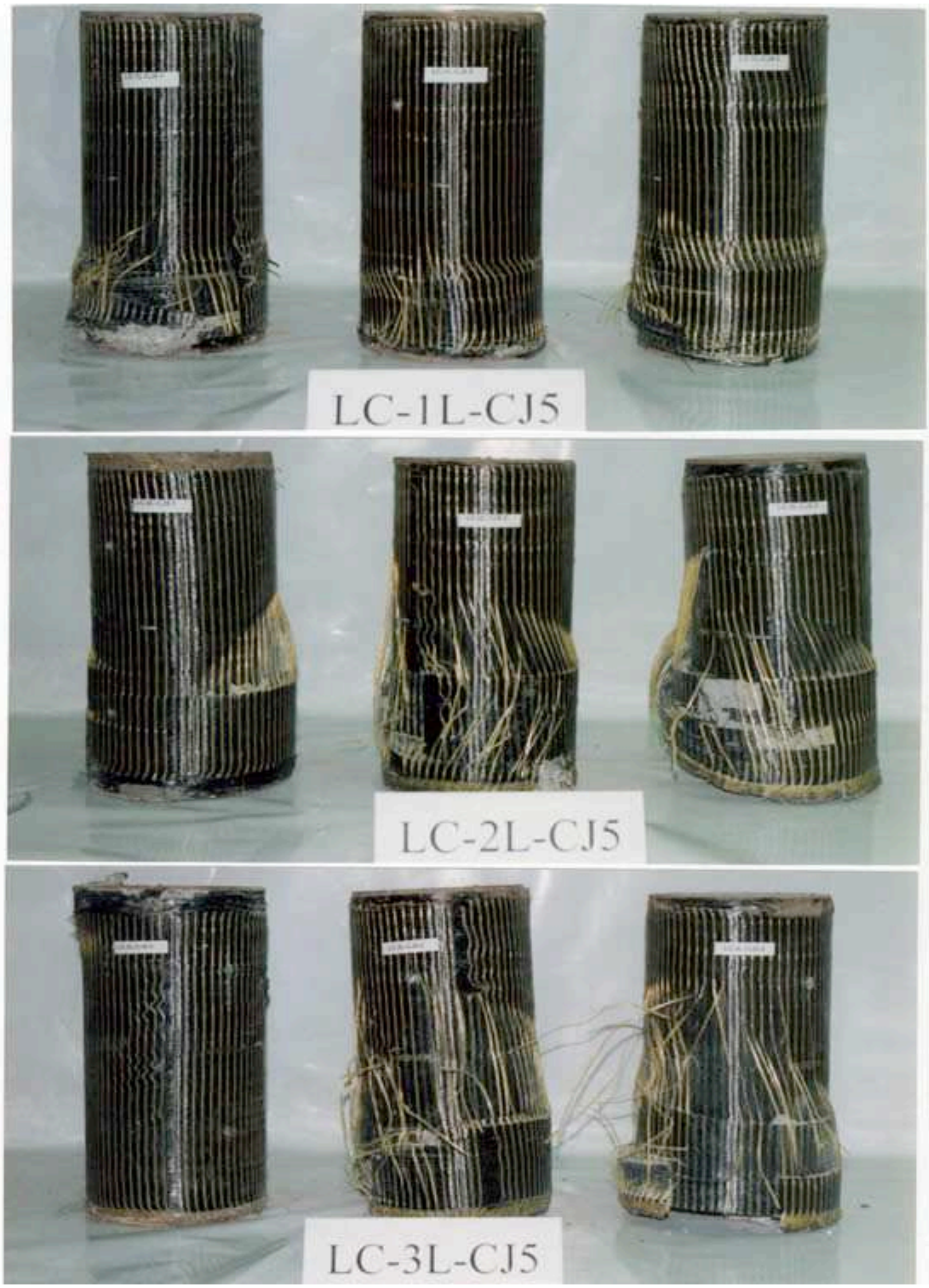

Fig.E-B5. Specimens after Testing

Part E-C Test Results of Medium Strength Concrete Cylinders

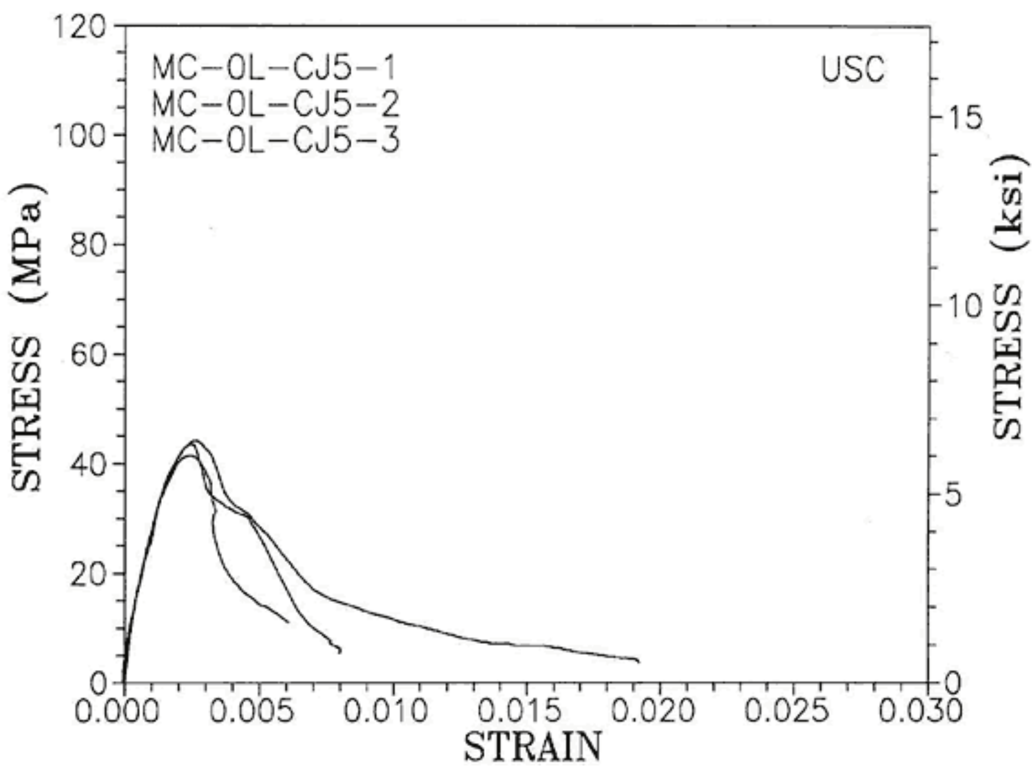

Fig.E-C1. Stress-Strain Relationship for Medium Strength Plain Concrete Cylinders

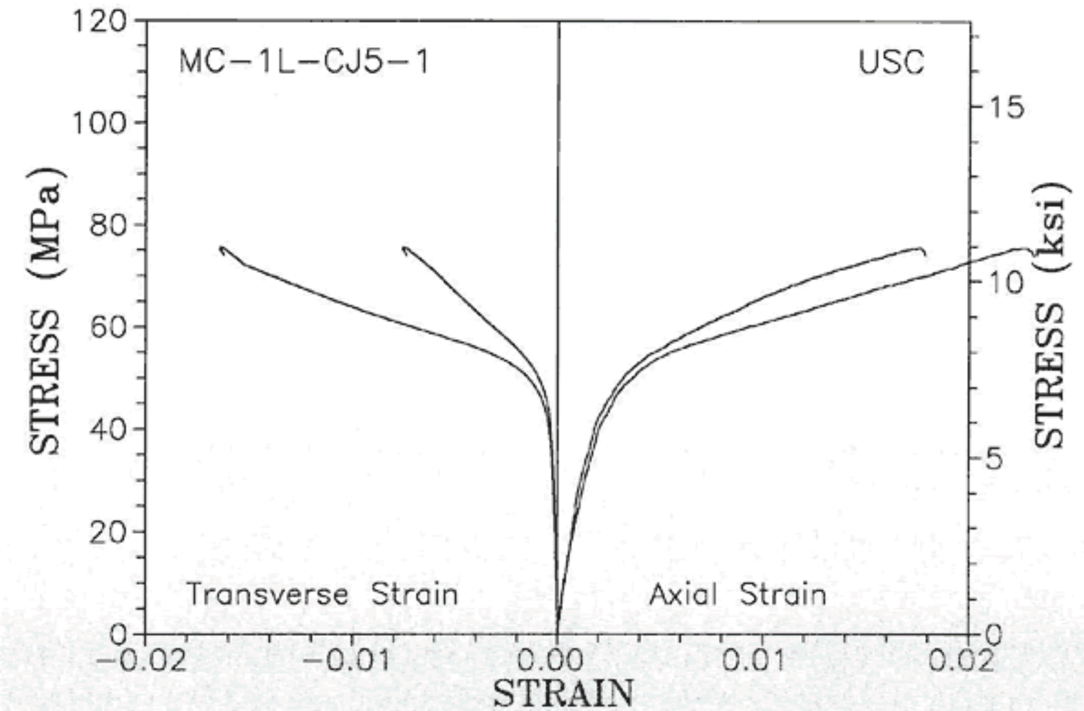

Fig E-C2.Stress-Strain Relationships for Medium Strength Concrete with One-layer Carbon Fiber Composite Jacket (MC-1L-CJ5-1)

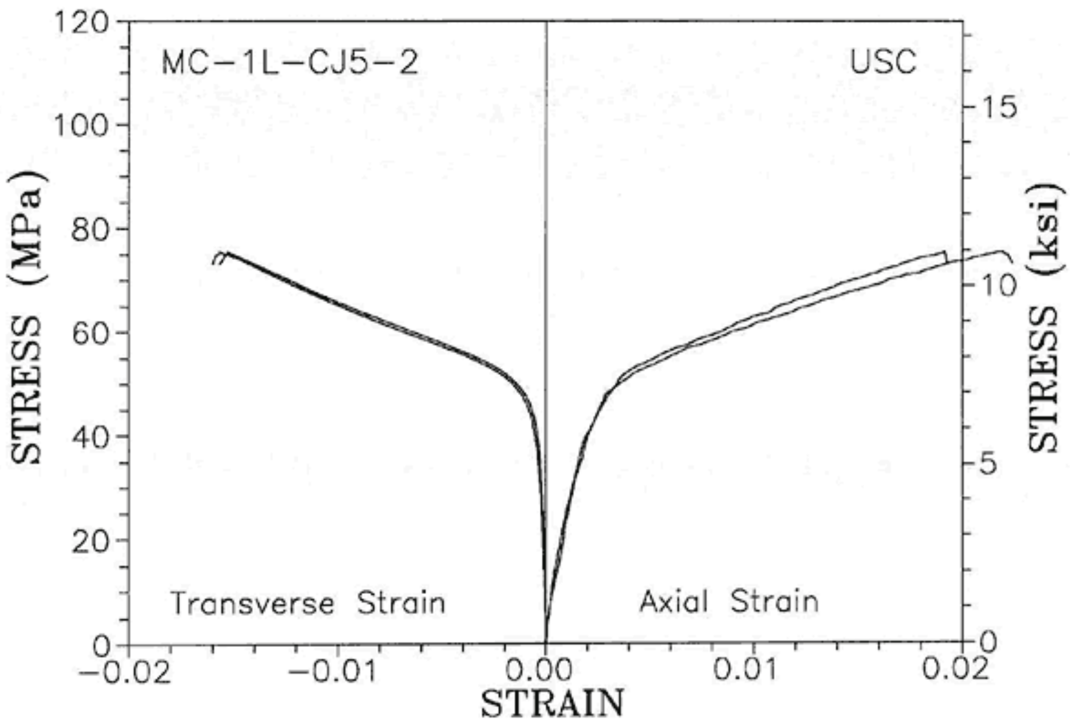

Fig E-C2.Stress-Strain Relationships for Medium Strength Concrete with One-layer Carbon Fiber Composite Jacket (MC-1L-CJ5-2)

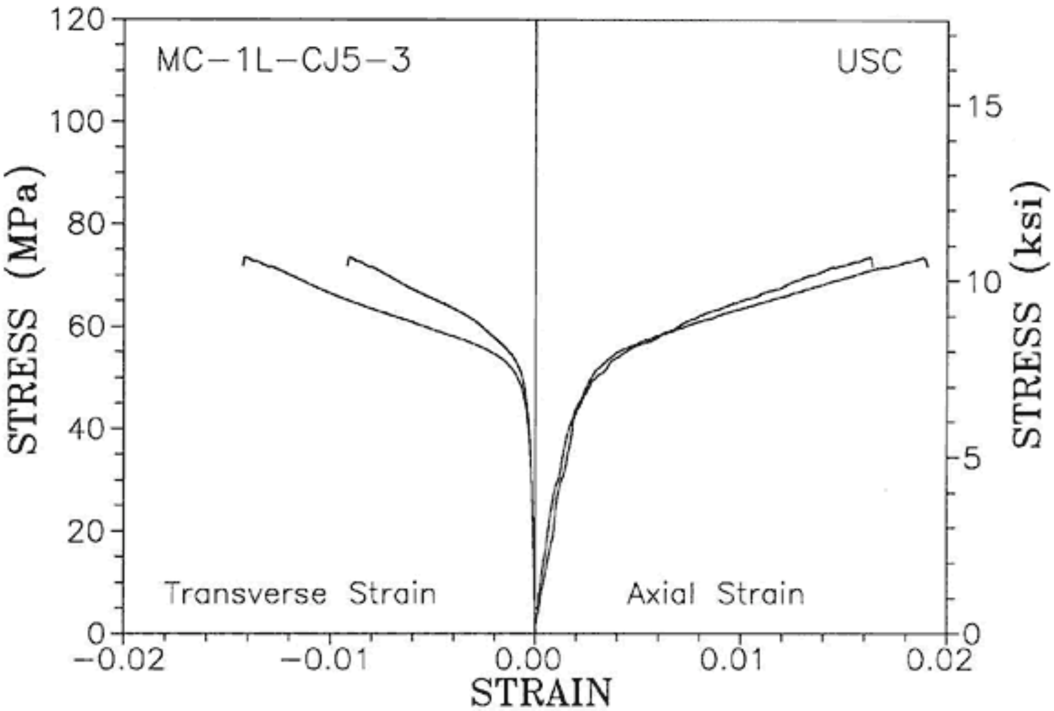

Fig E-C2.Stress-Strain Relationships for Medium Strength Concrete with One-layer Carbon Fiber Composite Jacket (MC-1L-CJ5-3)

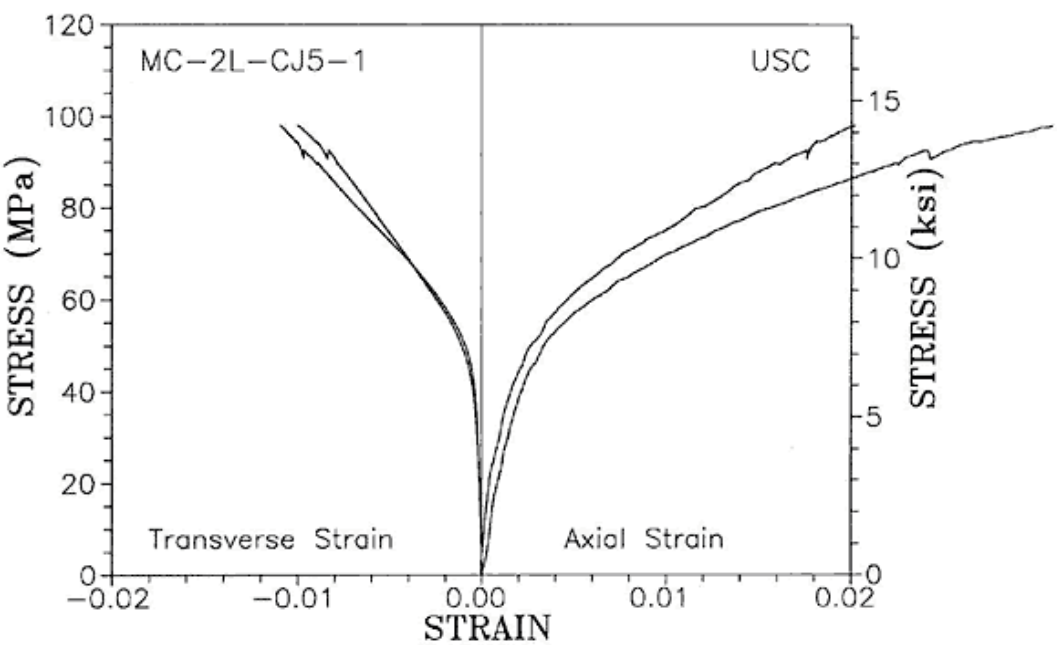

Fig E-C3.Stress-Strain Relationships for Medium Strength Concrete with Two-layer Carbon Fiber Composite Jacket (MC-2L-CJ5-1)

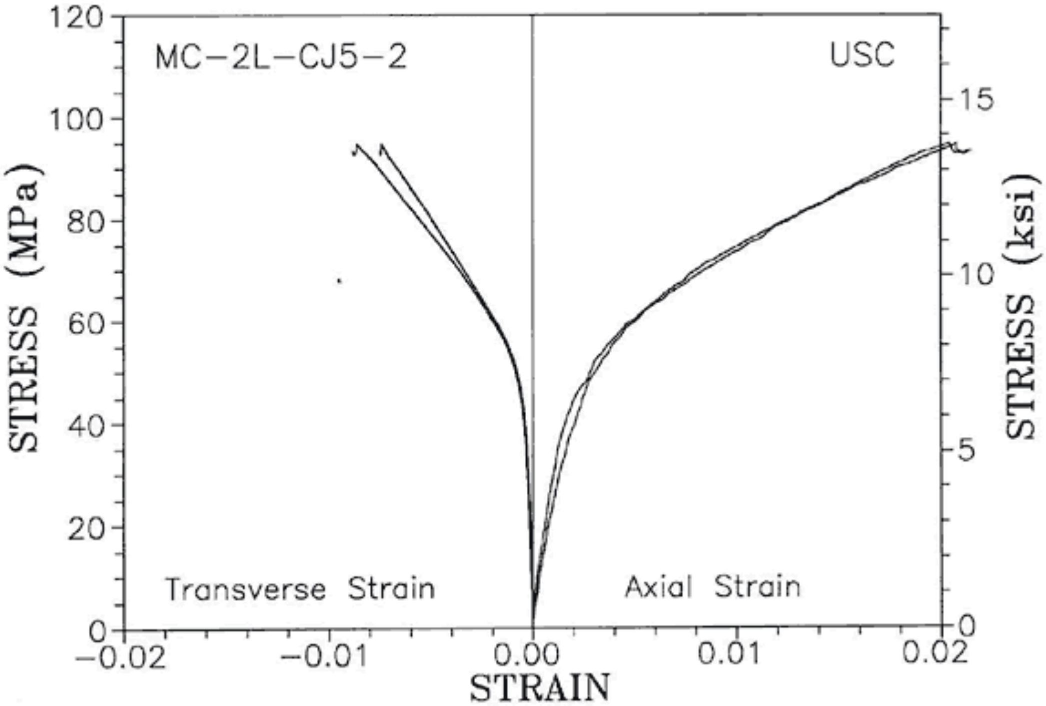

Fig E-C3.Stress-Strain Relationships for Medium Strength Concrete with Two-layer Carbon Fiber Composite Jacket (MC-2L-CJ5-2)

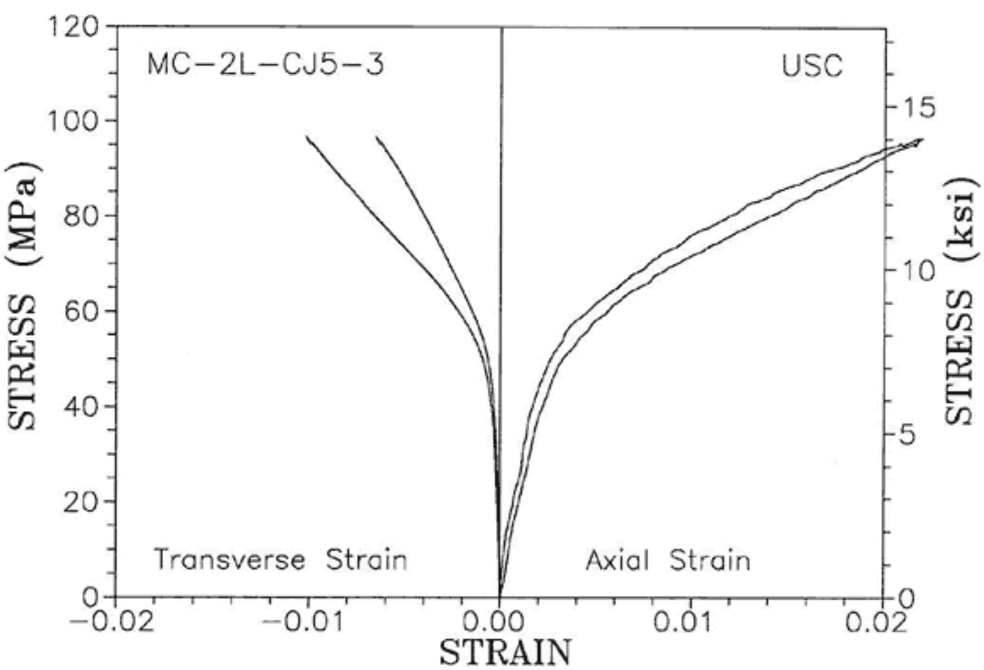

Fig E-C3.Stress-Strain Relationships for Medium Strength Concrete with Two-layer Carbon Fiber Composite Jacket (MC-2L-CJ5-3)

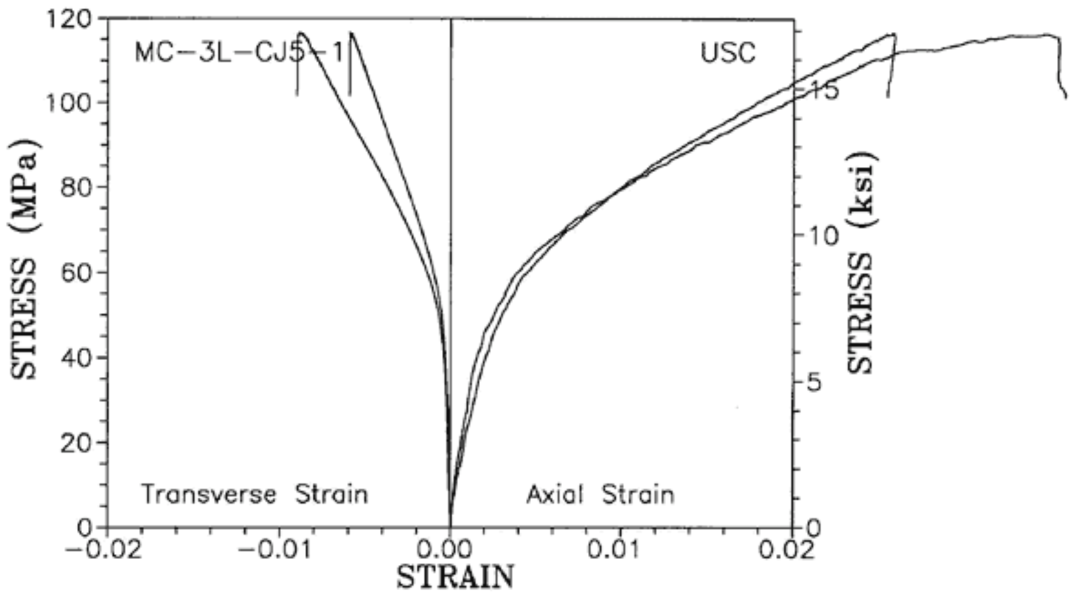

Fig E-C4.Stress-Strain Relationships for Medium Strength Concrete with Three-layer Carbon Fiber Composite Jacket (MC-3L-CJ5-1)

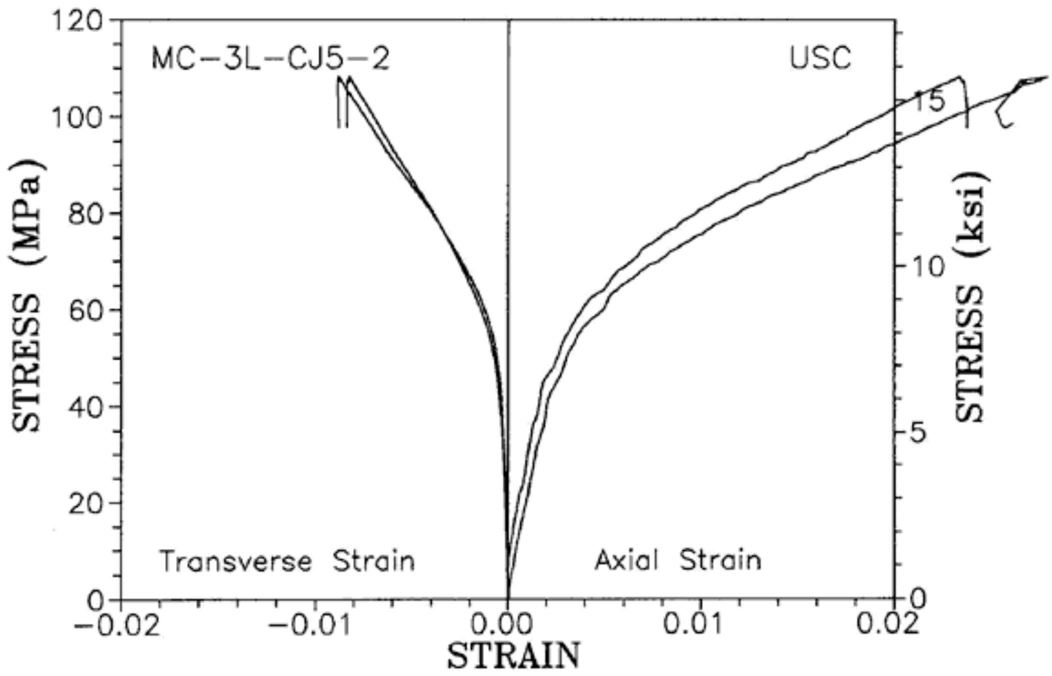

Fig E-C4.Stress-Strain Relationships for Medium Strength Concrete with Three-layer Carbon Fiber Composite Jacket (MC-3L-CJ5-2)

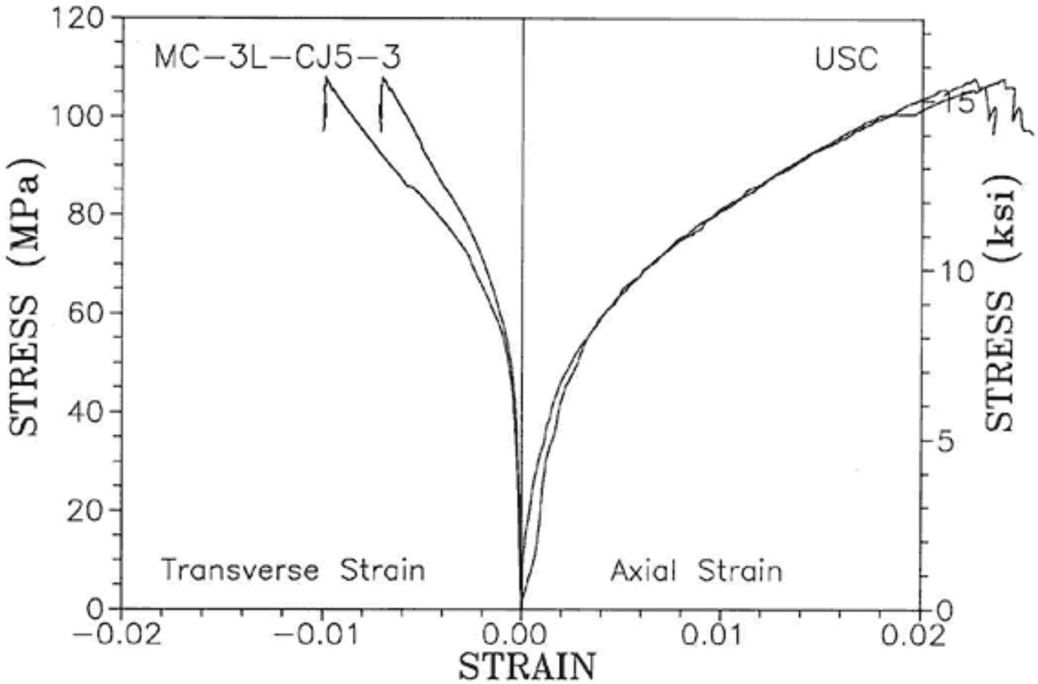

Fig E-C4.Stress-Strain Relationships for Medium Strength Concrete with Three-layer Carbon Fiber Composite Jacket (MC-3L-CJ5-3)

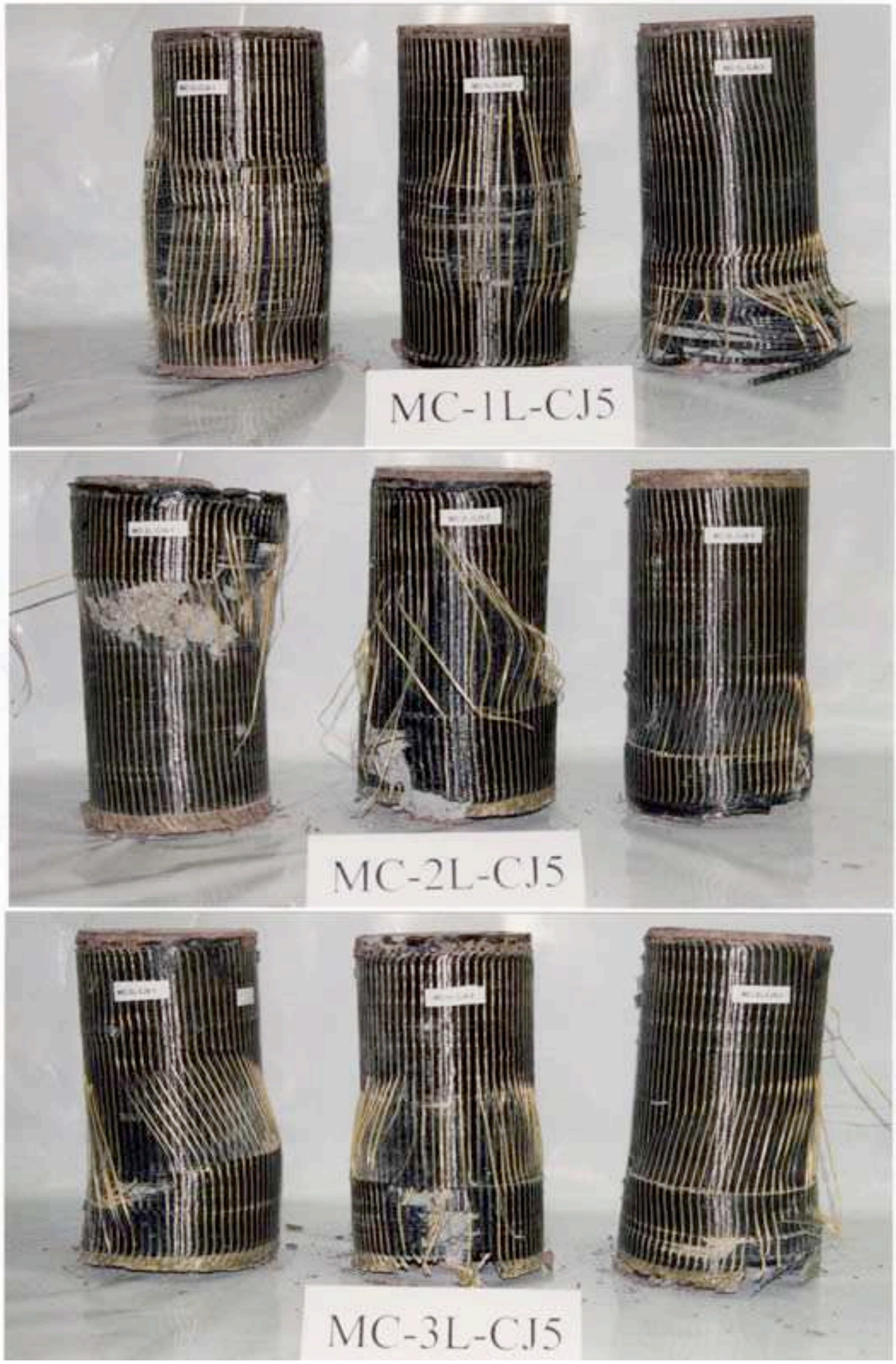

Fig.E-C5. Specimens after Testing

Part E-D Test Results of Higher Strength Concrete Cylinders

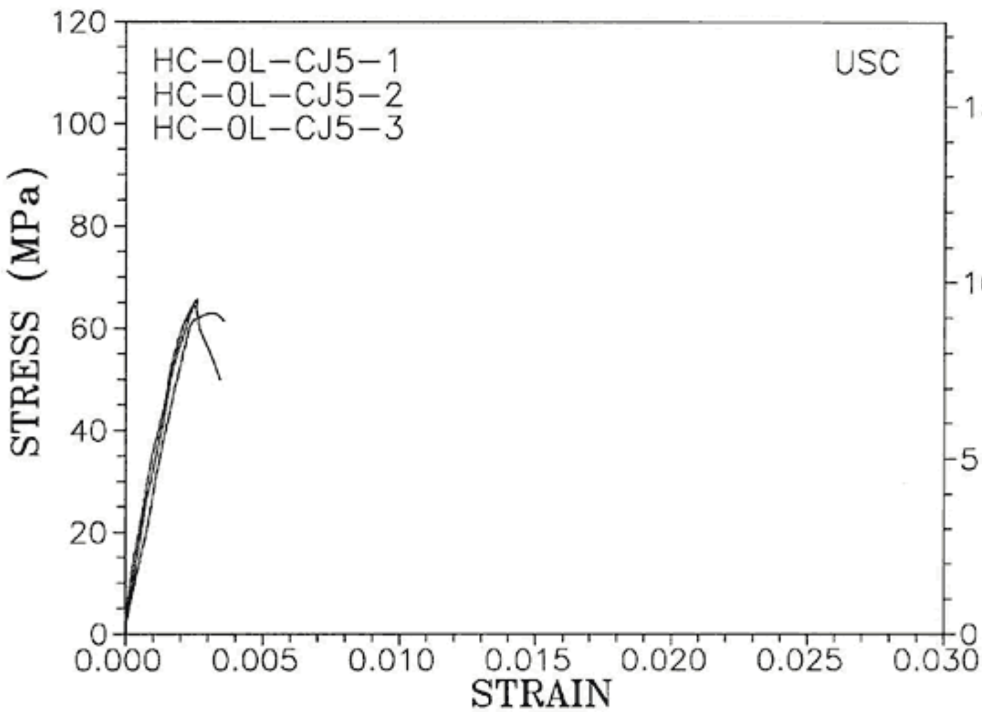

Fig.E-D1. Stress-Strain Relationships for Higher Strength Plain Concrete Cylinders

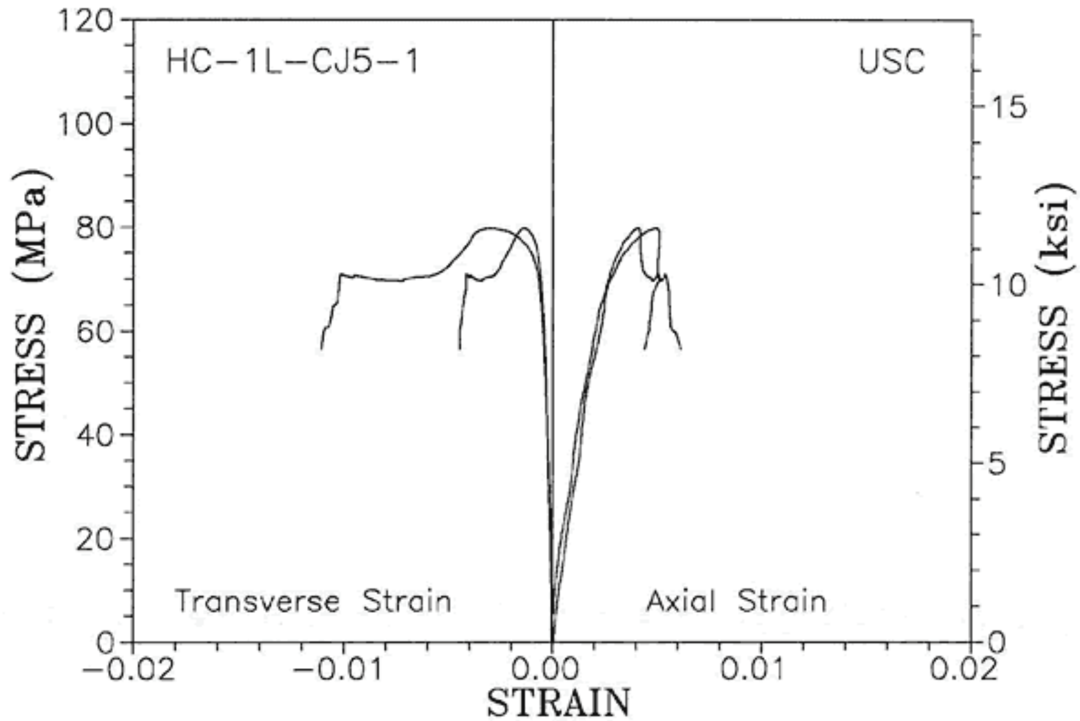

Fig E-D2.Stress-Strain Relationships for Higher Strength Concrete with One-layer Carbon Fiber Composite Jacket (HC-1L-CJ5-1)

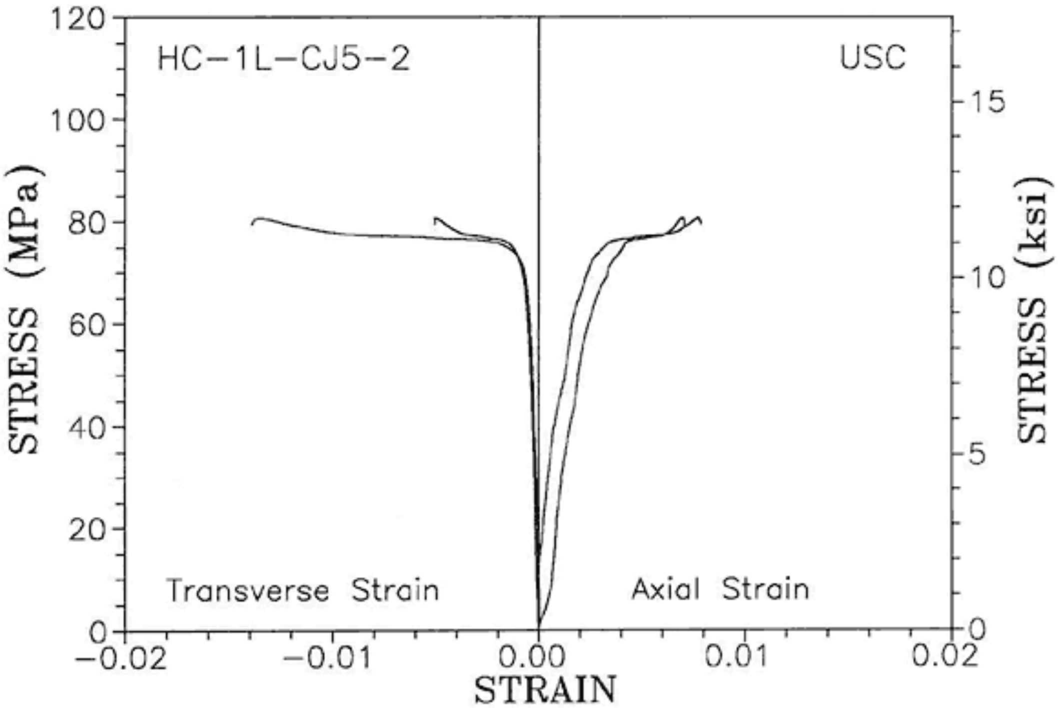

Fig E-D2.Stress-Strain Relationships for Higher Strength Concrete with One-layer Carbon Fiber Composite Jacket (HC-1L-CJ5-2)

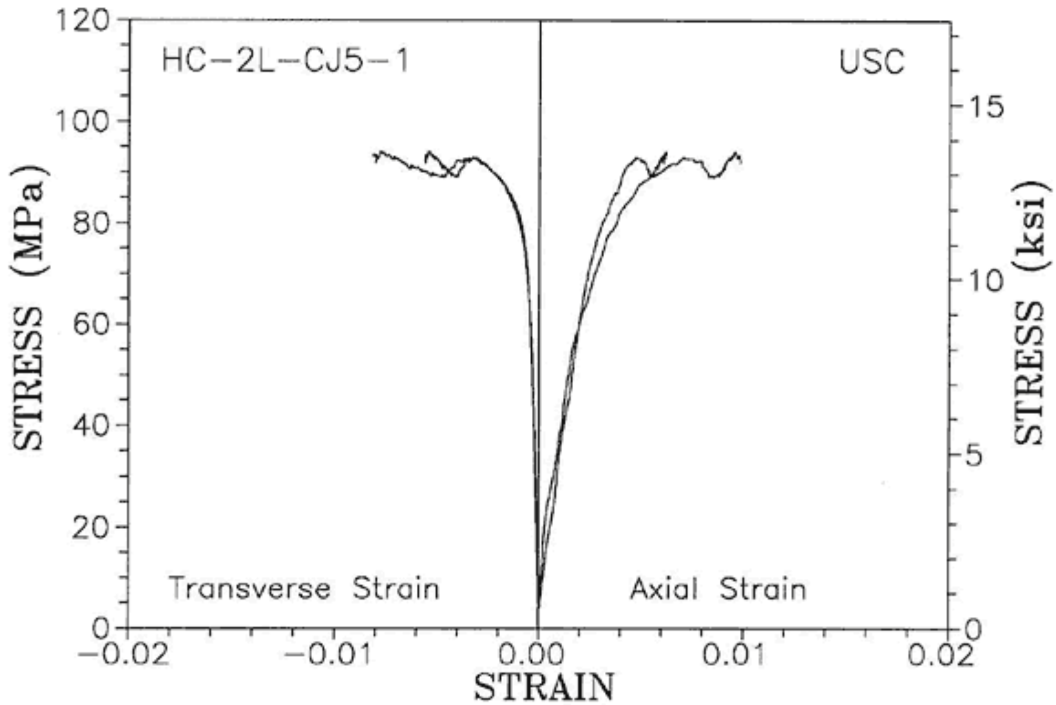

Fig E-D3.Stress-Strain Relationships for Higher Strength Concrete with Two-layer Carbon Fiber Composite Jacket (HC-2L-CJ5-1)

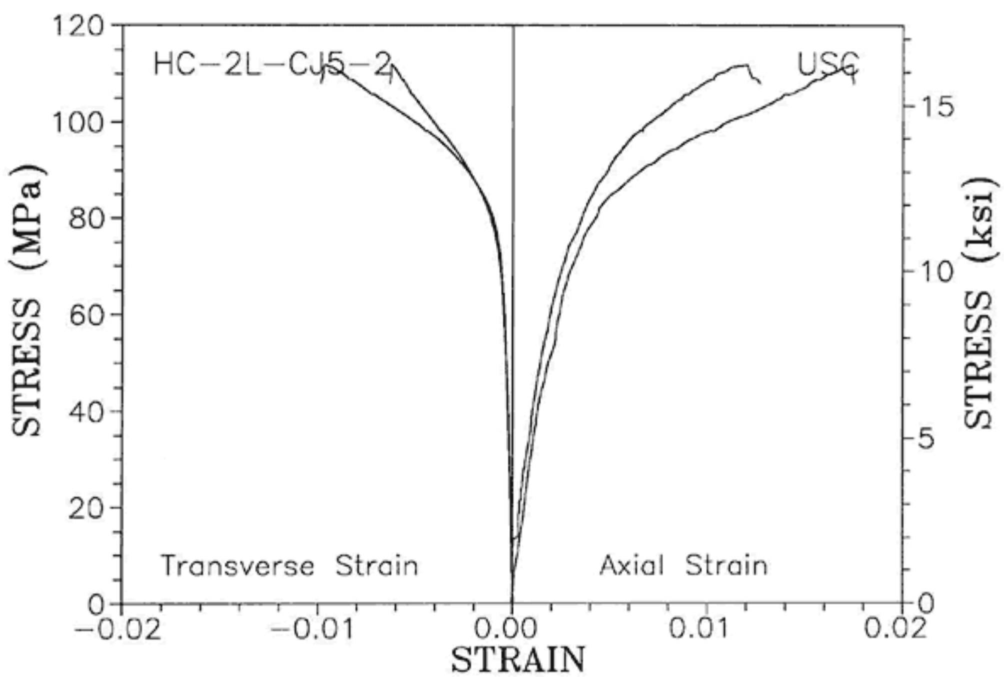

Fig E-D3.Stress-Strain Relationships for Higher Strength Concrete with Two-layer Carbon Fiber Composite Jacket (HC-2L-CJ5-2)

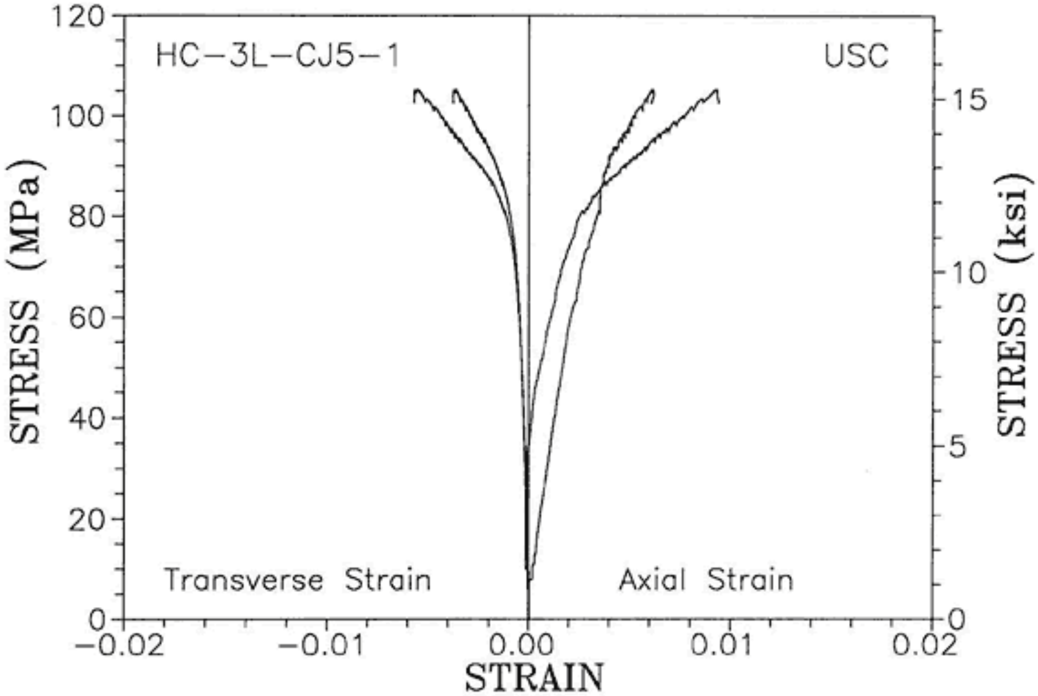

Fig D-D4.Stress-Strain Relationships for Higher Strength Concrete with Three-layer Carbon Fiber Composite Jacket (HC-3L-CJ5-1)

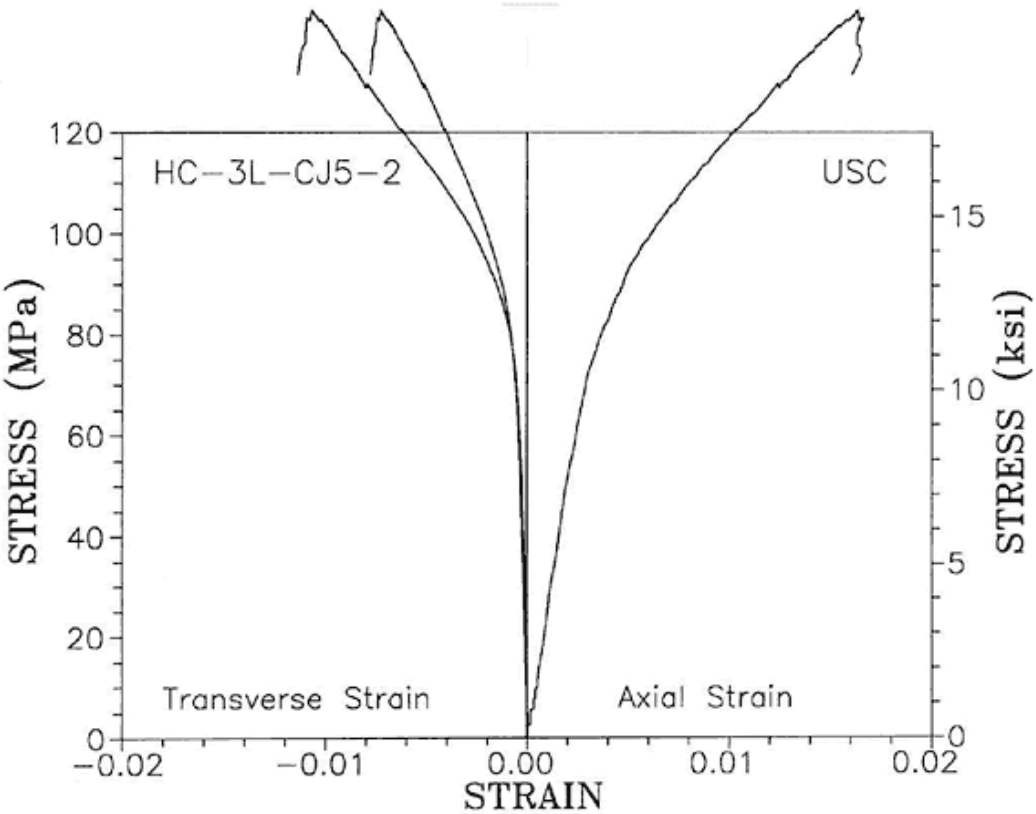

Fig E-D4.Stress-Strain Relationships for Higher Strength Concrete with Three-layer Carbon Fiber Composite Jacket (HC-3L-CJ5-2)

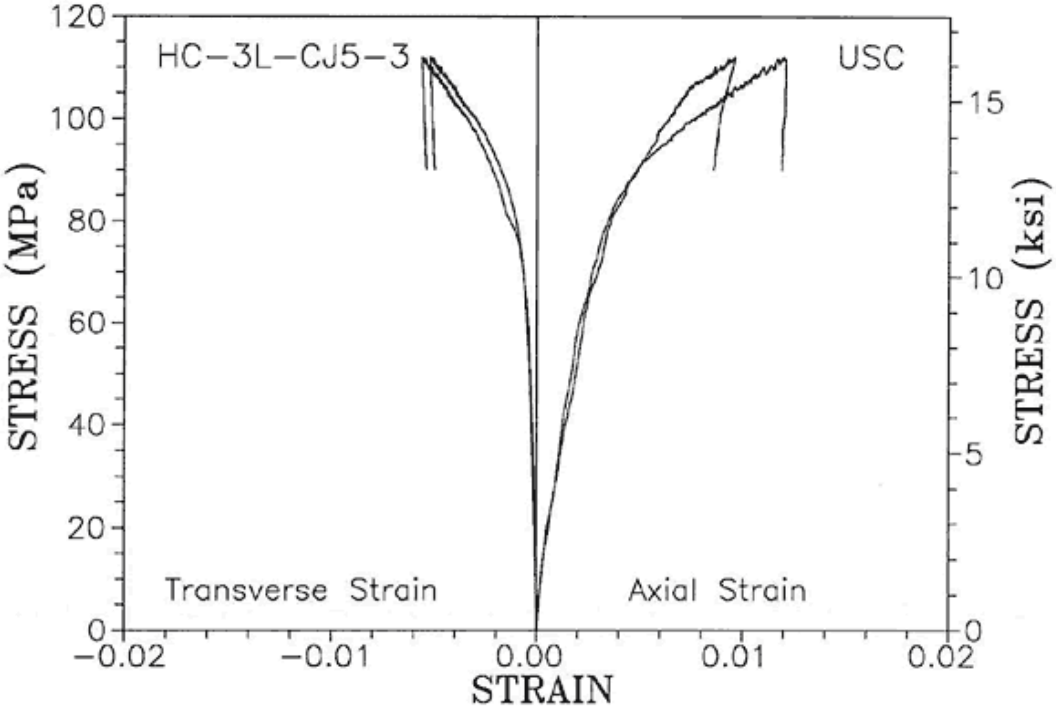

Fig E-D4.Stress-Strain Relationships for Higher Strength Concrete with Three-layer Carbon Fiber Composite Jacket (HC-3L-CJ5-3)

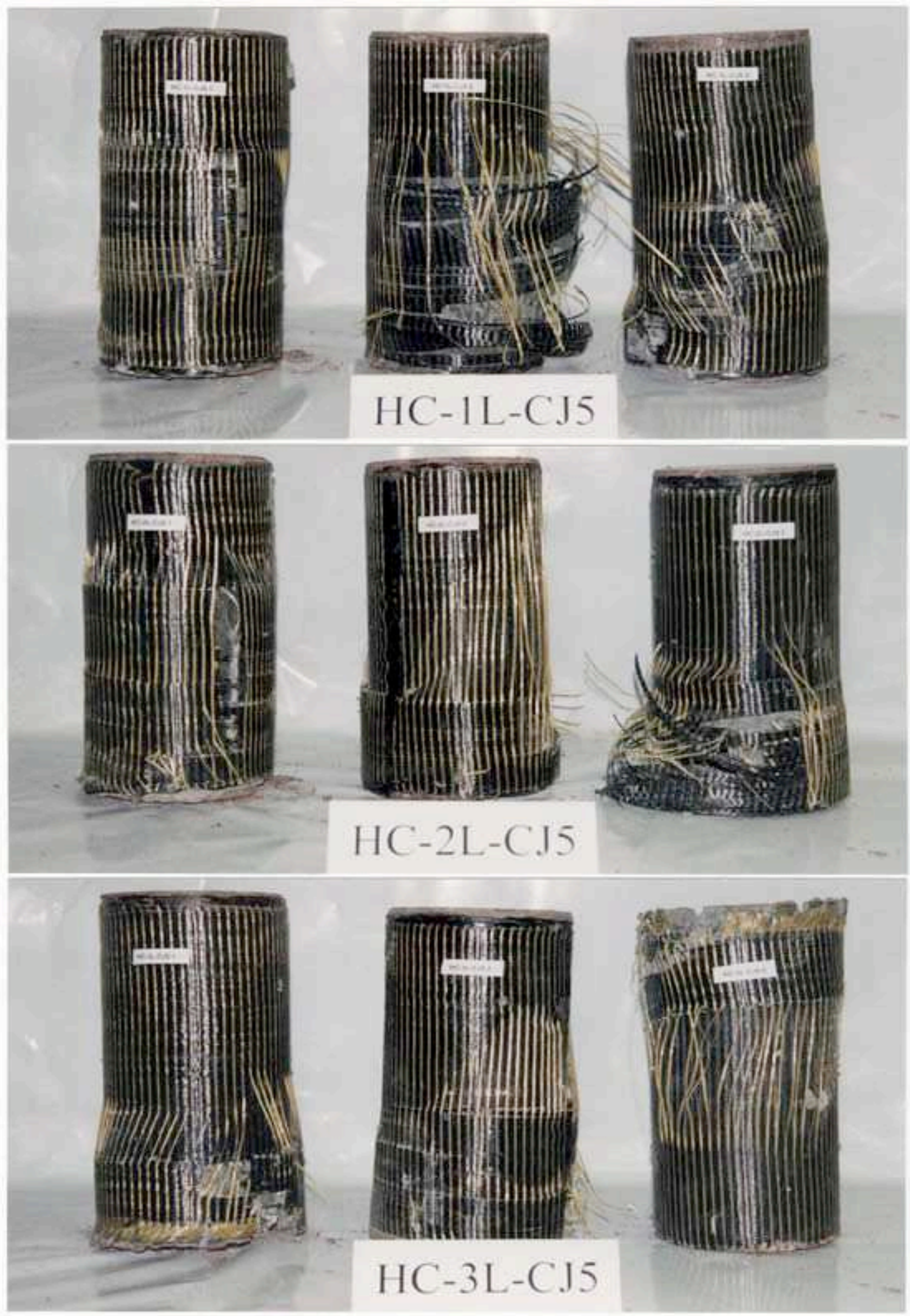

Fig.E-D5. Specimens after Testing

APPENDIX F: TEST RESULTS OF SYSTEM SIX

Part F-A General Information

Table F-A1 Test Matrix

Type of Jacket	Concrete Strength	Jacket Layers	Specimen Numbers
Glass fiber Reinforced composite	Lower	Plain concrete	3
		1-layer	5
		2-layer	4
	Medium	Plain concrete	3
		1-layer	5
		2-layer	4
	Higher	Plain concrete	3
		1-layer	5
		2-layer	4

Table F-A2 Mix Proportion of Concrete

Series	Target f'_{co} (MPa)	W/C	Water (kg/m^3)	Cement (kg/m^3)	Fine Aggregates (kg/m^3)	Coarse Aggregates (kg/m^3)
L	27.6	0.68	196	288	1087	853
M	37.9	0.48	196	408	986	853
H	48.2	0.38	197	515	857	853

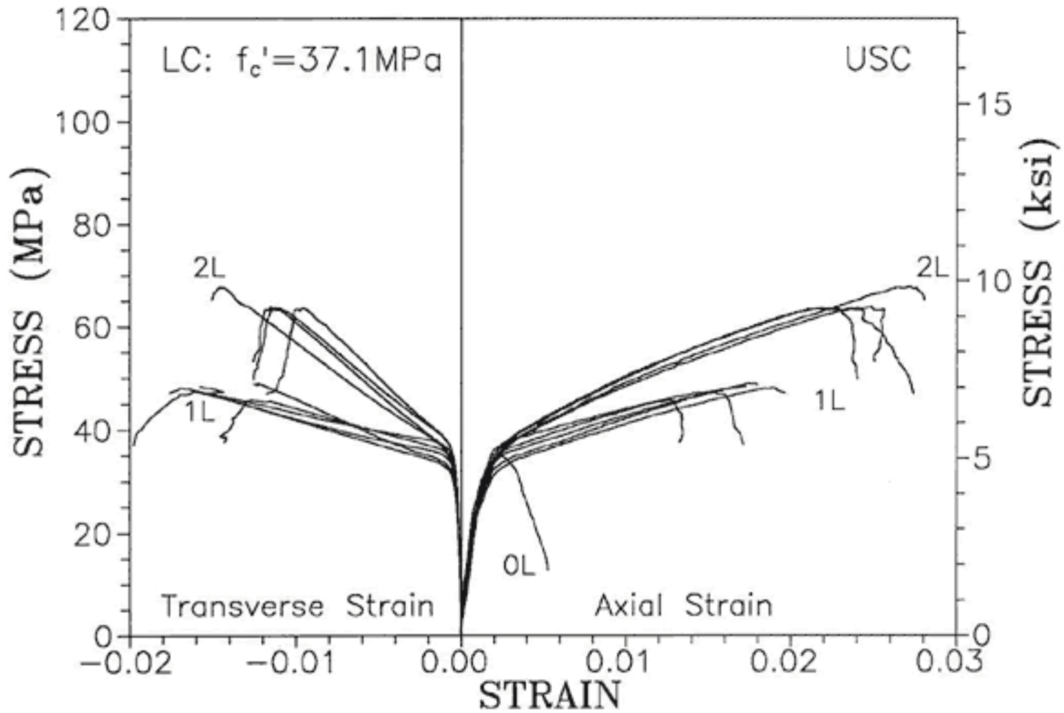

Fig.F-A1. Test Results of Lower-Strength Specimens

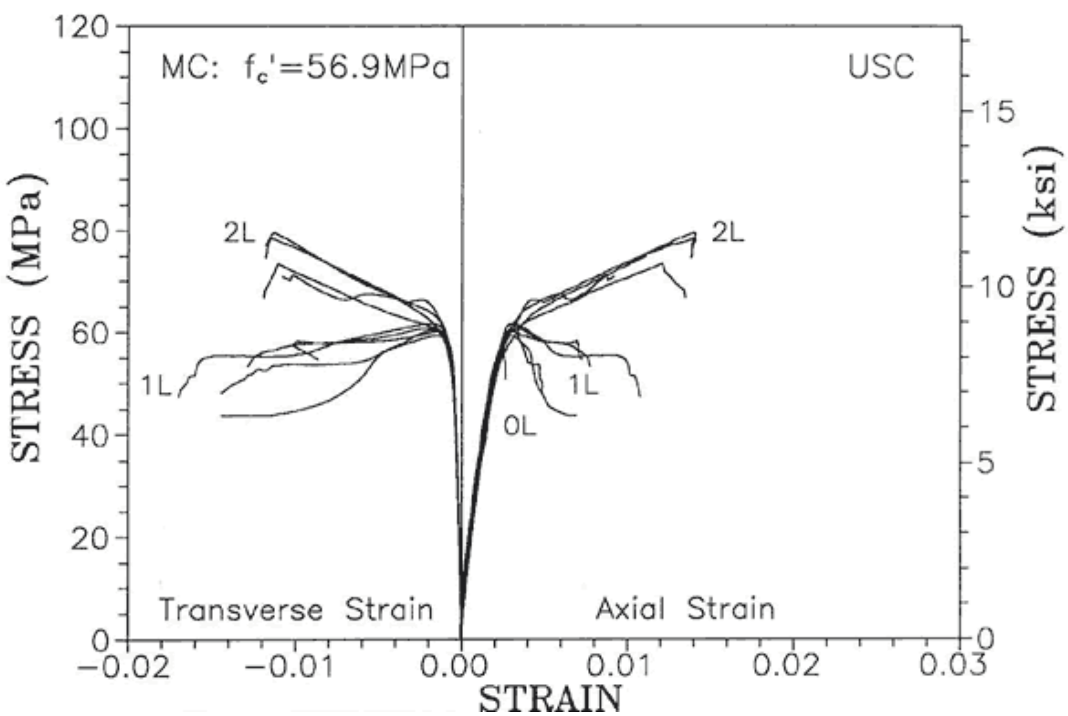

Fig.F-A2. Test Results of Medium-Strength Specimens

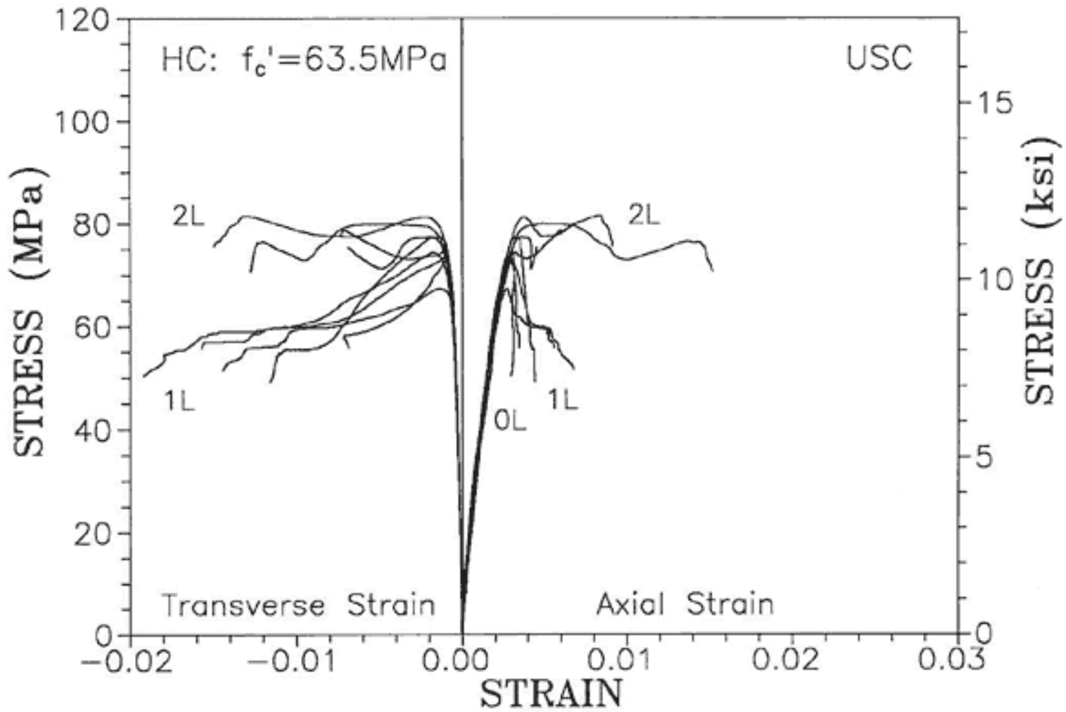

Fig.F-A3. Test Results of Higher-Strength Specimens

Table F-A4 Test Results

Series	Specimen	f_c' (MPa)	Jacket Layers	f_{cc}' (MPa)	ε_{cu}
L	LC-0L-GJ6-1	37.1	0	38.22	0.002609
	LC-0L-GJ6-2			34.87	0.002367
	LC-0L-GJ6-3			38.16	0.002228
	LC-1L-GJ6-1		1	48.81	0.012715
	LC-1L-GJ6-2			48.97	0.017447
	LC-1L-GJ6-3			48.40	0.017224
	LC-1L-GJ6-4			48.10	0.019018
	LC-1L-GJ6-5			47.42	0.015266
	LC-2L-GJ6-1		2	63.72	0.021822
	LC-2L-GJ6-2			63.56	0.021680
	LC-2L-GJ6-3			63.92	0.024826
	LC-2L-GJ6-4			63.73	0.026472
M	MC-0L-GJ6-1	56.9	0	60.07	0.002605
	MC-0L-GJ6-2			55.12	0.002072
	MC-0L-GJ6-3			55.62	0.002463
	MC-1L-GJ6-1		1	60.52	0.003005
	MC-1L-GJ6-2			60.18	0.003146
	MC-1L-GJ6-3			60.74	0.003496
	MC-1L-GJ6-4			59.33	0.002973
	MC-1L-GJ6-5			61.68	0.002980
	MC-2L-GJ6-1		2	79.59	0.013982
	MC-2L-GJ6-2			71.20	0.008680
	MC-2L-GJ6-3			78.52	0.013995
	MC-2L-GJ6-4			73.46	0.012079
H	HC-0L-GJ6-1	63.5	0	6515	0.002469
	HC-0L-GJ6-2			58.26	0.002105
	HC-0L-GJ6-3			67.19	0.002268
	HC-1L-GJ6-1		1	73.59	0.002907
	HC-1L-GJ6-2			77.22	0.003435
	HC-1L-GJ6-3			72.61	0.003064
	HC-1L-GJ6-4			67.24	0.002744
	HC-1L-GJ6-5			74.33	0.003088
	HC-2L-GJ6-1		2	77.40	0.003620
	HC-2L-GJ6-2			79.91	0.004984
	HC-2L-GJ6-3			81.47	0.008276
	HC-2L-GJ6-4			78.61	0.006011

ote: (i) Example for specimen name designation:
LC-2L-GJ6-1: LC designates Lower strength Concrete; 2L designates 2 Layers; GJ6 designates Glass fiber Jacket System 6; and the last number represents specimen number in same series.
(ii) f_c': Average plain concrete cylinder strength;
(iii) f_{cc}': Ultimate strength of confined concrete;
(iv) ε_{cu}: Ultimate strain

Part F-B Test Results of Lower Strength Concrete Cylinders

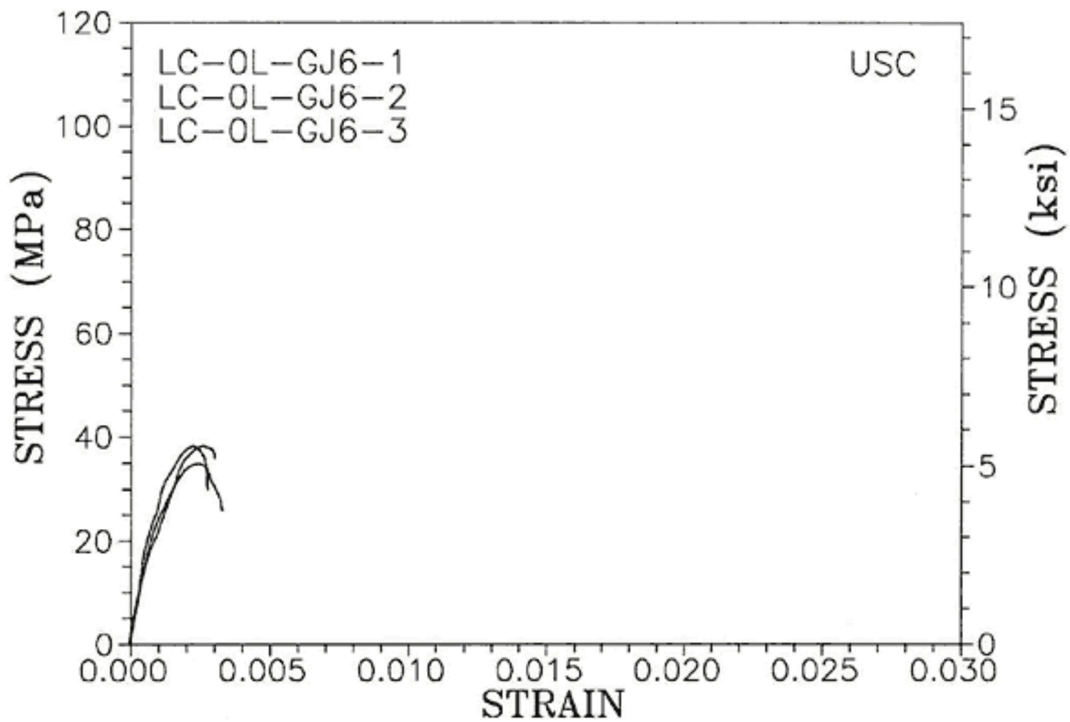

Fig.F-B1. Stress-Strain Relationship for Lower Strength Plain Concrete Cylinders

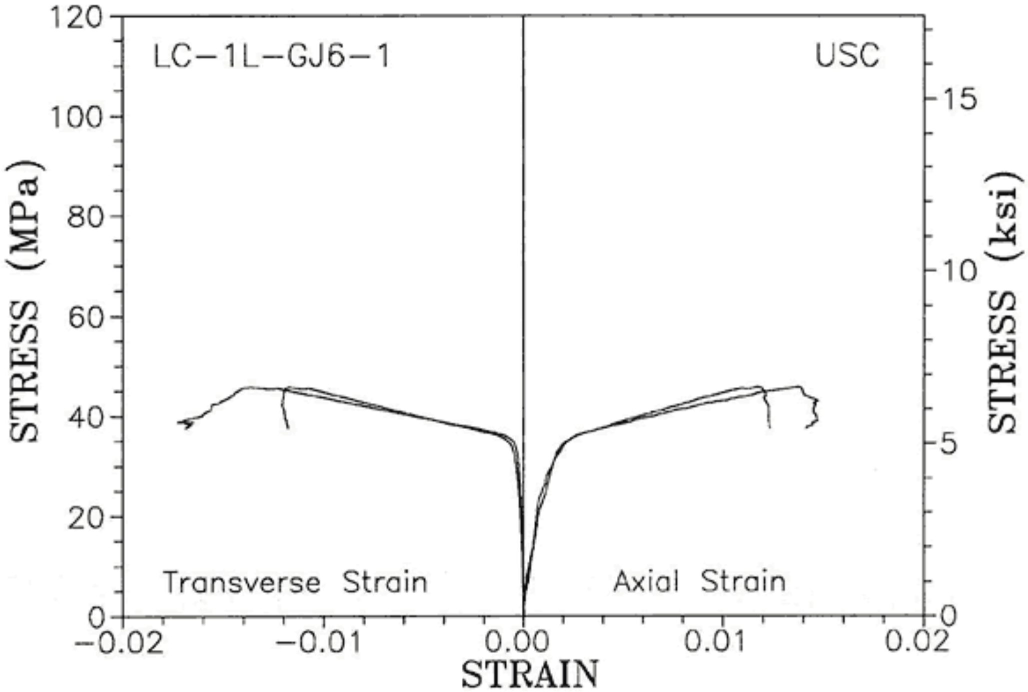

Fig F-B2.Stress-Strain Relationships for Lower Strength Concrete with One-layer Glass Fiber Composite Jacket (LC-1L-GJ6-1)

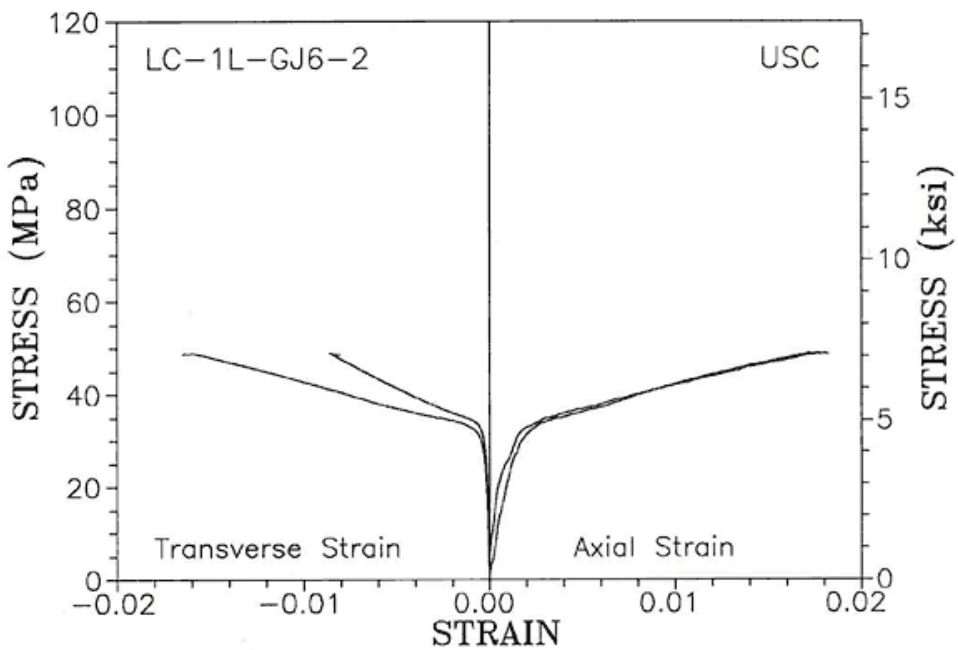

Fig F-B2.Stress-Strain Relationships for Lower Strength Concrete with One-layer Glass Fiber Composite Jacket (LC-1L-GJ6-2)

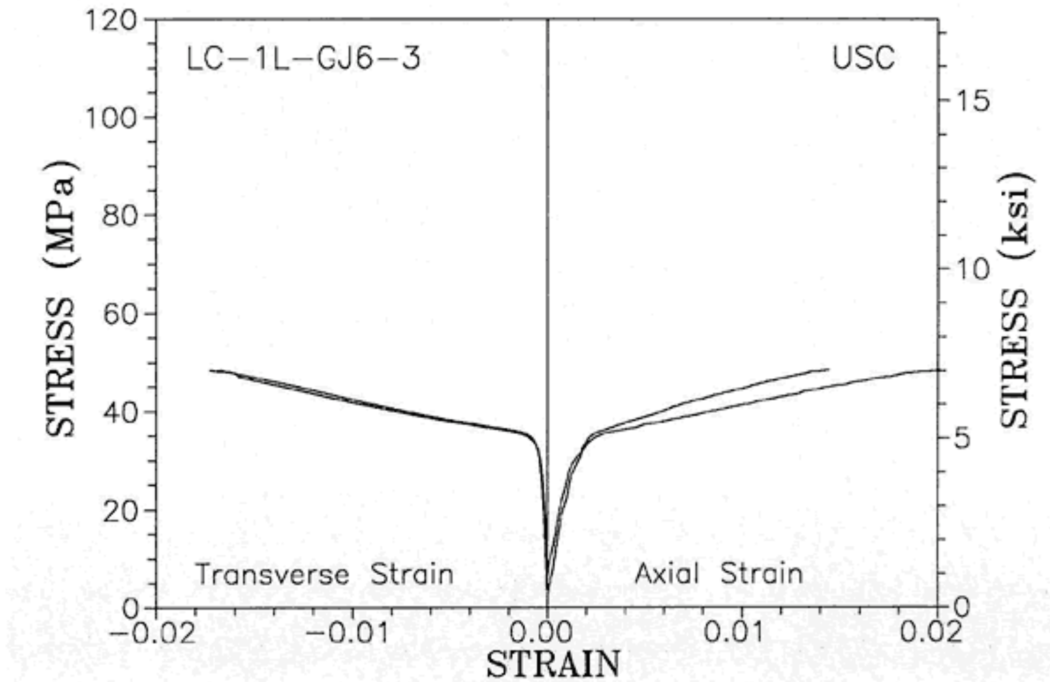

Fig F-B2.Stress-Strain Relationships for Lower Strength Concrete with One-layer Glass Fiber Composite Jacket (LC-1L-GJ6-3)

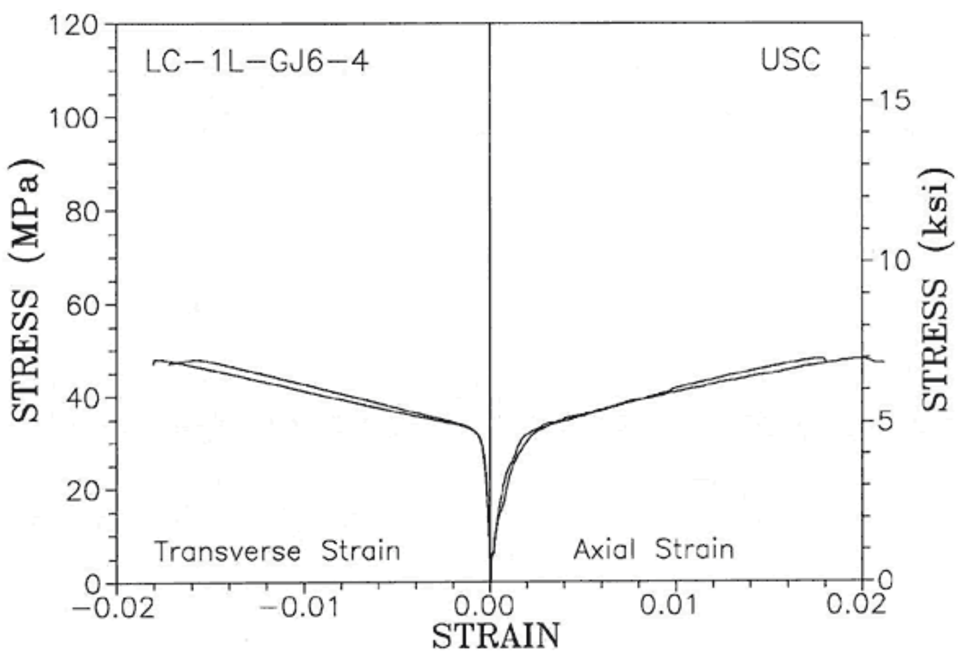

Fig F-B2.Stress-Strain Relationships for Lower Strength Concrete with One-layer Glass Fiber Composite Jacket (LC-1L-GJ6-4)

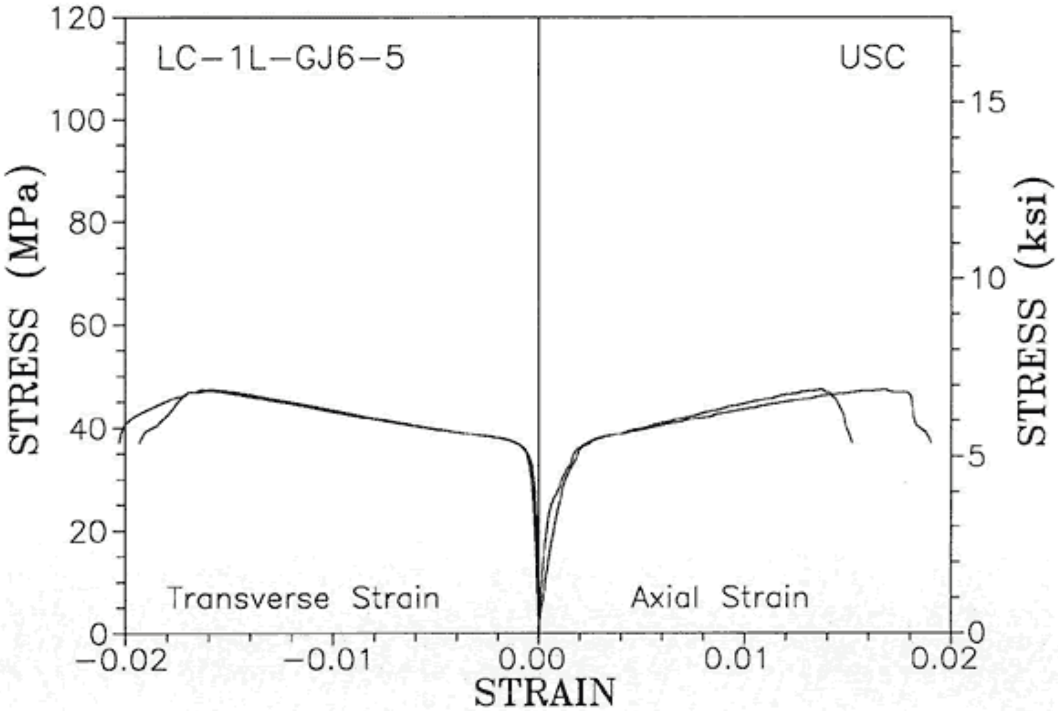

Fig F-B2.Stress-Strain Relationships for Lower Strength Concrete with One-layer Glass Fiber Composite Jacket (LC-1L-GJ6-5)

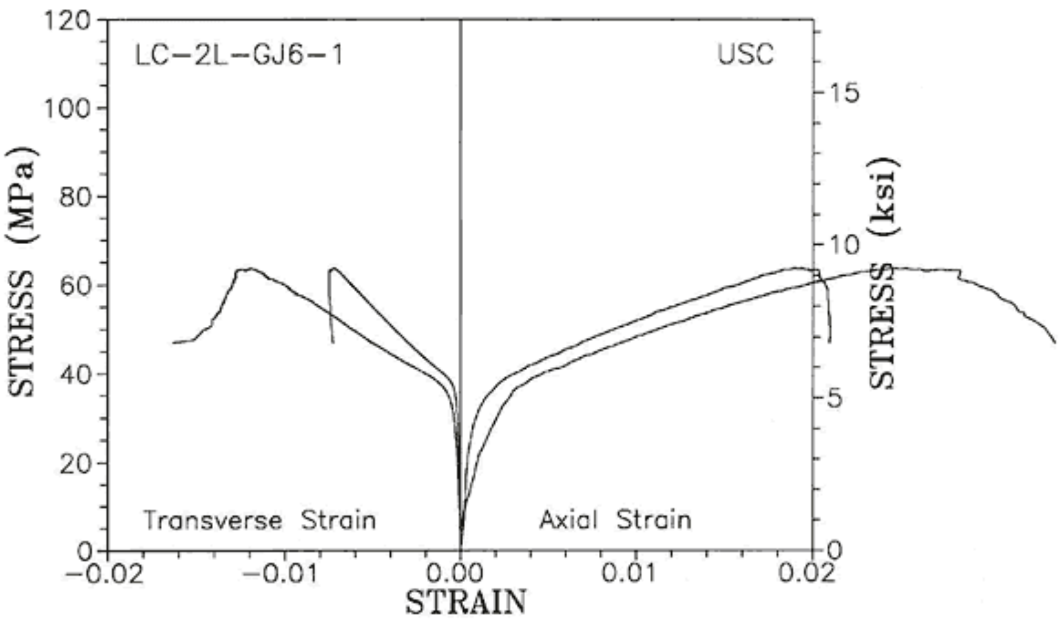

Fig F-B3.Stress-Strain Relationships for Lower Strength Concrete with Two-layer Glass Fiber Composite Jacket (LC-2L-GJ6-1)

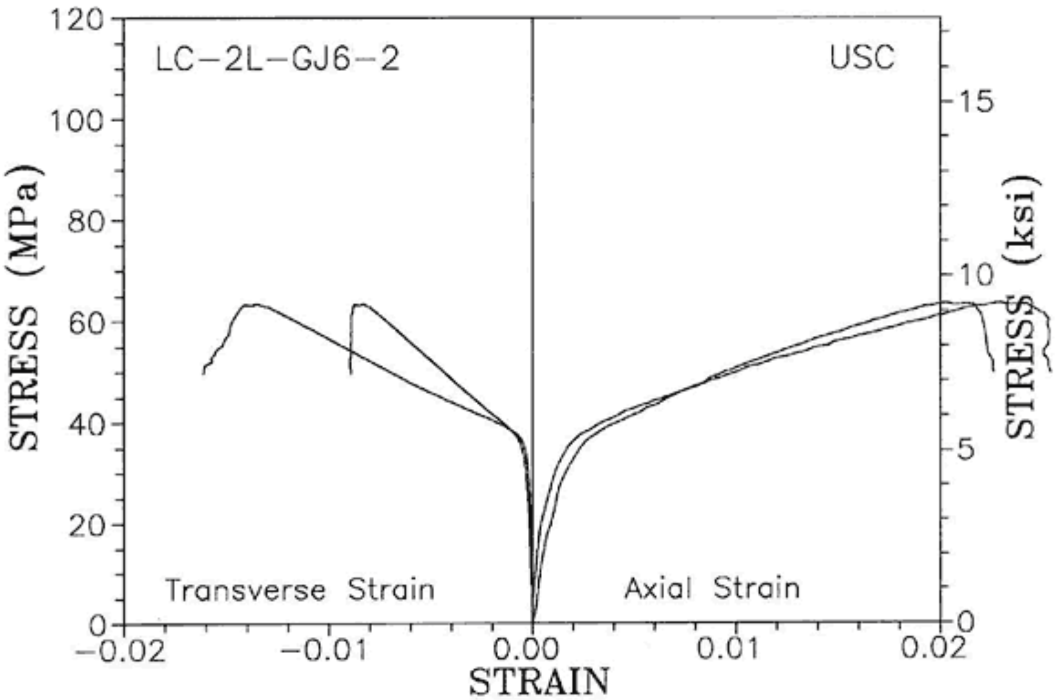

Fig F-B3.Stress-Strain Relationships for Lower Strength Concrete with Two-layer Glass Fiber Composite Jacket (LC-2L-GJ6-2)

Fig.F-B5. Specimens after Testing

Part F-C Test Results of Medium Strength Concrete Cylinders

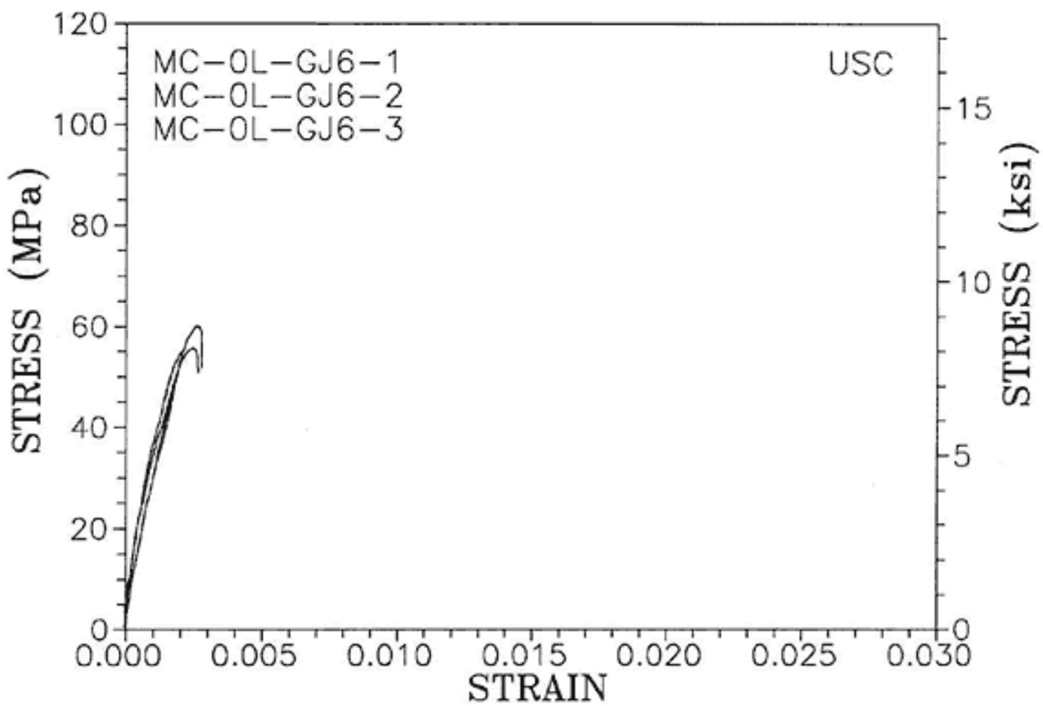

Fig.F-C1. Stress-Strain Relationship for Medium Strength Plain Concrete Cylinders

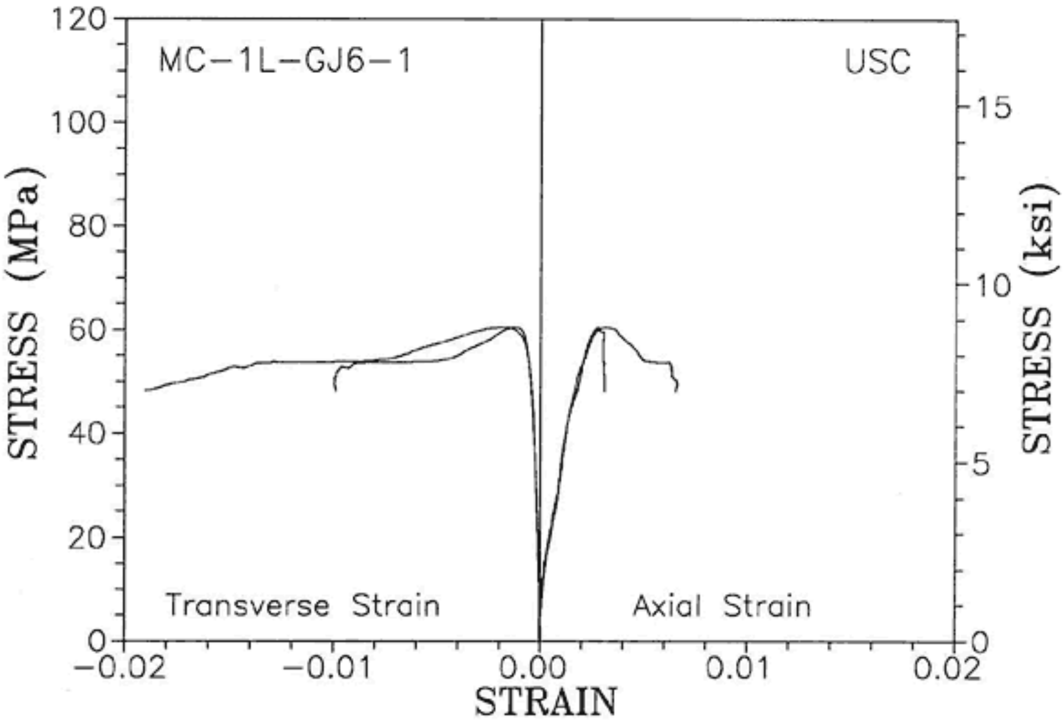

Fig F-C2.Stress-Strain Relationships for Medium Strength Concrete with One-layer Glass Fiber Composite Jacket (MC-1L-GJ6-1)

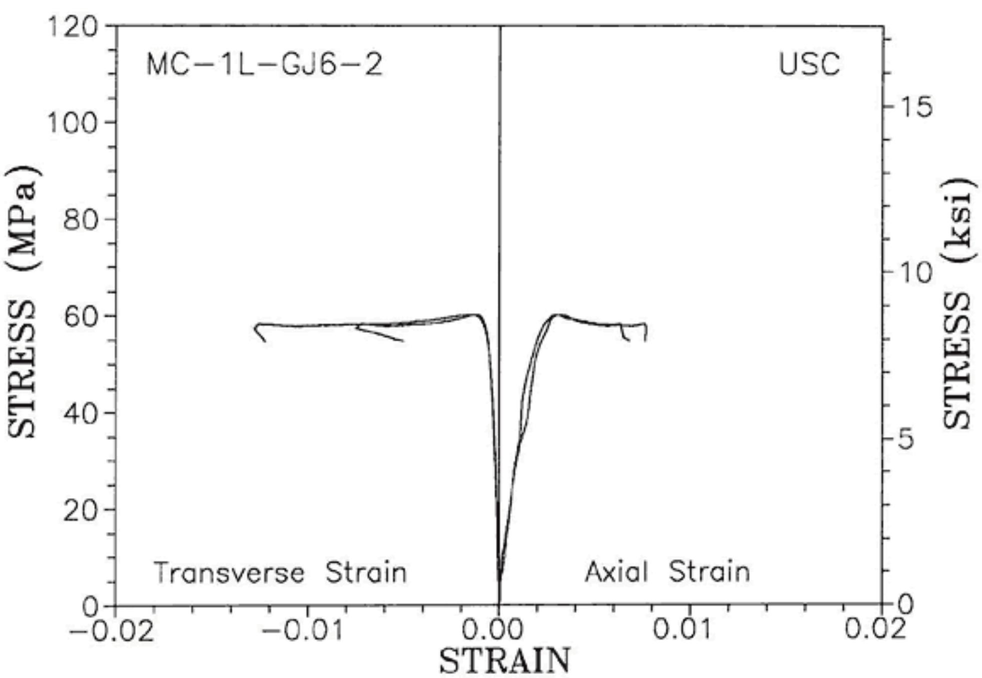

Fig F-C2.Stress-Strain Relationships for Medium Strength Concrete with One-layer Glass Fiber Composite Jacket (MC-1L-GJ6-2)

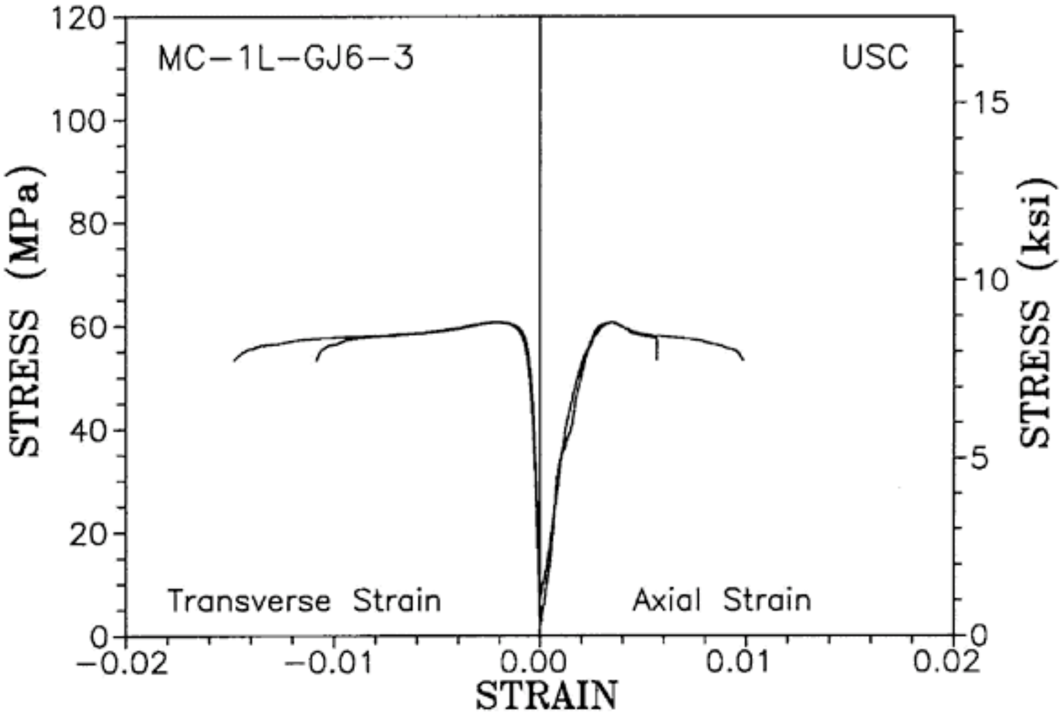

Fig F-C2.Stress-Strain Relationships for Medium Strength Concrete with One-layer Glass Fiber Composite Jacket (MC-1L-GJ6-3)

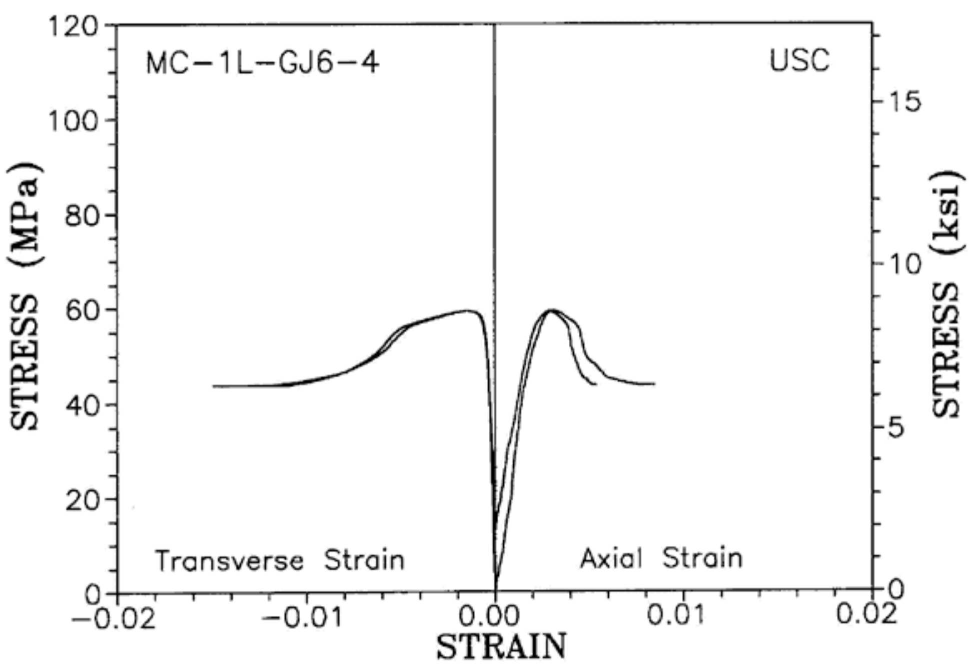

Fig F-C2.Stress-Strain Relationships for Medium Strength Concrete with One-layer Glass Fiber Composite Jacket (MC-1L-GJ6-4)

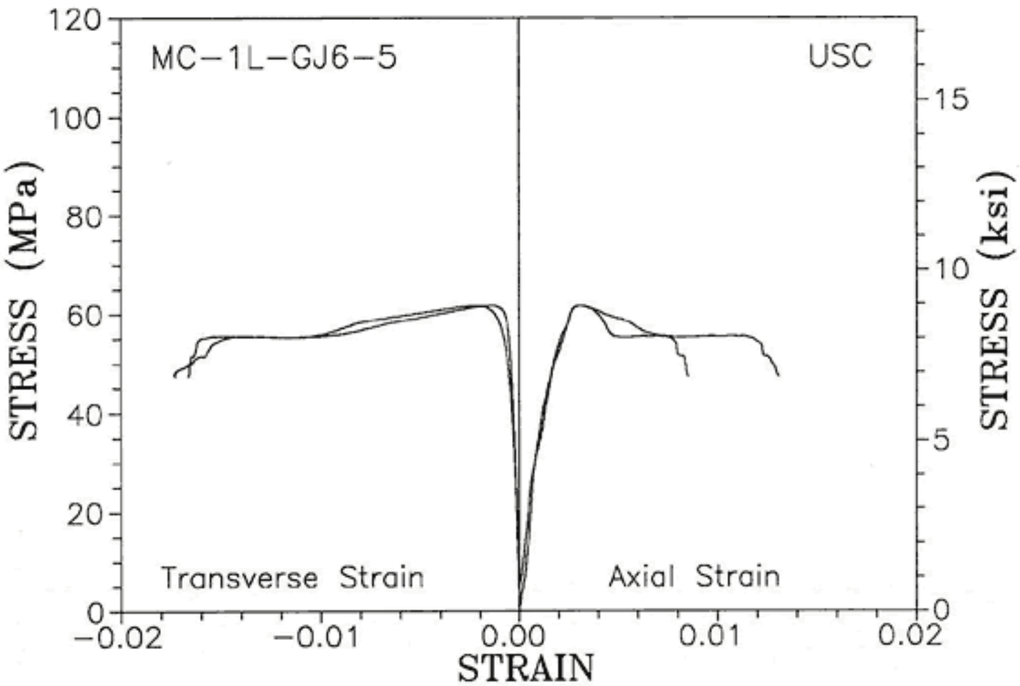

Fig F-C2.Stress-Strain Relationships for Medium Strength Concrete with One-layer Glass Fiber Composite Jacket (MC-1L-GJ6-5)

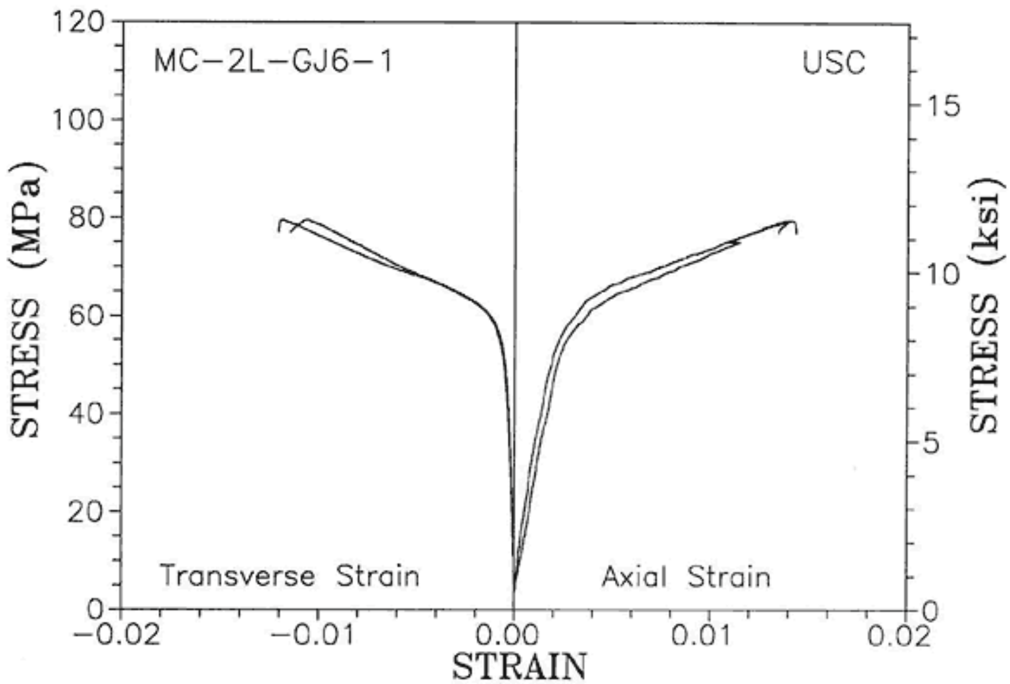

Fig F-C3.Stress-Strain Relationships for Medium Strength Concrete with Two-layer Glass Fiber Composite Jacket (MC-2L-GJ6-1)

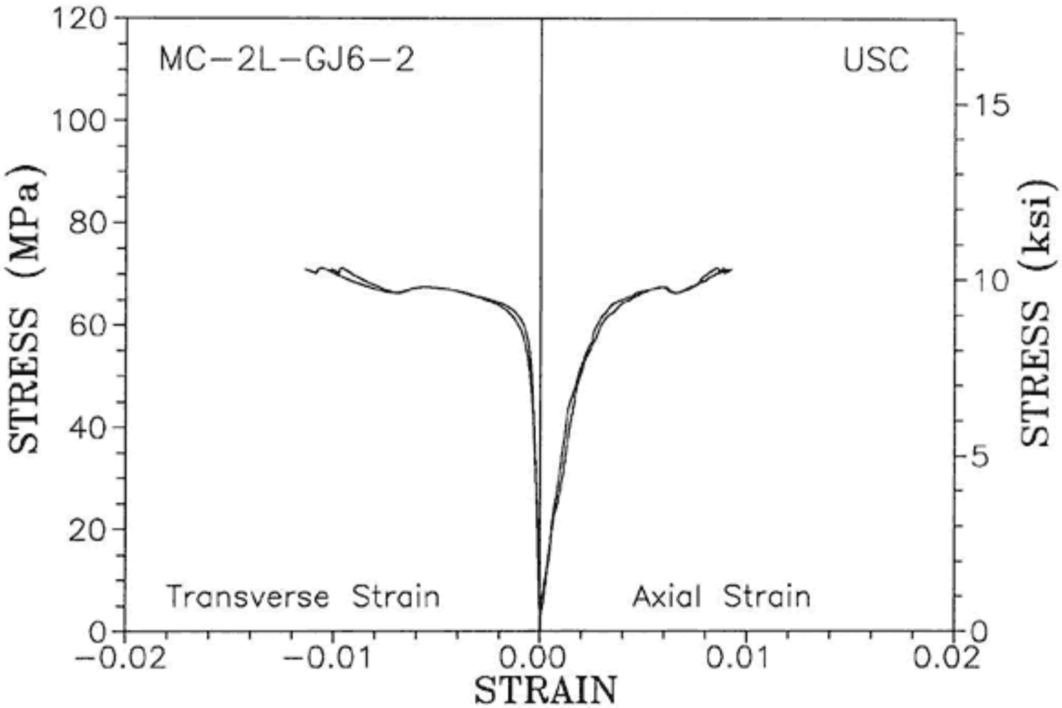

Fig F-C3.Stress-Strain Relationships for Medium Strength Concrete with Two-layer Glass Fiber Composite Jacket (MC-2L-GJ6-2)

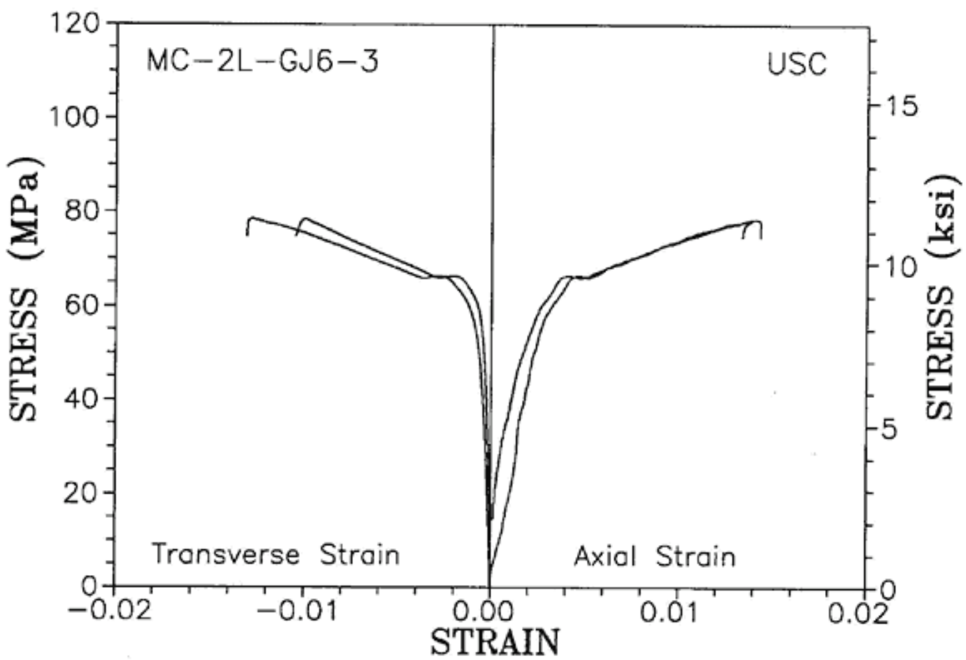

Fig F-C3.Stress-Strain Relationships for Medium Strength Concrete with Two-layer Glass Fiber Composite Jacket (MC-2L-GJ6-3)

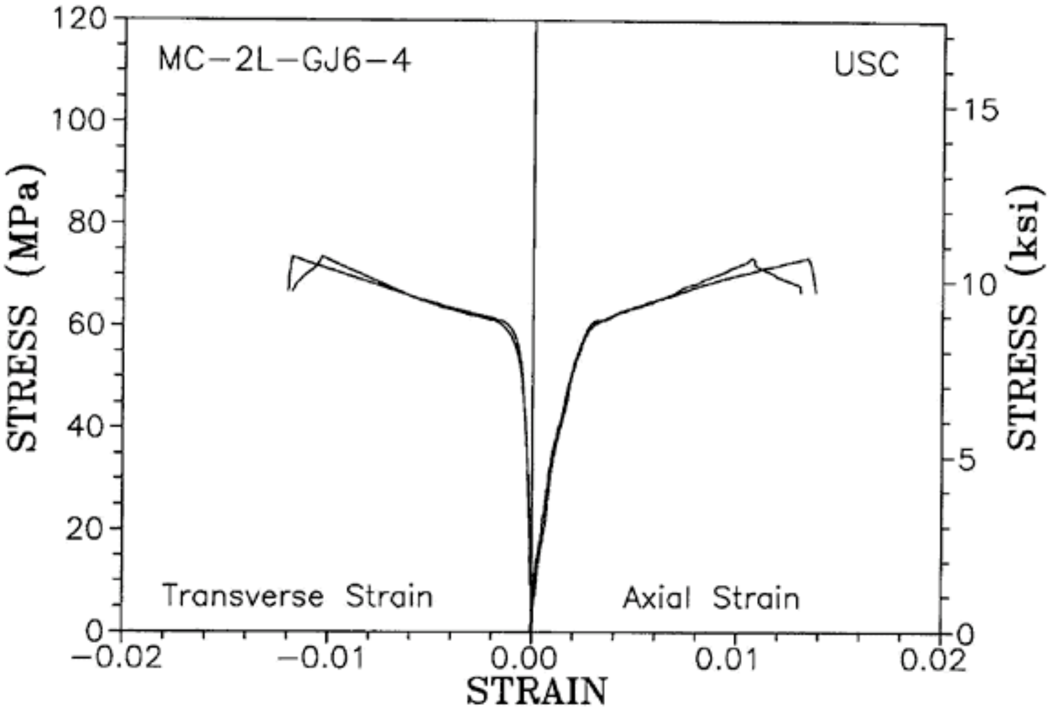

Fig F-C3.Stress-Strain Relationships for Medium Strength Concrete with Two-layer Glass Fiber Composite Jacket (MC-2L-GJ6-4)

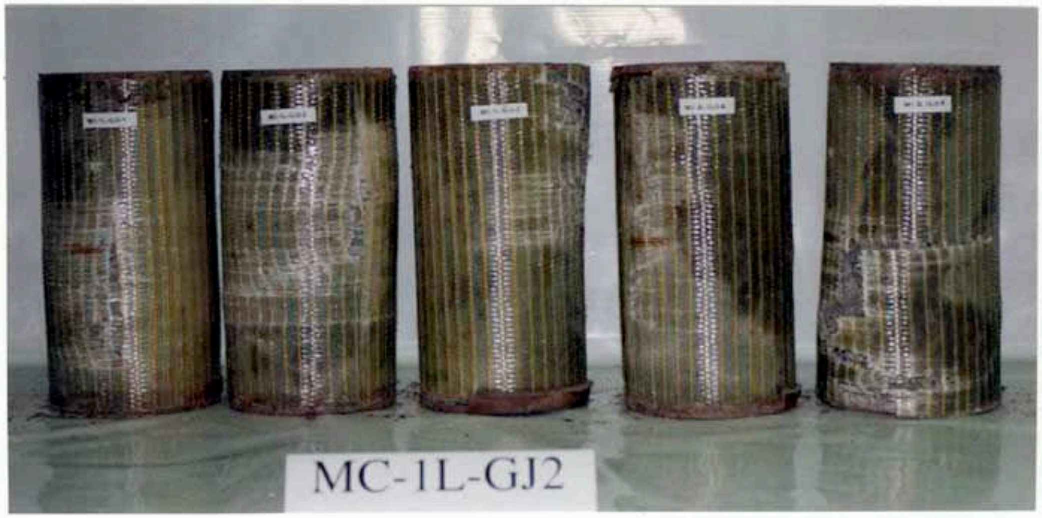

Fig.F-C5. Specimens after Testing

Part F-D Test Results of Higher Strength Concrete Cylinders

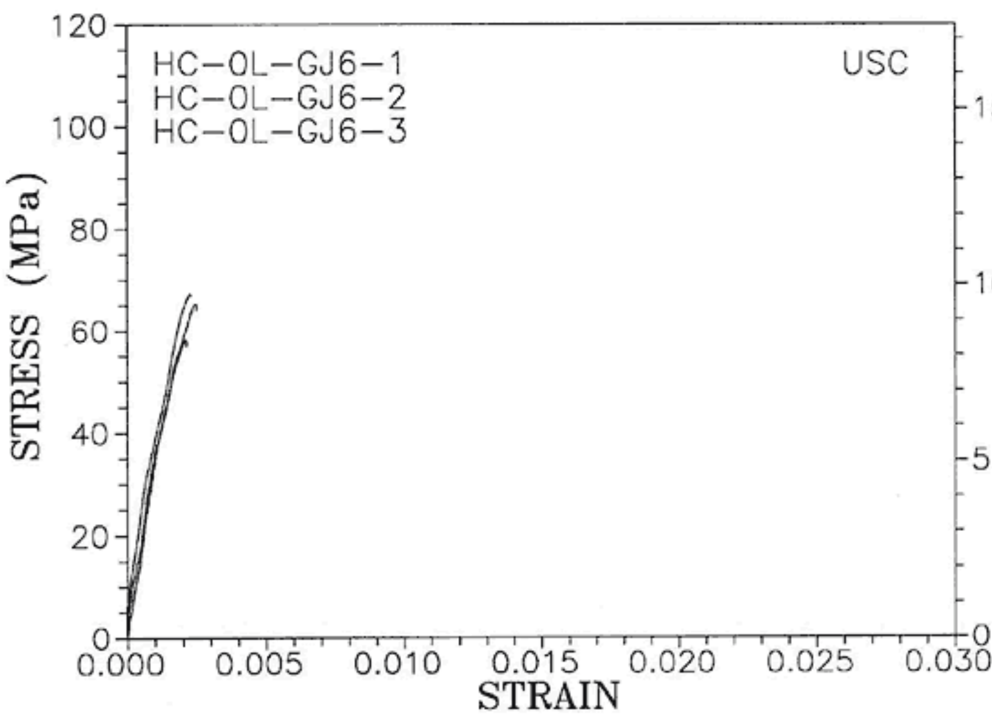

Fig.F-D1. Stress-Strain Relationships for Higher Strength Plain Concrete Cylinders

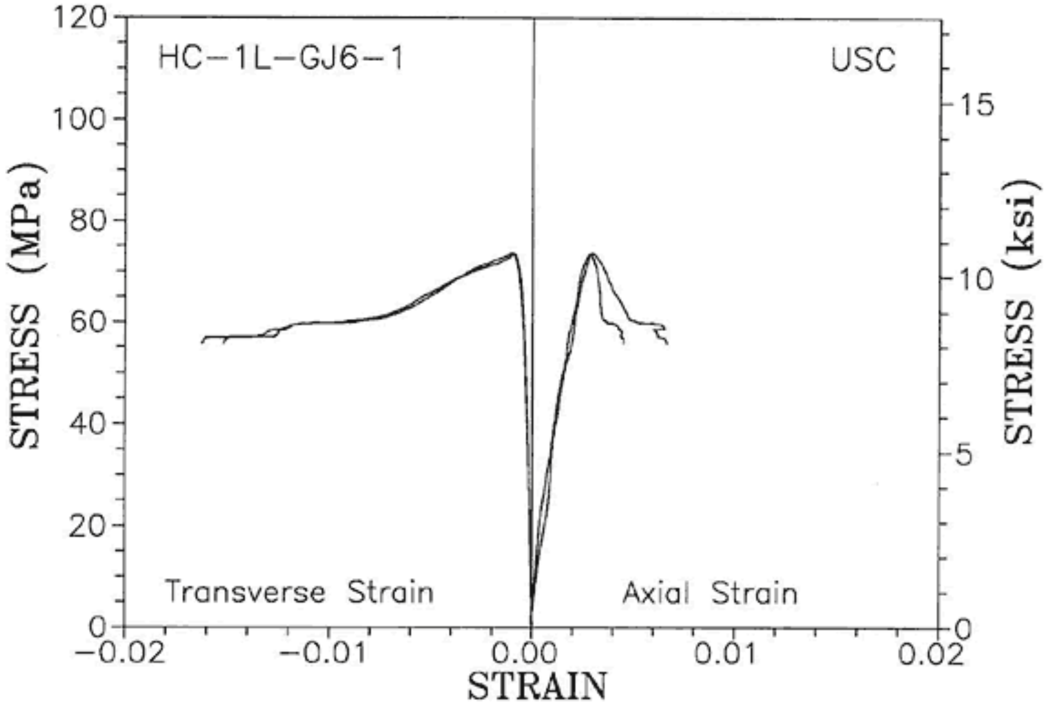

Fig F-D2.Stress-Strain Relationships for Higher Strength Concrete with One-layer Glass Fiber Composite Jacket (HC-1L-GJ6-1)

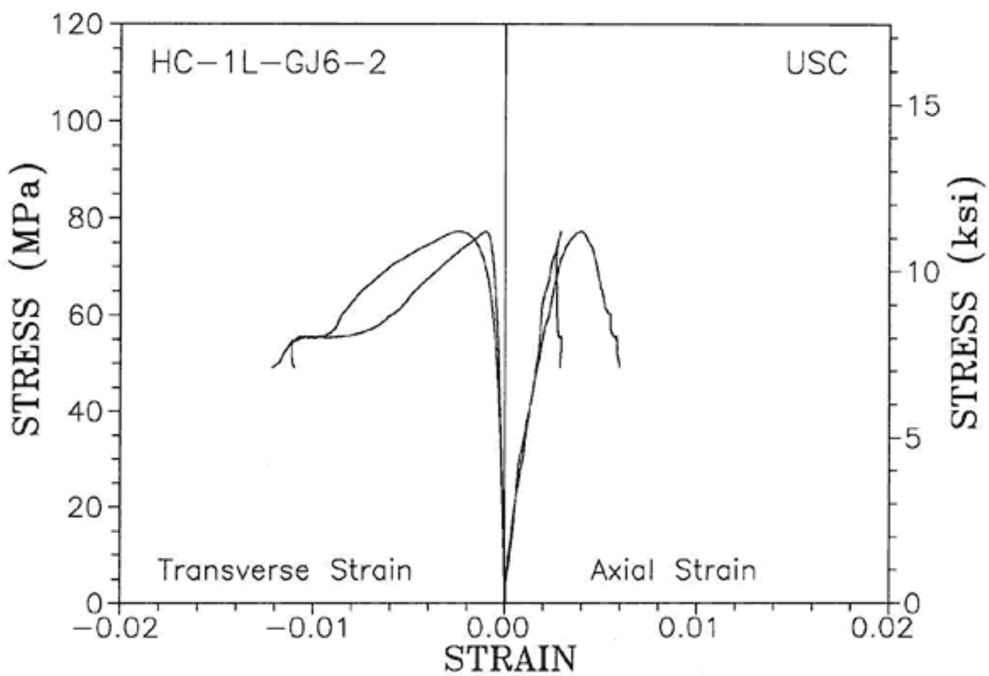

Fig F-D2.Stress-Strain Relationships for Higher Strength Concrete with One-layer Glass Fiber Composite Jacket (HC-1L-GJ6-2)

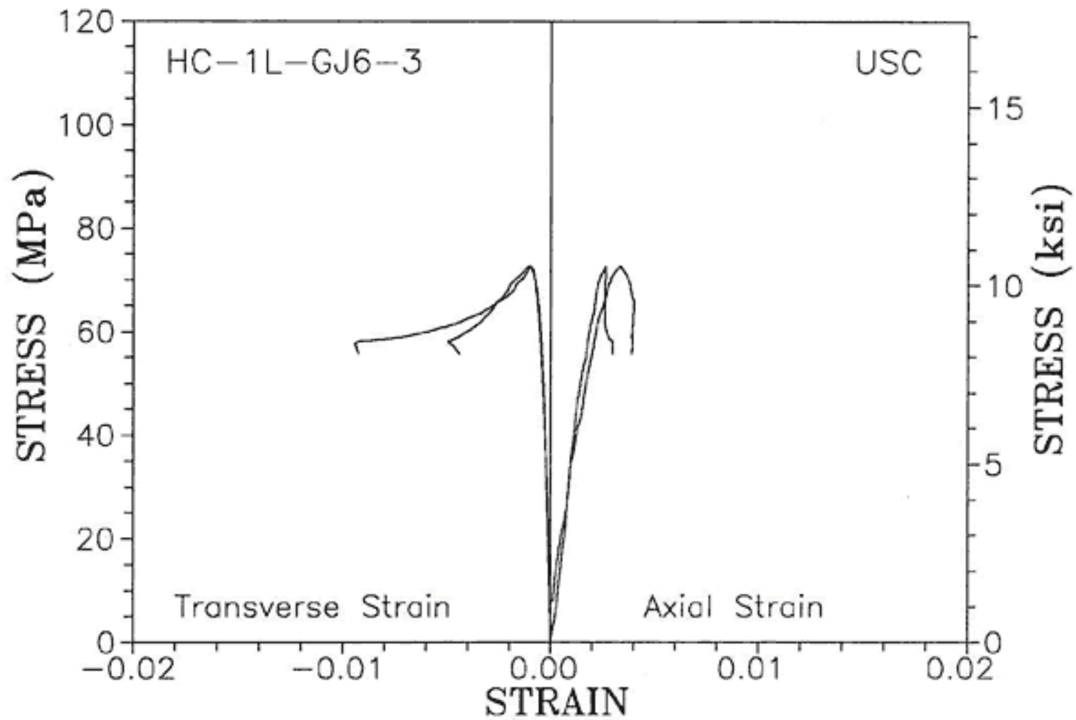

Fig F-D2.Stress-Strain Relationships for Higher Strength Concrete with One-layer Glass Fiber Composite Jacket (HC-1L-GJ6-3)

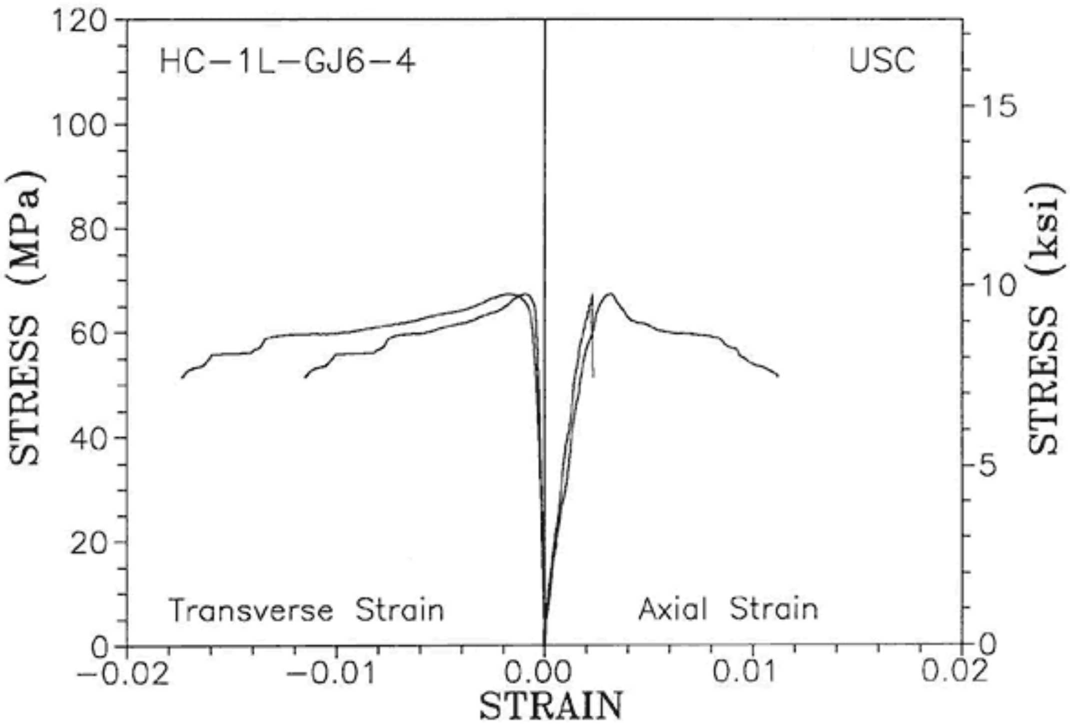

Fig F-D2.Stress-Strain Relationships for Higher Strength Concrete with One-layer Glass Fiber Composite Jacket (HC-1L-GJ6-4)

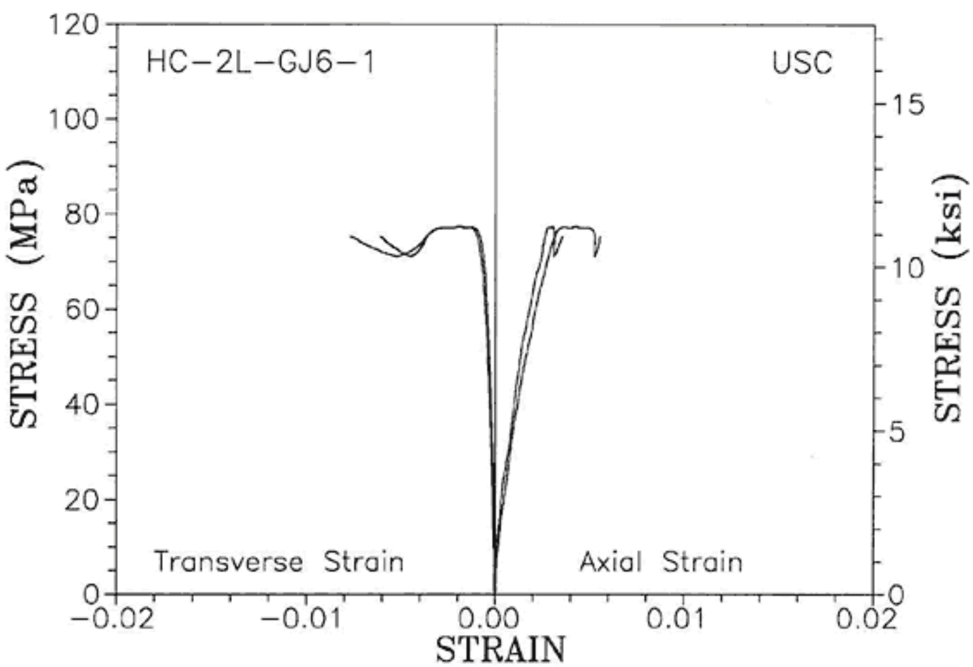

Fig F-D3.Stress-Strain Relationships for Higher Strength Concrete with Two-layer Glass Fiber Composite Jacket (HC-2L-GJ6-1)

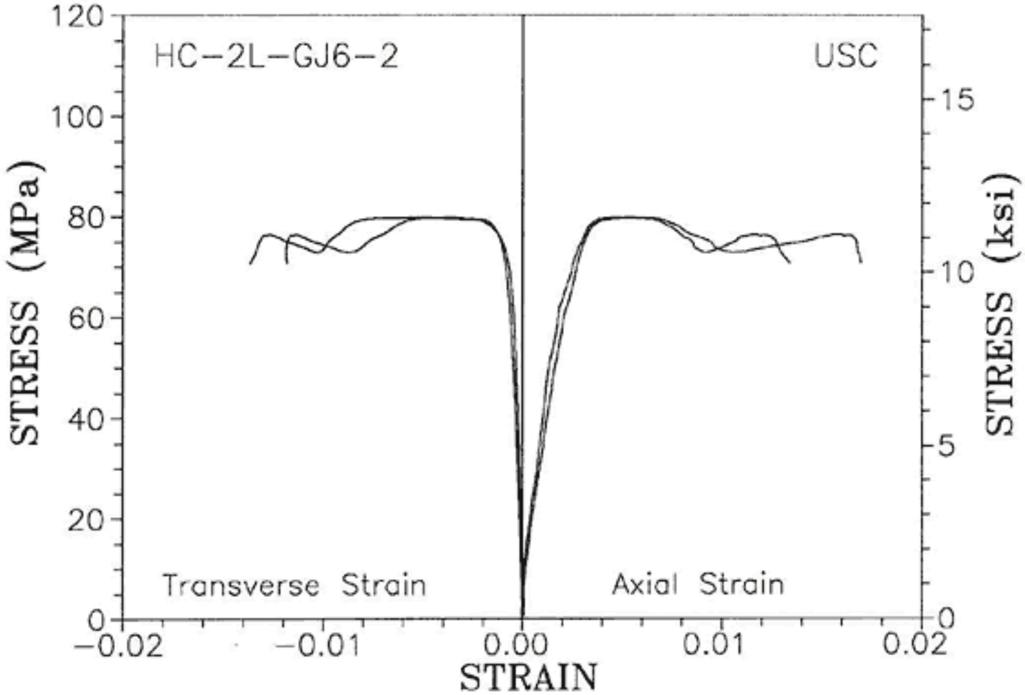

Fig F-D3.Stress-Strain Relationships for Higher Strength Concrete with Two-layer Glass Fiber Composite Jacket (HC-2L-GJ6-2)

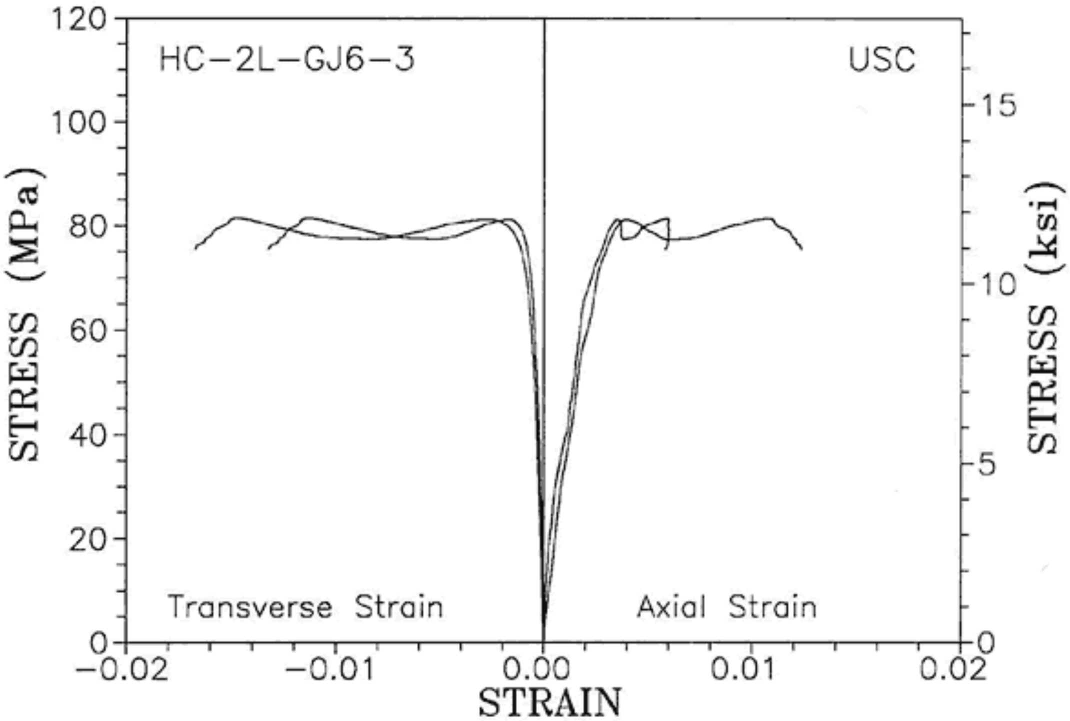

Fig F-D3.Stress-Strain Relationships for Higher Strength Concrete with Two-layer Glass Fiber Composite Jacket (HC-2L-GJ6-3)

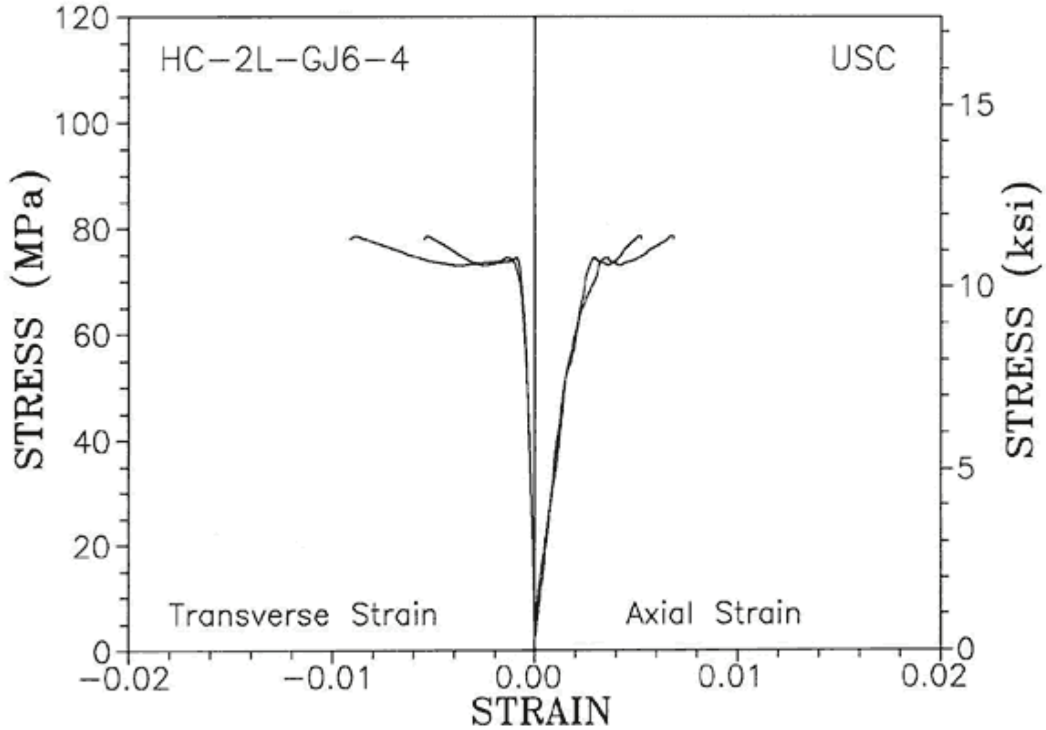

Fig F-D3.Stress-Strain Relationships for Higher Strength Concrete with Two-layer Glass Fiber Composite Jacket (HC-2L-GJ6-4)

Fig.F-D5. Specimens after Testing

APPENDIX G: TEST RESULTS OF SYSTEM SEVEN

Part G-A General Information

Table G-A1 Test Matrix

Type of Jacket	Concrete Strength	Jacket Equivalent Thickness (mm)	Specimen Numbers
Carbon fiber Reinforced composite	Lower	Plain concrete	3
		0.318	3
		0.635	3
		1.270	3
	Medium	Plain concrete	3
		0.318	3
		0.635	3
		1.270	3
	Higher	Plain concrete	3
		0.318	3
		0.635	3
		1.270	3

Table G-A2 Mix Proportion of Concrete

Series	Target f'_{co} (MPa)	W/C	Water (kg/m^3)	Cement (kg/m^3)	Fine Aggregates (kg/m^3)	Coarse Aggregates (kg/m^3)
L	27.6	0.68	196	288	1087	853
M	37.9	0.48	196	408	986	853
H	48.2	0.38	197	515	857	853

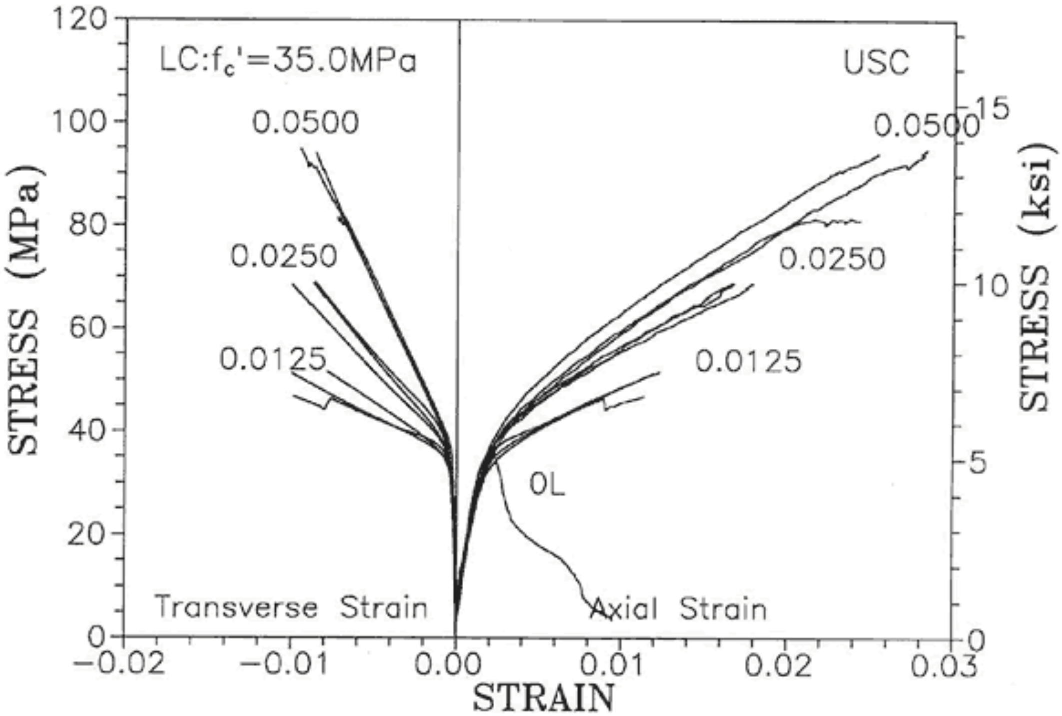

Fig.G-A1. Test Results of Lower-Strength Specimens

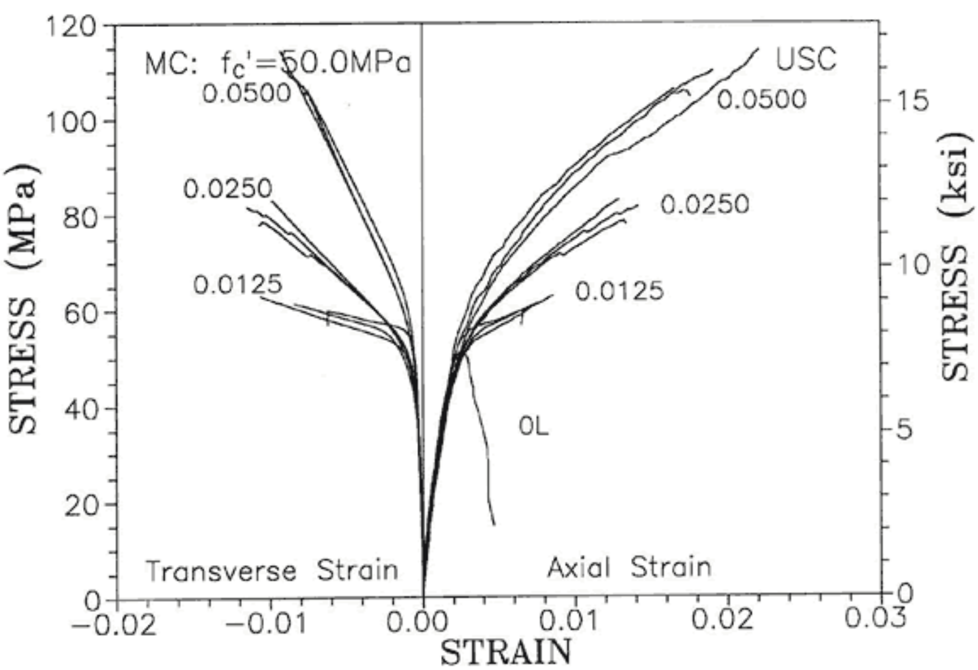

Fig.G-A2. Test Results of Medium-Strength Specimens

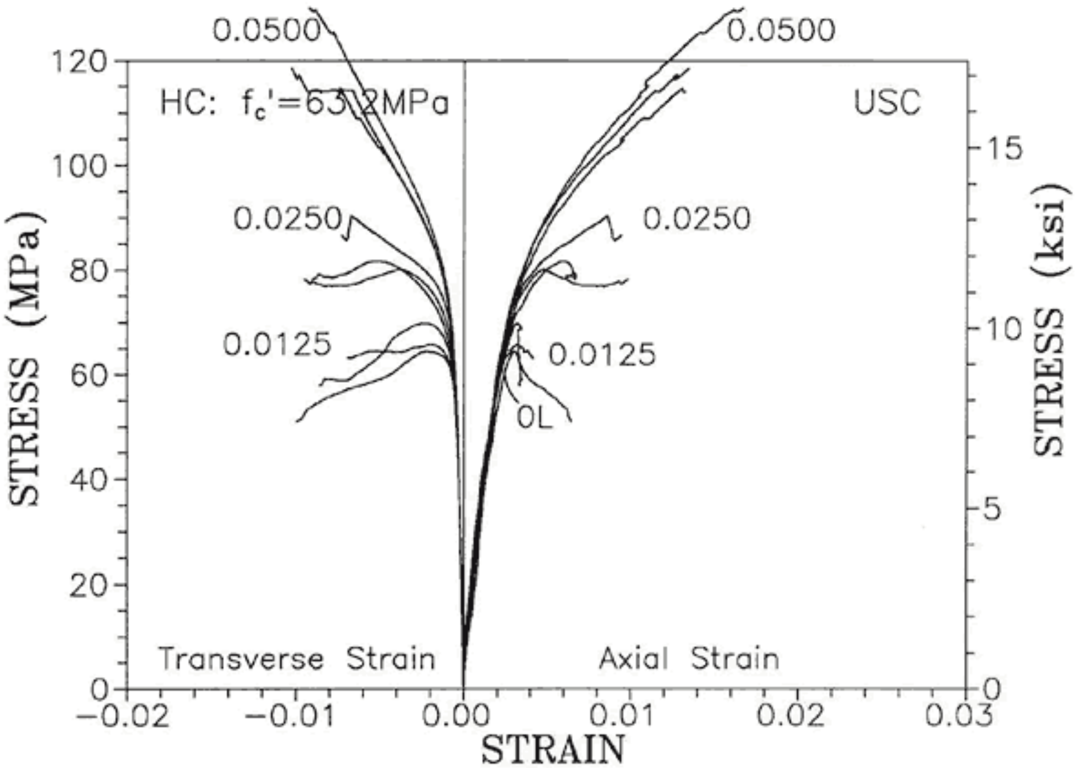

Fig.G-A3. Test Results of Higher-Strength Specimens

Table G-A4 Test Results

Series	Specimen	f_c' (MPa)	Jacket Equivalent Thickness (mm)	f_{cc}' (MPa)	ε_{cu}
L	LC-0L-CJ7-1	35.0	0	35.81	0.002062
	LC-0L-CJ7-2			37.15	0.002089
	LC-0L-CJ7-3			31.91	0.001649
	LC-0.0125-CJ7-1		0.318	51.23	0.011886
	LC-0.0125-CJ7-2			51.52	0.012269
	LC-0.0125-CJ7-3			46.71	0.011299
	LC-0.0250-CJ7-1		0.635	68.94	0.016742
	LC-0.0250-CJ7-2			68.44	0.016611
	LC-0.0250-CJ7-3			68.80	0.017898
	LC-0.0500-CJ7-1		1.270	94.75	0.028350
	LC-0.0500-CJ7-2			81.38	0.023747
	LC-0.0500-CJ7-3			93.92	0.025394
M	MC-0L-CJ7-1	50.0	0	47.65	0.002427
	MC-0L-CJ7-2			51.48	0.002572
	MC-0L-CJ7-3			50.74	0.002609
	MC-0.0125-CJ7-1		0.318	59.87	0.006471
	MC-0.0125-CJ7-2			61.40	0.007581
	MC-0.0125-CJ7-3			62.94	0.008547
	MC-0.0250-CJ7-1		0.635	78.67	0.013224
	MC-0.0250-CJ7-2			82.99	0.012878
	MC-0.0250-CJ7-3			81.70	0.014147
	MC-0.0500-CJ7-1		1.270	114.29	0.022076
	MC-0.0500-CJ7-2			105.85	0.017131
	MC-0.0500-CJ7-3			110.06	0.019049
H	HC-0L-CJ7-1	63.2	0	63.88	0.002344
	HC-0L-CJ7-2			60.00	0.002440
	HC-0L-CJ7-3			65.69	0.002615
	HC-0.0125-CJ7-1		0.318	65.87	0.003242
	HC-0.0125-CJ7-2			64.44	0.003023
	HC-0.0125-CJ7-3			69.85	0.003210
	HC-0.0250-CJ7-1		0.635	90.29	0.008567
	HC-0.0250-CJ7-2			81.70	0.005932
	HC-0.0250-CJ7-3			80.15	0.004764
	HC-0.0500-CJ7-1		1.270	114.65	0.013034
	HC-0.0500-CJ7-2			118.48	0.013383
	HC-0.0500-CJ7-3			130.14	0.016651

Note: (i) Example for specimen name designation:

LC-0.0250-CJ7-1: LC designates Lower strength Concrete; 0.0250 designates jacket equivalent thickness in inches; CJ7 designates Carbon fiber Jacket System 7; and the last number represents specimen number in same series.

(ii) f_c': Average plain concrete cylinder strength;

(iii) f_{cc}': Ultimate strength of confined concrete;

(iv) ε_{cu}: Ultimate strain

Part G-B Test Results of Lower Strength Concrete Cylinders

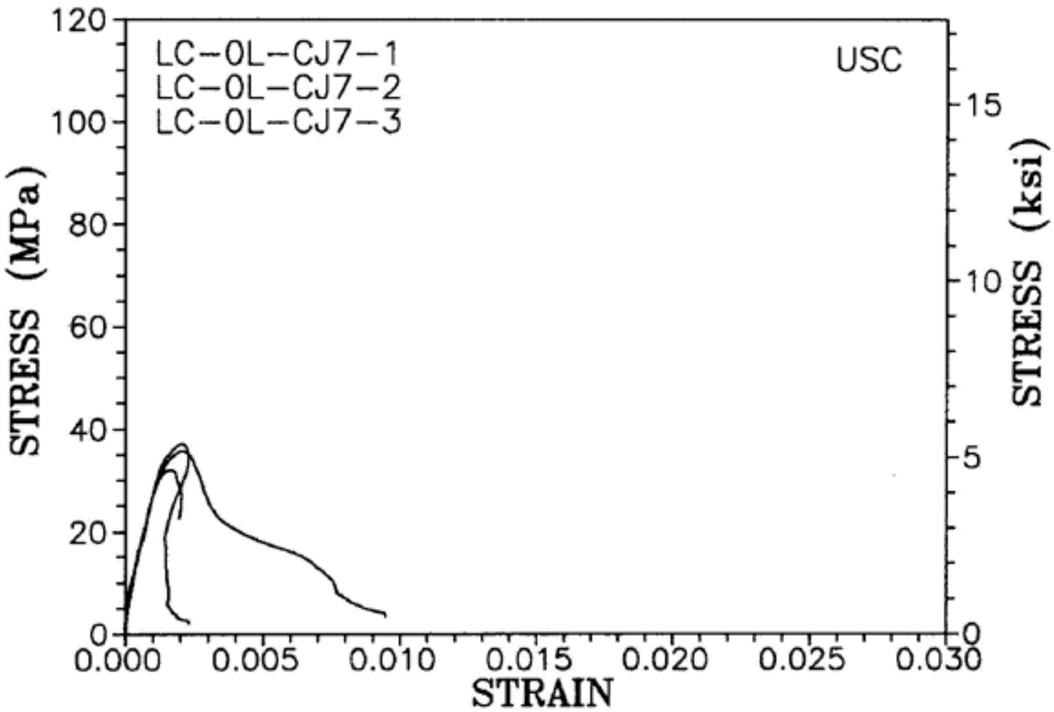

Fig.G-B1. Stress-Strain Relationship for Lower Strength Plain Concrete Cylinders

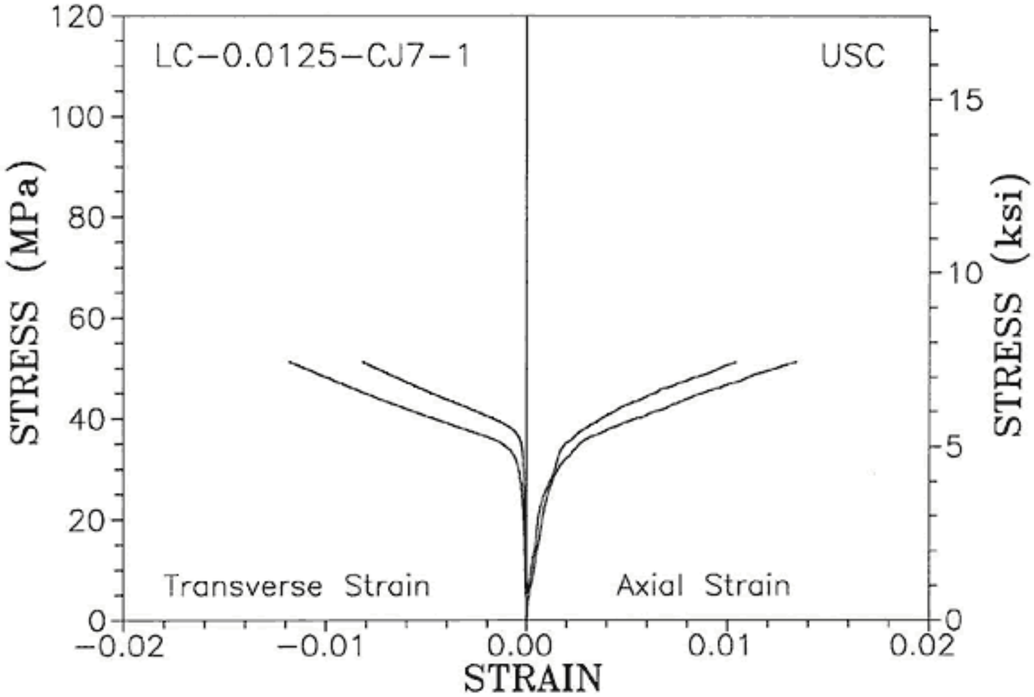

Fig G-B2.Stress-Strain Relationships for Lower Strength Concrete with 0.318mm Thickness Carbon Fiber Composite Jacket (LC-0.0125-CJ7-1)

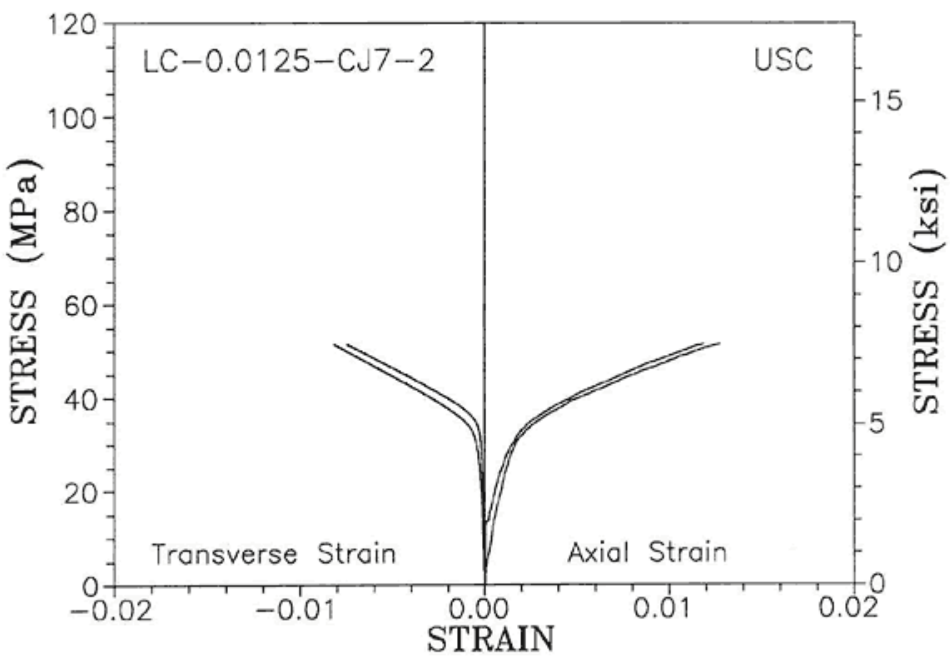

Fig G-B2.Stress-Strain Relationships for Lower Strength Concrete with 0.318mm Thickness Carbon Fiber Composite Jacket (LC-0.0125-CJ7-2)

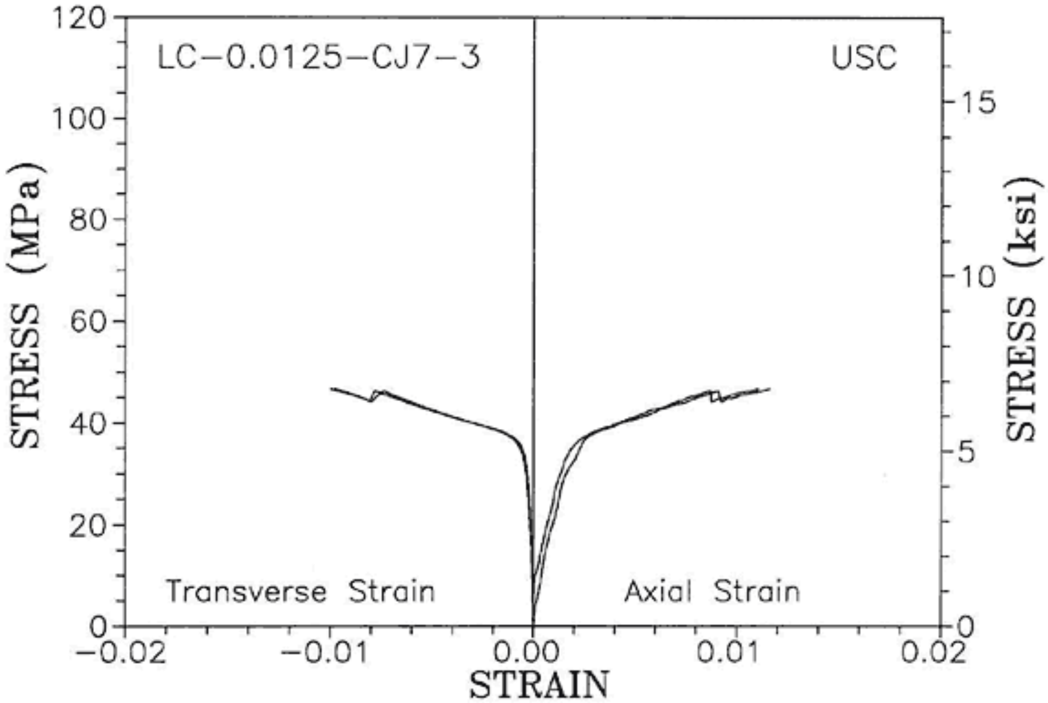

Fig G-B2.Stress-Strain Relationships for Lower Strength Concrete with 0.318mm Thickness Carbon Fiber Composite Jacket (LC-0.0125-CJ7-3)

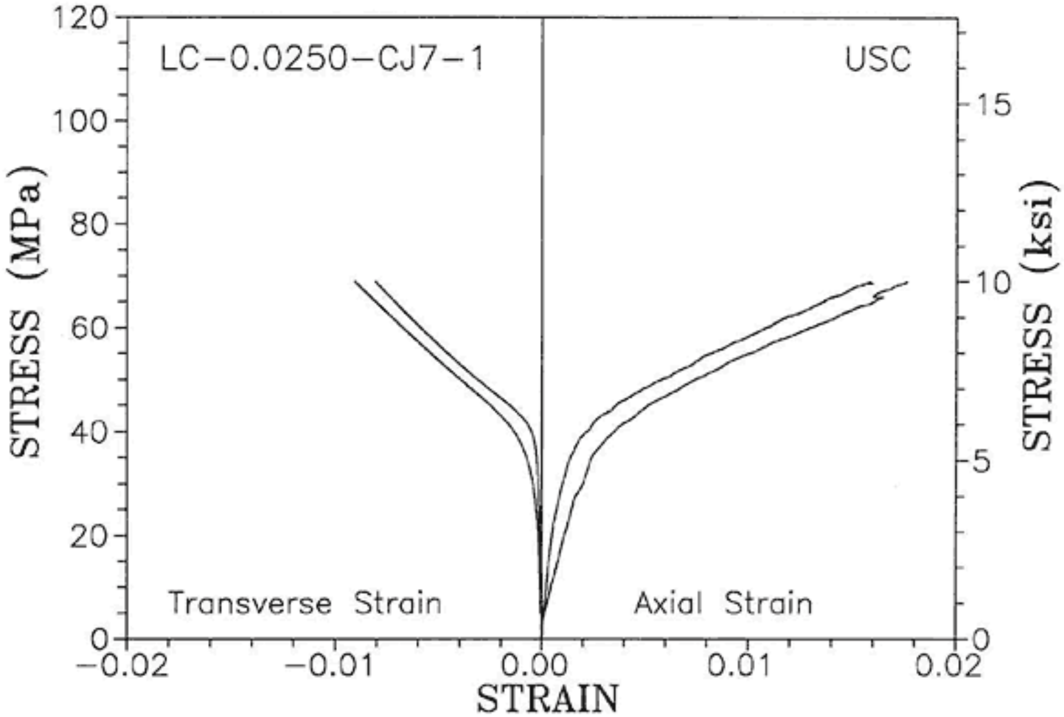

Fig G-B3.Stress-Strain Relationships for Lower Strength Concrete with 0.635mm Thickness Carbon Fiber Composite Jacket (LC-0.025-CJ7-1)

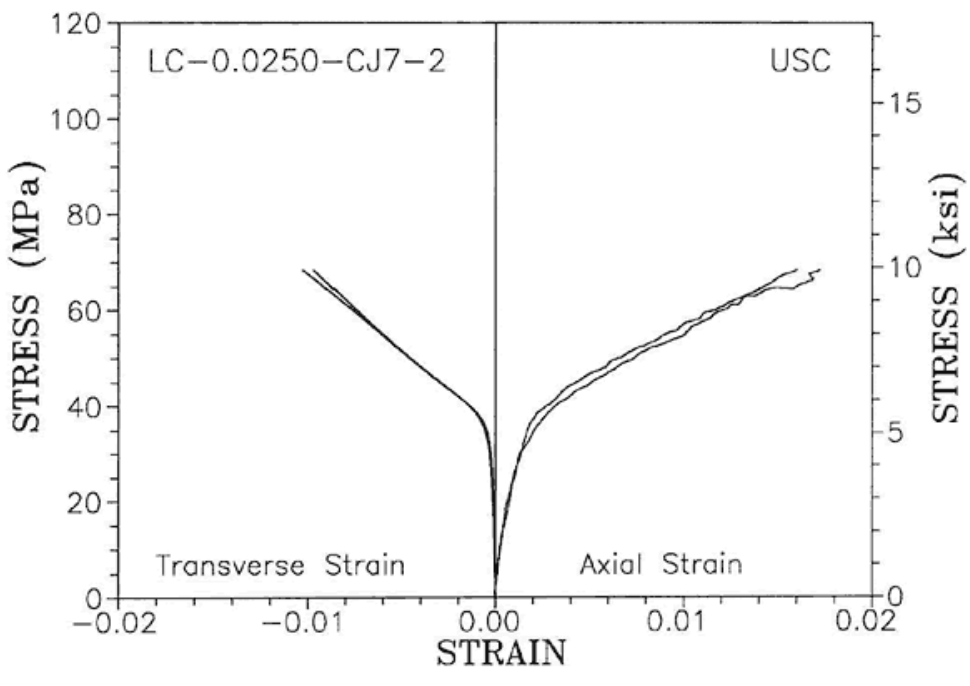

Fig G-B3.Stress-Strain Relationships for Lower Strength Concrete with 0.635mm Thickness Carbon Fiber Composite Jacket (LC-0.025-CJ7-2)

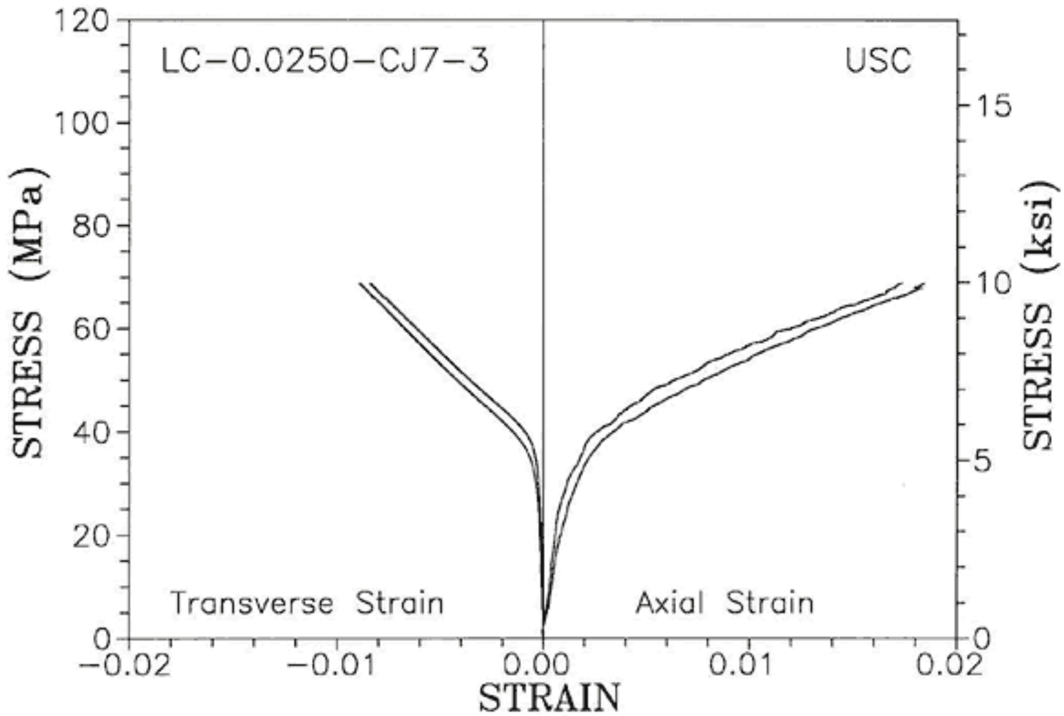

Fig G-B3.Stress-Strain Relationships for Lower Strength Concrete with 0.635mm Thickness Carbon Fiber Composite Jacket (LC-0.025-CJ7-3)

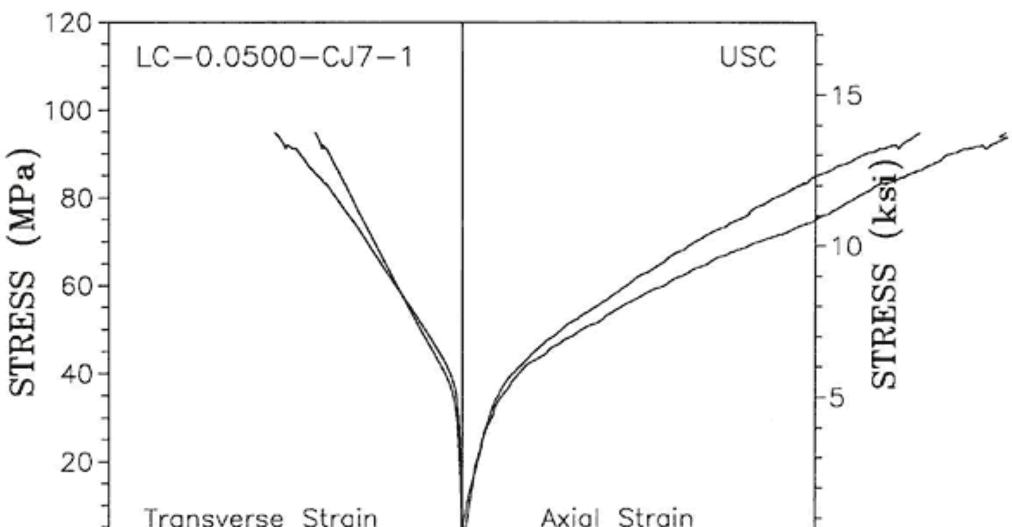

Fig G-B4.Stress-Strain Relationships for Lower Strength Concrete with 1.27mm Thickness Carbon Fiber Composite Jacket (LC-0.0500-CJ7-1)

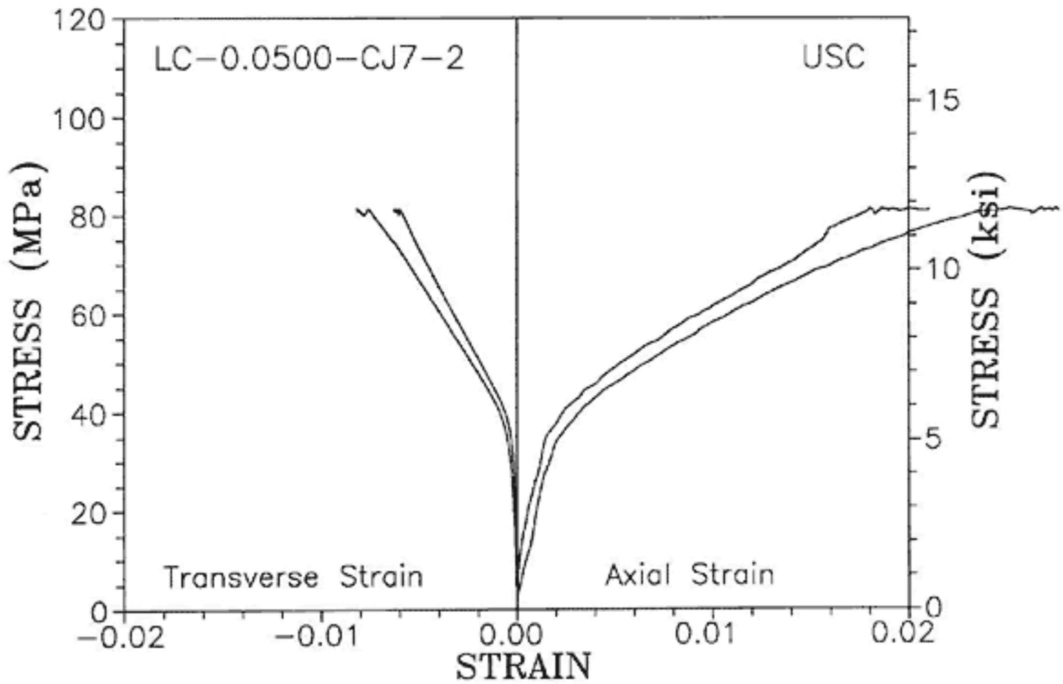

Fig G-B4.Stress-Strain Relationships for Lower Strength Concrete with 1.27mm Thickness Carbon Fiber Composite Jacket (LC-0.0500-CJ7-2)

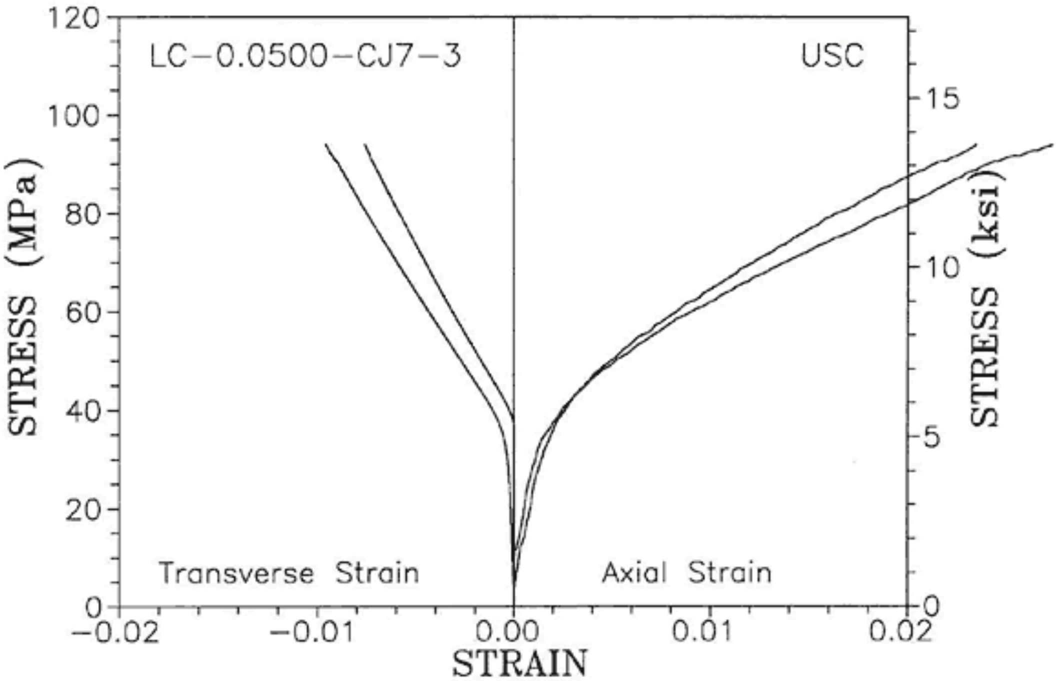

Fig G-B4.Stress-Strain Relationships for Lower Strength Concrete with 1.27mm Thickness Carbon Fiber Composite Jacket (LC-0.0500-CJ7-3)

Fig.G-B5. Specimens after Testing

Part G-C Test Results of Medium Strength Concrete Cylinders

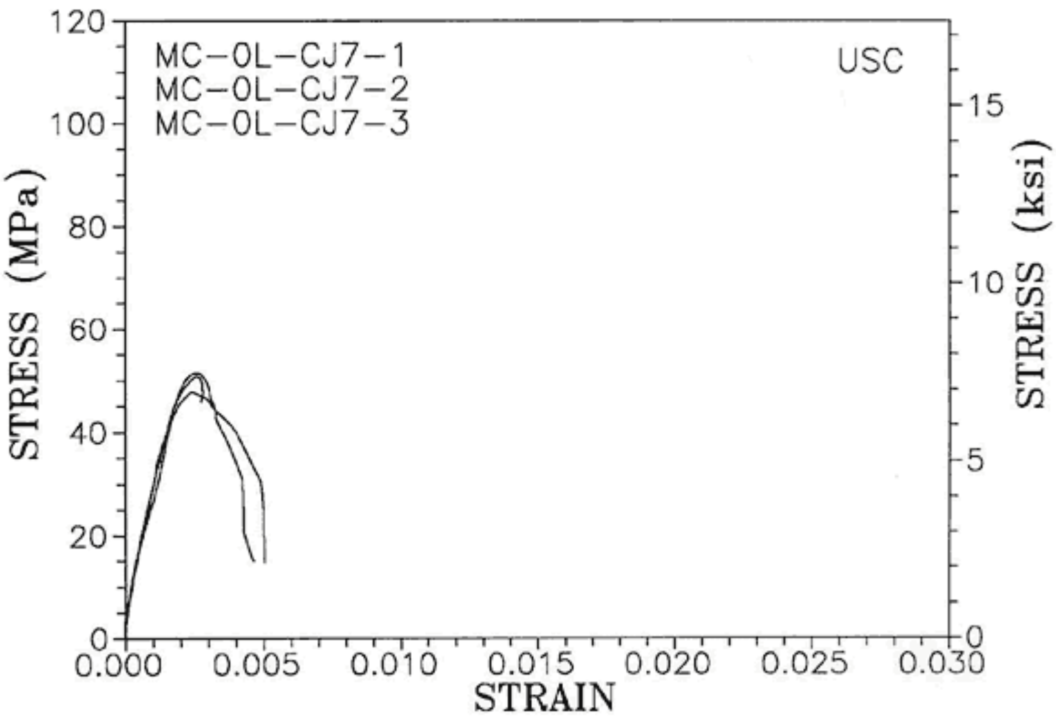

Fig.G-C1. Stress-Strain Relationship for Medium Strength Plain Concrete Cylinders

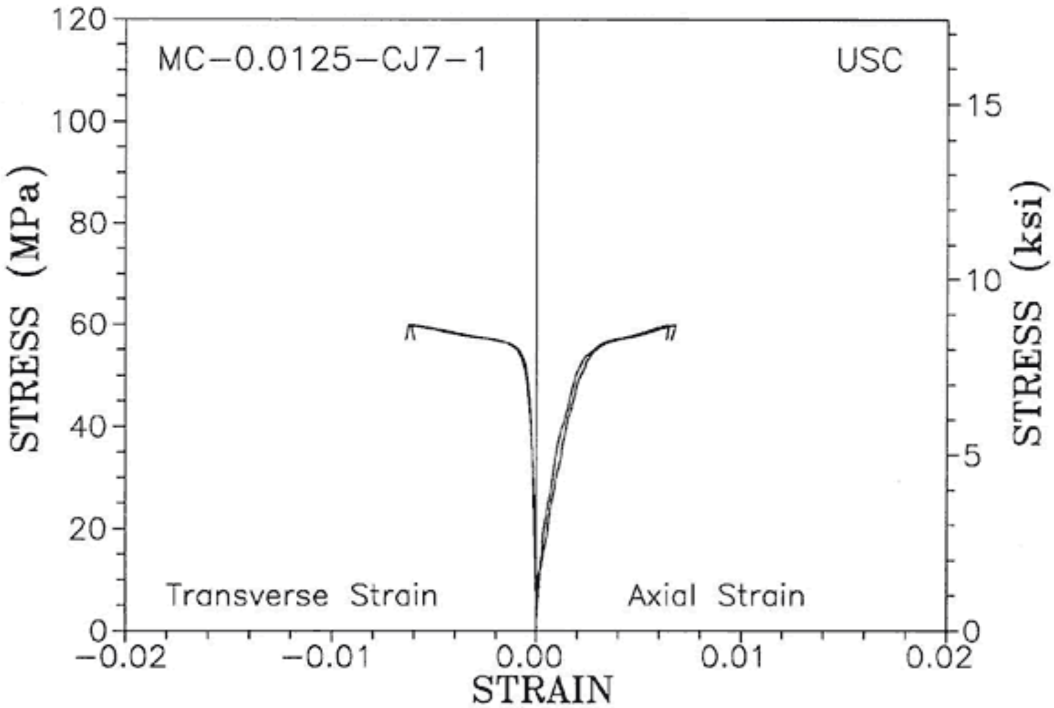

Fig G-C2.Stress-Strain Relationships for Medium Strength Concrete with 0.318mm Thickness Carbon Fiber Composite Jacket (MC-0.0125-CJ7-1)

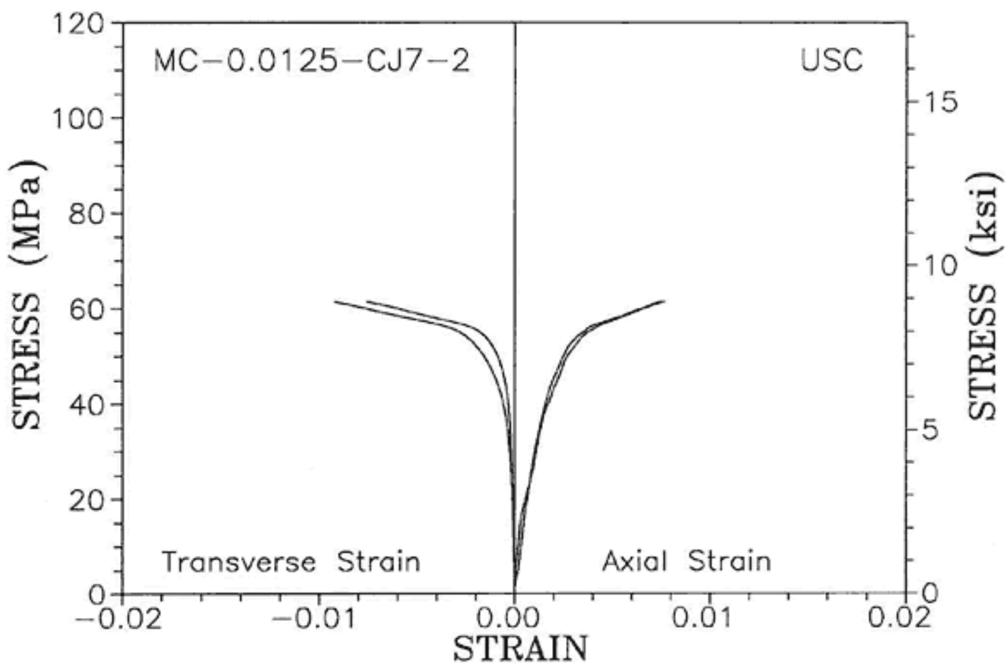

Fig G-C2.Stress-Strain Relationships for Medium Strength Concrete with 0.318mm Thickness Carbon Fiber Composite Jacket (MC-0.0125-CJ7-2)

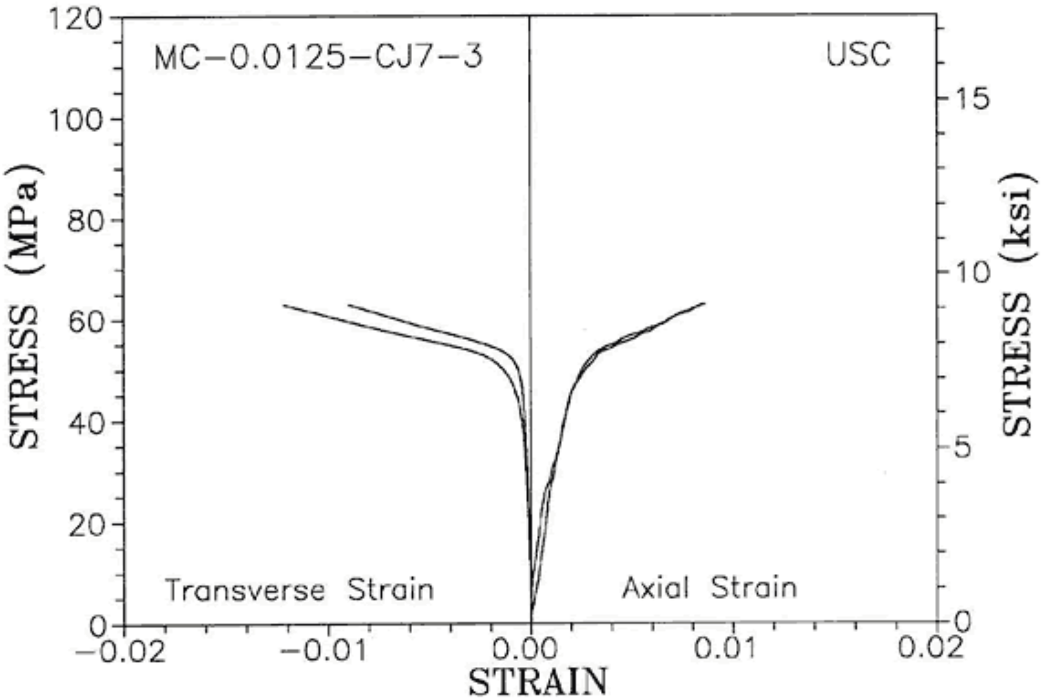

Fig G-C2.Stress-Strain Relationships for Medium Strength Concrete with 0.318mm Thickness Carbon Fiber Composite Jacket (MC-0.0125-CJ7-3)

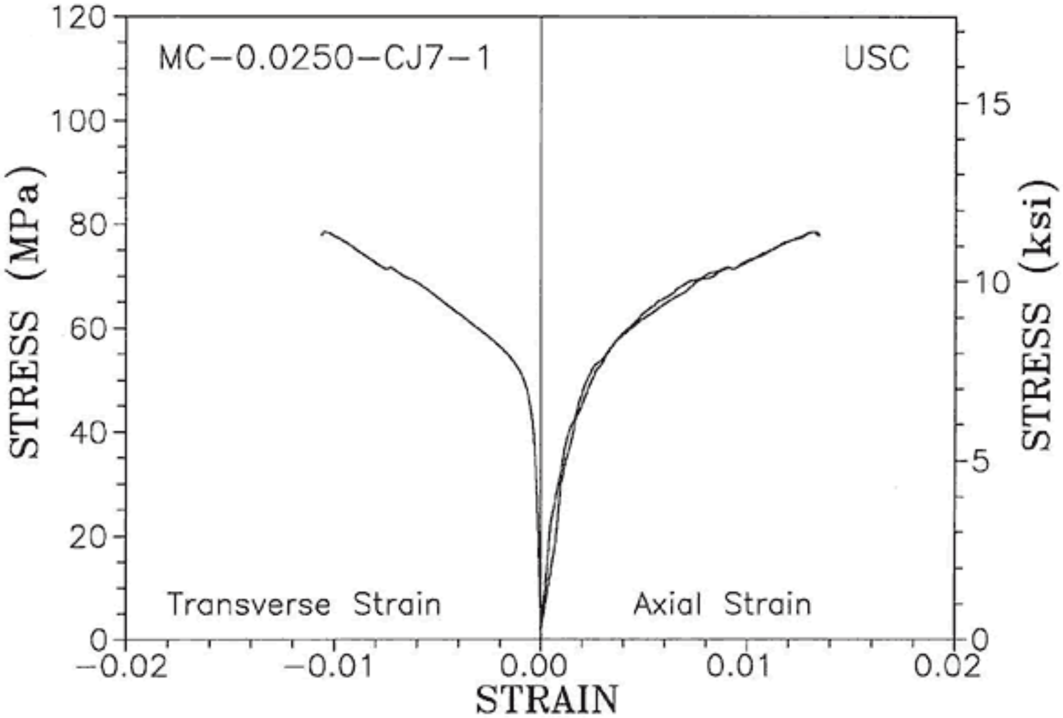

Fig G-C3.Stress-Strain Relationships for Medium Strength Concrete with 0.635mm Thickness Carbon Fiber Composite Jacket (MC-0.025-CJ7-1)

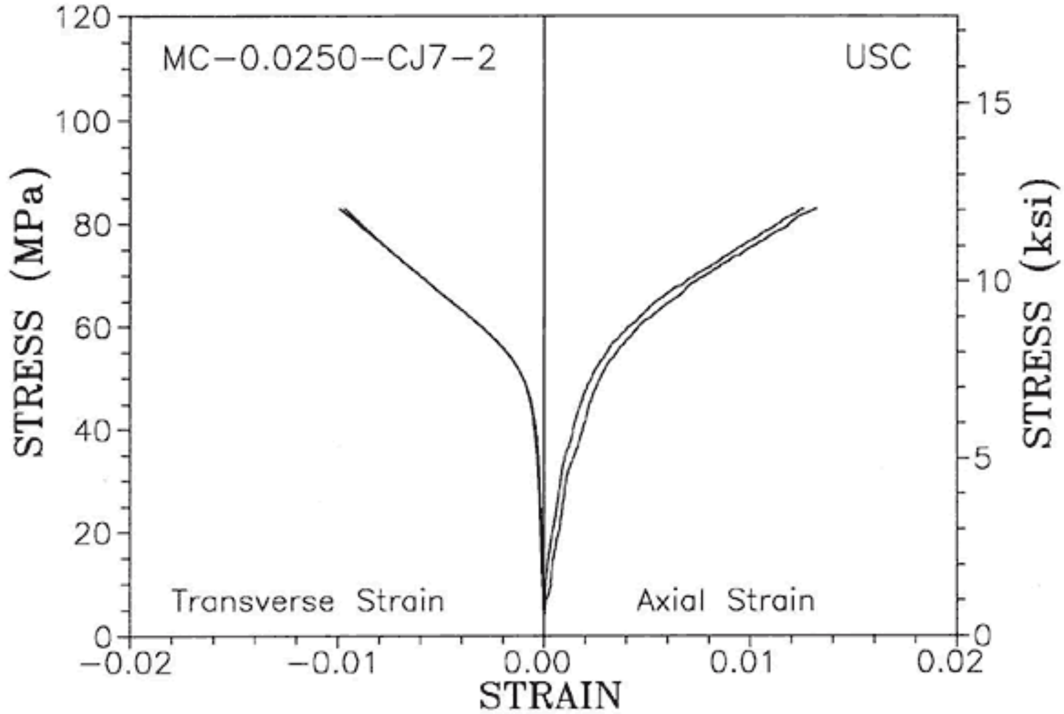

Fig G-C3.Stress-Strain Relationships for Medium Strength Concrete with 0.635mm Thickness Carbon Fiber Composite Jacket (MC-0.025-CJ7-2)

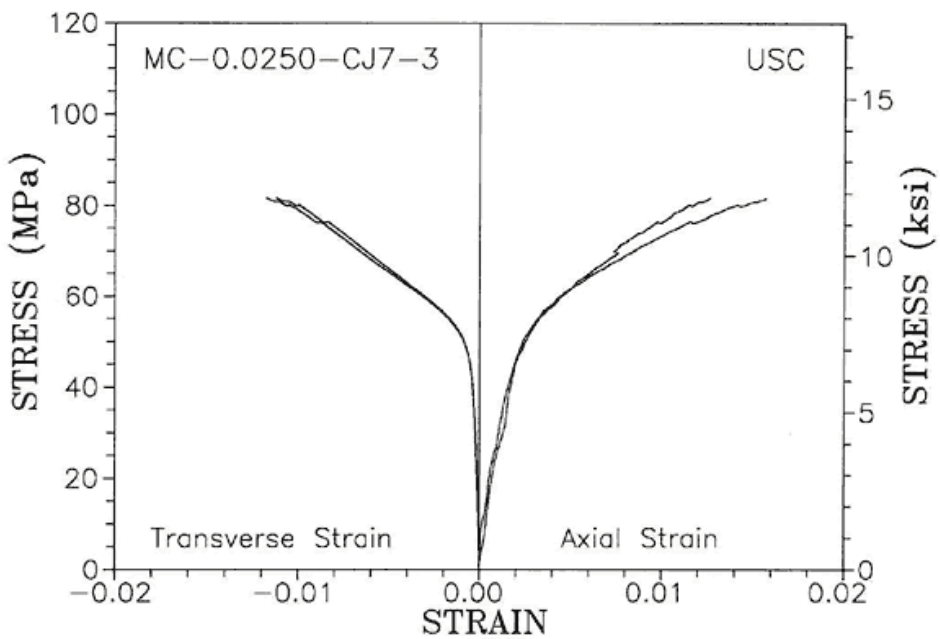

Fig G-C3.Stress-Strain Relationships for Medium Strength Concrete with 0.635mm Thickness Carbon Fiber Composite Jacket (MC-0.025-CJ7-3)

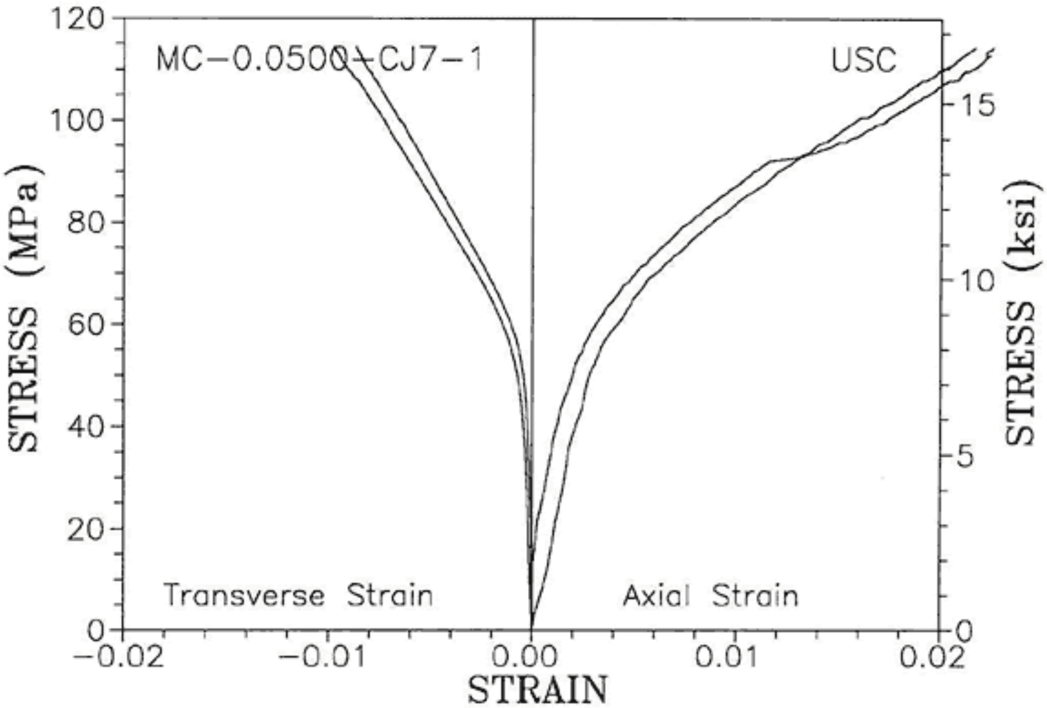

Fig G-C3.Stress-Strain Relationships for Medium Strength Concrete with 1.27mm Thickness Carbon Fiber Composite Jacket (MC-0.0500-CJ7-1)

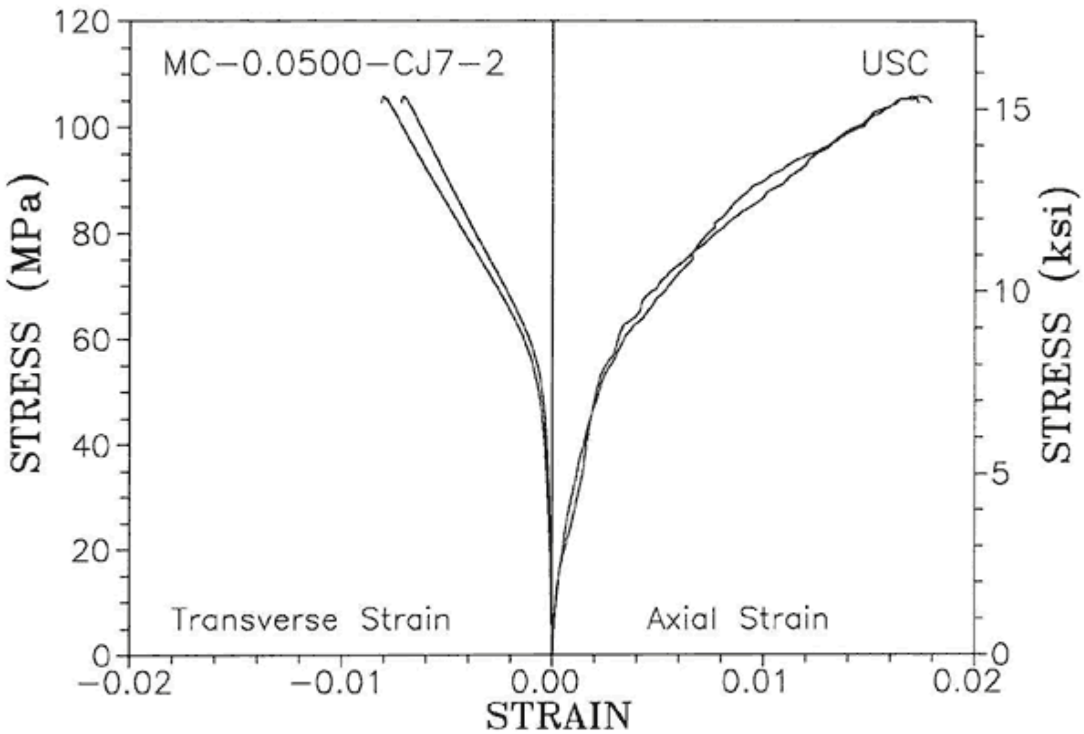

Fig G-C3.Stress-Strain Relationships for Medium Strength Concrete with 1.27mm Thickness Carbon Fiber Composite Jacket (MC-0.0500-CJ7-2)

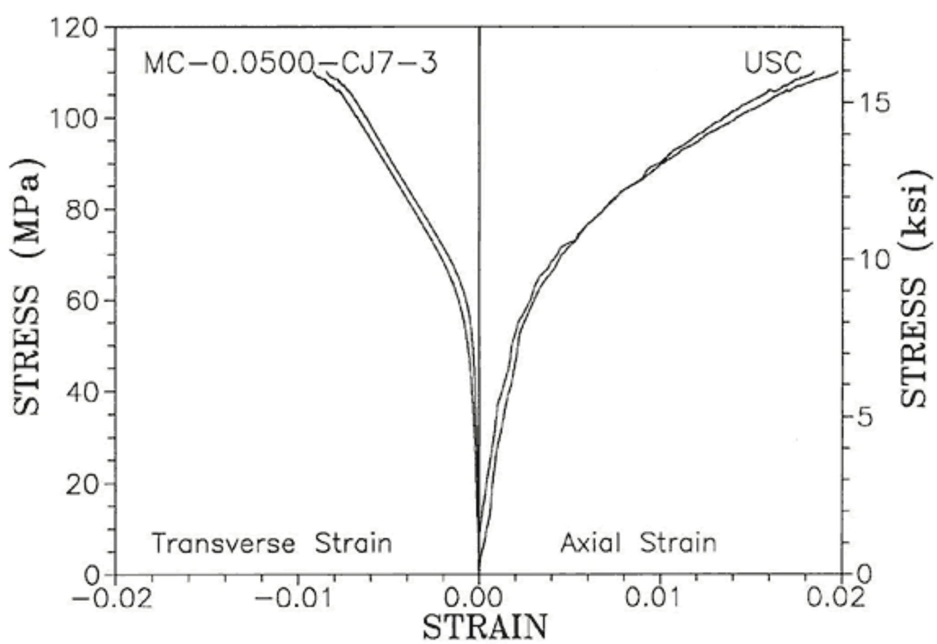

Fig G-C3.Stress-Strain Relationships for Medium Strength Concrete with 1.27mm Thickness Carbon Fiber Composite Jacket (MC-0.0500-CJ7-3)

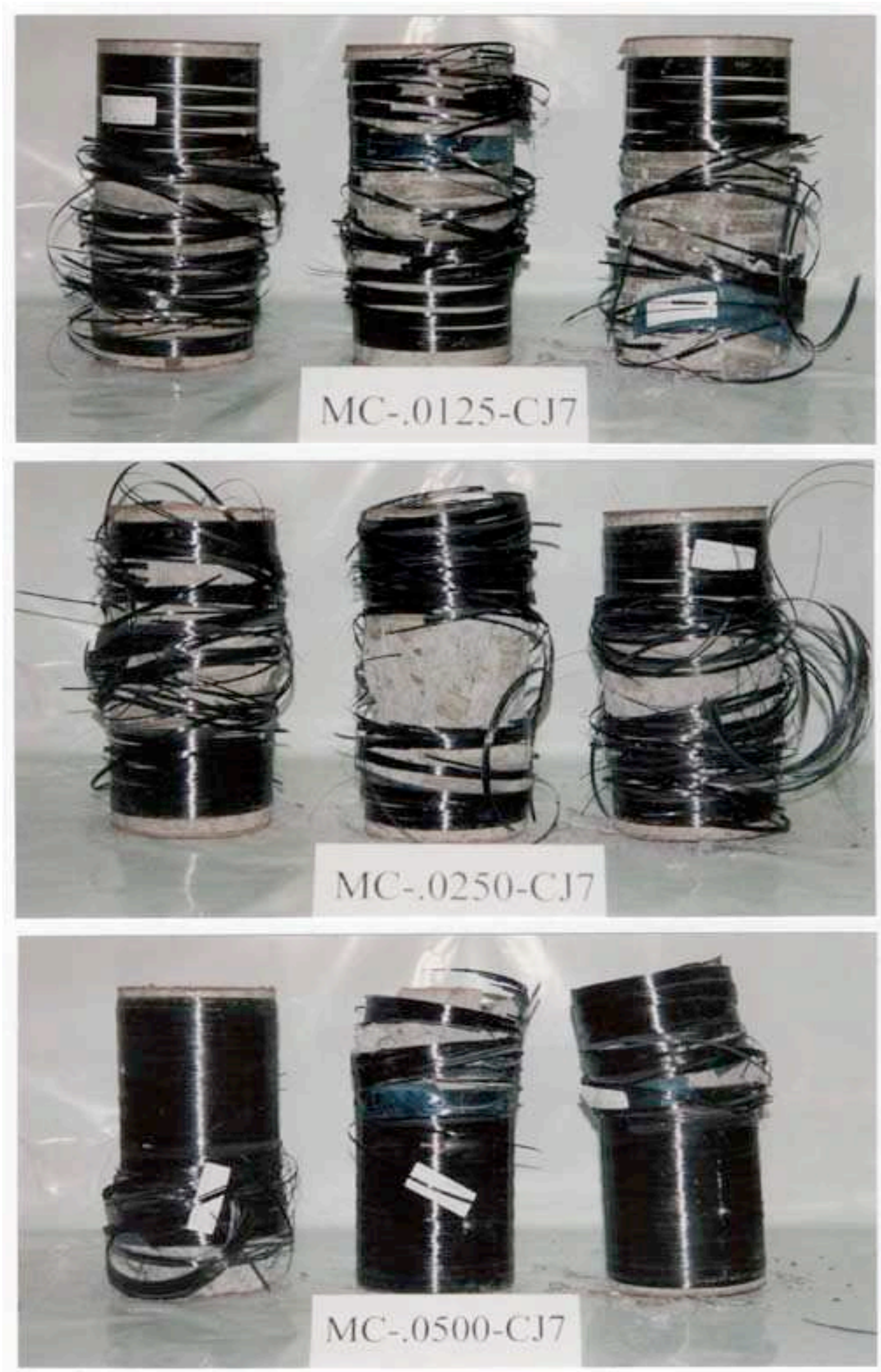

Fig.G-C5. Specimens after Testing

Part G-D Test Results of Higher Strength Concrete Cylinders

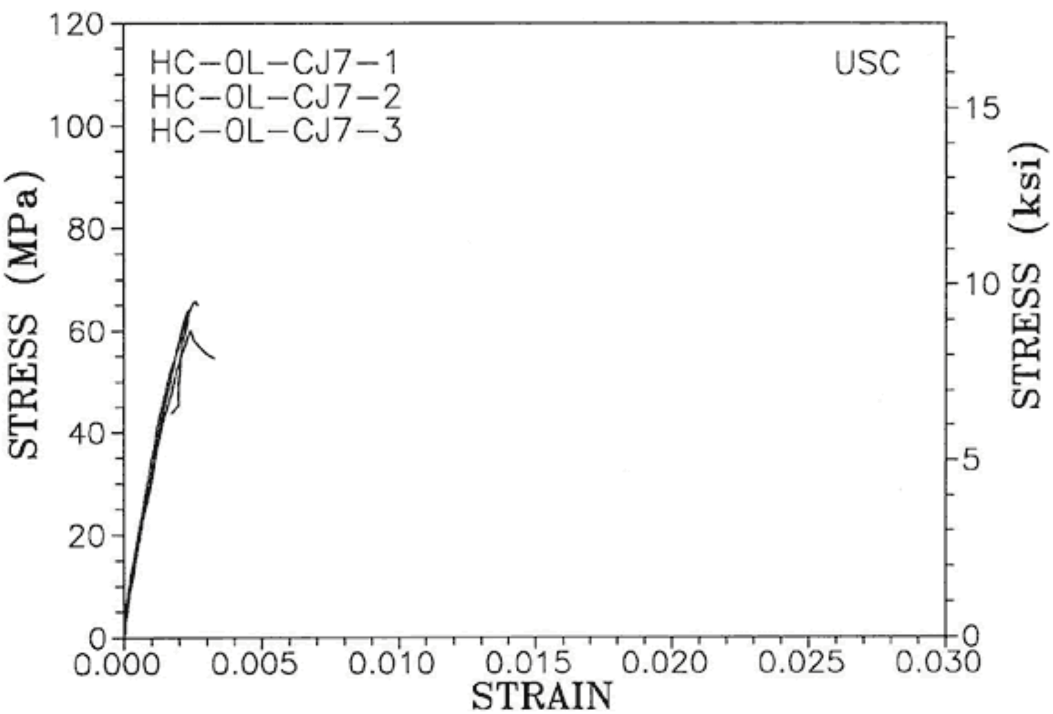

Fig.G-D1. Stress-Strain Relationships for Higher Strength Plain Concrete Cylinders

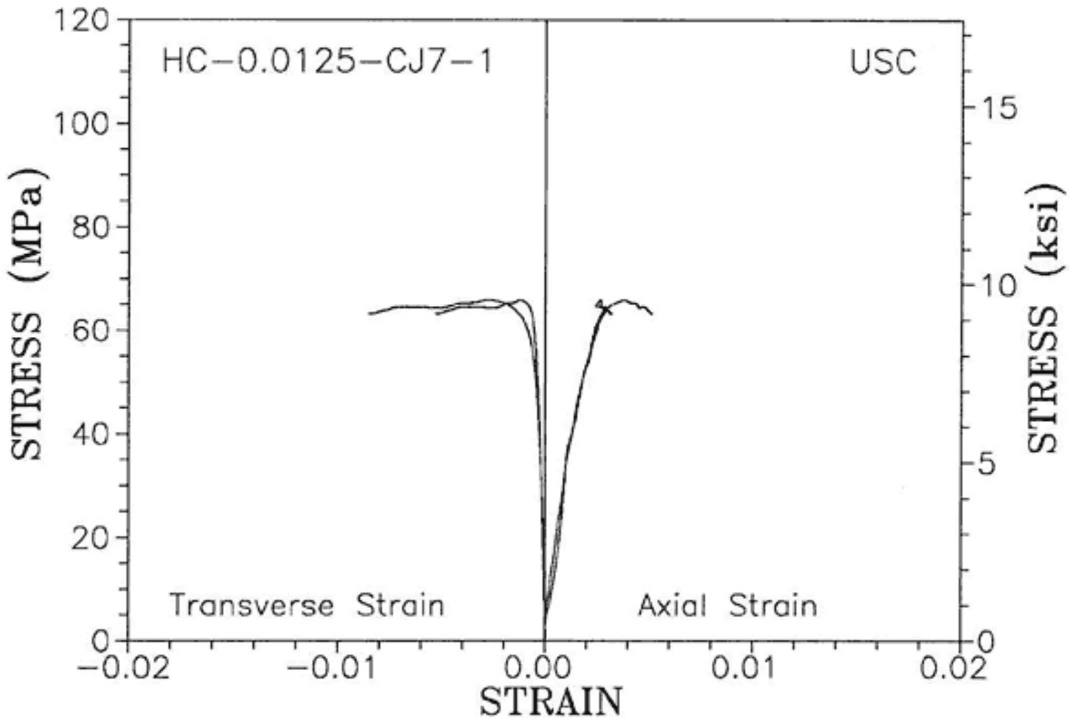

Fig G-D2.Stress-Strain Relationships for Higher Strength Concrete with 0.318mm Thickness Carbon Fiber Composite Jacket (HC-0.0125-CJ7-1)

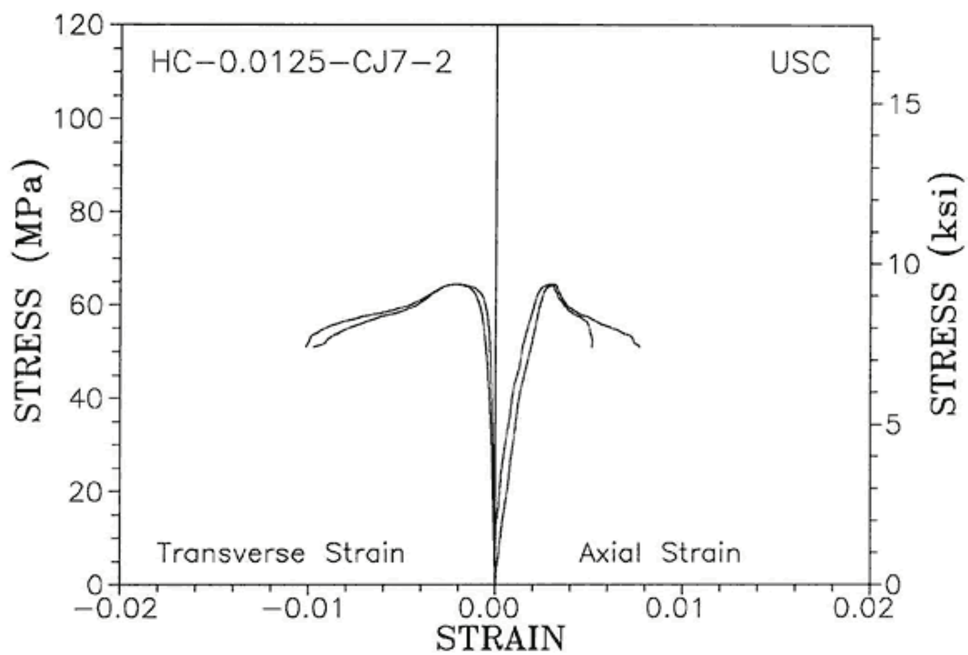

Fig G-D2.Stress-Strain Relationships for Higher Strength Concrete with 0.318mm Thickness Carbon Fiber Composite Jacket (HC-0.0125-CJ7-2)

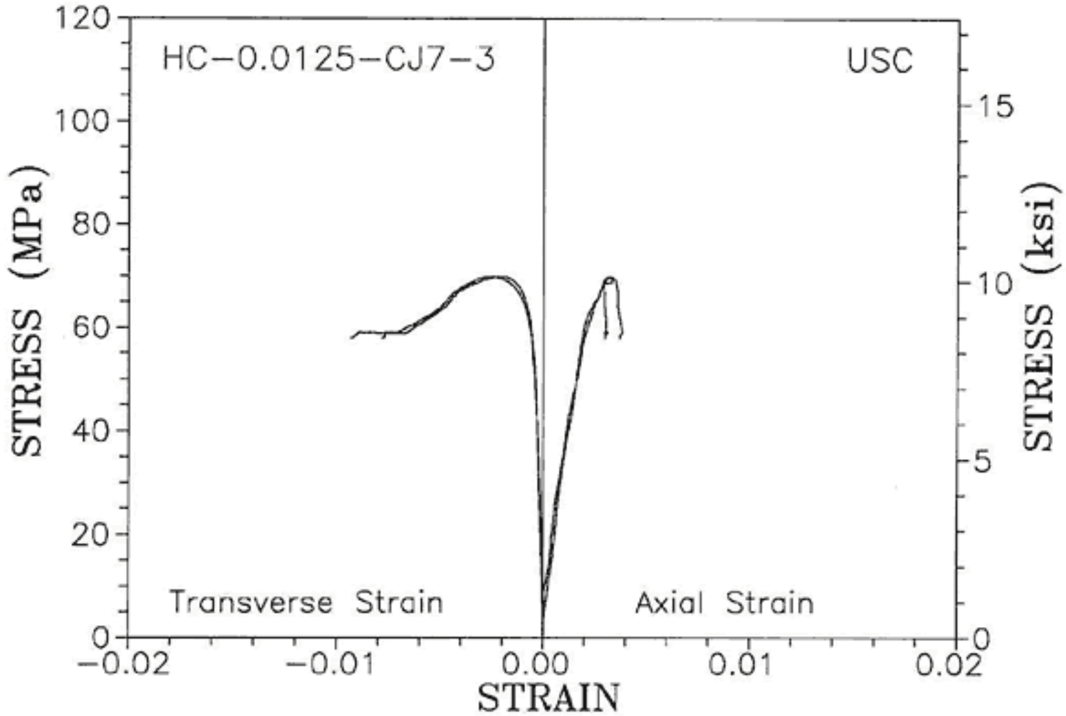

Fig G-D2.Stress-Strain Relationships for Higher Strength Concrete with 0.318mm Thickness Carbon Fiber Composite Jacket (HC-0.0125-CJ7-3)

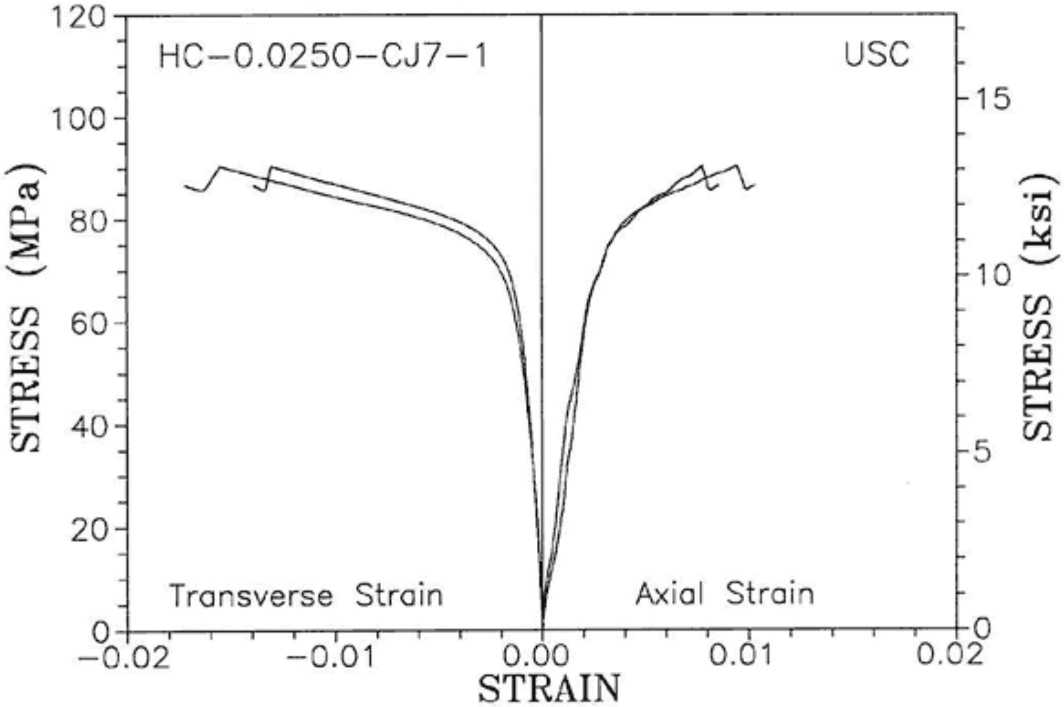

Fig G-D3.Stress-Strain Relationships for Higher Strength Concrete with 0.635mm Thickness Carbon Fiber Composite Jacket (HC-0.025-CJ7-1)

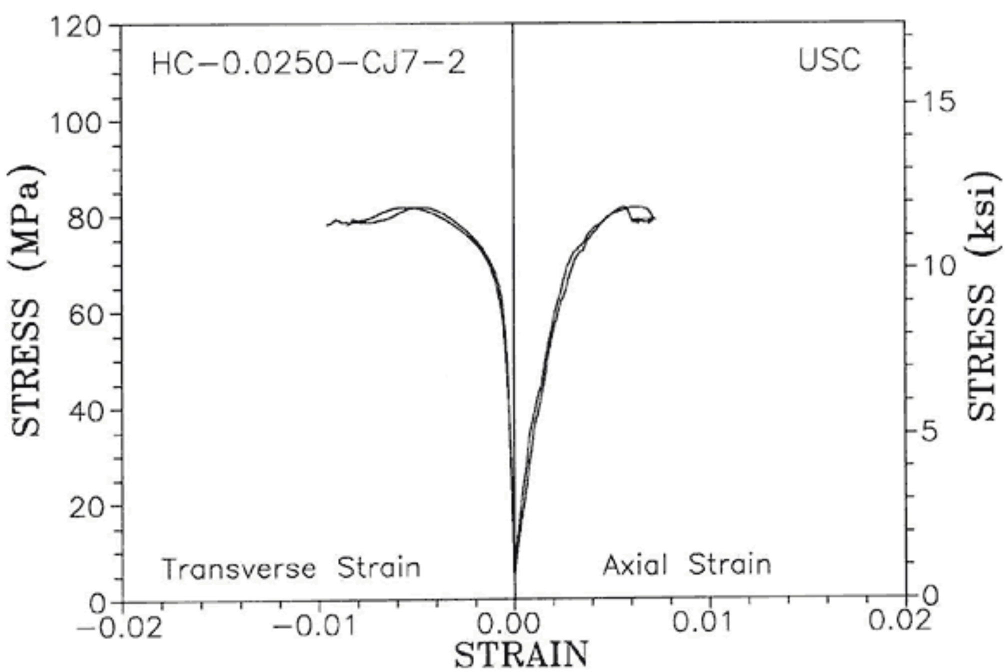

Fig G-D3.Stress-Strain Relationships for Higher Strength Concrete with 0.635mm Thickness Carbon Fiber Composite Jacket (HC-0.025-CJ7-2)

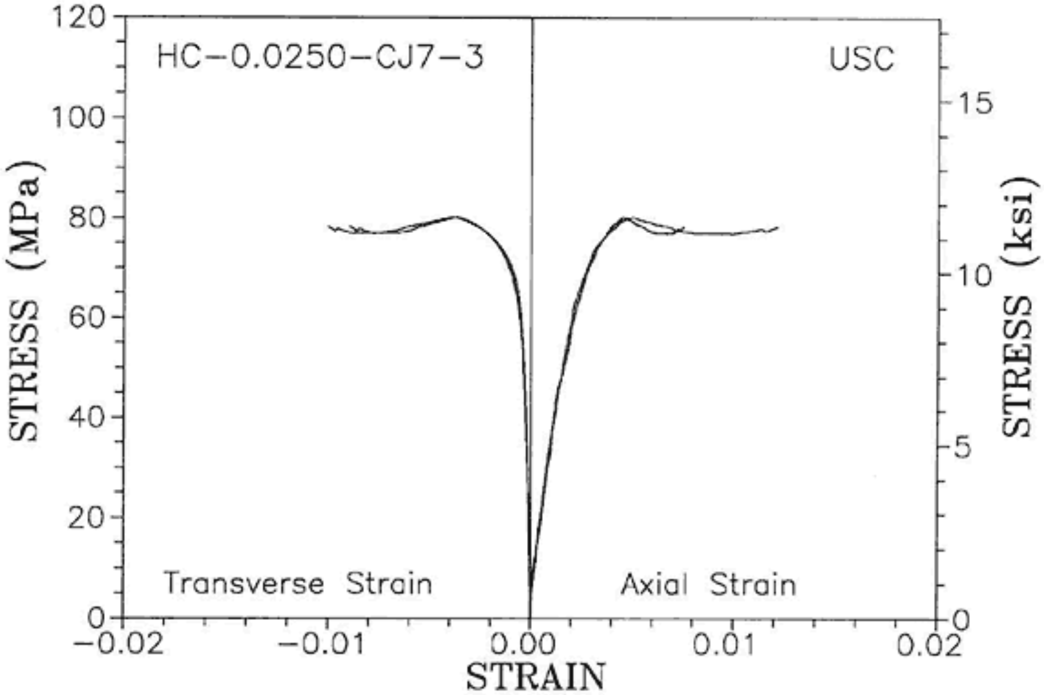

Fig G-D3.Stress-Strain Relationships for Higher Strength Concrete with 0.635mm Thickness Carbon Fiber Composite Jacket (HC-0.025-CJ7-3)

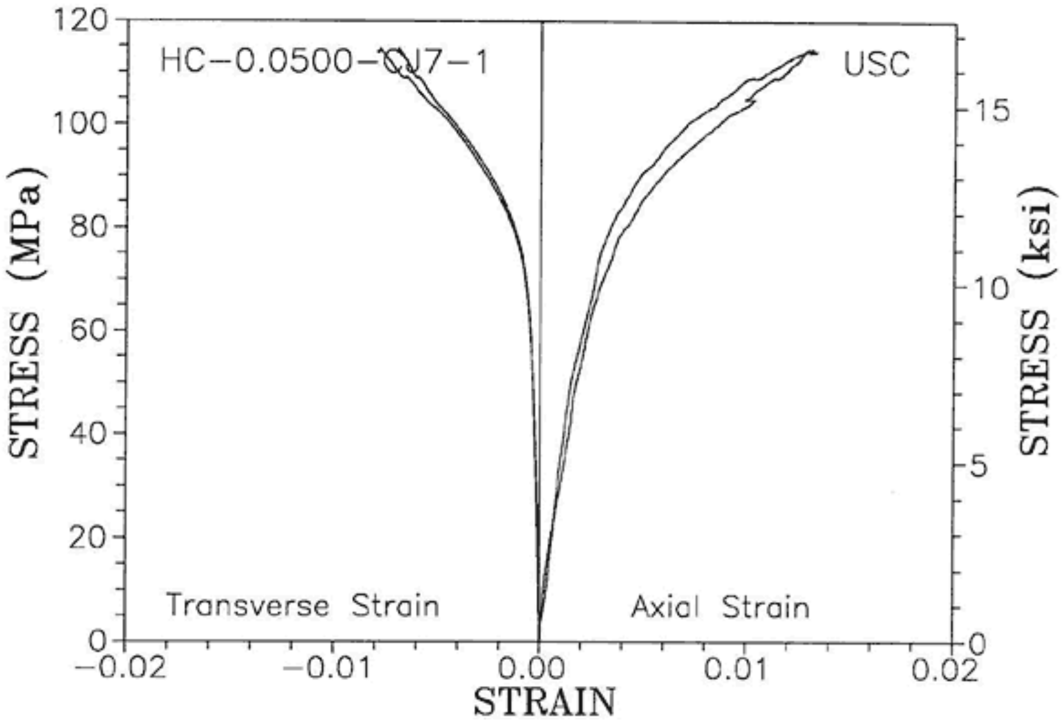

Fig G-D4.Stress-Strain Relationships for Higher Strength Concrete with 1.37mm Thickness Carbon Fiber Composite Jacket (HC-0.0500-CJ7-1)

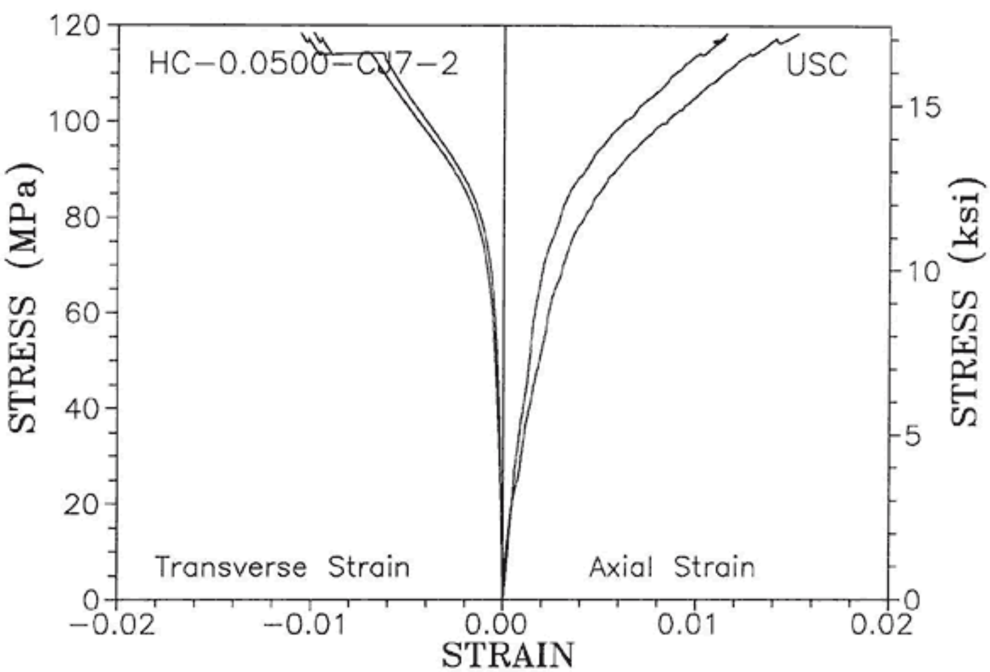

Fig G-D4.Stress-Strain Relationships for Higher Strength Concrete with 1.37mm Thickness Carbon Fiber Composite Jacket (HC-0.0500-CJ7-1)

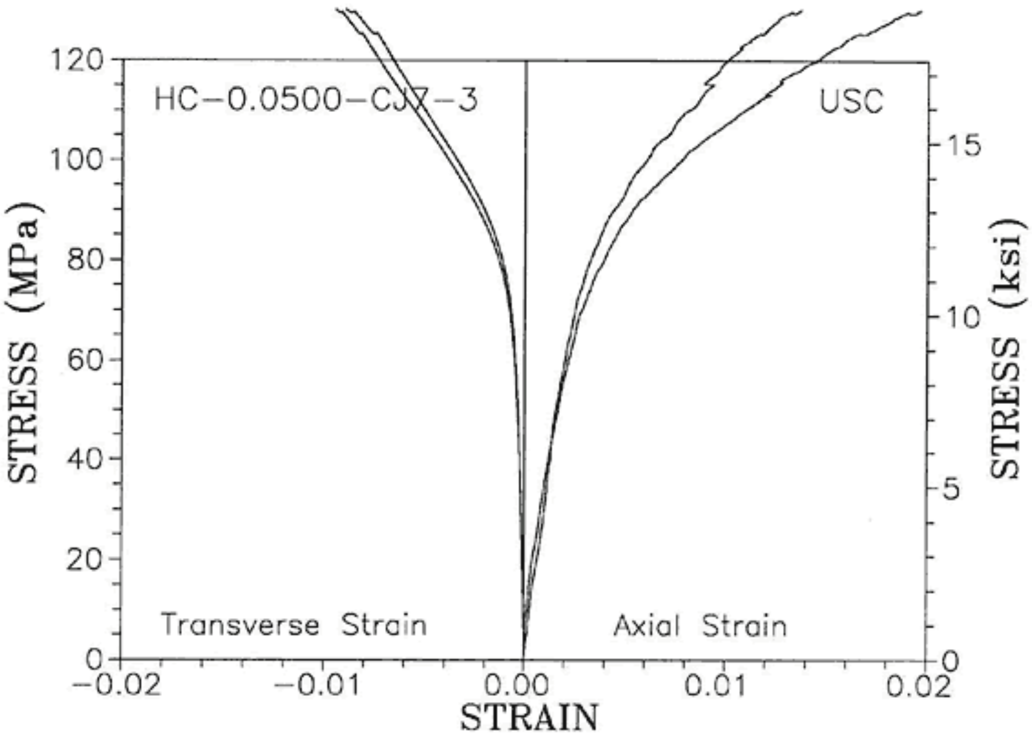

Fig G-D4.Stress-Strain Relationships for Higher Strength Concrete with 1.37mm Thickness Carbon Fiber Composite Jacket (HC-0.0500-CJ7-1)

Fig.G-D5. Specimens after Testing

APPENDIX H: TEST RESULTS OF SYSTEM EIGHT

Part H-A General Information

Table A-A1 Test Results

Series	Specimen	f_c' (MPa)	Jacket Equivalent Thickness (mm)	f_{cc}' (MPa)	ε_{cu}
L	LC-0L-CJ8-1	34.5	0	34.68	0.001569
	LC-0L-CJ8-2			36.03	0.001877
	LC-0L-CJ8-3			32.74	0.001513
	LC-0.0125-CJ8-1		0.318	49.93	0.009149
	LC-0.0125-CJ8-2			41.36	0.005343
	LC-0.0125-CJ8-3			49.33	0.009913
	LC-0.0250-CJ8-1		0.635	63.77	0.014026
	LC-0.0250-CJ8-2			59.85	0.013206
	LC-0.0250-CJ8-3			62.84	0.014535
	LC-0.0500-CJ8-1		1.270	96.05	0.031151
	LC-0.0500-CJ8-2			91.59	0.023993
	LC-0.0500-CJ8-3			76.12	0.022242
M	MC-0L-CJ8-1	48.8	0	46.35	0.002026
	MC-0L-CJ8-2			48.70	0.002102
	MC-0L-CJ8-3			51.32	0.002278
	MC-0.0125-CJ8-1		0.318	46.77	0.002381
	MC-0.0125-CJ8-2			53.58	0.003963
	MC-0.0125-CJ8-3			58.12	0.006554
	MC-0.0250-CJ8-1		0.635	56.51	0.003294
	MC-0.0250-CJ8-2			60.43	0.004222
	MC-0.0250-CJ8-3			75.14	0.009706
	MC-0.0500-CJ8-1		1.270	108.18	0.018290
	MC-0.0500-CJ8-2			105.36	0.020808
	MC-0.0500-CJ8-3			114.63	0.023628
H	HC-0L-CJ8-1	60.2	0	65.13	0.002887
	HC-0L-CJ8-2			53.56	0.001831
	HC-0L-CJ8-3			62.02	0.002569
	HC-0.0125-CJ8-1		0.318	57.45	0.002358
	HC-0.0125-CJ8-2			58.57	0.002767
	HC-0.0125-CJ8-3			57.50	0.002255
	HC-0.0250-CJ8-1		0.635	84.29	0.009113
	HC-0.0250-CJ8-2			67.70	0.004402
	HC-0.0250-CJ8-3			73.32	0.005954
	HC-0.0500-CJ8-1		1.270	124.05	0.013835
	HC-0.0500-CJ8-2			128.62	0.015697
	HC-0.0500-CJ8-3			103.12	0.006560

Note: (i) Example for specimen name designation:
LC-0.0250-CJ8-1: LC designates Lower strength Concrete; 0.0250 designates jacket equivalent thickness in inches; CJ8 designates Carbon fiber Jacket System 8; and the last number represents specimen number in same series.
(ii) f_c': Average plain concrete cylinder strength;
(iii) f_{cc}': Ultimate strength of confined concrete;
(iv) ε_{cu}: Ultimate strain.

Part H-B Test Results of Lower Strength Concrete Cylinders

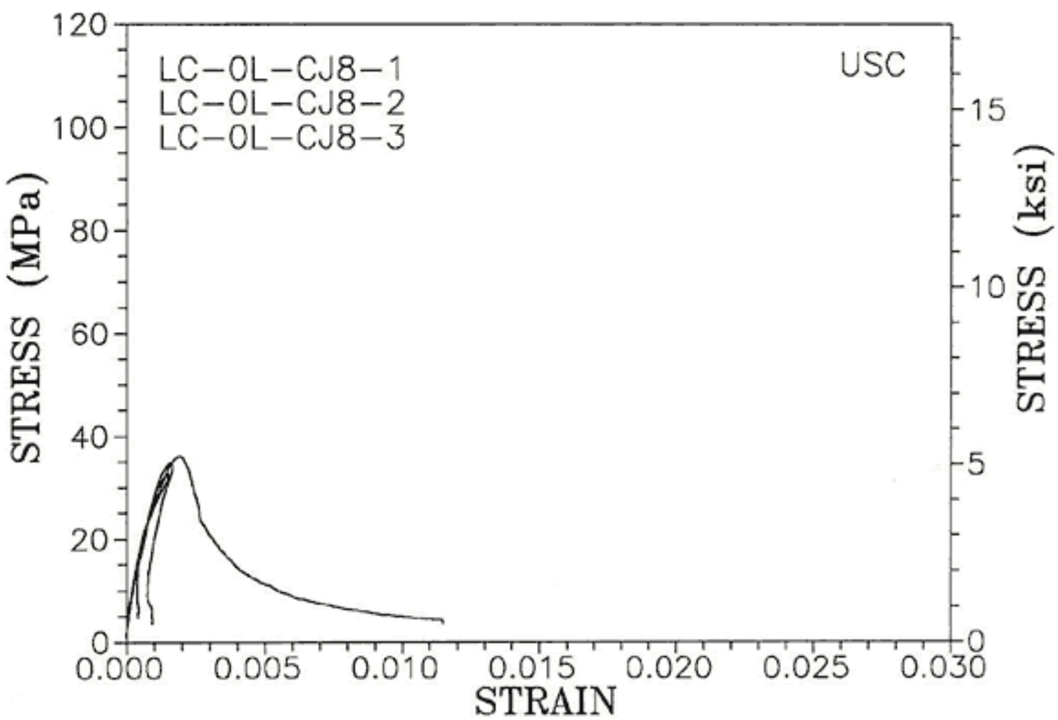

Fig.H-B1. Stress-Strain Relationship for Lower Strength Plain Concrete Cylinders

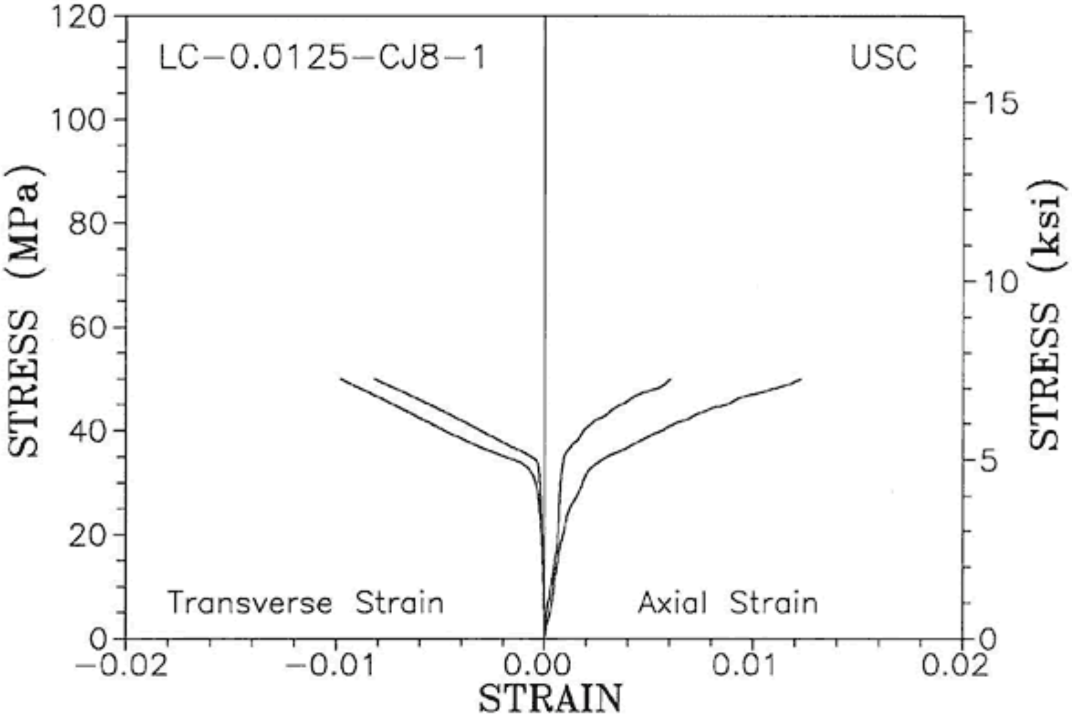

Fig H-B2.Stress-Strain Relationships for Lower Strength Concrete with 0.318mm Thickness Carbon Fiber Composite Jacket (LC-0.0125-CJ8-1)

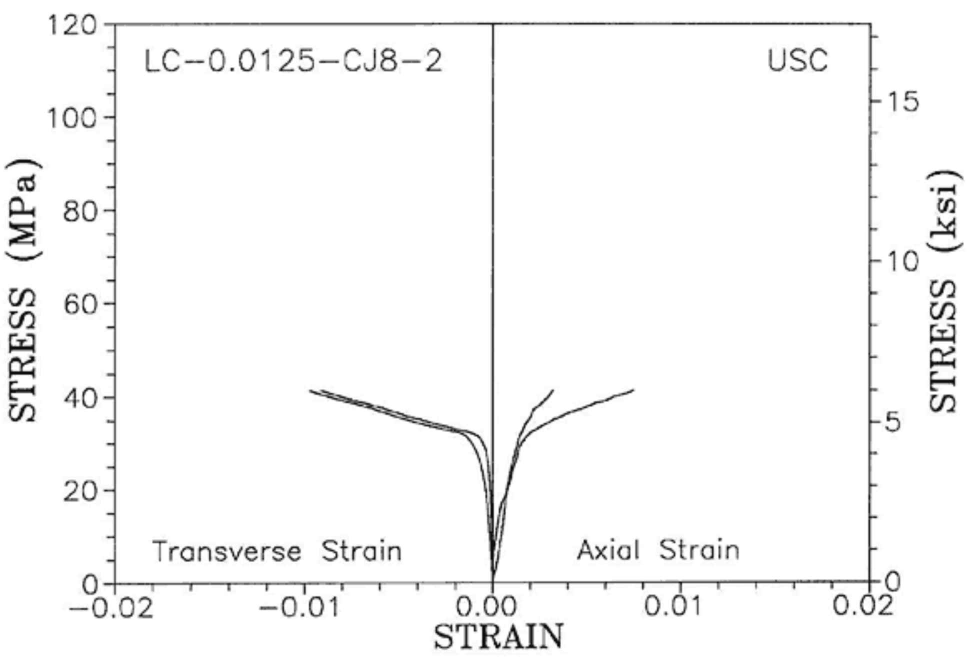

Fig H-B2.Stress-Strain Relationships for Lower Strength Concrete with 0.635mm Thickness Carbon Fiber Composite Jacket (LC-0.025-CJ8-2)

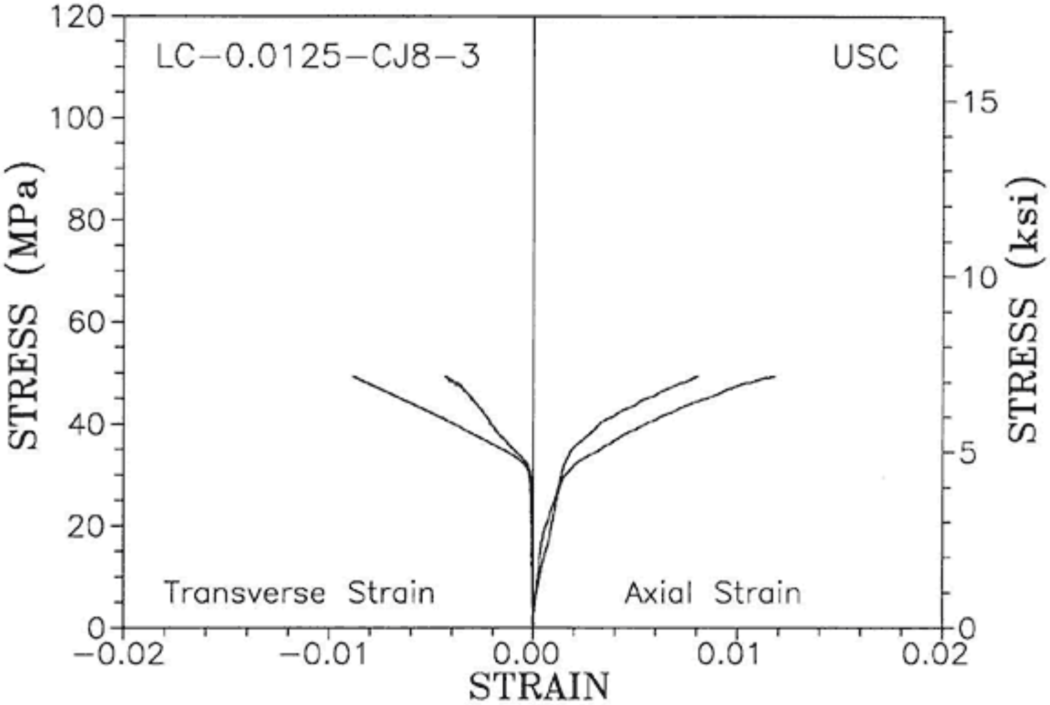

Fig H-B2.Stress-Strain Relationships for Lower Strength Concrete with 0.318mm Thickness Carbon Fiber Composite Jacket (LC-0.0125-CJ8-3)

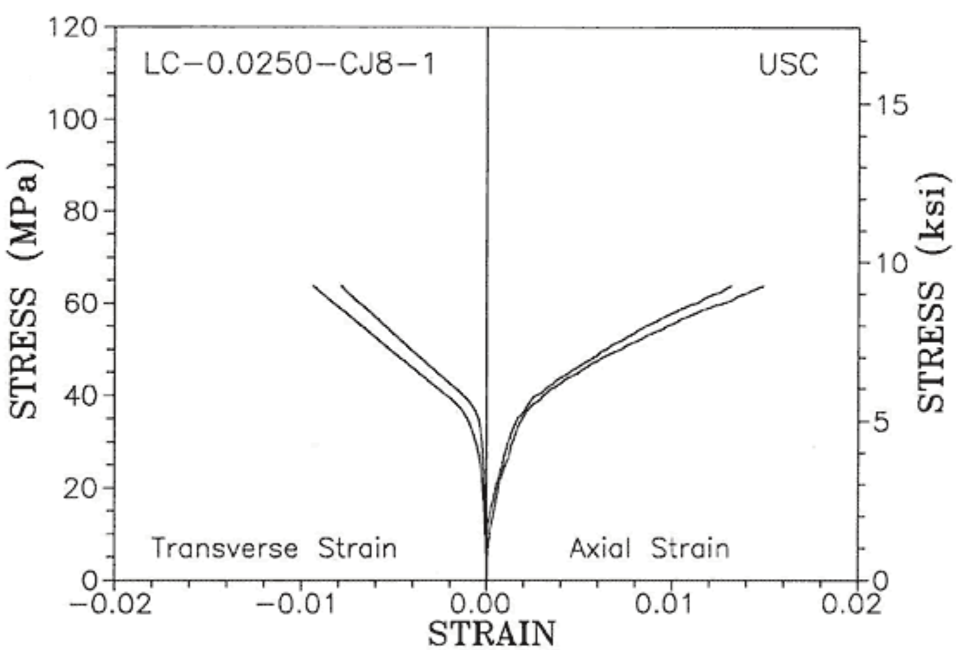

Fig H-B3.Stress-Strain Relationships for Lower Strength Concrete with 0.635mm Thickness Carbon Fiber Composite Jacket (LC-0.025-CJ8-1)

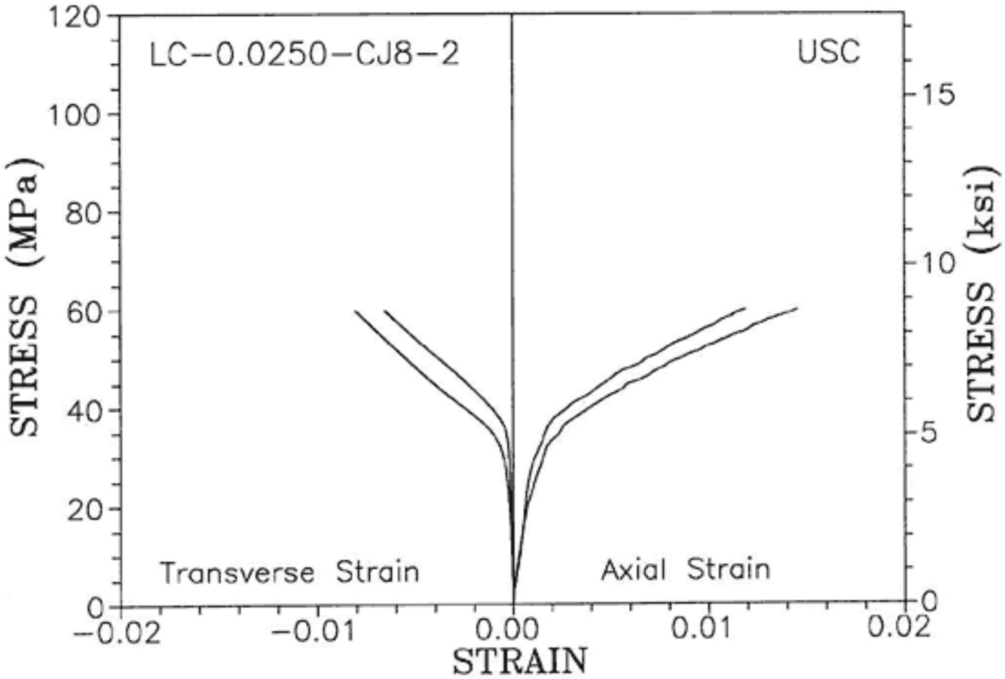

Fig H-B3.Stress-Strain Relationships for Lower Strength Concrete with 0.635mm Thickness Carbon Fiber Composite Jacket (LC-0.025-CJ8-2)

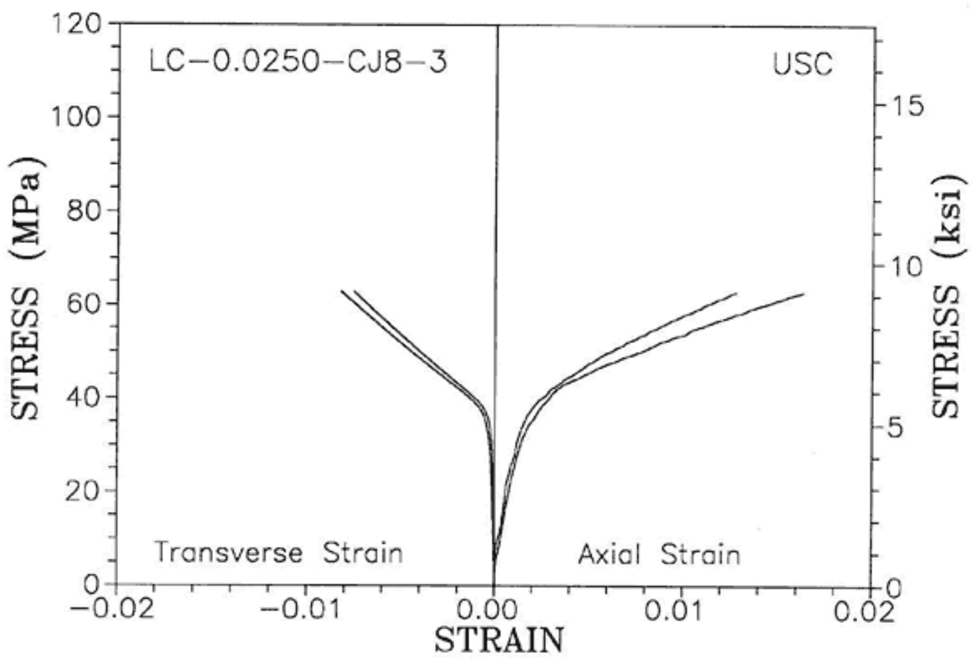

Fig H-B3.Stress-Strain Relationships for Lower Strength Concrete with 0.635mm Thickness Carbon Fiber Composite Jacket (LC-0.025-CJ8-3)

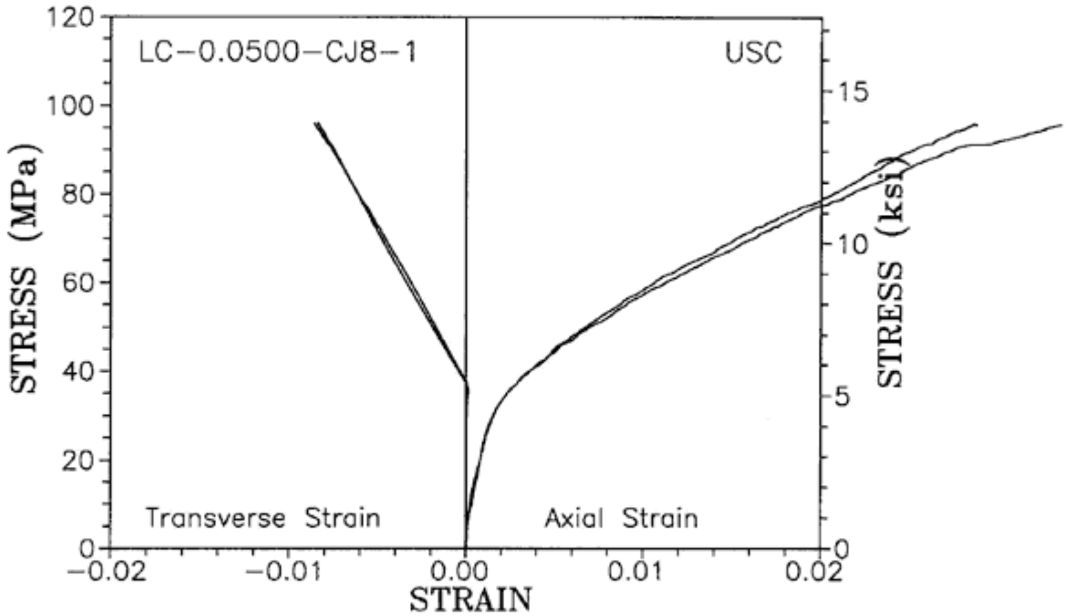

Fig H-B4.Stress-Strain Relationships for Lower Strength Concrete with 1.27mm Thickness Carbon Fiber Composite Jacket (LC-0.05-CJ8-1)

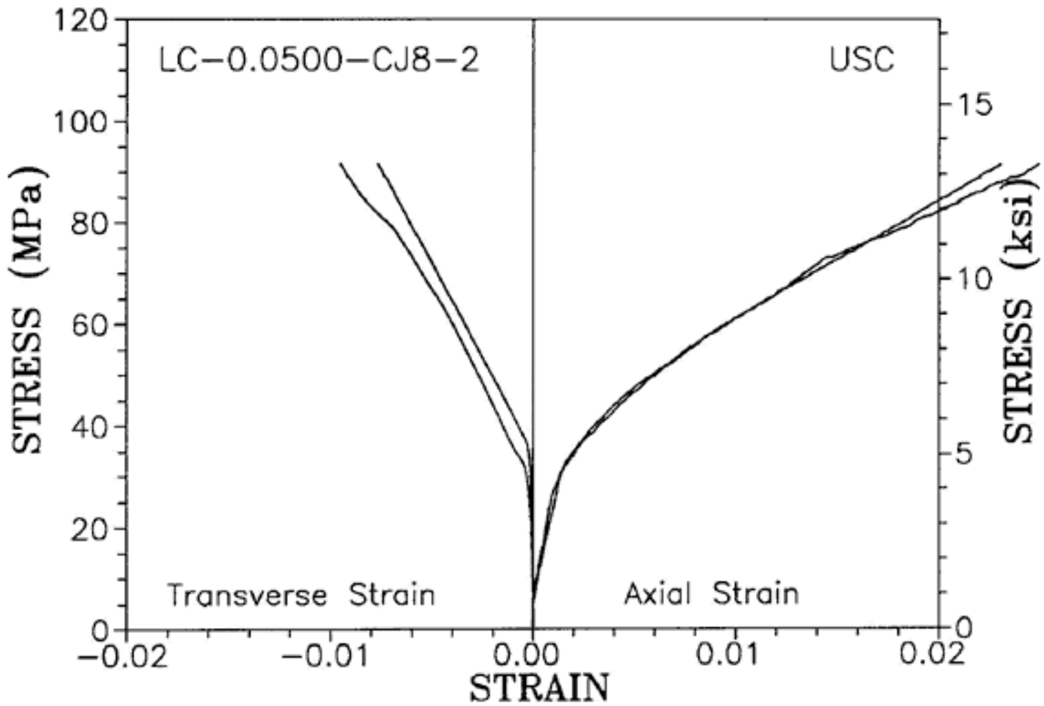

Fig H-B4.Stress-Strain Relationships for Lower Strength Concrete with 1.27mm Thickness Carbon Fiber Composite Jacket (LC-0.05-CJ8-2)

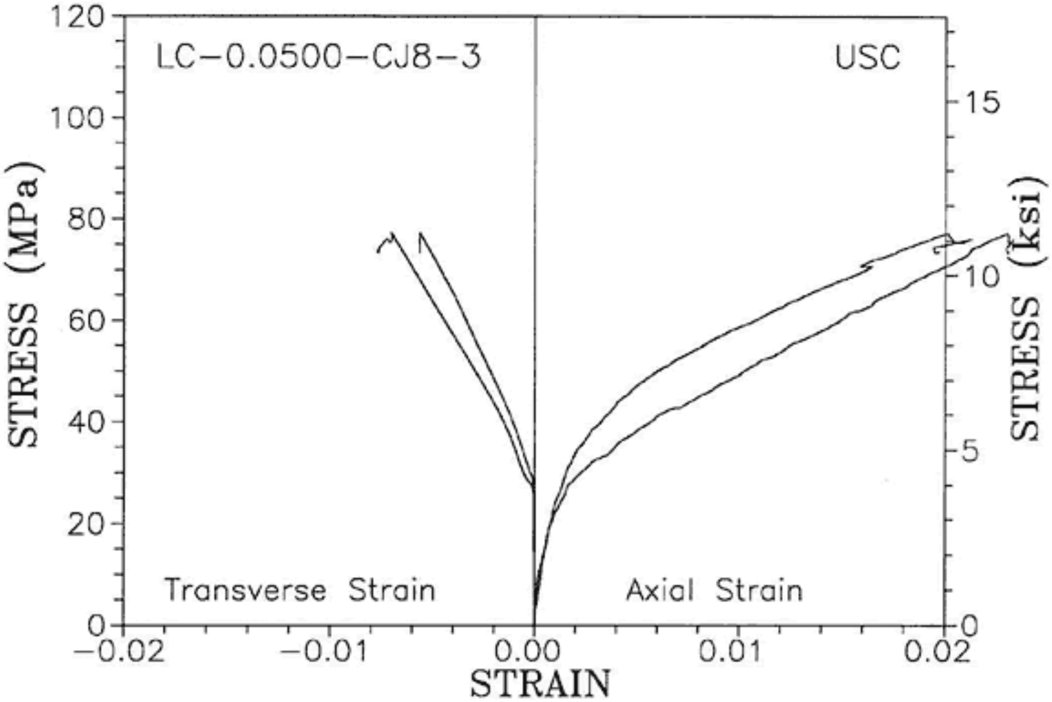

Fig H-B4.Stress-Strain Relationships for Lower Strength Concrete with 1.27mm Thickness Carbon Fiber Composite Jacket (LC-0.05-CJ8-3)

Fig.H-B5. Specimens after Testing

Part H-C Test Results of Medium Strength Concrete Cylinders

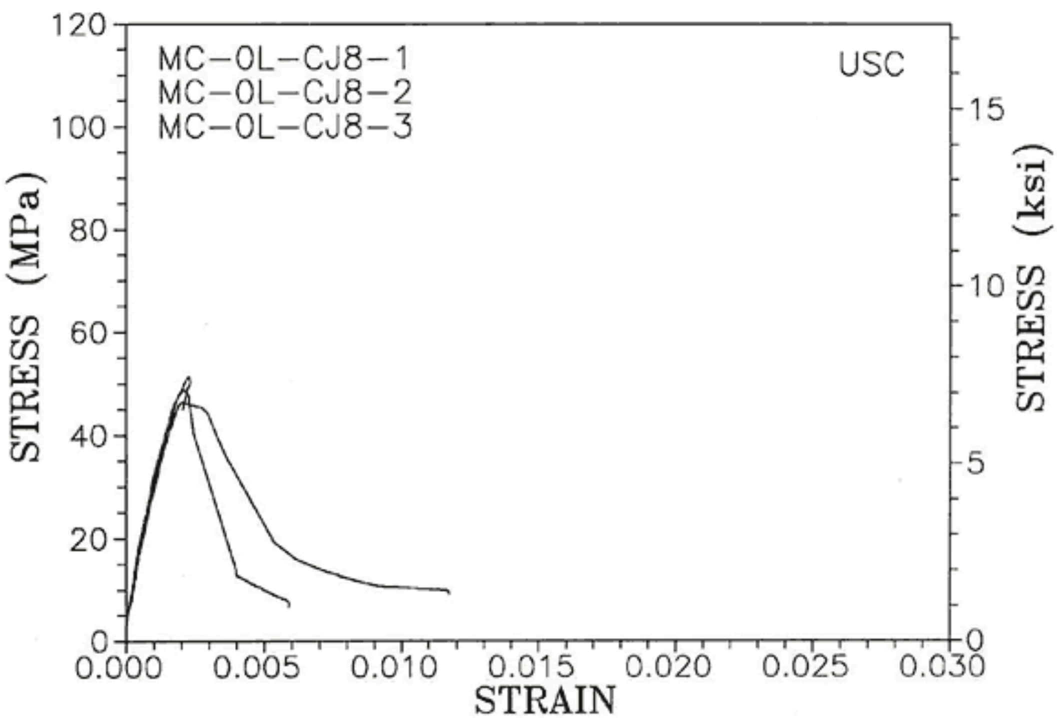

Fig.H-C1. Stress-Strain Relationship for Medium Strength Plain Concrete Cylinders

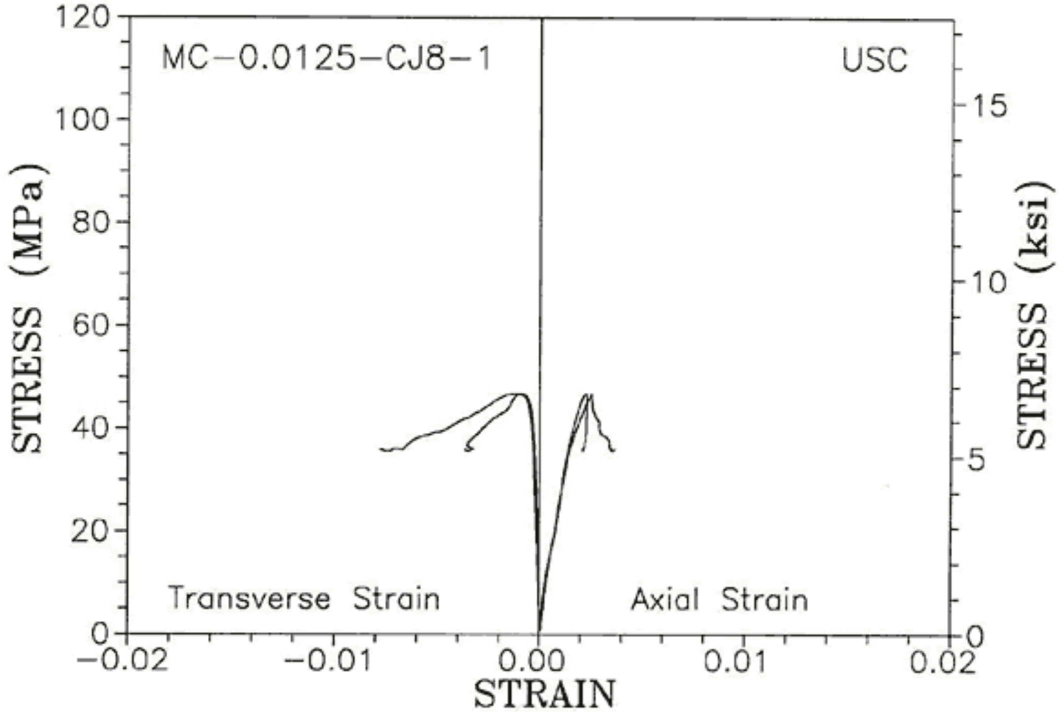

Fig H-C2.Stress-Strain Relationships for Medium Strength Concrete with 0.318mm Thickness Carbon Fiber Composite Jacket (MC-0.0125-CJ78-1)

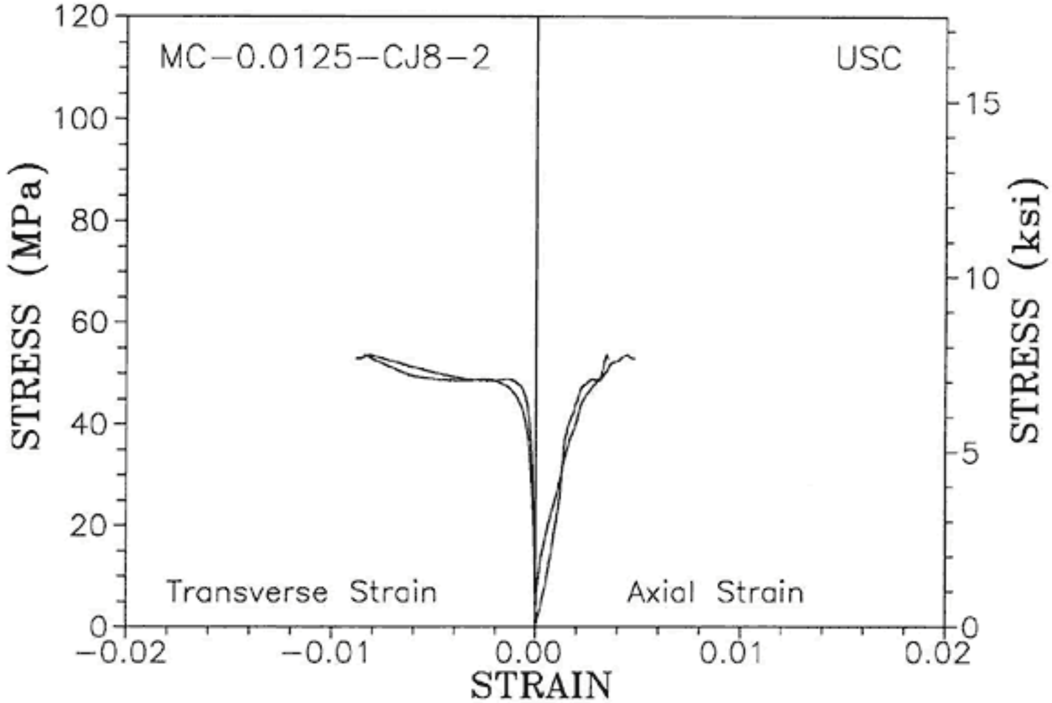

Fig H-C2.Stress-Strain Relationships for Medium Strength Concrete with 0.318mm Thickness Carbon Fiber Composite Jacket (MC-0.0125-CJ78-2)

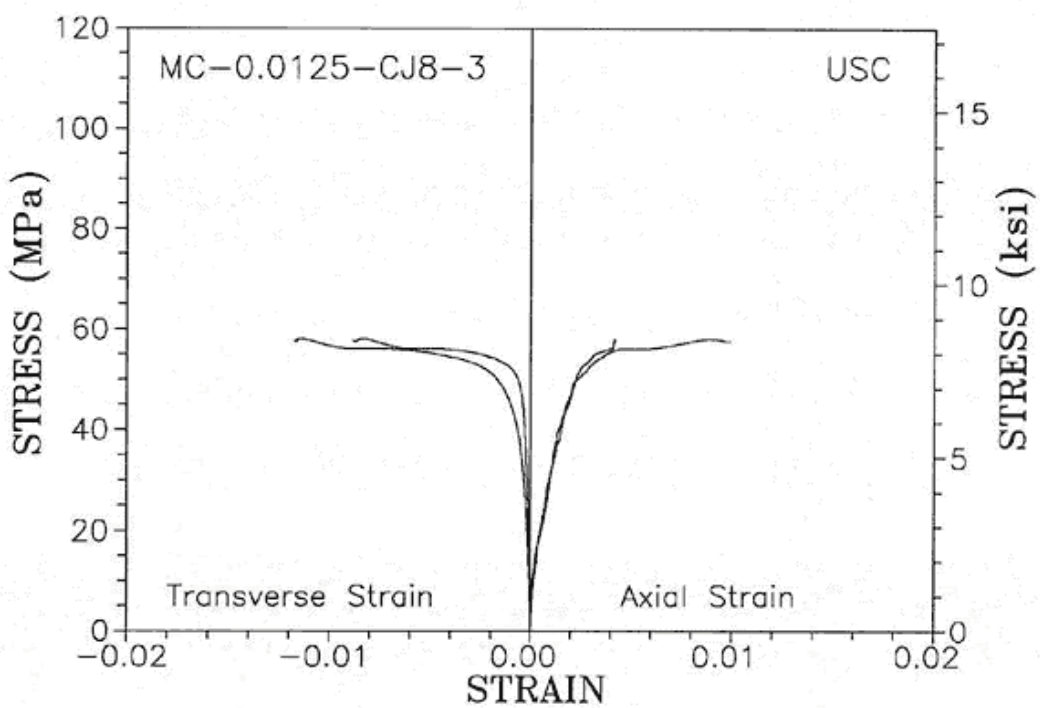

Fig H-C2.Stress-Strain Relationships for Medium Strength Concrete with 0.318mm Thickness Carbon Fiber Composite Jacket (MC-0.0125-CJ78-3)

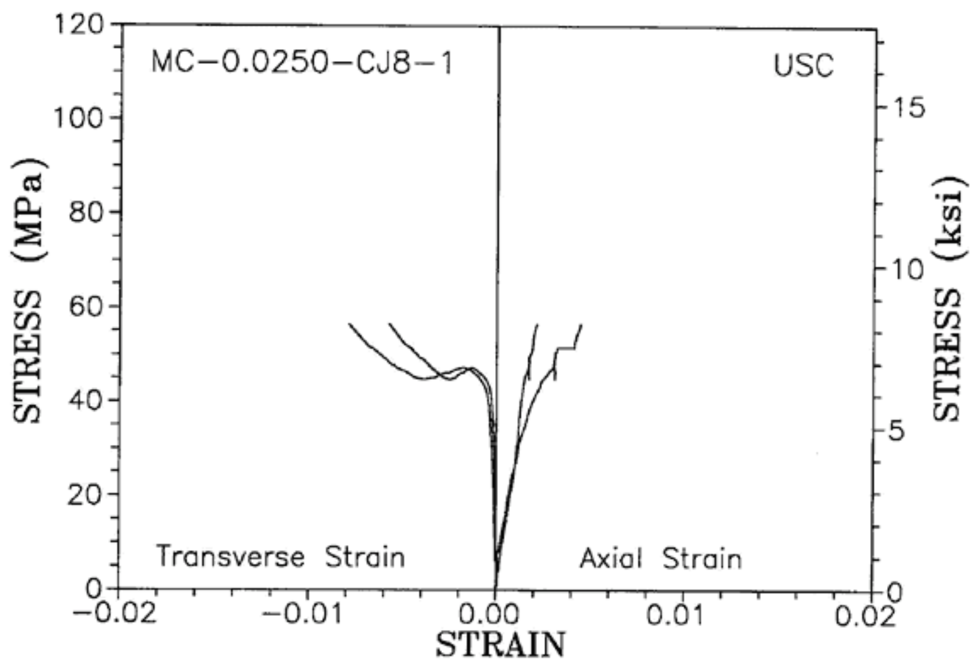

Fig H-C3.Stress-Strain Relationships for Medium Strength Concrete with 0.635mm Thickness Carbon Fiber Composite Jacket (MC-0.025-CJ78-1)

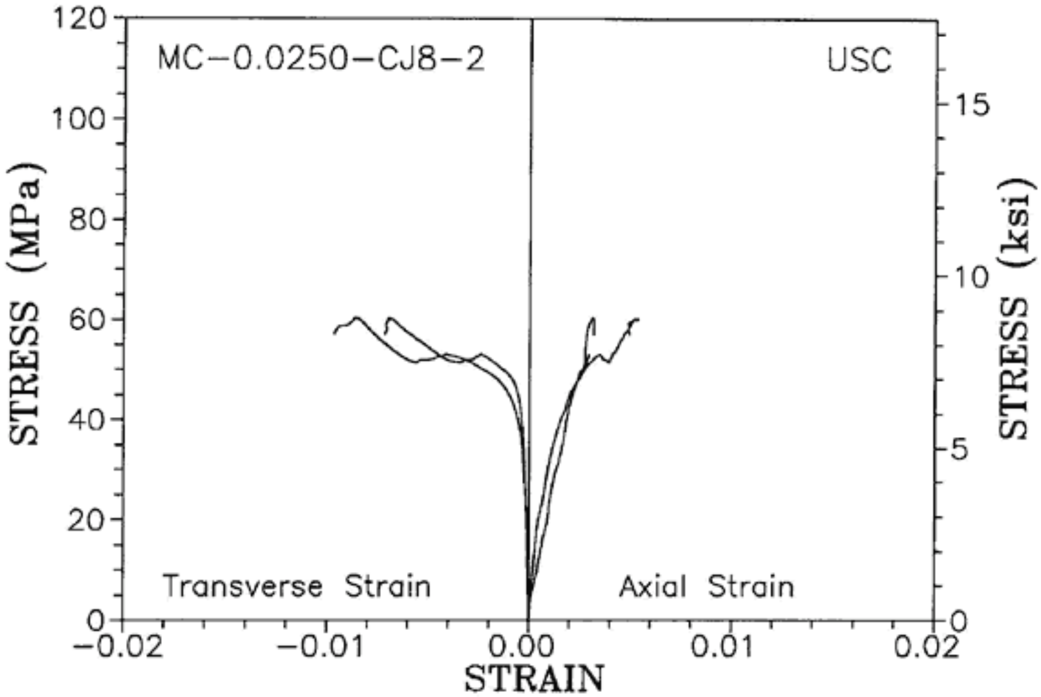

Fig H-C3.Stress-Strain Relationships for Medium Strength Concrete with 0.635mm Thickness Carbon Fiber Composite Jacket (MC-0.025-CJ78-2)

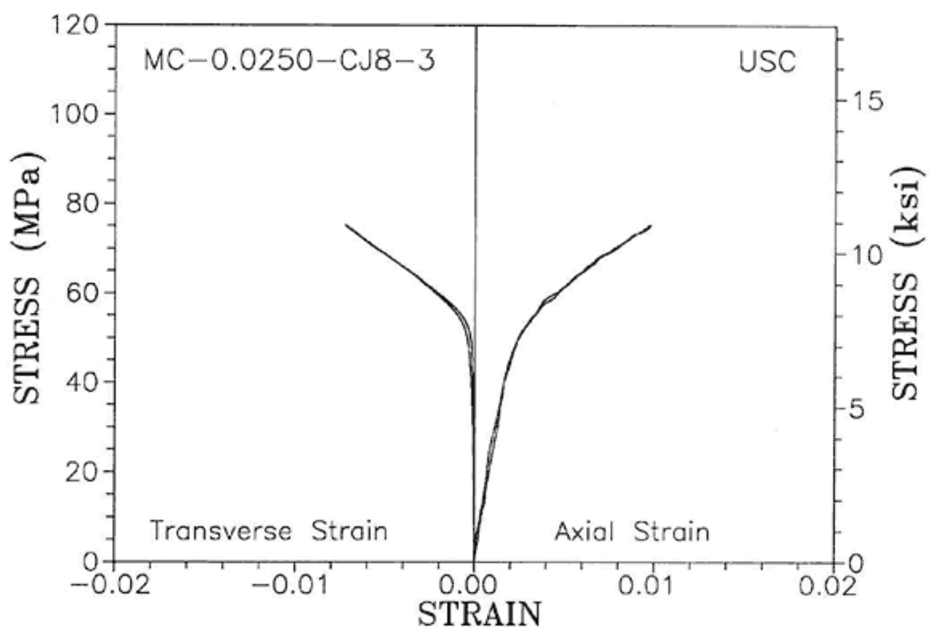

Fig H-C3.Stress-Strain Relationships for Medium Strength Concrete with 0.635mm Thickness Carbon Fiber Composite Jacket (MC-0.025-CJ78-3)

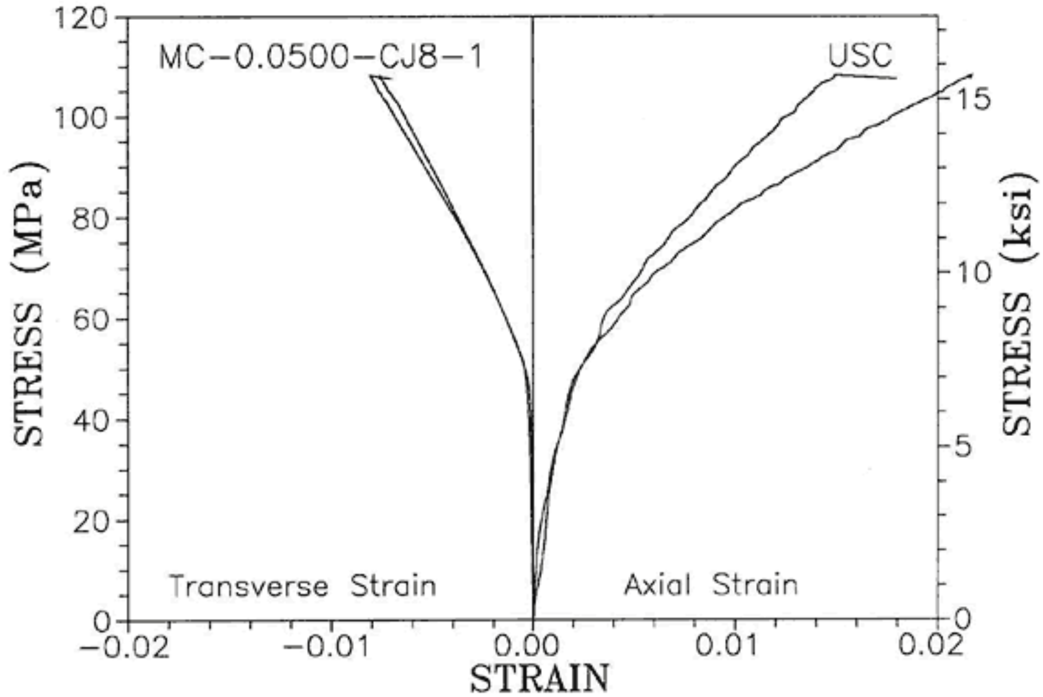

Fig H-C4.Stress-Strain Relationships for Medium Strength Concrete with 1.27mm Thickness Carbon Fiber Composite Jacket (MC-0.05-CJ78-1)

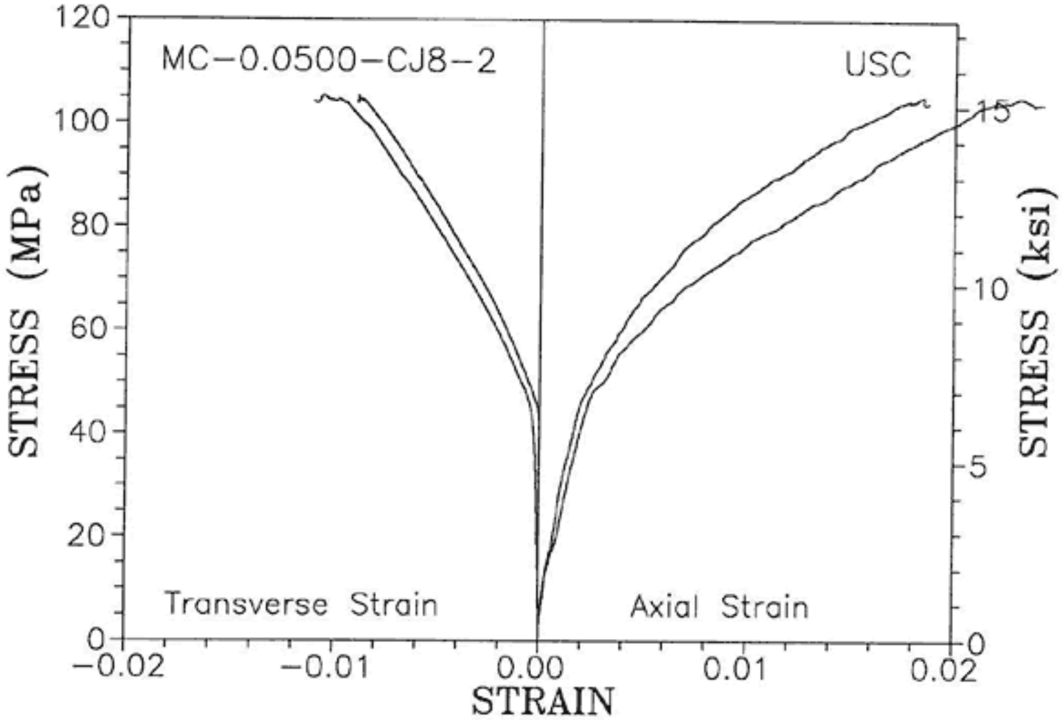

Fig H-C4.Stress-Strain Relationships for Medium Strength Concrete with 1.27mm Thickness Carbon Fiber Composite Jacket (MC-0.05-CJ78-2)

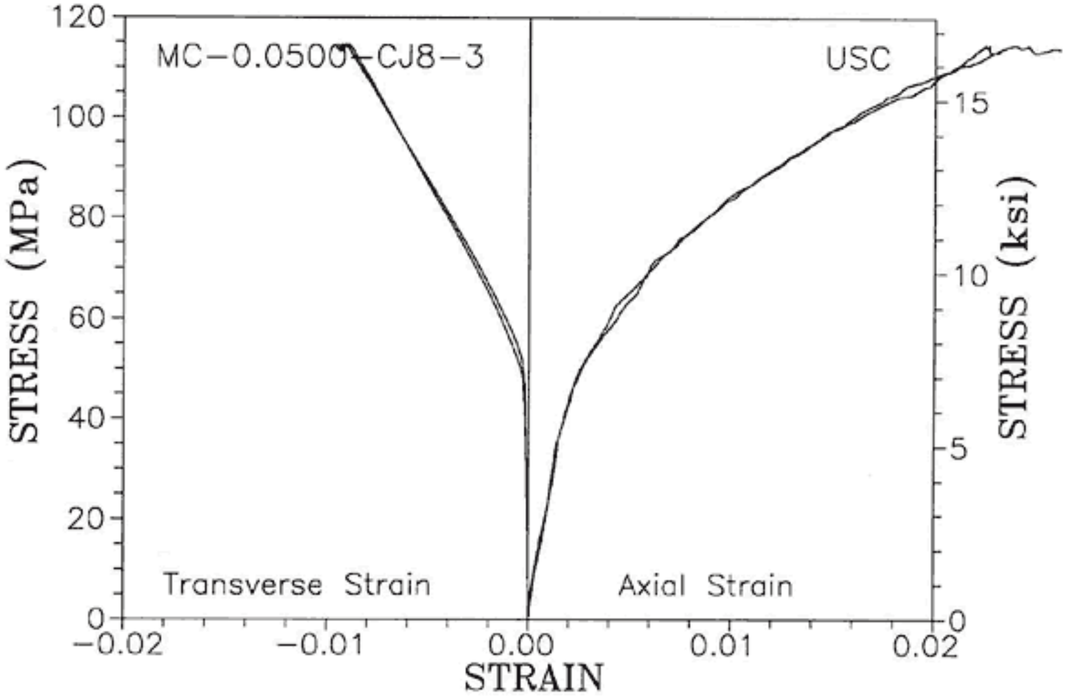

Fig H-C4.Stress-Strain Relationships for Medium Strength Concrete with 1.27mm Thickness Carbon Fiber Composite Jacket (MC-0.05-CJ78-3)

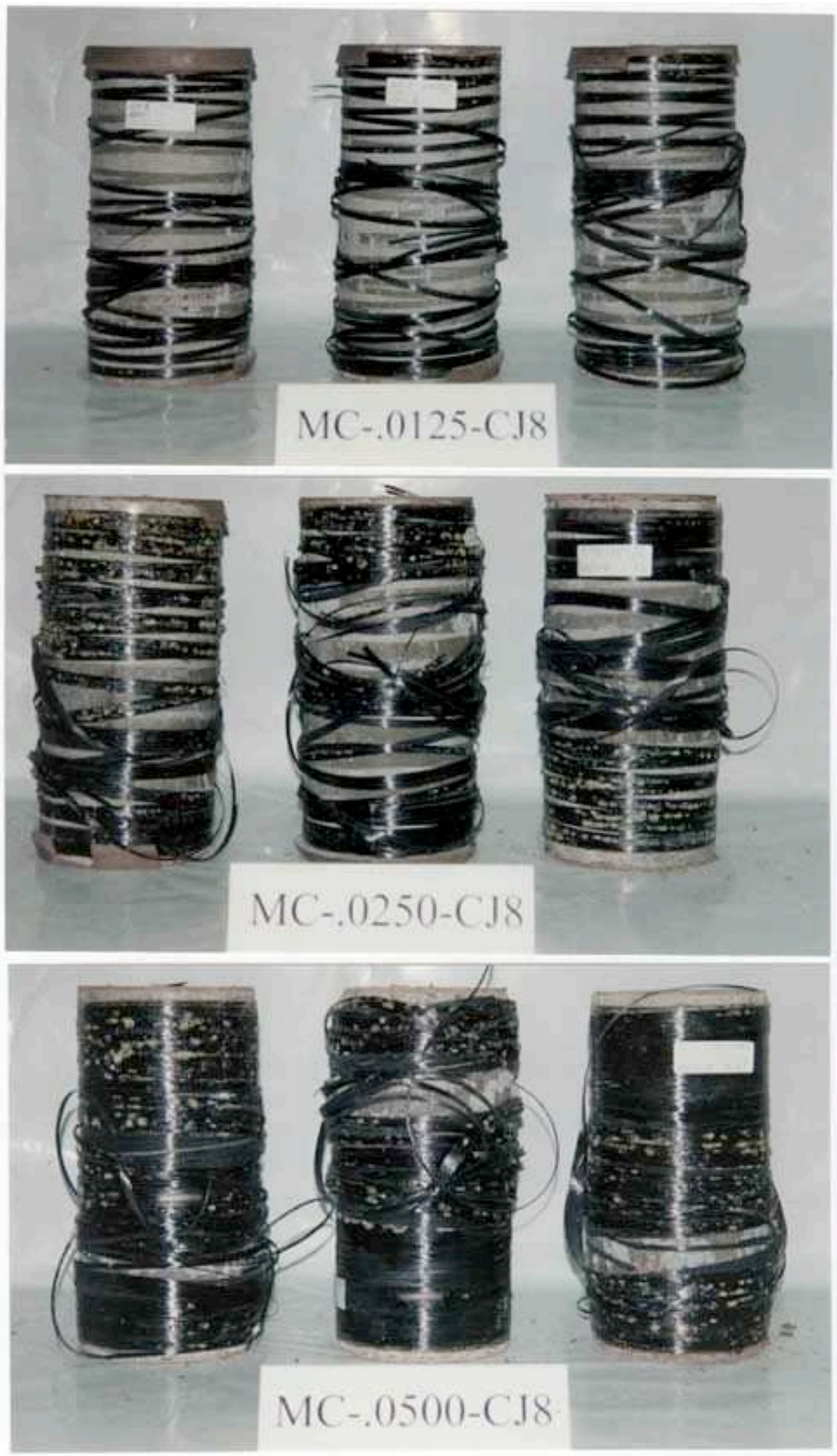

Fig.H-C5. Specimens after Testing

Part H-D Test Results of Higher Strength Concrete Cylinders

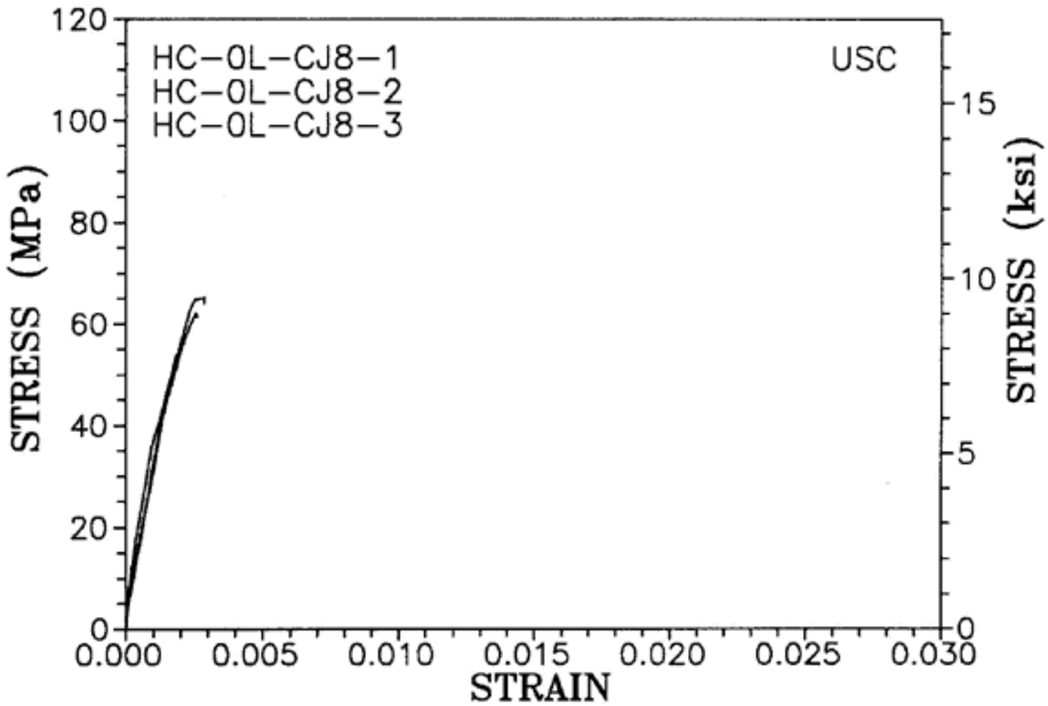

Fig.H-D1. Stress-Strain Relationships for Higher Strength Plain Concrete Cylinders

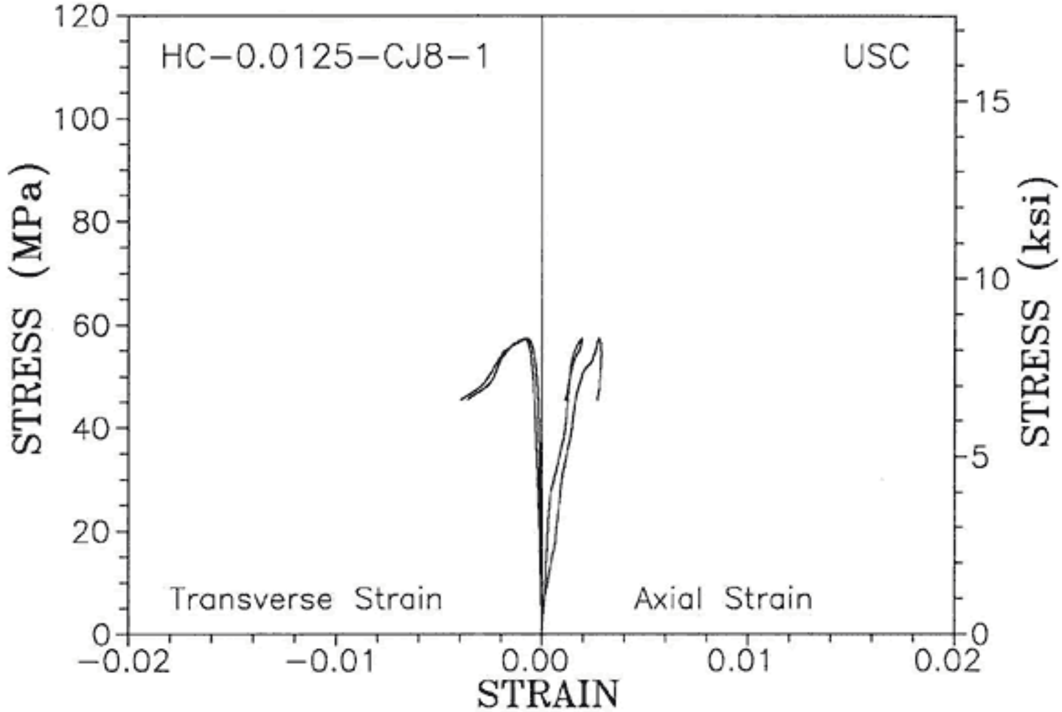

Fig H-D2.Stress-Strain Relationships for Higher Strength Concrete with 0.318mm Thickness Carbon Fiber Composite Jacket (HC-0.0125-CJ8-1)

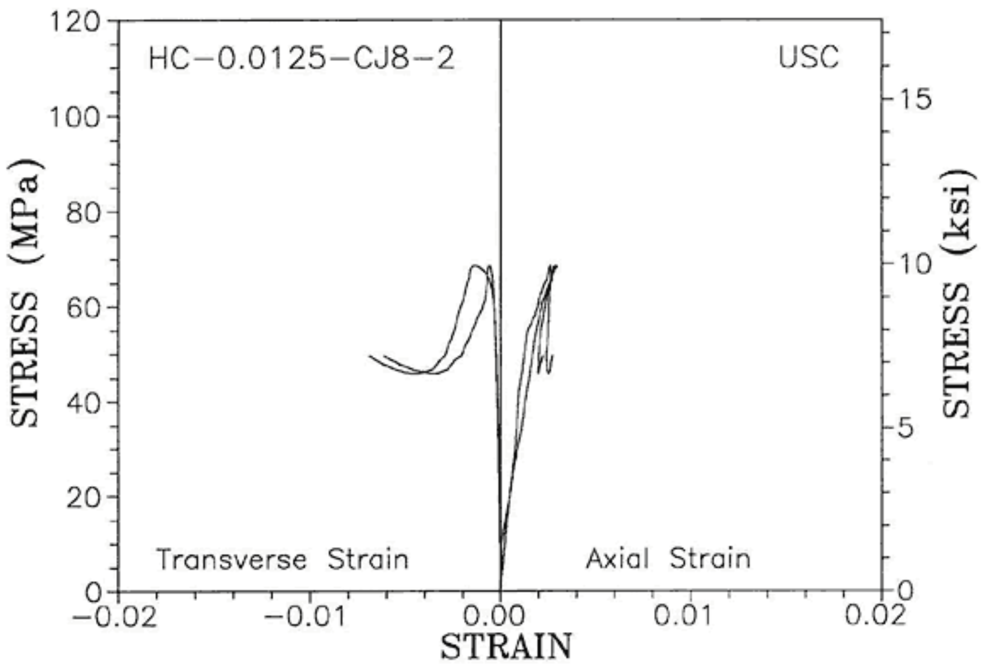

Fig H-D2.Stress-Strain Relationships for Higher Strength Concrete with 0.318mm Thickness Carbon Fiber Composite Jacket (HC-0.0125-CJ8-2)

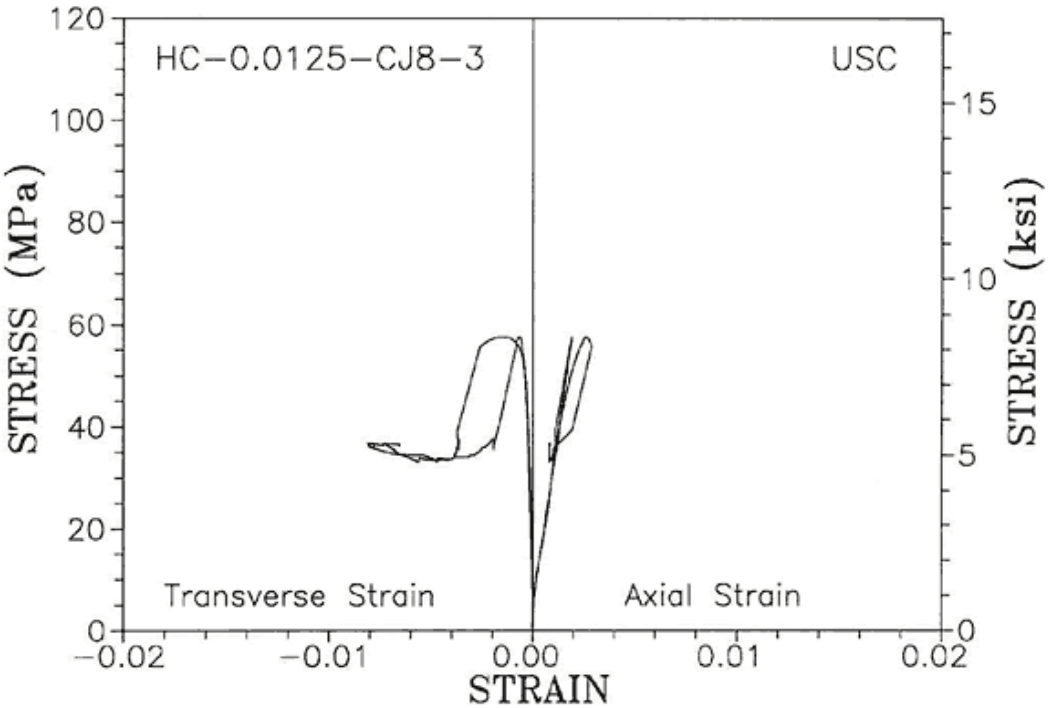

Fig H-D2.Stress-Strain Relationships for Higher Strength Concrete with 0.318mm Thickness Carbon Fiber Composite Jacket (HC-0.0125-CJ8-3)

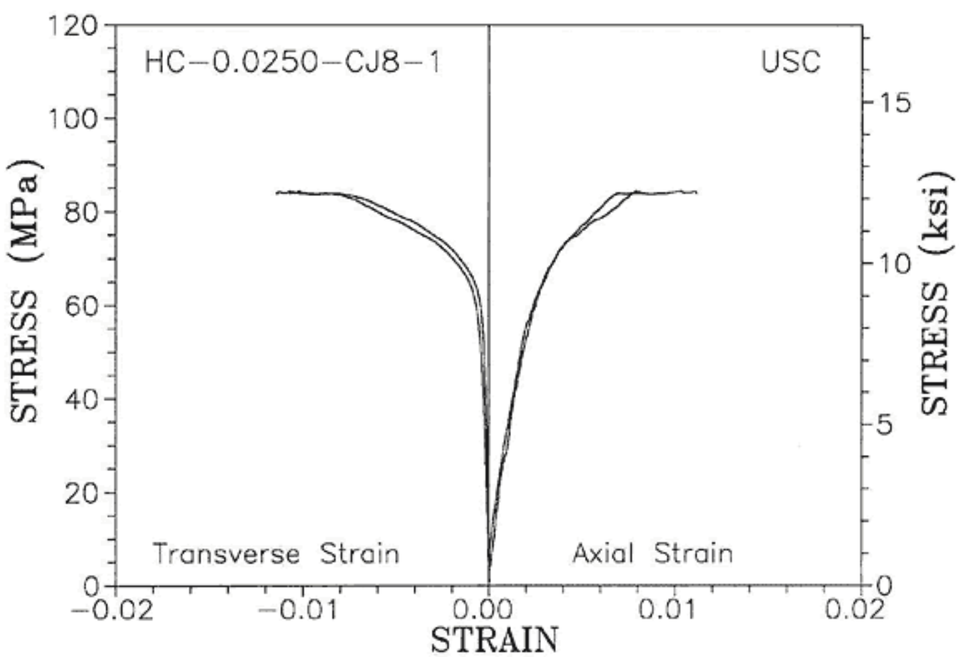

Fig G-D3.Stress-Strain Relationships for Higher Strength Concrete with 0.635mm Thickness Carbon Fiber Composite Jacket (HC-0.025-CJ8-1)

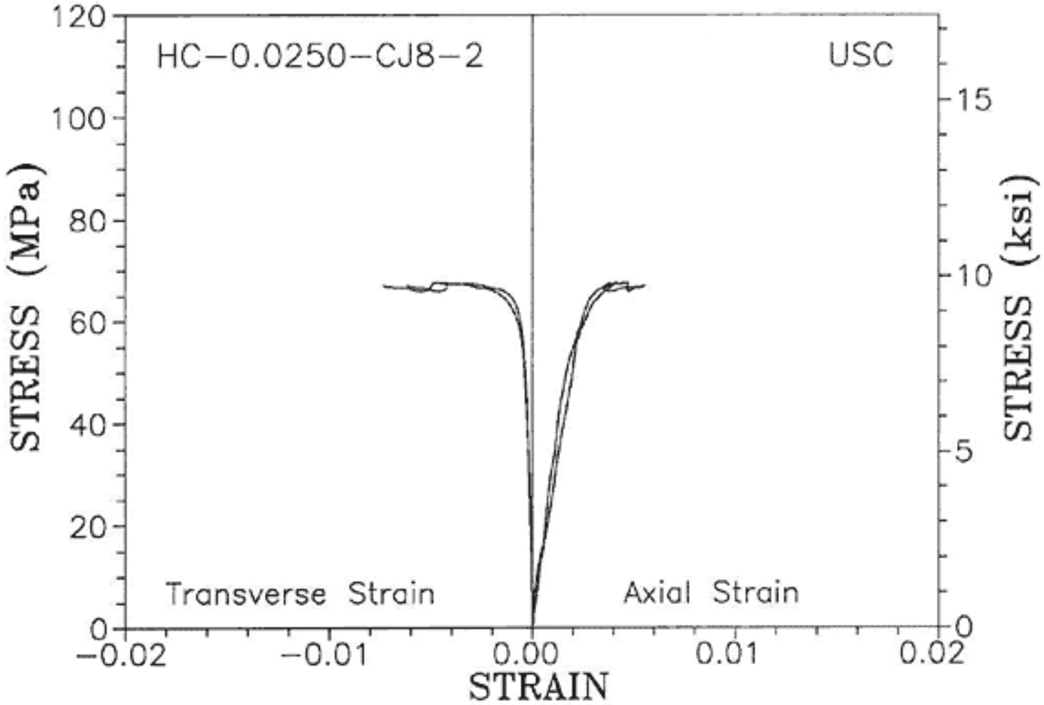

Fig H-D3.Stress-Strain Relationships for Higher Strength Concrete with 0.635mm Thickness Carbon Fiber Composite Jacket (HC-0.025-CJ8-2)

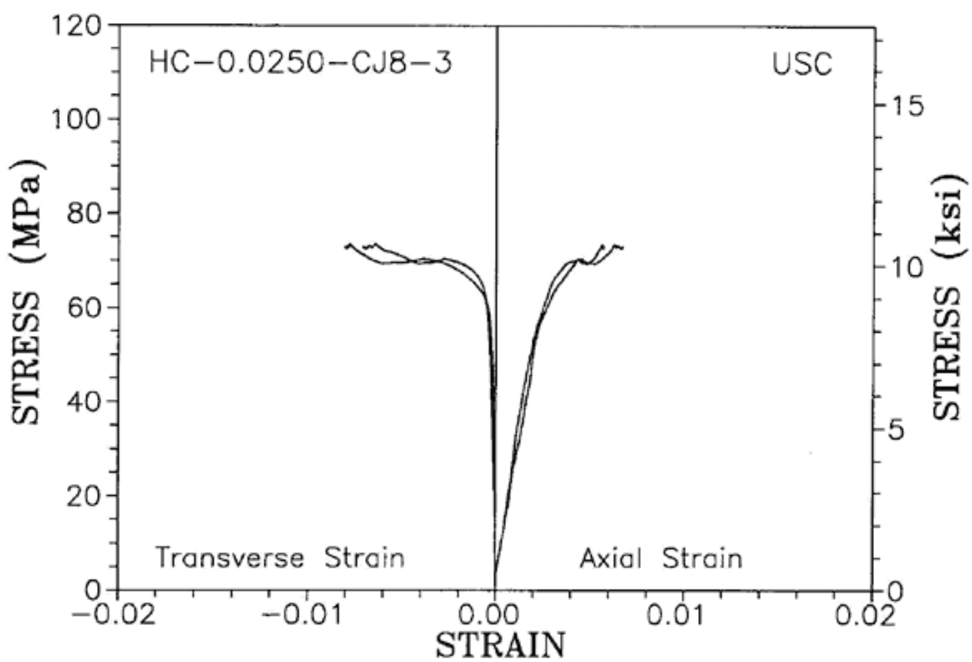

Fig H-D3.Stress-Strain Relationships for Higher Strength Concrete with 0.635mm Thickness Carbon Fiber Composite Jacket (HC-0.025-CJ8-3)

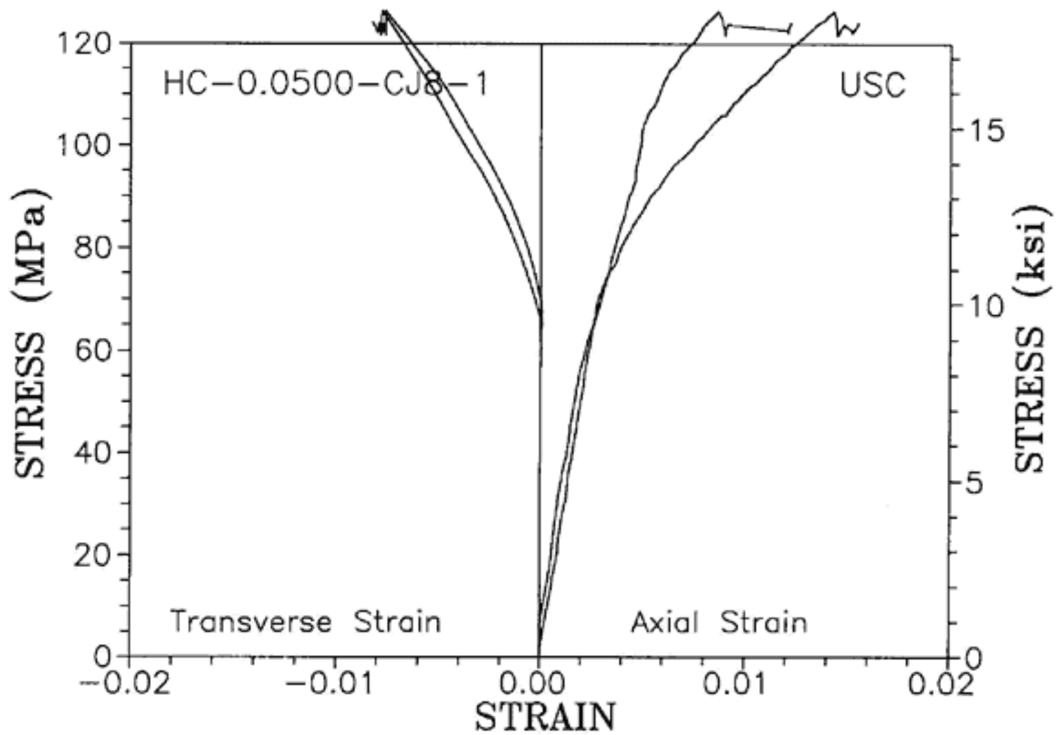

Fig H-D4.Stress-Strain Relationships for Higher Strength Concrete with 1.27mm Thickness Carbon Fiber Composite Jacket (HC-0.05-CJ8-1)

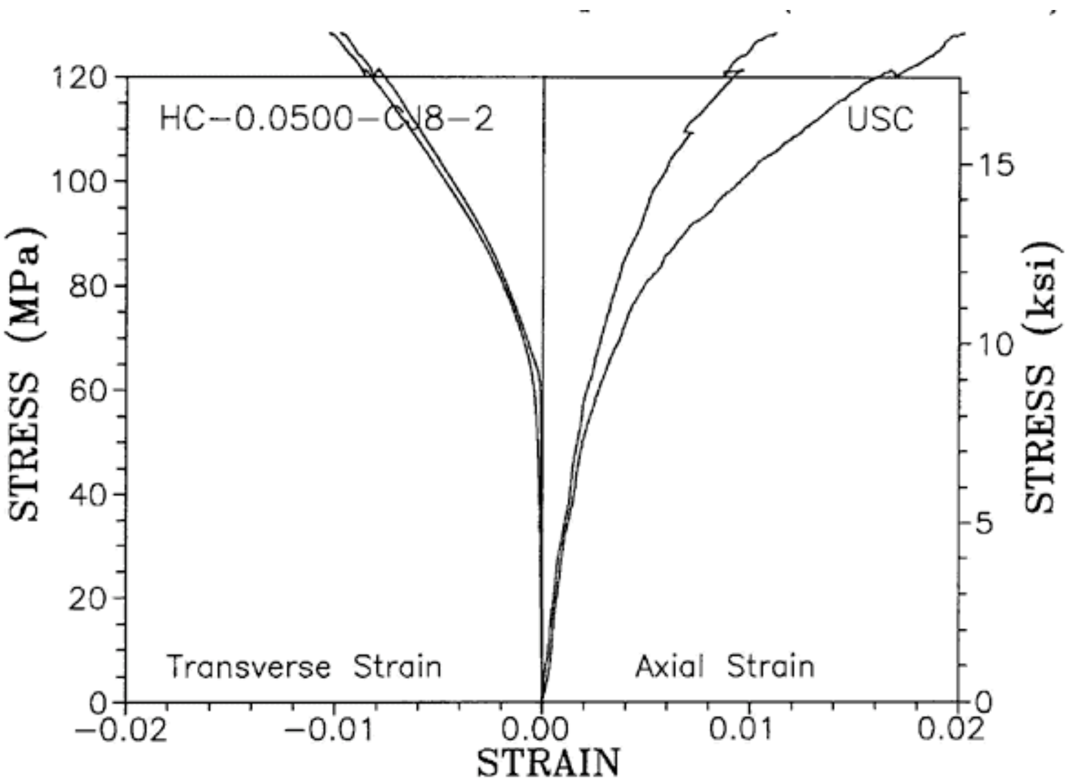

Fig H-D4.Stress-Strain Relationships for Higher Strength Concrete with 1.27mm Thickness Carbon Fiber Composite Jacket (HC-0.05-CJ8-2)

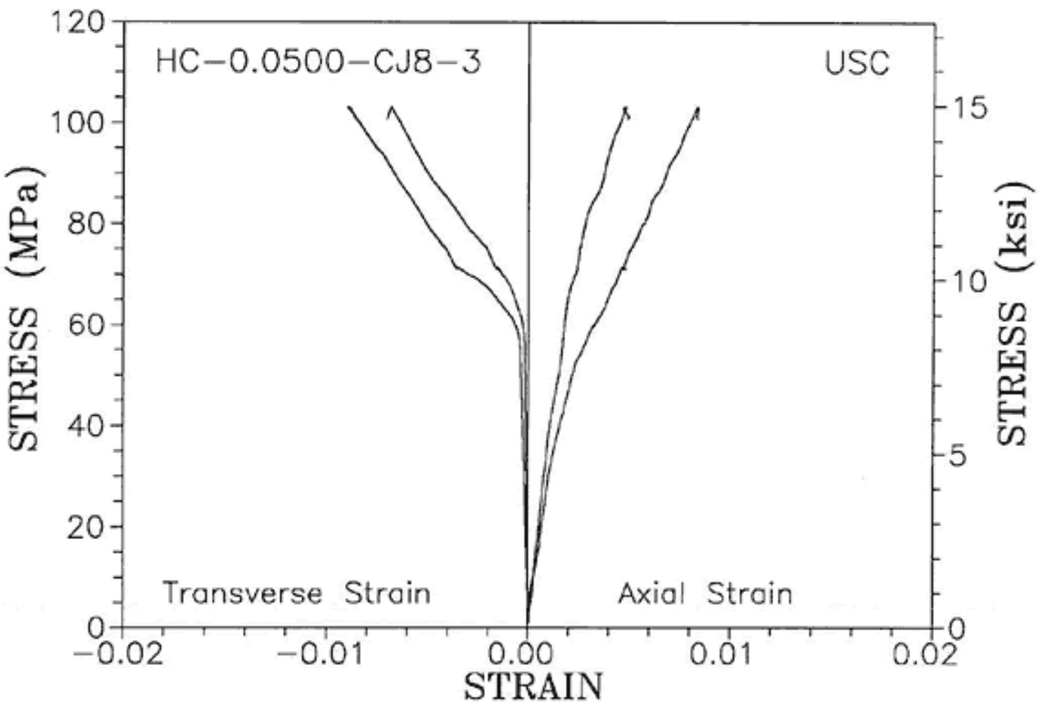

Fig H-D4.Stress-Strain Relationships for Higher Strength Concrete with 1.27mm Thickness Carbon Fiber Composite Jacket (HC-0.05-CJ8-3)

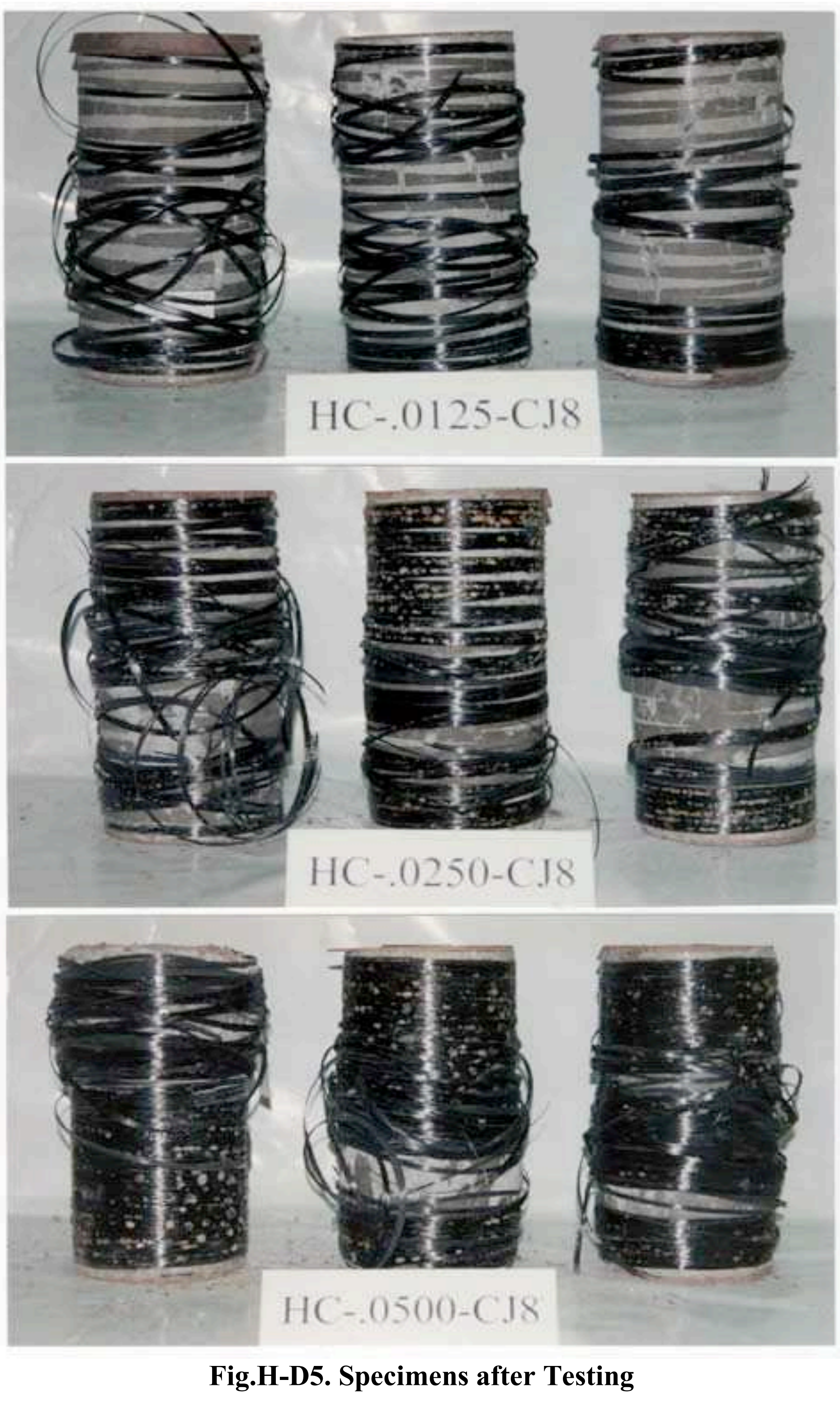

Fig.H-D5. Specimens after Testing

APPENDIX I: TEST RESULTS OF SYSTEM NINE

Part I-A General Information

Table I-A1 Test Results

Series	Specimen	f_c' (MPa)	Jacket Equivalent Thickness (mm)	f_{cc}' (MPa)	ε_{cu}
L	LC-0L-CJ9-1	34.7	0	33.19	0.002140
	LC-0L-CJ9-2			35.85	0.002440
	LC-0L-CJ9-3			34.91	0.001841
	LC-0.0125-CJ9-1		0.318	37.06	0.007121
	LC-0.0125-CJ9-2			35.09	0.002770
	LC-0.0125-CJ9-3			43.01	0.004712
	LC-0.0250-CJ9-1		0.635	60.01	0.016185
	LC-0.0250-CJ9-2			58.28	0.009641
	LC-0.0250-CJ9-3			54.40	0.012779
	LC-0.0500-CJ9-1		1.270	81.79	0.030770
	LC-0.0500-CJ9-2			61.95	0.013448
	LC-0.0500-CJ9-3			75.76	0.021571
M	MC-0L-CJ9-1	54.3	0	53.24	0.002585
	MC-0L-CJ9-2			56.29	0.002761
	MC-0L-CJ9-3			53.27	0.002830
	MC-0.0125-CJ9-1		0.318	53.51	0.002840
	MC-0.0125-CJ9-2			49.91	0.002206
	MC-0.0125-CJ9-3			50.85	0.002789
	MC-0.0250-CJ9-1		0.635	84.67	0.013935
	MC-0.0250-CJ9-2			67.95	0.007421
	MC-0.0250-CJ9-3			54.90	0.003690
	MC-0.0500-CJ9-1		1.270	96.14	0.014837
	MC-0.0500-CJ9-2			95.78	0.016359
	MC-0.0500-CJ9-3			109.46	0.020639
H	HC-0L-CJ9-1	61.9	0	64.55	0.002714
	HC-0L-CJ9-2			63.16	0.002685
	HC-0L-CJ9-3			57.97	0.002344
	HC-0.0125-CJ9-1		0.318	61.95	0.002467
	HC-0.0125-CJ9-2			59.69	0.002353
	HC-0.0125-CJ9-3			65.47	0.002829
	HC-0.0250-CJ9-1		0.635	68.67	0.003585
	HC-0.0250-CJ9-2			69.21	0.003119
	HC-0.0250-CJ9-3			69.14	0.003433
	HC-0.0500-CJ9-1		1.270	84.79	0.005570
	HC-0.0500-CJ9-2			98.93	0.007854
	HC-0.0500-CJ9-3			92.55	0.008013

te: (i) Example for specimen name designation:
LC-0.0250-CJ9-1: LC designates Lower strength Concrete; 0.0250 designates jacket equivalent thickness in inches; CJ9 designates Carbon fiber Jacket System 9; and the last number represents specimen number in same series.
(ii) f_c': Average plain concrete cylinder strength;
(iii) f_{cc}': Ultimate strength of confined concrete;
(iv) ε_{cu}: Ultimate strain.

Part I-B Test Results of Lower Strength Concrete Cylinders

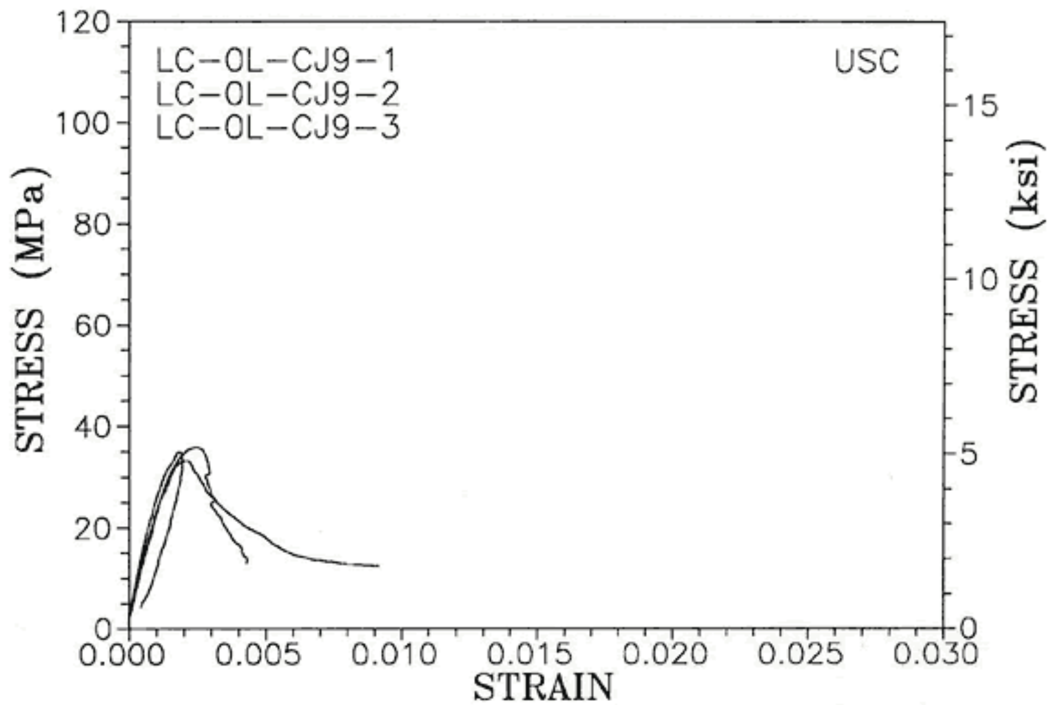

Fig.I-B1. Stress-Strain Relationship for Lower Strength Plain Concrete Cylinders

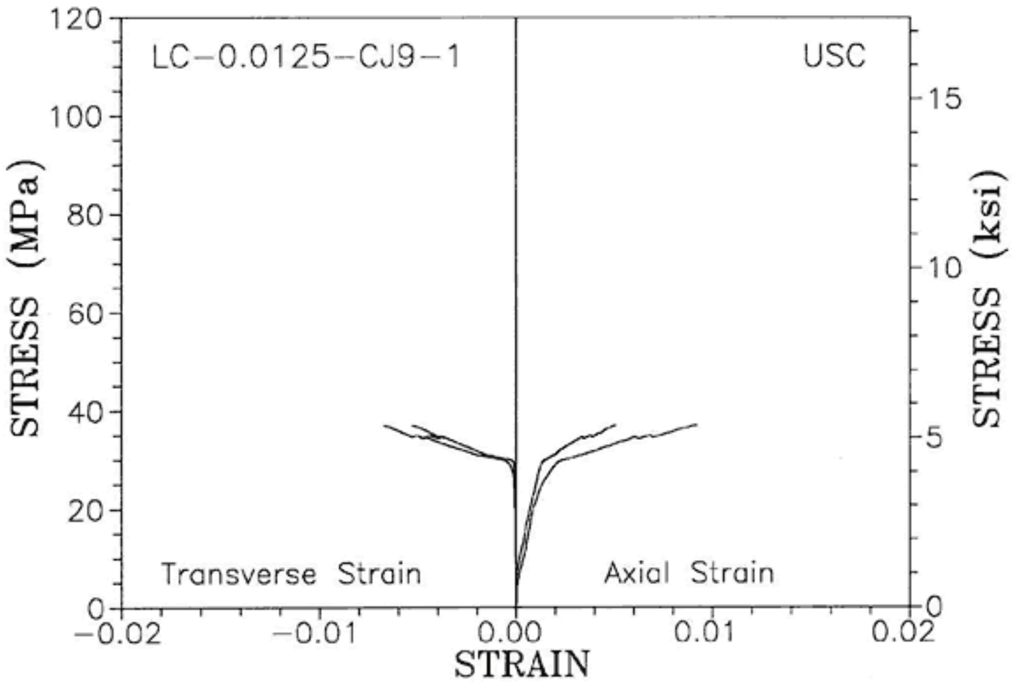

Fig I-B2.Stress-Strain Relationships for Lower Strength Concrete with 0.318mm Thickness Carbon Fiber Composite Jacket (LC-0.0125-CJ9-1)

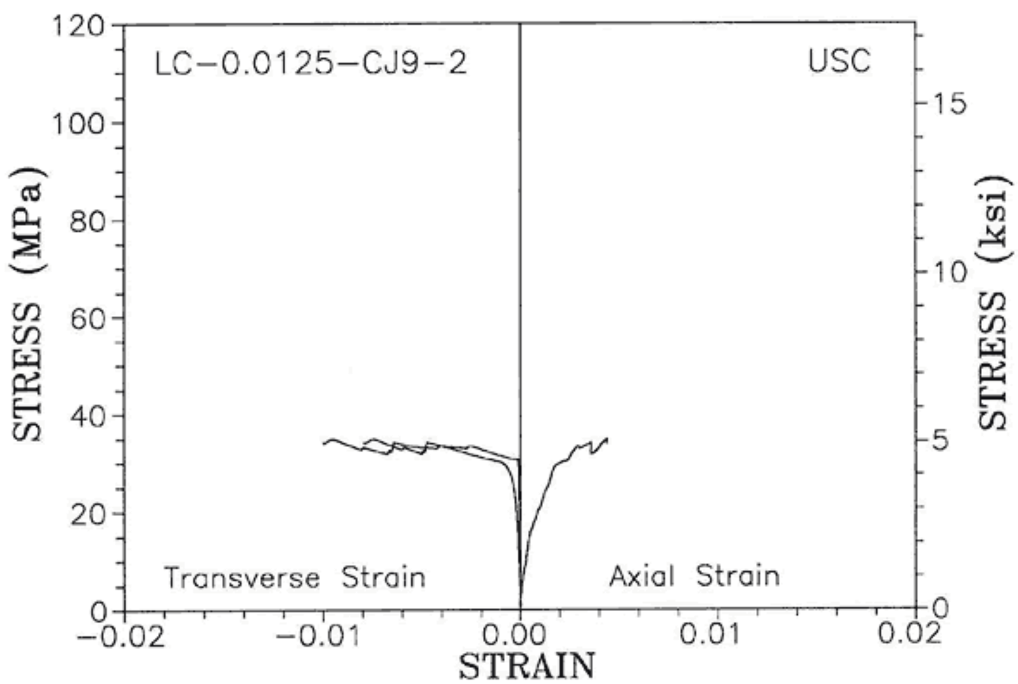

Fig I-B2.Stress-Strain Relationships for Lower Strength Concrete with 0.318mm Thickness Carbon Fiber Composite Jacket (LC-0.0125-CJ9-2)

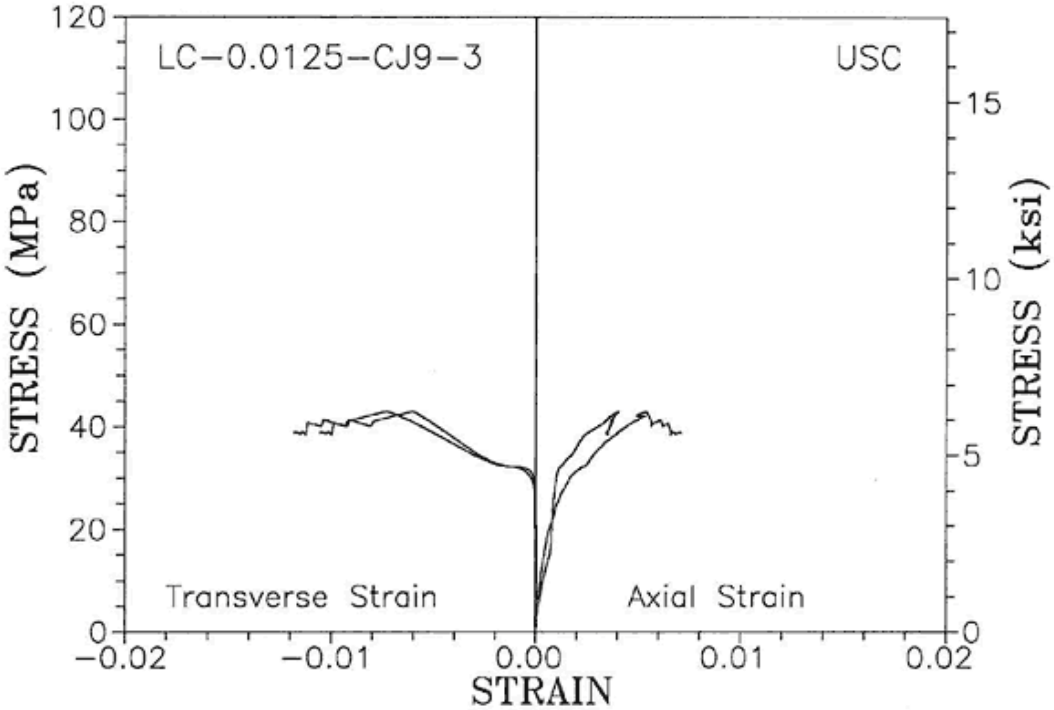

Fig I-B2.Stress-Strain Relationships for Lower Strength Concrete with 0.318mm Thickness Carbon Fiber Composite Jacket (LC-0.0125-CJ9-3)

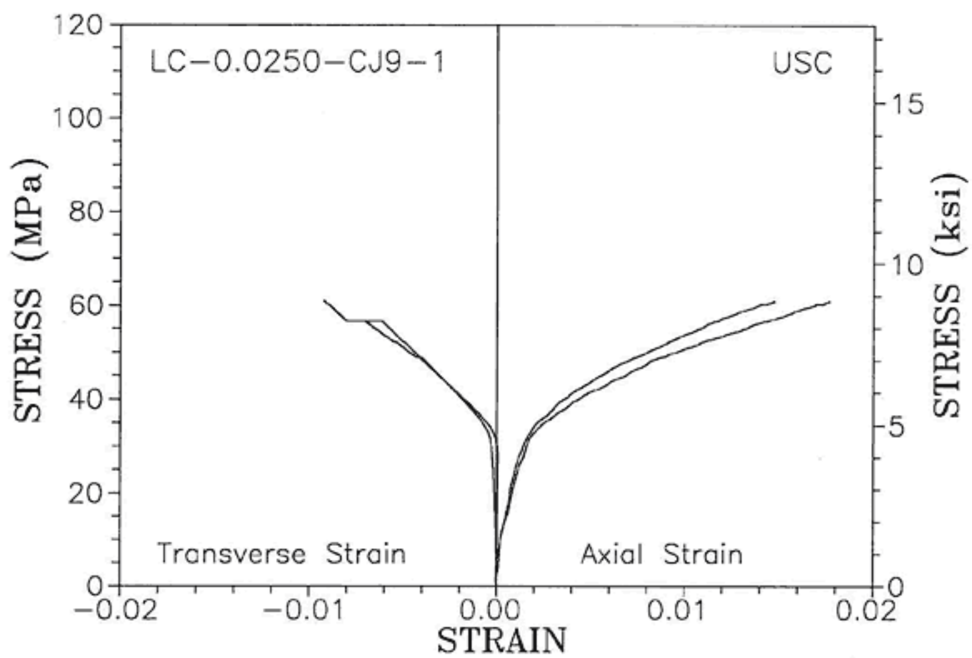

Fig I-B3.Stress-Strain Relationships for Lower Strength Concrete with 0.635mm Thickness Carbon Fiber Composite Jacket (LC-0.025-CJ9-1)

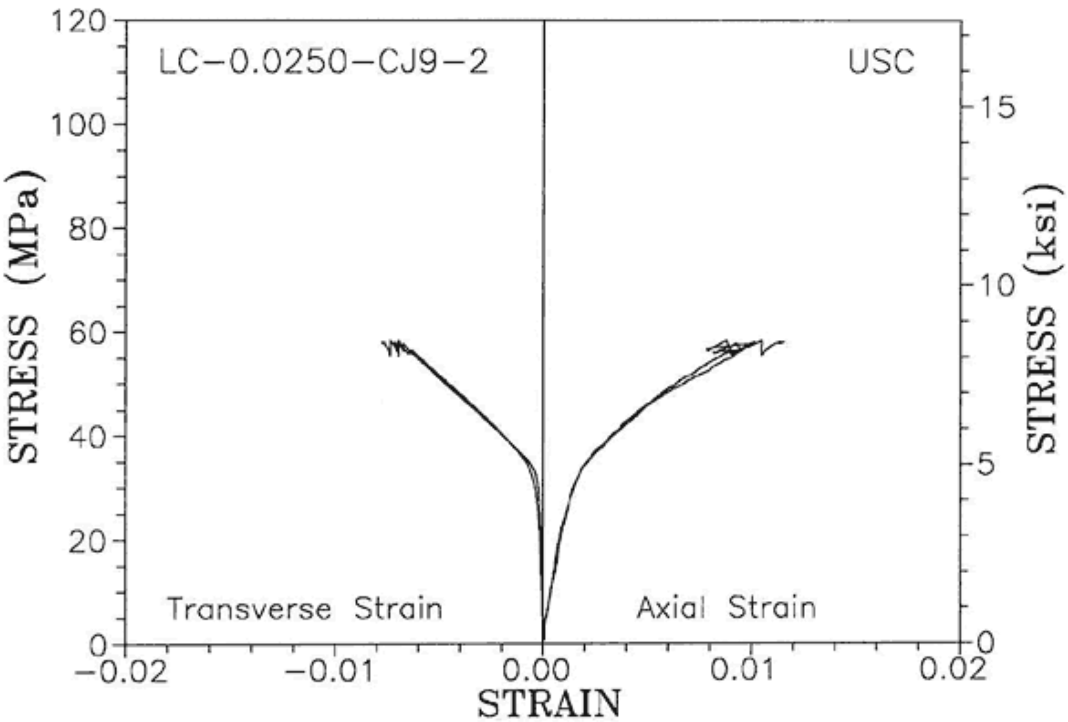

Fig I-B3.Stress-Strain Relationships for Lower Strength Concrete with 0.635mm Thickness Carbon Fiber Composite Jacket (LC-0.025-CJ9-2)

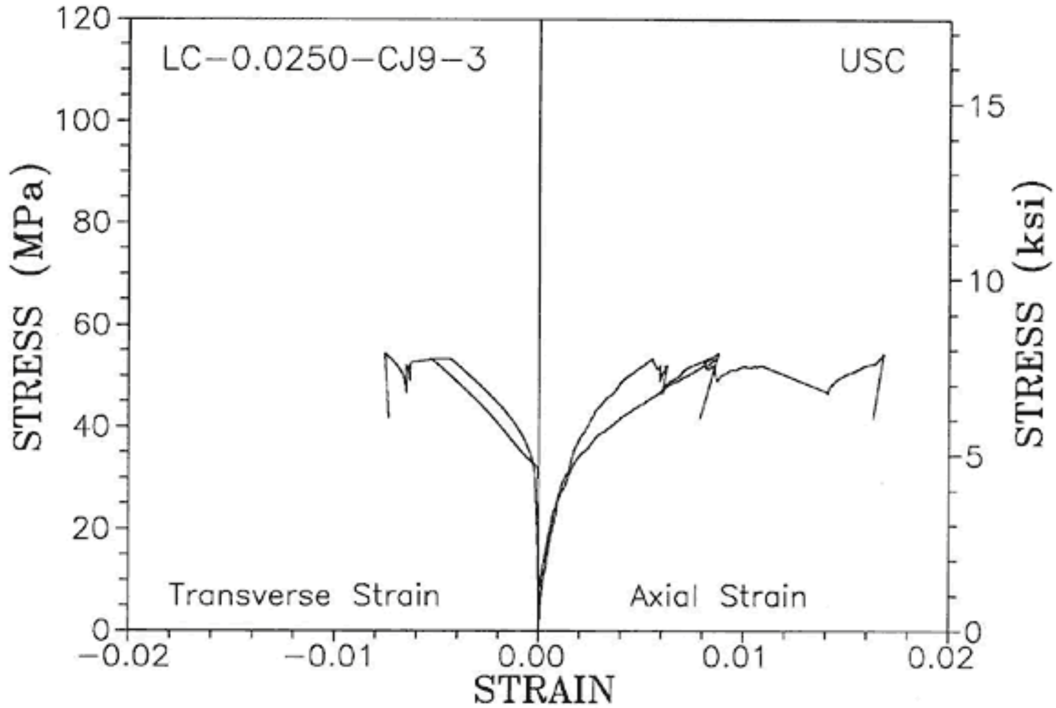

Fig I-B3.Stress-Strain Relationships for Lower Strength Concrete with 0.635mm Thickness Carbon Fiber Composite Jacket (LC-0.025-CJ9-2)

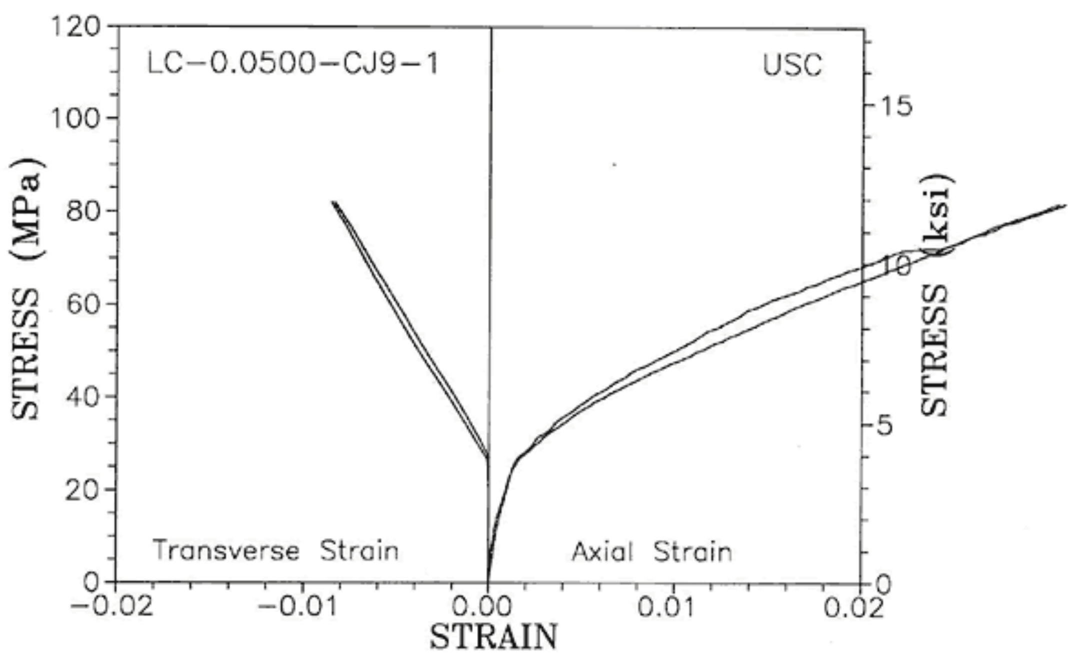

Fig I-B4.Stress-Strain Relationships for Lower Strength Concrete with 1.27mm Thickness Carbon Fiber Composite Jacket (LC-0.05-CJ9-1)

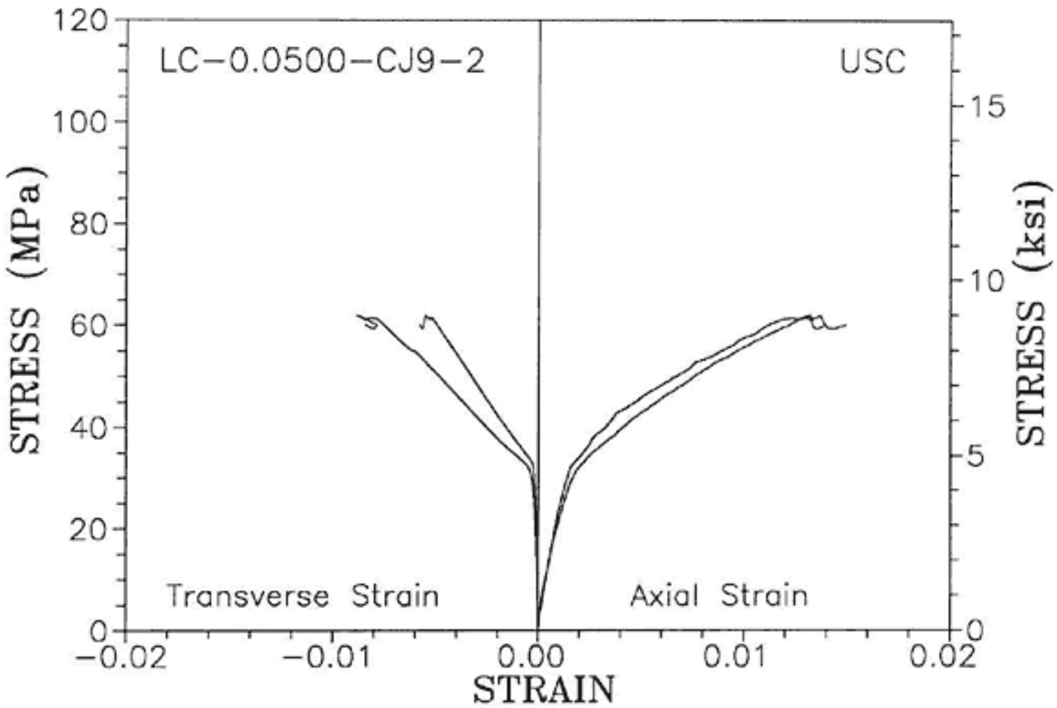

Fig I-B4.Stress-Strain Relationships for Lower Strength Concrete with 1.27mm Thickness Carbon Fiber Composite Jacket (LC-0.05-CJ9-2)

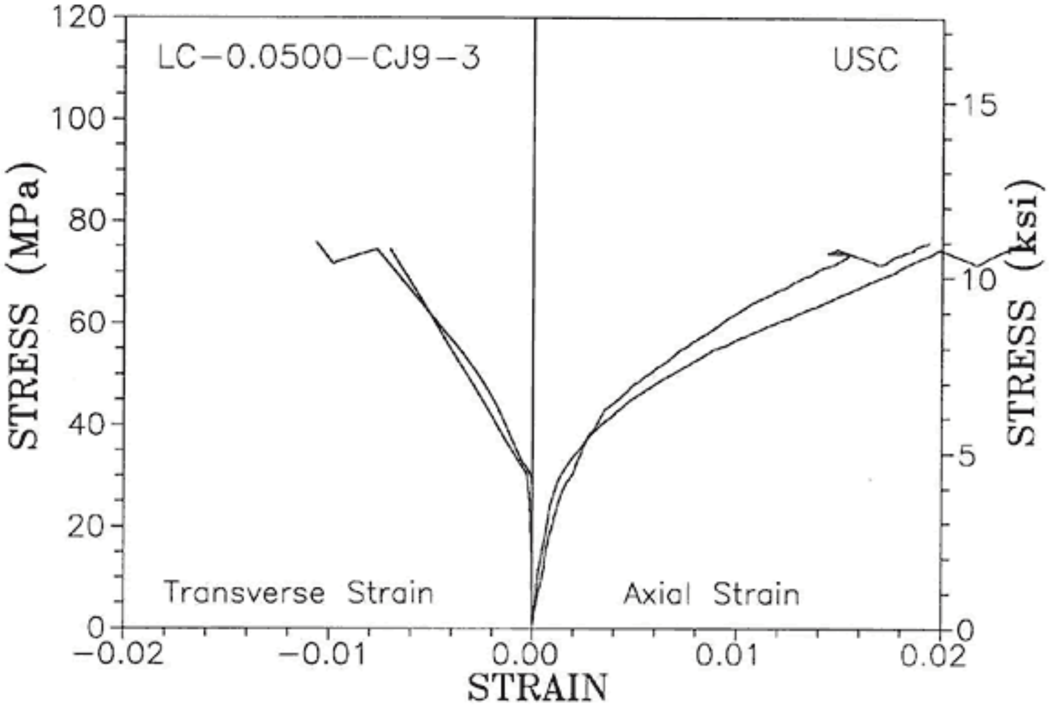

Fig I-B4.Stress-Strain Relationships for Lower Strength Concrete with 1.27mm Thickness Carbon Fiber Composite Jacket (LC-0.05-CJ9-3)

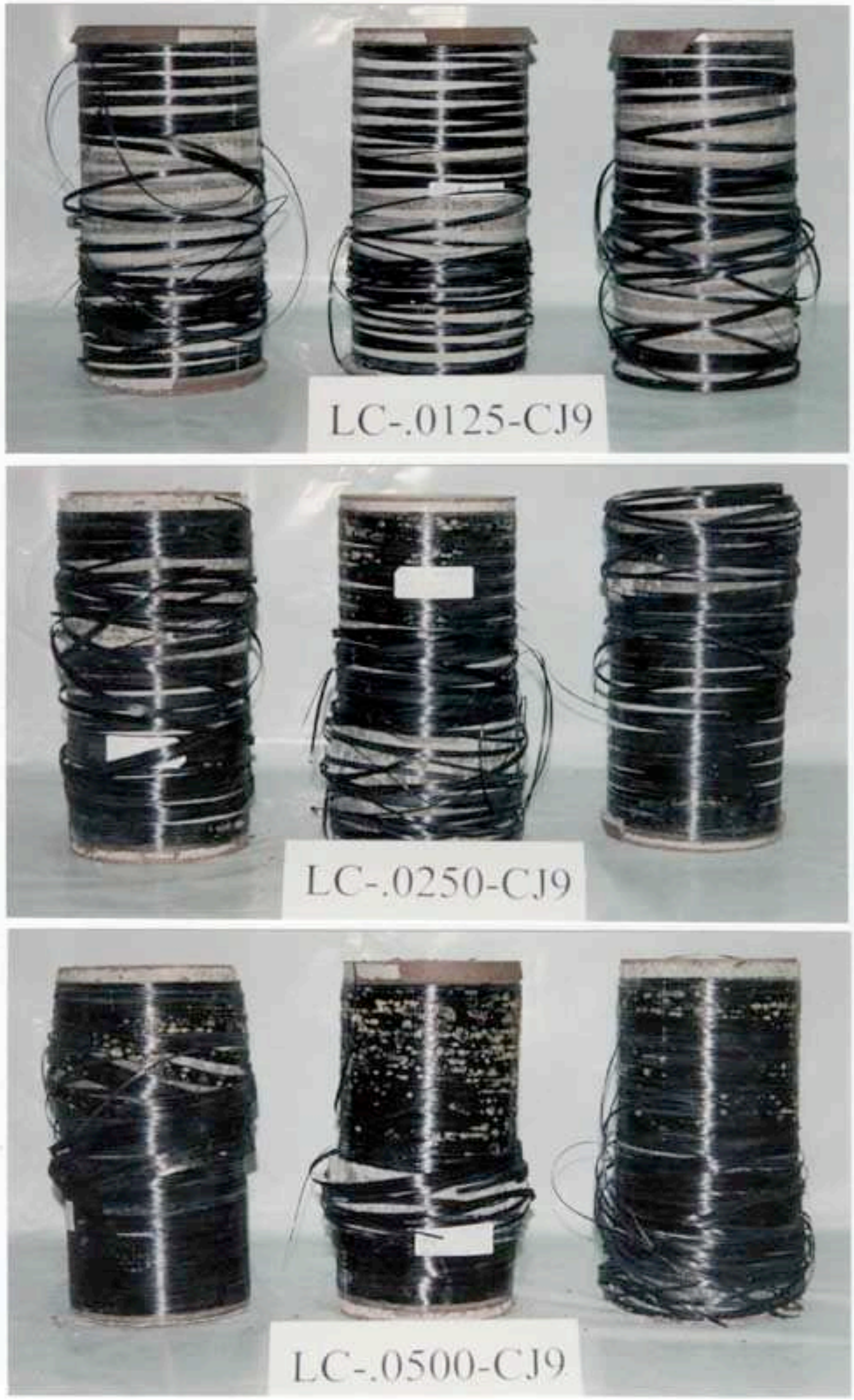

Fig.I-B5. Specimens after Testing

Part I-C Test Results of Medium Strength Concrete Cylinders

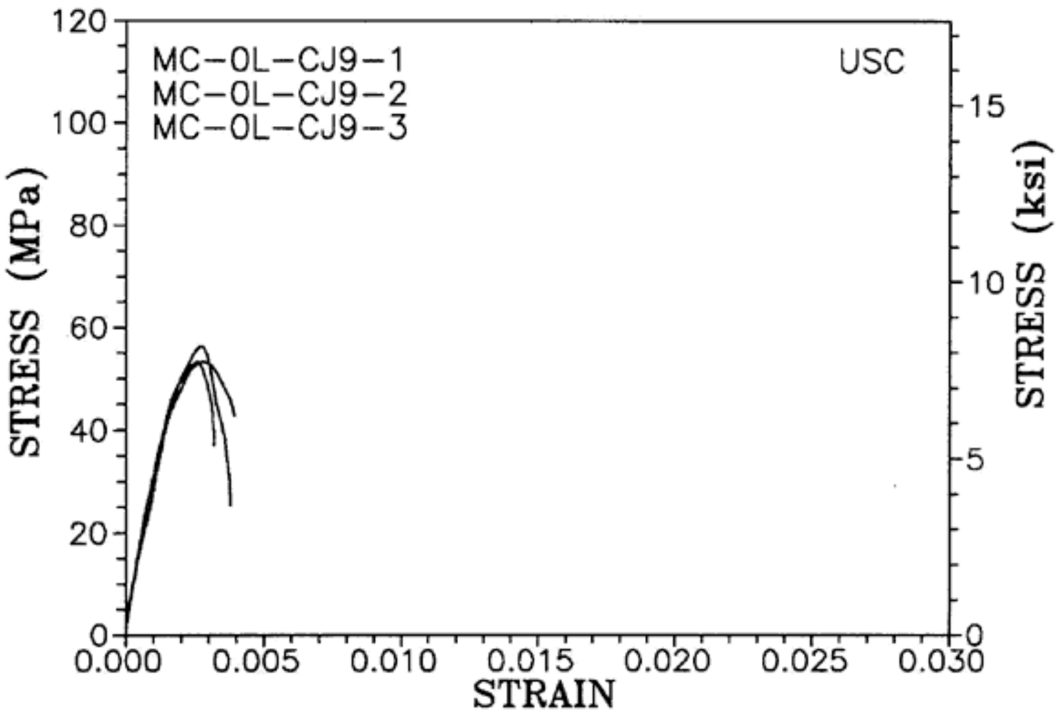

Fig.I-C1. Stress-Strain Relationship for Medium Strength Plain Concrete Cylinders

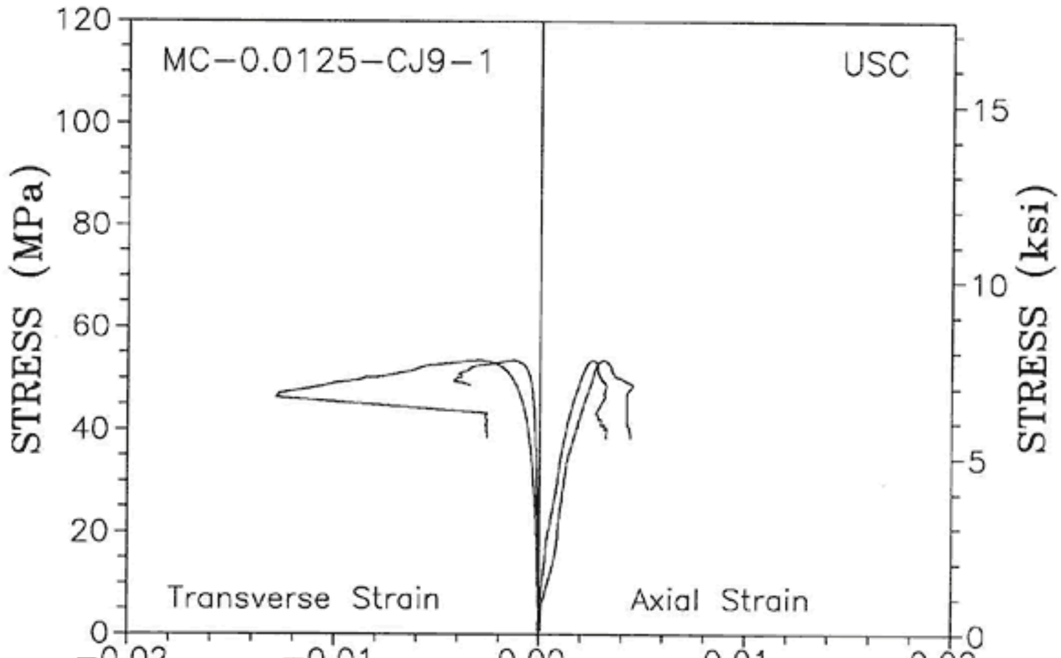

[redacted]

Fig I-C2.Stress-Strain Relationships for Medium Strength Concrete with 0.318mm Thickness Carbon Fiber Composite Jacket (MC-0.0125-CJ9-1)

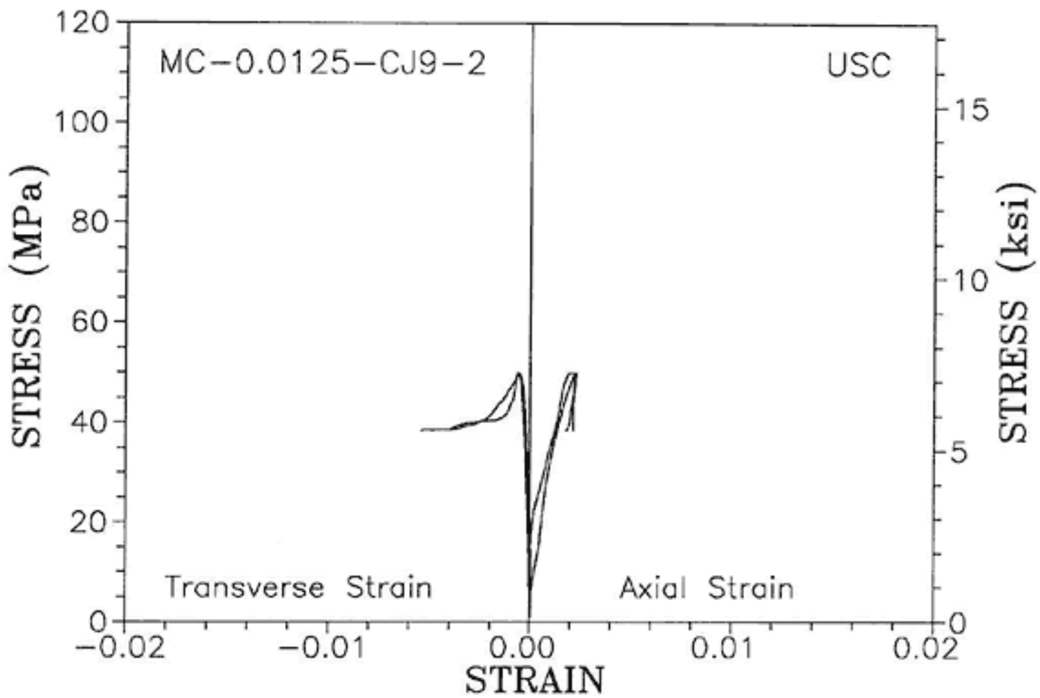

Fig I-C2.Stress-Strain Relationships for Medium Strength Concrete with 0.318mm Thickness Carbon Fiber Composite Jacket (MC-0.0125-CJ9-2)

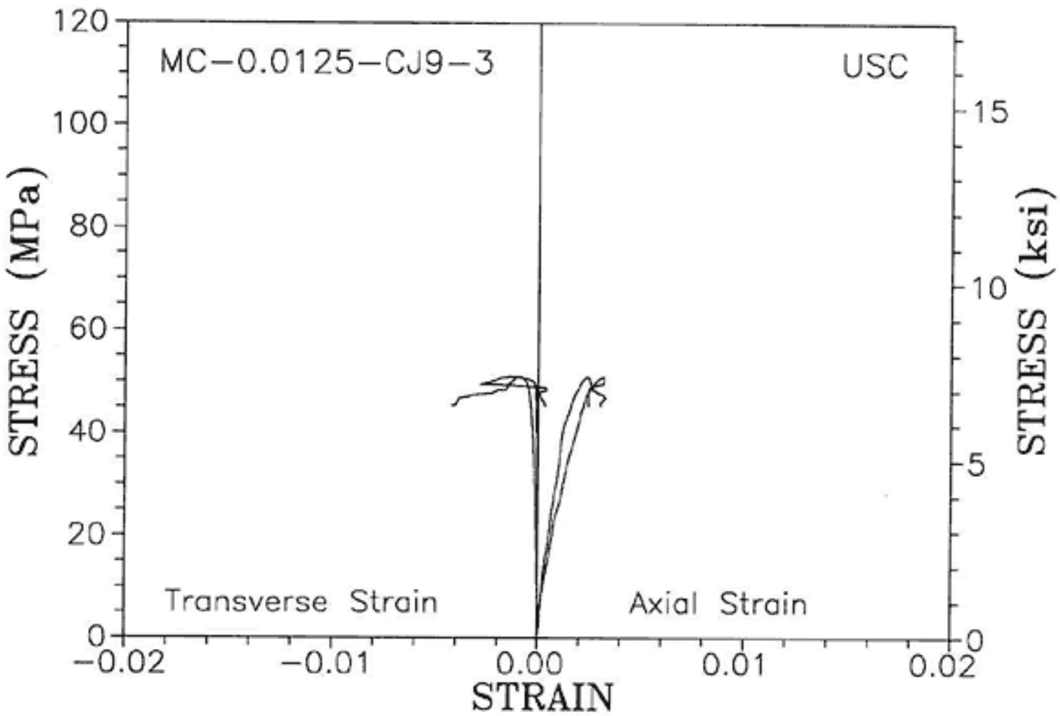

Fig I-C2.Stress-Strain Relationships for Medium Strength Concrete with 0.318mm Thickness Carbon Fiber Composite Jacket (MC-0.0125-CJ9-3)

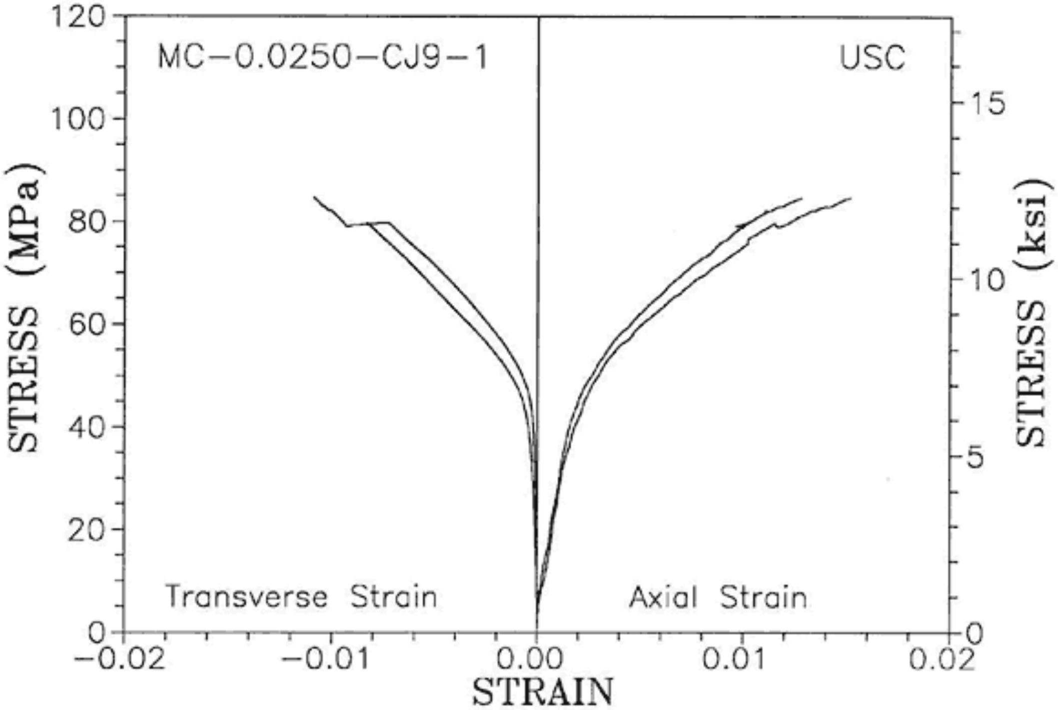

Fig I-C3.Stress-Strain Relationships for Medium Strength Concrete with 0.635mm Thickness Carbon Fiber Composite Jacket (MC-0.025-CJ9-1)

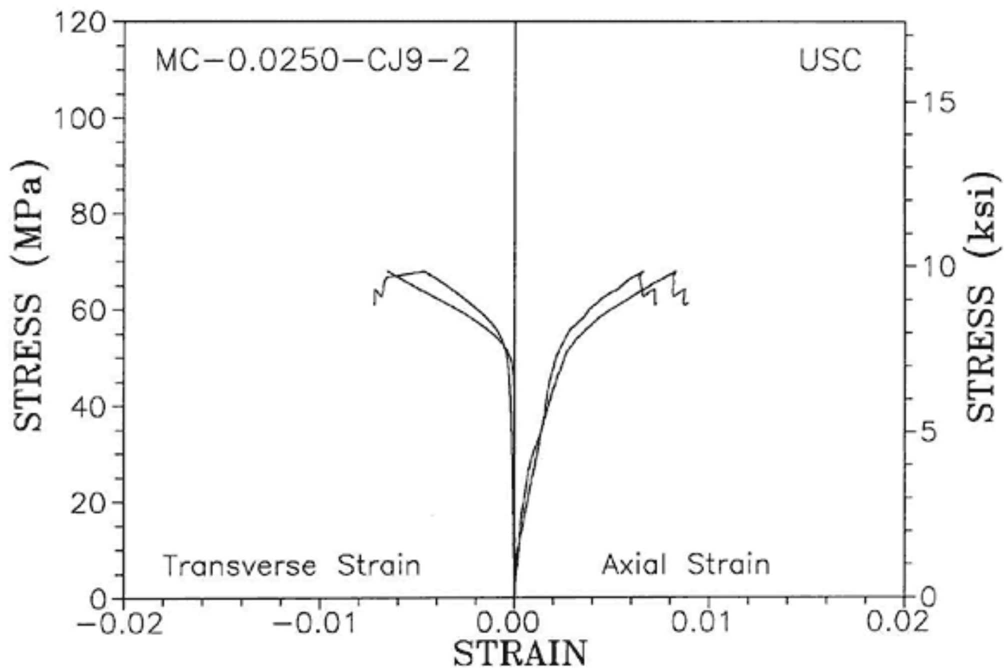

Fig I-C3.Stress-Strain Relationships for Medium Strength Concrete with 0.635mm Thickness Carbon Fiber Composite Jacket (MC-0.025-CJ9-2)

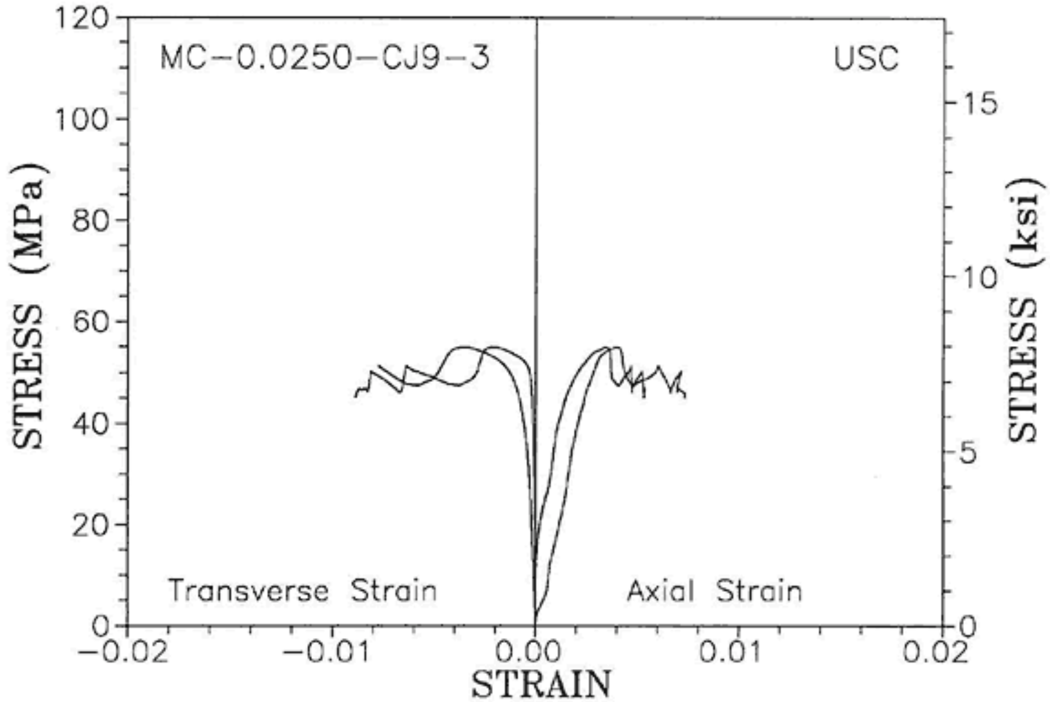

Fig I-C3.Stress-Strain Relationships for Medium Strength Concrete with 0.635mm Thickness Carbon Fiber Composite Jacket (MC-0.025-CJ9-3)

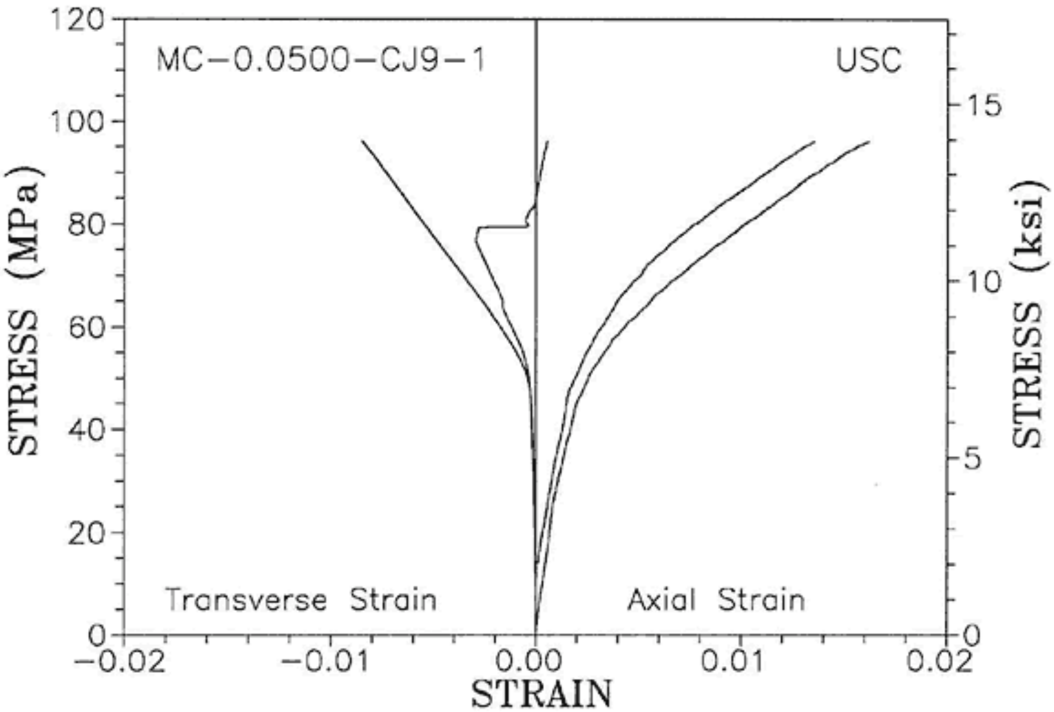

Fig I-C4.Stress-Strain Relationships for Medium Strength Concrete with 1.27mm Thickness Carbon Fiber Composite Jacket (MC-0.05-CJ9-1)

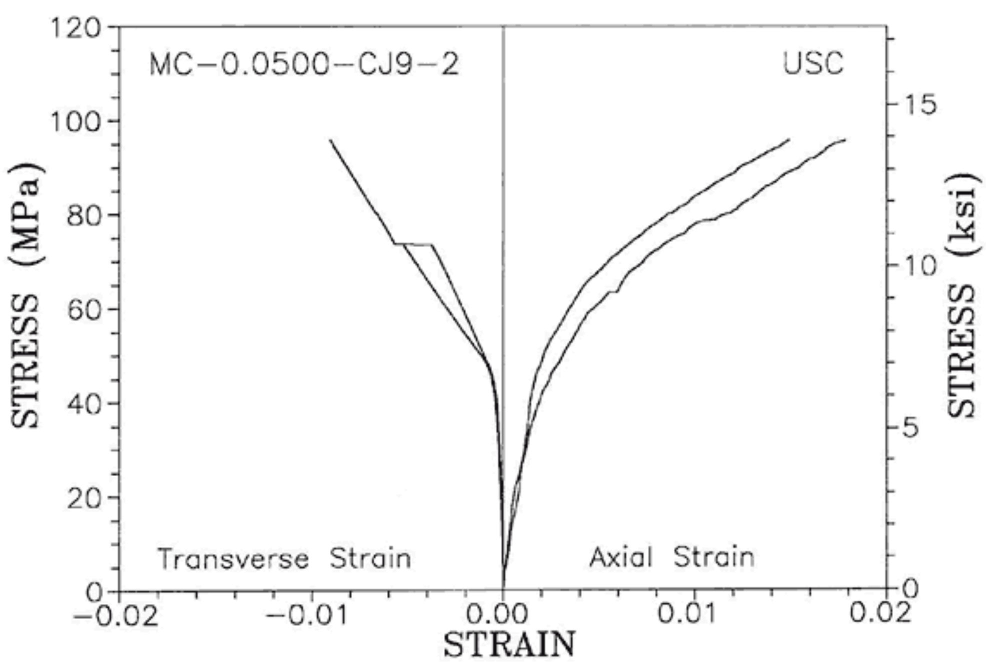

Fig I-C4.Stress-Strain Relationships for Medium Strength Concrete with 1.27mm Thickness Carbon Fiber Composite Jacket (MC-0.05-CJ9-2)

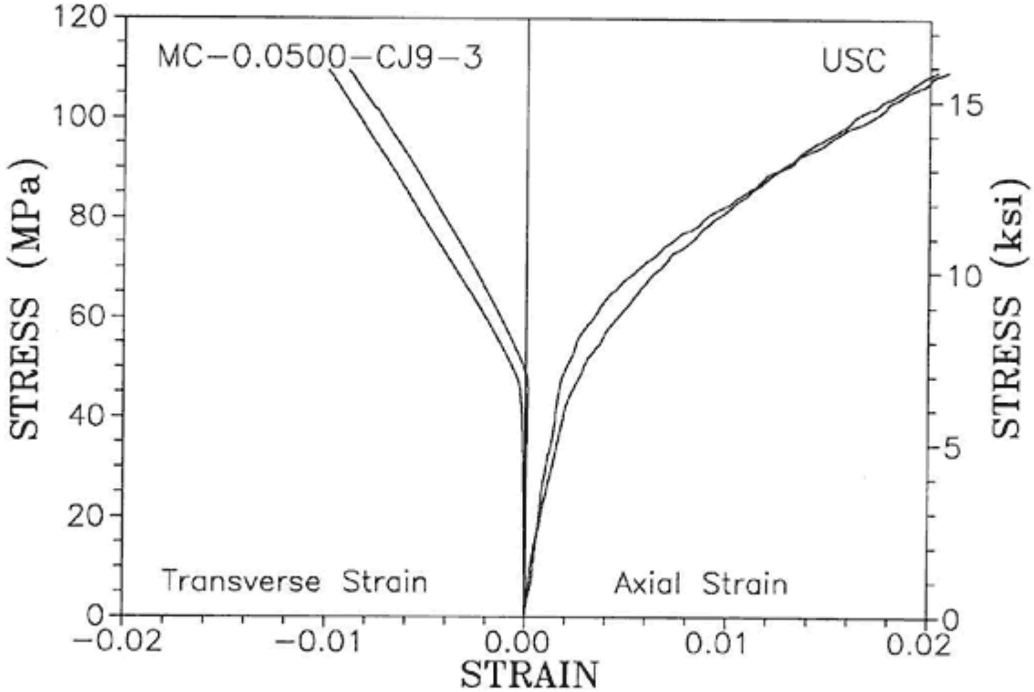

Fig I-C4.Stress-Strain Relationships for Medium Strength Concrete with 1.27mm Thickness Carbon Fiber Composite Jacket (MC-0.05-CJ9-3)

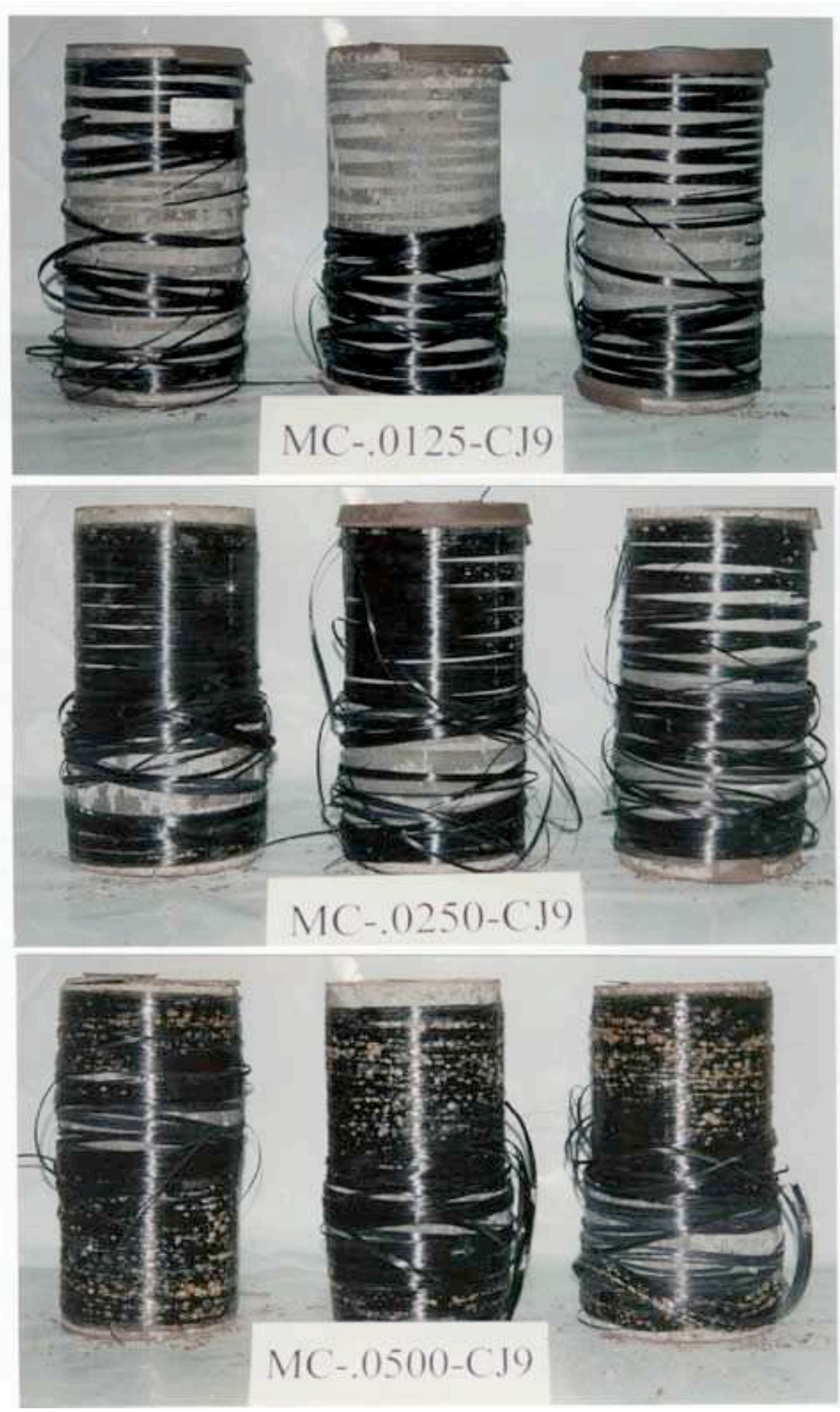

Fig.G-C5. Specimens after Testing

Part I-D Test Results of Higher Strength Concrete Cylinders

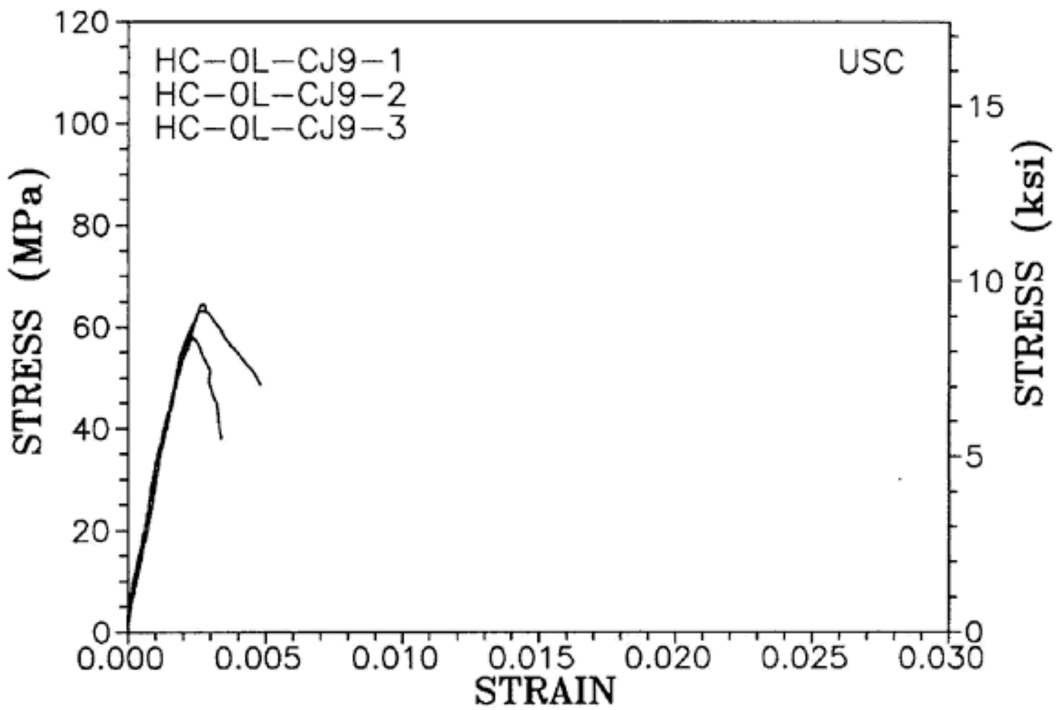

Fig.I-D1. Stress-Strain Relationships for Higher Strength Plain Concrete Cylinders

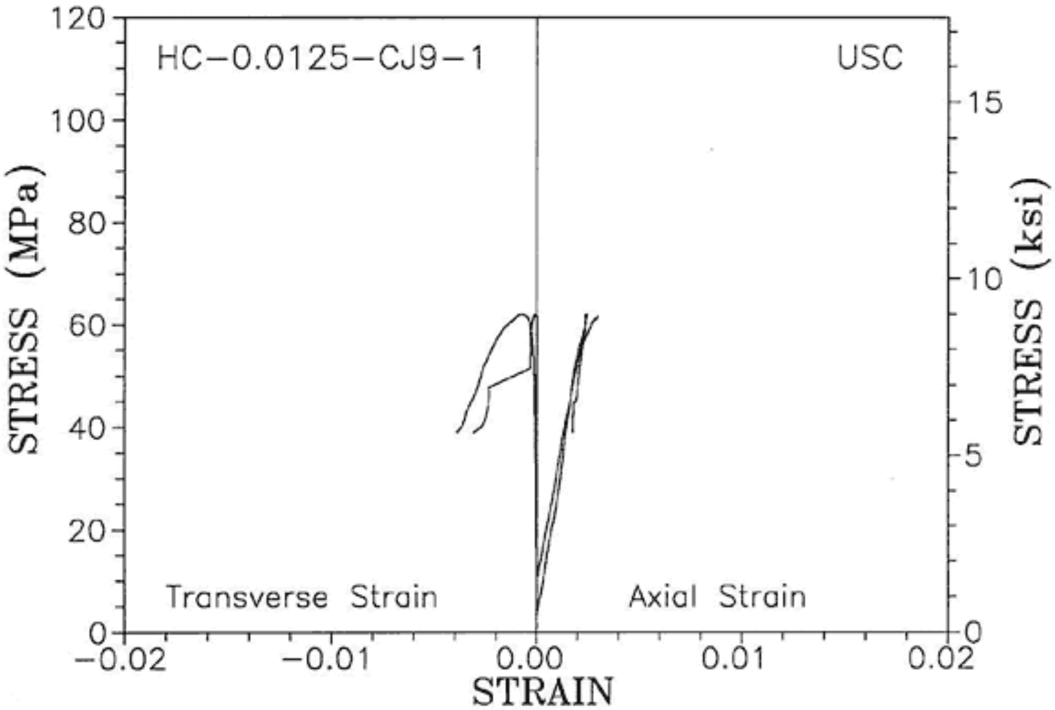

Fig I-D2.Stress-Strain Relationships for Higher Strength Concrete with 0.318mm Thickness Carbon Fiber Composite Jacket (HC-0.0125-CJ9-1)

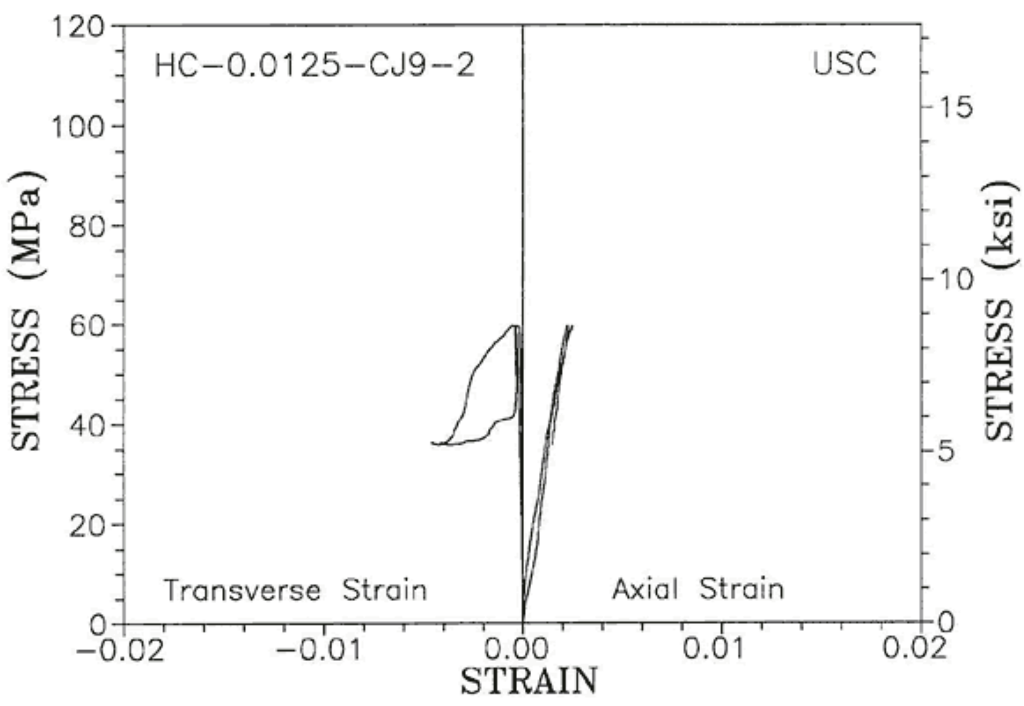

Fig I-D2.Stress-Strain Relationships for Higher Strength Concrete with 0.318mm Thickness Carbon Fiber Composite Jacket (HC-0.0125-CJ9-2)

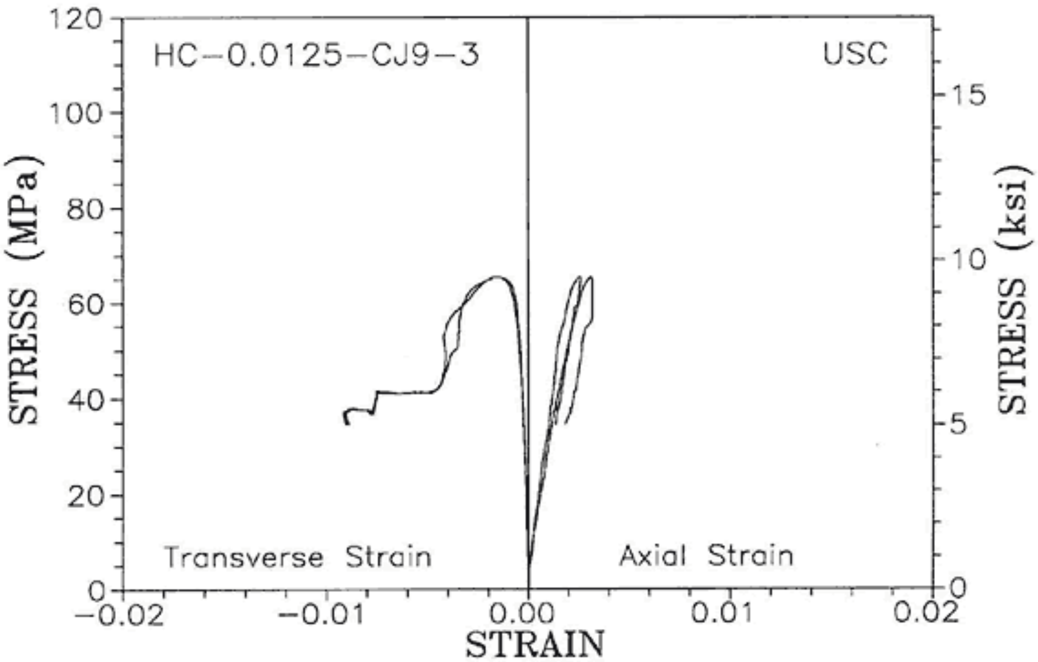

Fig I-D2.Stress-Strain Relationships for Higher Strength Concrete with 0.318mm Thickness Carbon Fiber Composite Jacket (HC-0.0125-CJ9-3)

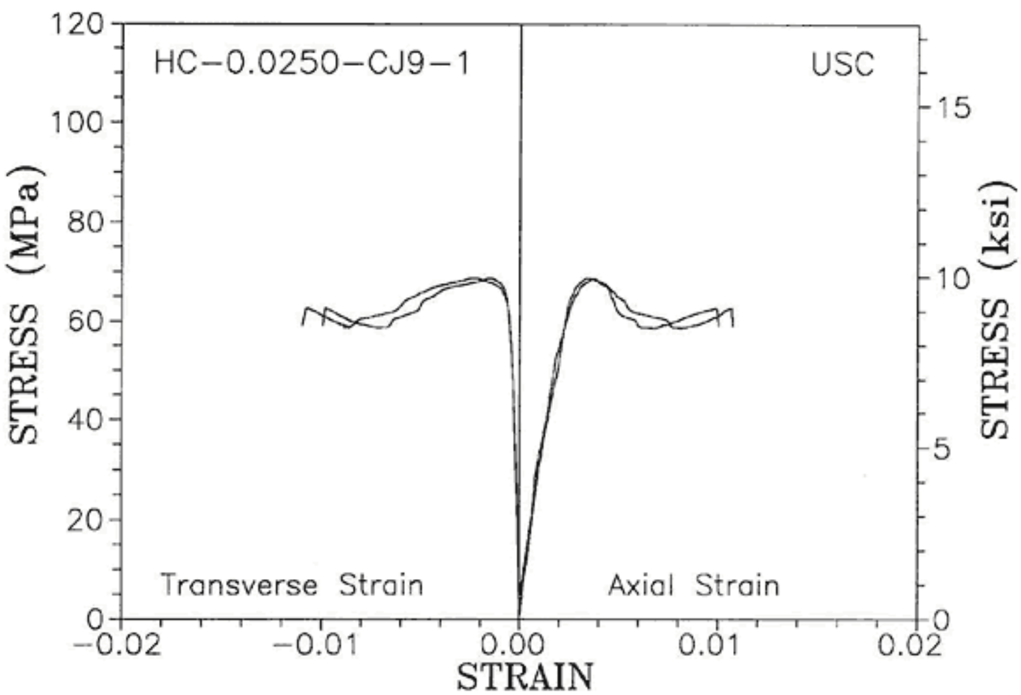

Fig I-D3.Stress-Strain Relationships for Higher Strength Concrete with 0.635mm Thickness Carbon Fiber Composite Jacket (HC-0.025-CJ9-1)

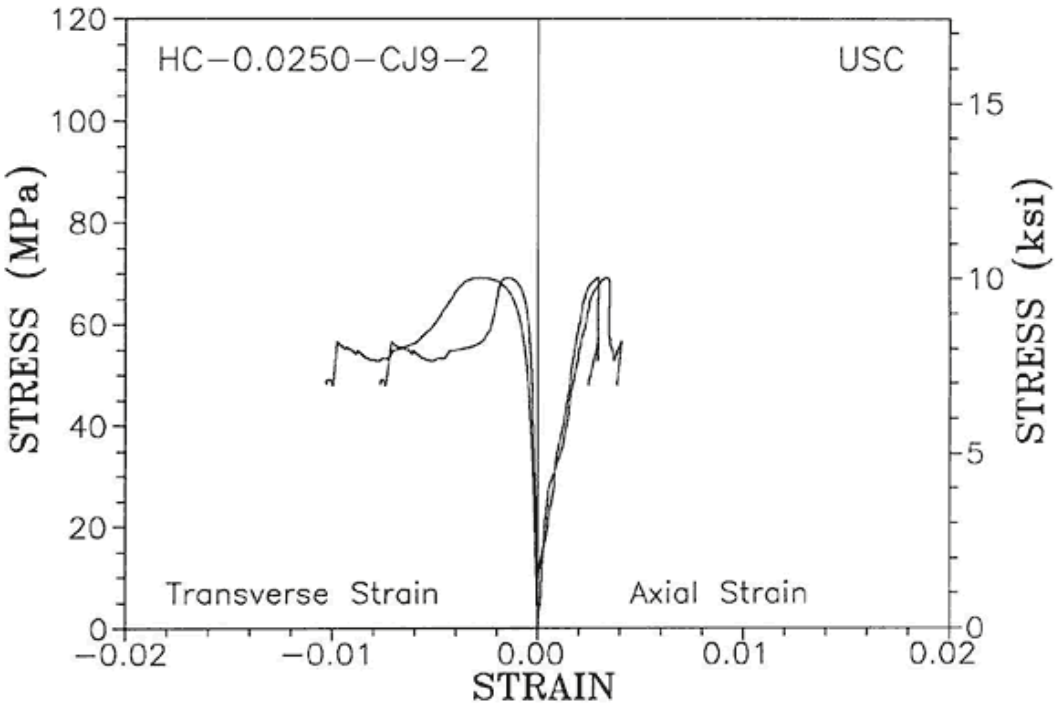

Fig I-D3.Stress-Strain Relationships for Higher Strength Concrete with 0.635mm Thickness Carbon Fiber Composite Jacket (HC-0.025-CJ9-1)

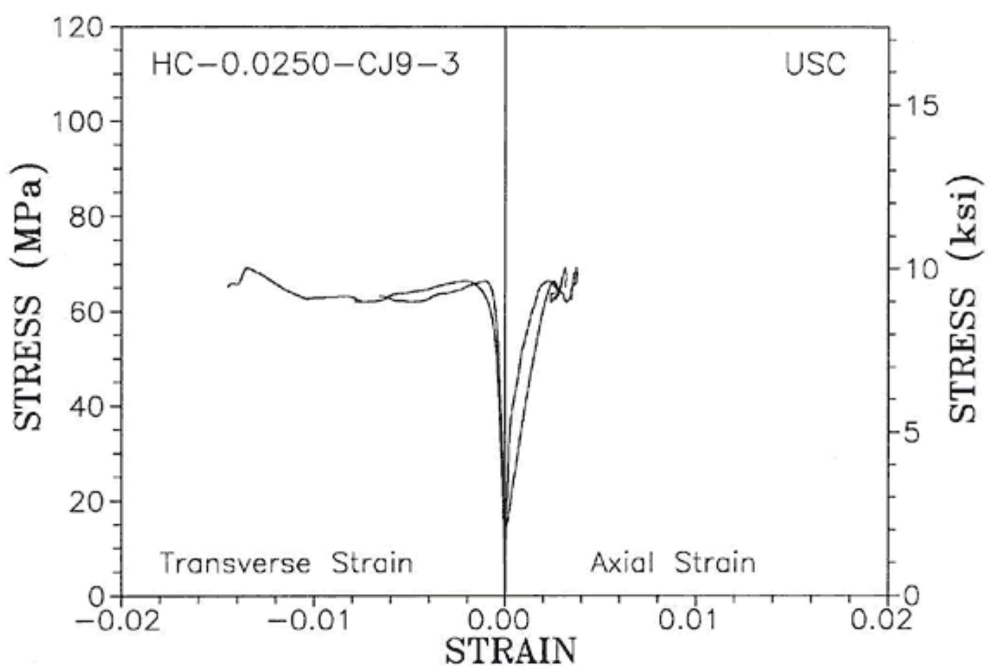

Fig I-D3.Stress-Strain Relationships for Higher Strength Concrete with 0.635mm Thickness Carbon Fiber Composite Jacket (HC-0.025-CJ9-3)

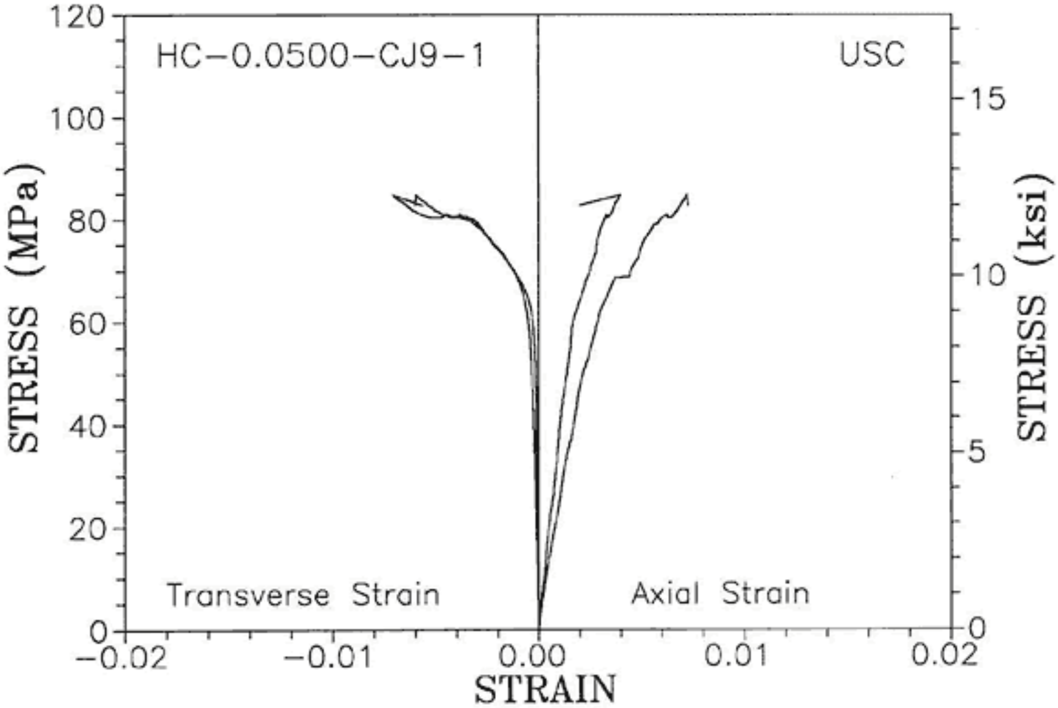

Fig I-D4.Stress-Strain Relationships for Higher Strength Concrete with 1.27mm Thickness Carbon Fiber Composite Jacket (HC-0.05-CJ9-1)

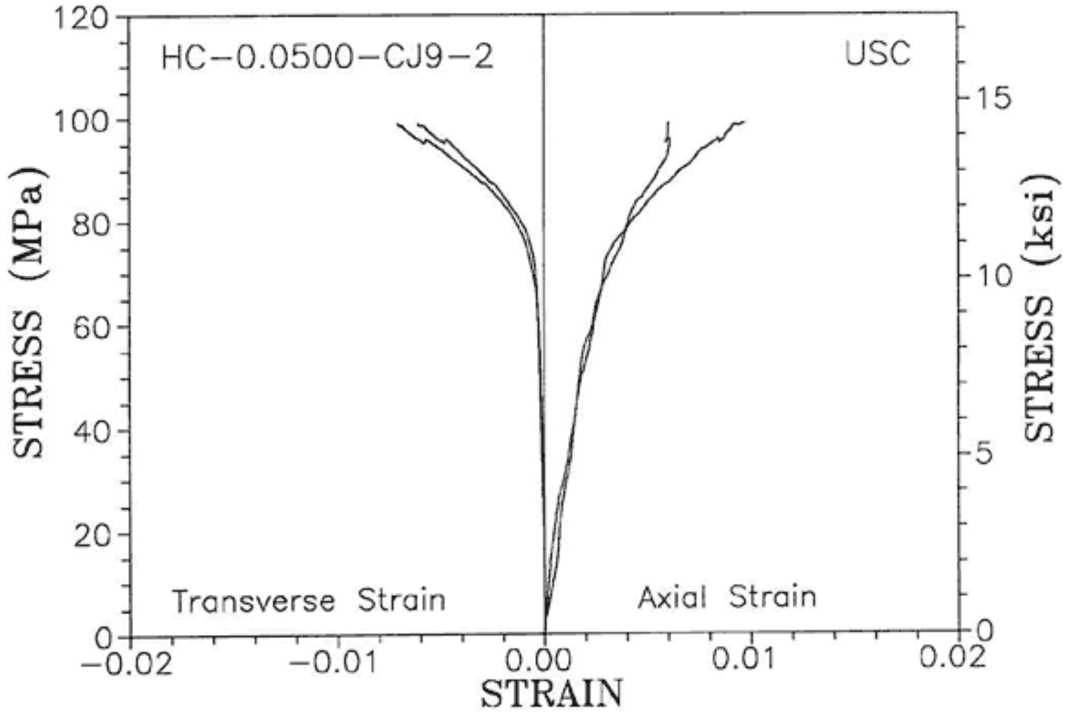

Fig I-D4.Stress-Strain Relationships for Higher Strength Concrete with 1.27mm Thickness Carbon Fiber Composite Jacket (HC-0.05-CJ9-2)

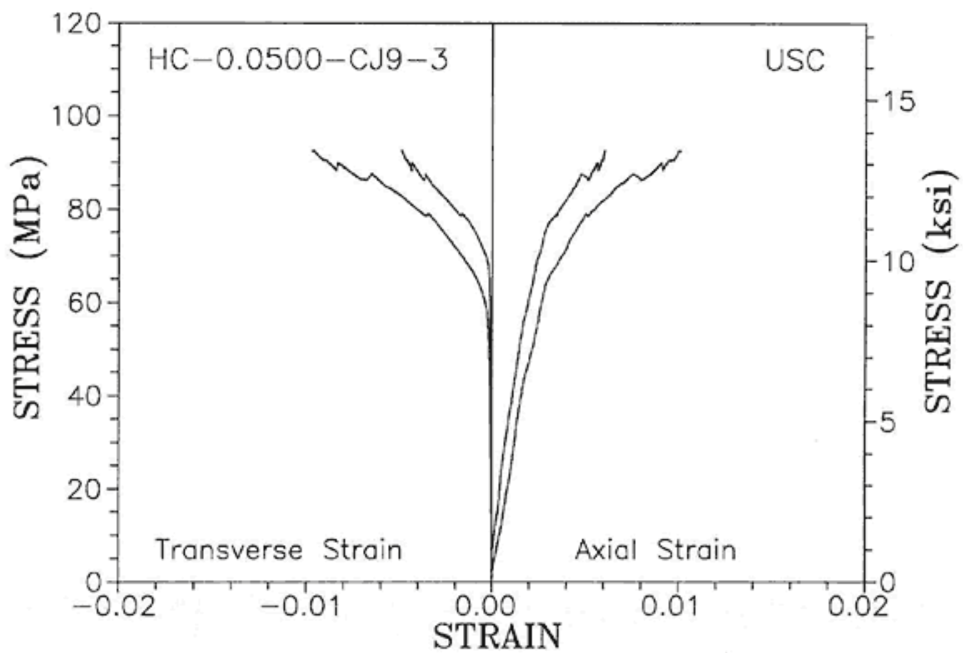

Fig I-D4.Stress-Strain Relationships for Higher Strength Concrete with 1.27mm Thickness Carbon Fiber Composite Jacket (HC-0.05-CJ9-3)

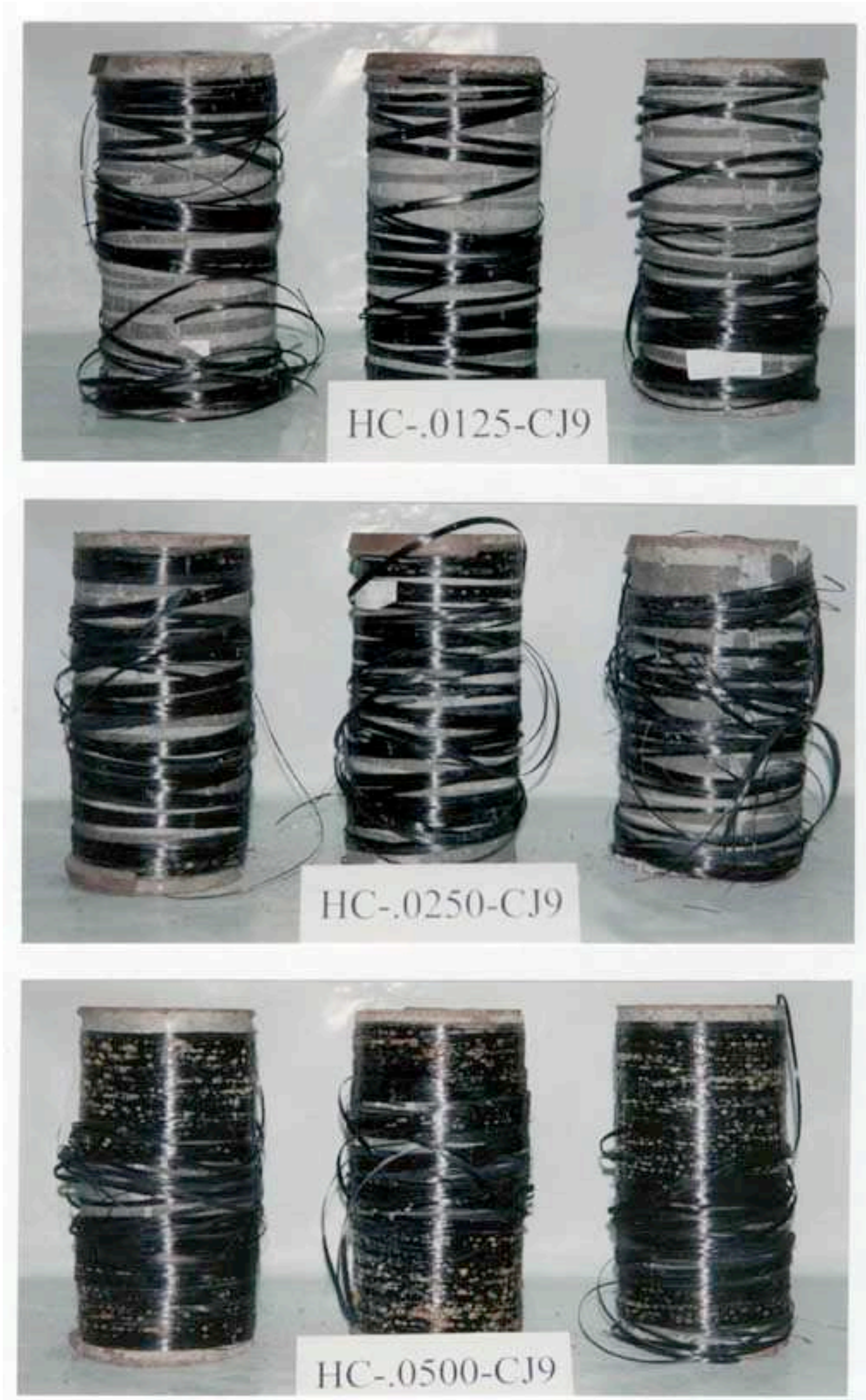

Fig.I-D5. Specimens after Testing